VOLUME 109 NUMBER 3

THE ASTROPHYSICAL JOURNAL

AN INTERNATIONAL REVIEW OF SPECTROSCOPY AND ASTRONOMICAL PHYSICS

MAY 1949

THE TEMPERATURE OF INTERSTELLAR MATTER. II — *Lyman Spitzer, Jr.* — 337

OBSERVATIONS OF INTERSTELLAR H AND K, MOLECULAR LINES, AND RADIAL VELOCITIES IN THE SPECTRA OF 300 O AND B STARS — *Walter S. Adams* — 354

AN UPPER LIMIT TO THE ELECTRON DENSITY NEAR THE EARTH'S ORBIT — *Fred L. Whipple and Joseph L. Greenstein* — 380

A STUDY OF M-TYPE STARS IN CYGNUS — *J. J. Nassau and C. B. van Albada* — 391

VARIATIONS IN THE STELLAR LUMINOSITY FUNCTION. III. A REGION IN AURIGA — *S. W. McCuskey* — 414

STELLAR SPECTRA IN MILKY WAY REGIONS. I. A REGION IN AQUILA — *S. W. McCuskey* — 426

SPECTROGRAPHIC OBSERVATIONS OF THE ECLIPSING VARIABLE SW LACERTAE — *Otto Struve* — 436

NEW SPECTROGRAPHIC INVESTIGATIONS OF THE ECLIPSING STAR XZ SAGITTARII — *Jorge Sahade* — 450

FURTHER NOTE ON THE DISTRIBUTION OF THE LONGITUDE OF PERIASTRON — *Elizabeth L. Scott* — 446

THE STARK EFFECT OF THE HIGHER BALMER LINES IN STARS OF SPECTRAL TYPES A AND B — *Elsa van Dien* — 452

ON THE PRESENCE OF POLARIZATION IN THE CONTINUOUS RADIATION OF STARS. II — *W. A. Hiltner* — 471

PHOTOGRAPHIC STUDIES OF NEBULAE. VI. THE GREAT NEBULOUS REGION IN CYGNUS PHOTOGRAPHED IN RED LIGHT — *John C. Duncan* — 479

SUPERTHERMIC PHENOMENA IN STELLAR ATMOSPHERES. III. THE CHROMOSPHERIC RADIATION FIELD — *Richard N. Thomas* — 480

SUPERTHERMIC PHENOMENA IN STELLAR ATMOSPHERES. IV. THE WOLF-RAYET ATMOSPHERE — *Richard N. Thomas* — 500

NONRADIAL OSCILLATIONS OF THE STANDARD MODEL — *Zdeněk Kopal* — 509

AN ATLAS OF IDENTIFICATION CHARTS OF WHITE DWARFS — *Willem J. Luyten* — 528

NOTES

A New Star of Large Proper Motion (L 726-8) — *Willem J. Luyten* — 532

A Large New Planetary Nebula — *F. D. Miller and E. van Dien* — 537

A New Variable Star — *Balfour S. Whitney* — 538

A Reflection Nebula and an Associated Variable Star — *Balfour S. Whitney* — 540

New Absorptions in the Uranus Atmosphere — *Gerard P. Kuiper* — 540

The Spectrum of AR Pavonis — *Jorge Sahade* — 541

Displaced Absorption Lines in the Spectrum of Upsilon Sagittarii — *W. P. Bidelman* — 544

A Catalogue of the Brighter Metallic-Line Stars — *Arne Slettebak* — 547

Upper Limits on the Abundances of Interstellar *Li* and *Be* — *Lyman Spitzer, Jr.* — 548

The Isothermal Function — *S. Chandrasekhar and Gordon W. Wares* — 551

Wave Lengths of the (0, 0) Band Heads in the Infrared System of *CN* — *C. C. Kiess* — 551

The Functions $G_{n,m}(\tau)$ and $G'_{n,m}(\tau)$ of Order 6 ($m = 6$ and $m \geqslant n$) — *S. Chandrasekhar* — 555

ERRATA — 555

INDEX — 557

THE UNIVERSITY OF CHICAGO PRESS
CHICAGO, ILLINOIS, U.S.A.

May 1949 Vol. 109, No. 3

THE ASTROPHYSICAL JOURNAL

AN INTERNATIONAL REVIEW OF SPECTROSCOPY AND ASTRONOMICAL PHYSICS

Edited by

W. W. MORGAN
Managing Editor
S. CHANDRASEKHAR
Yerkes Observatory of the University of Chicago

PAUL W. MERRILL
Mount Wilson Observatory of the Carnegie Institution of Washington
HARLOW SHAPLEY
Harvard College Observatory
Cambridge, Massachusetts

N. U. MAYALL
Lick Observatory
University of California

With the Collaboration of the American Astronomical Society

Collaborating Editors:

1947-49
LYMAN SPITZER, JR.
Princeton University Observatory
A. N. VYSSOTSKY
Leander McCormick Observatory
ALBERT E. WHITFORD
Washburn Observatory

1948-50
CECILIA H. PAYNE-GAPOSCHKIN
Harvard College Observatory
H. N. RUSSELL
Princeton University
ANDREW McKELLAR
Dominion Astrophysical Observatory, Victoria

1949-51
W. BAADE
Mount Wilson Observatory
LEO GOLDBERG
Observatory of the University of Michigan
G. HERZBERG
National Research Council, Ottawa

The Astrophysical Journal is published bimonthly by the University of Chicago at the University of Chicago Press, 5750 Ellis Avenue, Chicago, Illinois, during July, September, November, January, March, and May. ¶The subscription price is $12.00 a year; the price of single copies is $3.00. Orders for service of less than a full year will be charged at the single-copy rate. ¶Postage is prepaid by the publishers on all orders from the United States and its possessions, Argentina, Bolivia, Brazil, Chile, Colombia, Costa Rica, Cuba, Dominican Republic, Ecuador, Guatemala, Haiti, Republic of Honduras, Mexico, Morocco (Spanish Zone), Nicaragua, Panama, Paraguay, Peru, Rio de Oro, El Salvador, Spain (including Balearic Islands, Canary Islands, and the Spanish Offices in Northern Africa; Andorra), Spanish Guinea, Uruguay, and Venezuela. ¶Postage is charged extra as follows: for Canada and Newfoundland, 42 cents on annual subscriptions (total $12.42); on single copies, 7 cents (total $3.07); for all other countries in the Postal Union, 96 cents on annual subscriptions (total $12.96), on single copies 16 cents (total $3.16). ¶Patrons are requested to make all remittances payable to The University of Chicago Press, in United States currency or its equivalent by postal or express money orders or bank drafts.

The following is an authorized agent:

For the British Empire, except North America and Australasia: The Cambridge University Press, Bentley House, 200 Euston Road, London, N.W. 1, England. Prices of yearly subscriptions and of single copies may be had on application.

Claims for missing numbers should be made within the month following the regular month of publication. The publishers expect to supply missing numbers free only when losses have been sustained in transit, and when the reserve stock will permit.

Business correspondence should be addressed to The University of Chicago Press, Chicago 37, Illinois.

Communications for the editors and manuscripts should be addressed to: W. W. Morgan, Editor of THE ASTROPHYSICAL JOURNAL, Yerkes Observatory, Williams Bay, Wisconsin.

Line drawings and photographs should be made by the author, and all marginal notes such as co-ordinates, wave lengths, etc., should be included in the cuts. It will not be possible to set up such material in type.

One copy of the corrected galley proof should be returned as soon as possible to the editor, Yerkes Observatory, Williams Bay, Wisconsin. Authors should take notice that the manuscript will not be sent to them with the proof.

The cable address is "Observatory, Williamsbay, Wisconsin."

The articles in this journal are indexed in the *International Index to Periodicals*, New York, N.Y.

Applications for permission to quote from this journal should be addressed to The University of Chicago Press, and will be freely granted.

Entered as second-class matter, July 31, 1940, at the Post-Office at Chicago, Ill., under the Act of March 3, 1879.
Acceptance for mailing at special rate of postage provided for in United States Postal Act of October 3, 1917, Section 1103, amended February 28, 1925.

[PRINTED IN U.S.A.]

THE ASTROPHYSICAL JOURNAL

An International Review of Spectroscopy and Astronomical Physics

FOUNDED IN 1895 BY GEORGE E. HALE AND JAMES E. KEELER

EDITORS

W. W. MORGAN
Managing Editor
Yerkes Observatory of the University of Chicago

S. CHANDRASEKHAR

PAUL W. MERRILL
Mount Wilson Observatory of the
Carnegie Institution of Washington

HARLOW SHAPLEY
Harvard College Observatory
Cambridge, Massachusetts

N. U. MAYALL
Lick Observatory
University of California

With the Collaboration of the American Astronomical Society

COLLABORATING EDITORS

CECILIA H. PAYNE-GAPOSCHKIN, *Harvard College Observatory;* H. N. RUSSELL, *Princeton University;* ANDREW MCKELLAR, *Dominion Astrophysical Observatory, Victoria;* W. BAADE, *Mount Wilson Observatory;* LEO GOLDBERG, *Observatory of the University of Michigan;* G. HERZBERG, *National Research Council, Ottawa;* LYMAN SPITZER, JR., *Princeton University Observatory;* A. N. VYSSOTSKY, *Leander McCormick Observatory;* ALBERT E. WHITFORD, *Washburn Observatory*

VOLUME 109

JANUARY–MAY, 1949

THE UNIVERSITY OF CHICAGO PRESS
CHICAGO, ILLINOIS

CAMBRIDGE UNIVERSITY PRESS, LONDON

PUBLISHED JANUARY, MARCH, MAY, 1949

COMPOSED AND PRINTED BY THE UNIVERSITY OF CHICAGO PRESS
CHICAGO, ILLINOIS, U.S.A.

CONTENTS

NUMBER 1

Analysis of the First Rocket Ultraviolet Solar Spectra. E. Durand, J. J. Oberly, and R. Tousey 1

Telluric Bands of CH_4 in the Solar Spectrum. Robert R. McMath, Orren C. Mohler, and Leo Goldberg 17

New Solar Lines in the Spectral Region 1.52–1.75 μ. Leo Goldberg, Orren C. Mohler, and Robert R. McMath 28

Multiplet Intensities for the Nebular Lines $^4S - {}^2D$ of O II. L. H. Aller, C. W. Ufford, and J. H. Van Vleck 42

Theoretical Contours of Absorption Lines. Daniel L. Harris III 53

Exact Curves of Growth for the Formation of Absorption Lines According to the Milne-Eddington Model. I. Total Flux. Marshal H. Wrubel 66

The Wolf-Rayet Spectroscopic Binary HD 190918. O. C. Wilson 76

High-Dispersion Spectrograms of T Coronae Borealis. Roscoe F. Sanford . . . 81

Stellar Spectra with Emission Lines in the Obscuring Clouds of Ophiuchus and Scorpius. Otto Struve and Mogens Rudkjøbing 92

Spectrographic Observations of TW Andromedae. W. A. Hiltner, Burke Smith, and O. Struve 95

Radial-Velocity Observations with the Bruce Spectrograph. Daniel M. Popper . 100

Identification of a Molecular Band at λ 3682 in the Spectra of Late-Type Stars. George H. Herbig 109

Spectrographic Observations of the Eclipsing Variable RS Sagittarii. Jorge Sahade 116

Analysis of the Metallic-Line Stars. II. Jesse L. Greenstein 121

Variations in the Stellar Luminosity Function. II. A Region in Orion. S. W. McCuskey 139

The Oscillations of a Rotating Star. T. G. Cowling and R. A. Newing 149

Dynamical Friction. Marvin Lee White 159

A Nonhomogeneous Cosmological Model. Guy C. Omer, Jr. 164

Notes

Photoelectric Observations of W Virginis. Katherine C. Gordon and Gerald E. Kron 177

Note on the Paper, "The Absorption-Line Spectra of the Central Stars of the Planetary Nebulae." Lawrence H. Aller 179

Editor's Note 179

Reviews 180

NUMBER 2

An Analysis of Radial-Velocity Measures of Eight Stars Formerly Assigned to the Beta Cephei Group. John F. Heard . . . 185

Distribution of the Longitude of Periastron of Spectroscofic Binaries. Elizabeth L. Scott . . . 194

Radial Velocities of RR Lyrae from Coudé Spectrograms. Roscoe F. Sanford . . 208

The Radial Velocity of XZ Cygni. O. Struve and A. Van Hoof . . . 215

Stars Whose Spectra Have Bright H and K Lines of Calcium. Alfred H. Joy and Ralph E. Wilson . . . 231

The Atmosphere of Gamma Pegasi. Lawrence H. Aller . . . 244

Spectrophotometry of the F Stars Alpha Canis Minoris and Alpha Persei. III. Jesse L. Greenstein and W. A. Hiltner . . . 265

On the Formation of Absorption Lines by Noncoherent Scattering. Guido Münch 275

Oscillator Strengths for the Continua of *Ca* II. Louis C. Green . . . 289

Anharmonic Pulsations of the Standard Model. Martin Schwarzschild and Malcolm P. Savedoff . . . 298

The Structure of Degenerate Stellar Configurations near the Limiting Mass. Anders Reiz . . . 303

The Law of Planetary and Satellite Distances. Gerard P. Kuiper . . . 308

A Bright Region in Cepheus. A. Marguerite Risley . . . 314

The Predictability of the Probable Features of the Sunspot Cycles. W. Gleissberg . . . 321

Notes

Comparison of the *Na* and N_2^+ Flashes at Twilight and Dawn. P. Swings and M. Nicolet . . . 327

The Radial Velocity of Beta Cephei. Mogens Rudkjøbing . . . 331

New Bands in the Photographic Infrared Spectra of Long-Period Variables. J. J. Nassau, G. B. van Albada, and P. C. Keenan . . . 333

Erratum . . . 336

NUMBER 3

The Temperature of Interstellar Matter. II. Lyman Spitzer, Jr. . . . 337

Observations of Interstellar H and K, Molecular Lines, and Radial Velocities in the Spectra of 300 O and B Stars. Walter S. Adams . . . 354

An Upper Limit to the Electron Density near the Earth's Orbit. Fred L. Whipple and Joseph L. Gossner . . . 380

A Study of M-Type Stars in Cygnus. J. J. Nassau and G. B. van Albada . . . 391

Variations in the Stellar Luminosity Function. III. A Region in Auriga. S. W. McCuskey . . . 414

STELLAR SPECTRA IN MILKY WAY REGIONS. I. A REGION IN AQUILA. S. W. McCuskey . 426

SPECTROGRAPHIC OBSERVATIONS OF THE ECLIPSING VARIABLE SW LACERTAE. Otto Struve 436

NEW SPECTROGRAPHIC INVESTIGATIONS OF THE ECLIPSING STAR XZ SAGITTARII. Jorge Sahade 439

FURTHER NOTE ON THE DISTRIBUTION OF THE LONGITUDE OF PERIASTRON. Elizabeth L. Scott 446

THE STARK EFFECT OF THE HIGHER BALMER LINES IN STARS OF SPECTRAL TYPES A AND B. Elsa van Dien 452

ON THE PRESENCE OF POLARIZATION IN THE CONTINUOUS RADIATION OF STARS. II. W. A. Hiltner 471

PHOTOGRAPHIC STUDIES OF NEBULAE. VI. THE GREAT NEBULOUS REGION IN CYGNUS PHOTOGRAPHED IN RED LIGHT. John C. Duncan 479

SUPERTHERMIC PHENOMENA IN STELLAR ATMOSPHERES. III. THE CHROMOSPHERIC RADIATION FIELD. Richard N. Thomas 480

SUPERTHERMIC PHENOMENA IN STELLAR ATMOSPHERES. IV. THE WOLF-RAYET ATMOSPHERE. Richard N. Thomas 500

NONRADIAL OSCILLATIONS OF THE STANDARD MODEL. Zdeněk Kopal 509

AN ATLAS OF IDENTIFICATION CHARTS OF WHITE DWARFS. Willem J. Luyten 528

NOTES

A NEW STAR OF LARGE PROPER MOTION (L 726-8). Willem J. Luyten 532

A LARGE NEW PLANETARY NEBULA. F. D. Miller and E. van Dien 537

A NEW VARIABLE STAR. Balfour S. Whitney 538

A REFLECTION NEBULA AND AN ASSOCIATED VARIABLE STAR. Balfour S. Whitney . 540

NEW ABSORPTIONS IN THE URANUS ATMOSPHERE. Gerard P. Kuiper 540

THE SPECTRUM OF AR PAVONIS. Jorge Sahade 541

DISPLACED ABSORPTION LINES IN THE SPECTRUM OF UPSILON SAGITTARII. W. P. Bidelman 544

A CATALOGUE OF THE BRIGHTER METALLIC-LINE STARS. Arne Slettebak 547

UPPER LIMITS ON THE ABUNDANCES OF INTERSTELLAR *Li* AND *Be*. Lyman Spitzer, Jr. 548

THE ISOTHERMAL FUNCTION. S. Chandrasekhar and Gordon W. Wares 551

WAVE LENGTHS OF THE (0, 0) BAND HEADS IN THE INFRARED SYSTEM OF *CN*. C. C. Kiess 551

THE FUNCTIONS $G_{n,m}(\tau)$ AND $G'_{n,m}(\tau)$ OF ORDER 6 ($m = 6$ AND $m \geqslant n$). S. Chandrasekhar 555

ERRATA 555

INDEX 557

THE ASTROPHYSICAL JOURNAL

AN INTERNATIONAL REVIEW OF SPECTROSCOPY AND ASTRONOMICAL PHYSICS

VOLUME 109 MAY 1949 NUMBER 3

THE TEMPERATURE OF INTERSTELLAR MATTER. II

LYMAN SPITZER, JR.
Princeton University
Received November 29, 1948

ABSTRACT

The processes which tend to dissipate the kinetic energy of interstellar particles are discussed, and the rate of energy loss for each process is derived in a form suitable for numerical computation of interstellar temperatures. The phenomena considered are: free-free emission by electrons in encounters with protons and H atoms; inelastic encounters of electrons with atoms and with H_2 molecules; excitation of rotational states of H_2 molecules by encounters with H atoms and with H_2 molecules; and inelastic collisions of H atoms and H_2 molecules with solid grains. Application of these and previous results to the analysis of interstellar temperatures will be made in a subsequent paper.

In a previous paper[1] the various processes which tend to increase the kinetic temperature of interstellar matter were analyzed. The present discussion considers those processes which tend to decrease the kinetic temperature. For each process considered in Paper I, formulae were given for G_e, the rate of gain of kinetic energy, in ergs per free electron per second. Here we give the corresponding formulae for L_e, the rate of loss of kinetic energy in ergs per free electron per second. Since in some processes the kinetic energy is lost by atoms and molecules rather than by free electrons, we shall consider for such processes the rate of loss of kinetic energy per atom and per molecule.

The notation used will be the same as in Paper I. In particular, the subscripts e, p, H, i, m, and g refer to electrons, protons, neutral hydrogen atoms, ions of atoms other than hydrogen and helium, molecules, and grains, respectively. In addition, the subscript a will be used to denote neutral atoms other than hydrogen and helium. Thus L_{ea} will denote the loss of kinetic energy in ergs per free electron per second in encounters with such neutral atoms, while L_{Hm} will denote the corresponding loss per neutral H atom per second in encounters with molecules.

In the first of the following sections the energy losses L_{ep} and L_{eH} resulting from free-free electronic transitions in encounters with protons and H atoms are analyzed. Section II discusses the energy loss due to excitation of neutral and ionized atoms by electrons. Excitation of molecules by electrons and by atoms or other molecules is treated in Sections III and IV. In the final section consideration is given to the energy loss resulting from inelastic collisions between grains and either atoms or molecules. Application of

[1] L. Spitzer, Jr., *Ap. J.*, **107**, 6, 1948 (subsequently referred to as "Paper I").

these results to detailed computation of interstellar temperatures is postponed to a subsequent paper.

I. FREE-FREE ELECTRON TRANSITIONS

An electron which encounters an atom may radiate energy and still escape; since the electron thus performs a transition from one free state to another, the process is called a "free-free transition."

The rate at which energy is radiated by free-free transitions of electrons colliding with protons, or with any particle whose force on the electron follows the inverse-square law, has been computed by Cillié[2] and by Menzel.[3] From Cillié's equation (31) or from Menzel's equation (30), corrected by the insertion of a factor K/h, we have

$$L_{ep} = \left(\frac{2\pi kT}{3m}\right)^{1/2} \frac{2^5 \pi e^6}{3hmc^3} \bar{g} Z^2 n_i , \tag{1}$$

where n_i is the density of ions of charge Ze and T is the kinetic temperature. The quantity $\bar{g}$ is the average value of the Gaunt factor. Although g has a logarithmic infinity for zero frequency,[4] its average value may be assumed equal to unity; the error in this approximation probably does not exceed 20 per cent at the most. The other symbols in equation (1) have their usual meanings. Substituting numerical values and setting Z equal to 1, we have

$$L_{ep} = 1.42 \times 10^{-27} n_p T^{1/2} \text{ erg/sec} . \tag{2}$$

The energy loss in free-free transitions induced by other ions may be found by substituting $n_i Z^2$ for n_p in equation (2). Such losses are rarely important in interstellar space.

As a result of the overwhelming abundance of H, free-free transitions produced by H atoms may be important when the hydrogen is neutral. The value of L_{eH} may be determined from the absorption coefficient for this process, which has been computed by Chandrasekhar and Mrs. Breen.[5] Since the electrons have a Maxwellian velocity distribution, the total energy radiated in such free-free transitions, per cubic centimeter per second, is equal to the energy radiated in thermodynamic equilibrium at the same kinetic temperature and with the same density of electrons and H atoms. From the principle of detailed balancing, this number, in turn, equals the energy absorbed per cubic centimeter per second in thermodynamic equilibrium. Thus, if a_ν is the absorption coefficient per neutral atom per unit electron density, then

$$n_e L_{eH} = n_i n_e \int_0^\infty a_\nu B_\nu(T)\, d\nu . \tag{3}$$

Evidently, the absorption coefficient a_ν must include the effect of stimulated emissions, since these effectively diminish the amount of radiation absorbed. Values of $\kappa(\nu)$, the absorption coefficient per neutral atom per unit electron pressure, have been given by Chandrasekhar and Mrs. Breen; this quantity is equal to a_ν/kT. If we insert the usual Planck formula for $B_\nu(T)$, equation (3) yields

$$L_{eH} = \frac{8\pi hkT}{c^2} n_H \int_0^\infty \frac{\kappa(\nu)\nu^3 d\nu}{e^{h\nu/kT} - 1} . \tag{4}$$

If we use the values of $\kappa(\nu)$ uncorrected for stimulated emission, we find the simpler equation,

$$L_{eH} = \frac{8\pi hkT}{c^2} n_H \int_0^\infty \kappa(\nu)\nu^3 e^{-h\nu/kT} d\nu . \tag{5}$$

[2] *M.N.*, **92**, 820, 1932.

[3] *Ap. J.*, **85**, 330, 1937.

[4] D. H. Menzel and C. L. Pekeris, *M.N.*, **96**, 77, 1935.

[5] *Ap. J.*, **104**, 430, 1946.

The tabulated values of $\kappa(\nu)$ cover temperatures between 2520° and 10,080°K. Lower temperatures are also of interest in interstellar space, and for these we use an expansion for $\kappa(\nu)$ which is valid at low frequencies and temperatures. For sufficiently low electron velocities the matrix elements which enter into $\kappa(\nu)$ may be found from equation (23) and Table 1 in the paper by Chandrasekhar and Mrs. Breen. In accordance with a previous paper by these same authors,[6] the normalization factors, $A_0(k_0)$ and $A_1(k_1)$, which enter into the formulae for the matrix elements, may be determined by equating, at $r=5$ and 6 (atomic units), the asymptotic form of the free-electron state function for large r with the function found by numerical integration for small r. In this way we find

$$\frac{1}{A_0} = 20.96k(1-51.3k^2)\,, \tag{6}$$

$$\frac{1}{A_1} = 0.5626k^2(1+2.6k^2)\,. \tag{7}$$

If we neglect higher-order terms in k_0 and k_1, the absorption coefficient κ, uncorrected for stimulated emission, becomes

$$\kappa(\Delta k^2) = \frac{5.267\times10^{-30}}{(\Delta k^2)^3\theta^{1/2}}\int_0^\infty dx\, e^{-x}(xy)^{1/2}\left\{x+y-\frac{6.55}{\theta}\,xy+\frac{0.17}{\theta}(x^2+y^2)\right\}, \tag{8}$$

where

$$y = 31.32\theta k_1^2 = x+31.32\theta\Delta k^2 \tag{9}$$

and where $\theta = 5040°/T$. Except where otherwise specified, the notation in these equations is the same as that used by Chandrasekhar and Mrs. Breen. If equation (8) is substituted in equation (5), the resulting double integral can be evaluated exactly, and we find

$$L_{eH} = 9.02\times10^{-36}n_H T^{5/2}\left(1-\frac{T}{550°}\right)\text{erg/sec}\,. \tag{10}$$

This formula may be used only if T is much less than 550°, since for greater temperatures the neglected powers of k_0^2 and k_1^2 become important.

TABLE 1

ENERGY LOST IN FREE-FREE TRANSITIONS OF H^-

θ	0.5	1.0	2.0	5.0	10.0	20.0
L_{eH}/n_H (Erg Cm³/Sec)	6.74×10^{-27}	2.22×10^{-27}	6.57×10^{-28}	1.11×10^{-28}	2.6×10^{-29}	6.2×10^{-29}

θ	50	100	200	500	1000	2000
L_{eH}/n_H (Erg Cm³/Sec)	7.51×10^{-31}	1.47×10^{-31}	2.74×10^{-32}	2.85×10^{-33}	5.09×10^{-34}	9.05×10^{-35}

Values of L_{eH}/n_H for different values of θ, or $5040/T$, are listed in Table 1. For θ between 0.5 and 2.0 these were determined from equation (5) by numerical integration, based on the values of κ given by Chandrasekhar and Mrs. Breen. For θ equal to 50 or

[6] *Ap. J.*, **103**, 41, 1946.

more, equation (10) was used. The values for intermediate θ were determined by interpolation between these two limiting sets of values; since this interpolation extends over a large range of θ, the values so determined may be in error by perhaps as much as 10 per cent.

II. ELECTRON EXCITATION OF ATOMS

The familiar excitation of atomic energy levels by electron impact can lead to an important dissipation of kinetic energy in interstellar space. If other mechanisms producing atomic excitation are neglected, the basic equation for $n_e L_{ea}$, the total energy radiated per second per cubic centimeter in this process, is simply

$$n_e L_{ea} = n_B A_{BA} (E_B - E_A), \tag{11}$$

where A_{BA} is the spontaneous radiative probability for the electron transition from the excited state, denoted by a subscript B, to the lower state, denoted by a subscript A. The quantity n_B is the number of atoms in the excited level per cubic centimeter, while E_B and E_A are the energies, in ergs, of the two levels in question.

Before equation (11) may be used, however, the population of the upper level must be expressed in terms of the cross-sections σ_{AB} and σ_{BA} for collisional excitation and de-excitation, respectively. In most cases the assumption that the atom has only one excited level is an adequate approximation, and on this basis the equation for statistical equilibrium becomes

$$n_A n_e \int_{v_0}^{\infty} \sigma_{AB} v P(v)\, dv = n_B A_{BA} + n_B n_e \int_0^{\infty} \sigma_{BA} v P(v)\, dv, \tag{12}$$

where $P(v)$ is the distribution function for the electron velocities (see eq. [3] of Paper I). At velocity v_0 an electron has just enough kinetic energy to excite the atom. The first integral in equation (12) may be expressed in terms of the second by the condition that, when A_{BA} vanishes, the relative population of states A and B must follow the Boltzmann law,

$$\frac{n_B}{n_A} = \frac{g_B}{g_A} e^{-(E_B - E_A)/kT} = \frac{g_B}{g_A} 10^{-\mathfrak{E}_B \theta} \equiv f(\theta), \tag{13}$$

where g_B and g_A are the quantum weights of the two states and $\mathfrak{E}_B$ is the excitation potential of the state B in electron volts. Thus we find

$$\int_{v_0}^{\infty} \sigma_{AB} v P(v)\, dv = \frac{g_B}{g_A} 10^{-\mathfrak{E}_B \theta} \overline{\sigma_{BA} v}, \tag{14}$$

where $\overline{\sigma_{BA} v}$ denotes an average over all velocities. Since σ_{BA} tends to be more nearly constant with velocity, $\overline{\sigma_{BA} v}$ for a neutral atom may be written simply as $\sigma_{BA} \bar{v}$; for this reason the de-excitation cross-section is easier to work with than the corresponding excitation cross-section and will be used throughout. For any particular velocity, σ_{AB} and σ_{BA} are related by the following equation, readily derived from the principle of detailed balancing in thermodynamic equilibrium:

$$\sigma_{AB}(v_1) = \frac{g_B}{g_A} \left\{ 1 - \frac{E_B - E_A}{\frac{1}{2} m v_1^2} \right\} \sigma_{BA}(v_2), \tag{15}$$

where

$$\tfrac{1}{2} m v_1^2 = \tfrac{1}{2} m v_2^2 + E_B - E_A. \tag{16}$$

It may be noted that equation (14) also follows as a special case from equation (15).

If equation (14) is substituted in equation (12) and the resultant value of n_B/n_A is substituted in equation (11), we find

$$L_{ca} = \frac{n_a (E_B - E_A)\, \overline{v\sigma}_{BA} f(\theta)}{1 + K\{1 + f(\theta)\}}, \tag{17}$$

where

$$K = \frac{n_e \overline{v\sigma}_{BA}}{A_{BA}}. \tag{18}$$

The quantity n_a is the total number per cubic centimeter of the atoms under consideration, regardless of which state they are in; in the present instance n_a equals $n_A + n_B$. For ions an equation identical to (17) applies, with n_i replacing n_a.

To apply equation (17) to the excited states of all interstellar atoms would be a more complicated undertaking than our present knowledge warrants. To simplify the subsequent analysis, only a small number of states will be assumed. First, we shall discuss the excited states above about 10 volts. Such states are important only if the temperature is very high, above some 30,000° at least. It is not certain that such high temperatures exist anywhere in interstellar space; but, if they do, *H* is likely to be almost completely ionized, and other highly ionized atoms must be considered. In a typical atom, such as *O* II, excited levels converge to the ionization limit at 35 volts. We shall assume here that 25 volts is a typical energy loss for an electron striking an ion of this sort. The value of A_{BA} for such excited levels can be set equal to infinity in equation (17), since the downward radiative transitions from these high levels are mostly permitted. Both g_A and g_B will be arbitrarily set equal to 5.

Next we consider the lower-lying excited states. These are presumably of greater importance in interstellar space than are the higher states, and, since there are fewer of them, a more detailed consideration is both feasible and desirable. All the excited states of the most abundant elements, with excitation potentials of 5 volts or less, are therefore given in Table 2, together with their excitation potentials taken from Bacher and Goudsmit[7] and from Miss Moore,[8] their spontaneous downward transition probabilities from Pasternack,[9] and the values of g_A and g_B. As indicated in the table, the spontaneous radiative transitions in *Mg* I and *Mg* II are permitted, and the values of A_{BA} are correspondingly high. The values of g_A are computed on the assumption that all the levels in the ground term are populated in accordance with their statistical weights. The resultant values are the correct ones to use, even when this assumption is not fulfilled, provided, as seems to be the case, that the excitation cross-section σ_{AB} is the same for all the levels in the ground term *A*.

For energies above 1 electron-volt (e.v.) all levels were included for neutral, singly ionized, and doubly ionized atoms of *C*, *N*, *O*, *Ne*, and *Mg*. For excitation potentials less than 1 e.v. the somewhat less abundant elements, *Si*, *S*, and *Fe*, were also included. According to a recent tabulation by Unsöld,[10] these eight elements included in Table 2, together with *H* and *He*, are much the most abundant ones in the sun and the stars; each other element is apparently less than 1 per cent as abundant as *O*. Unsöld's quantitative abundances are not in complete agreement with either the investigation of the solar spectrum by Menzel and his collaborators[11] or the analysis of planetary nebulae by Aller and Menzel.[12] In particular, while Unsöld finds the abundance of *Ne* and *Mg*, by

[7] *Atomic Energy States* (New York and London: McGraw-Hill Book Co., 1932).

[8] *Contr. Princeton U. Obs.*, No. 20, 1945.

[9] *Ap. J.*, **92**, 129, 1940.

[10] *Zs. f. Ap.*, **24**, 306, 1948.

[11] Summarized by Goldberg and Aller, *Atoms, Stars, and Nebulae* (Philadelphia: Blakiston Co., 1943).

[12] *Ap. J.*, **102**, 239, 1945.

volume, to be 1.18 and 0.063, on the basis of 1.00 for *O*, the former is found to have a relative abundance of only 0.04 in the nebulae, while Goldberg and Aller[11] report a solar abundance of 0.68 for the latter. We shall here assume that the abundances of *Ne* and *Mg* are both 0.25 times that of *O*.

One of the most striking features of Table 2 is the absence of levels with excitation potentials between 0.11 and 1.1 volts. The *Fe* multiplets are the only ones in this region, and all but one of these lie close to either the upper or the lower limits.

The upper levels, between 1 and 5 volts, may be represented by a single level. Since *C* I, *N* I and *N* II, *O* I, *O* II, and *O* III, *Mg* I and *Ne* III all have levels between 1.2 and 3.6 volts, we shall take this "equivalent level" to be at 2.4 volts, and compute L_{ea} and L_{ei} on the assumption that every atom other than *H* and *He* in interstellar space has an excited level of this energy. The values of A_{BA} for the various lines are widely different,

TABLE 2

LOW-LYING LEVELS OF ABUNDANT ELEMENTS

E.P. (Volts)	Symbol	Element	A_{BA} (Sec^{-1})	g_A	g_B
5.00	$^2P_{3/2,\,1/2}$	*O* II	0.38	4	6
4.41	$^2P_{1/2,\,3/2}$	*Mg* II	Permitted	2	6
4.33	$^1P_1$	*Mg* I	Permitted	1	3
4.17	$^1S_0$	*O* I	2.3	9	1
4.04	$^1S_0$	*N* II	2.2	9	1
3.56	$^2P_{3/2,\,1/2}$	*N* I	0.24	4	6
3.31	$^2D_{5/2,\,3/2}$	*O* II	7.7×10^{-5}	4	10
3.19	$^1D_2$	*Ne* III	0.28	9	5
2.70	$^3P_0$	*Mg* I	Permitted	1	9
2.67	$^1S_0$	*C* I	1.4	9	1
2.50	$^1D_2$	*O* III	0.022	9	5
2.37	$^2D_{5/2,\,3/2}$	*N* I	1.8×10^{-5}	4	10
1.96	$^1D_2$	*O* I	0.010	9	5
1.89	$^1D_2$	*N* II	3.0×10^{-3}	9	5
1.26	$^1D_2$	*C* I	2.0×10^{-4}	9	5
0.98–1.09	$a^4D_{7/2-1/2}$	*Fe* II	.....	30	20
0.86–1.01	a^5F_{5-1}	*Fe* I	.....	25	35
0.23–0.38	$a^4F_{9/2-3/2}$	*Fe* II	.....	30	28
0.13	a^5D_0	*Fe* III	.....	9	1
0.12	$a^{5,\,6}D$	*Fe* I, II, III	.....	9, 10, 9	1, 2, 3
0.11	$a^{5,\,6}D$	*Fe* I, II	.....	9, 10	3, 4
0.11	$^3P_2$	*S* III	2.1×10^{-3}	1	5
0.11	$^3P_0$	*Ne* III	1.2×10^{-3}	5	1
0.096	$^2P_{1/2}$	*Ne* II	.....	4	2
0.08–0.09	$a^{5,\,6}D$	*Fe* I, II, III	.....	9, 10, 9	5, 6, 5
0.079	$^3P_1$	*Ne* III	6.0×10^{-3}	5	3
0.072	$^3P_0$	*S* I	3.0×10^{-4}	5	1
0.05	$a^{5,\,6}D$	*Fe* I, II, III	.....	9, 10, 9	7, 8, 7
0.045	$^3P_1$	*S* I	1.4×10^{-3}	5	3
0.038	$^3P_2$	*O* III	9.8×10^{-5}	1	5
0.037	$^3P_1$	*S* III	4.7×10^{-4}	1	3
0.035	$^2P_{3/2}$	*Si* II	.....	2	4
0.028	$^3P_0$	*O* I	1.7×10^{-5}	5	1
0.028	$^3P_2$	*Si* I	4.2×10^{-5}	5	5
0.020	$^3P_1$	*O* I	8.9×10^{-5}	5	3
0.017	$^3P_2$	*N* II	7.5×10^{-6}	1	5
0.014	$^3P_1$	*O* III	2.6×10^{-5}	1	3
0.010	$^3P_1$	*Si* I	8.2×10^{-6}	5	3
0.0062	$^3P_1$	*N* II	2.1×10^{-6}	1	3
0.0052	$^3P_2$	*C* I	2.8×10^{-7}	1	5
0.0018	$^3P_1$	*C* I	5.8×10^{-8}	1	3

but a value of 1.0×10^{-2} sec^{-1} represents about the mid-point of the distribution; similarly, values of 9 and 5 for g_A and g_B, respectively, will be adopted, since these are typical of *O* I, *O* III, and a number of other elements.

Next we consider the lower levels. To represent these adequately, at least two equivalent levels are required. To represent the excited states of *Fe* I, II, and III, *Ne* II and III, and *S* I and III, we shall assume a level at 0.10 volts, and with a value of 1.0×10^{-3} sec^{-1} for A_{BA} and with g_A and g_B set equal to 5 and 2, respectively. Five per cent of all neutral atoms (other than *H* and *He*, of course) and 15 per cent of all ionized atoms (again excluding *H* and *He*) will be assumed to possess this particular level. Finally, we shall assume one level at 0.015 e.v., with a value of 1.0×10^{-5} sec^{-1} for A_{BA}. For neutral atoms, g_A and g_B will be set equal to 5 and 3, respectively, while for ionized atoms the values 1 and 3 will be assumed. This assumed level represents the excited states of *Si* I, *O* I, *N* II, and *O* III between 0.010 and 0.020 volts. Since *N* I and *O* II have no levels in this region, we shall assume that half the neutral atoms and half the ionized atoms (other than *H* and *He*) possess this particular level. A summary of these four equivalent levels assumed, together with the properties of each level, is given in Table 3.

Finally, we must know the proper values of σ_{BA} before numerical values may be found for L_{ea} and L_{ei}. Unfortunately, these values are quite uncertain, and there is an almost complete lack of experimental information for the transitions of astrophysical interest. The laboratory data on other transitions, however, cast light on the magnitude of the cross-sections to be expected. Since, as indicated above, the de-excitation cross-section σ_{BA} for a neutral atom tends to be constant as the electron velocity approaches zero, equation (15) will be used to express the experimental results in terms of σ_{BA}. Moreover, since σ_{BA} is proportional to g_A, the results will be expressed in terms of the cross-section per unit weight of the ground state. Measurements on the D lines, made by G. Haft[13] and W. Christoph,[14] show that the value of σ_{BA} per unit weight for the 3^2P term is about 7.0×10^{-16} cm^2 for electrons with some 5–10 volts of kinetic energy, and gradually decreases to about half this value for 60-volt electrons. Thus for the resonance lines the excitation and de-excitation cross-sections are comparable with the gas-kinetic cross-section; for higher levels, however, the values of σ_{BA} seem to decrease rapidly with increasing excitation potential.

Measurements on *Hg* have been made by F. L. Arnot and G. O. Baines,[15] whose results on excitation cross-sections yield values of 4.6×10^{-16} cm^2 per unit weight for de-excitation of the $6s6p\,^3P_1$ level and about 2.5×10^{-16} cm^2 for the $6s6p\,^1P_1$ level. Thus the de-excitation of the metastable level is more probable than that of the nonmetastable one. This excitation and de-excitation of states of different multiplicity from the ground state is generally attributed to electron exchange, which is important only for electrons with a few volts of kinetic energy. Unfortunately, these precise numerical values are somewhat uncertain, since the other results referred to by Arnot and Baines vary from $\frac{1}{3}$ to 2.5 times the values found by these authors.

Absolute values of the cross-section for excitation of *He* by electron impact have been measured by J. H. Lees,[16] O. Thieme,[17] and J. P. M. Woudenberg and J. M. W. Milatz.[18] For the 3^1P_1 level the measures agree in giving a cross-section of about 9×10^{-19} cm^2 for optical excitation of the line at 5015 A by electron of 100-volts energy. According to data given by Goldberg,[19] only 2.4 per cent of the electrons excited to the 3^1P_1 level jump downward to the 2^1S_0 level, and thus the true excitation cross-section exceeds the optical values by a factor of 42. The final cross-section for the 3^1P_1 level, per unit weight of the ground state, becomes 1.7×10^{-17} cm^2. For the 3^3P term, no such correction is

[13] *Zs. f. Phys.*, **82**, 73, 1933.

[14] *Ann. d. Phys.*, ser. 5, **23**, 51, 1935.

[15] *Proc. R. Soc., London, A*, **151**, 256, 1935.

[16] *Proc. R. Soc., London, A*, **137**, 173, 1932.

[17] *Zs. f. Phys.*, **78**, 412, 1932.

[18] *Physica*, **8**, 871, 1941.

[19] *Ap. J.*, **90**, 414, 1939.

needed, since the spontaneous transition down to the 2^3S_1 level, with emission of radiation at 3888A, is the only one allowed. However, the measures for the excitation of this term are not at all in agreement, giving de-excitation cross-sections per unit weight which range from 7.0×10^{-18} cm^2 to 2.1×10^{-19} cm^2 for electrons with only a few volts of kinetic energy. The one set of measures available[18] for the excitation of the 2^3P term gives a de-excitation cross-section of 4.4×10^{-18} cm^2 for electrons of about 60 volts. For slower electrons a greater value would presumably be observed, but apparently the de-excitation cross-sections for the lowest excited states of *He* do not much exceed 10^{-17} cm^2 at most. These relatively low values may result in part from the relatively low geometrical cross-section of *He*.

Theoretical computations on the collisional excitation of the $^1D_2$ level in *O* I have been carried through by Yamanouchi, Inui, and Ameniya.[20] Their results indicate a de-excitation cross-section of 4.0×10^{-16} cm^2 per unit weight, or about half the value found for the D lines by W. Christoph.[14] However, these computations are based on first-order perturbation theory, whose validity is open to question when the computed cross-section is so large.

The collisional excitation of atomic ions is even less well explored than that of neutral atoms. From simple classical considerations one would expect that $\sigma_{BA}(i)$, the cross-section for de-excitation of an ion of charge Ze, would be related to $\sigma_{BA}(a)$, the corresponding cross-section for a neutral atom, by the formula

$$\sigma_{BA}(i) = \sigma_{BA}(a)\left\{1 + \frac{2Ze^2}{mv^2r}\right\}, \tag{19}$$

where m and v are the electron mass and velocity and r is the "atomic radius," which we shall here set equal to 10^{-8} cm. Except at very high velocities, the first, or unit, term in the braces is small compared with the second and may be neglected. If $\sigma_{BA}(a)$ is assumed constant, then we have

$$\overline{\sigma_{BA}(i)\, v} = \frac{2\sigma_{BA}(a)Ze^2}{r}\left\{\frac{2}{\pi mkT}\right\}^{1/2}. \tag{20}$$

A theoretical analysis of the collisional excitation and de-excitation of *O* III has been made by Hebb and Menzel.[21] If equation (20) is used to obtain values of $\sigma_{BA}(a)$ from their results, we find 2.1×10^{-17} cm^2 for the de-excitation cross-section per unit weight. The values for different terms have an average deviation of about 20 per cent from this mean value. These computations are based on the Born approximation, which should be valid when the cross-sections found are relatively small.

A similar theoretical analysis for *O* II, carried out by Aller,[22] gives 3.1×10^{-19} cm^2 for $\sigma_{BA}(a)$. This result is surprisingly small. As pointed out by Barbier,[23] the observed ratio of intensities of the forbidden *N* II and *O* II lines in planetary nebulae implies that the effective cross-sections for electron excitation of these two atoms are about equal. Since one would expect the cross-sections for *N* II to be roughly equal to the corresponding cross-section in the isoelectronic ion *O* III, one would therefore expect roughly equal values of σ_{BA} for *O* II and *O* III. Until further information is available on the validity of the approximations made in these theoretical studies, Aller's low value of the excitation cross-section for *O* II must be accepted with caution.

To summarize this survey of existing evidence, we have seen that the observed values of σ_{BA}/g_A for low excited states range from about 6×10^{-16} cm^2 for *Na* and *Hg* to about 10^{-17} cm^2 for *He*. For *O* atoms, which are of primary interest in interstellar space, only theoretical values are available, and these cover the much wider range from

[20] *Proc. Phys. Math. Soc. Japan*, **22**, 847, 1940.

[21] *Ap. J.*, **92**, 408, 1940.

[22] *Pub. A.S.P.*, **60**, 317, 1948; also *Ap. J.* (in press).

[23] *Ann. d'ap.* (in press).

4×10^{-16} cm² to 3×10^{-19} cm². It is very doubtful whether the attempt to take into account differences in $\sigma_{BA}(a)$ between different atoms would be warranted at the present time, and we shall arbitrarily take $\sigma_{BA}(a)/g_A$ to equal 2×10^{-17} cm² for all four equivalent atomic states specified above. This value may be compared with the geometrical means: 8×10^{-17} cm² for the extreme theoretical values, and 10^{-17} cm² for the extreme observational values. Obviously, no great accuracy can be claimed for this estimate; one may surmise that the average value of $\sigma_{BA}(a)/g_A$ for *N*, *C*, *O*, *Ne*, and *Mg* atoms in different stages of ionization probably does not differ from this assumed value by more than one order of magnitude at most.

If we now combine equations (16), (17), and (20) and insert numerical values, we find

$$L_{ea} = 1.4 \times 10^{-21} \frac{n_a}{\theta^{1/2}} \sum_{j=2}^{4} \frac{p_{aj} 10^{-\theta \mathfrak{E}_j}}{1 + \frac{n_e q_{aj}}{\theta^{1/2}}} \text{ erg/sec} , \tag{21}$$

$$L_{ei} = 7.1 \times 10^{-20} n_i \theta^{1/2} \sum_{j=1}^{4} \frac{p_{ij} 10^{-\theta \mathfrak{E}_j}}{1 + n_e \theta^{1/2} q_{ij} \left(1 + \frac{g_{Bj}}{g_{Aj}} 10^{-\theta \mathfrak{E}_j}\right)} \text{ erg/sec} , \tag{22}$$

where values of the constants p_{aj}, p_{ij}, q_{aj}, q_{ij}, and g_{Bj}/g_{Aj} are given in Table 3.

TABLE 3

VALUES OF CONSTANTS FOR ELECTRONIC EXCITATION OF ATOMS AND IONS

j	$\mathfrak{E}_j$	p_{aj}	p_{ij}	q_{aj}	q_{ij}	g_{Bj}/g_{Aj}
1	25	.....	170	.....	0	.....
2	2.4	12	12	8.0×10^{-7}	4.0×10^{-5}	5/9
3	0.10	0.01	0.03	4.5×10^{-6}	2.2×10^{-4}	2/5
4	0.015	0.023	0.023	4.5×10^{-4}	4.5×10^{-3}	3

In deriving equation (21), the quantity in braces in the denominator of equation (17) has been set equal to 1, since it cannot exceed 1.6 and is usually much nearer 1.0. In deriving equation (22), Z has been set equal to 2 for the highest level and to 1.5 for the other three levels. Evidently, p_{aj} equals $g_B \mathfrak{E}_j$, multiplied by the fraction of atoms assumed to possess the level j. The quantity p_{ij} is similarly defined, except that p_{i1} includes a factor 2/1.5 to take into account the greater nuclear charge assumed for this level.

A somewhat similar formula might also be derived for excitation of atoms by impact with other atoms. The cross-section for such a process may be expected to be very small, since transfer of energy from electron excitation to atomic translation is an improbable process, except under rather special conditions. For example, in the normal collision of the second kind between two molecules, excitation energy is transferred from one molecule to another, but the change of kinetic energy of the two molecules is generally very small. The loss of energy produced by inelastic collisions between atoms will therefore be neglected here.

III. ELECTRON EXCITATION OF MOLECULES

Most molecules have apparently a small influence on interstellar temperatures, if one accepts Dunham's[24] value of 10^{-6} per cubic centimeter as the average density of inter-

[24] *Pub. A.A.S.*, **10**, 123, 1941.

stellar *CH* and *CN*. It is possible that under some circumstances these and similar molecules might have a somewhat increased effect. However, the contribution of these molecules in such cases is almost certain to be overshadowed by that of H_2.

While it has been pointed out by Hoyle and Lyttleton[25] that collisions between electrons and H_2 molecules might reduce the kinetic temperature, the probable high abundance of H_2 in interstellar space does not seem to have been generally realized. As emphasized by van de Hulst,[26] one may expect the surface of a solid grain to form an excellent catalytic agent for the combination of two H atoms to form H_2. An appreciable fraction of the surface may be covered with adsorbed H atoms; thus it seems highly probable that an appreciable fraction of the H atoms striking a grain will leave as molecules. As pointed out in Paper I, any molecules found in H I regions cannot be dissociated by radiation, since the energy required is 14.5 volts; hence in any H I region there should be a steady trend toward the conversion of H into H_2. Between the clouds, where the density of grains may be small, the hydrogen may remain atomic during 3×10^9 years; but within a cloud, where a hydrogen atom should strike a grain within less than 10^9 years, on the average, an appreciable fraction of the hydrogen should become molecular within 10^8 years. While the lifetime of a cloud may be less than this, certainly a substantial ratio of H_2 to H within a cloud must at least be considered a possibility.

Since the excited electronic states of H_2 lie at least 11 volts above the ground state, it is evident that electronic transitions are not of great interest at the relatively low temperatures which will generally prevail in H I regions. Electrons cannot excite the rotational states, since the difference in angular momentum between adjacent rotational states is much greater than the angular momentum possessed by an electron which "strikes" the molecule and which has a kinetic energy of only a few volts. This theoretical conclusion has been verified experimentally by W. Harries[27] for electrons of 5.2 e.v. of energy striking N_2 and *CO* molecules.

Excitation of molecular vibrational levels is not subject to this difficulty and has been observed for many molecules. In particular, quantitative measurements of the vibrational excitation of H_2 molecules by electrons with energies between 3.5 and 7.2 e.v. have been made by H. Ramien.[28] As before, equation (15) will be used to give his results in terms of the de-excitation cross-section. If his values of η, the probability of excitation per collision, are combined with E. Brüche's[29] measured values of the cross-section for elastic scattering, we find that σ_{BA} increases from 2.9×10^{-17} cm^2 for 6-volt electrons to 5.4×10^{-17} for 3-volt electrons. As the velocity approaches zero, σ_{BA} presumably approaches a constant value, which we shall assume to be 7.0×10^{-17} cm^2. It should be noted that these derived values of σ_{BA} may be somewhat too large if excitations of the higher vibrational levels, neglected by Ramien, are of some importance.

The value of L_{em}, the loss of energy per free electron per second, resulting from impact with H_2 molecules, may be found from equations (17) and (18), applied to the first excited vibrational state only. At the temperature of some 10,000° necessary to excite the higher vibrational states, the H_2 molecules will dissociate. Since only one excited state need therefore be considered, equation (17) is applicable to the present problem. All the rotational levels for each vibrational state may be grouped together as a single state; since the rotational structure of adjacent vibrational states is nearly identical, the ratio g_A/g_B in equation (13) may be set equal to unity. The term in braces in the denominator of equation (17) may also be set equal to unity, since $f(\theta)$ is at most unity. The energy radiated may be set equal to 0.528 e.v., the energy difference between the

[25] *Proc. Cambridge Phil. Soc.*, **35**, 405, 1939; **36**, 424, 1940.

[26] *Centennial Symposia* ("Harvard Observatory Monographs," No. 7 [Cambridge: Harvard College Observatory, 1948]), p. 73.

[27] *Zs. f. Phys.*, **42**, 26, 1927.

[28] *Zs. f. Phys.*, **70**, 353, 1931.

[29] *Ann. d. Phys.*, ser. 4, **84**, 279, 1927.

vibrational states of zero rotational energy; the change of rotational energy which may accompany the vibrational transition is small and may be neglected.

To compute L_{em} from equation (17), one must also know the value of A_{BA} to be used in equation (18). Since H_2 has no dipole moment, the spontaneous radiative de-excitation of the excited vibrational states occurs only through electron quadrupole transitions. The probability of such transitions has been computed by H. M. James and A. S. Coolidge,[30] who give values for the Einstein coefficient $B(A, B)$ for induced upward transitions.[31] From these results the values of A_{BA} may be found by standard formulae. Adding up the probabilities for the downward transitions with $\Delta J = 2, 0$, and -2 from each level, one finds that the probability of radiative de-excitation of the first excited vibrational state is 1.7×10^{-7} sec^{-1} if the rotational quantum number, J_B, is zero. This de-excitation probability increases slowly with increasing J_B, reaching 2.7×10^{-7} sec^{-1} for $J_B, = 4$. As an average for the relevant rotational levels we shall set A_{BA} equal to 2.0×10^{-7} sec^{-1} for the first vibrational state.

It should be noted that transitions between levels of odd J and those of even J do not occur either by radiation or by electron collision. Hydrogen molecules in rotational states of odd and even J constitute orthohydrogen and parahydrogen, respectively. The abundance ratio of the first type of molecule to the second in interstellar space must be determined by the method of formation of H_2. If, as seems probable, these are formed at the surface of the grains, this ratio will equal $3 \times \exp(-E_0/kT)$, where E_0 is the energy of the ground state of orthohydrogen relative to that of parahydrogen, which equals 0.015 e.v. The temperature of the grains has been estimated by van de Hulst[32] to be about 10°–20° K. At these temperatures the ratio of orthohydrogen to parahydrogen will lie between 10^{-3} and 10^{-7}. Hence one may assume that virtually no orthohydrogen is present in interstellar space. This assumption does not appreciably affect the results obtained in the present paper.

We may now write down the resultant formula for L_{em}. On substitution of the usual formula for $\bar{v}$ and insertion of numerical values, we find

$$L_{em} = 2.6 \times 10^{-21} \frac{n_m}{\theta^{1/2}} \times \frac{10^{-0.528\theta}}{1 + \dfrac{1.5 \times 10^{-2} n_e}{\theta^{1/2}}} \text{ erg/sec} . \tag{23}$$

IV. EXCITATION OF MOLECULES BY ATOMS AND MOLECULES

The impact of a molecule against atoms or other molecules can also lead to excitation of the molecule. As we have already seen, only the H_2 molecule is abundant enough to be of much interest; the collision of H_2 with H atoms and other H_2 molecules must therefore be considered. Such collisions can excite the rotational levels of the H_2 molecule. The level whose angular quantum number is J has an energy E_J relative to the level of zero J, given by the formula

$$E_J = E_r J (J + 1) , \tag{24}$$

where E_r is 1.18×10^{-14} ergs, or 0.00736 e.v. As already noted, transitions from levels of even J to levels of odd J cannot occur, and we shall assume that orthohydrogen, composed of H_2 molecules in rotational states of odd J, is not present in appreciable amounts in interstellar space. These collisions of heavy particles can also excite vibrational transitions, but, as shown at the end of this section, this effect may be neglected.

Even with the problem restricted to the even rotational levels of the ground vibrational state, the solution of the equation of statistical equilibrium for this case offers many

[30] *Ap. J.*, **87**, 438, 1938.

[31] It should be noted that the notation used by James and Coolidge differs from the present one; they denote the ground state by B, the excited state by A.

[32] *Rech. Astr. de l'Obs. d'Utrecht*, Vol. 11, Part 1, 1946; also published separately as dissertation, *Optics of Spherical Particles.*

difficulties. Since the physical information on collision cross-sections is not very definite, an accurate and detailed solution of this problem is not possible at the present time. A number of simplifying assumptions will be made in order to obtain numerical results.

We shall restrict ourselves primarily to a consideration of the value of L_{Hm} in two limiting cases. In the first, the probabilities of radiative de-excitation of all states may be assumed less than the collisional de-excitation probabilities, while in the second the reverse is true for all states. In this first case, collisions will evidently establish a nearly Boltzmann distribution of molecules among the excited rotational states; and, if the values of the downward radiative probabilities A_{BA} are known, the total energy radiated may be computed very simply. We shall let Υ_1 be the energy radiated per H_2 molecule per second, computed for this limiting case. While $n_m\Upsilon_1$, the total energy radiated per cubic centimeter per second, is independent of n_H, the energy loss L_{Hm} is defined as the loss per H atom per second. Hence in this case $L_{Hm} = n_m\Upsilon_1/n_H$.

In the second case, collisional de-excitation may be neglected. The energy radiated then equals the number of collisions times the mean energy of excitation after each collision. If the cross-sections for collisional excitation of the various states are known, then the total energy radiated per second may again be computed. In this case the total energy loss per cubic centimeter is proportional to n_H as well as to n_m. If we define Υ_2 as the energy loss per H_2 molecule per H atom per second, then $L_{Hm} = n_m\Upsilon_2$.

It is evident physically that the actual rate of radiation will be intermediate between these two limiting cases. Moreover, if the first limiting case gives a much smaller rate of radiation than the second, this indicates that radiative de-excitation is much less probable than collisional de-excitation for most of the relevant states and that therefore the first limiting case gives essentially the correct rate of radiation. Similarly, if the second limiting case gives much the smaller result, then this is the correct value. These considerations indicate that half the harmonic mean of the values of L_{Hm} found in the two limiting cases should be a reasonably good approximation to the correct value. We may therefore write

$$L_{Hm} = n_m\Upsilon\,, \tag{25}$$

where, in accordance with the discussion in the two preceding paragraphs, we have

$$\frac{1}{\Upsilon} = \frac{n_H}{\Upsilon_1} + \frac{1}{\Upsilon_2}. \tag{26}$$

To compute Υ_1, we may write for n_j, the number of molecules per cubic centimeter in the Jth rotational level,

$$n_J = n_m F(J)\,, \tag{27}$$

where

$$F(J) = \frac{(2J+1)\, e^{-E_J/kT}}{\sum_J (2J+1)\, e^{-E_J/kT}}; \tag{28}$$

$(2J + 1)$ is simply the statistical weight g_J of the Jth level. Equations (27) and (28) are valid in thermodynamic equilibrium when the distribution of molecules among excited levels follows the Boltzmann law. Thus these equations apply to the first case under consideration, and Υ_1 may be written down at once, if we take into account the fact that A_{BA} is appreciable only when J_A equals $J_B - 2$; if we substitute from equation (24) for $E_J - E_{J-2}$, we have

$$\Upsilon_1 = 2E_r \sum_{J=2}^{\infty} F(J)\, A_{J,J-2}\,(2J-1)\,; \tag{29}$$

in equations (28) and (29) the summation extends over even values of J only.

Numerical values of $A_{J,J-2}$ may be obtained from an extension of the work by James and Coolidge.[30] Although these authors have not considered purely rotational transitions, their analysis may readily be applied to these. One needs compute only the value of the quadrupole moment averaged over the probability distribution for the lowest vibrational state. James and Coolidge consider the quadrupole moment to be a function of internuclear distance, r, and expand this moment as a power series in $(r - r_e)$, where r_e is the value of r at which the potential is a minimum. In the present instance the dominant term in the average quadrupole moment is the first term in the expansion, which is independent of $r - r_e$. The higher-order terms are small and may be computed to sufficient accuracy by the state function for a parabolic potential. The terms in $r - r_e$ and $(r - r_e)^3$ both vanish on this basis, while that in $(r - r_e)^2$ is 1.3 per cent of the first term and opposite in sign. Finally, then, one obtains for $A_{J,J-2}$ the equation

$$A_{J,J-2} = 7.52 \times 10^{-13} \frac{J(J-1)(2J-1)^4}{2J+1} \text{ sec}^{-1} . \tag{30}$$

These values increase rapidly with J, ranging from 2.4×10^{-11} sec^{-1} for the level $J = 2$ up to 1.1×10^{-6} sec^{-1} for the level $J = 12$.

Numerical values of Υ_1 are given in Table 4 for values of θ between 1 and 50. For

TABLE 4

VALUES OF Υ_1 AND Υ_2

θ	$_1\Upsilon$ (Erg/Sec)	$_2\Upsilon$ (Erg Cm^3/Sec)	θ	$_1\Upsilon$ (Erg/Sec)	$_2\Upsilon$ (Erg Cm^3/Sec)
1.0	2.08×10^{-19}	1.7×10^{-23}	12	2.20×10^{-23}	1.6×10^{-25}
1.2	1.15×10^{-19}	1.3×10^{-23}	15	1.23×10^{-23}	8.8×10^{-26}
1.5	5.45×10^{-20}	9.3×10^{-24}	20	3.16×10^{-24}	4.0×10^{-26}
2.0	2.08×10^{-20}	5.9×10^{-24}	25	1.02×10^{-24}	2.2×10^{-26}
3.0	5.21×10^{-21}	3.0×10^{-24}	30	4.43×10^{-25}	1.3×10^{-26}
4.0	1.89×10^{-21}	1.8×10^{-24}	40	1.47×10^{-25}	4.6×10^{-27}
5.0	8.52×10^{-22}	1.2×10^{-24}	50	5.48×10^{-26}	1.5×10^{-27}
6.0	4.34×10^{-22}	8.4×10^{-25}	60	1.94×10^{-26}	5.2×10^{-28}
8.0	1.49×10^{-22}	4.5×10^{-25}	80	2.56×10^{-27}	6.0×10^{-29}
10.0	6.30×10^{-23}	2.6×10^{-25}	100	3.35×10^{-28}	7.0×10^{-30}

greater values of θ, only the first term in the series in equation (29) need be considered, and we have

$$\Upsilon_1 = 8.62 \times 10^{-24-0.04418\theta} \text{ erg/sec} . \tag{31}$$

To compute values of Υ_2, we must make some assumption about excitation and deexcitation cross-sections. On a very simplified semiclassical picture one might expect that immediately after each collision the distribution of molecules among the various levels would follow the Boltzmann law. If this assumption were correct, one could then define an effective cross-section σ_{eff} so that the number of molecules per cubic centimeter excited to the Jth level per second by collisions would be given by the equation

$$\left(\frac{dn_J}{dt}\right)_{\text{exc}} = n_H n_m \sigma_{\text{eff}} \bar{v} F(J) . \tag{32}$$

In this equation n_m is the number of molecules in all states per cubic centimeter.

Equation (32) is somewhat of an oversimplification, since, as we shall see below, the value of σ_{eff} in equation (32) must vary with J to give correct results. As a next higher

approximation we may let σ_{eff} in equation (32) vary with J. We shall let σ_{eff} equal $\sigma_0 q_J$, where σ_0 is a constant for all levels and is taken to be a rough average value of σ_{eff}, while q_J varies with J. On this still rather simplified picture the expression for Υ_2 becomes

$$\Upsilon_2 = \sigma_0 \bar{v} E_r \sum_J q_J F(J) J(J+1). \tag{33}$$

Unfortunately, the accurate evaluation of σ_0 and q_J is apparently not possible at present. For high temperatures and highly excited levels, when the classical theory becomes valid, q_J should approach a constant value, which we may take equal to unity, and equation (32) should be at least a tolerable first approximation. The value of σ_0 would presumably be substantially less than the gas-kinetic cross-section[33] of about 1.8×10^{-15} cm^2; the internuclear distance in H_2 is only one-third the mean molecular diameter, and, in addition, the angular acceleration of the nuclei resulting from distortion of the electron cloud during collision should be less than for an ideally rigid molecule.

From the accurate standpoint of quantum mechanics, the quantities σ_0 and q_J must be expressed in terms of the detailed cross-sections for excitation and de-excitation. In the simplest case we assume that n_H is so small that all molecules are in the ground state; then only the values of σ_{0J}, the cross-section for excitation from the ground state, are relevant. The number of excitations per second to each state is given by an expression similar to the left-hand side of equation (12); and, if we use the relation in equation (14), we have

$$\left(\frac{dn_J}{dt}\right)_{\text{exc}} = n_H n_0 \overline{\sigma_{J0} v} \frac{g_J}{g_0} e^{-E_J/kT}. \tag{34}$$

Since g_0 is unity, and n_0 is here assumed to equal n_m, comparison of equations (32) and (34), with use of equation (28), shows that

$$\sigma_{\text{eff}} = q_J \sigma_0 = \sigma_{J0} \sum_J g_J e^{-E_J/kT}. \tag{35}$$

If, on the other hand, the lowest p states are all occupied according to the Boltzmann formula, then it is readily shown that

$$\sigma_{\text{eff}} = q_J \sigma_0 = \sum_{r=0}^{p} \sigma_{Jr}, \tag{36}$$

provided that $F(p)$ is negligible. When equation (36) applies, a molecule excited to level J may not cascade all the way down to the ground state, and the energy radiated may be less than the value E_J assumed in equation (33). This effect is not very large and will be neglected here.

Numerical values of the de-excitation cross-sections may be found from observations[34] on the dispersion of sound in parahydrogen at low pressures and high frequencies. These results give directly a quantity $(f/p)_0$, which is the sum of the probabilities for excitation up and de-excitation back down, at 1 atm. pressure, divided by 2π. By the use of equation (14) we find that the average cross-section for collisional de-excitation of the level with $J = 2$ is 4.0×10^{-18} cm^2 at 198° K, and 3.9×10^{-18} cm^2 at 298°. For the level with $J = 4$, the de-excitation cross-section at 298° is 2.0×10^{-17} cm^2, or 4.0×10^{-18} cm^2 per

[33] L. B. Loeb, *Kinetic Theory of Gases* (New York and London: McGraw-Hill Book Co., 1934), Appen. I.

[34] J. E. Rhodes, *Phys. Rev.*, **70**, 932, 1946.

unit weight of the lower state, in good agreement with the de-excitation cross-section for the lower level. These results refer, of course, to collisions between H_2 molecules. One may expect that the cross-sections for excitation of H_2 by impact with H atoms would not be widely different from these values.

From these results we see at once that for the level $J = 2$ the value of σ_{eff} is simply 4.0×10^{-18} cm^2 in accordance with equation (35). For the level $J = 4$, σ_{eff} depends on whether or not n_2 has its Boltzmann value. If n_2 is much less than $n_m F(2)$, then σ_{eff} will equal σ_{40}; the observational evidence does not determine σ_{40} directly, since σ_{42} is apparently a much larger quantity, but one would expect σ_{40} to be of the same order as σ_{20}. However, $A_{2,0}$ is so small that if n_H is as great as 10 per cubic centimeter, a reasonable value for an absorbing cloud, n_2/n_m will be about equal to $F(2)$. In this case σ_{eff} must be found from equation (36) and is about equal to 2.4×10^{-17} cm^2.

These values are applicable only at low temperatures. Specifically, when θ is less than about 15, the population of the level $J = 2$ in thermodynamic equilibrium becomes greater than that in the ground state and the value of σ_{eff} computed from equation (35) is increased by a factor of 2 or more, if σ_{J0} is independent of T. In fact, for large T, σ_{eff} varies as $T\sigma_{J0}$. Similarly, an increase of T increases the corresponding value of σ_{eff} found when the lowest p states are occupied according to the Boltzmann formula. This increase can certainly not be real for the relevant values of J, since it is evident from the correspondence principle that, as T increases, σ_{eff} must approach a limiting value substantially less than the geometrical cross-section, and probably less than 10^{-16} cm^2. Either σ_{Jp}/g_p must decrease as the temperature increases, or σ_{Jp}/g_J must fall off with decreasing J. In any event, one may expect that for the higher excited states and for higher temperatures, the value of σ_{eff} will approach a constant value somewhere between 10^{-16} and 10^{-17} cm^2.

In the lack of more definite information, we shall set σ_0 equal to 2.0×10^{-17} cm^2 in equation (33). To take into account the low value of σ_{eff} found for the level $J = 2$ at low temperatures, we shall take $q_2 = \frac{1}{5}$. For all other levels, however, q_J will be set equal to unity. Moreover, we shall assume that the cross-sections for collisions between H and H_2 are identical for those between H_2 and H_2. This procedure should give approximately correct results for the first two excited levels, when these make the dominant contribution; but for other levels the proper values of σ_0 and q_J might well differ by an order of magnitude from those adopted here.

With these assumptions, equation (33) for Υ_2 may be evaluated without further difficulty. Computed values of Υ_2 are given in Table 4 for values of θ between 1 and 50. For greater values of θ, only the first term in equation (33) need be considered, and we have

$$\Upsilon_2 = \frac{1.8 \times 10^{-24-0.0441\theta}}{\theta^{1/2}} \text{ erg cm}^3/\text{sec} . \tag{37}$$

In equation (37), as in Table 4, $\bar{v}$ has been set equal to the mean velocity of H atoms relative to H_2 molecules.

To find a value of L_{Hm}, an average of Υ_1/n_H and Υ_2 may be obtained in accordance with equation (26). While this procedure is obviously valid at the two extremes, it may be questioned for intermediate values of n_H; in view of the rapid increase of $A_{J,J-2}$ with increasing J, collisional de-excitation may be dominant for the lower levels and radiative de-excitation for the upper ones. The validity of equations (25) and (26) may be tested by solving the equation of statistical equilibrium for a few selected values of θ and n_e. If equation (32) is adopted for collisional excitation, and the corresponding equation for de-excitation, then the equation of transfer becomes

$$n_H \sigma_{\text{eff}} \bar{v} F(J)\, n_m + A_{J+2,J} n_{J+2} = n_J n_H \sigma_{\text{eff}} \bar{v}\, n_J + A_{J,J-2} n_J , \tag{38}$$

where n_J is the population in each excited state and n_m is the sum of n_J over all even values of J. Equation (38) has the solution

$$\frac{n_J}{n_m} = K_J \sum_{J} \frac{F(J')}{(1+K_{J'})} \prod_{J}^{J'} \frac{1}{(1+K_{J''})}, \tag{39}$$

where

$$K_J = \frac{n_H \sigma_{\text{eff}} \bar{v}}{A_{J,J-2}} \tag{40}$$

and where the sum and product are taken over even values only of J. For the total rate of radiation per cubic centimeter, which equals $n_H L_{Hm}$, we find

$$n_H L_{Hm} = n_m \sigma_{\text{eff}} \bar{v} \times 2E_r \times \sum_{2}^{\infty} F(J) \sum_{2}^{J} (2J'-1) \prod_{J}^{J'} \frac{1}{1+K_{J''}}, \tag{41}$$

where, by use of equation (24), $2E_r(2J'-1)$ has been substituted for $E_{J'} - E_{J'-2}$; it is assumed here that σ_{eff} is the same for all levels.

This equation has been applied in the computation of L_{Hm} for a number of intermediate cases. The resulting values were in some cases only about half those obtained from equations (25) and (26), together with Table 4, but this seems to be the maximum error for the relevant values of θ. Since σ_{eff} is not certain to within a factor of 2, we shall therefore use equations (25) and (26) rather than the more cumbersome equation (41). In addition, we shall also assume that L_{mm}, the energy loss per molecule in impacts with other molecules, is given with adequate accuracy by the equations obtained for L_{Hm}, provided that n_m replaces n_H throughout.

In addition, the impact of an H_2 molecule with either an H atom or another H_2 molecule can excite the vibrational levels of the molecule. The energy radiated in this way is at most no greater than that resulting from the excitation of rotational levels. Even at energies of 1 or more electron-volts the cross-section for vibrational excitation is not likely to exceed very much that for rotational excitation. Moreover, with decreasing energy, the cross-section for vibrational excitation falls off appreciably, as evidenced both by theory[35] and by observations[36] on CO_2 and other molecules. Since this process does not increase L_{Hm} very substantially and since under most conditions it is negligible, we shall neglect it.

V. INELASTIC ENCOUNTERS WITH GRAINS

When particles strike grains, there is a certain probability that they will go off again with a reduced kinetic energy, the energy being lost to the random motions of the grain. While low-energy electrons tend either to stick or to be reflected without loss of energy, as pointed out in Paper I, inelastic collisions of atoms and molecules with grains provide an important source of energy loss.

Transfer of heat in this way from a gas to a solid surface has been explored in the laboratory, and results reported in terms of an accommodation coefficient, α. If T is the temperature of the gas, T_g, that of the solid—here the internal temperature of the grain—and T_2 the kinetic temperature of the atoms or molecules leaving the surfaces, then α is defined by the equation

$$\alpha = \frac{T - T_2}{T - T_g}. \tag{42}$$

[35] J. M. Jackson and N. F. Mott, *Proc. R. Soc., London, A*, **137**, 703, 1932; L. Landau and E. Teller, *Phys. Zs. d. Sowjetunion*, **10**, 34, 1936.

[36] A. Eucken and collaborators, *Zs. f. phys. Chem.*, **B30**, 85, 1935; *ibid.*, **B36**, 163, 1937; A. Kantrowitz, *J. Chem. Phys.*, **14**, 150, 1946.

Thus if α is zero, the collisions with the solid surface are perfectly elastic, while if α is unity, complete equipartition of kinetic energy is established between the atoms in the solid and those in the gas.

For clean metallic surfaces, the measurements by J. K. Roberts[37] and the theory by A. F. Devonshire[38] indicate that α is very small and approaches zero at 0° K. For *He* on pure *W* at 79° K, Roberts found that α was 0.025 but increased to 0.058 at 298°. On the other hand, for surfaces on which adsorbed gases are present, α is much higher. For example, Roberts observed that α increased with time after a clean surface had been prepared, reaching values of about 0.50. In addition, while α decreases with T_g for clean surfaces, it apparently increases with decreasing T_g for surfaces covered with adsorbed gases. Thus, W. H. Keesom and G. Schmidt[39] observe that for H_2 on glass, presumably covered by adsorbed H_2O molecules, α increases from 0.28 at 273° K to 0.56 at 90° K, and to 0.98 and 1.05 at 17.9° and 14.3° K. For *He*, however, α increased only to 0.67 at 12.1°, the lowest temperature reached. Additional measurements of α are reported in a thorough study by van de Hulst,[40] who concludes that at the low temperature of interstellar grains α is unity for all atoms except *He*, for which it is 0.6.

There are two factors which give some uncertainty to this conclusion. In the first place, the density of interstellar gas is much lower than that of the gases used in most laboratory measurements of α. In the second place, the temperature difference between the gas and the grains may be orders of magnitude greater than the 2° difference at the lowest temperatures employed by Keesom and Schmidt. As a result of these two factors, the nature of the adsorbed layer and of the individual collisions may be somewhat different from those in the laboratory. While these factors might reduce α somewhat and reduce appreciably the capture probability for atoms, it is difficult to see how a value of α much less than 0.50 could result. The assumption that α is unity should therefore give a value of L_{Hg} which is of the correct order of magnitude.

With this assumption, the equation for L_{Hg} becomes

$$L_{Hg} = \frac{3\pi a^2 n_g \bar{v}_H k}{2}(T - T_g)\,, \tag{43}$$

where a is the radius of the grain and n_g the number of grains per cubic centimeter. If we let a equal 10^{-5} cm and insert the standard equation for $\bar{v}$, we find

$$L_{Hg} = 9.4 \times 10^{-22} n_g T^{1/2}(T - T_g)\ \text{erg/sec}\,. \tag{44}$$

For H_2 molecules the velocity is somewhat less, but, in view of the uncertainty in the precise value of α, we shall set L_{mg} equal to L_{Hg}.

Equation (44) applies only to neutral particles. For ions the effect is more complicated, since the charge on the grain must be taken into account. If the accommodation coefficient is unity, the ions will lose all their energy on impact, but if they leave, they may be assumed to carry off an electron. This process therefore forms part of the superelastic collisions considered in Paper I; and the loss of energy of the ion, on the average, will about equal the loss of energy of the electron which is captured. Hence the term in T in equation (57) in Paper I must be increased accordingly. However, this effect is at most rather small, and we shall therefore neglect it.

The author is indebted to Mr. William Buscombe for a thorough check of the manuscript and for a number of necessary computations.

[37] *Proc. R. Soc., London, A*, **129**, 146, 1930; **135**, 192, 1932.

[38] *Proc. R. Soc., London, A*, **158**, 269, 1937.

[39] *Physica*, **3**, 590, 1085, 1936; **4**, 828, 1937.

[40] *Rech. Astr. de l'Obs. d'Utrecht* (in preparation).

OBSERVATIONS OF INTERSTELLAR H AND K, MOLECULAR LINES, AND RADIAL VELOCITIES IN THE SPECTRA OF 300 O AND B STARS*

WALTER S. ADAMS
Mount Wilson Observatory, Carnegie Institution of Washington
Received March 3, 1949

ABSTRACT

Spectrograms of 300 stars of types O and B, observed with the coudé spectrograph and the 100-inch telescope in the region λλ 3600–4700, have been used in a study of the structure of the interstellar H and K lines, of the presence of interstellar molecular and additional atomic lines, and in the measurement of interstellar radial velocities. A dispersion of 2.9 A/mm was used for 231 stars and of 10 A/mm for 69 fainter stars.

About one star in two is found to have complex interstellar H and K lines, and about one star in four shows one or more interstellar lines of *CN*, *CH* I, *CH* II, *Ca* I, or *Fe* I. As many as four components of H and K are found in a few stars; 17 stars show triple lines. The radial velocity from individual components in 7 stars exceeds 50 km/sec and reaches nearly 100 km/sec in one case, but the strongest component nearly always gives a low velocity. Double stars and stars close together in position usually show the same structure for the H and K lines, and nearly the same radial velocities. The radial velocities derived from the molecular lines, with few exceptions, agree with those from the strongest component of H and K.

The stars in the Pleiades are remarkable in showing interstellar molecular lines that are exceptionally strong relative to H and K. The results for this group and other stars showing the molecular lines have been utilized for a discussion of a possible difference in the place of origin of the absorption of H and K and of the molecular lines, but the evidence is not altogether adequate to afford a decision.

The radial velocities, corrected for the solar motion, are used for a determination of the galactic rotation, although most of the stars are too near to be favorable for the purpose. A calculation based upon 171 near-by stars gives a value of 16.8 km/sec for the rotational constant, in good agreement with other determinations. More distant stars are too few in number to provide satisfactory results.

The discovery in 1936 by C. S. Beals[1] at the Dominion Astrophysical Observatory of the double character of the interstellar H and K lines of ionized calcium in the spectra of ρ Leonis and one or two other stars proved the existence of multiple discrete clouds of interstellar gas, which often could be identified through their radial velocities. Extension of such observations evidently required the use of the highest possible resolution in the spectrograph, since the separation of the components would in general be expected to be small. For this reason the coudé spectrograph of the 100-inch telescope of the Mount Wilson Observatory was used by R. F. Sanford[2] in 1939 to investigate the structure of interstellar H and K in the spectra of a number of stars of types O and early B. The 32-inch Schmidt camera, dispersion 10 A/mm, was employed, and about 10 additional stars were found to show a doubling of the *Ca* II lines.

In the meantime, further use of the 114-inch camera of the coudé spectrograph, dispersion 2.9 A/mm, had proved that the spectral region near H and K of stars of early type could be photographed in reasonable exposure time to stellar magnitude about 6.0. Since many stars brighter than this limit are available, systematic observations were begun with this instrument in 1941. A summary of the results for 50 stars was published in 1943.[3]

The total number of stars observed to January, 1946, including those for which results had been published, amounted to 300; these form the basis of the present *Contribu-*

* *Contributions from the Mount Wilson Observatory, Carnegie Institution of Washington*, No. 760.

[1] *M.N.*, **96**, 661, 1936. [2] *Pub. A.S.P.*, **51**, 238, 1939.

[3] W. S. Adams, *Mt. W. Contr.*, No. 673; *Ap. J.*, **97**, 105, 1943.

tion. Of this number, 231 were observed with the high dispersion of the 114-inch camera. They are mainly bright stars of spectral types O–B3, and some of types B5–B8, which could be observed with the telescope in the coudé form without too great loss of light. In addition, 69 stars were observed with the lower dispersion of the 32-inch Schmidt camera. These were nearly all stars fainter than magnitude 6.0, the few exceptions being brighter stars of large southern declination. The northern limit in declination for essentially all the observations was about +50°.

The portion of spectrum included on most of the photographs extends from about λ 3600 to λ 4700, but some of the strongly exposed negatives extend considerably farther into the ultraviolet. Two strips of plate, each 10 inches in length, are placed end to end in the plateholder and set on curved rails which provide the small amount of bending required to bring the entire region into focus. No correcting plate is needed for the focal ratio of the 114-inch camera, and hence the star's light undergoes no transmission through glass throughout the entire optical system of telescope and spectrograph.

The photographic emulsions used have been mainly Eastman 103-O and 103*a*-O. The first of these has proved especially useful when baked for a period of 48–72 hours in an electric oven at a temperature of 50° C. The gain in sensitivity is considerable for exposures exceeding 1 hour. A few bright stars of special interest, such as ζ Persei, χ^2 Orionis, ζ Ophiuchi, and 55 Cygni, have also been photographed on Cramer Contrast

TABLE 1

ADOPTED WAVE LENGTHS OF INTERSTELLAR LINES

3719.949	*Fe* I	3878.798	*CH* I	3968.494	*Ca* II
3745.330	*CH* II	3886.426	*CH* I	4226.742	*Ca* I
3859.924	*Fe* I	3890.220	*CH* I	4232.573	*CH* II
3874.025	*CN*	3933.684	*Ca* II	4300.338	*CH* I
3874.634	*CN*	3957.712	*CH* II		

emulsions. The finer grain and higher contrast have been most effective in resolving multiple H and K lines and in making visible faint components and the weaker atomic and molecular lines. For example, the two interstellar lines of neutral iron, λ 3720 and λ 3860, were first seen with certainty on a spectrogram of 55 Cygni taken on a contrasty emulsion and are doubtful objects on emulsions of higher photographic speed. Unfortunately, length of exposure time has prohibited the use of the more contrasty plates except in special cases.

The results for nearly 80 per cent of the stars observed depend upon a single spectrogram of good quality. Experience has shown that, because of the excellent character for measurement of most of the interstellar lines, additional spectrograms add comparatively little to the accuracy of the results. When the resolution of complex lines is uncertain or bright stars are of exceptional interest, more observations have been made.

In addition to H and K, the region of the spectrum under investigation includes several atomic interstellar lines and most of the recognized molecular lines. The wave lengths of all such lines were determined by referring them to the solar wave lengths of H and K. For this purpose 14 stars were used, selected for the quality and intensity of the lines present. The values for the *Fe* I lines and λ 4227 of *Ca* I proved to be in such close agreement with their values in the sun that the solar wave lengths were used. The complete list of adopted wave lengths is in Table 1. Except for H and K, λ 4232 and λ 4300 are the strongest of these lines in all spectra in which they occur. A very faint line at λ 3579.99, observed only in ζ Ophiuchi but agreeing in position with a *CN* line predicted by McKellar as a possible interstellar line, is not altogether certain.

The difficulty of distinguishing interstellar from stellar H and K in the range of spectral types B3 to B9, in which stellar lines would be expected to appear and finally

attain considerable strength, is a serious one. Numerous stars which have been observed are omitted from the published list because of this uncertainty. On the other hand, several factors may aid in reaching a decision. In the first place, an interstellar line may be sufficiently strong to be seen superposed upon a broad stellar line. The star α Cygni seems to be a case of this sort. In the second place, the lines in question may give a different radial velocity from that of the recognized stellar lines. Finally, the presence of the molecular lines affords definite evidence that interstellar H and K are to be expected. Most of the stars in the Pleiades belong to this category. Frequently, the character of H and K itself is the best criterion. Although unresolved components may produce the appearance of a broad line, sufficient structure is often visible to make a judgment possible. A few stars have been included in the list in which blending of stellar and interstellar lines may be present and may affect the radial velocities, but in all cases there seems to be sufficient evidence to warrant their inclusion.

The results of the observations and measurements are in Tables 2 and 3. Table 2 gives a complete list of all the stars. Table 3 lists additional data for stars whose spectra contain one or more molecular or atomic lines in addition to H and K; such stars are indicated in Table 2 by the symbol †.

Most of the data in Table 2 are self-explanatory. The spectral types are mainly those of the *Henry Draper Catalogue*. The intensities of K and its components are based upon an arbitrary scale, 1 indicating the faintest line which is well visible, and "tr" a line present with reasonable certainty but at the limit of visibility. The scale may be moderately accurate between 1 and perhaps 10, but for stronger lines it is of value chiefly for purposes of relative comparison.

The two columns of radial velocities are, respectively, the combined values from H and K, and these velocities corrected for a solar motion of 20 km/sec. The latter are termed "residual velocities" in accordance with the usual practice. Although the intensities of H and its components are not listed, the lines have been used throughout to check the reality of the components observed at K, and have been measured consistently. The intensity of H is nearly always nearly half that of K, but occasionally the wings of *He* are so broad as to affect seriously estimates of the intensity of H.

Table 3, which lists the stars in which one or more interstellar lines in addition to H and K have been observed and usually measured, gives the radial velocities from these lines; the radial velocity from H and K, for comparison; and the estimated intensities of the three most prominent molecular lines λ 3957 and λ 4232 of *CH* II, and λ 4300 of *CH* I. Stars containing other interstellar lines are designated by the letters "(a)," "(b)," "(c)," and "(d)." The line λ 3745 of *CH* II is usually visible when λ 4232 is well marked, the three lines, $\lambda\lambda$ 3745, 3957, and 4232, forming a group with intensities increasing in the order named. Neutral calcium, λ 4227, appears in several stars but is always faint. It is best seen in 55 Cygni. The *Fe* I lines, λ 3720 and λ 3860, have been observed with certainty in only two stars, χ^2 Orionis and 55 Cygni, which have been photographed on contrasty emulsions. Except for λ 4232 and λ 4300, the intensities of the additional interstellar lines exceed 1 in only a very few stars.

Of the 62 stars in Table 3, 54 have been observed with the higher dispersion and only 8 with the lower. Limiting the comparison to stars observed on the larger scale, which is more favorable for showing faint lines, we find 54 stars out of 231, or somewhat less than one star in four, in which molecular or atomic lines or both appear in addition to H and K. In many of these stars the lines are extremely faint. The *CH* II line λ 4232 is present in all but 2 of the stars listed and in a large majority is the strongest molecular line. On the other hand, λ 4300 *CH* I is stronger than λ 4232 in a few stars, the best examples being ζ Persei, X Persei, and the pair ρ Ophiuchi. Both AE Aurigae and ζ Ophiuchi show both lines in considerable strength and nearly equal. All stars in which λ 4300 of *CH* I is prominent show the group of three *CH* I lines between λ 3879 and λ 3890 and the three *CN* lines between λ 3874 and λ 3894. Such stars are characterized by H and K lines of moderate intensity; λ 4227 of *Ca* I is not present with certainty.

TABLE 2

STRUCTURE AND RADIAL VELOCITIES OF INTERSTELLAR H AND K LINES IN 300 STARS

NAME OR HD No.	1900 R.A.	1900 Dec.	m	Spec.	l	b	K INT.	RADIAL VELOCITY (KM/SEC)	RESIDUAL VELOCITY (KM/SEC)	NOTES
1337	0^h12^m5	+50° 58′	6.1	O8	86°	−11°	3, 3, 4, 10	−44.5, (−39.8), −34.8, −23.0, (−15.5), −11.1	−37.3, (−32.6), −27.6, −15.8, (−8.3), −3.9	c
1976	0 18.9	+51 28	5.4	B4	87	−10	1, 5	−69.6, −9.1	−62.5, −2.0	
ξ Cas	0 36.5	+49 58	4.8	B3	89	−12	6s	−10.8	−4.9	
4142	0 38.8	+47 19	5.6	B5	90	−15	4	−3.0	+2.4	
o_2 Cas	0 39.2	+47 44	4.7	B4e	90	−14	10s, 1	−6.5, +15.5	−1.2, +20.8	†
ν And	0 44.3	+40 32	4.4	B5	91	−22	5b	−3.0	+1.0	
6300	0 58.9	+50 29	6.5	B4	93	−11	4	−6.6	−1.7	*
φ Per	1 37.4	+50 11	4.2	B0e	99	−11	4s	−6.6	−3.5	
14633	2 16.7	+41 2	7.7	O8	109	−17	12s	−4.8	−5.6	*
ξ Ari	2 19.5	+10 9	5.5	B7	126	−45	4s	+4.3	−3.8	
35 Ari	2 37.6	+27 17	4.6	B3	120	−28	5	+4.6	−0.5	
π Ari	2 43.7	+17 3	5.3	B8	127	−36	6s	+13.3	+5.3	
30 Per	3 11.0	+43 39	5.4	B7	117	−10	4	+2.2	−0.2	
29 Per	3 11.5	+49 51	5.3	B3	113	− 5	6s	+2.8	+2.2	
31 Per	3 12.0	+49 43	5.1	B3	114	− 5	6s	+3.5	+2.9	
61 Ari	3 15.5	+20 47	5.2	B7	132	−28	6	+13.4	+4.8	
20809	3 16.1	+48 51	5.3	B3	115	− 6	7s	+1.6	+0.6	
21278	3 20.9	+48 43	4.9	B5	115	− 5	6s, 1	−0.4, +48.4	−1.5, +47.3	
34 Per	3 22.2	+49 10	4.7	B5	115	− 5	5s	+0.7	−0.4	
21856	3 26.3	+35 6	5.8	B3	124	−16	15s	+4.9	−0.5	
ψ Per	3 29.4	+47 51	4.3	B5e	117	− 5	6	−0.2	−2.0	‡
22780	3 34.6	+37 16	5.6	B8	124	−13	3s	+8.2	+3.2	
40 Per	3 36.0	+33 39	5.0	B2	127	−16	8s	+9.0	+2.9	†
o Per	3 38.0	+31 58	3.9	B2	128	−17	8s	+10.1	+3.5	†
16 Tau	3 38.9	+23 59	5.4	B7	134	−22	2	+17.5	+8.7	†
17 Tau	3 39.0	+23 48	3.8	B5e	134	−23	tr	+18.2	+9.4	†
19 Tau	3 39.3	+24 10	4.4	B8	134	−22	2	+14.0	+5.1	†
20 Tau	3 39.9	+24 4	4.0	B9	134	−22	4	+15.0	+6.1	†
21 Tau	3 39.9	+24 15	5.8	B9	134	−22	1	+16.0	+7.1	†
23 Tau	3 40.4	+23 39	4.2	B5e	135	−22	tr	(+16.9)	(+7.9)	†

TABLE 2—*Continued*

Name or HD No.	1900 R.A.	1900 Dec.	m_v	Spec.	l	b	K Int.	Radial Velocity (Km/Sec)	Residual Velocity (Km/Sec)	Notes
23478	3h40m4	+32° 0′	6.5	B5	129°	−16°	3	+8.6	+1.9	*
η Tau	3 41.5	+23 48	3.0	B5e	135	−22	1	+15.5	+6.5	†
23753	3 42.4	+23 7	5.5	B8	135	−23	1	+14.3	+5.1	†
30 Tau	3 42.8	+10 50	5.0	B3	145	−31	3	+18.9	+6.8	
27 Tau	3 43.2	+23 45	3.8	B9	135	−22	2	+14.5	+5.4	†
23923	3 43.8	+23 25	6.1	B8	135	−22	2	+13.9	+4.7	
24131	3 45.5	+34 3	5.7	B2	128	−14	6s	+12.3	+5.9	†
ζ Per	3 47.8	+31 35	2.9	cB1	130	−15	10s	+12.0	+4.8	†
X Per	3 49.1	+30 45	6.3	B0e	130	−16	12	+12.2	+4.8	†
24640	3 50.0	+34 47	5.5	B3	128	−13	10s	+10.8	+4.7	
ε Per	3 51.1	+39 43	3.0	B2	125	− 9	4,3	+7.6, +18.2	+2.8, +13.4	
ξ Per	3 52.5	+35 30	4.0	O7	128	−12	10, 1	+9.4, +25.4	+3.2, +19.2	†
λ Tau	3 55.1	+12 12	3.3	B3	146	−28	2	+20.8	+8.4	
25539	3 58.3	+32 18	6.7	B3	131	−13	3s	+11.8	+4.6	*
40 Tau	3 58.4	+ 5 9	5.3	B5	153	−32	4, 2	+22.6, (+26.2), +31.7	+8.7, (+12.3), +17.8	
25799	4 0.3	+32 6	6.9	B5	132	−13	3	+9.0	+1.6	*
25833	4 0.6	+33 11	6.6	B3	131	−12	4s	+14.0	+6.9	*
48 Per	4 1.4	+47 27	4.0	B3e	121	− 2	6s	+5.7	+2.9	
μ Tau	4 10.1	+ 8 39	4.3	B3	152	−27	5s	+21.9	+8.2	†
53 Per	4 14.3	+46 16	4.9	B4	124	− 1	8	+6.1	+2.6	†
ν Eri	4 31.3	− 3 33	4.1	B2	167	−30	1, 4	+2.5, +21.0	−15.9, +2.6	
29309	4 31.8	+31 48	7.1	B3	137	− 8	6s	+11.1	+2.8	*†
3 Ori	4 45.9	+ 5 26	3.8	B2	161	−22	5b	+22.3	+6.9	‡c
8 Ori	4 49.0	+ 2 17	3.9	B2	164	−23	3	+20.9	+4.9	
AE Aur	5 9.7	+34 12	5.8	O9	140	− 1	10b	+13.0	+4.7	†c
34656	5 14.0	+37 20	6.7	O6	138	+ 2	5, 7s	−7.6, (+0.9), +8.4	−15.0, (−6.5), +1.0	*†
ρ Aur	5 14.7	+41 42	5.1	B7	134	+ 4	3b	+8.2	+2.2	
λ Lep	5 15.0	−13 17	4.3	B1	182	−25	5b, 2	+2.4, +21.4	−16.4, +2.6	
22 Ori	5 16.7	− 0 29	5.0	B3	170	−18	6, 8	−5.2, +23.5	−22.3, +6.4	‡
23 Ori	5 17.6	+ 3 27	5.0	B3	167	−16	5	+21.1	+4.7	†

TABLE 2—*Continued*

Name or HD No.	1900 R.A.	1900 Dec.	m	Spec.	l	b	K Int.	Radial Velocity (Km/Sec)	Residual Velocity (Km/Sec)	Notes
35395	5h19m3	+20°30′	6.8	B2	152°	− 7°	15s	+15.0	+2.5	*†
η Ori	5 19.4	− 2 39	3.4	B0	172	−19	5, 2	+7.2, +24.2	−10.2, +6.8	
35708	5 21.6	+21 51	4.8	B3	152	− 6	2b, 12s	+1.1, +20.1	−11.0, +8.0	
ψ Ori	5 21.6	+ 3 0	4.7	B2	168	−16	2, 4b	+5.1, (+14.1), +22.9	−11.4, (−2.4), +6.4	
35921	5 23.0	+35 18	6.7	O9	140	+ 2	15	+3.9	−4.3	*
χ Aur	5 26.2	+32 7	4.9	cB3	143	+ 1	8, 10	+0.0, +10.6	−9.2, +1.4	*
36485	5 26.9	− 0 21	6.9	B3	171	−16	4b	+17.1	−0.1	*c
δ Ori br	5 26.9	− 0 22	2.5	B0	171	−16	4b	+15.2	−2.0	c
δ Ori ft	5 26.9	− 0 22	6.9	B	171	−16	5b	+15.1	−2.1	*c
υ Ori	5 27.1	− 7 23	4.6	B2	178	−20	1, 8	+7.9, +27.8	−10.3, +9.6	
120 Tau	5 27.6	+18 29	5.5	B3e	155	− 6	8b	+18.0	+4.9	c
36591	5 27.6	− 1 40	5.3	B2	173	−17	3, 6	+10.8, +23.9	−6.6, +6.5	‡
VV Ori	5 28.5	− 1 14	5.5	B2	173	−16	2, 6	+9.3, +25.6	−8.1, +8.2	
121 Tau	5 29.3	+23 58	5.3	B3	151	− 3	4	+19.3	+7.7	
ϕ^1 Ori	5 29.3	+ 9 25	4.5	B0	163	−11	3, 1, 8s	+2.6, +12.9, +21.7	−12.7, −2.4, +6.4	
λ^1 Ori	5 29.6	+ 9 52	3.7	O8	163	−11	4, 1, 7s	+5.6, +15.0, +23.3	−9.6, −0.2, +8.1	
λ^3 Ori	5 29.6	+ 9 52	5.6	B0	163	−11	4, 1, 6s	+6.9, +14.2, +21.3	−8.3, −1.0, +6.1	
36959	5 30.1	− 6 5	5.6	B1	177	−18	1, 7s	+15, +27.8	−3, +9.7	
36960	5 30.1	− 6 5	4.7	B1	177	−18	tr, 7	+15, +27.6	−3, +9.5	c
37016	5 30.4	− 4 29	6.3	B2	176	−17	1, 3	+2, +25.1	−16, +7.2	*
37017	5 30.4	− 4 34	6.5	B2	176	−17	1, 4	0, +26.4	−18, +8.5	*
42 Ori	5 30.4	− 4 54	4.6	B2	176	−18	1, 10s	+5.8, +27.9	−12.2, +9.9	
θ^1 Ori	5 30.4	− 5 27	5.4	O7	177	−17	2, 3, 4	+2.5, (+12.2), +18.5, +29.9	−15.5, (−5.8), +0.5, +11.9	
Bond 619	5 30.4	− 5 27	6.8	O	177	−17	4b	+20.9	+2	*c
Bond 640	5 30.4	− 5 27	6.7	O	177	−17	4b	+21.0	+2	*c
37040 br	5 30.5	− 4 26	6.3	B3	176	−17	1, 3s	−0.5, +26.8	−18.4, +8.9	
θ^2 Ori	5 30.5	− 5 29	5.2	O9	177	−18	1, 6	0, +23.0	−18.1, +4.9	
ι Ori	5 30.5	− 5 59	2.9	O8	177	−18	1, 5	+3.2, +27.9	−14.9, +9.8	
37061	5 30.6	− 5 20	9.1	B	177	−17	4s	+27.3	+9.3	*
ε Ori	5 31.1	− 1 16	1.8	cB0	173	−16	1, 3, 6	−0.3, +9.1, +25.0	−17.7, −8.3, +7.6	

TABLE 2—*Continued*

Name or HD No.	1900 R.A.	1900 Dec.	m	Spec.	l	b	K Int.	Radial Velocity (Km/Sec)	Residual Velocity (Km/Sec)	Notes
37150	5^h31^m3	− 5°43′	6.4	B3	177°	−18°	2	+27.2	+9.2	
ζ Tau	5 31.7	+21 5	3.0	B3e	153	− 4	4	+16.4	+4.0	
125 Tau	5 33.5	+25 50	5.0	B3	150	− 1	5s	+16.6	+5.5	
σ Ori	5 33.7	− 2 39	3.8	B0	174	−16	1, 5	+1.0, +22.9	−16.6, +5.3	
ω Ori	5 33.9	+ 4 4	4.5	B3e	168	−13	12b	+25.5	+9.1	c
126 Tau	5 35.5	+16 29	4.9	B3	158	− 6	4b	+20.9	+7.3	c
ζ Ori br	5 35.7	− 2 0	2.0	B0	174	−15	3, 5	−4.7, +21.1	−22.2, +3.6	
ζ Ori ft	5 35.7	− 2 0	4.2	B0	174	−15	3, 4	−3.4, +22.0	−20.9, +4.5	*
κ Ori	5 43.0	− 9 42	2.2	cB0	182	−17	4b, 2, 1	−1.4, +18.6, +31.4	−20.1, −0.1, +12.7	c
57 Ori	5 49.1	+19 44	5.9	B3	157	− 1	10b	+19.4	+6.5	c
139 Tau	5 51.8	+25 57	4.9	B0	152	+ 2	15s	+12.1	+1.0	
χ^3 Ori	5 58.0	+20 8	4.7	cB1e	157	+ 1	20b, 2	+14.4, +29.6	+1.6, +16.8	†c
41335	5 59.4	− 6 42	5.1	B2e	181	−12	2, 4	−3.9, +16.7	−22.3, −1.7	
ν Ori	6 1.9	+14 47	4.4	B3	163	− 1	5s, 1	+15.7, +30.4	+1.5, +16.2	
41943	6 2.9	+13 59	7.4	B2	163	− 1	10s	+17.7	+3.4	*
3 Gem	6 3.7	+23 8	5.8	B2	155	+ 3	3, 8, 9	−27.2, +5.7, (+12.3), +20.7	−39.2, −6.3, (+0.3), +8.7	c
69 Ori	6 6.2	+16 9	4.9	B3	162	0	10s	+15.4	+1.6	
ξ Ori	6 6.3	+14 14	4.4	B3	164	− 1	8s	+13.0	−1.3	
47129	6 32.0	+ 6 13	6.1	O8	174	+ 1	6b, 10	+7.9, (+14.2), +22.0	−8.0, (−1.7), +6.1	†c
S Mon	6 35.5	+ 9 59	4.7	O7	171	+ 4	5, 6	+7.7, (+13.6), +21.4	−7.4, (−1.5), +6.3	
48099	6 36.6	+ 6 27	6.2	O7	174	+ 2	15b	+17.7	+1.9	
48434	6 38.3	+ 4 2	5.8	B0	176	+ 2	20b	+19.5	+3.2	c
15 CMa	6 49.2	−20 6	4.7	B0	199	− 7	1, 4	+8, +21.0	−11, +1.7	
ι CMa	6 51.7	−16 55	4.4	B5	196	− 5	6b, 5b	+16.5, (+24.5), +32.6	−2.6, (+5.4), +13.5	c
52382	6 55.9	− 9 4	6.4	B2	190	− 1	8s	+32.2	+14.0	*
19 Mon	6 57.9	− 4 6	4.9	B3	186	+ 2	5	+24.1	+6.7	
o^2 CMa	6 58.8	−23 41	3.1	cB3	203	− 7	8b	+22.7	+3.4	c
54662	7 4.6	−10 11	6.2	O7	192	+ 1	10b	+25.9	+7.8	*c
55879	7 9.7	−10 8	6.0	O9	192	+ 2	5b	+25.8	+7.8	*
ω CMa	7 10.8	−26 36	3.8	B3	207	− 6	4	+22.2	+3.0	

TABLE 2—*Continued*

Name or HD No.	1900 R.A.	1900 Dec.	m	Spec.	l	b	K Int.	Radial Velocity (Km/Sec)	Residual Velocity (Km/Sec)	Notes
29 CMa	7^h14^m5	$-24°23'$	4.9	O7	205°	− 4°	15	+26.3	+7.3	c
30 CMa	7 14.5	−24 47	4.4	O9	206	− 4	10b	+25.9	+6.9	c
58050	7 18.8	+15 43	6.4	B3	170	+16	3b	+12.0	−1.0	*c
58343	7 20.1	−16 0	5.2	B3	199	+ 1	7s	+19.5	+1.1	
η CMa	7 20.1	−29 6	2.4	cB7	210	− 5	7, 6	+16.4, (+23.7), +31.0	−2.7, (+4.6), +11.9	
o Pup	7 43.9	−25 42	4.6	B3e	210	+ 1	4s	+24.0	+5.7	
67880	8 4.9	−15 57	5.5	B3	204	+10	3	+16.8	−0.2	
Nov. Pup	8 8.0	−35 0	.....	.....	221	0	6b	+20.4	+2.8	
87015	9 57.2	+22 26	5.6	B3	179	+53	5	+2.0	−2.4	
89688	10 15.9	+ 2 47	6.5	B3	210	+47	5s	+3.8	−3.3	
ρ Leo	10 27.5	+ 9 49	3.8	cB1	204	+54	5, 2, 3	−13.0, −3.5, +16.4	−18.0, −8.5, +11.4	
104337	11 55.7	−19 6	5.3	B4	256	+42	5b	−2.0	−5.6	c
1 Sco	15 45.0	−25 27	4.8	B4	314	+20	tr, 3	−33, −10.7	−25, −2.0	
λ Lib	15 47.5	−19 52	5.1	B4	319	+24	2, 3b	−26.4, (−18.7), −12.0	−16.2, (−8.5), −1.8	‡
142165	15 47.9	−24 14	5.4	B6	316	+21	3	−10.8	−1.7	
142184	15 48.0	−23 41	5.4	B4	316	+21	4b	−13.3	−4.1	
δ Sco	15 54.4	−22 20	2.5	B1	318	+21	4s	−13.6	−3.7	
β^1 Sco	15 59.6	−19 32	2.9	B1	321	+22	4s	−11.0	−0.2	
β^2 Sco	15 59.6	−19 32	5.1	B2	321	+22	4s	−10.7	+0.1	
ω^1 Sco	16 1.0	−20 24	4.1	B2	321	+21	4s	−9.5	+1.1	
ν Sco	16 6.2	−19 12	4.3	B3	323	+21	7s	−11.7	−0.6	
σ Sco	16 15.1	−25 21	3.1	B1	319	+16	6s	−8.5	+1.3	
147888	16 19.4	−23 14	6.6	B3	322	+16	3	−9.5	+1.0	*
ρ Oph br	16 19.6	−23 13	5.2	B3	322	+16	6s	−9.7	+0.8	†
ρ Oph ft	16 19.6	−23 13	5.9	B3	322	+16	6s	−9.8	+0.7	†
χ Oph	16 21.2	−18 14	4.8	B3e	326	+19	3, 5	−27.5, −11.1	−15.7, +0.7	†
ζ Oph	16 31.7	−10 22	2.7	B0	334	+22	1, 7s	−30.7, −16.3	−16.7, −2.3	†
149881	16 32.4	+14 40	6.6	B1	359	+35	15	−17.1	+1.0	c
154090	16 58.2	−33 59	4.9	cB1e	319	+ 3	8b	−3.8	+4.5	*
154445	17 0.4	− 0 45	5.6	B3	347	+21	8	−15.5	+1.0	†

TABLE 2—*Continued*

Name or HD No.	1900 R.A.	1900 Dec.	m	Spec.	l	b	K Int.	Radial Velocity (Km/Sec)	Residual Velocity (Km/Sec)	Notes
155806	17h 8m8	−33° 26′	5.5	O8	320°	+ 2°	2, 6	−43.7, −6.1	−35.1, +2.5	
U Oph	17 11.4	+ 1 19	6.0	B5	350	+20	8s	−16.2	+1.1	†
u Her	17 13.6	+33 12	4.8	B3	24	+32	4, 2	−27.2, −17.6	−7.6, +2.0	c
157857	17 20.7	−10 55	7.4	O7	341	+12.	10	−9.7	+5.2	*c
158148	17 22.5	+20 10	5.4	B5	10	+26	3	−20.1	−0.6	
159176	17 28.1	−32 31	5.7	O8	323	− 1	2, 7	−31.7, (−16.2), −5.1	−22.6, (−7.1), +4.0	*
μ Oph	17 32.4	− 8 3	4.6	B8	345	+11	8s	−16.5	−0.9	†
63 Oph	17 48.7	−24 52	6.1	B0	332	− 1	5, 8	−22.8, (−14.7), −8.1	−11.4, (−3.3), +3.3	†
163472	17 51.2	+ 0 42	5.7	B2	355	+11	15	−16.5	+0.9	†
163800	17 52.9	−22 30	6.9	B0	335	− 1	8	−4.6	+7.5	*c
66 Oph	17 55.3	+ 4 23	4.8	B5e	359	+12	1, 5, tr	−37, −17.4, +4	−19, +0.6, +22	
67 Oph	17 55.6	+ 2 56	3.9	cB3	357	+11	15, 1	−15.4, +2.5	+2.4, +20.3	
164402	17 55.8	−22 46	5.7	B0	335	− 2	1, 15	−53.3, −8.5	−41.3, +3.5	
164492	17 56.3	−23 1	6.9	O7	335	− 2	8s	−8.5	+2.9	*
164794	17 57.7	−24 22	5.9	O5	334	− 3	3, 8	−18.9, (−11.8), −7.4	−7.3, (−0.2), +4.2	†
165052	17 59.0	−24 24	6.8	O6	334	− 3	2, 10	−23, −6.7	−11, +4.9	*
165174	17 59.6	+ 1 55	6.1	B2	357	+10	20b, 1	−11.6, +12.6	+6.0, +30.2	†
165516	18 1.2	−21 27	6.2	B0	337	− 2	10, 3	−9.4, +7.7	+3.1, +20.2	*
102 Her	18 4.4	+20 48	4.3	B2	15	+17	7, 1	−25.7, −7.0	−6.0, +12.7	
μ Sgr	18 7.8	−21 5	4.0	cB8e	338	− 3	1, 15, 1, 2	−19, −8.2, +11.3, +27.1	−7, +4.4, +23.8, +39.6	†
16 Sgr	18 9.3	−20 25	6.0	B1	338	− 3	12, tr, 4	−10.5, +9.8, +26.1	+2.2, +23.5, +38.8	†
15 Sgr	18 9.3	−20 46	5.4	B0	338	− 3	12, 1, 4	−9.3, +8.4, +28.9	+3.3, +21.0, +41.5	†
167771	18 11.6	−18 30	6.4	O8	340	− 3	2, 8	−35.1, −9.4	−21.9, +3.8	*
167838	18 11.9	−15 28	6.6	B0	343	− 1	12b	−11.8	+2.2	*
167863	18 12.0	−18 51	6.6	B5	340	− 3	8s	−19.9	−6.8	*
167971	18 12.5	−12 17	7.3	O8	346	0	15b	−2.8	+12.0	*c
168021	18 12.7	−18 39	6.9	B0	340	− 3	3s, 7s	−35.1, −9.5	−21.9, +3.7	*
168797	18 16.5	+ 5 24	6.0	B5	2	+ 8	1, 10s	−35.7, −14.5	−17.6, +3.6	
169454	18 19.6	−14 2	6.8	B0e	345	− 2	15b, 3	−8.5, +81.3	+5.8, +95.6	*
170235	18 23.2	−25 19	6.2	B2e	336	− 8	12s	−9.5	+1.8	*

TABLE 2—*Continued*

Name or HD No.	1900 R.A.	1900 Dec.	m	Spec.	l	b	K Int.	Radial Velocity (Km/Sec)	Residual Velocity (Km/Sec)	Notes
170650	18^h25^m5	+23° 48′	5.7	B5	20°	+14°	8b	−16.5	+3.2	†
170740	18 25.9	−10 52	5.8	B3	349	− 2	6s	−12.9	+2.1	*
171012	18 27.3	−18 26	7.0	B0e	342	− 6	15s	−10.1	+3.0	c
171780	18 31.6	+34 22	5.9	B5	30	+17	5b	−17.4	+2.4	
4 Aql	18 39.8	+ 1 57	5.0	B9	2	+ 1	3	−19.5	−2.1	
174179	18 44.2	+31 39	5.8	B3	29	+13	10b	−16.6	+3.1	
8 Lyr	18 46.1	+32 42	5.8	B3	30	+14	6s	−17.6	+2.0	
β^1 Lyr	18 46.4	+33 15	3.8	Bp	31	+14	8s	−17.4	+2.2	c
174959	18 48.1	+36 25	6.0	B5	34	+15	6	−16.5	+3.1	c
δ^1 Lyr	18 50.2	+36 51	5.5	B3	34	+15	7s	−17.2	+2.3	
175754	18 51.7	−19 17	7.0	B0p	344	−11	2, 10, 2	−86.9, −8.2, +15.7	−77.0, +4.4, +28.3	*
175876	18 52.3	−20 33	6.7	O8	343	−12	12b	−7.4	+4.9	c
176162	18 53.8	−12 58	5.4	B7	350	− 9	15s	−11.6	+2.5	†
176818	18 57.0	+21 22	6.9	B3	21	+ 6	6s	−18.2	+3.0	*
176819	18 57.0	+20 42	6.6	B2	20	+ 6	6s	−17.4	+3.8	*
176871	18 57.2	+26 9	5.5	B3	25	+ 8	8s	−12.8	+6.6	
177109	18 58.2	+33 29	6.2	B3	32	+12	4s	−16.2	+3.2	
178175	19 2.4	−19 27	5.4	B3e	345	−14	20	−7.1	+5.3	c
ϵ Lyr	19 3.7	+35 57	5.1	B5	35	+12	5s	−14.4	+4.9	
20 Aql	19 7.3	− 8 7	5.4	B3	356	−10	2, 10	−24.2, −13.6	−9.2, +1.4	†
1 Vul	19 11.9	+21 13	4.6	B5	22	+ 3	5s	−16.2	+2.7	
2 Vul	19 13.5	+22 51	5.4	B0	24	+ 4	8s	−15.0	+4.0	
N. Aql 1945	19 13.7	+ 0 30	.....	.....	5	− 8	15b, 4b	−4.3, (+16.0), +35.4	+12.2, (+32.5), +51.9	*c
181409	19 15.3	+33 13	6.3	B3	33	+ 8	3	−13.3	+5.9	*
υ Sgr	19 16.0	−16 9	4.6	B8+F2	350	−15	10, 4	−11.6, +4.4	+1.3, +17.3	†
182180	19 18.3	−28 4	5.9	B3	338	−20	4	−7.8	+1.9	
2 Cyg	19 20.2	+29 26	4.9	B5	31	+ 6	6s	−14.6	+4.5	†
183143	19 23.0	+18 5	6.9	cB9e	21	− 1	20b, 1	−7.5, +41.6	+11.0, +60.1	*†c
183362	19 24.1	+37 44	6.4	B3e	38	+ 9	8b	−23.1	−4.3	
8 Cyg	19 28.1	+34 14	4.8	B5	36	+ 6	4	−15.0	+3.3	

TABLE 2—*Continued*

Name or HD No.	1900 R.A.	1900 Dec.	m	Spec.	l	b	K Int.	Radial Velocity (Km/Sec)	Residual Velocity (Km/Sec)	Notes
184279.....	19^{h}28^{m}6	+ 3°34′	6.8	B2e	9°	− 9°	10s	−11.2	+5.4	*
κ Aql.....	19 31.5	− 7 15	5.0	B0	0	−15	8, 4	−12.1, +8.2	+2.4, +22.7	
σ Aql.....	19 34.3	+ 5 10	5.2	B3	11	−10	7b	−13.3	+3.4	c
185859.....	19 36.1	+20 15	6.4	B0	24	− 2	12s	−11.0	+7.3	*
185936.....	19 36.5	+13 35	5.8	B5	19	− 6	5	−13.4	+4.2	
187459.....	19 45.0	+33 12	6.4	B0	36	+ 3	15s	−14.3	+4.1	*
187567.....	19 45.5	+ 7 39	6.4	B3e	15	−11	10s	−3.4	+13.2	*
187879.....	19 47.2	+40 20	5.6	B2	43	+ 6	3, 6, tr	−29.7, −16.2, −7	−11.5, +2.0, +11	
9 Sge.....	19 47.9	+18 25	6.3	O7	24	− .6	20b	−8.0	+9.8	c
188209.....	19 49.0	+46 47	5.5	O8	48	+ 9	10, 4	−23.4, −12.5	−5.6, +5.3	
188252.....	19 49.2	+47 41	5.7	B2	49	+10	20b	−14.3	+3.4	c
57 Aql br....	19 49.3	− 8 29	5.8	B5	0	−19	2	−13.9	−0.2	
57 Aql ft.....	19 49.3	− 8 29	6.5	B5	0	−19	2	−16	−2	*
188439.....	19 50.1	+47 34	6.2	B2	49	+10	15b	−15.3	+2.4	c
22 Cyg.....	19 52.3	+38 13	4.9	B7	41	+ 4	8s	−14.6	+3.5	†
189066.....	19 53.1	+35 59	6.0	B3	40	+ 3	6s	−15.9	+2.3	
189178.....	19 53.7	+40 6	5.4	B3	43	+ 5	7	−14.1	+3.9	
25 Cyg.....	19 56.2	+36 46	5.2	B3	41	+ 3	7	−18.2	−0.1	
190066.....	19 58.1	+21 52	6.6	cB0	28	− 6	20b	−7.2	+10.5	†c
190429 br....	19 59.8	+35 45	7.2	O5	40	+ 2	4, 12b	−79, −12.3	−60, +5.7	*
190429 ft....	19 59.8	+35 45	7.8	O	40	+ 2	4, 12b	−76, −10.7	−58, +7.3	*
190603.....	20 0.7	+31 56	5.7	cB0e	37	− 1	12, 10	−18.4, (−11.4), −2.7	−0.4, (+6.6), +15.3	†
190918.....	20 2.2	+35 31	7.0	O9	40	+ 1	20	−17.7	+0.2	*
+35°3955....	20 2.2	+35 31	7.3	B0	40	+ 1	20	−18.5	−0.6	*
190919.....	20 2.2	+35 24	7.3	cB1	40	+ 1	20	−15.3	+2.6	*
28 Cyg.....	20 5.7	+36 33	4.8	B3e	42	+ 1	3, 5	−23.2, (−18.6), −13.2	−5.4, (−0.8), +4.6	c
191877.....	20 7.0	+21 35	6.1	B0	29	− 8	20	−8.8	+8.5	†
192163.....	20 8.5	+38 3	7.4	O6	43	+ 2	2, 10s	−43.0, −13.9	−25.3, +3.9	*
192685.....	20 11.0	+25 17	4.8	B3	33	− 6	4s	−13.5	+3.9	
193007.....	20 12.9	+37 20	8.0	B	43	0	15s	−13.8	+3.7	*†

TABLE 2—*Continued*

Name or HD No.	1900 R.A.	1900 Dec.	m	Spec.	l	b	K Int.	Radial Velocity (Km/Sec)	Residual Velocity (Km/Sec)	Notes
P Cyg.....	20^h14^m1	+37°43′	4.9	B1eq	43°	0°	1, 12, 12, 2	−38, −18.6, (−13.9), −10.8, −1.2	−20, −1.1, (+3.6), +6.7, +16.3	†c
193322.....	20 14.6	+40 25	5.8	O8	46	+ 2	3, 2, 10, 10	−39.9, −23.4, −12.6, −2.5	−22.4, −5.9, +4.9, +15.0	†
193536.....	20 15.6	+46 0	6.3	B2	50	+ 5	2, 10	−20.5, −11.4	−3.3, +5.8	
193793.....	20 17.1	+43 32	6.8	O5	49	+ 3	1, 12	−36.6, −12.6	−19.4, +4.6	*†c
25 Vul.....	20 17.7	+24 7	5.4	B8e	33	− 8	5, 3	−13.8, (−8.4), −2.8	+3.3, (+8.7), +14.3	c
194279.....	20 19.7	+40 26	7.0	cB1	46	+ 1	4, 12	−54.8, −9.8	−37.6, +7.4	*†
194335.....	20 20.0	+37 10	5.7	B3e	44	− 1	5	−15.3	+2.0	
195089.....	20 24.1	+41 42	7.2	B3	48	+ 1	10s	−12.3	+4.7	*
ω Cyg.....	20 27.0	+48 37	4.9	B3	54	+ 5	2, 4	−21.4, (−14.1), −8.8	−4.7, (+2.6), +7.9	c
195592.....	20 27.2	+43 59	7.2	B0e	50	+ 2	2, 12, 2	−50.2, −13.3, +11.4	−33.6, +3.6, +28.3	*†
28 Vul.....	20 34.2	+23 46	5.0	B7	35	−11	3s	−14.4	+2.0	
196775.....	20 34.4	+15 29	5.9	B3	28	−16	8b	−11.8	+3.9	c
α Cyg.....	20 38.0	+44 55	1.3	cA2e	52	+ 1	2, 15	−25.7, −13.8	−9.2, +2.7	
51 Cyg.....	20 39.1	+49 59	5.4	B3	56	+ 4	5b	−12.5	+3.7	
λ Cyg.....	20 43.5	+36 7	4.5	B5e	46	− 5	6	−12.0	+4.4	
55 Cyg.....	20 45.5	+45 45	4.9	cB2e	53	+ 1	25, 2	−13.3, −5.8	+2.9, +10.4	†c
198846.....	20 48.1	+34 17	7.1	O9	45	− 7	2, 10s	−32.3, −7.6	−16.3, +8.6	*
57 Cyg.....	20 49.7	+44 0	4.7	B3	53	− 1	3	−17.1	−1.0	c
199140.....	20 50.1	+28 8	6.4	B1	41	−11	8s	−9.3	+6.6	*
199478.....	20 52.4	+47 2	5.8	cB8e	55	+ 1	10, 12, 2, 3	−19.5, (−14.5), −8.7, +24.9, +43.8	−3.6, (+1.4), +7.2, +40.8, +59.7	†
199579.....	20 53.1	+44 33	6.0	O6	53	− 1	15b	−13.2	+2.8	†c
59 Cyg.....	20 56.4	+47 8	4.9	B3e	56	0	3b	−17.3	−1.6	c
60 Cyg.....	20 57.6	+45 46	5.2	B3e	55	− 1	3b	−15.9	−0.2	
201819.....	21 7.0	+35 53	6.4	B1	49	− 9	3, 8	−19.6, −10.2	−4.1, +5.3	
σ Cyg.....	21 13.5	+38 59	4.3	cA0	52	− 8	5b	−12.9	+2.3	
υ Cyg.....	21 13.8	+34 29	4.4	B3e	49	−11	5	−16.3	−1.2	c
68 Cyg.....	21 14.8	+43 31	5.1	O8	55	− 4	25	−13.6	+1.5	
69 Cyg.....	21 21.7	+36 14	5.8	B0	51	−11	3, 10	−32.5, −15.4	−17.7, −0.6	
70 Cyg.....	21 23.2	+36 41	5.2	B3	52	−10	10b	−14.5	+0.2	c
204722.....	21 25.5	+43 54	7.5	B3e	57	− 6	8s	−12.5	+2.2	*

TABLE 2—*Continued*

Name or HD No.	1900 R.A.	1900 Dec.	m	Spec.	l	b	K Int.	Radial Velocity (Km/Sec)	Residual Velocity (Km/Sec)	Notes
ϵ Cap	21^{h}31^{m}5	−19°55′	4.7	B5ep	0°	−46°	4s, 1	−21.8, −6.1	−15.4, +0.3	
80 Cyg	21 38.6	+50 44	4.8	B3	63	− 2	10b, 3	−19.1, (−15.9), −12.2	−5.1, (−1.9), +1.8	c
81 Cyg	21 43.1	+48 51	4.3	B3	63	− 5	10s	−16.9	−2.9	
207563	21 44.8	+20 0	6.2	B3	44	−26	12	−11.4	+1.1	
16 Peg	21 48.5	+25 27	5.0	B3	48	−22	4	−4.3	+8.5	
o Aqr	21 58.1	− 2 38	4.7	B6e	26	−44	4s	−4.1	+4.2	
30 Peg	22 15.5	+ 5 17	5.4	B7	38	−42	1, 1, 8	−37.8, −19.2, −5.6	−29.3, −10.7, +2.9	
31 Peg	22 16.6	+11 42	4.9	B3e	44	−37	8	−7.6	+1.8	†
32 Peg	22 16.7	+27 50	4.9	B8	55	−24	5s	−8.5	+2.8	
2 Lac	22 16.9	+46 2	4.7	B5	66	− 9	5	−15.0	−2.6	
π Aqr	22 20.2	+ 0 52	4.6	B1e	35	−46	7, 2	−14.1, −3.9	−6.7, +3.5	
212978	22 23.1	+39 19	6.1	B3	63	−15	2, 10	−86.3, −12.7	−74.5, −0.9	†
6 Lac	22 26.1	+42 36	4.5	B3	65	−13	8	−13.8	−2.0	
8 Lac ft	22 31.4	+39 7	6.6	B2	64	−16	1, 6	−32, −16.1	−20, −4.8	*
8 Lac br	22 31.4	+39 7	5.8	B3e	64	−16	1, 8	−31.2, −13.9	−19.9, −2.6	
10 Lac	22 34.8	+38 32	4.9	O9	65	−17	2, 2, 8	−36.3, (−31.6), −27.3, −12.5	−25.2, (−20.5), −16.2, −1.4	
12 Lac	22 37.0	+39 43	5.2	B1	66	−17	1b, 10	−33.4, −11.6	−22.3, −0.5	c
215191	22 38.4	+37 17	6.2	B3	65	−19	8b	−12.8	−1.9	
14 Lac	22 45.8	+41 26	5.8	B3	68	−16	tr, 8, 1	−12.0, −1.4	−1.1, +9.5	
16 Lac	22 51.9	+41 4	5.5	B3	69	−17	1b, 8b	−38.1, −12.6	−27.7, −2.2	c
217101	22 53.1	+38 48	6.1	B2	68	−19	8	−11.0	−0.8	†c
217227	22 54.2	+43 18	7.0	B3	70	−15	7b	−9.5	+1.0	*
217543	22 56.3	+38 10	6.4	B3e	69	−20	5b	−9.1	+0.8	c
o And	22 57.3	+41 47	3.6	B5	70	−16	4s	−10.3	−0.2	
β Psc	22 58.8	+ 3 17	4.6	B5e	48	−50	2	−3.0	+2.1	
218674	23 4.8	+49 7	6.5	B3	74	−10	10	−8.2	+2.1	*
219188	23 8.9	+ 4 27	6.9	B2	52	−51	6s	−9.1	−4.5	*
64 Peg	23 17.0	+31 16	5.4	B8	70	−28	3, 1	−12.4, +0.9	−4.5, +8.8	
223229	23 42.6	+46 16	5.8	B3	80	−15	2b, 6s	−23.9, −6.9	−15.8, +1.2	
224559	23 53.8	+45 52	6.5	B3e	80	−15	5	−16.1	−8.6	*

NOTES TO TABLE 2

Letters and symbols have the following meanings:
s, sharp; b, broad; tr, trace; c, complex.
*, stars observed with 32-inch Schmidt camera.
†, stars with one or more additional molecular or atomic lines.
‡, stellar lines present which may affect radial velocities.
The letter "c" is attached to stars in which H and K are so broad as to indicate complexity, and also to some stars in which components are measured but not fully resolved. Occasionally, components and the unresolved blend are both measured, the value for the blend being given in parentheses.

Items below refer in general to the character of H and K. Radial velocities of suspected components noted here are not corrected for solar motion.

HD 1337	Structure most complex.
23 Tauri	Radial velocity derived from *CH* II 3957 and 4232. K too faint for measurement.
ζ Per	Many molecular lines; resembles ζ Oph.
X Per	Similar to ζ Per.
AE Aur	Probably complex.
δ Ori	Broad, probably double.
χ Aur	*CN* 3875 present.
θ^1 Ori	*He* I 3888, sharp and double.
Bond 619 Bond 640 θ^2 Ori	*He* I 3888, sharp and strong.
ι Ori	Possibly triple.
κ Ori	Quadruple?
3 Gem	Quadruple?
ξ Ori	Red component?
HD 54662	H and K double.
δ Sco	Possible violet component, −29 km/sec.
ω^1 Sco	Possible violet component, −29 km/sec.
ζ Oph	All recognized interstellar lines present except those of *Fe* I and *Ca* I 4227.
HD 164492	*He* I 3888 sharp and narrow, −7.1 km/sec.
4 Aql	Possible component, −35 km/sec.
β^1 Lyr	Faint red fringe.
HD 175754	Components 2 and 3 not fully resolved.
N. Aql 1945	Probably triple.
HD 183143	Strong component complex.
HD 183362	Complex?
HD 190429	Triple?
HD 193007	Radial velocity agrees with mean of two strong components of P Cygni.
P Cyg HD 193322	These two stars, about 4° apart, show interesting relationships in the interstellar clouds. HD 193322 has four well-separated components. P Cygni appears to have two strong, not fully resolved components, with fainter components on either side. The radial velocities seem to identify the clouds as common to both stars, but their intensities differ greatly. *CH* II 4232 is double in HD 193322, the radial velocities agreeing with those from two components of H and K.
HD 201819	First component seen as fringe on main line.
8 Lac br	Faint component probably double.

TABLE 3

STARS WITH ADDITIONAL INTERSTELLAR LINES, INTENSITIES OF PRINCIPAL LINES, OBSERVED RADIAL VELOCITIES, AND VELOCITIES FROM H AND K

NAME	MOLECULAR LINES				H AND K VELOCITY (KM/SEC)	NAME	MOLECULAR LINES				H AND K VELOCITY (KM/SEC)
	Intensity			Velocity (Km/Sec)			Intensity			Velocity (Km/Sec)	
	3957	4232	4300				3957	4232	4300		
o Cas	1	2	....	−9.4 (2)	− 6.5, +15.5	47129	tr	1	tr	+24.9 (2)	+ 7.9, (+14.2), +22.0
40 Per	....	tr	....	.....	+ 9.0						
o Per (a)	....	tr	1	+ 9.6 (1)	+10.1	ρ Oph br	....	1	3	−10.0 (2)	− 9.7
16 Tau (b)	2	3	....	+16.7 (3)	+17.5	ρ Oph ft	....	1	2	−9.4 (2)	−9.8
17 Tau	....	tr	....	.....	+18.2	χ Oph	1	2	3	−11.4 (3)	−27.5, −11.1
19 Tau	tr	2	....	+16.4 (1)	+14.0	ζ Oph (a, b)	2	4	3	−16.4 (10)	−30.7, −16.3
20 Tau (b)	2	4	....	+16.2 (3)	+15.0	154445	1	2	1	−16.0 (3)	−15.5
21 Tau	tr	2	....	+17.0 (1)	+16.0	U Oph	1	2	1	−16.8 (3)	−16.2
23 Tau	1	3	....	+16.9 (2)	.....	μ Oph	....	1	....	−17.1 (1)	−16.5
η Tau	....	tr	....	.....	+15.5	63 Oph	....	tr	....	.....	−22.8, (−14.7), −8.1
23753	....	1	....	+14.5 (1)	+14.3	163472	....	1	1	−16.2 (2)	−16.5
27 Tau	....	tr	....	.....	+14.5	164794	tr	1	....	−7.3 (2)	−18.9, (−11.8), −7.4
24131	....	tr	....	.....	+12.3	165174	....	tr	....	.....	−11.6, +12.6
ζ Per (a)	....	1	3	+11.9 (7)	+12.0	μ Sgr	....	1	....	−7.5 (1)	−19, −8.2, +11.3, +27.1
X Per (a)	....	tr	3	+11.6 (6)	+12.2						
ξ Per (b)	1	3	1	+ 7.1 (3)	+ 9.4, +25.4	16 Sgr	....	tr	....	−8 (1)	−10.5, +9.8, +26.1
μ Tau	....	tr	1	+22.9 (1)	+21.9	15 Sgr	....	tr	....	.....	−9.3, +8.4, +28.9
53 Per	1	2	1	+ 7.3 (3)	+ 6.1	170740	1	2	2	−10.4 (3)	−12.9
29309	....	tr	....	.....	+11.1	176162	....	1	....	−15.0 (1)	−11.6
AE Aur (a, b)	2	4	3	+14.0 (6)	+13.0	20 Aql (a)	....	....	1	−15.2 (3)	−24.2, −13.6
34656	....	tr	tr	.....	− 7.6, (+0.9), +8.4	υ Sgr	tr	2	1	−13.1 (1)	−11.6, +4.4
23 Ori	....	1	....	+22.1 (1)	+21.1	2 Cyg	....	....	1	−12.1 (1)	−14.6
35395	....	1	....	+14.6 (1)	+15.0	183143	....	1	tr	−5.2 (1)	−7.5, +41.6
χ Aur (c)	....	tr	1	*CH* I +9.6 (1) *CH* II +5.3 (1)	0.0, +10.6	22 Cyg	....	1	....	−12.3 (1)	−14.6
						190066 (c)	....	1	....	−6.4 (2)	−7.2
χ^2 Ori (b, c, d)	1	2	1	+15.6 (8)	+14.4, +29.6						

TABLE 3—*Continued*

Name	Molecular Lines				H and K Velocity (Km/Sec)	Name	Molecular Lines				H and K Velocity (Km/Sec)
	Intensity			Velocity (Km/Sec)			Intensity			Velocity (Km/Sec)	
	3957	4232	4300				3957	4232	4300		
190603 (b, c)	2	3	tr	−16.8 (3)	−18.4, (−11.4), −2.7	195592	....	tr	tr	.....	−50.2, −13.3, +11.4
191877 (c)	....	tr	....	−7.0 (2)	−8.8	55 Cyg (a, b, c, d)	1	3	1	−15.2 (11)	−13.3, −5.8
193007	....	1	tr	−14.0 (1)	−13.8	199478	1	3	1	−19.0 (3)	−19.5, (−14.5), −8.7, +24.9, +43.8
P Cyg (b)	2	4	tr	−14.4 (2)	−38, −18.6, (−13.9), −10.8, −1.2						
193322	2	2, 2	tr	−23.8, −11.7 (2)	−39.9, −23.4, −12.6, −2.5	199579	tr	2	1	−12.1 (2)	−13.2
193793	1	2	tr	−12.5 (2)	−36.6, −12.6	31 Peg	....	tr	....	.....	−7.6
194279	....	tr	....	.....	−54.8, −9.8	212978	1	2	1	−14.0 (2)	−86.3, −12.7
						217101	....	tr	....	.....	−11.0

NOTES TO TABLE 3

(a) One or more of the following lines present: *CN*, 3874.0, 3874.6, 3875.8; *CH* I, 3878.8, 3886.4, 3890.2.
(b) *CH* II 3745.3 present.
(c) *Ca* I 4226.7 present.
(d) *Fe* I 3719.9 and 3859.9 present.
Figures in parentheses in the column "Velocity for Molecular Lines" indicate the number of lines upon which the results depend.

In contrast, the stars in which λ 4227 is seen have very strong H and K lines, and only in such stars have the *Fe* I lines been detected. Except in the stars of the Pleiades, there is some slight indication that λ 4232 of *CH* II, if present, correlates in intensity with H and K, but the evidence is by no means adequate. It is of some interest to note that most of the comparatively few stars with strong neutral *CH* lines lie in the general areas of Perseus and Ophiuchus, while the more numerous stars with strong lines of ionized *CH* are mainly in Sagittarius and especially Cygnus.

Table 3 also indicates that double stars and often stars close together in position usually show the same interstellar lines. Examples are the stars observed in the Pleiades and pairs like ζ and X Persei, the double star ρ Ophiuchi, P Cygni, HD 193322, and some others. The intensities of the molecular lines in such pairs usually differ but slightly. This subject will be considered further when the complexity of the H and K lines and their radial velocities are discussed.

STRUCTURE OF THE H AND K LINES

Table 2 shows that in 87 of the stars the H and K lines have been measured as double, in 17 as triple, and in 4 as quadruple—a total of 108 stars in which components have been observed. In 40 additional stars H and K are sufficiently broad, or present structure enough, to indicate almost certain complexity. If these stars are included, essentially

TABLE 4

MEAN $m-M$ AND MEAN INTENSITY OF K

Limits of $m-M$	Mean $m-M$	Mean Intensity of K	Limits of $m-M$	Mean $m-M$	Mean Intensity of K
≲ 6.0 (23)	5.6	4.4	8.0– 8.9 (63)	8.4	8.9
6.1–6.9 (57)	6.5	5.6	9.0– 9.9 (44)	9.4	11.6
7.0–7.9 (72)	7.4	7.5	≳ 10.0 (38)	10.8	14.6

one star in two of those observed shows complex H and K lines. Several stars, of which HD 1337, κ Orionis, 3 Geminorum, and probably P Cygni are examples, have components which themselves appear complex. Hence the complete structure of the H and K lines in such stars may be even more complex than is indicated in Table 2.

Reference has already been made to the uncertainties of the arbitrary scale used in estimating the intensities of the K line and its components, especially when the lines are strong. As an approximate test of the consistency of the scale, the stars were divided into six groups according to their values of $m - M$, the absolute magnitude, M, being taken from R. E. Wilson's table relating M directly to spectral type.[4] The mean values of the estimated intensity of K or the sum of its components was then compared with the mean value of $m - M$ for each group. A total of 297 stars was used, the 3 stars omitted being 2 novae of uncertain apparent magnitude and v Sagittarii of peculiar spectrum. The results are given in Table 4.

For a comparison in which so many uncertainties are involved, the results are fairly consistent. The apparent increase in the rate of change of intensity for the faintest stars may well be due to some difference in the scale of estimates. Lower dispersion was used for many more of these stars than for those in the brighter groups.

A few of the conclusions which may be drawn from an inspection of the results for the H and K lines in Table 2 are as follows:

1. Stars with complex lines are most numerous in Orion, Sagittarius, and Cygnus; and, in general, the most complex lines are found in these areas. Complex lines are by no

[4] *Mt. W. Contr.*, No. 631; *Ap. J.*, 92, 170, 1940.

means limited to these regions, however, as is shown by such examples as HD 1337, ρ Leonis, and 10 Lacertae.

2. The intensities of interstellar H and K increase as the plane of the galaxy is approached. This is especially true in Sagittarius and Cygnus, where stars of very low galactic latitude show H and K lines roughly twice as strong as those of stars in higher latitudes.

3. Most of the stars in Orion have interstellar lines of moderate intensity but complex in many cases. The absence of molecular lines in these stars is striking.

4. All the double stars and frequently stars near one another in galactic position show the same structure in H and K and often the same intensities for the components. Table 5, given later in this discussion, lists a number of examples with the radial velocities from the lines and components.

5. The brighter stars of the Pleiades, with the single exception of 20 Tauri, are unique in showing stronger lines of molecular *CH* II relative to H and K than any other stars in the list. In 23 Tauri, for example, K is scarcely visible, while λ 4232 has an intensity of 3, and λ 3957, also of *CH* II, an intensity of 1. The exceptional star, 20 Tauri, has nearly equal intensities of 4 for K and λ 4232, K being very slightly the stronger.

RADIAL VELOCITIES FROM THE H AND K LINES

The average velocity from H and K, after elimination of the solar motion, is small, but considerable motion is occasionally indicated by one or more components. With very few exceptions, the small velocity corresponds to the strongest component of H and K, while the large velocity belongs to a fainter component. In the complete list, 21 components show radial velocities exceeding 30 km/sec, and 7 of these exceed 50 km/sec. The largest velocity observed is +96 km/sec for a well-marked component of HD 169454. The next largest is −77 km/sec for a component of HD 175754. The star HD 199478 has two well-resolved components, giving velocities of +41 km/sec and +60 km/sec, respectively.

In contrast to these fast-moving clouds, we find that the average radial velocity given by the K line or its strongest component for all the stars in the list is about 4.5 km/sec, regardless of sign. Even this low value would be reduced if the clouds in Orion and the Pleiades, which show a velocity systematically higher than average, were omitted.

The radial velocities in combination with the structure of the K line afford a means for the identification of the individual clouds in the direction of double stars and of close groups. Table 5 gives the results for the 8 double stars included in Table 2 and for a few other pairs or groups of stars fairly close together in the sky. Most of the fainter stars have been observed with lower dispersion, and the velocities are subject to larger errors.

The structure and intensity of the K line and its components in the double stars, together with their residual radial velocities, are given in the first part of Table 5 and the same for some representative groups and pairs in the latter part. The large group in Orion illustrates the difficulty of analysis of the complex lines in many of these stars.

The results for the double stars listed in Table 5 show close agreement in the intensities and structure of the H and K lines and in the radial velocities derived from them. As might be expected, more variation is found within the groups of more widely separated stars in the latter part of the table. Some of the differences in the large group in Orion may be due either to diversity in the clouds producing the lines or to differences in the analysis of the more complex lines. The 4 stars in Sagittarius form an interesting group with three, and probably four, interstellar clouds involved. The apparent relationship of the clouds in the direction of P Cygni and HD 193322 is discussed in a note to Table 2. An interesting feature is that, while the molecular lines are present in the spectra of both stars in about the same intensity, λ 4232 of *CH* II is distinctly double in HD 193322. The radial velocities of the two components agree with those from two components of H and K.

The radial velocities, derived from interstellar H and K in the spectra of ζ, X, and ξ Persei, are nearly equal. The first two stars, which are about 1° apart, show nearly identical interstellar spectra, containing all the molecular lines of *CH* I and *CN*, and λ 4232 of *CH* II only faintly. On the other hand, ξ Persei, about 4° distant, which has H and K lines of intensity comparable to those of the other two stars, shows very weak lines of *CH* I and *CN* but a prominent line at λ 4232. Such a reversal of intensities of stars relatively near together in position is exceptional.

As already stated, in the brighter stars of the Pleiades the ratio of the intensities of the *CH* II lines to those of H and K is remarkably high. The absolute intensities of the two sets of lines are not great, nor would they be expected to be for such comparatively nearby stars. The range in intensity, however, among the different stars is large. In η Tauri, K has an intensity of 1, while λ 4232 is barely visible; in 23 Tauri, K is a mere trace and λ 4232 has an intensity of 3; in 20 Tauri both lines have an intensity of 4. The average radial velocity from the interstellar lines corrected for the solar motion for the 9 stars

TABLE 5

RESIDUAL K-LINE RADIAL VELOCITIES FOR DOUBLE STARS AND OTHER GROUPS

NAME	K	*V* (KM/SEC)	NAME	K	*V* (KM/SEC)
δ Ori br.	4c	−2.0	β^1 Sco	4s	−0.2
δ Ori ft.	5c	−2.1	β^2 Sco	4s	+0.1
λ^1 Ori	4, 1, 7s	−9.6, −0.2, +8.1	ρ Oph br.	6s	+0.8
λ^2 Ori	4, 1, 6s	−8.3, −1.0, +6.1	ρ Oph ft.	6s	+0.7
HD 36959	1, 7s	−3, +9.7	57 Aql br.	2	−0.2
HD 36960	tr, 7c	−3, +9.5	57 Aql ft.	2	−2
ζ Ori br.	3, 5	−22.2, +3.6	8 Lac br.	1, 8	−19.9, −2.6
ζ Ori ft.	3, 4	−20.9, +4.5	8 Lac ft.	1, 6	−20, −4.8
Pairs or Groups of Stars					
29 Per	6s	+2.2	P Cyg	1, 12, 12, 2	−20, −1.1, +6.7, +16.3
31 Per	6s	+2.9	HD 193322	3, 2, 10, 10	−22.4, −5.9, +4.9, +15.0
HD 20809	7s	+0.6			
HD 21278	6s, 1	−1.5, +47.3			
34 Per	5s	−0.4	HD 37016	1, 3	−16, +7.2
			HD 37017	1, 4	−18, +8.5
ζ Per	10s	+4.8	42 Ori	1, 10s	−12.2, +9.9
X Per	12	+4.8	θ^1 Ori	2, 3, 4	−15.5, +0.5, +11.9
			Bond 619	4b	+2
29 CMa	15c	+7.3	Bond 640	4b	+2
30 CMa	10c	+6.9	HD 37040 br.	1, 3s	−18.4, +8.9
			θ^2 Ori	1, 6	−18.1, +4.9
HD 165516	10, 3	+3.1, +20.2	ι Ori	1, 5	−14.9, +9.8
μ Sgr	1, 15, 1, 2	−7, +4.4, +23.8, +39.6	HD 37061	4s	+9.3
			HD 37150	2	+9.2
16 Sgr	12, tr, 4	+2.2, +23.5, +38.8			
15 Sgr	12, 1, 4	+3.3, +21.0, +41.5			

observed is +6.9 km/sec. The average radial velocity of the stars themselves is −2.4 km/sec. Hence we must conclude that the clouds which produce the interstellar lines must be moving relatively to the stars with a radial velocity of more than 9 km/sec.

PLACE OF ORIGIN OF THE MOLECULAR INTERSTELLAR LINES

Reference to the Pleiades suggests the interesting question first raised by P. W. Merrill[5] whether there may not be a difference in the place of origin of the H and K lines and the D lines of sodium, on the one hand, and the molecular and perhaps some of the faint atomic lines, on the other. The relatively strong calcium and sodium lines would, on this hypothesis, be assumed to originate in what might be called the "true" interstellar clouds, usually far away from the stars by which they are observed, while the molecular lines would be produced in clouds relatively near the stars and thus subject to strong radiation. Differences in constitution from those found in the more distant clouds might also be assumed. The clouds near to the stars might be separate and discrete clouds independent of those which absorb H and K, or they might be portions of the H and K clouds which approach a star closely and are stimulated by its radiation to absorb the molecular lines.

The evidence afforded by the present observations seems on the whole to be somewhat against the view that the molecular lines originate in clouds distinct from those which produce H and K. The argument, which is based upon the radial velocities, would be stronger if the range in the peculiar motions of the clouds were larger and if the apparent motions were not, as appears to be the case, governed predominantly by galactic rotation. As it is, the quantities involved are small. With this consideration in mind, however, we may say that the assumption that the clouds producing H and K and those producing the molecular lines, in stars in which both sets of lines appear, always have equal radial velocities wherever the stars are observed seems hardly probable. The question, then, is primarily one of the accuracy of the differences in radial velocity between H and K and the molecular lines.

Two not wholly independent tests may be made, based upon the material available. As stated previously, the wave lengths of the molecular and faint atomic lines used in this investigation were derived on the assumption that they show the same displacements as H and K. The two most important lines are λ 4232 of *CH* II and λ 4300 of *CH* I. Their wave lengths, as determined from 11 and 10 stars, respectively, in various regions of the sky, were

$$4232.573A \pm 0.002\ ;\ 4300.338A \pm 0.002\ .$$

The smallness of the probable error, amounting to 0.15 km/sec in radial velocity, shows that the differences in velocity between the clouds producing H and K and those producing the molecular lines, if they are separate, must be relatively small. These wave lengths were then applied to all other stars in which the molecular lines could be measured satisfactorily, with the following results:

	Molecular − H and K
λ 4232	+0.21 km/sec ±0.30
λ 4300	+0.20 km/sec ±0.40

The probable errors for these stars naturally are larger than for the stars selected for determinations of wave length, since the molecular lines are fainter and less well measurable. The differences in velocity still remain small, however.

An inspection of Table 3 shows 43 stars in which the radial velocity determined from the molecular lines may be compared directly with that from H and K or from one of

[5] *Ap. J.*, **95**, 268, 1942; *Pub. A.S.P.*, **58**, 354, 1946.

their strongest components. The average deviation, regardless of sign, is slightly less than 1.2 km/sec, a satisfactory value, since the molecular velocity in numerous stars depends upon a single faint line. The average difference for all the stars, taken with regard to sign, is

$$\text{Molecular velocity} - \text{H and K velocity} = +0.24 \text{ km/sec}.$$

The accuracy of these results seems to be sufficient to indicate fairly strongly that the molecular lines and H and K originate in clouds having the same motions and hence probably in the same clouds. This conclusion is strengthened by the observational evidence that numerous clouds have very appreciable peculiar motions apart from those due to galactic rotation. It would appear hardly reasonable to assume that, if the clouds producing the molecular lines are distinct from those producing H and K and are widely distributed in galactic longitude, a few of them at least would not share in these peculiar motions to an extent sufficient to distinguish them from the H and K clouds. Such differences of motion not only should result in larger differences than have been found between the molecular and the H and K results for the individual stars of Table 3 but should also influence the probable errors of the adopted wave lengths for the molecular lines.

The hypothesis that both molecular lines and H and K originate in the same clouds but that the molecular lines are absorbed in the portions nearest the stars avoids the difficulty of assuming separate clouds in the two cases. It would, however, place the clouds which absorb both sets of lines relatively near the stars and in some cases, in which differences of motion between the stars and the clouds are observed, would require considering the presence of the molecular lines as a somewhat temporary feature, dependent upon the motion of the clouds relative to that of the stars whose radiation is involved. In time, changes in the interstellar spectrum might be expected which would be more rapid than if larger-scale phenomena were assumed. Such changes may, of course, be possible.

An observational fact bearing upon the question is that the molecular lines, when present, almost invariably correspond to one of the components of a complex H and K line. This component is, with very few exceptions, the strongest one. Table 3 contains 20 stars with complex interstellar H and K lines in which molecular lines have been measured. In 18 of these the molecular lines agree with the strongest component of H and K; in P Cygni they correspond in position with the mean of the two strongest but not fully resolved components of H and K; and in the neighboring star, HD 193322, in which λ 4232 is measured as double, one component agrees with a strong component of the calcium lines, but the other with one which is relatively faint. The interstellar lines of χ Aurigae are of special interest. The H and K lines are strong, well-resolved doublets of nearly equal intensity. Of the molecular lines, those of *CH* I agree in position with the red component of each pair, but the less well-defined lines of *CH* II appear to correspond more closely with the mean of the two components. These and similar comparisons which might be made show how close is the relationship between the calcium lines and those of molecular origin, as regards both position and, in most cases, relative intensities as well.

One of the chief arguments for concluding that the molecular lines have a somewhat different place of origin than the H and K lines is that, on the basis of existing observations, they do not seem to show the increase in intensity with distance of the stars by which they are observed, which is a well-marked characteristic of the calcium lines. The present material is not well suited for a discussion of this question. The stars observed are for the most part bright, the range in distance is not very great, and the comparatively few more distant stars have been observed on a smaller scale, making the detection of the faint molecular lines more difficult and uncertain. This effect is seen in Table 2, where molecular lines are found in about one star in four of those observed with the higher dispersion, but in only about one star in eight of those observed on the smaller scale, and then as very faint lines. With the exception of the stars in the Pleiades, no star

in Table 2 shows molecular lines comparable in intensity with K, and in only two or three stars, such as ζ Persei, AE Aurigae, and ζ Ophiuchi, do they approach the strength of H. Many stars with strong interstellar H and K lines do not show the molecular lines at all. Since the absorption of the molecular lines in interstellar clouds seems to be much less frequent and abundant than that of H and K, it appears quite possible that observations must be carried to considerably fainter stars and greater distances in order to detect any correlation between intensity and distance. This is due to the slower rate of building-up of intensity for the molecular lines. Unfortunately, the practical necessity of using lower dispersion adds to the difficulties of such an investigation.

If the radiation of the stars is peculiarly effective in producing the absorption of the molecular lines in the portions of the gaseous clouds which approach the stars most closely, it might be expected that the absorption of these lines would vary with the temperatures and spectral types of the stars concerned. The observations indicate that the strongest molecular lines are usually found when the stars are of type O–B1, but this is by no means always the case. In the Pleiades, for example, the spectral types range from B5 to B9, and the strongest molecular lines are found in 20 Tauri of type B9. HD 199478, classified as cB8, has well-marked λ 4232 of *CH* II, and the same is true of υ Sagittari of composite type B8p and F2p. Numerous stars of types B3–B5 also show λ 4232 distinctly. In general, there seems to be no marked relationship between spectral type and intensity of the molecular lines.

The Pleiades form a group of stars which perhaps supports most strongly the view of some kind of difference in origin of the calcium and the molecular lines. The cluster has much nebulosity connected with it, and the intensity of the *CH* II lines relative to H and K is abnormally high. The absolute intensities of both sets of lines differ so greatly from star to star that it is necessary to assume a highly spotted distribution of relatively small gaseous clouds and marked differences in their composition or similar differences in the absorption induced by the radiation of the different stars. The comparatively low intensity of the H and K lines in all the stars, except possibly 20 Tauri, is to be expected because of the nearness of the cluster. In contrast to the Pleiades, no star has been found in the great nebulous areas of Orion which shows the molecular lines with certainty.

In summarizing these results, it seems reasonable to conclude that the closeness of the agreement of the radial velocities from the molecular lines with those from H and K in all observed regions of the sky favors the conclusion that the same interstellar clouds are involved in their production. Moreover, the fact that, with almost no exception, the molecular lines agree in position with the strongest component, or the mean of two strong components, of the H and K lines supports the view that the two sets of lines originate not only in the same clouds but also in the same general portions of these clouds. Other considerations are the presence of the same molecular lines with nearly the same intensities in wide double stars and numerous pairs of physically unrelated stars, as well as the lack of evidence that the occurrence of the lines is related to the spectral types of the stars which appear to lie nearest to them. From this point of view interstellar clouds would differ greatly in size and depth and probably, as well, in the distribution and relative abundance of the various atoms and molecules. The assumption of such differences can hardly be avoided on any hypothesis of the formation of interstellar lines because of the wide differences in relative intensity observed between star and star.

On the other hand, it is clear that the present material is inadequate to answer the important question whether the molecular lines increase in average intensity with the distance of the stars observed, although some evidence is afforded why such an increase might be expected to be more gradual than for the calcium lines. Of particular importance, however, is the behavior of the molecular lines in the stars of the Pleiades cluster. Here the character of the group, the intermingled nebulosity, and especially the very considerable range in intensity of the molecular lines observed in the different stars are all strongly suggestive of influences of the radiation of the stars themselves.

GALACTIC ROTATION

The stars listed in Table 2 are, for the most part, bright and too near to show large effects of galactic rotation in the intervening interstellar clouds. The complexity of the H and K lines in the spectra of nearly half the stars also reduces considerably the quality of the material for any calculation of the rotational velocity. A preliminary plot of the radial velocities, however, showed results of sufficient interest to warrant some slight analysis.

As a first step, the absolute magnitudes of the stars and the corresponding distances were determined from the spectral types by the aid of the table of mean absolute magnitude for each type given by R. E. Wilson.[4] The stars were then divided into three groups with distances less than 600 parsecs, 600–1000 parsecs, and greater than 1000 parsecs. The first group contained 171 stars, the second 43 stars, and the third 30 stars—a total of 244 stars. Of the 56 stars omitted, 25 have galactic latitudes greater than 25°, and the remaining 31 show uncertainties in the analysis of the complex H and K lines which were noted at the time of measurement, or other characteristics which tend to make the results unreliable. In general, the attempt was made to utilize all material of reasonable quality. One exceptional case is that of η Orionis, which shows double interstellar H and K lines of unequal intensity. The stronger component gives a very discordant velocity when compared with that of other stars in the same general region, but the fainter component gives an accordant value. Such behavior is most exceptional, and the star has been omitted. Almost invariably the strongest component of a complex interstellar line is that which yields the galactic rotation.

The first group of 171 stars with distances less than 600 parsecs was divided into sixteen subgroups arranged according to galactic longitude, and the mean residual radial velocity of each subgroup was plotted against its mean longitude. The two other groups of 43 and 30 stars, with distances of 600–1000 parsecs, and greater than 1000 parsecs, respectively, were treated similarly, except that only nine subgroups could be formed in each case. The small number of subgroups, their distribution in galactic longitude, and the very limited number of stars in several of the subgroups make the results for these two groups of more distant stars of relatively low weight. The probable error of the mean radial velocity for a subgroup of 10 stars averages about ± 0.6 km/sec, which does not appear excessive in view of the intrinsic motions of the interstellar clouds, especially in the Pleiades and Orion, and the uncertainties and dispersion in distance. The values for the three groups and their subgroups are listed in Table 6, and the corresponding curves are shown in Figure 1.

All the curves show positive maxima at about 10° and 170°–180°, and a minimum at about 90°, in fairly good agreement with theory. The difference in group 1 in the height of the maximum near 170° from that at 10° is almost certainly due to the inclusion of numerous stars in the Pleiades and Orion of galactic longitudes 130°–180°. The clouds in these regions have very appreciable peculiar motions of positive sign. The more distant stars of groups 2 and 3 in this general direction appear, as might be expected, to show less of this effect, but the curves from these relatively few stars are none too well defined. The curves all show a fair approximation to double sine-curves.

A peculiar feature of the results is the lack of symmetry of the curves with reference to the axis of zero velocity. This is due to an excess of positive over negative velocities, and the curves require a displacement downward of approximately 2 km/sec to produce symmetry. A large amount of available evidence indicates that the quantity involved, amounting to 0.026 A in wave length, cannot be ascribed to the adopted wave lengths of H and K[6] or to any systematic error in the spectrograph. Its explanation may lie in the character of the distribution of the stars observed or possibly in the value of the solar

[6] The use of laboratory wave lengths would increase the asymmetry.

motion applied as a correction to the directly observed radial velocities. A reduction from 20 to 18 km/sec would go far toward producing symmetry about the zero axis of velocities for the positive maximum at 10° of galactic longitude; it would affect the negative maximum at 90° but slightly but would raise the positive maximum at about 170° by nearly the full amount of 2 km/sec, thus making this portion of the curve still less symmetrical to the axis. Since this is the portion of Figure 1 determined largely by the motions of the interstellar clouds in the direction of the Pleiades and Orion, with their considerable peculiar motions of positive sign, an increase of this amount does not seem altogether unreasonable.

TABLE 6

MEAN GALACTIC LONGITUDES AND RESIDUAL RADIAL VELOCITIES

No. Stars	l	V (Km/Sec)	No. Stars	l	V (Km/Sec)
	Group 1—Mean Distance 320 Parsecs				
7	91°	−1.6	14	324°	− 0.6
7	115	+0.2	14	348	+ 2.1
11	126	+2.8	13	17	+ 5.1
12	134	+5.4	12	33	+ 3.3
8	154	+5.6	11	44	+ 2.4
9	164	+5.5	7	54	+ 1.4
18	174	+6.5	12	66	− 1.5
12	200	+3.7	4	77	− 1.6
	Group 2—Mean Distance 770 Parsecs				
1	86	−3.9	2	342	+ 3.0
7	145	+4.2	6	17	+ 5.7
8	181	+7.1	4	41	+ 4.5
2	320	+3.2	7	57	+ 1.2
6	336	+3.5			
	Group 3—Mean Distance 1290 Parsecs*				
1	109	−5.6	6	343	+ 5.6
2	150	+2.0	2	24	+10.8
3	177	+5.1	9	44	+ 4.3
4	319	+4.5	2	52	+ 3.2
5	336	+5.1			

* Two stars of abnormally great distance omitted in the mean.

For the determination of galactic rotation the amplitudes of the curves are, of course, the essential feature. Accordingly, the values for the three groups of stars listed in Table 6 have been reduced by a least-squares solution. The equations of condition have been set up in the form given by R. E. Wilson[4] which uses rA and K as the quantities to be determined, r being the mean distance in kiloparsecs of the stars in each subgroup, A the rotational radial velocity at 1 kiloparsec, and K a quantity introduced to equalize the areas on the two sides of the zero axis. A uniform correction of −2.0 km/sec has been applied to the radial velocities of Table 6 in order to reduce the value of K; this, of

course, does not affect the result for A, which is the quantity sought. Weights were accordingly assigned to the number of stars in each subgroup. The results of the solutions are given in Table 7.

The probable errors of rA and K in group 1 are large in view of the number of stars included. This is due mainly to the effect of two or three subgroups which contain clouds with considerable peculiar motions. The fourth subgroup, which consists chiefly of stars

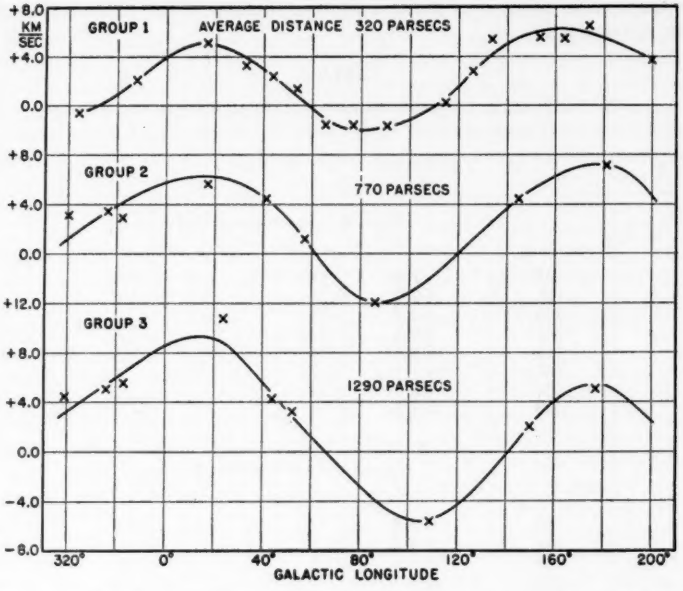

FIG. 1.—Mean residual radial velocities of stars grouped according to distance and galactic longitude

TABLE 7

VALUES OF rA AND K FROM STARS AT DIFFERENT DISTANCES

Group	No. Stars	No. Subgroups	Mean Distance (Kpc)	rA (Km/Sec)	K (Km/Sec)
1.....	171	16	0.320	2.69±0.63	0.23±0.40
2.....	43	9	0.770	4.12± .65	.51± .39
3.....	30	9	1.290	6.56±0.83	0.01±0.43

in Orion, accounts by itself for more than one-quarter of the probable error for the entire group of 171 stars.

It is difficult to evaluate the effect of general absorption and scattering in reducing the brightness of the stars observed, and hence making their photometric distances greater than they actually are, because of uncertainties in the value of the coefficient of absorption. The first group of stars is probably too near to be affected more than very slightly by general absorption. If we assume with Wilson a coefficient of 0.65 mag/kpc and apply

it to the other two groups, we obtain for the three groups, reduced to a distance of 1 kiloparsec, the following values of *A:* 8.41 km/sec; 6.81 km/sec; 6.84 km/sec. Multiplying by a factor of 2, on the usual assumption that the mean place of origin of the interstellar absorption lies halfway from the observer to the star, we have for the final values of *A:* group 1, 16.8 km/sec; group 2, 13.6 km/sec; group 3, 13.7 km/sec.

The results for the last two groups are of very low weight because of the small number of stars and unsatisfactory distribution in galactic longitude. The result for group 1 differs by less than 1 km/sec from Wilson's final value based upon a wide variety of objects; and even this slight difference would be eliminated by the use of a slight correction for general absorption affecting the brightness and hence the distances of the stars in this group.

This discussion of galactic rotation, which is mainly a by-product of the study of the structure of the interstellar H and K lines, makes no particular contribution to the numerical accuracy of the rotational constant. It may have some interest, however, as dealing with the rotational effect in near-by interstellar clouds and in indicating the influence of peculiar motions of clouds in certain parts of the sky. In the case of complex lines it also aids in the selection of the component to be used for a study of the rotation.

AN UPPER LIMIT TO THE ELECTRON DENSITY NEAR THE EARTH'S ORBIT

FRED L. WHIPPLE AND JOSEPH L. GOSSNER
Harvard College Observatory
Received February 14, 1949

ABSTRACT

Brightness and polarization observations of the zodiacal light are used to determine the upper limit of the interplanetary electron density at one astronomical unit. The value depends on the assumed distribution law of the electrons, a $1/R$ law giving 800/cm³; $1/R^2$, 900/cm³; $1/R^3$, 1000/cm.³. It is further shown that the observed polarization can probably be accounted for by reflection of sunlight by dust particles. Hence the upper limits for the electron density are probably much greater than the actual value. Certain consequences of these results are discussed briefly.

The brightness and polarization of the zodiacal light provide an upper limit to the possible density of electrons near the earth's orbit if one assumes (*a*) that the zodiacal light is scattered sunlight, (*b*) that the polarized component arises entirely from electron scattering, (*c*) a reasonable range of electron density distributions, in which the electron density decreases outwardly from the sun near the ecliptic, and (*d*) that other possible scattering processes cannot produce polarization of the opposite sense to that produced by electron scattering.

The observational data are reviewed below and the well-known laws of electron scattering are applied to the problem. In addition it is shown that scattering from small particles may account for a considerable fraction, if not all, of the polarization observed in the zodiacal light. Hence the calculated upper limits for the electron density may well be much greater than actuality.

A knowledge of the electron density in interplanetary space is of importance in setting limits to the density of ionized particles and in studying the possible resistance of interplanetary material on small particles moving about the sun.

I. BRIGHTNESS OF THE ZODIACAL LIGHT

If we accept the hypothesis that the Fraunhofer component of the corona is caused by zodiacal light, we might use data on its brightness within a degree or two from the sun obtained during eclipse observations.[1] Polarization measures, however, are not available for the purpose.

In the range of solar elongations from 2° to 30° we have no information on the surface brightness of the zodiacal light. During a solar eclipse, however, Smiley has observed and photographed the zodiacal light, but no one has made photometric measures. Van de Hulst suggests that infrared observations with photocells be made on this region during total eclipse. These observations might be made from aircraft to escape atmospheric scattering.[2]

Japanese amateurs during the 1930's made extensive observations of the brightness of the zodiacal light, comparing its brightness to that of several Milky Way fields.[3] These observations, by a large number of observers, contain numerous personal errors. Elvey has analyzed the available observations and has found a seasonal variation in the brightness.[4] The maximum light for the evening observations occurred near the middle of

[1] S. Baumbach, *A.N.*, **263**, 121, 1937.

[2] *Ap. J.*, **105**, 471, 1947.

[3] Reported in various issues of the *Bull. Kwasan Obs.*, 1928–1936.

[4] *Ap. J.*, **86**, 84, 1937.

January, while the morning observations gave a peak at the end of October. The Japanese observations contain some estimates of shape and color as well. Elvey has further attempted to show a correspondence of the seasonal variation with positions of cometary orbits. These observations are more or less in agreement with the position of the greater Taurid stream of meteors and might possibly be observations of this phenomenon.

Earlier photometric work was carried out by Fessenkopf[5] both at Nice and at Meudon. The observations cover elongations of 34°–58° and from 0° to 20° in a direction perpendicular to the axis. The measures are given in terms of the brightness of the night sky taken as 10.0. Variations of the brightness of the night sky affect these observations.

Accurate observations have been made photoelectrically by Elvey and Roach.[6] On several nights they made isophotal maps of the intensity along the ecliptic as part of their study of the general brightness of the Milky Way. Their contour maps show a seasonal variation of about 20 per cent around the average brightness, but in the range from 40° to 180° the mean curve is well defined. The brightness at various elongations from the sun on the ecliptic is given in Table 1 in terms of the number of tenth-magnitude stars per square degree.

A second set of extensive observations is due to Hoffmeister.[7] The range is from 30° to 180°. The values he found are similarly listed in Table 1.

TABLE 1

OBSERVED BRIGHTNESS OF THE ZODIACAL LIGHT

Elongation	Elvey and Roach	Hoff-meister	Mean	Mag/Sq Sec	Elongation	Elvey and Roach	Hoff-meister	Mean	Mag/Sq Sec
40°	912	912	912	20.38	70°	332	228	280	21.65
50°	618	565	592	20.84	80°	261	155	208	21.98
60°	436	319	378	21.32	90°	213	109	166	22.28

As there is undoubtedly a variation in the intensity of the zodiacal light, we may best use the mean of the values by Elvey and Roach and by Hoffmeister. This mean is given in the fourth column of Table 1 and in the last column, after being transformed to magnitudes per square second of arc.

II. SPECTRUM AND COLOR OF THE ZODIACAL LIGHT

Numerous attempts have been made to observe the spectrum of the zodiacal light. The low intensity of the surface necessitates long exposures, even with low dispersion. Care must further be taken during the exposure to avoid the effects of moonlight and twilight. The first observations of the spectrum were made by Liais, Vogel, Piazzi-Smith, and Wright.[8] These observers found only the night-sky lines and a continuous background. In 1908, Fath[9] succeeded in obtaining an integrated exposure of 12^h31^m in the course of many nights. His spectrum showed the H and K lines and possibly the G band. He concluded that the spectrum was probably identical with that of the sun.

Color observations tend to confirm Fath's conclusion. The zodiacal light is now gen-

[5] *C.R.*, **157**, 1913. [6] *Ap. J.*, **85**, 231, 1937.

[7] *Veröff. U. Sternw. Berlin-Babelsberg*, Vol. **8**, No. **2**, 1930; Vol. **10**, No. 1, 1932.

[8] Visual observations are given in *Observatory*, **13**, 77, 1890; *C.R.*, **74**, 262, 1872; *A.N.*, **79**, 327, 1872; and *Amer. J. Sci.*, Ser. 3, **8**, 39, 1874. Photographic observations are reported in *Proc. R. Soc. Edinburgh*, **17**, 142, 1883.

[9] *Lick Obs. Bull*, **5**, 141, 1909.

erally attributed to the presence of meteoric particles concentrated in the plane of the ecliptic. If the particles had diameters of the order of a wave length, Rayleigh scattering should make the light bluer than the sun's light. Should the particles be large compared to the wave length of light, then the reflected light should be largely independent of color.

Elvey[10] made color observations at Yerkes Observatory, but his results suggested a variation in color. Later, Elvey and Rudnick repeated the observations at the higher altitude of the McDonald Observatory, calibrating the measures by means of bright stars. The color was found to be +0.28 mag. on Becker's scale, corresponding to a star of spectral type G1, with no evidence of Rayleigh scattering. From this observation Elvey and Rudnick concluded that the number of small particles was negligible, those of meteoric dimension, much greater than a wave length of light, being the principal cause of the zodiacal light.

III. POLARIZATION OF THE ZODIACAL LIGHT

Another method of studying the nature of the interplanetary particles involves the amount of light polarized by reflection from their surfaces. Thus observations of the polarization of the zodiacal light might tell of the nature and constitution of the particles responsible. Observationally this field has been the most neglected because of the difficulties involved.

TABLE 2

POLARIZATION OF THE ZODIACAL LIGHT (DUFAY)

Elongation	Per Cent	Elongation	Per Cent	Elongation	Per Cent
30°	12.5	60°	15.0	80°	6
40°	12.5	70°	13.0	85°	4
50°	13.0	75°	10	90°	2.5

Several attempts were made to measure the polarization, the earliest being that of Wright.[11] His work was done in 1874 with a Savart polariscope, which unfortunately absorbs a good deal of the light. The results showed a definite polarization of as much as 15 per cent and certainly not more than 20 per cent. By comparison with the percentage of light polarized from various surfaces, he attributed the cause of the polarization to particles that were meteoric in nature. For some sixty years afterward, few attempts were made. Several English observers did make some investigations and detected polarization, but they could give no numerical data concerning their observations.[12]

The only quantitative determination is that of Dufay.[13] From photographic observations he found the polarization to vary with elongation from the sun. Table 2 gives the percentages at elongations from 30° to 90° along the ecliptic. Dufay saw in these observations an indication that the zodiacal light was merely diffused sunlight.

Japanese observers attempted to get further polarization measures with cameras of quartz-sphere lenses. Dr. Take-uchi confirms the value of 15 per cent found by Dufay at 60° elongation.[14] The I.A.U. commission on zodiacal light in 1938 recommended strongly that further attempts be made to obtain such observations. The new Schmidt-type meteor cameras might prove useful in this respect because of their speed. A check of Dufay's values at large elongations particularly is needed.

[10] *Ap. J.*, **86**, 342, 1937.

[11] *Amer. J. Sci.*, **107**, 451, 1874.

[12] *M.N.*, **31**, 171, 1871.

[13] *C.R.*, **181**, 399, 1925.

[14] *Trans. I.A.U.*, **6**, 173, 1938.

IV. RECENT WORK ON THE INTERPLANETARY MEDIUM

Van de Hulst has investigated the relation between the zodiacal light and the corona.[15] From known observations of brightness he attempted to find the sizes and distribution of particles outward from the sun. Near the sun he points out the importance of diffraction as well as of reflection effects. The particles are found to have a distribution function of radii of $n(a) = 3.5 \times 10^{-20}\, a^{-2.6}$. Particles larger than radius 0.035 cm would be less abundant than smaller ones. The comparison to the zodiacal light at 90° elongation shows either that the albedo is less than 1 per cent or that the particles are concentrated closer to the sun. As the particles probably have albedos of about 10 per cent, we might accept the latter conclusion as fitting the case. Van de Hulst finds, furthermore, that the space density of the interplanetary medium is about 5×10^{-21} gm/cm^3, so that within the earth's orbit the total mass amounts to 5×10^{18} gm, or 10^{-9} that of the earth, too small to produce measurable gravitational effects. In an independent investigation Allen[16] comes to somewhat similar conclusions. He finds that the observations are satisfied by a 1/R law with particles of 10^{-3} cm radius. Further studies along the lines set by van de Hulst and Allen are now under way at Harvard to determine the possible ranges of such solutions.

V. UPPER LIMIT TO THE ELECTRON DENSITY

We shall now apply the observational data to find the following: (1) the upper limit of the density of electrons at the distance of the earth on the basis of the observed brightness and polarization of the zodiacal light, and (2) the amount of polarized light which may be produced in the zodiacal light by reflection from solid particles rather than from electrons.

In order to obtain the upper limit to the number of electrons in the vicinity of the earth, we assume that all the polarized zodiacal light is caused by the scattering of sunlight by electrons. From a knowledge of the brightness of the zodiacal light as well as the percentage polarized, we may determine the number of electrons at each value of elongation. There appears to be good evidence, however, that reflection from particles accounts for most of the polarization.

Compton and Allison,[17] following J. J. Thomson, derive the expression for the light, dI, scattered through an angle θ by a single electron of charge e and mass m in an unpolarized beam of intensity I_0/R^2 as

$$dI = \frac{I_0}{R^2}\frac{e^2}{mc^2}\tfrac{1}{2}(1+\cos^2\theta)\,. \tag{1}$$

The scattering cross-section, $d\alpha$, is thus

$$d\alpha = \frac{e^2}{mc^2}(\tfrac{1}{2})(1+\cos^2\theta)\,d\omega\,, \tag{2}$$

or

$$d\alpha = \frac{3}{16\pi}\,\sigma_e(1+\cos^2\theta)\,d\omega\,, \tag{3}$$

as

$$\sigma_e = \frac{8\pi}{3}\left(\frac{e^2}{mc^2}\right)^2,$$

[15] *Ap. J.*, **105**, 471, 1947.

[16] *M.N.*, Vol. **106**, No. 2, 1946.

[17] *X-Rays in Theory and Experiment* (New York: D. Van Nostrand, 1946).

where $d\omega$ is the solid angle of observation and R is the distance from the sun. Equation (3) is the scattering function for the case under study. We also consider the scattering to be done in a volume of space subtending a solid angle $\Delta\Omega$ at the earth and of length $d\Delta$ at distance Δ (see Fig. 1). Further, let us write

$$n = \text{Number of electrons per cubic centimeter,}$$

$$U\,c = \text{Flux from the sun} = \frac{U_0 c}{R^2},$$

and

N = Total number of scattering electrons in a volume of space $\Delta\Omega d\Delta$ (see Fig. 1).

Then

$$N = n\Delta\Omega\Delta^2 d\Delta\,. \tag{4}$$

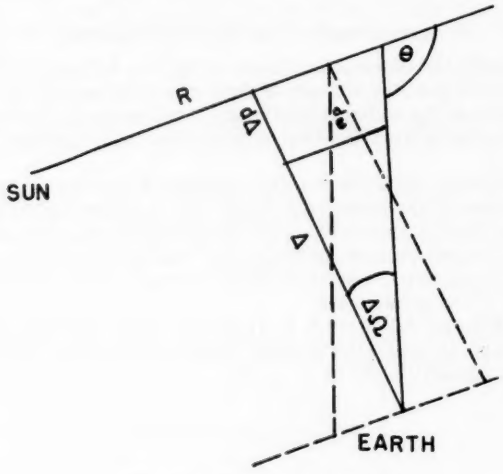

FIG. 1.—Geometry of the ecliptic

The light scattered from this volume in the direction θ into the solid angle $d\omega$, then, is

$$\frac{U_0 c N\,d\alpha}{R^2} = \frac{n\Delta^2}{R^2}\,\Delta\Omega d\Delta\,\frac{3}{16\pi}\,\sigma_e(1+\cos^2\theta)\,U_0 c\,d\omega\,, \tag{5}$$

where R is the distance from the sun. The flux at the earth, f_e, then becomes

$$f_e = \frac{\text{Light scattered}}{\text{Area of } d\omega} = \frac{\text{Light scattered}}{\Delta^2 d\omega}, \tag{6}$$

or

$$f_e = \frac{3}{16\pi}\,U_0 c n\Delta\Omega\left(\frac{1+\cos^2\theta}{R^2}\right)\sigma_e d\Delta\,. \tag{7}$$

The total flux at the earth, F_e, from all volumes is obtained by integrating over all values of Δ, so that

$$F_e = \frac{3}{16\pi} U_0 c \sigma_e \Delta\Omega \int_0^\infty n \frac{1+\cos^2\theta}{R^2} d\Delta . \tag{8}$$

The distribution of electrons about the sun is not known, so that, to allow for several reasonable solutions, we assume the law of distribution of electrons to be $n = n_e/R^p$, where n_e is the number of electrons at 1 a.u. We may thus satisfy any inverse-power law that appears applicable.

Putting R and Δ in terms of astronomical units, we have

$$F_e = \frac{3}{16\pi} \frac{U_0 c}{1 \text{ a.u.}} \sigma_e \Delta\Omega n_e \int_0^\infty \frac{1+\cos^2\theta}{R^{p+2}} d\Delta . \tag{9}$$

Equation (9) represents the total flux at the earth of the light scattered by the electrons. Now, in solving the above equation, we wish to express flux in terms of magnitudes

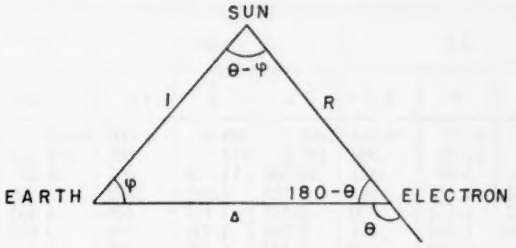

FIG. 2.—Definition of angles

per square second of arc, so that $\Delta\Omega = 1.86 \times 10^{-12}$. Also, $\sigma_e = 6.57 \times 10^{-25}$ (c.g.s.). Define L by the equation

$$L = \int_0^\infty \frac{1+\cos^2\theta}{2R^{p+2}} d\Delta . \tag{10}$$

Hence

$$\frac{\text{Scattered light}}{\text{Sunlight}} = 2.18 \times 10^{-24} n_e L . \tag{11}$$

In terms of magnitudes, if the magnitude of the sun is -26.72, the light scattered by electrons, L_e, becomes:

$$L_e(\text{mag.}) = +32.41 - 2.514 \log_{10}(n_e L) . \tag{12}$$

The integral, L (eq. [10]), cannot be solved in its present form. To solve, we write the integral in terms of θ. The relation between Δ and θ can be seen from Figure 2. Thus

$$\frac{d\Delta}{d\theta} = \frac{\sin\phi}{\sin^2\theta} \tag{13}$$

and

$$R = \frac{\sin\phi}{\sin\theta} . \tag{14}$$

The integral (eq. [10]) then becomes

$$L = \frac{1}{2 \sin^{p+1}\phi} \int_{\phi}^{\pi} (1 + \cos^2 \theta) \sin^p \theta \, d\theta \,. \tag{15}$$

The integral for the polarized light, P, scattered by the electrons, then becomes

$$P = \frac{1}{2 \sin^{p+1}\phi} \int_{\phi}^{\pi} \sin^{p+2} \theta \, d\theta \,, \tag{16}$$

since

$$\frac{\text{Polarized light}}{\text{Total light}} = \frac{\sin^2 \theta}{1 + \cos^2 \theta} \,. \tag{17}$$

These expressions can be solved for all angles of ϕ; the results for equation (15), luminosity, and equation (16), polarized component, as well as the ratio P/L are presented in

TABLE 3

ELECTRON SCATTERING AND POLARIZATION

ϕ	1/R			1/R²			1/R³		
	L	P	P/L	L	P	P/L	L	P	P/L
5°	175.0	87.7	0.501	1482.	889.5	0.600	13860.	9240.	0.667
10	43.72	22.10	.506	187.2	112.5	.601	879.6	586.5	.667
20	10.90	5.68	.522	24.209	14.714	.608	58.23	38.98	.669
30	4.832	2.632	.545	7.519	4.685	.623	12.549	8.509	.678
40	2.722	1.553	.570	3.359	2.168	.646	4.432	3.083	.696
50	1.760	1.040	.591	1.839	1.232	.670	2.063	1.483	.719
60	1.250	0.750	.600	1.153	0.792	.687	1.150	0.850	.739
70	0.956	0.564	.589	0.801	0.549	.685	0.732	0.545	.745
80	0.778	0.432	.556	0.605	0.398	.657	0.518	0.374	.723
90	0.667	0.333	.500	0.491	0.295	.600	0.400	0.267	.667
100	0.597	0.255	.427	0.423	0.219	.518	0.333	0.193	.580
120	0.528	0.139	.263	0.358	0.115	.321	0.272	0.098	.361
140	0.505	0.061	.121	0.338	0.050	.146	0.254	0.042	.164
160	0.500	0.015	.030	0.334	0.012	.037	0.251	0.010	.041
180	0.500	0.000	0.000	0.333	0.000	0.000	0.250	0.000	0.000

Table 3 for several values of the solar elongation ϕ. Figure 3 portrays graphically the calculated data of Table 3.

From the ratios P/L we can obtain the relative amount of polarization from electrons for any of the three laws. We also know the observed brightness of the zodiacal light and the observed polarization according to Dufay. We can thus determine what percentage of the zodiacal light is caused by electron scattering. For example, at 60° elongation the P/L for the 1/R law is 0.600; Dufay finds that the observed polarization is 0.15. Hence

$$0.60 L_e \leq 0.15 \text{ zodiacal light} \,, \tag{18}$$

so that the electron scattering is

$$L_e \leq 0.25 \text{ zodiacal light} \,. \tag{19}$$

Knowing the value L_e in terms of magnitudes, we can readily solve equation (12) for n_e. The values given in Table 4 represent upper limits. The values at 90° elongation are the lowest found and are therefore taken as the upper limit for the number of electrons at 1 a.u.

VI. POLARIZATION BY SMALL PARTICLES

The upper limits to the electron density seem rather high. Inasmuch as it is generally accepted that reflection from solid particles is the major cause of the zodiacal light, let us investigate how well we can account for the observed polarization by means of polarization by reflection from interplanetary dust.

The best data on the polarization by reflection for various minerals and substances is found in Lyot's thesis.[18] From this we have chosen data for a number of particles of low albedo ($\sim$0.1) and have carried out a numerical integration for elongations of 60° and 90° in order to determine what percentage of the zodiacal light would be polarized by reflection if the interplanetary medium were composed of these substances.

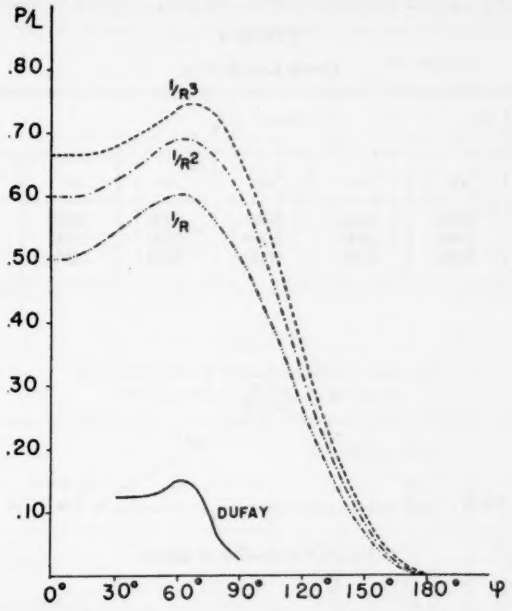

FIG. 3.—Polarization of electron-scattered light for three electron distributions at various elongations from the sun.

For elongations greater than 60° van de Hulst finds diffraction to be negligible, all the light coming from reflection. In these regions he gives as the phase function that of Lambert for spheres

$$I(\theta') = \frac{2\gamma}{3\pi^2}(\sin\theta' - \theta'\cos\theta'), \tag{20}$$

where γ = Albedo and θ' = Supplement of the scattering angle, θ. The angles are defined in Figure 4.

A column (σ, $d\Delta$) of n particles (of radius a) per cubic centimeter receives a flux of solar radiation,

$$\frac{U_0 c}{R^2}\,\sigma\, d\Delta\, \frac{n}{R^p}\,\pi a^2, \tag{21}$$

[18] Thesis, Paris: Orléans, 1929.

of which $I(\theta')\Delta^{-2}$ is scattered to 1 cm² at the surface of the earth. The surface brightness, H_{col}, of the column as seen from the earth is

$$H_{col} = \frac{U_0 c}{R^{p+2}} n\pi a^2 I(\theta')\, d\Delta . \tag{22}$$

By integrating over the length of the column, we get the surface brightness at an elongation ϕ. This is done by changing the integral to one in θ' as above, since (from eq. [13])

$$R = \frac{\sin\phi}{\sin\theta'} \quad \text{and} \quad d\Delta = \frac{\sin\phi}{\sin^2\theta'}\, d\theta' , \tag{23}$$

TABLE 4

UPPER LIMIT TO n_0

DISTRIBUTION LAW	ϕ					
	40°	50°	60°	70°	80°	90°
$1/R$.....	5400	5600	6000	4800	2040	830
$1/R^2$.....	3600	4600	5000	4500	2200	930
$1/R^3$.....	2500	3600	5000	4500	2400	1030

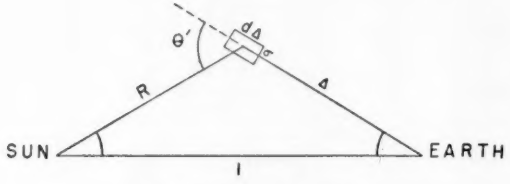

FIG. 4.—Definition of angles

we have

$$H_{col} = U_0 c n\pi a^2 I(\theta') \frac{\sin^p\theta'}{\sin^{p+1}\phi}\, d\theta' . \tag{24}$$

If $n = n(a)da$ and $I(\theta')$ is of the form of equation (20), then

$$H(\phi) = \frac{2\gamma}{3\pi} \frac{U_0 c}{\sin^{p+1}\phi} \int_{a_1}^{a_2} a^2 da \int_{\phi}^{\pi} n(a) \sin^p(\theta') (\sin\theta' - \theta'\cos\theta') . \tag{25}$$

For $\phi = 90°$ we have numerically integrated equation (25) for pulverized volcanic lava (silicate), pyrite, lead sulphide, and granite. In each case the polarization comes out much greater than that observed. It thus seems evident that a good part of the polarization may be caused by reflection from particles other than electrons. Further, at the large angles involved there are no processes giving opposite polarization to electrons. The values are given in Table 5, along with other data concerning the particles.

For $\phi = 60°$, where the polarization is a maximum, the problem has also been solved; the values found by numerical integration are given in Table 6. From both sets of results it appears that particle scattering could well account for most of the polarization.

VII. BRIGHTNESS OF THE $H\alpha$ LINE

We can further consider the results of an extrapolation of the maximal values of electron densities to the vicinity of the sun. Van de Hulst[2] has corrected Baumbach's earlier observational values, which are interesting for comparison. Though an agreement

TABLE 5

PERCENTAGE OF POLARIZATION AT $\phi = 90°$ (OBSERVED VALUE 2.5 PER CENT)

SUBSTANCE	ALBEDO	DISTRIBUTION			
		Uniform	1/R	$1/R^2$	$1/R^3$
B, grayish crystalline lava	0.15	5.3	7.9	9.7	10.5
B' pulverized	.17	2.5	3.9	4.8	5.4
Pyrite	.15	4.6	8.1	9.9	11.5
Lead sulphide	.11	4.6	8.1	9.9	11.5
Basalt	.08	4.6	7.2	8.4	9.5
Gray granite	0.14	2.2	3.5	4.2	4.6

TABLE 6

PERCENTAGE OF POLARIZATION AT $\phi = 60°$
(OBSERVED VALUE 15 PER CENT)

SUBSTANCE	DISTRIBUTION LAW			
	Uniform	1/R	$1/R^2$	$1/R^3$
Lava *B*	6.8	10.2	12	12.6
Lava *B'*	3	4.6	5.5	5.9
Pyrite	6.5	9.6	13.2	14.9
Lead sulphide	6.5	9.6	13.2	14.9
Basalt	5.8	9.0	10.5	11.5
Granite	2.8	4.7	5.5	6.2

of values by such an extrapolation may be mere coincidence, it is useful as a guide in selecting the most appropriate law of electron distribution.

As a whole the $1/R^2$ law provides the best agreement. The 1/R law seems to be ruled out. We must point out that the source of electrons near the sun may differ completely from that near the earth; the apparent agreement there is possibly no more than coincidence.

Finally, we must look to see whether the calculated electron densities would lead to detectable bright lines of H, if the density of H^+ corresponds to that of the electrons. The energy per cubic centimeter per second arising from transitions in the hydrogen atom is given by Menzel.[19] We have $n_e = 10^3$ per cubic centimeter and further assume that the electron temperature, T_e, is $10^4°$ K in the vicinity of the earth.

[19] *Ap. J.*, **85**, 330, 1937.

To get the value of b_n, we take the region around the sun as transparent to Lyman line radiation with the Gaunt factor equal to unity (Case A_1).[20] The value of E_{32} ($H\alpha$) is then 1.05×10^{-19} ergs/cm^3/sec. We may now compare this radiation with the brightness of the night sky. The energy density crossing a sphere of radius 1 a.u. is then 2.8×10^{-18} ergs/cm^{-2}/sec^{-1}/$\square''^{-1}$ compared with the energy density of sunlight at the earth, 1.38×10^6 ergs/cm^{-2}/sec^{-1}. At best, then, the $H\alpha$ radiation would be some 10 mag. fainter than the night sky, making its observation improbable if not impossible, even though the $H\alpha$ radiation is concentrated in a line of the spectrum.

TABLE 7

EXTRAPOLATED ELECTRON DENSITIES

	$R=1\odot$	$R=2\odot$	$R=3\odot$
Baumbach	4.3×10^8	2×10^6	0.2×10^6
1/R	1.7×10^8	8.6×10^4	5.7×10^4
$1/R^2$	4.1×10^7	1×10^7	2.1×10^6
$1/R^3$	9.8×10^9	1.2×10^9	3.6×10^8

In conclusion we suggest that, if corpuscular streams from the sun are responsible for the aurora polaris, a high concentration of free electrons in these streams might scatter sufficient solar radiation to be detectable. Variations in the brightness and polarization of the zodiacal light at low or moderate latitudes might correlate with solar, auroral, or magnetic activity. Lack of such correlations would set an upper limit to the density of free electrons in large streams or else limit the dimensions of streams with high electron density (see, e.g., Chapman and Ferraro).[21]

[20] Menzel, *Ap. J.*, **88**, 52, 1938.

[21] *Terr. Mag. and Atm. Elec.*, **36**, 77 and 171, 1931; **37**, 147 and 421, 1932; **38**, 79, 1933.

A STUDY OF M-TYPE STARS IN CYGNUS

J. J. NASSAU AND G. B. VAN ALBADA
Warner and Swasey Observatory, Case Institute of Technology
Received December 31, 1948

ABSTRACT

The present investigation is based on objective-prism spectra taken with the 2° and 4° prisms attached to the 24-inch Schmidt-type telescope, with I-N emulsion and Wratten No. 89 filter.

The classification of the M stars was established solely on the *TiO* bands, while the carbon stars were identified from the bands of *CN*. A new band near λ 7950 is utilized in the identification of S stars. A band in the same spectral region has been observed in several late M stars—notably variables. The limiting magnitude for which we believe our data to be complete is 13.5 infrared, although a number of stars are classified down to 14.5.

The search for M stars was carried out in a relatively clear region in Cygnus at galactic longitude 41°.2 and latitude 3°.7. The area is in the form of a rectangle perpendicular to the celestial equator and covers 2.28 square degrees. In this area 709 M stars were identified, 4 carbon stars, and 2 S stars; of the total we found several new variables. The number of M stars per square degree is 311, while at galactic latitude of 9°.2 and approximately at the same longitude the corresponding number is 31.

Infrared magnitudes were established by assuming that the infrared intrinsic color for an A5 star is equal to zero. The median apparent infrared magnitude of the M0 stars at galactic latitude 3°.7 is 13.1, which value decreases with advancing spectral type to 11.3 at M4. This is in agreement with the absolute infrared magnitudes derived from the Mount Wilson spectroscopic absolute magnitudes, which give −1.2 for M0 and −3.0 for M4. For the late M types this relation does not seem to exist, since the observed median magnitudes remain stationary after M4.

From our material it was possible to obtain the spectrum-intrinsic color relation for all the M stars; they are given in Table 2. An estimate of the interstellar absorption of the region was found to give 0.10 mag. per kiloparsec (infrared). The unevenness in the surface distribution of M stars indicates local regions of much heavier obscuration.

A density analysis has been made from 627 stars (M0–M4). At a distance of 2 kpc from the sun the number of stars is 16×10^{-6} per cubic parsec and at a distance of 6 kpc, 8×10^{-6}. For 107 stars from M2.5 to M4 the corresponding values are 4×10^{-6} and 0.7×10^{-6}, respectively. In comparison, at a distance of 8 kpc the density was found to be 0.1×10^{-6} or less.

I. INTRODUCTION

This investigation deals with the study of M-type stars in an apparently clear region in Cygnus. In a sense it constitutes the first report of a general survey of M-type stars in our galaxy. The survey will cover several fields approximately equally spaced in galactic longitude and fields at different latitudes at longitudes of 41°–47°.

The volume of the material already collected is such that we felt a part of it should be published as soon as possible and thus made available to other investigators. This part is concerned with the classification of M stars, the determination of their photographic magnitudes and their infrared magnitudes in one field, as well as with a general discussion of this observational material. The latter includes the determination of provisional intrinsic infrared magnitudes of M-type stars and the amount of interstellar absorption in this region. Our results reveal more than 700 M-type stars in an area of 2.28 square degrees, a few carbon and S stars, and a number of new variables. Among these stars is a number of unusually high color.

II. OBSERVATIONAL MATERIAL

The program was carried out mostly with the infrared sensitive Kodak I-N plates; a Wratten No. 89 filter was used in connection with these plates. For spectral classification nearly all plates were hypersensitized by bathing them for 1 minute in a 4 per cent solution of 28 per cent ammonia at a temperature no higher than 5° C. Recently, however,

hypersensitization before exposure by means of a 2-minute bath in cold water has been tried and found to be satisfactory.

The spectra were obtained with the 4° and the 2° objective prisms, attached to the Burrell telescope. Those obtained with the 4° prism extend about 0.6 mm to either side of the atmospheric A-band. The dispersion for this prism at the A-band is 1700 A/mm. The dispersion for the 2° prism is double this value. The wave-length range is from λ 6800 to about λ 8800.

In the beginning of our survey with the 4° prism the spectra were widened by taking plates near the meridian and permitting differential refraction to widen the spectra. A half-hour exposure produced spectra varying from 0.08 to 0.20 mm in width, depending on the declination of the field. Later, and particularly when the 2° prism was employed with an exposure of 1 hour, plates were guided. The somewhat narrower spectra thus obtained did not diminish the accuracy of classification. Our present practice for reaching the intermediate and faint stars is to guide for all plates and to take a half-hour exposure with the 4° prism and a 1-hour exposure with the 2° prism. To secure spectra in case of overlaps, plates are taken with the prisms turned 90°, i.e., with the dispersion in the direction of right ascension.

III. LIMITING MAGNITUDES

With the 4° prism we were able to observe stars of spectral class M0 to about 13.2 infrared mag. and, with the 2° prism, more than 1 mag. fainter. The limiting photographic magnitude of our plates is about 18.0, and for some of the stars no blue direct image could be obtained. Bright sky is not the only factor which limits our exposures to 1 hour; an appreciable part of the plate fog is due to overlapping spectra of very faint stars. Plates in the Cygnus region having stars as faint as 14.5 infrared mag. show as many as 400 spectra per square centimeter. The influence of the faint stars is also apparent from the great reduction of background fog in obscured regions.

The spectra of the brighter stars were secured mostly from nonsensitized plates. In this case the spectra were sometimes widened.

IV. CRITERIA FOR CLASSIFICATION OF SPECTRA

Owing to low dispersion, our classification criteria are based on the absorption bands only. Indeed, no definite evidence of a single absorption line has been found. On rare occasions, however, some emission lines have been observed.

a) Telluric bands.—Of the telluric bands, the A-band of oxygen is by far the strongest and most easily observed in nearly all spectra, provided that they are not overexposed. In plates obtained with the 2° prism it is not so prominent and is sometimes difficult to see. In early-type spectra this band usually appears as a sharp line of considerable depth, although occasionally it appears somewhat diffused.

The oxygen B-band at λ 6800 usually defines the short-wave-length end of the spectrum, and it is visible only in heavily exposed spectra, since the transparency of the filter in this region is decreasing rapidly. The infrared side of this band merges with a weak band of water vapor, producing a weakening effect on the continuum up to wave length λ 7100. This effect is particularly apparent in late-type stars. The H_2O band at about λ 7190 causes considerable difficulty; on many of the plates this band is rather strong, and care must be taken to avoid confusion with the TiO band appearing at λ 7054.

In general, it is necessary to examine each plate for the intensity of the H_2O absorption, which is readily determined by observing early-type stars. Serious errors may be made in the classification of early M-type stars if the strength of the H_2O bands is not taken into account properly. Other telluric bands present in the region covered are omitted from the discussion, as they do not appear to interfere with our classification.

b) Classification of M-type stars.—The main group of stars which are readily classifi-

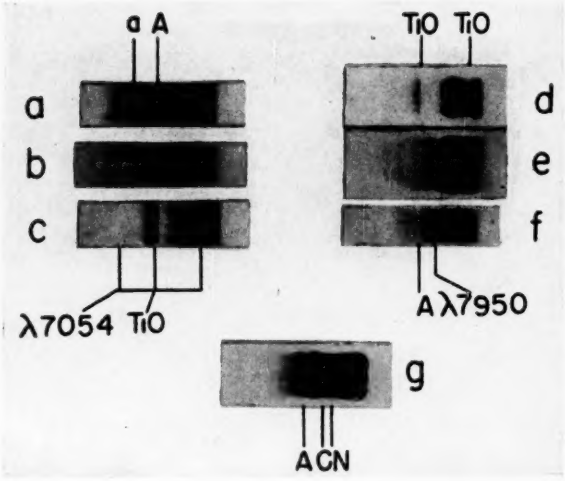

FIG. 1.—Principal features in infrared spectrum of M stars. *a*, ϕ Ser (K4); *b*, 8 UMa (M2); *c*, α Her A (M5); *d*, BD+49°2999 (M7); *e*, U Her, April 8, 1947 (S2e) shows *LaO* band; *g*, Y CVn, April 8, 1947 (N3 or $C5_4$).

able from our infrared spectra are the M-type stars, as the wave-length region from λ 6800 to λ 8800 shows several strong *TiO* bands. These bands are wide enough to be detected even in the narrowest spectra. The subclassification of these stars is carried out on the basis of the strength of the *TiO* bands. The main features (Fig. 1) are as follows:

(1) *The group with head at λ 7054.*—The main band of this group corresponds to the transition from the vibrational ground state of the molecule and appears at class M0.

(2) *The group at λ 7589.*—The first appearance of this group occurs at M2 as a slight widening of the A-band and becomes increasingly apparent with later classes. The first band of this group arises from the second vibrational level and is probably masked by the A-band in spectra earlier than M2.

(3) *The group at λ 8432.*—The wave length given here does not correspond to the first head of this band arrangement but rather to its strongest feature. The group becomes apparent at M5 or slightly earlier. In late spectral types the width and strength of all three features are greatly enhanced. In some very late M stars, notably variables, a band has been observed near λ 7900, the origin of which is unknown. The principal features of the M spectra are shown in Figure 1.

These features enable us to classify stars to an accuracy of half a spectral division. This degree of precision was also obtained when stars were classified from two plates of different exposure times.

Figure 2 shows the internal consistency of our criteria and the accuracy attainable for the resulting classification. Sixty field stars in one plate were observed independently by both of us. The open circles indicate that the classification was considered doubtful by one or both observers on account of overlap or faintness of the spectrum. A small number of stars which either of us classed as being earlier than M0 are not included in the figure. The probable error of one estimate in our classification was found to be 0.3 of a spectral division.

To avoid errors in the classification of early M stars, great care was exercised not to confuse the first appearance of *TiO* with the atmospheric a-band. In the band group of *TiO* two band heads nearly coincide at λ 7126,[1] and it is here rather than at λ 7054 that the group is first observed. The distance between λ 7126 and the a-band is less than 0.05 mm in our 4° prism spectra and only half this distance in the 2° prism spectra. The task of classifying early M stars becomes still more difficult for faint and space-reddened stars when the spectral region under consideration approaches the limit of visibility and the graininess of the plate becomes important. In general, we have been able to overcome this difficulty by classifying from the two plates simultaneously, with an observer at each plate, although we are not certain in every individual case. In stars of type M1 the chances of error are greatly reduced, and at M2 they completely disappear.

No luminosity effects have been observed in our spectra. Hence the M-type stars identified in different regions form a mixture of all luminosities. However, it follows from Kuiper's[2] survey of the stars in the neighborhood of the sun that the number of dwarfs present per square degree to the limiting magnitude of our survey must be negligible. This conclusion is also confirmed by the exceedingly high galactic concentration of M stars. In the Cygnus region, more than 300 M stars per square degree have been observed, while at the galactic pole less than one M star per square degree appears. We are also unable to distinguish supergiants from giants.

c) Carbon stars.—The presence of *CN* bands of considerable strength (Fig. 1, *g*) in the infrared region provides a means for classifying carbon stars. No detailed study of their spectra has been made.

d) S-type stars.—Stars of this class which lack strong *TiO* bands show an absorption band near λ 7950[3,4] (Fig. 1, *f*), which is visible in our spectra.

[1] Christy, *Ap. J.*, **70**, 1, 1929.

[2] *Ap. J.*, **95**, 201, 1941.

[3] Nassau and van Albada, *Ap. J.*, **107**, 418, 1948.

[4] Keenan, *Ap. J.*, **107**, 420, 1948.

e) Emission objects.—Wolf-Rayet stars and certain O stars show some of their infrared emission lines on our plates.

f) Stars with peculiar spectra.—Sometimes we have observed spectra showing features which do not fit into the pattern of classification described above. These spectra do not form a homogeneous group. On the contrary, they show a great variety among themselves. No systematic effort has been made to classify or describe their features.

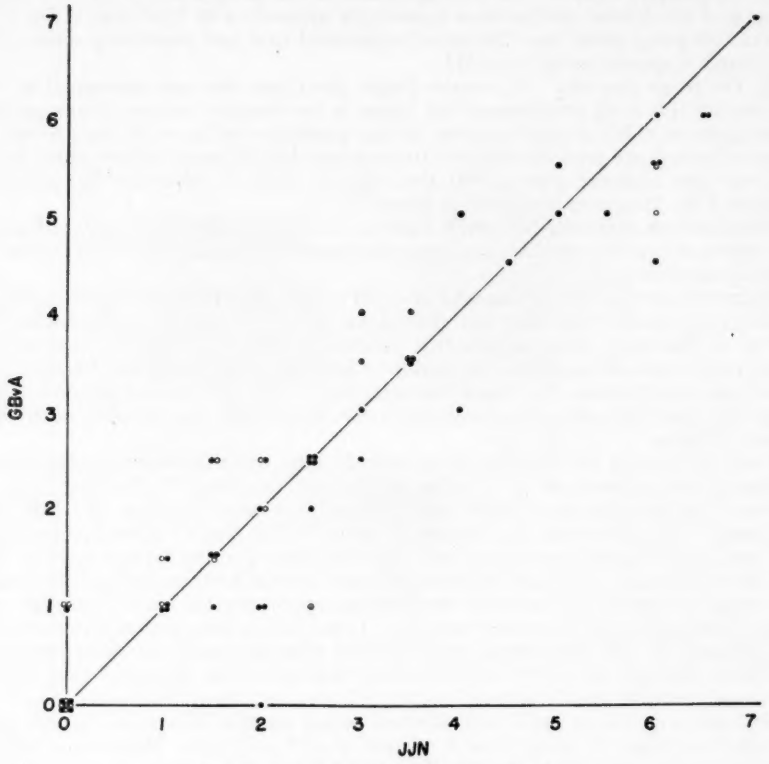

FIG. 2.—Internal consistency of classification

V. COMPARISON WITH THE MOUNT WILSON SYSTEM

In the establishment of criteria of classification of the M-type stars we have made use of the Mount Wilson system[5] and have drawn from the material in the infrared portion of the spectrum published by Christy,[1] Merrill,[6] Keenan and Hynek,[7] and Dobronravin.[8]

At the beginning of our classification we used stars from the Mount Wilson list for the establishment of a memory scale of spectral class based upon the evolution of the strength of the *TiO* bands. This scale is described in the previous section.

[5] Adams, Joy, and Humason, *Ap. J.*, **64**, 225, 1926.

[6] *Ap. J.*, **79**, 183, 1934; also *Spectra of Long-Period Variable Stars* (Chicago: University of Chicago Press, 1940).

[7] *Ap. J.*, **101**, 265, 1945.

[8] *Poulkova Obs. Circ.* No. **24**, p. 3, 1938.

A comparison of our system with that of Mount Wilson was made finally from 72 M stars. Usually we took three exposures for each infrared spectrum, in order to avoid systematic errors due to exposure time. Figure 3 shows the comparison between the two systems. It appears that our classification is systematically later by about half a division between M0 and M2 and earlier by nearly one division for stars between M3 and M7. The figure also shows an apparent discontinuity between the two systems at about M2.5, which, however, is not apparent in our spectrum-color relation, to be described in Section XIII.

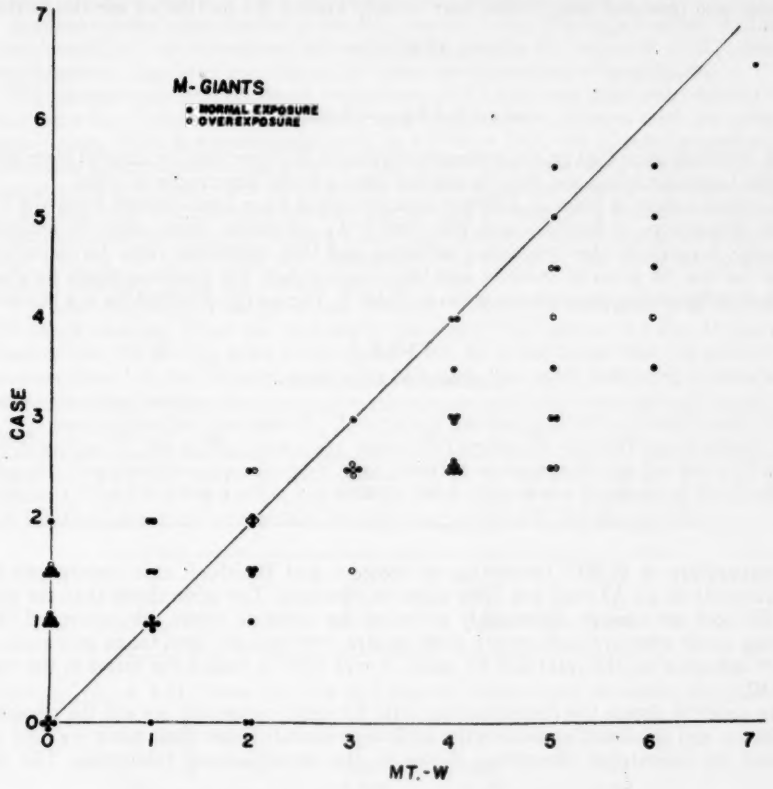

FIG. 3.—Comparison of Mount Wilson and Case spectral types

VI. INFRARED MAGNITUDES

In this paper we make use of infrared magnitudes which are obtained from direct exposures on I-N plates with a Wratten No. 89 filter. No hypersensitization was applied to the plates used for photometry.

The effective wave length for the infrared system is about λ 7700. The effective wave lengths for the international photographic and for photored magnitudes are approximately λ 4240 and λ 6200, respectively. These figures refer to early-type stars. We denote the

photographic, the photored,[9] and infrared magnitudes by m_{pg}, m_{pr}, and m_{ir}, respectively, and define the photored and infrared color indices by

$$RI = m_{pg} - m_{pr}\,, \qquad II = m_{pg} - m_{ir}\,.$$

The zero point for the infrared magnitude scale is obtained by assuming that the infrared intrinsic color is equal to zero for A5 stars if they are free from interstellar reddening. The same assumption had previously been made for the photored zero point.[9] To determine our infrared sequences, we have used stars with small color index for which photographic and photored magnitudes were already known. To do this we use the relation

$$II = 1.40\,RI\,,$$

or

$$m_{ir} = 1.40\,m_{pr} - 0.40\,m_{pg}\,.$$

First, we shall show that an approximate relation of this type may be derived from independent considerations and may be applied over a fairly large range of color.

Intrinsic colors of stars of different spectral types have been derived from the six-color photometry of Stebbins and Whitford.[10] We determine these colors by applying Planck's formula to the continuous radiation and then correcting them for deviations from the law, as given in Stebbins and Whitford's paper. The resulting colors for giant stars of different temperature are given in Table 1. The energy distribution in a star with

TABLE 1

COLORS FOR GIANT STARS

T	RI	II	II/RI	T	RI	II	II/RI
8000	0.26	0.36	1.39	5000	1.01	1.44	1.43
6000	0.69	0.96	1.39	4000	1.48	2.17	1.47

a temperature of 10,000° (according to Stebbins and Whitford, this corresponds approximately to an A5 star) has been taken as standard. The table shows that the ratio II/RI does not change appreciably as far as the intrinsic colors are concerned. The change in the effective wave length with spectral type has not been taken into account, as its influence on the ratio will be small; it will tend to reduce the trend in the ratio II/RI.

In order to obtain the corresponding ratio for space reddening, we use the results of Stebbins and Whitford's photometry of B-type stars.[11] From their table we find the values for interstellar absorption shown in the accompanying tabulation. The cor-

λ	4240	6200	7700
$1/\lambda$	2.36	1.60	1.30
Abs.	0.817	0.411	0.215

responding color excesses are: $E_r = 0.406$ and $E_{ir} = 0.602$, and therefore $E_{ir}/E_r = 1.48$.

[9] Nassau and Burger, *Ap. J.*, **103**, 25, 1946.

[10] *Ap. J.*, **102**, 318, 1945.

[11] *Ap. J.*, **98**, 20, 1943.

A similar calculation may be made by using the theoretical curve due to Oort and van de Hulst,[12] with the following results:

λ	4240	6200	7700
Abs.	1.024	0.562	0.360

and hence $E_{ir}/E_r = 1.44$. We may conclude that the ratio E_{ir}/E_r for space reddening is nearly equal to that of II/RI determined from intrinsic colors.

Because of some uncertainties in the data, especially in the assigned values of effective wave lengths, it was considered advisable to determine the value of II/RI, once its near-constancy had been established, by direct measurements of magnitudes.

The photographic and photored magnitudes of A5 stars and other stars having little color were first determined in the usual way by direct comparisons with the polar sequence stars. With the provisional value of $II/RI = 1.40$, the infrared magnitudes of these stars were computed. Since the average value RI for these stars was only 0.29 mag., a slight error in the ratio will not affect the resulting infrared magnitudes. Later this sequence was used to determine infrared magnitudes of stars with relatively high color. From the measured infrared, photored, and photographic magnitudes of these stars the value 1.40 for the ratio II/RI was confirmed. With this as a final value we established our final sequence, using the stars of low color only.

The near-constancy of the ratio does not apply for M-type stars later than M0, where *TiO* bands seriously affect the continuous spectrum. The value of RI and II has been measured for 101 M-type stars in the region of SA 39. It was found that the ratio II/RI increases from 1.37 for M0 stars to 2.12 for M7 stars. The space reddening is included in these values of the ratio.

It is conceivable that the ratio E_{ir}/E_r for space reddening of M-type stars is also different from that of the earlier-type stars, since the presence of the *TiO* bands affects considerably the effective wave lengths. The effective wave lengths for the early M stars are about λλ 4550–4600, λ 6600, and λ 7900. With these wave lengths and the Stebbins and Whitford material,[11] we obtain the following values for the absorption:

λ	4575	6600	7900
$1/\lambda$	2.19	1.52	1.27
Abs.	0.739	0.355	0.196

Hence, $E_{ir}/E_r = 1.41$. From the Oort and van de Hulst[12] curve we obtain the following values:

λ	4575	6600	7900
Abs.	0.929	0.501	0.341

and $E_{ir}/E_r = 1.37$. These values are still close to the assumed value of 1.40. From Oort and van de Hulst's data the ratio of infrared absorption to infrared excess for M stars is $0.341/0.588 = 0.58$. This latter ratio cannot be obtained from Stebbins and Whitford's data, as the proper normalization of the curve cannot be performed. According to Oort and van de Hulst, the ratio of photographic absorption (at λ 4240) to the infrared excess is $1.024/0.588 = 1.74$.

[12] *B.A.N.*, **10**, 187, 1946.

From an extensive investigation of the B-star cluster near P Cygni, Nassau and Harris[13] have found the ratio of photographic absorption to red excess equal to 2.6, and, since $E_{ir}/E_r = 1.4$, we have, for the ratio of the infrared absorption to infrared excess, 0.86. This value is greater than the one obtained from theoretical considerations of Oort and van de Hulst; but, since it is derived from uniform material secured from the same part of the Milky Way, it was thought advisable to use it in our statistical studies.

VII. ABSOLUTE MAGNITUDES

Our adopted absolute magnitudes have been secured from the Mount Wilson list,[14] which at present is the only source for such data. The calibration of these magnitudes presents many difficulties. Here we use the most recent calibration, derived by Russell and Moore,[15] which is expressed by the formula

$$M'_v = M_v + A\,(M_v - S_1)\,,$$

where M_v is the observed absolute magnitude, S_1 is a standard absolute magnitude for which separate values are given for every spectral subdivision, and A is a constant. For giants the value of this constant is 0.33. Our adopted visual absolute magnitudes for different spectral classes are given in Table 2, third column. They were secured from the

TABLE 2

ABSOLUTE MAGNITUDES

Case Class	Mt. W. Class	M_{vis}	CI_i	M_{ps}	II_i	M_{ir}
M0	M0	+0.05	1.48	1.53	2.75	−1.22
M1	M0.5	+0.04	1.49	1.53	2.88	−1.35
M1.5	M1.2	−0.02	1.51	1.49	2.99	−1.50
M2	M2	−0.24	1.57	1.33	3.24	−1.91
M2.5	M2.8	−0.30	1.55	1.25	3.43	−2.18
M3	M3.5	−0.42	1.47	1.05	3.66	−2.61
M3.5	M4	−0.53	1.38	0.85	3.80	−2.95
M4	M4.5	−0.42	1.31	0.89	3.88	−2.99
M4.5	M5	−0.32:	1.25	0.93	4.08	−3.15:
M5	M5.5	−0.31:	1.20	0.89	4.33	−3.44:
M5.5	M6	−0.30:	1.15	0.85	4.29	−3.44:

Mount Wilson list[14] and corrected by means of the above formula. For classes M4.5 (Mount Wilson system) and later, the number of stars available is small. Hence their assigned absolute magnitudes are very uncertain. All stars of visual magnitude 6 and brighter and north of −26° declination were included. For these stars the Mount Wilson catalogue claims completeness. We have omitted the twelve supergiants.

To obtain infrared absolute magnitudes (M_{ir}), we have used the color scale given in Gabovitš'[16] paper, which corresponds nearly to the ordinary photovisual wave length. Its zero point was obtained as follows: Seares and Joyner[17] give for CI_i for a gM0 star the value of 1.48; Nassau and Seyfert[18] give 1.42; and Gabovitš,[16] 1.63. Since the first of these

[13] Unpublished data.

[14] Adams, Joy, Humason, and Brayton, *Ap. J.*, **81**, 187, 1935.

[15] *Ap. J.*, **92**, 354, 1940.

[16] *Tartu Pub.*, Vol. **28**, No. 5, 1936.

[17] *Ap. J.*, **98**, 261, 1943.

[18] *Ap. J.*, **103**, 117, 1946.

values was obtained directly from photographic and photovisual magnitudes of a relatively larger number of stars and refers to recent material, it was adopted. Thus the modified Gabovitš colors given in the fourth column of Table 2 have been corrected for zero point by the amount of 0.15. The fifth column gives the resulting photographic absolute magnitudes. Our data provide the infrared colors of the sixth column, as determined in Section XIII. The last column gives the resulting infrared absolute magnitudes. The small systematic differences between the temperature classification of Mount Wilson and Case have been considered in our calculations. The first two columns of Table 2 give the corresponding spectral classes.

We have also determined the spread in absolute magnitude of the Mount Wilson material, and, after accounting for the scale error, the resulting average value of σ for the different subclasses is equal to 0.47 mag. This value consists of two components, i.e., spread in intrinsic brightness and observational errors. The value of the latter for the giants as a whole is given by Russell and Moore as 0.53 mag., not much different from the value given above. Hence it appears that the spread in intrinsic brightness is probably smaller than 0.25 mag. However, this result is uncertain, as the calibration factor and the observational spread of 0.53 mag. refer to giants in general. It will be appropriate, therefore, in computing space densities to make two solutions—one with σ equal to 0.50 and another with σ equal to 0.25.

The number of supergiants brighter than 6.0 apparent mag. and north of $-26°$ declination is too small to affect our statistical studies. Here, again, uncertainties are present, as Stromberg,[19] in a study of proper motion of stars brighter than 6.0 mag., finds a significant number of M supergiants.

VIII. INVESTIGATION OF THE CYGNUS REGION

It is obvious that only by detailed investigation of many fields can the distribution of M stars be appraised; but, because of their great numbers, the regions must necessarily be limited in size.

This paper deals with one such region. The field has its center at R.A. = 20^h0^m and Dec. = $38\overset{\circ}{.}0$ (1950). It is in low galactic latitude ($l = 3\overset{\circ}{.}1$) and relatively free from interstellar absorption.[20] It is one of the fields in our luminosity function program, having the designation LF3b. On account of the great number of M-type stars present, we have limited ourselves to two rectangles of 2.28 square degrees each, one centered $1\overset{\circ}{.}2$ west and the other $1\overset{\circ}{.}2$ east of the center of the field (Fig. 4). The present study deals with the west rectangle, which was divided into eight squares. Two digits identify each square, the first digit changing in the direction of right ascension and the second with declination. Table 3 gives the co-ordinates of the centers of the squares with the galactic pole taken at R.A. = 18^h40^m, Dec. = $+28\overset{\circ}{.}0$ (1900). For convenience in finding the stars, each square was divided into three equal rectangles, with the numbering consecutive in the direction of increasing R.A. within each rectangle; thus a star is designated by a number of four digits, the first two giving the square. In cases where more than 100 M stars are in a square, five digits are used. Figure 4, *a–h*, gives the reproduction in infrared of the eight squares with the numbering of the stars as described above. In each square three BD stars are indicated by the letters *A*, *B*, and *C*; their identification is given in Table 3*a*.

IX. IDENTIFICATION OF M-TYPE STARS

The process of identifying M-type stars has been carried out in several steps. The first step consisted in the study of a 4° prism plate, secured with a half-hour exposure. About 300 M stars were identified from this plate. As a second step, a 2° prism plate with 1-hour

[19] *Ap. J.*, **71**, 175, 1930.

[20] Oort and Oosterhoff, *B.A.N.*, **9**, 325, 1942.

exposure was studied for faint stars, which augmented our list by more than 30 per cent. However, some stars are missed with this procedure, especially faint early-type M stars and many others whose spectra overlap, particularly with bright stars. For this reason a third step has been taken by comparing direct-exposure plates, one infrared and the other blue. All stars having an infrared index in excess of about 2.8 mag. were marked and their spectra examined. Of these stars, about 30 per cent were rejected as not M stars; presumably they were space-reddened K stars. Three hundred new M stars were

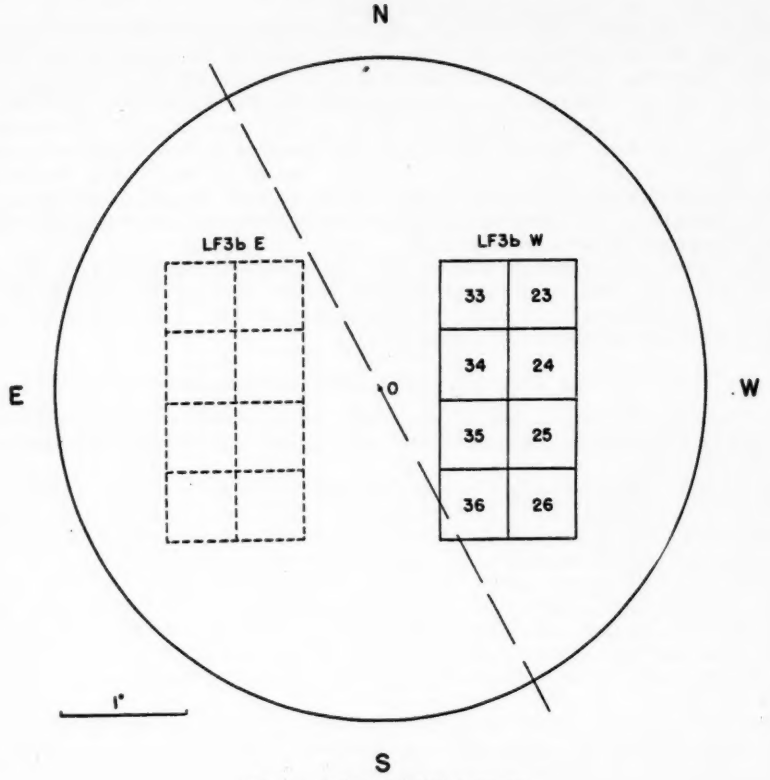

FIG. 4.—Region included in survey

found by this method. Finally, all stars given an M classification were examined on two plates simultaneously, with an observer at each plate. One of the plates was taken with the prism rotated 90° with respect to the other position. This procedure proved very satisfactory, as local defects and overlaps in spectra were eliminated as far as possible.

In spite of all precautions taken, a number of stars were difficult to classify and were marked very doubtful, owing mostly to faintness, overlaps, or plate defects. This is particularly true in the case of M0 stars, where only the band at λ 7054 provides a means of classification. Any accidental fluctuation in the grain of the plate in this region may be almost as strong as the band itself.

For classifying the spectra of very bright stars, short-exposure plates were taken.

FIG. 4a

FIG. 4b

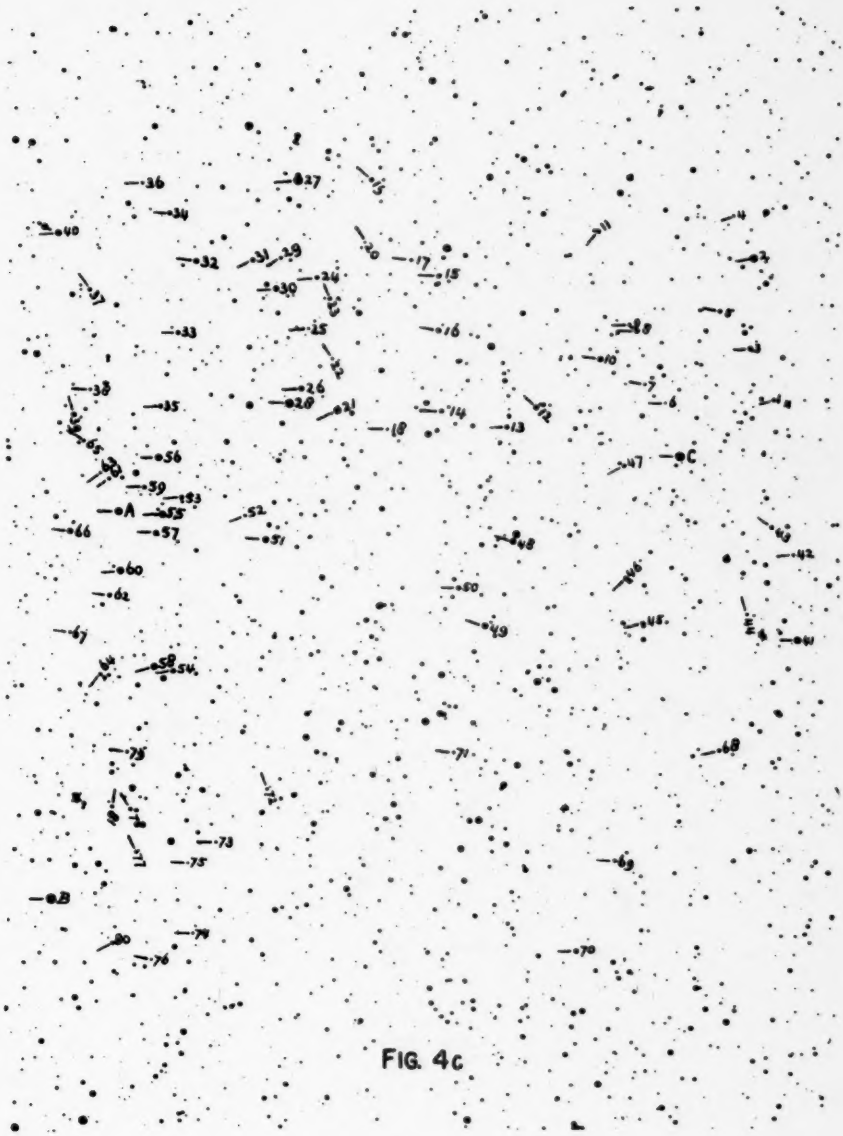

FIG. 4c

FIG. 4d

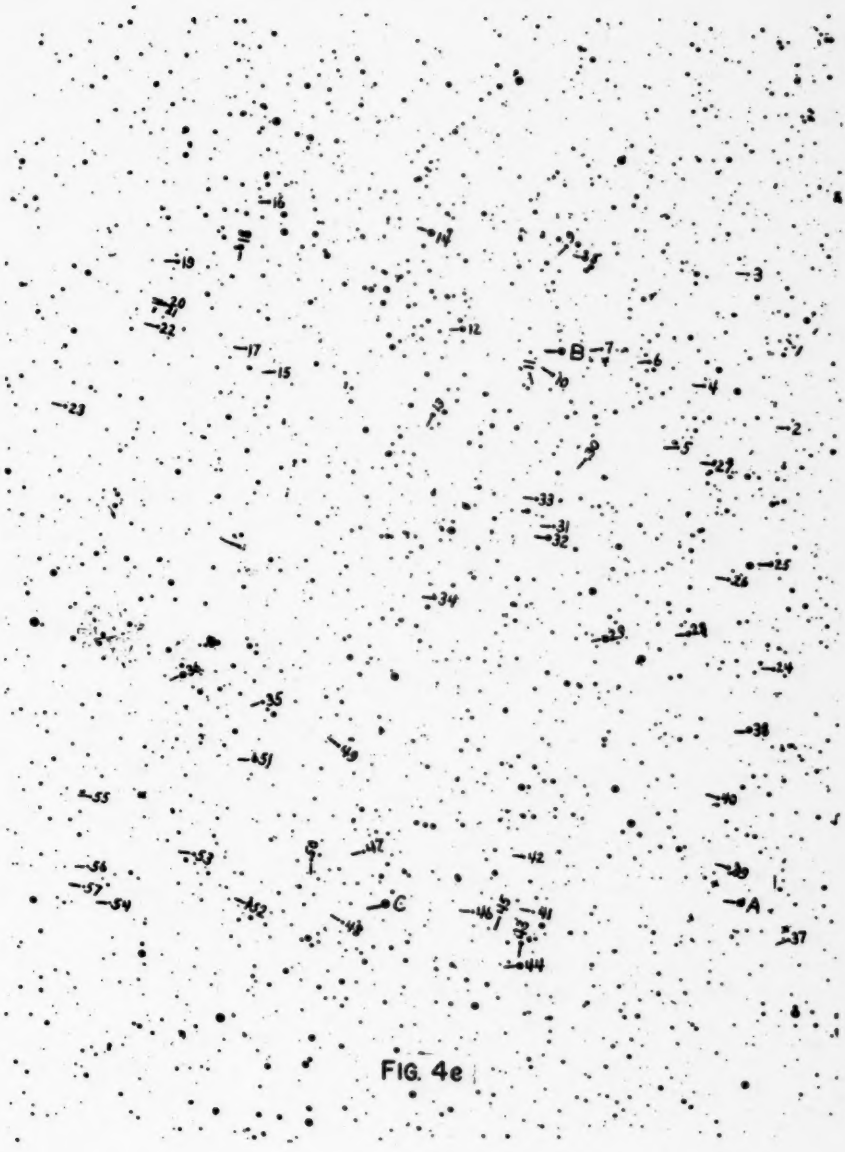
16
14
19
20
21
22
17
15
23
12
B
7
6
10
4
2
5
22
33
31
32
25
26
34
29
28
24
35
38
51
49
55
40
53
47
42
39
56
57
54
52
C
46
41
A
37
43
44

FIG. 4e

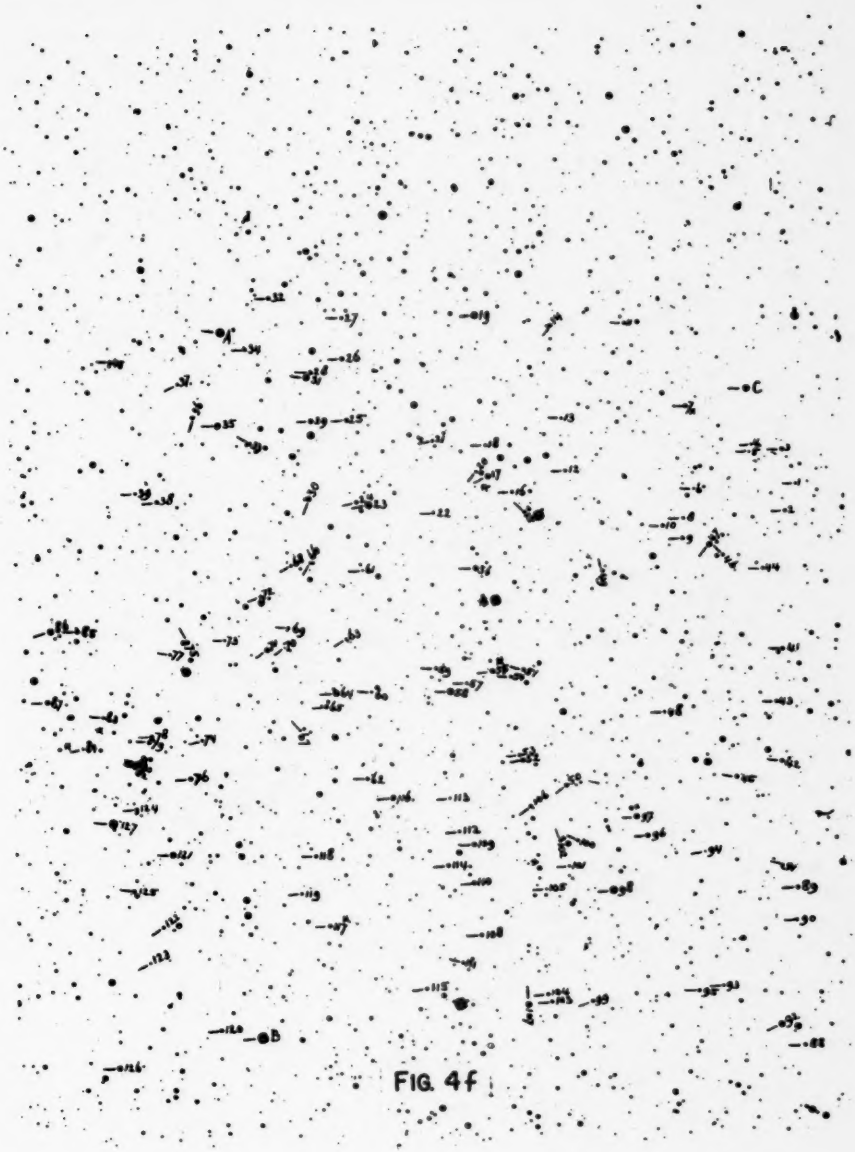

FIG. 4f

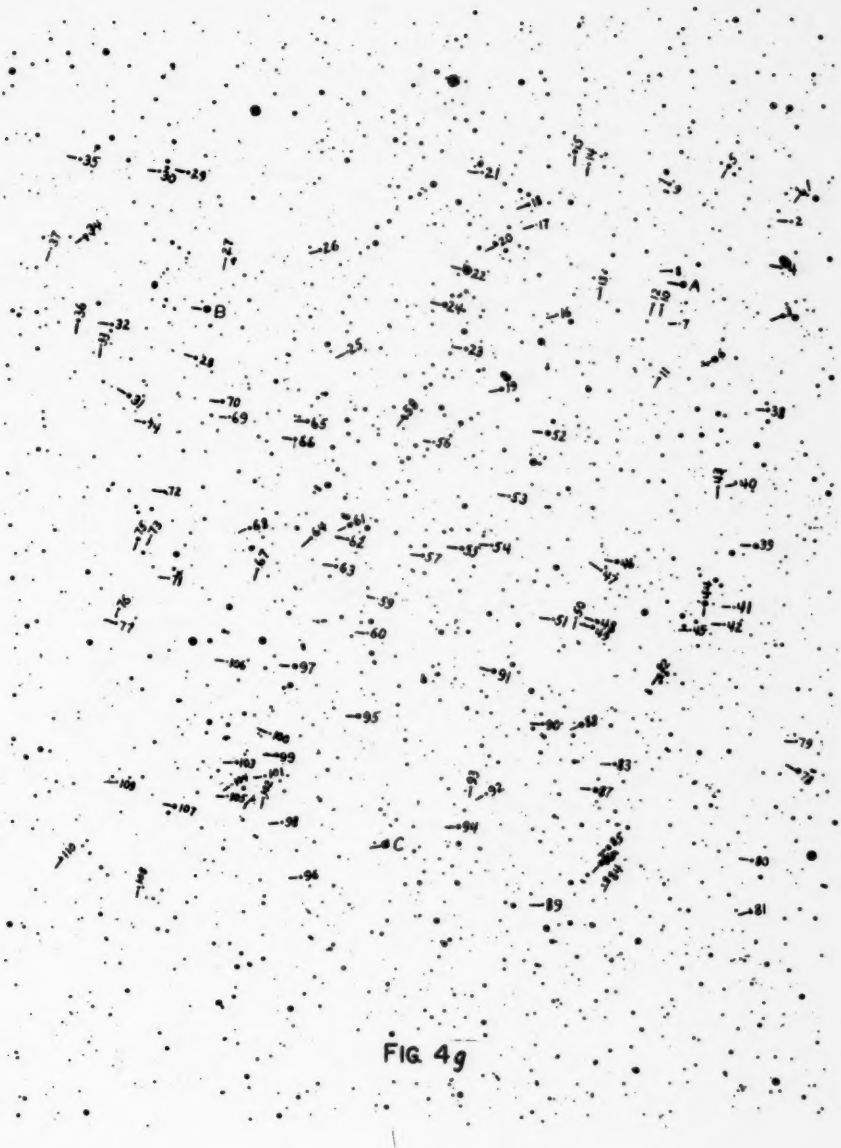

FIG. 4g

FIG. 4h

These plates also provided means for examining systematic errors in our classification due to exposure, since many stars had weak spectra on one plate and strong on another.

X. THE CATALOGUE

Table 4 gives the data of all the M stars classified in the field under investigation. The area of the field is 2.28 square degrees. The list contains 709 M stars; 4 carbon stars, of which 3 are new; and 2 S-type stars, both new. Seventy-one stars are marked with doubtful spectra (:) and 40 with very doubtful (::). The first column gives the number of the star as explained in a previous section; the second, the spectrum with the letter M omitted; the third, the infrared magnitude; and the fourth, the infrared color index.

TABLE 3

DATA FOR FIELD

Square	α	δ	l	b	Square	α	δ	l	b
23	$19^h\,51^m.7$	38° 36′	41° 45′	4° 38′	33	$19^h\,54^m.4$	38° 37′	42° 3′	4° 12′
24	19 51.7	38 4	41 18	4 20	34	19 54.3	38 5	41 36	3 54
25	19 51.8	37 32	40 52	4 2	35	19 54.5	37 33	41 10	3 36
26	19 51.8	37 0	40 25	3 44	36	19 54.5	37 1	40 43	3 18

TABLE 3*a*

STANDARD REFERENCE STARS

FIGURE	SQUARE	BD STARS		
		A	B	C
4, *a*	23	38° 3818	38° 3819	38° 3809
4, *b*	24	38 3817	38 3810	37 3672
4, *c*	25	37 3685	37 3688	37 3670
4, *d*	26	36 3766	37 3687	37 3673
4, *e*	33	38 3822	38 3831	38 3839
4, *f*	34	38 3847	37 3703	38 3823
4, *g*	35	37 3691	37 3705	37 3701
4, *h*	36	36 3798	36 3778	37 3712

When a star has a close companion or is too bright for accurate photometry or when there is a plate defect, the infrared magnitude is given to one decimal; and when the star is altogether too bright, a dash is given. When a star has a weak image in the blue or has too close a companion for accurate photometry, the color is given to one decimal. If the star is variable, the letter *v* is given, while if the star is fainter than photographic magnitude 18 (the limit of our plates), a dash is placed in the color column.

XI. VARIABLE STARS

This paper does not include a systematic study of variables in the region; nevertheless, during the course of the work, a number were detected and were excluded from our color studies. Undoubtedly several remain unidentified; but, since the total number of M stars is so great, we believe that our statistics will not be materially affected. Only obvious variations in magnitude could be detected, and only those which occur between

Table 4

Observational Data

23	Sp	m_{ir}	II
1	1	11.46	2.86
2	2	10.33	2.99
3	5	12.75	4.31
4	3	12.25	4.34
5	1.5	12.25	2.7
6	1.5	12.52	3.66
7	2	12.32	4.04
8	3	12.38	3.84
9	2	11.67	3.91
10	1	12.25	2.91
11	0	11.76	2.81
12	2.5	11.90	3.86
13	2:	13.07	4.00
14	1:p	13.34	4.1
15	0::	12.69	3.42
16	1.5	13.23	3.49
17	1	12.82	3.40
18	1.5:	13.27	3.35
19	6.5	11.73	5.17
20	1:	13.12	3.42
21	1.5	11.34	2.99
22	2	12.72	3.12
23	1.5:	12.85	3.43
24	1::	13.11	3.85
25	2	10.76	3.56
26	1.5p	12.60	3.64
27	1	12.76	3.60
28	0	13.11	3.59
29	1.5	13.15	3.73
30*	4.5	11.88	v
31	1:p	13.01	3.19
32	1	12.58	3.53
33	3	11.18	3.97
34	1.5	10.37	2.79
35	0p	11.39	2.84
36	1	12.48	3.12
37	0p	12.83	3.59
38	1	11.00	3.0
39	1.5	10.89	3.18
40	1.5	12.28	3.64
41	0	10.6	2.8
42	2	11.05	3.35
43	0	13.50	3.85
44	4	11.65	3.93
45	1.5	12.69	3.73
46	2.5	10.89	3.55
47	4	10.47	4.07
48	0	13.55	3.33
49	1	12.44	2.82
50*	6.5	13.12	v

23	Sp	m_{ir}	II
51	1	13.14	3.2
52	1	10.76	3.17
53	2	9.3	3.3
54	6	12.61	4.39
55*	3	12.69	v
56	2	9.0	3.2
57	2.5	12.60	4.16
58	1.5	13.22	3.07
59	4.5p	12.03	4.56

24	Sp	m_{ir}	II
1	1.5	12.66	3.39
2	S	10.24	6.95
3	1.5	11.47	2.81
4	3.5	11.31	4.99
5	1	10.73	3.01
6*	2	12.11	v
7	4	11.12	5.12
8	2:	13.18	3.64
9	1.5	11.70	2.91
10	1.5	11.02	3.63
11	1.5	12.87	3.41
12	3	9.3	4.0
13	4	11.88	4.36
14	1.5	9.90	3.06
15	2	9.4	3.5
16	5	11.92	5.9
17	2	11.77	4.29
18	3	11.18	3.43
19	2p	12.44	4.70
20	2	11.82	3.94
21	1.5	11.77	2.67
22	0	13.14	3.46
23	1	12.28	3.69
24	0	13.61	3.37
25	1.5	12.23	2.92
26	1.5	11.45	3.09
27	0	12.87	3.37
28	6.5	11.18	5.20
29	1.5	12.06	3.09
30	3	12.37	3.89
31	C	14.08	3.09
32	1.5	12.53	3.35
33	6	11.88	4.45
34	2p	12.99	3.39
35	1.5	12.66	3.49
36	0	12.45	3.46
37	5.5	10.62	4.53
38	3.5	8.7	3.7
39	6	10.13	5.57
40*	5.5	13.42	v

24	Sp	m_{ir}	II
41	1.5p	12.99	3.37
42	1.5p	12.47	3.69
43	1	12.25	3.63
44	6.5	11.10	6.5
45	1	12.84	3.18
46	6.5	11.88	5.10
47	1.5	11.10	3.12
48	1	10.59	2.94
49	1.5	12.38	4.14
50	1.5	12.95	3.82
51	6.5	11.31	6.2
52	1.5	11.40	3.43
53	1	13.07	3.64
54	3	10.56	4.09
55	2	12.75	3.89
56	3	11.12	3.97
57	2.5	10.89	2.96
58	2	9.60	3.86

25	Sp	m_{ir}	II
1	1.5	12.31	3.28
2	3	9.4	3.0
3	2.5	11.29	3.61
4	1	12.90	3.13
5	2	11.88	3.69
6	1	13.44	3.13
7	1.5	13.18	2.82
8	2	10.97	3.51
9	2	12.70	3.62
10	2	11.00	2.75
11	1	11.67	3.03
12	1.5	11.00	2.87
13	0	11.82	3.12
14	1	11.90	3.12
15	2	11.90	4.28
16	0	11.08	3.39
17	1.5	12.97	3.81
18	1	13.48	3.13
19	3	11.48	4.26
20	1:	13.52	3.20
21	4.5	9.2	4.4
22	0	13.21	3.13
23	4	12.80	4.58
24	1.5	11.85	3.13
25	0	13.36	3.06
26	6	10.89	5.33
27*	1.5	8.6	2.4
28	5.5	8.9	4.2
29	1.5p	12.86	3.26
30	4	10.70	3.80

Table 4

Observational Data (Cont'd)

25	Sp	m_{ir}	II
31	1.5	11.37	3.43
32	5	11.02	4.96
33	1	11.83	2.97
34	4	11.45	4.06
35	6	11.77	5.23
36	2	12.86	3.68
37	2	12.17	3.25
38	2.5	13.13	3.37
39	4	11.18	4.16
40	3	10.05	4.07
41	5.5	9.5	5.2
42	1.5	13.23	4.03
43	2.5	12.32	4.05
44	1	13.21	3.43
45	1.5	12.66	2.97
46	2.5p	11.56	4.65
47	3	12.38	3.78
48	4.5	10.62	4.13
49	2	10.43	3.15
50	0p	11.95	3.21
51	4	10.47	4.39
52	1.5	13.28	3.72
53	1.5	12.08	3.92
54	3.5	11.34	4.06
55	3	9.81	3.63
56*	C	9.5	v
57	3	11.05	4.40
58	3.5	10.05	4.13
59	3	11.92	4.24
60	6.5	9.81	5.77
61	2	12.78	3.47
62	7	12.17	5.5
63	0	13.21	2.97
64	2	12.83	3.35
65	2	12.85	4.07
66	1.5	10.70	3.48
67	0	13.26	3.46
68	1.5	12.85	2.90
69	1.5	12.47	4.27
70	5	11.51	5.19
71	1	13.32	3.83
72	1.5	13.28	3.6
73	1.5	13.22	3.34
74	1:	13.32	3.60
75	1	13.67	3.30
76	2.5	13.32	3.53
77	1	12.86	3.10
78	2	12.45	3.32
79	2	12.89	3.83
80	1	12.62	4.16
81	1.5	12.85	3.84

26	Sp	m_{ir}	II
1	0::	13.99	2.97
2	1.5	13.17	2.73
3	4	9.1	3.9
4	4	11.82	4.20
5	1	10.09	2.95
6	1.5	10.61	2.45
7	1	11.68	3.34
8	2.5	12.28	3.84
9	1	13.19	3.42
10	5.5	10.43	4.43
11	1	13.17	3.05
12	1.5	12.97	3.07
13	0:	13.34	3.34
14	0:	12.89	2.98
15	1	12.78	3.0
16	0	11.51	3.83
17	0:	12.10	2.59
18	0	9.63	2.67
19	1	13.54	3.18
20	5	11.62	4.89
21	1	12.67	3.20
22	1.5	11.51	3.35
23	4.5	12.72	4.38
24	C	13.14	3.62
25	0	12.67	2.99
26	2	10.78	3.52
27	1	13.19	3.21
28	1.5	12.85	3.08
29	1	12.74	2.64
30*	5	11.56	v
31	1	12.32	3.34
32	4	12.41	4.47
33	1.5	13.44	3.42
34	2	13.32	4.00
35	1.5	13.25	3.33
36	1p	10.67	2.69
37	1	12.35	3.10
38	1.5	10.62	3.03
39	0	12.75	2.93
40	1.5	12.36	3.6
41	1	12.77	3.35
42	1::	12.63	3.08
43	1	13.31	3.54
44	6.5	11.18	4.82
45	0	12.21	3.07
46	0:	12.82	3.30
47	1	13.34	3.34
48	5.5	11.40	4.29
49	1.5	12.00	3.56
50	0	10.52	2.94

26	Sp	m_{ir}	II
51	1	11.65	3.03
52	3	12.85	3.91
53	1:	11.94	3.43
54	2	12.38	3.78
55	1	11.73	2.79
56	0::	12.75	2.55
57	5	11.51	4.13
58	1	11.53	3.05
59	0	13.21	3.4
60	4.5	11.59	4.47
61.	0:	13.04	3.64
62	4.5	9.2	4.3
63	1	13.23	3.50
64	0	13.15	3.00
65	6.5	12.11	4.75
66	0	13.23	4.2
67	2	12.00	3.98
68	1	12.89	2.97
69*	7p	8.3	v
70	4	8.8	4.3
71	1	12.48	3.20
72	3	12.69	3.75
73	1	12.32	3.17
74	3	10.30	3.9
75	2	11.02	3.78
76	1::	13.49	3.8
77	0:	13.15	3.53
78	0p	13.42	3.18
79	6	12.20	5.3
80	5.5	9.77	4.95
81	0:	11.18	2.72
82*	7p	10.50	6.70
83	2.5	12.17	4.21
84	1	12.00	3.86

33	Sp	m_{ir}	II
1	1:	13.18	3.58
2	1	13.14	3.16
3	2	13.05	3.71
4	1:	12.95	3.77
5	1:	13.33	3.26
6	0	12.35	3.04
7	1.5	12.95	3.55
8	5	10.67	4.23
9	7	13.00	4.6
10	2p	12.32	3.15
11	2	13.83	4.0
12	2	11.15	3.50
13	1	12.18	2.76
14	5	9.77	4.5
15	1:	13.22	3.07

Table 4

Observational Data (Cont'd)

33	Sp	m_{ir}	II
16	1	12.85	3.15
17	1.5p	13.17	3.75
18	2	10.70	3.38
19	1.5	11.61	3.41
20	1:	13.37	3.6
21	1:	13.05	3.0
22	5.5	12.08	4.86
23	1	12.14	3.10
24	1	12.38	2.78
25	4.5	11.88	4.58
26	0:	13.05	2.45
27	1:	12.87	3.68
28	1	11.86	2.3
29	2.5	9.94	3.18
30	1	13.22	3.25
31	1	13.11	3.48
32	4	10.82	3.86
33	2	12.74	3.19
34	1.5	12.80	3.85
35	1.5p	12.77	3.11
36	3.5	8.94	4.42
37	1.5p	13.21	3.68
38	1	10.56	2.82
39	C	12.62	4.40
40	2	12.73	3.66
41	1:	13.22	3.9
42	2	12.95	3.55
43	6.5	11.22	5.81
44	2.5	9.89	3.55
45	0::	13.30	3.23
46	1	12.91	2.41
47	2	13.07	3.54
48	3.5	12.88	3.96
49	2p	12.97	3.56
50	1	12.80	3.48
51	3	10.30	4.28
52	6.5	11.22	5.4
53	2	12.21	4.51
54	1.5	13.30	3.68
55	1:	13.14	4.5
56	1::	13.34	3.78
57	0::	13.42	4.1

34	Sp	m_{ir}	II
1	0	13.34	3.75
2	5	12.73	5.0
3	2	11.98	3.72
4	1	13.42	4.3
5	1:	13.76	3.9

34	Sp	m_{ir}	II
6	0:p	13.59	3.25
7	1	12.14	2.88
8	1	13.21	3.72
9	1	12.36	2.80
10	0::	12.76	3.06
11	2	12.81	3.50
12	1	12.91	3.16
13	0:	13.42	4.18
14	1.5	12.47	3.73
15	1::	12.84	3.61
16	3	13.09	4.31
17	0	10.77	3.19
18	2	13.18	3.80
19	0	9.4	3.5
20	1.5:p	13.21	3.74
21	1	12.95	3.33
22	0::	13.37	3.40
23	4	9.3	4.7
24	1p	12.50	3.30
25	1	12.06	3.0
26	3	11.70	4.36
27	3p	12.85	4.11
28	0	11.86	2.18
29	3	11.15	4.55
30	2.5	10.92	4.28
31	2	9.73	3.65
32	2	12.25	4.73
33	1.5:	12.87	3.99
34	3	12.81	4.5
35	1.5	10.30	5.0
36	0::	12.80	4.0
37	0:	12.99	3.73
38	1p	12.14	3.06
39	1.5	13.15	3.40
40	0	12.25	3.45
41	1	12.39	3.53
42	2.5	11.92	4.34
43	1.5	12.58	3.28
44	2	12.93	4.03
45	1	11.92	3.42
46	2p	12.79	3.91
47	1.5	10.76	3.64
48	1.5	13.55	3.65
49	0::	13.18	3.36
50	1::	12.10	3.48
51	0	12.43	3.73
52	4.5	11.75	4.99
53	2	12.85	4.26
54	1p	13.06	2.98
55	1.5	11.45	1.47

34	Sp	m_{ir}	II
56	2.5	11.22	3.42
57	0:	13.22	3.36
58	3	9.98	4.21
59	5	13.02	4.7
60	0	13.79	3.29
61	0:	14.37	-
62	1	12.79	3.05
63	0	13.31	3.09
64	2.5	10.26	4.32
65	3	12.41	4.37
66	1::	13.26	3.68
67	2	13.63	-
68	0:	13.42	3.20
69	1	13.17	3.51
70	1::	14.47	3.1
71	1.5	11.05	3.56
72	0::	12.84	3.26
73	1.5	13.42	3.8
74	1	13.22	4.1
75	1:	12.25	3.7
76	1	11.90	2.38
77	2	13.36	3.50
78	1.5	11.77	3.43
79	2	12.08	4.30
80	1	12.57	3.52
81	1.5	12.27	3.51
82	2	12.17	3.11
83	1	12.84	3.20
84	1	13.30	3.48
85	1:	11.67	3.24
86	1.5	9.68	3.54
87	2	11.10	3.55
88	1	12.24	2.91
89	0	11.95	3.15
90	1	12.85	2.91
91	1	13.31	3.86
92	6	9.94	5.5
93	0	13.15	3.15
94	1:	13.95	-
95	1	12.39	2.71
96	3.5	11.45	4.57
97	1.5	10.79	3.83
98	4	9.0	5.1
99	5	12.62	4.46
100	0::	12.91	3.35
101	2:	13.41	2.85
102	1.5	13.03	3.30
103	1	12.69	3.43
104	1	12.73	3.82
105	1	13.47	3.45

Table 4

Observational Data (Cont'd)

34	Sp	m_{ir}	II
106	1	12.83	3.69
107	0	10.14	2.68
108	0	12.39	3.03
109	1	11.29	3.42
110	1.5	11.65	2.93
111	1::	12.99	4.41
112	0	13.07	3.99
113	6.5p	14.4	-
114	1.5	12.44	3.90
115	1.5	12.85	3.31
116*	2.5	11.53	-
117	6.5	11.98	5.30
118	2p	12.77	3.87
119	2	13.14	4.24
120	1	12.53	4.33
121	3	10.26	4.04
122	1.5p	12.81	4.05
123	0:	13.36	3.36
124	2	12.74	3.83
125	1.5	12.16	3.68
126	3.5	10.94	3.70
127*	3	8.5	v

35	Sp	m_{ir}	II
1	2.5	9.77	3.88
2	1.5	12.99	3.17
3	4	11.31	4.45
4	1p	13.00	3.85
5	2.5	11.34	3.86
6	0	9.56	2.68
7	0	13.97	3.28
8	0	13.60	2.98
9	2.5	12.35	4.47
10	1.5	12.99	3.89
11	1.5	12.71	2.79
12	1.5	12.99	3.8
13	1	13.03	3.86
14	0	13.19	3.39
15	1.5	11.37	3.21
16	0	13.23	3.77
17	1	13.99	3.7
18	1.5	11.90	3.12
19	0	11.70	3.46
20	5p	12.41	4.77
21	1	13.15	3.72
22*	1.5	-	-
23	4.5	12.17	4.68
24	2.5	10.65	3.93
25	1.5	13.52	3.46

35	Sp	m_{ir}	II
26	1	12.85	3.31
27	2.5	13.43	3.93
28	1	12.02	3.54
29	3.5	12.20	4.76
30	1	12.79	3.85
31	1	11.08	3.18
32	1	12.47	3.29
33	1::	13.36	3.94
34	2	11.00	3.94
35	3.5	12.29	4.73
36	5	11.95	4.79
37	0	13.25	3.51
38	1.5:	12.30	3.56
39	5.5	10.33	5.05
40	1:	14.26	3.4
41	2	13.47	3.51
42	1	13.27	3.33
43	1.5	13.11	3.81
44	2	10.43	3.29
45	0:	13.68	3.20
46*	5	11.18	v
47	1.5	13.19	3.5
48	2	11.77	3.92
49	0	11.48	2.99
50	0	13.27	3.11
51	1.5	13.07	2.99
52	1.5	10.56	3.45
53	1.5	13.23	3.11
54	0	12.91	3.35
55	6	11.73	5.05
56	1::	13.47	3.13
57	2	12.80	4.0
58	1	12.77	3.4
59	1	14.35	3.3
60	1	13.39	3.47
61	2.5	11.02	4.78
62	0:	13.25	3.36
63	1p	12.71	3.33
64	2.5	12.82	4.58
65	1.5	12.34	4.52
66	1:p	12.32	3.92
67	1.5	13.00	4.40
68	1	12.39	3.37
69	2p	13.13	3.34
70	2	11.82	3.94
71	4.5	13.47	4.5
72	4	12.83	4.47
73	1:	14.22	3.6
74	2.5	12.85	3.79
75	1	11.62	3.21

35	Sp	m_{ir}	II
76	0::	13.09	4.03
77	0:	12.83	3.58
78*	6.5p	11.98	v
79	0	13.19	3.27
80	3	12.50	3.98
81	1	12.16	2.90
82	2.5	12.42	4.18
83	1	12.01	2.97
84	1	12.86	2.64
85	1	10.73	3.28
86	1.5	10.40	3.61
87	2	10.20	3.27
88	3.5	10.47	4.00
89	2	13.27	4.17
90	0:	12.79	3.85
91	2.5	11.06	3.42
92	1	12.95	3.71
93	0:	13.31	3.42
94	2.5	11.43	4.03
95	3	11.05	4.22
96	1.5	12.60	4.07
97	3	10.92	4.18
98	0	13.02	3.62
99	1	11.59	3.61
100	1.5	13.39	3.81
101	1.5	13.25	3.23
102	1::	13.28	3.10
103	1	12.06	3.88
104	0::	13.75	3.4
105	2	13.25	3.45
106	0	13.52	3.10
107	6.5	11.29	5.59
108	1.5p	13.13	4.23
109	1.5:	13.36	3.6
110	4	12.08	4.66

36	Sp	m_{ir}	II
1	3	11.34	4.26
2	0	12.95	2.95
3	3	11.75	3.76
4	6	11.56	5.11
5	0	12.91	3.03
6	0:	13.61	3.46
7	1	13.34	3.10
8	0	11.87	2.79
9	1	12.95	3.66
10	4.5	12.71	4.9
11	2p	12.90	3.41
12	1.5	12.53	4.0
13	0:	13.50	3.15
14	2	12.63	3.8
15	2	11.31	2.91

Table 4

Observational Data (Cont'd)

36	Sp	m_{ir}	II
		S	
16	0::	13.42	3.12
17	0	13.20	3.52
18	1.5	13.15	3.71
19	3	12.84	-
20	0:	13.34	3.68
21	1.5p	12.37	4.98
22	0	11.71	3.10
23	4.5	12.50	4.83
24	4.5	11.05	4.29
25	3.5	13.39	3.86
26	0:	14.08	3.45
27	1:	12.85	3.37
28	0::	13.04	3.24
29	0:	13.78	3.52
30	1	13.25	3.7
31	1.5	13.13	4.07
32	1	10.56	3.27
33	2	12.65	5.1
34	1.5:	13.06	2.86
35	0	13.11	2.96
36	1::	14.44	2.8
37	0::	13.59	3.72
38	1	12.97	3.63
39	1	11.93	3.26
40	0::	10.61	2.81
41	0:	11.05	2.96
42	1:	13.42	3.21
43	2	10.99	3.42
44	5.5	12.23	5.13
45	1	13.25	3.77
46	3	12.20	5.00
47	1	12.14	3.73
48	1.5	14.14	3.8
49	4p	11.40	4.72
50	0::	14.32	3.12
51	1	11.75	3.35
52	4	13.15	4.15
53	1:	13.38	3.50
54	1	13.62	3.55
55	6.5	12.78	4.9
56	4	11.67	4.59
57	0	12.48	3.43
58	1.5::	13.15	3.48
59	2.5	12.77	3.84
60	6.5	12.32	

36	Sp	m_{ir}	II
61	1.5	13.12	3.2
62	3	12.84	4.62
63	0	12.81	3.71
64	6p	12.74	4.61
65	3	11.82	4.39
66	0	13.20	2.98
67	1.5	11.05	2.85
68	0::	13.62	3.22
69	5.5	12.35	2.30
70	0:	12.61	3.03
71	0	12.66	2.44
72	2p	12.98	3.7
73	5	12.80	4.9
74	0	11.68	2.58
75	4.5	11.05	4.46
76	0::	13.34	3.40
77	1	12.11	3.13
78*	1.5	-	-
79	1	12.78	3.68
80	0:	12.25	3.84
81*	S	12.95	v
82	0:	13.69	3.65
83	0	13.80	3.37
84	1	11.85	3.72
85	3	11.85	4.41
86	6.5	10.70	5.94
87	0	13.42	3.18
88	1.5	9.63	3.25
89	1.5p	12.30	3.47
90*	7	11.22	v
91	1.5	11.22	3.20
92	1	12.89	3.61
93	1	10.92	3.74
94	1	10.37	2.75
95	4	10.67	4.05
96	1:	13.25	3.4
97	1:	13.47	3.13
98	1.5	12.00	3.46
99	1.5:	13.00	3.60
100	0	11.92	3.24

36	Sp	m_{ir}	II
101	2	8.6	3.3
102	1	13.20	2.80
103	1	12.96	3.67
104	5.5	11.80	5.08
105	2	12.47	4.04
106	6	12.68	5.0
107	2	12.34	3.35
108	0:	12.19	2.80
109	3	12.25	4.31
110	5.5	12.29	5.15
111	0	11.93	2.65
112	3	10.13	4.17
113	2	12.25	3.71
114	1	11.08	3.18
115	2.5	12.95	3.87
116*	5	10.23	v
117	1	13.45	3.79
118	0	13.81	3.46
119	1	12.81	3.63
120	1.5	12.95	3.42
121	5.5	11.43	4.94
122	5	11.43	5.31
123	0	11.31	3.19
124	0	14.32	3.23
125	1	12.02	3.74
126	0::	13.80	3.75
127	5.5	13.37	3.79
128	1	10.37	3.38
129	1.5	11.00	3.04
130	0::	13.73	3.7
131	1:	12.59	3.27
132	0::	13.73	3.23
133	0::	13.42	3.26
134	1.5	12.17	3.87
135	0	12.95	3.09
136	0	12.68	3.05
137	0:	12.15	2.65
138	2::	13.06	4.49
139	1::	14.00	3.31

NOTES TO TABLE 4*

Number	Name	Remarks on Sp.	m_{pg}			m_{ir}		Var.
			1	2	3	4	5	
23– 30	OY Cyg	June 1947 M4.5 May 1948 M2	.....	16.14	16.23	11.88	11.80	v
23– 50	.....	M6.5	.....	Invis.	Invis.	13.12	11.20	v
23– 55	PT Cyg	M3	.....	17.6	Invis.	12.69	.....	v
24– 6	.....	M2	16.37	16.36	16.63	12.11	11.20	v
24– 40	PR Cyg	June 1947 M5.5 May 1948 M2.5	Invis.	17.78	17.80	13.42	13.29	v
25– 27	BD+37°3679	M1.5	.....	11.07	11.04	8.6	.....	.....
25– 56	PU Cyg	C	13.30	13.62	13.32	9.5	9.47	v
26– 30	.....	June 1947 M5 May 1948 M6.5	.....	15.57	16.38	11.56	10.67	v
26– 69	IZ Cyg	M7p Strong λ 7900 band	.....	11.43	13.74	8.3	11.31	v
26– 82	.....	M7p λ 7900 present λ 7589 shallow	.....	17.21	17.19	10.50	.....	.....
34–116	.....	M2.5	Blue image obscured			11.53	.....	.....
34–127	QZ Cyg	M3	.....	11.77	11.93	8.5	.....	v
35– 22	BD+37°3696	M1.5	.....	11.07	10.60	.....	.....	.....
35– 46	.....	M5	.....	15.42	16.38	11.18	.....	v
35– 78	PX Cyg	M6.5p λ 7900 present	.....	Invis.	16.47	11.98	12.08	v
36– 78	BD+36°3792	M1.5	.....	10.42	.....	.....	.....	.....
36– 81	.....	S	Invis.	Invis.	Invis.	12.95	14.19	v
36– 90	.....	M7	.....	16.71	17.06	11.22	10.57	v
36–116	.....	M5	.....	16.14	16.28	10.23	12.00	v

* Magnitudes on the following dates: 1, Oct. 15, 1946; 2, May 23, 1947; 3, July 17, 1947; 4, June 29, 1947; 5, Dec. 15, 1947.

the few dates at which direct photographs were taken. Of the 14 variables given, 7 are new. Only 3 or 4 of the 12 variable M stars have a spectrum earlier than M4.5; one star is of class S, and one is an N star. The name designations of the known variables are given in notes to Table 4. Of the known variables, 4 are irregular, and none of these would have been discovered from our magnitude measures. A comparison of our measured blue magnitudes with the range given in Schneller's Catalogue shows that the stars OY Cyg, PR Cyg, and PU Cyg were outside the published range. PR Cyg was as much as 1.7 mag. fainter than the catalogue value.

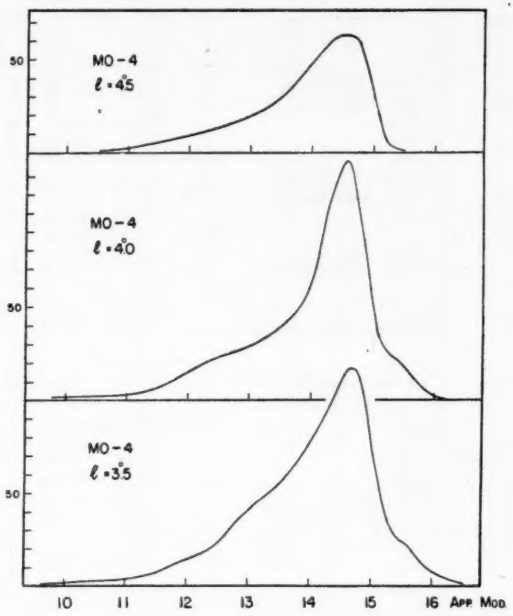

FIG. 5.—Numbers of M stars in various galactic latitudes

XII. DISTRIBUTION OF M-TYPE STARS

The 709 M stars within the area of 2.28 square degrees are not evenly distributed. The squares of the higher galactic latitudes show definitely fewer stars. Figure 5 shows this clearly. Here the ordinate represents the number of M stars between M0 and M4 in intervals of 0.5 mag. per square degree. It appears also that a number of subareas within the regions of higher galactic latitude are completely free of M stars. These areas strongly suggest isolated small clouds of interstellar material, although the space reddening in these squares does not differ materially from that in the region nearer to the galactic equator, as the color excesses show. The number of M stars in each square is given in Table 5, while the co-ordinates of their centers are shown in Table 3.

In spite of the surface distribution irregularities, we are forced to assume uniformity and proceed with a study of the number of stars in different spectral subdivisions. The subclasses between M0 and M4 are shown in Figure 6; the ordinate gives the number of stars in intervals of 0.4 mag., and the abscissa is the infrared apparent magnitude. The

number of stars from M0 to M1.5 remains about the same if we consider the fact that at M1 the interval is 50 per cent greater than at the other classes. From M1.5 to M3 the number of stars gradually diminishes, and from M3.5 to M6.5 the number of stars is about the same, with an average value of 15 stars.

The median apparent magnitude in each subclass is shown by full circles in the figure. A gradual shift to brighter magnitudes with advancing spectral type is indicated. The apparent modulus of 14.3 shown by the dotted line, which was obtained from the data of Table 2, follows this trend in median magnitudes. From this we may infer that the scale of our absolute magnitudes for M0–M4 stars is satisfactory and that the stars from M0 to M4 have essentially the same distribution in space. The stars later than M4

TABLE 5

NUMBER OF M STARS

Square	No. of M Stars	Square	No. of M Stars	Square	No. of M Stars	Square	No. of M Stars
23.....	59	25.....	81	33.....	57	35.....	110
24.....	58	26.....	84	34.....	127	36.....	139

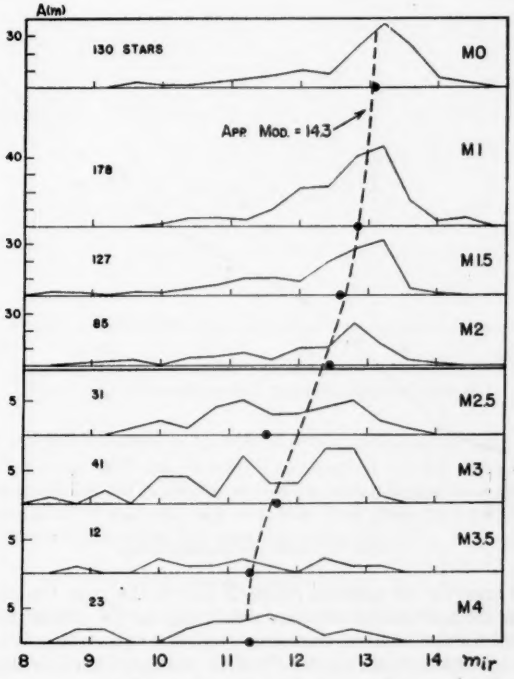

FIG. 6.—Numbers of M stars of various spectral subdivisions

fail to show the increase in brightness with advancing spectral class. This might be due either to the assigned value of absolute magnitudes, as given in Table 2, or to a different space distribution.

XIII. THE SPECTRUM-COLOR RELATION

Infrared colors (*II*) have been determined for nearly all M stars in our survey. Since the space distribution of the stars with spectral range from M0 to M4 appears to be the same, it is possible to determine their relative intrinsic colors by assuming that the space

TABLE 6

RELATIVE INTRINSIC COLORS

Spectrum	*II'*	Weight	Spectrum	*II'*	Weight	Spectrum	*II'*	Weight
M0	−0.13	81	M3	+0.78	33	M5.5	+1.41	12
M1	0.00	.....	M3.5	+0.92	11	M6	+1.64	8
M1.5	+0.11	78	M4	+1.00	20	M6.5	+2.12	12
M2	+0.36	61	M4.5	+1.20	11	M7	+2.37	1
M2.5	+0.55	28	M5	+1.45	12			

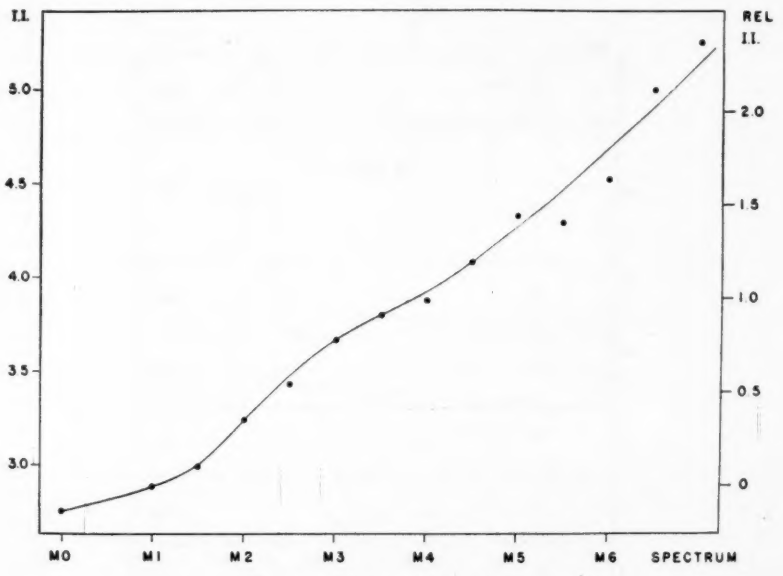

FIG. 7.—Relative intrinsic colors

reddening is the same for all spectral types. If this is the case, the average of all these stars will show a certain amount of space reddening, which, although its absolute value is unknown, may be assumed to be the same for all spectral classes. We will choose for an arbitrary zero point the intrinsic color (*II'*) of an M1 star, since this class has the greatest number of stars. Table 6 or Figure 7 gives the relative intrinsic colors obtained by subtracting from the average infrared index of the stars in each spectral subclass the cor-

responding average of the M1 stars. The assigned weights in each case represent the number of stars used in forming the averages; stars with uncertain color or classification are given half-weight.

Since for stars later than M4 there is no direct evidence that the assumption of equal space distribution is valid, it is possible that the relative colors for these types still need a correction for space reddening. Since the total absorption in the region under consideration is not very large, this correction is probably not great.

The absolute values of the intrinsic infrared colors (II_i) of M stars, which are given in Table 2, were obtained by adding to the relative colors of Table 6 the intrinsic color of

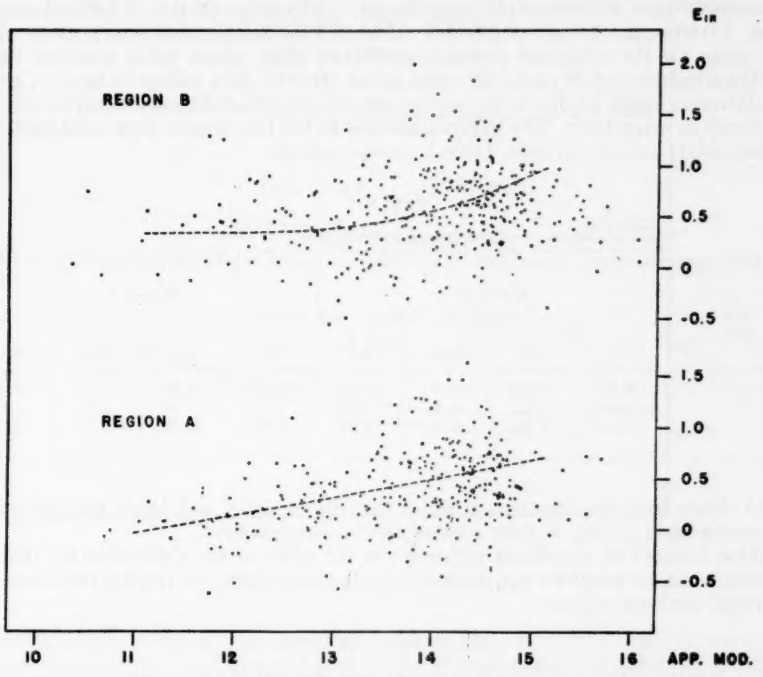

FIG. 8.—Infrared excess and apparent distance modulus

an M1 star. This value was taken to be 2.88 and was obtained as follows. The adopted intrinsic color index of an M0 star is 1.48. To reduce it to the corresponding infrared index, we make use of the ratio $II/RI = 1.40$, a value found to hold approximately true up to M0 stars, and the ratio $RI/CI = 1.33$.[21] This gives for an M0 star $II_i = 2.75$, and from Table 6 we obtain for an M1 star the value of 2.88.

XIV. SPACE ABSORPTION

In the previous section we obtained the intrinsic infrared colors of stars from the observed colors. From the same observational data we shall obtain in this section an estimate of the interstellar absorption. In determining the absorption, we use the com-

[21] Cf. n. 9 and unpublished material.

bined material of all nonvariable stars from M0 to M4 by reducing them to the M1 class. The data of Table 2 furnished the necessary means for this reduction.

A systematic difference in the amount of reddening was observed between the different parts of the region under investigation. The squares 23, 24, 25, 26, and 33, which are designated as "region A," showed, on the average, 0.17 mag. less reddening than did region B, which includes squares 34, 35, and 36. The average galactic latitude of region A is 4°.2 and that of region B, 3°.6.

Figure 8 shows the apparent modulus as abscissa plotted against the infrared excess as ordinate for each of the two regions. The spread of E_{ir} is composed of the following: (*a*) probable error of photographic magnitudes, ± 0.09 mag.; (*b*) p.e. of infrared magnitudes, ± 0.06 mag.; (*c*) p.e. of intrinsic colors due to classification error, ± 0.17 mag. This gives for the combined probable error 0.20 mag., which value does not differ significantly from ± 0.28 mag., the value found directly. As a matter of fact, a part of this difference might be due to the unevenness of interstellar absorption and to systematic errors in magnitudes. The infrared excesses in the two regions were combined into normal points and are given in Table 7, second column.

TABLE 7

INFRARED EXCESSES

App. Mod.	Region A				Region B			
	E_{ir}	A_{ir}	r(kpc)	A_{ir}/r	E_{ir}	A_{ir}	r(kpc)	A_{ir}/r
11.8	0.05	0.04	2.3	0.02	0.35	0.30	2.0	0.15
13.3	.29	.25	4.1	.06	.40	.34	3.9	.09
14.4	0.51	0.44	6.2	0.07	0.65	0.56	5.9	0.10

To obtain from the apparent modulus the true modulus, and hence the distance r, we use the ratio $A_{ir}/E_{ir} = 0.86$, a value previously considered.

Table 7 shows no significant difference in the value of the absorption for the two regions; hence we adopt for our statistical studies the values of 0.10 mag. per kiloparsec (infrared) for both regions.

XV. DENSITY ANALYSIS

The density analysis of the 627 stars between M0 and M4 was undertaken by reducing the material to the M1 class, in accordance with the data of Table 2. The interstellar absorption was taken equal to 0.10 mag. per kiloparsec (infrared) and $\sigma = \pm 0.50$ mag., which gives the value of $M_0 = -1.00$ (infrared) for M1 stars. This value refers to the mean absolute magnitude of stars in a given volume of space, while that of Table 2 has been determined from stars given apparent magnitude. The resulting densities show (upper half of Fig. 9) a value of 16×10^{-6} per cubic parsec at 2 kpc, decreasing to half this value at 4 kpc and a relatively constant density up to 6 kpc. At 8 kpc we find density zero, but this result might be due to incompleteness in our material for faint stars. To avoid the effect of incompleteness, a solution was made utilizing the 107 stars from M2.5 to M4. This produces densities which satisfy the number of observed stars up to a distance of 6 kpc, where the density is equal to 0.7×10^{-6} per cubic parsec, while at 2 kpc the corresponding density is 4×10^{-6}. At a distance of 8 kpc the density was found to be 0.1×10^{-6} or less. It might be pointed out that the stars which determine this

value are of 13.0 apparent infrared magnitude and of spectral class from M2.5 to M4, which could hardly have been missed in great numbers.

A number of other solutions was made by dividing the material into different groups or by assuming different absorption or different values for σ. In all these cases the density gradient was found to be about the same, namely, a rapid decrease from 2 kpc to half the original value at about 4 kpc and a gradual decrease beyond this distance. Figure 9

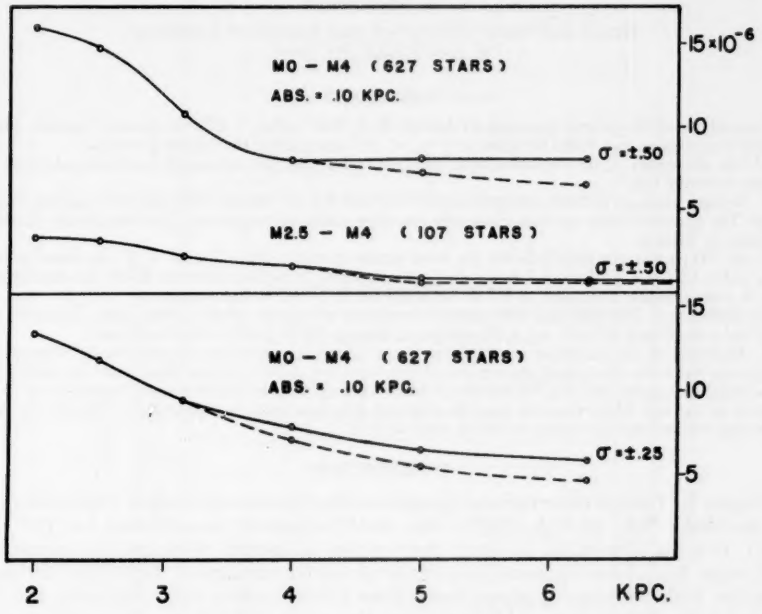

FIG. 9.—Density gradients for M stars

shows two solutions. One of these was made by assuming $\sigma = \pm 0.25$, with the resulting densities shown in the lower half of Figure 9. The other was made by assuming that the interstellar absorption does not extend beyond 5 kpc or 350 psc distance from the galactic plane. The dotted lines show the densities resulting for these solutions.

Since our field is at a latitude of 4°, a distance of 6 kpc from the sun corresponds to a separation of more than 500 psc from the galactic plane. In our density analysis, real distance effects and latitude effects will be intermingled. Investigation of fields at other latitudes are under way in order to separate these two effects.

VARIATIONS IN THE STELLAR LUMINOSITY FUNCTION
III. A REGION IN AURIGA

S. W. McCuskey
Warner and Swasey Observatory, Case Institute of Technology
Received February 25, 1949

ABSTRACT

An analysis of the galactic structure in Auriga (R.A. 5^h01^m; Dec. $+42°$) by means of spectra, photographic magnitudes, and colors for stars with $m_{pg} < 12.5$ has yielded the following results:

1. The absorption of photographic light amounts to 1.2 mag. per kiloparsec, beginning at about 200 parsecs from the sun.

2. Density analyses indicate concentrations of B5 and B8–A0 stars at 1000 and 1500 parsecs, respectively. The giants of other spectral classes do not show such concentrations. Detailed density functions are given in Table 6.

3. At 100 parsecs the data indicate the same excess of stars with $-1 < M < +1$ as found in other fields (LF1, LF2, LF8), about 0.3 in log $\phi(M)$ as compared to the standard van Rhijn luminosity function. A corresponding deficiency of 0.3 in log $\phi(M)$ for $M > +2$ is also present.

At distances of 200, 400, and 600 parsecs, the excess of brighter stars is very slight. For stars with $M > +1$ a deficiency of 0.4 in log $\phi(M)$ relative to the van Rhijn function has been found.

4. Variation of the parameter σ_0, the dispersion in absolute-magnitude distribution for a given spectral group, has little effect upon the computed functions, log $\phi_s(M)$. On the other hand, by making the mean absolute magnitude, M_0, for the dwarf stars 0.5 mag. fainter, the deficiency found for $M > +3$ relative to the van Rhijn function may be removed. No reasonable reassignment of M_0 for the early-type stars will remove the excess noted for stars with $M < +1$.

INTRODUCTION

Region LF7 in the observational program of the Warner and Swasey Observatory lies in the Milky Way at R.A. 5^h01^m; Dec. $+41°.6$ (galactic co-ordinates $l = 133°$, $b = +2°$). It is the fifth region in which observations of spectra, photographic magnitudes, and colors have been combined in a study of the fluctuations of the stellar luminosity function with distance. Analyses for regions LF1 (Aquila), LF2 (Cygnus), and LF8 (Orion) have already been published,[1] while the results of LF3b are now being prepared for publication. The center of LF7 is just north of η Aur. On its northern boundary, in the vicinity of ϵ Aur, there is a small, sharply outlined, obscuring nebulosity. The rest of the region is relatively smooth as regards stellar population, with possibly a trace of obscuring cloud in the southwest sector of the field. An analysis of the galactic structure in the region will be given in the present paper.

OBSERVATIONAL DATA

Spectral types have been determined for nearly 2000 stars in the 16.9 square degrees comprising LF7. Many of these are fainter than $m_{pg} = 12.5$ and hence are not included in the analysis. Disregarding these and also those unclassifiable because of overlaps and other causes, there remain about 1800 stars on which to base an analysis. The distribution of spectral types as a function of photographic magnitude is given in Table 1. A catalogue of the spectral types and other observational data will be published separately.

As indicated by the next to last column of the table, very few stars brighter than $m_{pg} = 12.5$ were omitted in the region. Primary classification was made on plates taken with the 4° prism attached to the 24–36-inch Burrell telescope. Overlapping spectra in most cases could be classified on plates taken with the 2° prism arrangement.

[1] *Ap. J.*, **106**, 1, 1947; **109**, 139, 1949.

TABLE 1

OBSERVED SPECTRAL DISTRIBUTION IN LF7
(Area 16.9 Sq. Deg.)

m_{pg}*	B0	B2	B3	B5	B8	B9	A0	A2, 3	A5	F0 III	F0 V	F2 III	F2 V	F5 III	F5 V	F8 III	F8 IV	F8 V	G0 III	G0 IV	G0 V
≤ 6.00	0	0	1	0	0	0	0	0	0	0	0	0	0	0	0	0	0	0	0	0	0
6.25	0	0	0	0	0	0	1	0	0	1	0	0	0	0	0	0	0	0	0	0	0
6.75	0	0	0	0	0	0	0	0	0	0	0	0	0	0	0	0	0	0	0	0	0
7.25	0	0	1	1	1	0	0	1	0	0	0	0	0	0	0	0	0	1	0	0	0
7.75	0	0	2	5	4	2	0	0	0	0	1	0	0	0	0	0	0	0	0	0	0
8.25	0	1	3	4	5	1	2	1	0	0	1	1	0	0	0	1	0	1	2	0	0
8.75	0	0	3	6	6	2	4	3	1	0	1	0	0	1	1	0	0	0	0	0	0
9.25	0	0	2	11	7	6	4	5	1	1	3	0	5	1	1	0	0	0	0	0	1
9.75	0	1	0	13	14	7	8	5	2	0	4	1	0	0	2	0	0	0	0	0	1
10.25	0	0	2	13	27	12	15	9	7	1	10	1	2	2	2	0	1	2	2	0	7
10.75	0	0	2	10	44	30	16	18	7	2	11	1	3	1	(2)† 2	1	0	7	6	(3)	12
11.25	0	0	1	10	57	33	30	13	2	10		3		5		8			19		
11.75	0	1	1	13	94	74	46	21	11	19		9		10		8			57		
12.25	0	0	0	12	93	75	67	38	16	18		6		7		12			73		
Total	0	3	18	98	352	242	193	114	47	83		32		37		42			183		

* The intervals in m_{pg} designated 6.25, 6.75, etc., refer to 6.01–6.50, 6.51–7.00, etc.

† Parentheses around entries for the late-type faint stars indicate the numbers of stars for which no luminosity classification could be made.

TABLE 1—*Continued*

m_{pg}	G2			G5			G8			K0			K2, 3			K5–M8		Unclassified‡	All Stars
	III	IV	V	III	IV	V	III	IV	V	III	IV	V	III	IV	V	III	V		
≤ 6.00	0	0	0	0	0	0	0	0	0	0	0	0	0	0	0	0	0	1	2
6.25	0	0	0	0	0	0	0	0	0	0	0	0	0	0	0	0	0	0	2
6.75	0	0	0	0	0	0	0	0	0	0	0	0	0	0	0	0	0	0	0
7.25	0	0	0	1	0	0	0	0	0	0	0	0	0	0	0	0	0	0	6
7.75	0	0	0	0	0	0	0	0	0	0	0	0	1	0	0	0	0	0	15
8.25	0	0	0	0	0	0	0	0	0	1	0	0	0	0	0	1	0	0	25
8.75	0	0	0	0	0	0	0	1	0	2	0	1	2	0	0	0	0	0	34
9.25	1	0	0	1	0	0	0	4	0	3	0	0	1	0	2	0	0	0	60
9.75	0	0	2	2	1	1	0	1	1	2	0	0	3	0	1	2	0	1	75
10.25	1	1	0	2	1	2	1	3	1	2	3	0	1	0	1	0	1	1	136
10.75	1	0	1	5	1	5	6	2	0	5	3	3	3	0	0	2	0	2	217
11.25		6		13	(2)	5	9	2(3)	2	13	(1)	1	0	(2)	0	2	(1) 0	7	260
11.75		9		8	(3)	10	13	1(11)	4	10	(7)	2	2	(7)	0	5	(2) 0	13	471
12.25		6		12	(17)	1	10	(17)	1	4	(10)	0	1	(17)	0	0	(2) 0	108	623
Total	28			93			93			73			44			18		133	1926

‡ Included in the "Unclassified" column are stars with composite spectra, peculiar spectra, and spectra unclassifiable because of overlap.

Luminosity classes on the Yerkes system[2] have been assigned for all stars of type F0 and later and brighter than $m_{pg} = 11.0$. Among the fainter stars a luminosity class could not always be assigned. The number of such stars in each spectral group is indicated by parentheses in Table 1. Criteria for luminosity classification have been given by Nassau and van Albada.[3]

Photographic magnitudes for all classifiable stars were determined on Eastman II*a*-O plates, a final magnitude depending on measures of three plates. Double-exposure and series plates made with the North Polar Sequence were used to establish a sequence in LF7. All measures were made with a graduated scale of images. The probable error of a final magnitude for a field star is ± 0.05 mag.

Photored magnitudes for 1000 stars of spectral type earlier than, and including, A5 have been measured on Eastman 103*a*-E plates taken with a No. 22 Wratten filter. The effective wave length of the combination is about λ 6200. Photored magnitudes established for the North Polar Sequence stars by Nassau and Burger[4] were used for calibration of a photored sequence in LF7. Four plates were used for the measurements of the red magnitudes of the field stars, a final magnitude having a probable error of ± 0.04 mag.

TABLE 2

DISTRIBUTION OF SPECTRAL TYPES FROM *Henry Draper Catalogue*
(100 Sq. Deg. Surrounding LF7)

m_{pg}	B0–B2	B5	B8–A0	A2–A5	F0–F5	F8–G0	G5	K0–K2	K5–M	All Stars
6.25	0	0	1	0	2	0	0	2	1	6
6.75	0	1	3	3	2	0	1	0	0	10
7.25	5	2	9	3	0	4	0	2	1	26
7.75	5	1	32	1	3	2	3	3	2	52
8.25	0	4	25	16	22	3	3	6	0	79
8.75	0	1	62	15	18	8	9	14	5	132
9.25	0	0	33	12	12	3	7	15	7	89

In order that the stellar population at great distances might be investigated, star counts have been made on Eastman 103*a*-O plates of 10-minute exposure time. These counts, in four sample areas situated symmetrically with respect to the field center, extend to $m_{pg} = 17.0$. The four areas total 1.15 square degrees and contain 4800 stars brighter than the limit mentioned. Summation of the spectral-type data for the whole region provides added statistical strength for the magnitude range 6–12.

The spectral-type data given in Table 1 have been regrouped for analysis and supplemented for the brighter stars by distributions obtained from the *Henry Draper Catalogue*. For the stars with $m \leqslant 7.0$, values of $\log A'(m)$ deduced[5] from Seydl's[6] counts have been used. These are tabulated in Paper I[7] of this series and refer to the galactic latitude zones 0 to $\pm 10°$ at all longitudes. Corrections to the photovisual magnitude intervals of Table 4, Paper I, have been applied to reduce them to the photographic system of the fainter stars.

For the intermediate range in magnitude, $6.0 \leqslant m_{pg} \leqslant 9.5$, counts according to spectral type for a 100-square degree area surrounding LF7 have been made in the *Henry Draper Catalogue*. The resulting distribution is given in Table 2. In this table, as in

[2] *An Atlas of Stellar Spectra* (Chicago: University of Chicago Press, 1943).

[3] *Ap. J.*, **106**, 20, 1947.

[4] *Ap. J.*, **103**, 25, 1946.

[5] $A'(m)$ is the number of stars per 100 square degrees with m_{pg} between $m - \frac{1}{4}$ and $m + \frac{1}{4}$.

[6] *Pub. Obs. Nat. Prague*, No. 6, 1929.

[7] *Ap. J.*, **106**, 1, 1947, Table 4.

Table 1, a magnitude entry such as 7.75 refers to the range 7.51–8.00. The grouping of spectral classes conforms to that adopted in Papers I and II.

Table 3 summarizes the color data for this region. Average observed red indices (R.I.) are given as a function of spectral class and photographic magnitude. Parentheses indicate the number of colors entering into each average. In order to check the zero point of the color system, data for a few late-type dwarfs are included. Normal red indices and mean absolute photographic magnitudes are given in the second and third columns. These are the same as those used in the analyses presented in Papers I and II. Colors for 15 stars of classes B2 and B3 were also measured. Most of these stars are relatively bright, however, and their colors are uncertain. They have not been included in the table. The probable error of a red index for $m_{pg} > 9$ is ± 0.06 mag.

TABLE 3

AVERAGE OBSERVED RED INDICES IN LF7

SPECTRUM	NORM.	$\bar{M}$	m_{pg}						
			8.01–9.00	9.01–10.00	10.01–10.5	10.51–11.0	11.01–11.5	11.51–12.0	12.01–12.5
B5	−0.53	−1.0	−0.37(9)	−0.38(24)	−0.33(12)	−0.34(10)	−0.14(8)	+0.05(12)	+0.24(5)
B8	−0.46	−0.5	− .18(11)	−0.38(21)	− .36(24)	− .25(45)	−0.15(53)	+ .30(92)	+ .19(71)
B9	−0.32	0.0	− .09(3)	−0.27(12)	− .22(13)	− .17(28)	−0.09(33)	+ .07(87)	+ .25(66)
A0	−0.20	+0.5	+ .08(6)	−0.17(12)	− .11(15)	− .13(14)	−0.04(29)	+ .20(43)	+ .31(46)
A2,3	−0.07	+1.5	+ .17(4)	+0.09(9)	+ .01(9)	+ .04(18)	+0.15(11)	+ .25(18)	+ .40(27)
A5	0.00	+1.7	+ .08(1)	+0.07(3)	+ .04(7)	+ .03(6)	+0.14(2)	+0.39(7)	+0.36(5)
F8V	+0.40	.....	+ .51(1)	.....	+ .26(3)	+ .39(3)	.....	.....	.....
G0V	+0.46	.....	.....	+0.34(2)	+ .28(5)	+ .40(7)	+0.41(3)	+0.56(3)	.....
G2V	+0.60	.....	.....	+0.33(1)	+ .41(1)	+ .46(1)	.....	.....	.....
G5V	+0.84	.....	.....	+0.49(1)	+ .76(2)	+ .80(3)	+0.80(2)	.....	.....
G8, K0V	+1.08	.....	.....	+1.14(1)	+0.60(1)	+0.96(1)	+1.10(1)	.....	.....

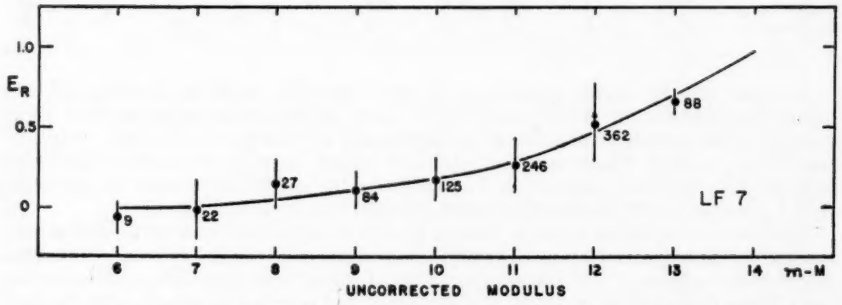

FIG. 1.—The distance modulus–red color excess relation for LF7. The number beside each point indicates the number of values of E_r entering into the mean $\bar{E}_r$ plotted. Vertical lines represent the total range in individual color excesses used in computing the average. Abscissa is uncorrected distance modulus.

ANALYSIS OF THE OBSERVATIONAL DATA

COLOR EXCESSES AND PHOTOGRAPHIC ABSORPTION

Color excesses, E_r, computed from the data of Table 3 for the late-type dwarf stars and the late A stars in the modulus range 5.5–6.5 indicate that the present red indices are too blue by about 0.05 mag. This is apparent from the curve $\bar{E}_r$ against uncorrected distance modulus $m - M$ shown in Figure 1. In this figure the number of color excesses entering into the average $\bar{E}_r$ for each plotted point has been indicated. Vertical lines

through the points represent the *total spread* in the individual values whose weighted average is shown. The groupings have been made according to a 1-mag. range in $m - M$.

From the average values of E_r shown in Figure 1, the photographic absorption, A_{pg}, has been computed by use of the previously adopted ratio, $A_{pg}/E_r = 2.6$.[1] In Figure 2 the values of A_{pg} have been plotted against corrected distance in parsecs. The data are consistent with a uniform absorption of 0.7 mag/kpc to 1000 parsecs followed by a cloud absorbing about 0.7 mag. in the next 250 parsecs and again a uniform increase of 0.7 mag/kpc. Or, alternatively, we may use a uniformly increasing absorption, beginning at 200 parsecs from the sun and amounting to 1.2 mag/kpc. The analysis for space densities will not differ materially if we use one or the other of the two hypotheses. Therefore, we shall adopt an absorption of 1.2 mag/kpc setting in at 200 parsecs distance.

Kiefer and Baker[8] have made extensive star-count analyses in a broad region which covers LF7. In fact, LF7 includes their area F and some of the surrounding area G. Colors were determined by them, and the interstellar absorption was evaluated in a

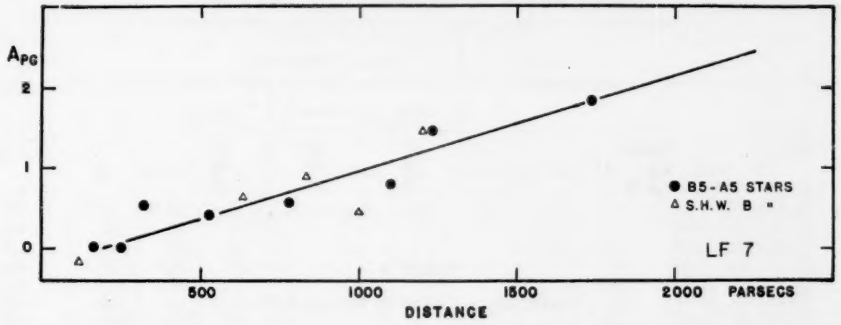

FIG. 2.—The absorption-distance relation in LF7. Abscissae are corrected distances in parsecs; ordinates are total photographic absorptions deduced from Fig. 1 by application of the ratio $A_{pg}/E_r = 2.6$.

manner similar to that described above. They reached the conclusion that the absorption over area G was produced by two clouds, at 300 and 800 parsecs, each absorbing about 0.4 mag. In region F, however, the absorption was found to be zero to a distance of 700 parsecs and 0.8 mag. beyond. The authors pointed out, however, that the data could be represented equally well by a continuous absorption of 0.7 mag/kpc for region F and 1.3 mag/kpc for G. The satisfactory agreement between these absorption values and those deduced from our colors is evident.

One further bit of evidence strengthening the results of our color analysis is provided by the photoelectric color excesses published by Stebbins, Huffer, and Whitford.[9] Five stars of their list lie within LF7. Color excesses, E_1, for these stars, multiplied by a factor of 9 to reduce them to A_{pg}, are plotted in Figure 2. The agreement between our data and the photoelectric color data is excellent. Just to the south of LF7, however, there is an abrupt increase in the absorption, as shown by the photoelectric data. The colors of five stars in this obscured area indicate about 1.5 mag. absorption at 500 parsecs.

SEPARATION OF GIANTS AND DWARFS

In order to analyze the data for the late-type stars, the percentage of dwarf stars among a given group has been estimated as in Papers I and II. The statistical work of

[8] *Ap. J.*, **94**, 482, 1941.

[9] *Ap. J.*, **91**, 20, 1940.

others[10] has been used for the separation among the brighter stars. For the fainter stars, percentages in agreement with the data of Table 1 have been adopted. The percentages of dwarfs in LF7 are given in Table 4. A noteworthy feature of the distribution in LF7 is the high percentage of dwarfs among the stars of intermediate brightness in the spectral group G8–K3. This value, 20 per cent, is about double that found in LF1, LF2, and LF8. All stars in the K5–M8 group will be assumed to be giants.

VALUES OF LOG $A'(m)$ FOR ANALYSIS

Table 5 summarizes the values of log $A'(m)$ for the same spectral groups used in the analyses already published. These numbers have been derived from freehand curves drawn through the points obtained by grouping the entries of Table 1 together with the data in Table 2 and with the Seydl data. Corrections to the photographic magnitudes of

TABLE 4

PERCENTAGES OF DWARFS AMONG LATE-TYPE STARS

Spectral Group	m_{pg}		
	$\leqslant 8.5$	8.5–10.5	>10.5
F8–G2	32	50	70
G5	20	40	50
G8–K3	4	20	15

TABLE 5

VALUES OF LOG $A'(m)$ IN REGION LF7

m_{pg}	Spectrum											
	B2–B3	B5	B8–A0	A2–A5	F0–F5	F8–G2		G5		G8–K3		K5–M
						g	d	g	d	g	d	
4.0	9.20	9.12	9.18	9.30	9.00	9.03	8.70	8.30	7.70	9.26	7.88	8.95
4.5	9.40	9.27	9.52	9.50	9.29	9.10	8.78	8.65	8.05	9.52	8.14	9.12
5.0	9.60	9.40	9.89	9.70	9.53	9.16	8.82	9.00	8.40	9.78	8.40	9.32
5.5	9.82	9.61	0.20	9.90	9.80	9.28	8.96	9.34	8.74	0.01	8.63	9.52
6.0	0.04	9.85	0.56	0.12	0.05	9.44	9.13	9.61	9.01	0.23	8.85	9.73
6.5	0.30	0.11	0.81	0.33	0.30	9.68	9.35	9.90	9.30	0.40	9.02	9.91
7.0	0.54	0.50	1.05	0.55	0.55	9.93	9.60	0.10	9.50	0.56	9.18	0.10
7.5	0.88	0.90	1.28	0.74	0.77	0.22	9.89	0.30	9.70	0.66	9.28	0.30
8.0	12.0	1.32	1.50	0.92	1.00	0.50	0.17	0.48	9.88	0.78	9.40	0.46
8.5	1.30	1.59	1.71	1.15	1.20	0.76	0.43	0.59	0.13	1.08	9.90	0.60
9.0	1.15	1.70	1.93	1.35	1.45	0.92	0.92	0.72	0.42	1.40	0.60	0.73
9.5	0.95	1.79	2.15	1.56	1.67	1.20	1.20	0.90	0.68	1.60	1.00	0.82
10.0	0.90	1.80	2.38	1.74	1.86	1.50	1.50	1.13	0.95	1.76	1.16	0.94
10.5	0.92	1.82	2.59	1.91	2.00	1.75	1.75	1.38	1.20	1.92	1.32	1.02
11.0	0.95	1.83	2.80	2.09	2.10	1.81	2.14	1.52	1.52	2.13	1.38	1.13
11.5	0.98	1.84	2.98	2.25	2.20	2.02	2.35	1.74	1.74	2.32	1.57	1.23
12.0	1.01	1.85	3.14	2.38	2.30	2.18	2.51	1.98	1.98	2.45	1.70	1.32
12.5	1.04	1.87	3.30	2.50	2.38	2.32	2.65	2.20	2.20	2.61	1.86	1.41

[10] See Paper I, *Ap. J.*, **106**, 9, 1947.

the *Henry Draper Catalogue* have been applied for $m_{pg} < 8$. These are necessary because of the differences between the color indices used in forming the photographic magnitudes of the *Catalogue* and the more recent normal color indices assigned to the various spectral types.

SPACE-DENSITY FUNCTIONS

Analyses for the space density of stars as a function of distance were made by the (m, log π) tabular method. The mean absolute magnitudes and dispersions required for the analysis were taken from Paper I, Table 12. The space densities were then corrected by Seeliger's formula[11] for the total absorption shown in Figure 2. The resulting density functions are given in Table 6.

The galactic structure in this region may be described briefly as follows:

a) The density function for the B5 stars shows a marked clustering of these stars with its maximum at 1000 parsecs from the sun. The density at the peak is five times the

TABLE 6

DENSITY FUNCTIONS IN LF7
(Number of Stars per 1000 Cubic Parsecs)

Distance (Parsecs)	Spectral Group											All Stars
	B5	B8–A0	A2–A5	F0–F5	dF8–G2	dG5	dG8–K3	gF8–G2	gG5	gG8–K3	gK5–M	
100....	0.02	0.08	0.40	1.0	0.8	2.0	3.0	0.07	0.10	0.40	0.20	8.07
200....	.005	.08	.10	0.7	1.0	2.0	1.0	.03	.07	.10	.05	5.14
300....	.001	.10	.14	0.7	2.8	1.4	.....	.04	.04	.07	.04	5.33
400....	.002	.10	.16	0.6	1.7	1.7	.....	.07	.02	.06	.03	4.44
500....	.002	.13	.13	0.4	2.1	2.1	.....	.11	.02	.09	.01	5.09
600....	.008	.13	.13	0.3	1.1	2.0	.....	.03	.03	.19	.01	3.93
800....	.023	.15	.04	0.1	.....	.....	.....	.04	.04	.19	.01	0.59
1000....	.03	.06	.12	0.1	.....	.....	.....	.06	.03	.06	.006	0.47
1200....	.01	.10	.09	0.07	.....	.....	.....	.07	.01	.09	.01	0.45
1400....	.001	.26	.10	.....	.....	.....	.....	.05	.05	.10	.01	0.57
1600....	.002	.27	0.04	.....	.....	.....	.....	0.02	0.15	.06	0.006	0.55
1800....	.003	.17	.....	.....	.....	.....	.....	.....	.....	.28	.....	0.45
2000....	0.004	0.04	.....	.....	.....	.....	.....	.....	.....	0.29	.....	0.33

average density in the first 500 parsecs. One might have anticipated this result from the presence in Table 1 of an excessive number of stars of magnitude 10 as compared to the number of magnitude 12. Beyond 1250 parsecs these early-type stars appear to be very scarce.

b) A similar clustering tendency, but at a greater distance, is evident among the B8–A0 stars. The density for this group remains sensibly constant in the first 1000 parsecs from the sun. From that point on, however, it rises to a value at 1500 parsecs, nearly three times its value in the solar neighborhood. Beyond 1500 parsecs the density decreases rapidly.

c) In the first 250 parsecs from the sun, the A2–A5 stars, as well as the giant stars of the late spectral groups, diminish in number very rapidly. The density at 250 parsecs is approximately one-quarter that in the solar neighborhood. Beyond this point the density slowly decreases for the A2–A5 stars and remains sensibly constant for the late-type giants.

d) The number of stars of types dF8–G2 and dG5 appears to be nearly constant in

[11] See Bok, *The Distribution of the Stars in Space* (Chicago: University of Chicago Press, 1937), p. 14.

the first 500 parsecs from the sun. The abrupt increase in density for the former group at 300 parsecs distance is of doubtful reality.

e) One feature of the density function for the dG8–K3 stars does not show in Table 6 because of the 100-parsec interval used. It would appear from the table that the density decreases rapidly to nearly zero at 300 parsecs. The analysis for this group was extremely difficult, and it was necessary to use a density of 10 at 125 parsecs, coupled with nearly zero density at 300 parsecs and beyond, in order to represent the star numbers at all. This peak in density does not show in the table. For this group the results must be considered very uncertain because of the small number of stars actually observed.

Schalén[12] has made an extensive study of several galactic regions by means of spectral-type distributions of stars brighter than $m_{pg} = 10.5$. Region LF7 is situated on the edge of his Auriga field, which is centered at 5^h00^m and $+39°$. A comparison of the density functions of Table 6 with those published by Schalén shows good agreement in general, except for the F0–F5 group. Only the regions labeled *N* and *B* by Schalén—the relatively

TABLE 7

LUMINOSITY FUNCTIONS LOG $\phi_s(M)$ IN REGION LF7

M	DISTANCE (PARSECS)				STANDARD
	100	200	400	600	
−2	4.79	4.41	4.34	4.64	4.75
−1	5.36	5.13	5.17	5.33	5.07
0	6.00	5.71	5.75	5.84	5.68
+1	6.54	6.14	6.14	6.18	6.34
+2	6.81	6.43	6.42	6.36	6.77
+3	6.85	6.59	6.61	6.45	6.86
+4	6.92	6.78	6.84	6.68	7.19
+5	7.12	7.01	7.03	6.95	7.35
+6	7.25	7.10	7.04	7.03	7.50
+7	7.16	6.93	6.74	6.76	7.53

clear regions—were used in the comparison. In the F0–F5 group, the considerably higher densities found in the analysis for LF7 arise from the use of a mean absolute magnitude 1.5 mag. fainter than that used by Schalén. The brighter absolute magnitude, $M_0 = +2$, used by him was based on the supposition that the proportion of giant and supergiant stars among the group is large. Unpublished material here does not confirm the high proportion of giants among these stars.

VARIATIONS IN THE LUMINOSITY FUNCTION

The luminosity function at distances of 100, 200, 400, and 600 parsecs has been computed from the densities given in Table 6 in the following way. The densities for each spectral group at a given distance were spread out with a dispersion σ_0 about the mean absolute magnitude M_0, and the results for half-magnitude intervals in M were summed to obtain the total number of stars per 1000 cubic parsecs between $M - \frac{1}{4}$ and $M + \frac{1}{4}$. Reduction to a volume of 1 cubic parsec and to an interval $M - \frac{1}{2}$ to $M + \frac{1}{2}$ yielded a luminosity function at each distance which has been designated log $\phi_s(M)$. These luminosity functions, together with the standard van Rhijn function generally used in star-count analyses, are exhibited in Table 7. The van Rhijn function is certainly the best that we have for comparison at the present time.

[12] *Upsala Medd.*, No. 37, 1928; No. 55, 1932.

In region LF7, as in the other areas so far investigated, at 100 parsecs there appears to be an excess of about 0.3 in log $\phi_s(M)$ for $M < +1$ and a deficiency of 0.25–0.4 for $M > +2$ relative to log $\phi(M)$ as deduced by van Rhijn. At the greater distances the excess for the brighter stars largely disappears. The functions at 200, 400, and 600 parsecs are in good agreement among themselves, and all show the defect from the standard function for $M > +1$.

When we compare the values of log $\phi_s(M)$ given in Table 7 for $r = 200$ parsecs with those deduced by Bok and Wright[13] from Schalén's data for his regions N and B in Auriga, we find some discordance. At the values of M equal to 0, 1, 2, 3, the differences, in the sense Bok-Wright log $\phi(M)$ minus LF7 log $\phi_s(M)$, are +0.26, +0.12, +0.13, +0.11, respectively. An examination of the numbers of B, A, and F stars given by Schalén reveals no striking differences in surface density of stars with $m_{pg} < 10.5$ between his data and the data for LF7. The systematically higher values for log $\phi(M)$ deduced from Schalén's data have undoubtedly arisen from the use of a larger value of the photographic absorption in this large area than was found in LF7.

In view of the rather serious fluctuations in the functions log $\phi_s(M)$ found thus far in our study of five regions of the Milky Way, we might inquire how changes in the assumed values of mean absolute magnitude, M_0, and dispersion, σ_0, would influence the results. Obviously, the *relative* functions so far observed should be indicative of actual fluctuations in stellar population. But the defect with respect to the van Rhijn function for $M > +2$, even at 100 parsecs, needs investigation.

TABLE 8

THE EFFECTS OF CHANGES IN M_0 AND σ_0 ON THE VALUES OF LOG $\phi_s(M)$ COMPUTED FOR LF7

M_{pg}	LOG $\phi_s(M)$				M_{pg}	LOG $\phi_s(M)$			
	(2)*	(3)	(4)	(5)		(2)*	(3)	(4)	(5)
−2.....	4.79	4.76	4.38	4.75	+3.....	6.85	6.92	6.85	6.86
−1.....	5.36	5.25	5.36	5.07	+4.....	6.92	7.09	6.90	7.19
0.....	6.00	5.90	5.86	5.68	+5.....	7.12	7.31	7.12	7.35
+1.....	6.54	6.50	6.57	6.34	+6.....	7.25	7.51	7.25	7.50
+2.....	6.81	6.80	6.98	6.77	+7.....	7.16	7.53	7.16	7.53

* See text for explanation of columns.

The effects on log $\phi_s(M)$ of changing the adopted M_0 and σ_0 within reasonable limits are shown in Table 8. Column 2 gives the values of log $\phi_s(M)$ computed for LF7, at 100 parsecs, from the adopted M_0 and σ_0 already published.[1] Column 3 has been computed by making M_0 for the B5 and B8–A0 groups 0.5 mag. brighter and M_0 for the dF8–G2, dG5, dG8–K3 groups 0.5 mag. fainter. For the giants of all classes and for the A2–A5 stars, the value of M_0 was used, as published, viz., +2.0. In each case the published σ_0 was used. Column 4 was obtained by using the published values of M_0 with varied values of σ_0 as follows: B5, $\sigma_0 = \pm 0.5$; B8–A0, A2–A5, giants, $\sigma_0 = \pm 0.7$; dwarfs, published σ_0. These are reasonable lower limits to σ_0 for the groups considered. Column 5 gives the standard van Rhijn function.

We conclude by inspection of Table 8 that it is quite possible to account for the deficiency of stars with $M > +2$, as compared to the van Rhijn function, by making the mean absolute magnitudes for the dwarf stars 0.5 mag. fainter. However, it would require unreasonable changes in M_0 to remove the excess of stars with $M < +1$. When the re-

[13] *Ap. J.*, **101**, 311, 1945.

sults for all the "luminosity function" regions are at hand, a more thorough study of these effects is contemplated. It is sufficient to note here that the values adopted for M_0 for the dwarf stars in the present series of papers are about 0.5 mag. brighter than those used by van Rhijn and Schwassman.[14] In view of the uncertainty in M_0, the relative defects of our functions log $\phi_s(M)$ for $M > +2$ cannot be considered too significant.

A decrease in the dispersion, σ_0, for the absolutely brighter stars has little influence on log $\phi_s(M)$ as is evident from column 4. The principal change is an increase in the value at $M = +2$ and a corresponding decrease at $M = 0$. The latter is not sufficient to remove the difference between the standard function and our log $\phi_s(M)$.

TABLE 9

GENERAL STAR-COUNT DATA IN REGION LF7

m_{pg}	LOG $N(m)$			m_{pg}	LOG $N(m)$		
	LF7 Counts	Kiefer and Baker	van Rhijn Zone		LF7 Counts	Kiefer and Baker	van Rhijn Zone
8	0.15	.....	0.00	13	2.30	2.33	2.01
9	0.70	0.50	0.48	14	2.64	2.66	2.41
10	1.16	0.92	0.93	15	2.97	2.99	2.81
11	1.58	1.56	1.31	16	3.30	.....	3.17
12	1.97	1.95	1.66	17	3.62	.....	3.53

TABLE 10

RELATIVE DENSITY FUNCTIONS IN LF7

Distance (r) (Parsecs)	$D(r)$ Counts	$D(r)$ Spectra	$D(r)$ Keifer and Baker	$D(r)$ Schalén (N, B)	Distance (r) (Parsecs)	$D(r)$ Counts	$D(r)$ Spectra	$D(r)$ Keifer and Baker	$D(r)$ Schalén (N, B)
100	1.00	1.00	1.00	1.00	600	1.10	0.53	0.80	.....
200	1.60	0.70	1.00	0.52	1000	0.70	.....	0.45	.....
300	1.57	0.63	0.90	0.29	1500	0.95	.....	0.25	.....
400	1.50	0.57	0.90	0.21	2000	1.20	.....	0.15	.....
500	1.35	0.55	0.90	.....	2500	1.50	.....	0.10	.....

GENERAL STAR-COUNT ANALYSIS IN LF7

Star counts to the seventeenth magnitude in four sample areas, symmetrical about the plate center, strengthened by the totals from the distribution of spectral types for the entire region, are summarized in Table 9. Log $N(m)$ is the number of stars per square degree brighter than magitude m.

Kiefer and Baker[15] have published an extensive star-count analysis for the Auriga region. As indicated before, their region F is very close to LF7 but embraces only 3 square degrees as compared to 16.9 for the latter. Log $N(m)$ deduced by them for region F is given in the third column of Table 9. The agreement with the counts in LF7 from

[14] *Zs. f. Ap.*, **10**, 161, 1935.

[15] *Ap. J.*, **94**, 482, 1941.

$m = 11$ to $m = 15$ is excellent. For the stars with $m_{pg} < 11$, the systematic difference between these two sets of data seems to be due to a magnitude difference of about 0.3 in the calibrations.

For a second comparison with our counts in LF7, I have listed in the fourth column the values given by van Rhijn in *Groningen Publications*, No. 43, Table 10, for the appropriate latitude zone. The surface density of stars in LF7 is considerably higher than in the surrounding region.

A relative space-density function, computed on the assumption that the standard van Rhijn luminosity function is valid for the entire space considered, is exhibited in Table 10, second column. An (m, log π) analysis, with corrections for absorption based upon Figure 2, was used. For comparison, a summation of the densities given in the last column of Table 6 and reduced to relative $D(r)$ is also shown. The striking difference in behavior of the two density functions in the first 500 parsecs reflects the excess of stars predicted by the standard function as compared to the observed log $\phi_s(M)$ for $M > +2$ in this region.

The relative density functions obtained by Kiefer and Baker[8] and by Schalén[12] are given in the fourth and fifth columns of Table 10. Not only the excess of stars with $m < 10$ but also the higher absorption in LF7 contribute to the greater densities for LF7 as compared to the values found by the investigators mentioned.

At the present time we shall limit our discussion and conclusions to the above comparisons. Only when the data for all the LF regions are available can an adequate study of the average effect of these local irregularities on the luminosity function be made.

STELLAR SPECTRA IN MILKY WAY REGIONS

I. A REGION IN AQUILA

S. W. McCuskey
Warner and Swasey Observatory, Case Institute of Technology
Received March 11, 1949

ABSTRACT

Observations of spectra, photographic magnitudes, and red color indices are presented for a region in Aquila R.A. 19^h27^m; Dec. $+6°.9$. The area covered is 14.3 square degrees. Table 1 lists the data for 989 stars. Identification charts are shown in Fig. 1, *a–f*.

OBSERVATIONAL DATA

Observations of stellar spectra, photographic magnitudes, and colors are being accumulated at the Warner and Swasey Observatory for studies of galactic structure in selected regions of the Milky Way. The purpose of the program is to evaluate the variations in the stellar luminosity function with galactic longitude and with distance from the sun and thereby to strengthen our knowledge of this important function. The areas selected for study are relatively smooth in stellar population. Centers for these "LF" regions, as they are called, have been published,[1] together with a detailed analysis of the space densities and fluctuations of the luminosity function in the Aquila, Cygnus, and Orion regions, LF1, LF2, and LF8. The present paper gives the observational data for region LF1, R.A. = 19^h27^m; Dec. = $+6°.9$; $l = 12°$; $b = -7°$. Data for the other regions will follow in succeeding papers of this series.

The spectra have been taken with the 4° and the 2° prisms attached separately to the Burrell 24–36-inch Schmidt-type telescope. Eastman 103*a*-O and II*a*-O plates have been used. With a 30-minute exposure on II*a*-O plates, spectra of nearly all stars with $m_{pg} < 12.5$ can be classified. In some instances, particularly for the early-type stars, a much fainter limit can be attained. While the survey in each area is aimed at a completeness limit of $m_{pg} = 12.5$, there are obvious difficulties due to overlapping spectra which preclude the assignment of spectral types to all stars. In LF1 the number of stars brighter than $m_{pg} = 12.5$ for which no spectral type could be assigned is 38. The total number of spectra observed is 989.

For identification purposes, a series of charts of the region are shown in Figure 1, *a–f*. A key chart indicating the sectioning of the field is shown in the upper left-hand corner of Figure 1, *a*. The co-ordinates for 1950 are indicated, and the stars are numbered approximately in order of right ascension for each degree zone of declination. The zone serial numbers correspond to those given in Table 1, first column. An asterisk following a serial number in Table 1 indicates that the star is a BD star. An "R" following the star number refers to remarks at the end of the table. The area of the sky involved is 14.3 square degrees.

Table 1, second and third columns, gives the photographic magnitudes for all stars observed and the red color indices (R.I.) for the majority of the stars with spectral type earlier than A5. The probable error of a tabulated blue magnitude is ± 0.09 mag., on the average. Red magnitudes on which the colors are based were determined on 103*a*-E plates used with a No. 22 Wratten filter. The resulting effective wave length of the combination is λ 6200. The red-magnitude system is believed to be consistent with that

[1] *Ap. J.*, **106**, 1, 1947; **109**, 139, 1949.

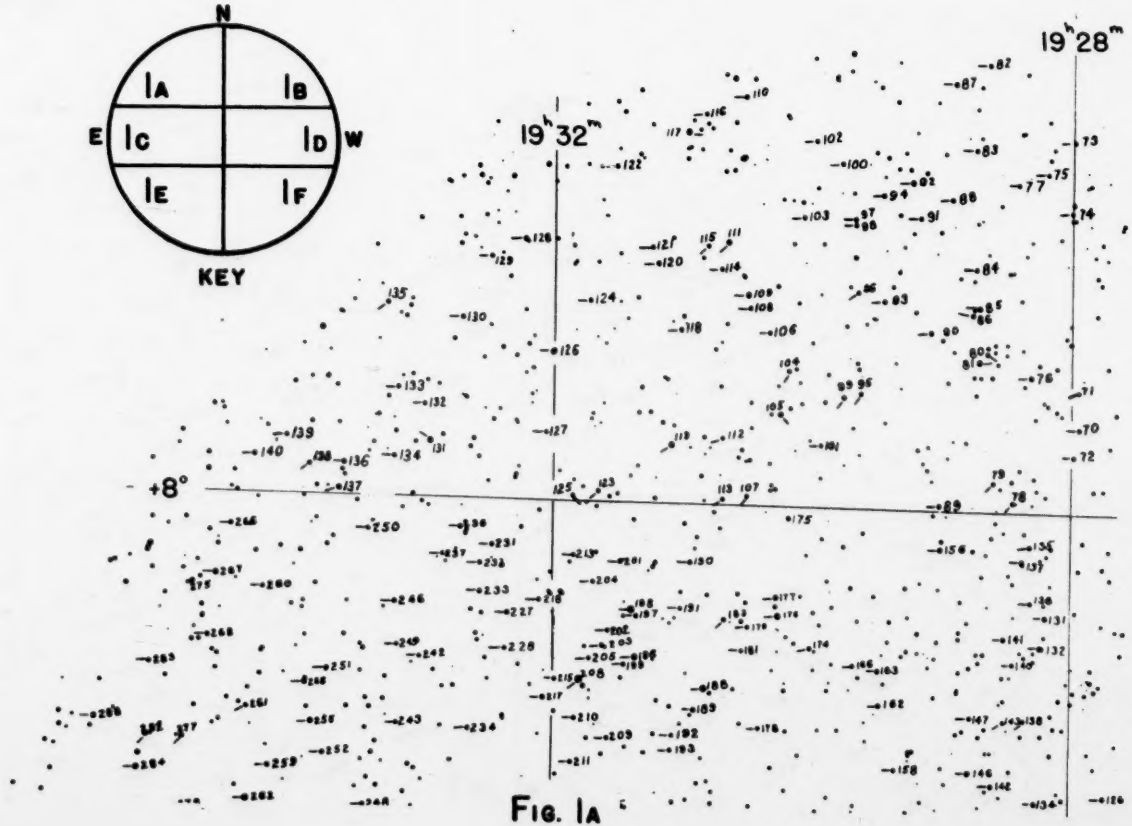

FIG. 1A

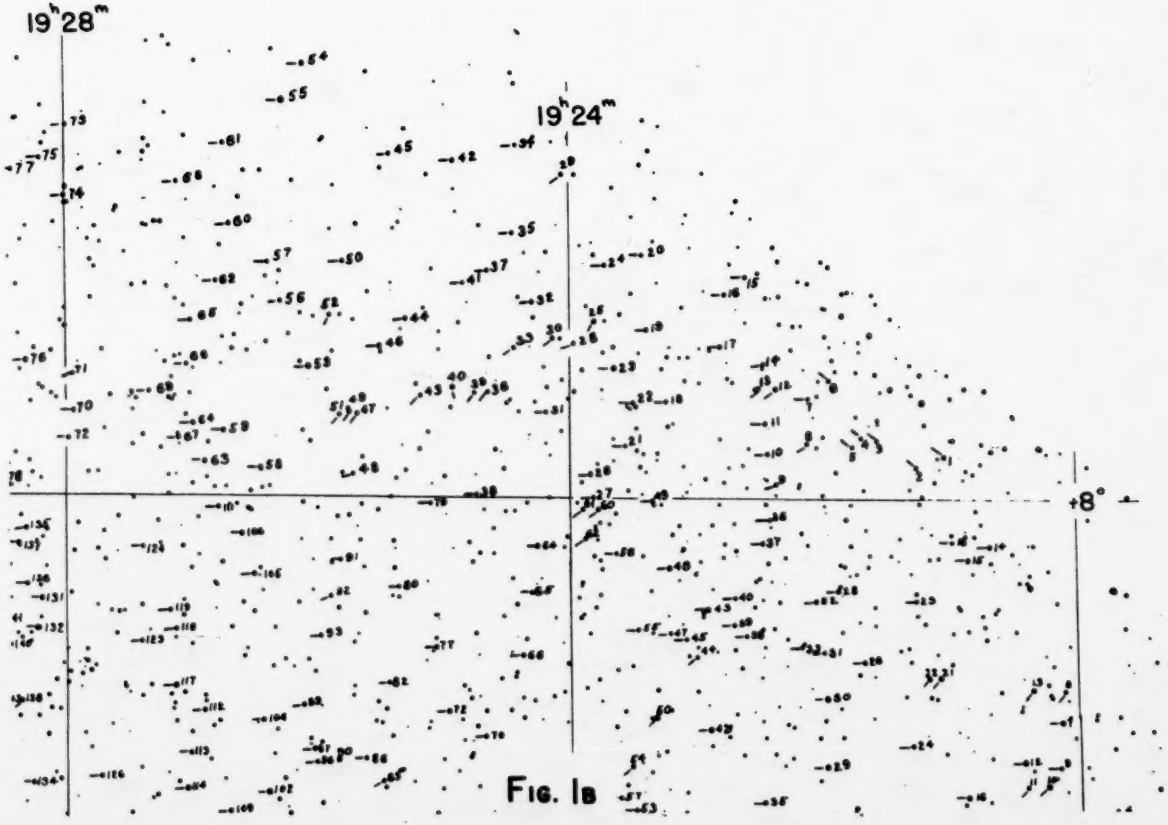

FIG. 1B

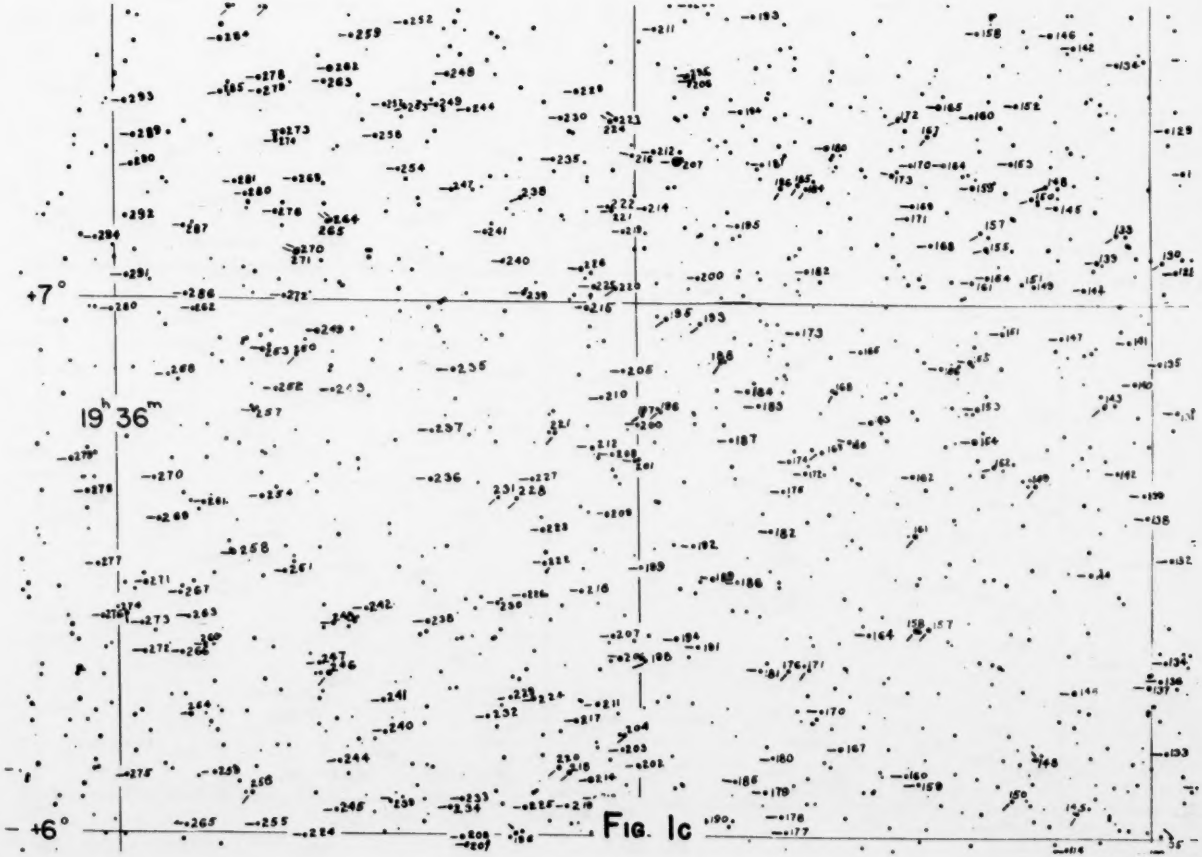

Fig. 1c

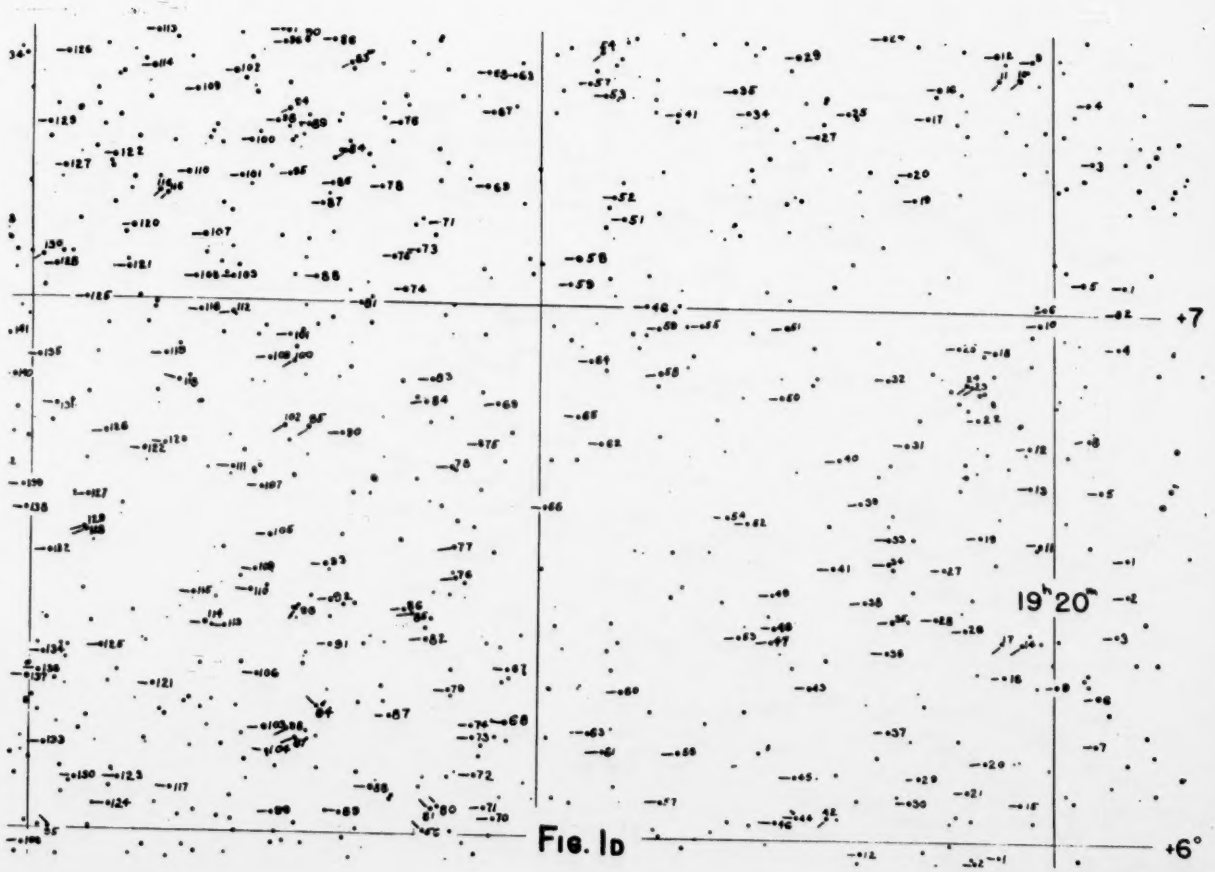

Fig. 1b

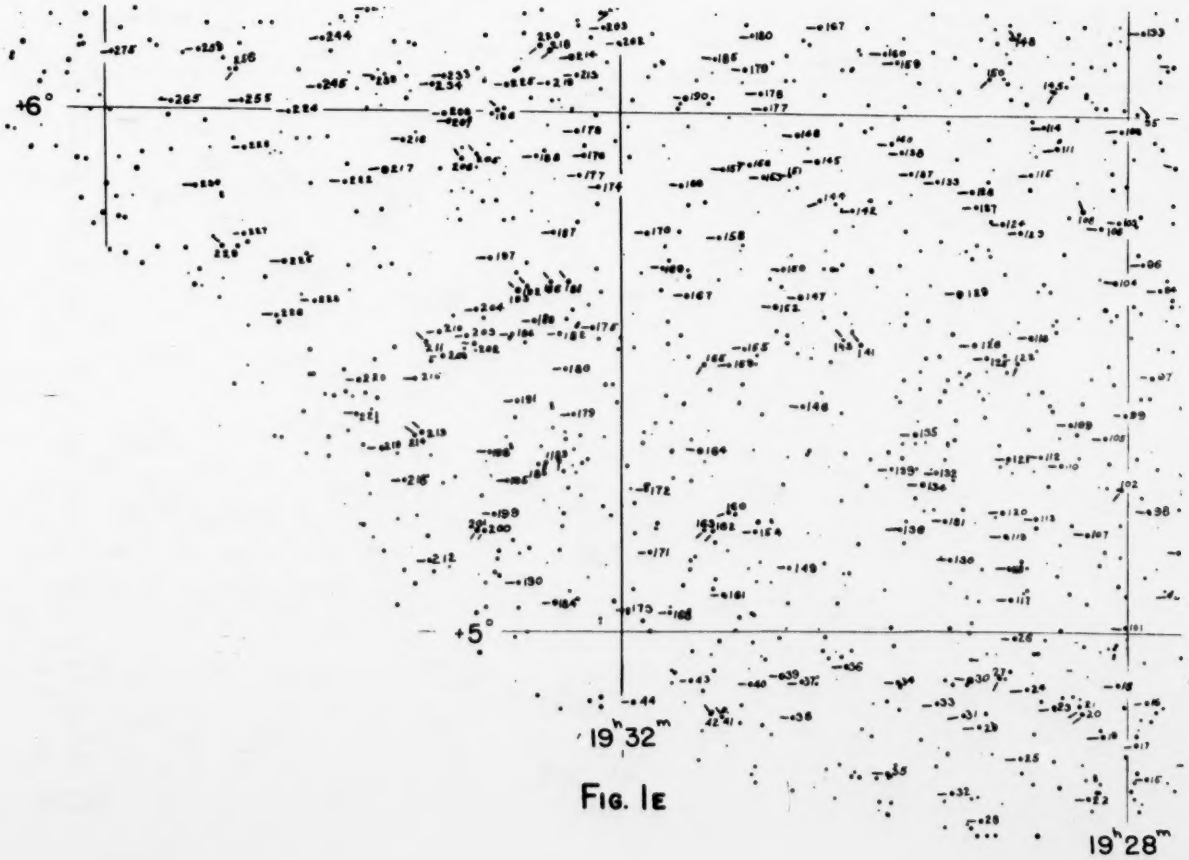

FIG. 1E

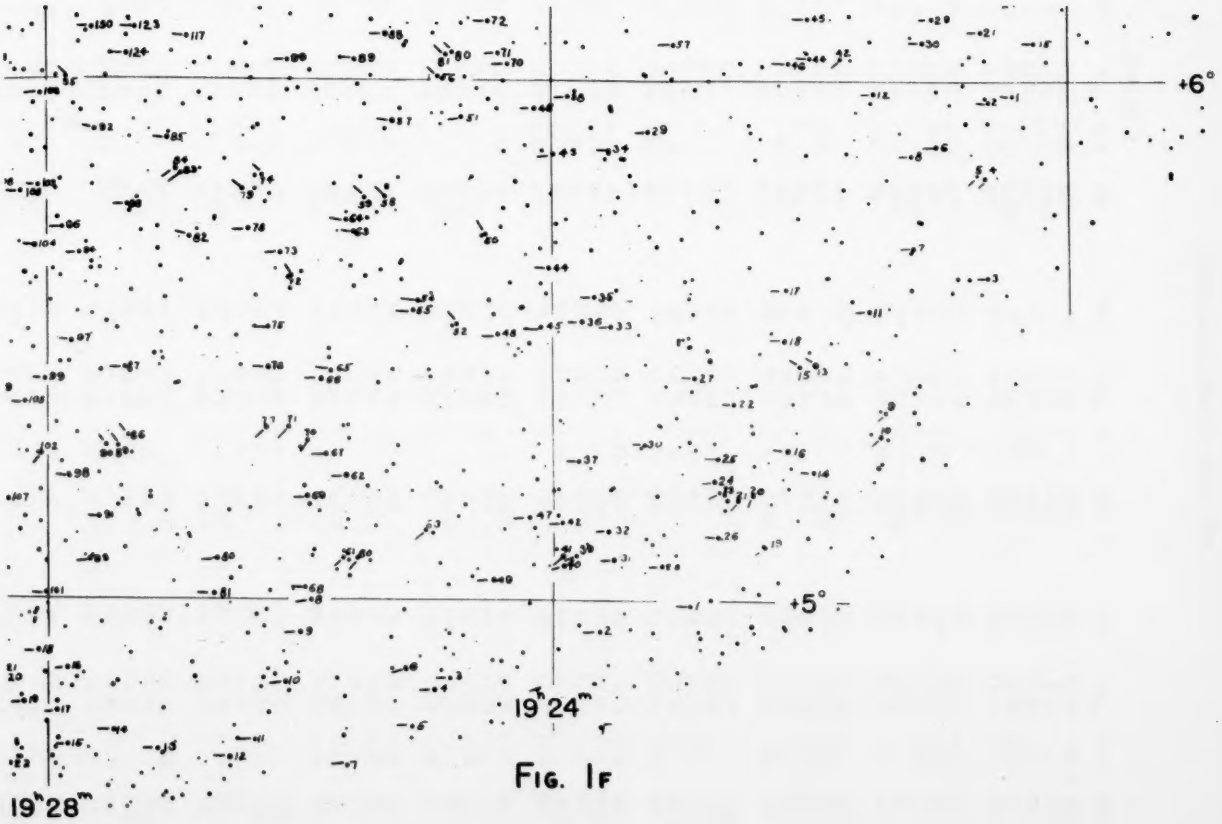

FIG. 1F

Table 1

Observational Data for Region LF1

Zone +4°

No.	m_{pg}	R. I.	Sp.	No.	m_{pg}	R. I.	Sp.	No.	m_{pg}	R. I.	Sp.
1	12.18	-.07	B9	6*	11.60	...	G5V	56	12.33	+.09	B8
2	11.74	...	G8III	7	11.78	...	G2V	57*	9.49	...	K0III
3	12.19	...	G0	8	12.67	+.54	A0	58*	11.84	...	F5
4*	10.80	...	K5III	9	12.30	+.05	B8	59	12.58	+.24	A0
5	12.19	...	F8	10*	10.85	-.33	B9	60	11.78	...	G5V
6	12.22	+.06	A0	11	11.83	...	G5V	61	12.14	+.15	A2
7	12.28	+.50	A5	12	11.78	+.55	A5	62*	8.73	-.23	B9
8*	11.78	...	G8III	13*	7.99	...	G0V	63	11.77	-.31	B8
9*	10.53	...	G5V	14*	11.83	...	G8III	64	12.10	...	F5
10	11.52	+.15	B9	15	12.06	+.20	A0	65	12.13	...	G0:
11	12.89	...	M5	16*	9.03	...	F5V	66*	10.80	...	M5III
12*	10.32	-.21	A0	17	12.17	...	G8III	67*	10.32	+.19	A3
13	12.10	...	F2	18	12.34	...	F0:	68	12.46	+.17	B8
14*	11.36	-.46	B9	19	12.25	-.21	A0	69*	10.80	...	F5V:
15	11.95	...	F0	20*	10.90	...	K0III	70	12.31	+.19	A5
16*	11.17	...	G5III	21	11.34	...	F0	71	11.78	...	G5III
17	11.64	...	F8	22	11.83	-.04	B8	72*	12.03	...	K2III
18*	11.32	...	G0	23	11.87	+.10	B9	73	12.01	+.59	A5
19*	10.83	+.06	A3	24*	10.25	-.12	A3	74	12.58	...	K0III:
20	12.04	+.21	B9	25*	12.13	...	G5:	75	11.94	+.20	B8
21	12.25	+.13	A2	26	12.07	+.29	B8	76*	9.74	-.08	B8
22	12.10	+.06	B8	27	10.61	...	G5V	77*	10.08	...	G0IV
23	11.64	-.13	B8	28*	11.41	...	K5III	78	11.47	...	A0
24	12.73	+.11	A0	29*	11.78	+.18	B8	79*	12.06	...	K0III
25	12.06	+.33	A0	30	12.10	...	G5:	80*	11.06	-.08	B9
26*	11.15	+.43	A3	31*	9.65	...	K0IV	81	11.36	+.27	B9
27	11.15	...	G0	32*	10.26	-.11	B8	82	11.60	...	F0
28*	11.36	...	G5V	33*	12.06	...	F0	83	12.06	+.02	A0
29	12.75	...	K0III	34*	10.95	...	G8III	84*	11.23	...	F8
30*	7.16	...	B9	35	12.10	...	G0	85*	10.67	-.42	B9
31	12.26	-.07	B8	36	11.15	...	F0	86	12.79	+.21	B9
32	11.90	...	G5III	37*	11.78	...	K2III	87	12.47	+.47	B8
33	12.00	+.13	A0	38	12.24	...	F0	88	12.73	+.39	A0
34*	11.25	...	F8	39	12.10	...	M2III	89	12.48	+.44	B9
35*	11.05	...	G5V	40	9.98	.00	A2	90	12.31	+.10	B9
36*	10.64	+.16	B8	41*	9.30	-.16	B9	91*	11.83	...	G5V
37	12.22	+.10	A3	42	12.13	-.07	B8	92	11.95	...	G5III
38	12.04	+.01	B9	43	12.42	+.17	A0	93	11.17	+.31	B9
39*	7.84	...	M5III	44*	11.78	...	K0III	94	12.25	+.13	B9
40	11.36	...	G0	45*	12.06	...	G8III	95	12.37	...	F8
41	11.88	...	F8	46*	10.89	...	F8IV	96	12.35	-.02	B8
42	12.16	...	K5III	47	11.15	-.45	B8	97*	10.61	...	F8IV
43	11.90	...	B9	48	11.64	+.08	B8	98	12.28	...	G8III:
44*	10.09	-.33	B5	49*	10.10	+.02	A0	99	12.47	+.18	A0
				50	12.25	+.29	A0	100	12.06	+.23	A5

Zone +5°

1R	12.66	...	K5	51	12.53	+.15	A0	101	12.27	...	F0
2*	12.26	...	K0III	52	12.13	+.31	A5	102	11.64	-.27	B8
3	12.25	+.47	B8	53*	12.13	-.04	B8	103	12.10	...	F0:
4	12.38	...	G8III:	54	11.57	...	F8	104*	9.93	-.30	B9
5	13.06	...	M5III	55	12.70	...	A0	105	12.13	...	K0III

Table 1

Observational Data for Region LF1 (Cont'd)

Zone +5° (Cont'd)

No.	m_{pg}	R. I.	Sp.	No.	m_{pg}	R. I.	SP.	No.	m_{pg}	R. I.	Sp.
106	11.84	...	G5V	156	12.04	+.38	A5	206	12.04	...	F0
107*	11.12	+.17	A0	157	11.83	+.23	A5	207	11.65	...	F0:
108*	9.93	...	F0III	158	12.00	...	G5III	208*R	10.12	-.46	B8
109	11.36	...	F8	159	12.04	+.01	B9	209*	10.95	...	G5III
110R	12.06	...	F8	160	11.83	-.20	A0	210	11.15	...	F0
111	12.25	...	G8III:	161*R	10.80	+.44	A5	211	11.66	+.05	A2
112	12.48	+.32	B8	162	12.13	+.14	A0	212	12.04	+.08	A0
113*	11.52	+.24	A3	163	12.59	...	M2	213	10.99	...	F0III
114	12.13	...	F0	164*	7.65	...	M8V	214	12.43	+.26	A0
115	12.35	+.32	A0:	165*	11.45	...	F8	215	12.17	+.05	A0
116*	9.43	...	F0III	166*	11.83	...	G8III	216	11.25	-.07	B9
117*	11.66	...	G8III	167*	9.77	+.26	A5	217*	7.24	...	G8III
118*	10.72	...	F8V:	168	12.26	+.01	B9	218	12.04	...	F0
119*	10.61	...	G5V	169	11.78	-.04	A0	219*	10.26	...	F8III
120*	10.35	...	F8III	170	10.70	...	F8III	220*	10.81	...	G8III
121*	9.86	...	K0IV	171	12.13	...	M0III	221	11.88	-.11	B8
122	12.15	+.19	B8	172*	12.00	...	K2III	222	12.07	...	K0III
123	11.78	...	F2	173	12.13	-.22	A0:	223	12.34	+.17	B9
124*	11.16	...	K0III	174	12.13	-.03	A2	224	12.27	-.19	A0
125R	11.72	+.44	A3	175*R	11.25	...	G5V:	225*	10.57	...	F5III
126*	9.93	...	K2III	176	11.45	-.06	A0	226	12.13	+.53	A0
127	12.17	...	K3III	177	12.42	+.14	A0	227*	12.36	-.02	A0
128*	10.35	-.22	A0	178*	11.05	...	K0III	228	12.31	...	G5:
129*	7.04	...	F2III	179	12.17	...	G5III	229*	11.71	...	G2V
130	12.13	...	G8V	180	11.88	...	G0	230*	11.92	...	G5III
131	11.88	...	K0III	181	10.47	+.61	B8	Zone +6°			
132	11.66	...	F0	182	11.45	...	G0	1	12.56	-.49	B8
133	12.31	...	G5:	183	10.93	-.03	A2	2	12.66	+.49	B8
134*	9.15	...	G8IV	184*	8.71	+.32	A5	3	12.31	+.36	A0
135*	9.94	...	G8III	185	12.13	...	K0III	4*	12.32	...	K0:
136	12.55	+.05	A0	186	12.17	...	F8	5*	11.49	...	G5V
137	12.31	+.05	B8	187	12.13	...	G8III	6*	8.91	+.08	A5
138	12.10	+.32	A2	188	12.13	-.37	A0	7	11.65	+.19	B8
139	12.25	...	A5	189*	10.80	...	G8III	8	12.04	+.50	A3
140	11.78	...	G8III	190	11.83	-.43	B9	9*	11.43	...	K2III
141*	10.99	...	F8III:	191	11.88	...	K0III	10*	10.55	...	G5III
142	12.33	+.37	A3:	192	12.35	...	K0III:	11	12.25	+.26	B8
143	12.10	...	G5V	193*	8.80	-.22	B8	12	11.88	...	G5V
144	11.88	+.02	B9	194	11.92	...	G5V:	13*	11.87	...	M2III
145*	9.40	...	K0III	195	12.08	...	G5V:	14*	12.35	...	G8III
146*	11.88	...	K5III	196R	11.45	...	F2	15*	12.13	...	G8III
147*	8.79	...	F5V	197*	11.15	...	G2V	16	12.08	...	K0:
148*R	10.00:	...	K3III	198	11.83	...	F2	17	12.47	+.51	A0
149	12.52	+.31	A0:	199	11.95	-.22	B9	18*	10.70	-.21	B8
150	10.71	-.43	B8	200	11.83	...	F5	19	12.13	...	G8V
151	12.22	+.02	A0	201*	10.22	...	G5III	20	12.17	...	G5V
152*	9.05	...	K0III	202	11.49	...	G8III	21	11.67	+.48	A3
153	11.83	-.25	B8	203	12.00	...	F0	22	12.86	+.78	B8
154*	11.15	...	G5III	204*	11.66	+.15	A0	23	12.69	+.53	A0
155	12.62	+.29	A2	205	12.90	...	K0III:	24	11.87	...	G8V
								25	12.31	+.14	A0

Table 1

Observational Data for Region LF1 (Cont'd)

Zone +6° (Cont'd)

No.	m_{pg}	R. I.	Sp.	No.	m_{pg}	R. I.	Sp.	No.	m_{pg}	R. I.	Sp.
26	11.83	+.28	B8	76	12.06	+.32	B8	126*	12.01	...	G2V
27	12.08	...	G0:	77	11.59	+.36	A2	127*	11.66	...	G8III
28*	10.79	-.17	B9	78*	10.79	...	K0III	128*	9.94	...	K0III:
29	12.10	+.46	A0	79	12.19	+.07	B9	129	11.95	+.09	A0
30*	10.79	-.07	A2	80	12.35	+.44	A0	130*	11.72	...	G8III
31*	11.15	...	F8	81*	11.89	+.25	A0	131	12.37	+.33	A0
32	12.73	+1.08	B8	82*	11.94	+.03	B5	132	11.15	...	G0
33*	11.34	+.02	B8	83*	11.36	...	M2III	133	11.32	+.23	B8
34*	11.06	-.08	B8	84	11.81	...	F0	134	12.14	+.02	B9
35*	10.11	+.03	B8	85	12.10	+.02	A0	135	12.43	...	G8III
36	12.27	...	G0:	86	12.35	...	K5III	136*	11.90	...	G0
37	11.41	-.10	B8	87	11.57	+.06	B8	137*	9.87	...	G5III
38	12.00	+.01	B8	88*	8.87	+.12	B9	138	11.90	...	F0
39	12.74	+.45	A0	89	12.06	...	G0	139	12.87	...	K0III
40*	12.08	...	M5III	90	12.50	...	F0	140	11.15	...	F0
41*	11.83	...	F0	91*	11.94	...	G8III	141	12.13	+.09	A0
42	12.60	+.43	A0	92*	10.35	-.02	B8	142	12.06	...	F0
43	11.28	+.23	A0	93*	10.80	...	G5V	143*	11.27	...	F2
44	12.77	...	G5:	94	12.28	...	G8V	144*	11.59	...	K0III
45	12.49	...	G0:	95	11.34	+.34	A3	145	12.13	...	F0
46*	12.54	...	K0III	96	12.25	-.01	B8	146*	8.96	...	G2Ib
47	12.13	...	K2:	97	12.22	...	G2V	147	12.36	+.24	B9
48*	11.15	...	K0V	98	12.10	+.11	B9	148	12.06	+.07	A0
49	12.60	+.52	B9	99	12.63	...	K0III	149	11.36	+.13	A3
50*	11.49	...	K0III	100*	12.22	...	K0:	150	12.36	+.02	A0
51*	9.30	-.27	A0	101*	12.84	...	K0:	151	11.45	...	F8
52*	12.25	...	G8III	102*	11.66	...	K3III	152	11.96	+.18	B9
53	12.03	...	G8III:	103*	8.30	-.13	B9	153*	9.86	...	G5III
54*	11.83	+.27	A0	104	12.13	...	G5V:	154*	7.75	-.23	B8
55	12.17	+.09	B9	105*	10.81	-.05	A0	155*	9.34	-.23	B9
56	11.45	...	F8	106	11.25	-.02	B8	156	11.52	-.17	B9
57	12.15	+.07	B5	107	11.89	-.02	B8	157*	10.09	-.44	B9
58*	10.43	+.55	A2	108	11.94	+.07	B8	158*	7.85	-.60	B8
59*	12.30	...	G5III	109	12.10	...	G8III	159	11.78	...	F5
60*	10.61	+.08	A0	110	11.71	...	F0	160	12.06	...	F8
61	12.28	...	F0	111*	12.10	...	K5III	161*	9.15	...	F2V
62	11.83	...	G0	112*	11.45	...	F8	162*	11.90	...	F8
63*	11.90	...	F2	113	12.47	...	G5III:	163*	9.13	-.43	B9
64	12.34	...	G5III	114*	10.10	+.43	A5	164	11.05	+.24	A3
65	12.24	+.16	B9	115	11.99	+.48	A3	165	12.22	...	G0:
66*	12.73	...	K0III	116	12.10	+.06	B8	166*	10.61	-.11	B8
67*	12.20	...	K0III	117	11.73	+.13	A0	167*	10.09	...	G8III
68*	9.12	-.19	B9	118	11.78	+.32	B9	168*	11.32	...	F0
69	11.96	+.22	A0	119	12.19	+.11	B8	169	11.27	.00	B9
70	12.22	+.05	B8	120	12.82	+.24	B8	170*	12.04	...	K5III
71	12.28	...	G0	121*	11.69	+.46	A5	171	12.08	...	G5V
72*	11.52	+.19	A0	122	12.27	-.17	B8	172*	11.15	...	F2
73	12.10	+.19	A0	123*	11.97	+.37	A0	173	12.26	...	K0III
74	12.19	+.19	A0	124*	11.21	-.11	B5	174	11.88	...	F2
75	11.64	+.78	A5:	125*	9.94	-.29	B8	175	12.46	-.08	A0

Table 1

Observational Data for Region LF1 (Cont'd)

Zone +6° (Cont'd)

No.	m_{pg}	R. L	Sp.	No.	m_{pg}	R. L	Sp.	No.	m_{pg}	R. L	Sp.
176	12.00	-.08	B5	226	12.21	...	A5	276*	11.36	...	G8V
177	12.25	+.05	A0	227	12.08	...	G5V	277*	11.66	...	G5V
178	11.45	-.41	B8	228	12.88	...	G5III	278*	10.23	+.15	A5
179*	10.89	...	G8V:	229	12.11	...	G0	279*	10.43	...	F0V
180	12.51	...	M5V:	230	11.50	-.45	B8	280	11.79	-.16	A0
								Zone +7°			
181	12.04	...	G0	231	11.96	...	M2III	1	12.38	-.01	B8
182*	11.41	-.06	A3	232	11.88	...	G0	2*	8.60	...	F2V
183	11.05	...	G0	233*	10.86	...	G0V:	3	12.13	...	A5
184*	10.08	-.25	B9	234*	11.05	...	K0III	4	10.95	-.42	B8
185	12.31	+.11	B8	235*R	10.09	-.48	B9	5*	10.06	+.03	B8
186	12.25	-.04	A0	236*	11.15	...	M2III	6*	11.44	...	G2V
187	11.36	-.10	A0	237	11.92	-.24	B9	7*	8.82	-.69	B8
188	11.78	...	G0:	238*	10.72	+.34	A0	8	12.04	...	K0III
189*	9.74	...	G8IV	239	12.39	...	G5III	9*	11.60	+.27	B9
190*	9.15	...	G5III	240*	11.79	...	G5V	10*	8.48	+.29	A0
191	11.88	...	F8	241*	10.78	...	G2V	11*	11.24	...	G8V
192	12.08	...	G5V	242	12.13	-.03	A0	12*	9.33	-.44	B9
193*	11.05	...	G5V	243	12.32	+.12	A0	13*	9.77	...	G2V
194*	9.92	+.10	B9	244	11.67	+.07	A0	14*	10.13	-.09	B8
195*	10.73	-.60	B9	245	11.96	...	G0	15*	11.76	...	K0III
196	11.36	-.51	A0	246*	9.40	...	K2III	16*	9.43	...	K5V
197*	11.96	...	M2III	247	12.05	+.01	A5	17*	11.56	...	G8V
198	11.66	...	G8III	248*	10.81	...	G2IV	18	12.60	+.23	B8
199	12.10	-.02	B9	249*	9.40	-.26	B9	19	12.38	...	G8III
200	11.41	-.61	B8	250	12.32	...	G8III	20	11.35	+.30	A2
201*	12.18	...	K0III	251*	11.16	...	G5V	21*	8.73	-.68	B8
202	12.26	...	K0III	252	11.15	...	G0	22	10.61	-.01	B9
203	12.59	...	M2	253*	9.75	-.23	B9	23	12.38	+.30	B8
204*	11.34	...	G5III	254*	10.60	...	F8V	24	10.61	-.44	B8
205	12.00	-.15	B8	255	12.46	...	K0III	25	12.13	...	G5III
206*	9.05	+.05	A0	256	11.71	...	K2V	26	11.46	-.18	A0
207*	11.05	...	G5V	257	11.88	+.02	A5	27	11.90	+.48	B8
208	12.17	...	G0:	258*	8.94	-.57	B5	28*	10.04	...	G5III
209	12.26	...	F5:	259*	11.71	...	G5III	29*	8.78	-.47	B8
210	12.37	...	K0III	260*	11.79	...	G0	30*	8.23	-.48	B8
211*	10.61	...	G5V	261*	11.05	-.28	B9	31	12.10	+.36	A3
212*	10.33	...	K0III	262	12.10	+.03	A5	32*	10.22	+.24	A0
213	12.13	+.01	B9	263	12.43	...	K0III	33	11.88	+.23	A0
214*	7.75	+.23	A2	264*	10.09	...	K3III	34*	11.15	...	G8III
215*	9.49	-.23	A0	265	12.17	...	G0	35*	11.45	...	G5III
216	11.14	...	F2	266*	11.83	...	F5	36	12.28	+.29	A0
217*R	10.12	...	F2III	267	12.17	+.75	A0	37	11.25	...	F0
218*	10.26	...	M0III	268	12.49	-.09	A0	38	12.45	+.10	A0
219	12.17	...	G8III	269*	10.26	...	G8IV	39	12.01	...	G5III
220	10.44	-.38	B8	270	11.92	...	F2	40	12.08	-.35	B8
221*	11.53	...	K5III	271*	10.37	...	G5III	41*	10.80	+.03	B9
222	11.23	...	F0:	272	11.88	+.37	B9	42*	8.70	-.07	A2
223*	10.09	-.13	B9	273	12.47	...	K0III	43*	10.07	-.06	B9
224*R	10.09	+.11	B8	274*	11.77	...	G8III	44	12.28	+.11	B9
225	10.61	-.11	B9	275	12.08	...	K0III	45	12.28	+.15	B8

Table 1

Observational Data for Region LF1 (Cont'd)

Zone +7° (Cont'd)

No.	m_{pg}	R. I.	Sp.	No.	m_{pg}	R. I.	Sp.	No.	m_{pg}	R. I.	Sp.
46	12.30	...	G8III	96	12.06	...	G0:	146*	10.00	...	G8V
47	12.28	+.33	A2	97	11.89	...	G0	147	12.04	-.08	A0
48*	8.97	...	F2III	98	11.94	+.03	B8	148*	11.16	+.11	A3
49	12.06	-.02	B8	99*	11.05	...	G8III	149	12.25	...	G5III
50*	9.10	...	F2V	100	11.94	-.02	B8	150*	11.52	...	G5III
51	12.00	+.35	A0	101*	11.78	...	G5III	151	12.25	-.05	A0
52	12.18	+.44	A5	102*	8.54	-.40	A2	152	10.99	-.15	B9
53	12.27	...	G0:	103*	11.83	...	G2V	153*	11.12	...	G0
54	11.27	-.20	B8	104*	11.36	-.28	A0	154	11.66	...	G2III
55	12.10	+.07	B8	105	10.70	-.07	A2	155*	9.25	...	G0V
56	12.46	+.60	B8	106*	10.17	...	M0III	156*	10.09	-.54	B9
57	12.25	...	G5III:	107*	9.38	-.14	A0	157	11.57	+.01	A5
58*	8.29	...	F0III	108*	12.13	...	M0III	158	11.88	...	F8
59	12.18	+.06	B8	109*	11.64	...	K2III	159*	9.37	+.04	A0
60	11.23	-.14	B9	110*	10.73	...	K0III	160	10.80	-.34	B9
61	12.10	...	G0	111	11.64	...	G8III	161	11.60	-.39	B8
62	12.25	+.13	B8	112	11.57	+.06	B8	162*	10.99	...	G8III:
63*	11.96	...	F0	113	11.27	+.32	A0	163*	10.84	+.07	A0
64*	9.84	...	G5III	114*	9.68	...	F0III	164*	11.06	...	G8V
65	12.37	...	G5:	115	12.10	+.10	A0	165*	7.94	...	K2III
66*	11.02	-.40	B8	116*	12.00	...	G5III	166	12.10	-.09	A0
67	12.09	...	G0	117*	9.40	-.18	B9	167	11.78	...	F8
68	12.06	...	G5V	118	12.01	...	F0	168	11.83	...	G0
69*	10.54	+.16	A5	119	12.06	...	F0:	169	11.52	...	G0
70*	11.64	...	K0III	120*	9.94	-.17	B5	170	12.31	...	K0III
71	12.50	+.24	A3	121	11.06	...	G0	171	12.13	...	G0:
72*	10.37	+.14	B9	122*	10.90	...	G8III	172	12.10	...	G5III
73*	12.38	...	K3V:	123	12.27	+.19	B9	173*	10.09	-.44	B8
74*	10.35	-.12	B8	124	12.25	...	K2III	174	12.00	-.04	A0
75*	10.99	...	F5V	125	12.46	+.33	A0	175*	11.40	-.06	B8
76	11.89	...	G5III	126	11.36	...	F0	176*	8.04	...	F2III
77	11.64	-.16	B8	127	11.36	...	F5	177*	10.35	-.27	A2
78	12.18	...	G0	128*	10.89	-.02	A2	178	12.13	...	G5V
79	12.31	...	F0:	129*	12.06	...	K0III	179	12.22	...	K0III
80	12.37	+.11	B8	130	12.13	+.09	A0	180*	10.08	...	G5V
81	12.10	...	G5V	131*	10.09	+.11	A2	181	12.16	...	K0III:
82	12.34	+.17	A5:	132*	10.09	...	K0IV	182*	10.56	-.54	B8
83	11.65	-.26	B8	133*	11.45	...	K0III	183*	11.05	...	F8
84	12.06	+.11	A3	134	10.83	-.31	B9	184	11.90	...	F0
85R	11.89	+.07	A2	135*	11.23	.00	B8	185*	10.93	-.21	B9
86	12.10	...	G8III	136	12.10	...	G8III	186	10.68	-.46	B8
87	12.06	+.06	B9	137*	9.93	.00	B8	187	12.13	-.25	A0
88*	11.78	...	K2III	138	11.78	...	G5III	188*	7.50	...	B8
89	11.96	+.19	B9	139*	10.15	+.17	B9	189	10.54	-.27	A0
90*	9.86	-.02	A0	140	12.10	...	G5V	190	11.05	-.14	A2
91	12.27	...	G5V	141*	10.25	-.42	B9	191	12.40	...	A0:
92	12.13	...	G5III	142*	10.83	-.03	A2	192	12.08	-.05	A0
93	12.06	...	G5V	143	12.36	+.09	B8	193	11.83	-.15	A0
94*	11.57	...	G0	144*	11.19	...	G2V	194	10.80	-.72	B8
95	11.94	+.08	B8	145	11.61	-.60	B8	195R	11.72	-.32	B8

Table 1

Observational Data for Region LF1 (Cont'd)

Zone +7° (Cont'd)								Zone +8°			
No.	m_{pg}	R. I.	Sp.	No.	m_{pg}	R. I.	Sp.	No.	m_{pg}	R. I.	Sp.
196*	7.75	...	B8	246*	10.95	...	G5V	1*	10.43	...	F0III
197	11.36	-.20	B8	247	11.88	...	G5III	2*	11.25	...	G0
198*R	6.89	-.78	B2	248	11.24	-.77	B8	3	12.12	...	G0
199	11.45	...	G0	249	10.85	...	G0V	4	12.20	+.11	B8
200	11.83	-.25	A0	250	11.92	...	G5III	5	12.31	...	K0III
201*	10.80	...	G8III	251	12.32	...	G8III	6*	11.88	...	G5III
202	11.71	...	G5V	252	11.35	-.56	A0	7	12.19	+.02	B8
203	11.05	-.28	A3	253	11.57	...	F5	8	12.38	...	G5III
204	12.04	+.04	A0	254	12.10	...	G0	9	12.13	...	G0
205	11.52	...	F2	255*	9.15	-.72	B8	10	11.78	...	G5V
206	11.45	...	F2	256*	10.47	...	F0V	11	11.15	-.13	B8
207*R	5.65	...	K0III	257	11.96	...	G0	12*	10.54	...	K0V
208*	6.60	...	B5	258*	10.95	...	K0V	13*	11.05	...	K0III
209	11.96	...	K0III	259	11.24	-.32	B9	14	12.22	+.31	A5
210	11.52	...	F0	260	12.21	...	G8III	15	11.96	...	F2
211	12.00	...	G5III	261	11.97	-.07	A5	16	11.90	+.16	B8
212*	10.61	...	G8IV	262*	7.40	-.46	A3	17	11.38	-.27	B8
213	12.34	...	K2III	263	10.88	...	F2III	18	12.24	+.20	A0
214	12.04	-.12	B9	264	11.63	-.15	A0	19	11.95	+.53	B8
215	11.78	-.13	A0	265*	10.88	+.20	A2	20	12.22	+.14	A0
216	12.10	...	F0	266	11.66	...	G8III	21	12.57	...	M5
217	10.54	-.41	A0	267*	9.30	...	F0III	22	11.84	+.42	A5
218*	11.66	...	G8III	268	11.24	-.54	B9	23*	9.15	-.21	B8
219	11.34	-.03	A2	269*	10.73	...	K0V	24	12.06	-.07	A0
220	11.05	...	F8	270	10.22	...	F8	25*	10.73	+.15	B9
221	11.66	+.15	A3	271*	8.70	...	G0IV	26*	12.28	...	G5III
222	12.13	-.01	A2	272	12.22	+.02	B8	27	12.31	...	K0:
223	11.05	-.46	B8	273*R	9.89	-.19	B8	28*	12.25	...	K2III
224*R	10.26	-.17	A0	274	11.91	...	F5:	29	11.90	-.05	B9
225*R	10.31	...	M5III	275	11.33	...	G0	30	12.06	...	K0III
226*	9.56	...	K0IV	276*	10.41	+.13	A5	31	12.28	...	F0:
227*	10.72	+.19	A3	277	11.87	...	G0	32	11.24	-.13	B8
228	12.13	...	B8	278*	10.63	...	K5III	33	12.10	...	G0
229*	9.93	...	G0IV	279*	11.33	-.33	B8	34	12.38	...	G0
230	11.92	-.12	A5	280	11.96	...	G2V	35	12.22	...	G8III
231*	11.15	...	F0	281	11.93	...	F5	36*	12.06	+.37	A0
232*	11.45	...	G0	282	11.76	+.25	B8	37	12.10	...	G8III
233*	10.89	...	G5V:	283	11.60	...	G5V	38	12.47	...	G0:
234	11.78	...	G0	284*	9.53	+.15	A2	39	12.67	...	K0III:
235	12.04	-.12	A0	285	11.61	-.11	B8	40*	10.10	+.07	A3
236*	11.34	...	F2	286R	11.68	-.10	A0	41	12.87	...	M2
237	12.04	...	G0	287	12.00	...	G0	42*	10.47	...	F5V
238*	11.71	...	G5III	288*	9.63	-.35	B9	43	12.18	+.10	B8
239*	9.73	...	F0III	289*	10.46	-.27	B8	44	11.06	...	G2III
240	12.08	...	G5V	290	11.28	-.27	A0	45	12.06	...	G0
241*	10.26	-.78	B8	291*	10.57	...	G8III	46*	10.01	...	G5III
242	12.53	...	K5III	292	11.60	...	K0III	47*	11.90	...	G5V
243	12.13	...	K0III	293*	10.47	+.03	A5	48	12.31	...	G5III
244	11.82	...	G5V	294	11.84	...	G0	49*	10.46	...	G8IV
245	12.50	-.31	B9	295	11.81	...	K5III	50*	11.78	...	G5III

Table 1

Observational Data for Region LF1 (Cont'd)

Zone +8° (Cont'd)

No.	m_{pg}	R. I.	Sp.	No.	m_{pg}	R. I.	Sp.	No.	m_{pg}	R. I.	Sp.
51	12.10	...	G5V	81*	8.45	...	G0IV	111*	9.25	-.32	B8
52	12.22	+.35	A0	82*	12.06	...	G5V	112	12.13	+.05	B9
53*	8.52	...	G2IV	83	11.78	...	G0	113	12.00	...	G0
54*	10.03	...	B8	84*	11.34	...	G5III	114	11.72	...	F9:
55*	7.65	...	F0III	85*	9.86	...	G2V:	115	12.11	...	G5III
56	11.60	-.09	B9	86	11.15	...	G8III	116	12.13	...	K0V
57	12.22	...	F0	87*	10.80	+.23	A5	117*	8.17	-.80	B8
58	11.15	...	A5	88	11.52	...	G0	118*	11.15	...	F2
59*	10.80	-.16	B8	89	10.90	-.47	B9	119*	8.38	...	K0III
60	11.15	-.17	B8	90	10.74	+.45	A0	120*	10.47	-.39	B8
61*	11.95	...	G8III	91	12.00	...	G0	121	11.57	-.12	B8
62	12.36	...	B8	92*	9.67	...	G5V	122	11.84	...	F8
63	10.46	+.13	B9	93	11.15	...	F5	123	11.46	...	G5V
64*	10.99	-.01	A0	94*	11.05	...	K2III	124	12.04	...	G8III
65	11.88	...	G2V	95	11.83	+.14	A0	125	12.00	...	G5V
66	12.31	...	G5V:	96	11.83	-.08	B9	126*R	9.30	...	A3-F5
67*	11.05	...	F5V	97	11.78	-.13	A0	127	12.29	...	K0III
68	12.25	...	F0	98	11.67	+.17	A5	128	10.74	-.03	A0
69	12.13	+.12	A5	99*	10.54	...	G8IV	129	12.10	...	G5III
70	11.15	-.50	B9	100	12.04	...	G5III	130	11.83	...	K5V
71	12.06	+.07	B9	101	12.17	...	G5V	131*	9.15	-.21	B5
72*	11.25	...	K0III	102*	11.92	...	G8III	132	12.26	...	K0III
73	11.86	-.27	A2	103	11.64	-.35	B9	133	11.76	...	F5
74*	11.88	...	G5V	104	11.78	+.55	A5	134*	12.13	...	K5III
75	12.31	+.18	A0	105*	11.15	-.27	A0	135	11.89	...	F8
76*	9.86	+.14	B9	106	11.95	...	G5V	136	10.80	-.64	B8
77	12.16	...	G8III	107	11.53	-.46	A0	137*	9.82	...	F0III
78	11.15	-.08	A2	108	11.37	...	G5III	138	12.04	+.04	A2
79*	11.95	...	G5III	109*	8.87	-.16	A3	139	12.26	...	K2III
80	11.90	-.18	B8	110	11.46	-.33	A0	140	11.41	...	G5V

NOTES TO TABLE 1

ZONE +5°

1—Suspect variability.
110—$H\delta$ strong.
125—$H\gamma$, $H\delta$ sharp.
148—Suspect variability.
161—Hydrogen lines sharp.
175—50″ s.p. No. 175 is NGC 6807, a planetary nebula with stellar image on our plates. Emission lines of $H\alpha$, $H\beta$, $H\gamma$, $H\delta$, $H\epsilon$, [O III], [Ne III] are present; no continuum is evident.
196—$H\delta$ very strong.
208—Hydrogen lines sharp.

ZONE +6°

217—HD 184569 Sp. K0; appears to be in error in *HDC*.
224—Hydrogen lines sharp.
235—Hydrogen lines sharp.

ZONE +7°

85—Hydrogen lines sharp.
195—Hydrogen lines sharp.
198—HD 184362 Sp. A0; appears to be in error in *HDC*.
207—HD magnitude given.
224—Hydrogen lines sharp.
225—HD 184542 Sp. K2; appears to be in error in *HDC*.
273—Hydrogen lines sharp.
286—Hydrogen lines sharp.

ZONE +8°

126—Composite spectrum; K line weak, G band strong; hydrogen lines strong in ultraviolet.

established for the stars of the North Polar Sequence by Nassau and Burger.[2] Since the red magnitudes have a probable error of ± 0.08 mag., the resulting red indices have an internal probable error of about ± 0.12 mag.

The fourth column of Table 1 gives the spectral type and luminosity class of the star. Criteria for classification of the spectra have been published by Nassau and Seyfert,[3] while criteria for a more detailed luminosity classification of the F0–K5 stars have been published by Nassau and van Albada.[4] These criteria have been applied to the F0–G0 stars brighter than $m_{pg} = 11.0$ and also to the fainter stars of later spectral classes. The resulting luminosity classes on the system of Morgan, Keenan, and Kellman[5]

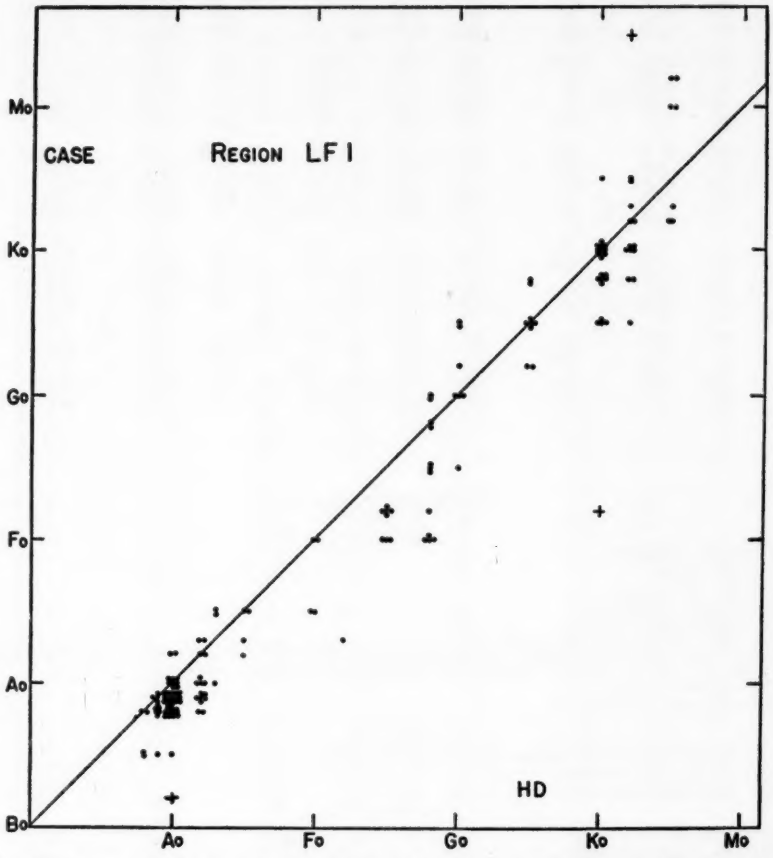

FIG. 2.—A comparison between the spectral classes determined at the Warner and Swasey Observatory with those of the *Henry Draper Catalogue*. Ordinate is the Case spectral class. Abscissa is the HD spectral class.

[2] *Ap. J.*, **103**, 25, 1946.

[3] *Ap. J.*, **103**, 117, 1946.

[4] *Ap. J.*, **106**, 20, 1947.

[5] *An Atlas of Stellar Spectra* (Chicago: University of Chicago Press, 1943).

are those included in Table 1. Class G5 III, for example, refers to an ordinary G5 giant, G5 V to an ordinary dwarf. Intermediate classes are assigned for the brighter stars where the details of the spectrum can be studied more accurately. The luminosity classes for stars with $m_{pg} > 12$ are uncertain.

COMPARISON WITH THE *Henry Draper Catalogue*

A comparison of the spectral types for 164 stars with those of the *Henry Draper Catalogue* is shown in Figure 2. There is a tendency for our spectral classes to be 0.1 or 0.2 earlier than those of the *HDC* at A0 and also at K0. A part of the latter trend may be due to the absence of class G8 in the *HDC*. The most serious departure, however,

TABLE 2

DISTRIBUTION OF LATE-TYPE STARS IN LUMINOSITY CLASSES

Sp.	$m_{pg} \leq 10.5$				$10.5 < m_{pg} < 12.5$	
	I	III	IV	V	III	V
F0	0	8	0	2	(1)	
F2	0	4	0	3	(1)	
F5	0	0	0	3	.....	
F8	0	2	0	0	(1)	
G0	0	0	4	2	(2)	
G2	1	0	1	2	2 (1)	11
G5	0	8	0	2	43 (3)	50
G8	0	3	4	1	50 (1)	9
K0	0	7	4	0	43 (2)	4
K2	0	3	0	0	11 (1)	1
K3	0	2	0	0	2	1
K5	0	0	0	1	12	1

appears to occur at class F. A re-examination of the spectra for six of these stars indicates definitely that they cannot be so late as F8, the type given in the *HDC*. Three very marked discrepancies where the HD class seems to be in error are shown by crosses in Figure 2. These stars are HD 184362, 184542, and 184569.

DISTRIBUTION OF GIANTS AND DWARFS

Table 2 summarizes the separation of the stars with spectral types F0–K5 into luminosity classes for two magnitude groups. Numbers in parentheses indicate the number of stars for which no luminosity class could be assigned.

SPECTROGRAPHIC OBSERVATIONS OF THE ECLIPSING VARIABLE SW LACERTAE*

OTTO STRUVE
Yerkes and McDonald Observatories
Received January 25, 1949

ABSTRACT

From twenty-seven spectrograms we find $\gamma = -22.5$ km/sec; $K_1 = 202.5$ km/sec, $K_2 = 172.5$ km/sec; $m_1/m_2 = 1.17$. The less massive component is eclipsed at principal minimum. The intensities of the components of the absorption lines vary in such a way that the advancing hemisphere of each star may be considered as having stronger lines and, therefore, probably an absorbing layer of greater thickness. There is an indication that the spectral type of each star is somewhat later at the tidal bulges than at the sides.

SW Lacertae is an eclipsing variable of the W Ursae Majoris type. Its position for 1950 is: $\alpha = 22^h51^m4$; $\delta = +37°39'$; and its apparent magnitude at maximum is 9.0. The period and epoch are given by the photometric observers as

$$\text{Principal minimum} = \text{JD } 2423372.780 + 0.32071561E .$$

The depth of the principal light-minimum is 0.8 mag.; that of the secondary is 0.7 mag. A few preliminary radial velocities were obtained at the Mount Wilson Observatory by

TABLE 1

STAR LINES

Fe I	4005.26	*Fe* I	4143.72
Fe I	4045.82	*Ca* I	4226.74
Fe I	4063.62	*Fe* I	4260.48
Fe I	4071.74	*Sc* II + *Fe* I	4325.64
Sr II	4077.73	*Hγ*	4340.49
Hδ	4101.75		

Adams, Joy, and Sanford,[1] and the spectra of both the two components visible in the spectrum of this system were given by Wyse[2] as G3p and G3p, respectively.

The purpose of this new investigation is to determine the orbital elements and the spectroscopic features of the components. Twenty-five spectrograms were obtained with the Cassegrain quartz spectrograph of the McDonald Observatory, giving a linear dispersion of 40 A/mm at λ 3933, and two with a camera of slightly smaller dispersion.

Table 1 gives the wave lengths of the star lines used in determining the radial velocities, and Table 2 lists the radial velocities. The times are geocentric, in accordance with my previous practice. The results of my measurements are plotted in Figure 1. Phase

* *Contributions from the McDonald Observatory, University of Texas*, No. 165.

[1] *Pub. A.S.P.*, **36**, 137, 1924.

[2] *Lick Obs. Bull.*, **17**, 37, 1934.

zero corresponds to principal mid-eclipse. The best circular elements of the orbit are as follows:

$$\begin{aligned}
\gamma &= -22.5 \text{ km/sec}, \\
K_1 &= 202.5 \text{ km/sec}, \\
K_2 &= 172.5 \text{ km/sec}, \\
m_1 \sin^3 i &= 0.28\odot, \\
m_2 \sin^3 i &= 0.33\odot, \\
a_1 \sin i &= 0.89 \times 10^6 \text{ km} \\
a_2 \sin i &= 0.76 \times 10^6 \text{ km}, \\
\frac{m_2}{m_1} &= 1.17, \\
T \text{ (min. vel.)} &= \text{Phase } 0.30P.
\end{aligned}$$

The shift in T from the predicted phase of $0.25P$ to the observed phase of $0.30P$ may be due to a small error (or a change) in the period. The departures of the observed radial velocities from the curves are somewhat systematic in character, but the precision of the measurements is not sufficient to warrant the computation of an elliptical orbit. The less massive component undergoes eclipse at principal light-minimum—a phenomenon which has already been commented upon in the case of several other W Ursae Majoris systems. But the mass ratio, $a = 1.17$, is much closer to 1 than is the

TABLE 2

RADIAL VELOCITIES OF SW LACERTAE

Plate	Date 1948	U.T.	Phase	Velocity (Km/Sec)	
				I	II
CQ 7161	Nov. 16	3:15	0.689	+176	−167
62	16	3:53	.773	+176	−191
63	16	4:22	.836	+176	−190
64	16	4:50	.895	+147	−158
65	16	5:19	.960	+110	−103
66	16	5:50	.025	− 33	.....
67	16	6:21	.094	− 44	.....
G *f*/2 11378	19	5:44	.368	−205	+138
79	19	6:16	.437	− 98	+130
CQ 7200	20	6:05	.527	− 29	.....
05	21	2:31	.184	−196	+114
06	21	3:19	.287	−228	+176
65	30	1:44	.143	−191	+128
66	30	2:10	.200	−211	+177
67	30	2:40	.265	−215	+130
68	30	3:08	.327	−216	+121
69	30	3:36	.387	−194	+116
70	30	4:05	.449	−121	+135
71	30	4:34	.511	− 29	.....
72	30	5:02	.574	+ 10	.....
97	Dec. 4	3:56	.904	+176	−147
98	4	4:23	.963	+109	− 94
99	4	4:56	.034	− 3	.....
7319	6	1:20	.801	+196	−194
20	6	1:55	.876	+193	−191
21	6	2:31	.954	+131	−119
22	6	3:06	0.031	− 29	.....

case in the other W Ursae Majoris systems. It is rather amusing that, after several astronomers, including myself, had recently commented upon the remarkable prevalence of values in the neighborhood of $\alpha = m_1/m_2 = 2$ among the W Ursae Majoris stars, the very first new orbit should give a perfectly "normal" ratio of 1.2. But it would be wrong to conclude that the former indications were spurious. On the contrary, the large average value of α is so well substantiated that it cannot be seriously doubted. The present result only shows that the dispersion of the mass ratios must be quite large—about between 1 and 3.[3]

Several representative spectra are reproduced in Figure 2. At phases in the vicinity $0.30P$ the violet component is very much stronger than the red component, but at

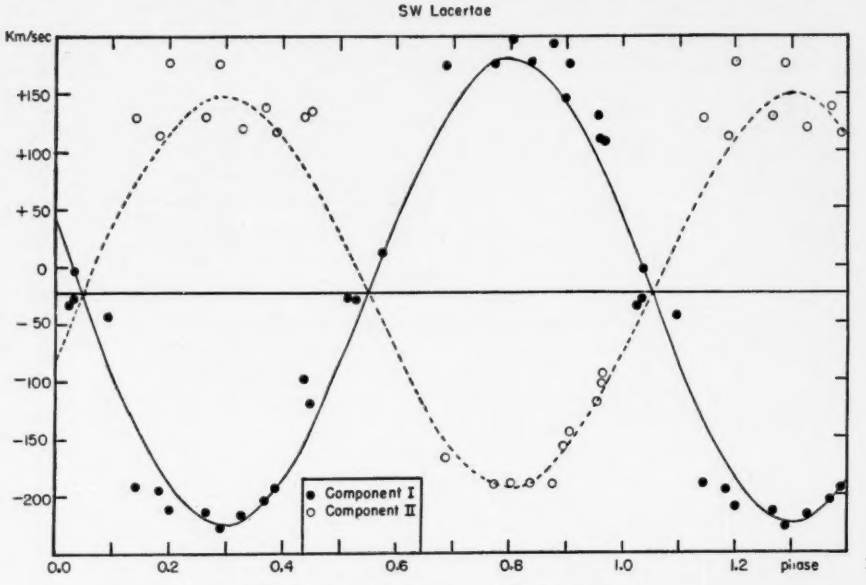

FIG. 1.—The velocity-curves of SW Lacertae

phases near $0.80P$ the difference in intensity is much smaller, the red component predominating in the plate at $0.773P$, while at $0.801P$ the two are almost identical. This is again the old phenomenon of variable line intensities which results in making each star appear relatively stronger when it approaches than when it recedes.

Perhaps the most interesting feature in Figure 2 is the great intensity of *Ca* I 4227 at phases $0.0P$ and $0.5P$ when the lines are single. During the double-line stages the *Ca* I lines do not predominate at all. In fact, *Fe* I 4045 is then appreciably stronger, and several other lines, including $H\delta$, are just as strong. I believe that this is a manifestation of the gravity effect, so that both components seen "end-on" have later spectral types than when they are seen at the elongations. I believe that there may also be a strengthening of the G band at the two eclipses, but the structure of this feature is so complex that it is difficult to be certain.

The absorption lines are quite diffuse and are clearly broadened by rotation, the amount of this broadening being about the same for both components.

[3] Nine other systems of the W UMa class give $\alpha = 1.4, 1.9, 2.0, 1.6, 1.5, 3.1, 2.4, 2.1$, and 2.5, respectively.

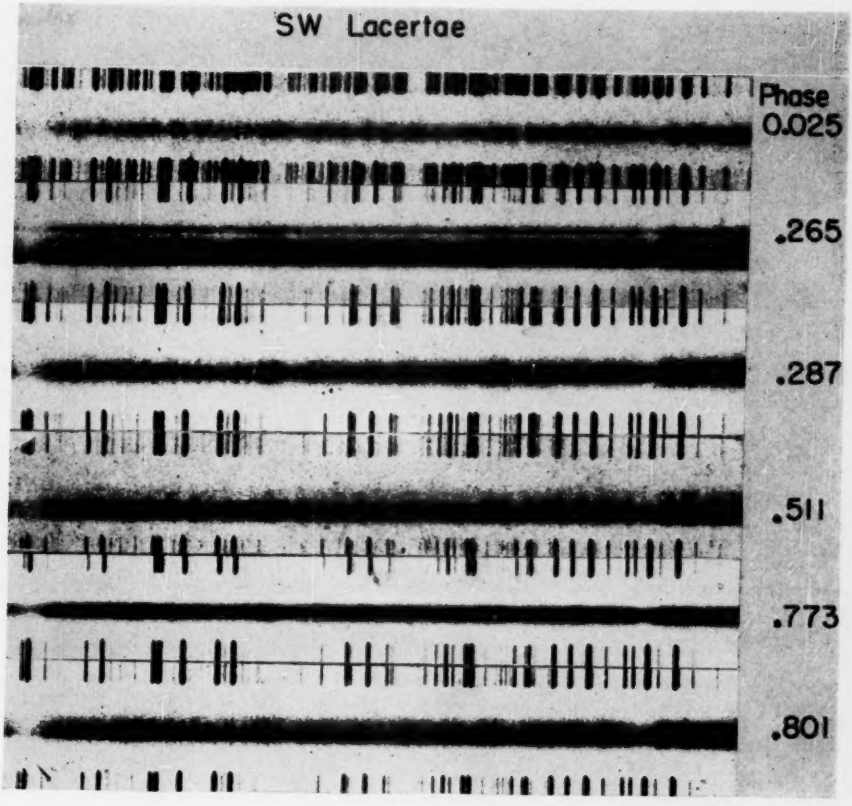

FIG. 2.—The spectrum of SW Lacertae

NEW SPECTROGRAPHIC INVESTIGATIONS OF THE ECLIPSING STAR XZ SAGITTARII

JORGE SAHADE
Observatorio Astronómico de Córdoba, Argentina
Received December 16, 1948

ABSTRACT

Spectrographic observations of XZ Sagittarii at Bosque Alegre show more clearly and convincingly than earlier work that we are dealing with an eclipsing system of very small amplitude in radial velocity, considering that the period is about $3\frac{1}{4}$ days. The assumption that the radial velocities result from the orbital motion of the primary star leads to a contradiction with the mass-luminosity relation. It is shown once more that the possibility of blending of the spectra of the two components must be discarded. The possibility of distortion of the velocity-curve is also considered.

THE PROBLEM

The eclipsing star XZ Sagittarii[1] was studied spectrographically for the first time in 1945 by the writer,[2] at the McDonald Observatory. The spectrograms taken at that time extended from $H\beta$ to about λ 3900; at maximum light they showed an A3 spectrum, when on a plate taken during predicted totality this spectrum appeared blended with one which was estimated as being of a late F or an early G type. As for the radial velocities, only four lines, namely, *Mg* II 4481, $H\gamma$, $H\delta$, and *Ca* II K were measurable; but the results from the *H* lines were so badly scattered that it was decided to rely only upon the lines of *Ca* II and *Mg* II, which were easier to measure. The plot of the mean values from *Ca* II K and *Mg* II 4481 still showed a large scatter but suggested that we were dealing with a system with an extraordinarily small amplitude in velocity, considering that the period is about $3\frac{1}{4}$ days. In fact, a tentative velocity-curve drawn through the plotted radial velocities indicated a value of *K* of 11.5 km/sec, which yielded a mass function $f(m)$ of 0.0005 $\odot$. The discussion of the photometric data showed that such a small amplitude could not be due to blending of the spectra of the two components of the system and, therefore, that it should be considered as resulting from the orbital motion of the primary star.

A mass function of such smallness imposes severe restrictions upon the mass ratio and/or the total mass. In our earlier paper it was shown that, assuming for the brighter star a mass of 3$\odot$, which was reasonable for an A3 star of normal spectrum, the mass of the secondary should be 0.16 $\odot$; furthermore, that reasonable values of the masses require a mass ratio somewhere between 17 and 44. All the evidence, therefore, points toward the fact that this system belongs to a group of objects which contradict the mass-luminosity relation; Struve has elaborated this point in two recent papers.[3, 4] Evidently such an important system deserved further investigation.

In recent correspondence, Dr. O. Struve pointed out to the writer his own opinion and that of Dr. H. N. Russell of Princeton that XZ Sagittarii should be reobserved and suggested that this be done at Bosque Alegre. Consequently, the star was placed on the spectrographic program of the 60-inch reflecting telescope at the Astrophysical Station of the Córdoba Observatory.

[1] $\alpha = 18^h19^m0$; $\delta = -25°16'$ [1950.0]. CD$-25°13054$ (8.9 mag.) HD 168710 (A2). Algol. $M = 8.5$ mag.; $A_1 = 2.8$ mag.; $A_2 = 0$; $D = 7$ hours; $d = 2.2$ hours (from Schneller's *Katalog für 1941*).

[2] *Ap. J.*, **102**, 474, 1945; *McDonald Contr.*, No. 116.

[3] *Ap. J.*, **108**, 497, 1948.

[4] *Ann. d'ap.*, **11**, 117, 1948.

THE NEW MATERIAL

Most of the Bosque Alegre spectrograms were obtained in the interval between July 25 and August 1, 1948; a few additional plates were secured in September and October, 1948. A Wood-grating spectrograph was used, giving a dispersion of about 42 A/mm, and the exposures were made on Eastman 103*a*-O emulsion, except for Plate I 250, which was on 103*a*-F emulsion. For the O plates secured at maximum light, the exposure times were of the order of 50 minutes, in fair seeing, and with the equivalent slit-width of 1.5 A; for those taken during eclipse the exposure times were of the order of 2^h40^m, with the equivalent slit-width of 1.8 A. Except in one case (Pl. I 214), the star was never trailed along the slit.

The total number of spectrograms used in this investigation is 45. Most of them are of very good quality and extend from $H\beta$ to beyond λ 3600.

For the computation of the phases we have adopted the photometric elements obtained by Lange[5] in 1926, which are quoted in Schneller's *Katalog für 1941* and, more recently, in the new *Russian Catalogue of Variable Stars* by B. V. Kukarkin and P. P. Parenago,[6] namely,

$$\text{Epoch of minimum} = \text{JD } 2420311.519,$$
$$\text{Period} = 3.275537 \text{ days.}$$

THE SPECTRUM

The new observations confirm the spectral type attributed to the star at maximum light. The lines are sharp; the metallic lines are faint, *Fe* II being considerably stronger than *Fe* I. The Balmer series is seen up to *H* 20, a fact which locates the A3 star in the main sequence.[7]

On the plates secured at phases 3.172, 3.265, and 0.054 days, that is, during eclipse, the A3 spectrum appears blended with one of later spectral type, which is estimated as G, in agreement with our earlier estimation. At phases 3.082 and 0.071 days the spectrum of late type already does not affect the one which is observed at maximum light.

Except at around eclipse, the spectrograms of XZ Sagittarii do not show noticeable changes with phase or with cycle.

The 103*a*-F plate, obtained at maximum light, extends up to about λ 6000 and does not show any trace of the late-type spectrum.

THE RADIAL VELOCITIES

The stellar lines used for radial-velocity determination were $H\theta$, $H\eta$, $H\zeta$, $H\delta$, $H\gamma$, *Ca* II K, and *Mg* II 4481. The metallic lines were too faint for measurement; however, on some plates it was also possible to measure *Fe* II 4233, *Fe* II 4549, and/or *Ca* I 4227. On the plate at phase 3.172 days, in addition to the ten lines already mentioned, *Sr* II 4078, *Fe* II 4352, *Fe* I 4005, *Fe* I 4046, and *Fe* I 4384 were also measured. The adopted wave lengths are listed in Table 1.

The radial velocities obtained from each element and the mean from all the measured lines are given in Table 2. Figures 1, 2, 3, and 4 show the plot of the radial velocities from *H*, *Ca* II, *Mg* II, and the mean of all the measured lines, respectively, against phase. Our radial velocities do not show any systematic variations with cycle.

The plate taken at phase 3.172 days yields, for every measured element, a radial velocity which is above the value suggested by the neighboring velocities. Furthermore, except for *H*, the velocities from this plate are higher than at any other phase.

[5] *A.N.*, **228**, 71, 1926.

[6] I am indebted to Dr. O. Struve for this reference.

[7] Unsöld and Struve, *Ap. J.*, **91**, 365, 1940.

The dispersion shown by the Bosque Alegre spectrograms is still large, but the trend of the velocity-curves is more clearly and more convincingly shown than from the McDonald plates.

Looking at the plottings in Figures 1, 2, and 3, we notice that the scatter shown by *Mg* II is the largest, which is very likely due to the fact that sometimes the line is not very easy to measure. As for the amplitudes, *H* and *Mg* II suggest approximately the same amplitude, while that of *Ca* II K is smaller by a few kilometers per second; the difference is probably not significant.

Orbital elements representing the plotted radial velocities from "all lines" (not taking into account the result from plate I 224 at phase 3.172 days) have been derived by the Wilsing-Russell method; they are listed in Table 3, and the corresponding velocity-curve is drawn in Figure 4.

TABLE 1

ADOPTED WAVE LENGTHS FOR RADIAL-VELOCITY MEASUREMENTS

H	*Ca* II	*Mg* II	*Fe* II	*Fe* I	*Sr* II	*Ca* I
3797.90	3933.67	4481.23	4233.17	4005.25	4077.71	4226.73
3835.39			4351.76	4045.82		
3889.05			4549.47	4383.55		
4101.74						
4340.47						

DISCUSSION

The present spectrographic observations of XZ Sagittarii confirm the theory that we are dealing with an eclipsing system which shows a very small amplitude in radial velocity, considering the period, and therefore has a low value of the mass function. The amplitude obtained at McDonald from *Ca* II K and *Mg* II 4481 was of the order of 12 km/sec and the one from the radial velocities of all the measured elements on the Bosque Alegre spectrograms is somewhat larger, being of the order of 23 km/sec. In view of the scatter of the individual points, the agreement is satisfactory.

Let us consider the value of $f(m)$ obtained in the present work. If we again assume a value of $3\odot$ for the mass of the A star, this being the average mass of a normal A3 star, the secondary star would have a mass of $0.35\odot$. An assumption of $1\odot$ for the mass of the secondary star, which seems to be of G type according to the observations at eclipse, leads, instead, to a value of $m = 16\odot$ for the A star. The conclusion is that reasonable values for the masses of the stars of the system require that the mass ratio be somewhere between 8 and 16. Furthermore, the consideration of the mass-luminosity relation, as derived by Russell and Moore, implies, for $m_A = 3\odot$ and $m_G = 0.35\odot$, that $M_{vis}(A) = +1.7$ and $M_{vis}(G) = +9.0$, that is, a difference of 7.3 mag. between the brightnesses of the two star. The case $m_G = 1\odot$ and $m_A = 16\odot$ leads to a much larger difference in magnitude between the two components of the system. And yet, at eclipse, the spectrum of the G star appears on the plate with relatively short exposures, of the order of four times the exposure time needed for obtaining the A3 spectrum. Hence, one of the components of XZ Sgr or both contradict the mass-luminosity relation.

In the above considerations we have assumed that the radial velocities result from the orbital motion of the A star around the center of gravity of the two stars of the eclipsing system. But we could think either that the small amplitude in radial velocity shown by XZ Sgr is produced by the blending of the spectra of the two components or that it results from a distortion of the velocity-curve of the A3 component caused by an effect similar to those often encountered in eclipsing binary systems.

TABLE 2

RADIAL VELOCITIES OF XZ SAGITTARII

PLATE	DATE (1948)	U.T.	PHASE (DAYS)	RADIAL VELOCITY IN KM/SEC FROM							
				Ca II K	*H*	*Mg* II	*Fe* II	*Ca* I	*Fe* I	*Sr* II	All Lines
I 263	Oct. 16	0:02	0.054	− 2	+ 3	.....	.....	.....	.....	.....	+ 2
202	July 26	3:08	0.071	+ 3	+11	−12	− 9	.....	.....	.....	+ 5
264	Oct. 16	1:25	0.112	− 4	+ 8	+18	− 2	.....	.....	.....	+ 7
243	Sept. 17	0:31	0.554	−19	−22	− 7	.....	.....	.....	.....	−19
227	July 29	23:41	0.633	+14	− 8	−20	.....	.....	.....	.....	− 5
244	Sept. 17	2:32	0.663	−28	.....	− 4	.....	.....	.....	.....	−16
228	July 30	0:16	0.676	−10	.....	−16	.....	.....	.....	.....	−13
229	30	1:24	0.723	−17	−21	−10	.....	.....	.....	.....	−20
230	30	2:34	0.772	−17	−26	−37	.....	.....	.....	.....	−26
231	30	3:48	0.823	−20	− 2	.....	+17	.....	.....	.....	− 2
232	30	5:04	0.876	+13	− 1	.....	.....	.....	.....	.....	+ 5
203	26	23:25	0.916	−13	−21	−20	.....	.....	.....	.....	−19
233	30	6:22	0.930	−13	.....	.....	.....	.....	.....	.....	−13
204	27	0:18	0.953	−27	−24	−46	−16	−22	.....	.....	−24
249	Sept. 23	23:45	0.971	−15	−14	− 2	.....	.....	.....	.....	−12
205	July 27	1:22	0.997	+ 1	+ 9	+20	.....	.....	.....	.....	+ 9
206	27	2:16	1.035	−37	−18	−29	.....	.....	.....	.....	−22
250	Sept. 24	1:48	1.056	−14	−13	+17	−10	.....	.....	.....	− 8
279	Oct. 17	0:18	1.065	− 9	−10	−15	.....	.....	.....	.....	−11
207	July 27	3:08	1.071	− 2	+ 3	.....	.....	.....	.....	.....	+ 2
208	27	4:00	1.107	−14	+ 2	+14	.....	.....	.....	.....	+ 1
209	27	4:54	1.144	−16	− 7	+14	.....	.....	.....	.....	− 4
210	27	5:50	1.183	− 1	.....	.....	.....	.....	.....	.....	− 1
234	30	23:28	1.643	−25	+16	− 5	.....	−18	.....	.....	+ 2
212	27	23:14	1.908	+23	+15	+21	.....	.....	.....	.....	+18
213	28	0:31	1.962	+29	+38	+15	.....	.....	.....	.....	+33
254	Sept. 24	23:46	1.972	+25	+29	+22	.....	.....	.....	.....	+26
214	July 28	2:24	2.040	+31	+38	+26	+13	.....	.....	.....	+33
255	Sept. 25	2:20	2.078	+17	+14	+31	.....	.....	.....	.....	+20
215	July 28	4:00	2.107	+ 7	+16	+27	+42	+27	.....	.....	+21
216	28	5:04	2.149	+16	+21	+46	.....	.....	.....	.....	+25
217	28	6:20	2.204	+15	+20	+10	.....	.....	.....	.....	+18
199	25	2:34	2.323	+25	.....	.....	.....	.....	.....	.....	+25
237	31	23:53	2.660	+16	+33	.....	.....	.....	.....	.....	+30
238	Aug. 1	0:47	2.698	+29	+25	.....	.....	.....	.....	.....	+26
239	1	1:40	2.734	+32	+25	+29	.....	.....	.....	.....	+28
240	1	2:38	2.775	− 8	.....	+26	.....	.....	.....	.....	+ 9
241	1	3:50	2.825	+23	+46	+27	.....	.....	.....	.....	+35
242	1	5:12	2.882	+54	+35	+38	.....	.....	.....	.....	+41
220	July 29	0:26	2.958	+25	+14	− 1	+ 6	.....	.....	.....	+12
221	29	1:26	3.000	+16	+ 4	.....	.....	.....	.....	.....	+ 6
222	29	2:24	3.040	+ 6	− 7	− 6	.....	.....	.....	.....	− 5
223	29	3:24	3.082	+17	+15	+23	+ 1	.....	.....	.....	+15
224	29	5:34	3.172	+64	+38	+72	+48	+56	+73	+61	+55
201	26	1:11	3.265	− 8	− 2	+35	.....	+20	.....	.....	+ 7

TABLE 3

ORBITAL ELEMENTS OF XZ SAGITTARII

$P = 3.275537$ days (assumed)
$K = 22.7$ km/sec
$\omega = +66°8$
$e = 0.12$
$T =$ phase 3.029 days

$\gamma = +8.2$ km/sec
$a \sin i = 1.0 \times 10^6$ km
$\dfrac{m_2^3 \sin^3 i}{(m_1 + m_2)^2} = 0.004\odot$

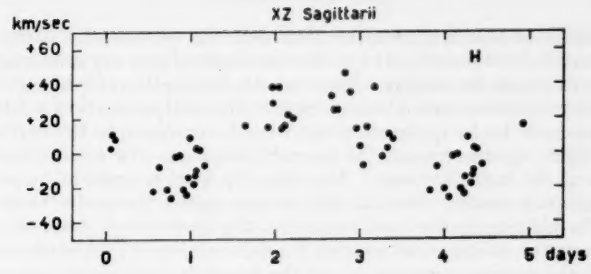

FIG. 1

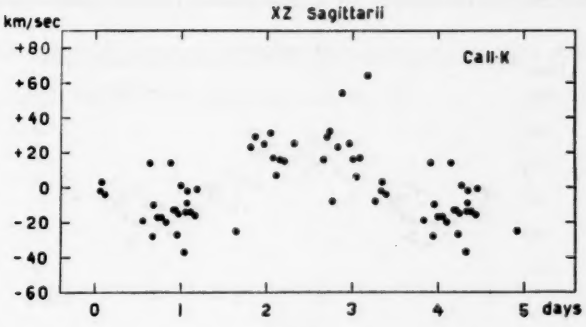

FIG. 2

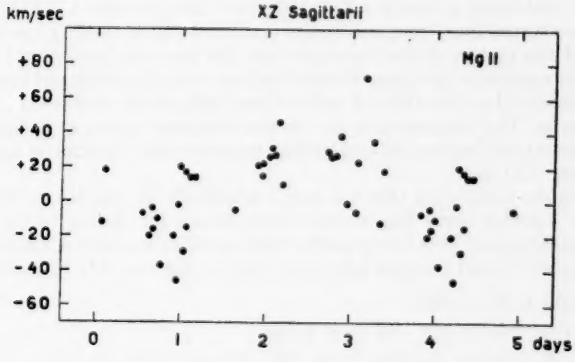

FIG. 3

The possibility of blending must be discarded. The photometric data, based upon visual observations by Zinner,[8] indicate that the depth of primary minimum is 2.8 mag., no secondary minimum having been observed. An assumption of 0.1 mag. for the depth of the secondary minimum and a total or nearly total eclipse leads to a ratio of the surface brightnesses of the two stars of about 10 and, therefore, to the earlier conclusion that "at full light, the spectrum of the primary star cannot be noticeably blended with the spectrum of the secondary star." The case of partial eclipse and/or a depth of the secondary minimum smaller than 0.1 mag. is even more unfavorable for the possibility of blending. In addition to the consideration of the photometric data, the internal consistency between the radial velocities from the different lines in the whole range λλ 3790–4550 in which the measures were made and the fact that the F plate, taken at maximum light, does not show any trace of the late-type spectrum are certainly arguments against the possibility of blending.

The time of mid-eclipse deserves some comments. The epoch of minimum and the period which are quoted in the latest catalogues, as was mentioned in the section headed "The New Material," were derived by Lange from his visual observations, and they

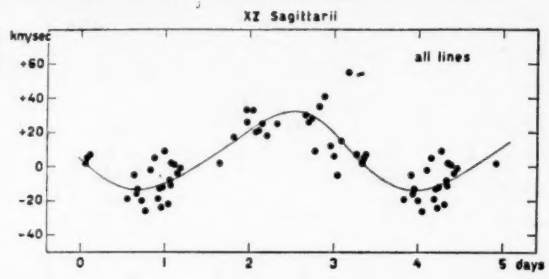

FIG. 4

have been confirmed by the observation of four minima by Zessewitsch.[9] There is a difference, however, in the duration of totality, 1.9 hours was found by Zessewitsch as against 2.2 hours by Lange. A light-curve also has been determined at Harvard,[10] and the period was indicated as being 3.2755338 days; Lange's was 3.275537 days. In our earlier paper we stated that "long before the predicted end of totality the writer noticed through one of the finders of the telescope that the star was becoming brighter." The same statement applies to the present observations, with the additional remark that we had the impression that the time of mid-eclipse falls much earlier than predicted by adopted elements. The examination of the spectrograms taken at around eclipse apparently confirms that impression and further suggests that the time of mid-eclipse falls at around phase 3.20 days.

Attention to the possibility that the small amplitude in velocity is caused by a distortion of the velocity-curve has already been drawn by Struve in his paper in the *Annales d'astrophysique*.[4] It is just possible that an effect similar to, but in the opposite sense from, the one found in some eclipsing systems, such as AU Monocerotis,[11] for in-

[8] *Astr. Abh.*, Vol. **4**, No. 3, 1922.

[9] *Astr. Circ. Acad. Sci. U.S.S.R.*, No. 18, p. 4, 1943.

[10] H. Shapley, *Rice Institute Pamphlet*, **18**, 81, 1931 (*Harvard Reprint*, No. 68).

[11] Sahade and Cesco, *Ap. J.*, **101**, 235, 1945; *McDonald Contr.*, No. 106. See also Struve, *Ap. J.*, **102**, 81, 1945; *McDonald Contr.*, No. 110; and Sahade and Struve, *Ap. J.*, **102**, 482, 1945; *McDonald Contr.*, No. 117.

stance, would yield a velocity-curve of abnormally small K. However, neither the result of the inspection of the spectrograms nor that of the plot of the radial velocities favors the possibility. Nevertheless, there is a fact which apparently deserves attention, namely, the radial velocity from Plate I 224 at phase 3.172 days. Even if mid-eclipse actually falls at about phase 3.20 days, this high velocity cannot be interpreted as due to rotation effect because Plate I 201 at phase 3.265 days fails to give a high radial velocity in the opposite sense. Furthermore, all the measured lines on Plate I 224 give a high radial velocity, even those which are strengthened because they presumably belong mostly to the G star. Are we actually dealing at eclipse with a "prominence action" as in the case of UX Monocerotis?[12] The available material taken at minimum is too meager to allow any conclusion. It is very unfortunate that the dispersion of the spectrograph at our disposal is not suitable to obtain relatively short-exposure spectrograms during minimum, so as to be able to find out the behavior of the radial velocities during eclipse.

We may conclude by saying that, while the available evidence favors the conclusion that XZ Sagittarii must be grouped among those objects which contradict the mass-luminosity relation, the conclusion should be accepted with caution.

Mr. Julio Albarracín assisted me during the process of reduction of the spectrograms.

[12] Struve, *Ap. J.*, **106**, 255, 1947; *McDonald Contr.*, No. 138.

FURTHER NOTE ON THE DISTRIBUTION OF THE LONGITUDE OF PERIASTRON*

ELIZABETH L. SCOTT
Statistical Laboratory, University of California
Received February 18, 1949

ABSTRACT

The distribution of ω, the longitude of periastron, was analyzed for 85 eclipsing and 330 noneclipsing spectroscopic binaries listed in the Fifth Catalogue as having elliptic orbits. The analysis was performed separately for various categories of binaries obtained from classifications and cross-classifications according to spectral class, semi-amplitude, period, and eccentricity. In general, the results of the analyses are consistent with the Struve hypothesis that the catalogue values of ω are distorted by systematic errors due to some phenomenon occurring in the vicinity of the binary. However, some curious results were obtained. The most striking of these is that there is strong evidence of nonuniformity in the distribution of ω among binaries with period from 2 to 5 days, while there is no such evidence for binaries with period shorter than 2 days.

I. INTRODUCTION

In a recent paper[1] the author considered the distribution of ω, the longitude of periastron, of spectroscopic binaries classified according to e, the eccentricity of the orbit, and showed that for several categories of eccentricity it is safe to assert that the distribution of ω is not uniform between 0° and 360°. The analyses were made with reference to Struve's hypothesis that the catalogue values of ω differ from the true longitude by systematic errors ascribable to some phenomenon occurring in the immediate vicinity of each binary, such as the absorption of radiation by gas streaming from and encircling the binary. The results obtained appear to be generally consistent with Struve's hypothesis.

When this first study had been completed, the author learned that, following the suggestion of Dr. J. H. Moore, tables of the distribution of ω and of various other parameters of the binary orbit were being prepared by V. M. Blanco and A. D. Williams with the data in the forthcoming Fifth Catalogue of Spectroscopic Binaries.[2] Dr. Moore suggested that an extension of the previous work to consider the distribution of ω for various periods and spectral classes would be of interest, especially with regard to Struve's hypothesis. The purpose of the present note is to present this analysis.

II. DATA

The 85 eclipsing and 330 noneclipsing binaries listed in the Fifth Catalogue as having elliptical orbits were classified according to various characteristics relevant to Struve's hypothesis, such as their catalogue value of eccentricity, spectral class, semi-amplitude, and period. They were also classified as eclipsing or noneclipsing, and various further divisions were made. For each category the distribution of ω in 5° intervals was obtained.

Simultaneously, some of these distributions of ω for the same stars in similar categories were produced by Blanco and Williams.[3] However, these distributions are in 30° intervals of ω, which is too coarse for the present purpose. Since the two tabulations were carried out independently, the tables of Blanco and Williams, whenever they overlap, provide a partial check against errors in our classification, and also our tables form a

* This work was done in part with the support of the Office of Naval Research.

[1] E. L. Scott, *Ap. J.*, **109**, 194, 1949.

[2] J. H. Moore and F. J. Neubauer, *Lick Obs. Bull.*, **20**, 1, 1949.

[3] V. M. Blanco and A. D. Williams, *Pub. A.S.P.*, Vol. **61**, 1949 (in press).

stronger check against errors in their tables. To avoid partial repetition and to save space, our tables are not reproduced here.

III. RESULTS OF TEST FOR UNIFORMITY OF DISTRIBUTION OF ω

The data just described are used to test the hypothesis—say, H—that the distribution of ω is uniform between 0° and 360°, that is, that the probability of a binary star having its ω in any 5° interval is 1/72. The test performed is an adaptation of the Neyman smooth test for goodness of fit.[4] The procedure used and, in particular, the significance of the four orders of the modified test are described in the previous paper.[1]

The test was performed separately for the several categories of binaries. Tables 1–5 give, for each category, the results of the test in the form of the probability of committing an error in rejecting hypothesis H. The smaller the probability in any given case, the greater the ground for rejecting hypothesis H and thus for asserting that the true distribution of the catalogue values of ω is not uniform.

The line marked n in Tables 1–5 gives the number of stars in the category. The subsequent lines refer to the four orders of the smooth test of hypothesis H. Which test to use depends upon the class of alternative hypotheses against which we desire the test to be most sensitive. As in the previous publication, we consider that the fourth-order test is probably the appropriate test to use.

In analyzing the data with reference to the Struve hypothesis, it is desirable to make the classifications and cross-classifications as fine as possible in an effort to determine the combinations of various factors for which the departure from uniformity of the distribution of ω is most pronounced. However, in treating a large number of classes with but a few stars in each class and in treating various combinations of these classes, we encounter difficulties.

1. If there are but few binaries in each category and H is only moderately false, then the test performed separately for each category may fail to detect the falsehood of H. On the other hand, if some of the categories are combined, there may be enough observations to detect that the actual distribution of the catalogue values of ω is not uniform.

2. However, combining two categories leads to combining two distributions of ω. There is, then, the possibility that, while each distribution is nonuniform, their combination may approach uniformity.

3. Also, if the test of hypothesis H is performed many times, then, even when H is true, we may expect H to be rejected occasionally by chance.

In this connection it is emphasized that, although not all the tables computed are reproduced in this paper, the only reason for omitting certain tables is that these tables lead to conclusions which are essentially the same as those suggested by some of the tables published. No table was omitted simply because it shows no reason for rejecting the hypothesis H.

A number of the tables obtained but not reproduced here refer to the classification of binaries according to their catalogue value of *eccentricity*. These tables, based on Moore and Neubauer's data, are not identical with, but are very similar to, the published tables based on material provided by Struve. They are omitted because they lead to conclusions which coincide with those already published.[1]

Table 1. Classification according to spectral class.—Of the three sections *a*, *b*, and *c* of Table 1, the clearest picture of the influence of spectral class on the distribution of ω is derived from *c*. In agreement with the Struve hypothesis, the early spectral classes provide evidence of the nonuniformity of the distribution of ω, and the later spectral classes do not. Part *a* of the table, relating to eclipsing binaries only, reveals a similar picture. Surprisingly, the picture in part *b* is less clear in spite of the fact that there are many stars in each category. The classes B5 and earlier and B6–A3 do not provide sufficient

[4] J. Neyman, *Skand. Aktuarietidskrift*, **20**, 149, 1937.

evidence against uniformity by themselves. Such evidence becomes apparent only when the two categories are combined into one category containing 150 stars.

Table 2. Classification according to semi-amplitude.—In cases in which the Struve effect is pronounced, the catalogue value of the semi-amplitude has a tendency to be larger than the true value (see Fig. 4 in Struve[5]). For this reason and also because larger semi-amplitudes indicate close binaries, the results shown in Table 2 are consistent with the Struve hypothesis. Binary stars with large semi-amplitude provide evidence of the nonuniformity of the distribution of ω, while those with smaller semi-amplitude do not.

TABLE 1*

PROBABILITY OF COMMITTING AN ERROR IN REJECTING HYPOTHESIS *H* THAT THE DISTRIBUTION OF ω IS UNIFORM

	(*a*) Eclipsing			(*b*) Noneclipsing						(*c*) Both Eclipsing and Noneclipsing				
Spectrum	≦B5	B6–A3	≧A5	≦B5	B6–A3	≦A3	A5–F2	F3–G0	G5–K2 K5–M	≦B5	B6–A3	A5–F2	F3–G0	G5–K2 K5–M
n	25	41	18	65	85	150	31	71	69	90	126	38	77	74
Test:														
1	0.0060	0.48	0.17	0.034	0.055	0.0045	0.035	0.74	0.62	0.0012	0.048	0.041	0.93	0.54
2	.0096	.16	.12	.11	.078	.011	.019	.87	.52	.0036	.019	.009	.95	.31
3	.024	.30	.20	.17	.16	.026	.046	.33	.62	.0096	.048	.022	.74	.48
4	0.042	0.45	0.30	0.27	0.13	0.041	0.059	0.49	0.77	0.019	0.054	0.023	0.86	0.64

* Binaries classified according to *spectral class* (Harvard classification).

TABLE 2*

PROBABILITY OF COMMITTING AN ERROR IN REJECTING HYPOTHESIS *H* THAT THE DISTRIBUTION OF ω IS UNIFORM

	(*a*) Eclipsing				(*b*) Noneclipsing								
Semi-amplitude	10–50	50–85	≧85	≧50	0–10	10–20	20–30	30–40	40–50	50–60	60–70	70–100	≧100
n	30	27	27	54	43	58	56	39	32	22	23	26	25
Test:													
1	0.97	0.32	0.061	0.043	0.34	0.42	0.097	0.98	0.63	0.042	0.75	0.0026	0.0092
2	.098	.24	.044	.013	.46	.64	.25	.28	.77	.049	.69	.0070	.033
3	.13	.33	.099	.030	.51	.76	.30	.28	.52	.084	.33	.0053	.061
4	0.22	0.40	0.16	0.062	0.42	0.70	0.44	0.34	0.62	0.12	0.21	0.0041	0.088

* Binaries classified according to *semi-amplitude* in km/sec.

Table 3. Classification according to period.—The results presented in Table 3 are surprising. Assuming Struve's hypothesis, one would expect that binaries with long period would show little if any evidence of nonuniformity of the distribution of ω and that such evidence would become more pronounced as the period is decreased. In part *c* of the table, where the number of stars in each category is the largest, we note the striking fact that the only category of binaries in which there is clear-cut evidence of nonuniformity is the category with period from 2 to 5 days. Furthermore, parts *a* and *b*, referring to eclipsing and noneclipsing binaries separately, seem to agree only in the category 2–5 days, where there is evidence of nonuniformity of the distribution of ω, and in the cate-

[5] O. Struve, *Ap. J.*, **99**, 95, 1944.

gory 0–2 days, where there is no such evidence. For longer periods, with one exception, the noneclipsing binaries show no evidence of nonuniformity, while the relatively few eclipsing binaries suggest nonuniformity. The exceptional category of noneclipsing binaries is that of period 10–15 days. Here there is an indication of nonuniformity. However, this indication is slight and not consistent with the results in the adjoining categories and in part *c*.

The lack of evidence of nonuniformity among the stars with period between 0 and 2 days may be due to the fact that there are relatively few such stars. If, in reality, the distribution of ω in this class is nonuniform, and the character of the nonuniformity is similar to that in the adjoining class with period 2–5 days, then, by combining the two

TABLE 3*

PROBABILITY OF COMMITTING AN ERROR IN REJECTING HYPOTHESIS *H* THAT THE DISTRIBUTION OF ω IS UNIFORM

	(*a*) Eclipsing					(*b*) Noneclipsing									
Period	0–2	2–5	≧5	≧10	0–5	0–2	2–5	5–10	10–15	15–35	35–365	≧365	≧5	≧10	0–5
n	14	40	31	19	54	20	47	56	32	40	62	73	263	207	67
Test:															
1	0.96	0.034	0.70	0.23	0.079	0.029	0.002	0.51	0.11	0.50	0.33	0.061	0.26	0.25	0.0001
2	.54	.009	.011	.033	.084	.089	.002	.34	.20	.59	.31	.17	.20	.37	.0003
3	.55	.020	.029	.044	.18	.18	.007	.40	.064	.67	.47	.30	.36	.57	.0012
4	0.72	0.044	0.056	0.089	0.29	0.23	0.016	0.56	0.048	0.66	0.64	0.62	0.50	0.67	0.0022

	(*c*) Both Eclipsing and Noneclipsing									
Period	0–2	2–5	5–10	10–15	15–35	35–100	100–365	≧365	≧5	≧10
n	34	87	68	40	44	32	34	76	294	226
Test:										
1	0.063	0.00036	0.18	0.27	0.46	0.35	0.90	0.13	0.28	0.57
2	.16	.00006	.061	.54	.69	.44	.42	.26	.046	.29
3	.26	.00023	.12	.25	.73	.63	.61	.35	.10	.48
4	0.34	0.00046	0.21	0.18	0.78	0.67	0.62	0.47	0.16	0.64

* Binaries classified according to *period* in days.

categories, we may expect to obtain a distribution showing strong evidence of nonuniformity. It is curious that the procedure gives contradictory results for eclipsing and noneclipsing binaries: eclipsing binaries show no evidence of nonuniformity, whereas the noneclipsing show strong evidence.

The above discussion brings out two interesting points—the striking role of the period 2–5 days and a difference between the eclipsing and noneclipsing binaries which was noted by Scott[1] in connection with the classification according to eccentricity. Since there seem to be several factors which influence the distribution of ω and these factors are sometimes correlated, it is interesting to study this distribution for categories of stars in a two-way classification. Unfortunately, since there are but few stars, this cross-classification cannot be very fine.

Table 4. Classification according to period and spectral class.—The uniformity of the distribution of ω was tested for categories of binaries cross-classified according to period

and spectral class for eclipsing and noneclipsing binaries separately. However, no clear-cut evidence of difference between the two types of binaries was noted, perhaps because the number of stars in the particular subclasses was extremely small. For this reason Table 4 gives only the results for both eclipsing and noneclipsing binaries considered together.

The results of Table 4 indicate that both spectral class and period play a role in the nonuniformity of the distribution of ω. The table does not seem to offer an explanation

TABLE 4*

PROBABILITY OF COMMITTING AN ERROR IN REJECTING HYPOTHESIS *H* THAT THE DISTRIBUTION OF ω IS UNIFORM

	Both Eclipsing and Noneclipsing															
Period.....	0–2				2–5				5–15				≧15			
Spectrum..	≦B5	B6–A3	≦A3	≧A5	≦B5	B6–A3	A5–F2	≧A5	≦B5	B6–A3	A5–F2	≧A5	≦B5	B6–A3	A5–F2	≧A5
n.....	12	11	23	11	25	42	12	20	24	47	9	36	29	26	12	122
Test:																
1.....	0.47	0.40	0.27	0.24	0.0008	0.044	0.22	0.23	0.0029	0.91	0.58	0.98	0.57	0.34	0.37	0.87
2.....	.69	.52	.24	.40	.0031	.016	.17	.12	.0037	.74	.84	.92	.64	.28	.065	.16
3.....	.83	.45	.42	.17	.0092	.041	.20	.23	.010	.81	.84	.98	.82	.28	.14	.28
4.....	0.92	0.59	0.50	0.25	0.015	0.048	0.12	0.21	0.023	0.88	0.80	0.96	0.91	0.35	0.14	0.43

* Binaries classified according to *period* and *spectral class*.

TABLE 5*

PROBABILITY OF COMMITTING AN ERROR IN REJECTING HYPOTHESIS H THAT THE DISTRIBUTION OF ω IS UNIFORM

	(*a*) Eclipsing				(*b*) Noneclipsing			
Period.....	0–2		2–5		0–2		2–5	
Eccentricity...	0.00–0.12	0.12–1.00	0.00–0.12	0.12–1.00	0.00–0.12	0.12–1.00	0.00–0.12	0.12–1.00
n.....	10	4	29	11	16	4	40	7
Test:								
1.....	0.80	0.49	0.81	0.00037	0.041	0.43	0.0006	1.00
2.....	.53	.75	.50	.00009	.12	.71	.0007	0.95
3.....	.70	.83	.71	.00012	.21	.81	.0022	0.53
4.....	0.84	0.92	0.79	0.00032	0.32	0.67	0.0055	0.63

* Binaries classified according to *period* and *eccentricity* of orbit.

for the still persisting difference in the outcome of the test when applied to the category 0–2 days and the category 2–5 days. In particular, the lack of evidence of nonuniformity in the category from 0 to 2 days cannot be attributed to a preponderance of late-type binaries in this category.

Table 5. Classification according to period and eccentricity.—For binaries of period 2–5 days classified according to eccentricity, Table 5 indicates that the hypothesis of uniformity is rejected for eclipsing binaries of eccentricity 0.12 and above but is accepted for those of smaller eccentricity. For noneclipsing binaries the situation is reversed. This is

again the phenomenon which was noticed[1] in relation to all binary stars, irrespective of period.

As in Tables 3 and 4, Table 5 offers no evidence against the uniformity of the distribution of ω for binaries with period between 0 and 2 days. The difference between the categories 0–2 and 2–5 persists, yet their distributions of eccentricity are essentially the same. Although no explanation is offered for the acceptance of the hypothesis of uniformity for the category with period 0–2 days, we note that the number of binaries in the category is not large and remark that the problem of determining an orbit for such close binaries is complex.

General remarks.—The above discussion of Tables 1–5 was based on the results of the fourth-order test. The reason is that this test is particularly sensitive to departures from uniformity in which the distribution of ω has three extremes. It was expected that nonuniformity of the distribution may be caused not only by the Struve effect but also by other factors. For example, additional extremes in the observed distribution of ω may appear because binaries with certain values of the longitude of periastron are more easily identified than others. In this case the distribution of the catalogue values of ω would have at least three extremes, and the fourth-order test would be more unfavorable to the hypothesis of uniformity than the other tests would be. However, in the great majority of categories in Tables 1–5, the second-order smooth test is less favorable to the hypothesis of uniformity than is the fourth-order test. This is an indication that, if the distribution of the catalogue values of ω is nonuniform, then it has one pronounced maximum (or minimum) which overshadows all the others. Furthermore, an examination[3] of the data shows that, in all cases where the hypothesis of uniformity is rejected, the distribution of ω is not symmetrical about 180°. Of the possible sources of nonuniformity discussed in the previous paper,[1] only the Struve effect seems compatible with a distribution of ω which has one pronounced maximum (or minimum) and is not symmetrical.

It is a pleasure to thank Dr. J. H. Moore for suggesting this further analysis of the distribution of ω and for providing the data in advance of their publication. The author is also deeply indebted to Dr. J. Neyman and Dr. O. Struve for their encouragement and interest in the work.

THE STARK EFFECT OF THE HIGHER BALMER LINES IN STARS OF SPECTRAL TYPES A AND B

ELSA VAN DIEN
Harvard College Observatory
Received April 19, 1948

ABSTRACT

The purpose of the investigation was to compute the number of Balmer lines which should be visible in a stellar spectrum on the following assumptions: (1) the stellar atmosphere consists of hydrogen only; (2) the static Stark effect is the only agent of line broadening; (3) the stellar atmosphere is uniformly stratified in gravitational equilibrium.

For the probability distribution of the field strength in an ionized gas, Holtsmark's theoretical results were used, as modified by Verweij. For the Stark pattern of the higher Balmer lines a simplifying assumption was introduced, suggested by Pannekoek. Eddington's equations of radiative transfer were integrated numerically for a number of wave lengths between 3660 A and 3750 A and for the following atmospheres: surface temperatures 10,080°, 12,600°, 16,800°, and at each temperature surface gravities 10^2, 10^4, 10^6, 10^8. The values of the coefficient of continuous absorption for hydrogen were taken from published computations by Pannekoek.

The theoretical results were compared with three groups of observational data: bright stars, eclipsing binaries, and two white dwarfs. The white dwarfs seem to conform to the theoretical expectations; but here the data on mass, radius, and temperature are more uncertain than for the two other classes of objects. It was found that in a large number of stars of the first two groups more hydrogen lines can be observed than are predicted by theory. In many of these stars the effective surface gravity seems to be only one one-hundredth of the dynamical value, or less. This agrees with results of Schalén and of Pannekoek and Reesinck.

Several possibilities are investigated which might account for the discrepancy found. Radiation pressure and electron scattering may, in a few cases, have some effect but not to an extent sufficient to explain all the disagreement. In the temperature range considered, the absorption by negative hydrogen ions is negligible. It is suggested that stellar atmospheres are not built according to the model, which assumes equilibrium and stratification under the influence of gravitation and radiation pressure.

1. It has been recognized for a long time that the Balmer lines of hydrogen in stellar spectra cannot be observed as far as the theoretical limit at 3647 A. The transition from line spectrum to continuum has been found to occur around wave length 3700 A in main-sequence stars, and the Balmer continuum extends to the red of 3647. It is generally assumed that the lines are broadened by Stark effect, which causes the lines to overlap and finally to merge into a continuum.

The present investigation is an extension of work by Verweij[1] and by Pannekoek.[2] Verweij has treated the Stark effect of the first four Balmer lines in great detail and has computed line profiles for a wide range of values of surface gravity and surface temperature. Pannekoek has given a simplified treatment for the higher Balmer lines.

The aim of the work presented in the following sections is to derive, from theoretical considerations, the number of Balmer lines visible, in its dependence on surface temperature and surface gravity. Three basic assumptions underlie the computations: (1) the atmosphere consists of hydrogen only; (2) the static Stark effect is the only broadening agent; and (3) the stellar atmosphere is uniformly stratified in gravitational equilibrium.

The following problems will be dealt with successively: (1) What is the strength of the electrical field active in a gas mixture of neutral atoms, ions, and electrons? (2) In what way is each Balmer line affected by it? (3) How does the field change in successive layers of the atmosphere? (4) What is the integrated effect on the observed lines?

2. In this section the first of these problems is considered. In an atmosphere consisting of neutral atoms, ions, and electrons in thermal motion, the electric field at any

[1] *Pub. Astr. Inst. U. Amsterdam*, No. 5, 1936. [2] *M.N.*, **98**, 701, 1938.

point is not constant but changes continuously. The problem is to find the statistical distribution of the field strength as a function of density.

As a first approximation we can suppose that the field at a point is caused by the nearest neighbor only and that the effects of the more distant particles are negligible. Chandrasekhar[3] has given a simple derivation for the probability distribution of the field strength in that case. Since the distance by which the Stark components are displaced with respect to the original line is proportional to the field strength, the probability distribution of the field strength yields that of the line width $\Delta\lambda$. The latter distribution is then given by $e^{-(\Delta\lambda_1/\Delta\lambda)^{3/2}}d(\Delta\lambda_1/\Delta\lambda)^{3/2}$, in which $\Delta\lambda_1$ depends on the line under consideration and on temperature and pressure. A probability distribution of this form was first given by Russell and Stewart[4] and has been applied by Elvey and Struve[5] in the computation of the contour of $H\gamma$ due to Stark effect.

Holtsmark[6] has treated the problem in a more general way, taking into account the contributions to the field of all the charged particles in the gas. Holtsmark's results cannot be expressed in a closed analytical form but are evaluated from series expansions. Verweij[1] improved on one of these, and his values have been used in the present work.

It should be pointed out here that the quantity for which the statistical distribution is actually computed is not the field strength itself but its ratio β to a standard field strength F_0. The quantity $\beta = F/F_0$, where $F_0 = 2.61\, n^{2/3}e$, in which n is the number of charged particles per cubic centimeter and e the charge of the electron. $F_0 = [1.87](P/T)^{2/3}$, in which the brackets indicate the logarithm on the base 10 of the coefficient.

Hence, once the probability distribution $W(\beta)$ of β is known, we can, for every temperature and pressure, compute the distribution of the field strength. $W(\beta)$ satisfies the relation

$$\int_0^\infty W(\beta)\, d\beta = 1 .$$

3. This section deals with the Stark effect caused by the electrical field discussed above. After Stark had, in 1913, discovered the effect of a strong electrical field on the light emitted by atoms, theoretical treatments of the phenomenon were given by Sommerfeld,[7] Epstein,[8] and many others, first on the basis of the classical Bohr theory and later by the application of wave-mechanical methods. Both methods agree in giving, for the first-order effect in hydrogen,

$$\Delta E = \frac{3h^2}{8\pi m e}\, n\,(n_2 - n_1)\,F \qquad \text{or} \qquad \Delta E = Cn\,(n_2 - n_1)\,F , \tag{1}$$

where ΔE is the change in energy of the level of principal quantum number n; n_1 and n_2 are parabolic quantum numbers, integers, subject to the conditions $0 \leqslant n_1, n_2 \leqslant n-1$. The quantity that determines the possible transitions is $m = n - n_1 - n_2 - 1$. Only transitions $\Delta m = 0, \pm 1$, are allowed. It is clear from the formula for ΔE that, for each positive value of ΔE, there is a corresponding negative value. Consequently, the pattern of lines originating from the combination of two levels, both split by Stark effect, will be symmetrical around the position of the undisturbed line. In all computations the fine structure of each hydrogen line has been disregarded.

The largest positive value which ΔE in equation (1) can have for any value of n occurs for $n_2 = n-1$, $n_1 = 0$, which yields $\Delta E = CFn\,(n-1)$. Similarly, for $n = 2$, the largest negative value of ΔE is $-2CF$. In both cases $m = 0$, and hence the extreme components, arising from a transition between these states, does exist. It follows that

[3] *Rev. Mod. Phys.*, No. 1, 1943.

[4] *Ap. J.*, **59**, 204, 1924.

[5] *Ap. J.*, **72**, 277, 1930.

[6] *Ann. d. phys.*, **58**, 576, 1919.

[7] *Quantummechanics*, chap. ii, § 2.

[8] *Ann. d. phys.*, **50**, 489, 1916.

the maximum extension of the Stark pattern for the nth Balmer line at either side of the unperturbed line is determined by

$$\Delta E_{2n} = CF\{n(n-1)+2\}. \tag{2}$$

Since

$$\Delta E_{2n} = h\Delta\nu$$

and

$$\Delta\nu = \frac{-c}{\lambda^2}\Delta\lambda,$$

we obtain, by inserting the values of the constants and the expression for the wave length of the Balmer line,

$$\Delta\lambda_m = 0.00256\left(\frac{n^2}{n^2-4}\right)^2\{n(n-1)+2\}F \tag{3}$$
$$= s_n\beta F_0,$$

where s_n is defined by equation (3) (cf. Pannekoek, *loc. cit.*). The quantity $\Delta\lambda_m$ is the maximum extension of the Stark pattern, expressed in angstroms.

Because the number of components increases greatly with n, the simplifying assumption, suggested by Pannekoek,[2] was made, that each absorption line is spread out into a band of uniform absorption of width $2\Delta\lambda_m$ and so that the total absorption of the band is equal to the total absorption of the original Balmer line. If a_n' is the total atomic absorption in the realm of the nth line, then the atomic absorption in the band caused by any strength F of the field amounts to

$$\frac{a_n'}{2\,s_n\beta F_0} = a_n''$$

per unit of wave length. This a_n'' has the weight $W(\beta)$. The total atomic absorption at distance $\Delta\lambda$ from the line center, originating from that line, is then found by integration of all the contributions arising from fields which spread the line as far as $\Delta\lambda$ or farther. Hence a_n is equal to

$$a_n = \int_{\beta_{\Delta\lambda}}^{\infty} \frac{W(\beta)\,a_n'}{2\,s_n\beta F_0}\,d\beta$$

$$= \frac{a_n'}{2\,s_n F_0}\int_{\beta_{\Delta\lambda}}^{\infty}\frac{W(\beta)\,d\beta}{\beta},$$

in which the lower limit, $\beta_{\Delta\lambda}$, is that value of β which is just large enough to spread the line to a width $\Delta\lambda$ from the line center.

In order to find the function

$$U(\beta) = \int_{\beta}^{\infty}\frac{W(\beta)\,d\beta}{2\beta},$$

$W(\beta)/\beta$, as given by Verweij,[1] was plotted on a sufficiently large scale to permit of graphical integration. Table 1 gives the values of $U(\beta)$.

The quantity called a_n' should now be considered more carefully. This quantity stands for the rate at which one atom absorbs energy in the realm of a Balmer line. This amount is, by a well-known relation, equal to

$$\frac{\pi e^2}{mc}f_{2n}, \quad \text{or to} \quad \frac{\pi e^2}{mc}\cdot\frac{\lambda^2}{c}10^{-8}\cdot f_{2n},$$

if the energy is expressed per unit of frequency or per unit of wave length (angstroms), respectively. In these formulae, f_{2n} is the oscillator strength for the transition from the second to the nth level. The quantities f_{2n} have been computed by Menzel and Pekeris.[9] For the transition between the n'th and the nth level, f is given by the formula

$$f_{nn'} = \frac{2^6}{3\sqrt{3}\pi}\frac{1}{\varpi_n}\frac{1}{\left[\left(\frac{1}{n'}\right)^2-\left(\frac{1}{n}\right)^2\right]^3}\left|\frac{1}{n^3}\frac{1}{n'^3}\right| g\,,$$

where $\varpi_{n'}$ = weight of the n'th level and g = correction factor of the order 1. A very important point which is brought out by the treatment as given by Menzel and Pekeris is the equivalence of the discrete and continuous spectra or between the bound-bound,

TABLE 1

β	$U(\beta)$	β	$U(\beta)$	β	$U(\beta)$
0.0	0.287	1.9	0.0928	4.6	0.0091
0.1	.286	2.0	.0839	4.8	.0080
0.2	.283	2.1	.0758	5.0	.0071
0.3	.278	2.2	.0684	6	.0041
0.4	.271	2.3	.0617	7	.0027
0.5	.262	2.4	.0557	8	.0018
0.6	.252	2.5	.0502	9	.0014
0.7	.240	2.6	.0454	10	.0011
0.8	.228	2.7	.0411	11	.0008
0.9	.215	2.8	.0373	12	.0006
1.0	.202	2.9	.0338	13	.0005
1.1	.188	3.0	.0310	14	.0004
1.2	.174	3.2	.0260	15	.0003
1.3	.161	3.4	.0220	16	.0003
1.4	.148	3.6	.0187	17	.0002
1.5	.135	3.8	.0160	18	.0002
1.6	.124	4.0	.0238	19	.0002
1.7	.113	4.2	.0120	20	.0002
1.8	0.1024	4.4	0.0104	30	0.0001
				40	.....

bound-free, and free-free transitions. The only change which the above formula undergoes for bound-free transitions is the substitution of ik for n, where k is no longer limited to integer values, and a similar change in the expression for g. It follows, then, that for large n there is a smooth transition from the line spectrum to the continuous spectrum, with the absorption coefficient proportional to $1/\nu^3$. In the region of the higher Balmer lines, from a certain line number on, which depends on the value of F_0, the lines are spread out by the Stark effect so strongly as to form one continuous band of absorption. This band merely acts as an extension of the Balmer continuum into the region to the red of the theoretical Balmer limit at 3647. The absorption in this continuum varies as $1/\nu^3$.

The steps in the computation of the absorption arising from the broadened Balmer lines are as follows:

1. Compute at each λ under consideration the $\Delta\lambda$ for the lines which contribute.
2. From $\Delta\lambda = \beta F_0 s_n$, find β for each value of F_0 used.
3. Find $U(\beta)$ from Table 1.
4. Multiply $U(\beta)$ by $f_{2n}/s_n F_0$. A factor of 10^{-4}, occurring in the quantities f_{2n}, was added to the other multiplicative constants.

[9] *M.N.*, **96**, 77, 1935.

5. Sum the contributions of all the lines for which the value mentioned in 4 is appreciable (e.g., larger than 0.01); this gives the final absorption a. This sum is found to become a constant, independent of the wave length and of F_0 in the region where the lines overlap completely.

The factor $\pi e^2/mc \cdot \lambda^2/c \cdot 10^{-12}$ was omitted throughout these preliminary computations. It was assumed to be constant in the short region of wave lengths considered and was taken care of as explained in section 5.

TABLE 2

LOG a AS A FUNCTION OF λ AND LOG F_0

λ	LOG F_0							REMARKS
	−1	0.70−1	0.30	0.70	1.00	1.40	2.00	
3659.42...	0.11	0.08	0.08	0.08	0.08	0.08	0.08	*H* 33
63.41...	0.32	0.08	.08	.08	.08	.08	.08	*H* 29; 1
68.35...	0.32−1	0.06	.08	.08	.08	.08	.08	
73.76...	0.80	0.16	.08	.08	.08	.08	.08	*H* 23
75.25...	0.73−2	0.94−1	.085	.085	.085	.085	.085	
76.37...	0.90	0.23	.085	.085	.085	.085	.085	*H* 22
77.74...	0.54−2	0.85−1	.085	.085	.085	.085	.085	
79.36...	1.00	0.31	.085	.085	.085	.085	.085	*H* 21
81.10...	0.30−2	0.60−1	.085	.085	.085	.085	.085	
82.81...	1.11	0.42	.09	.09	.09	.09	.09	*H* 20
84.92...	0.15−2	0.40−1	.07	.09	.09	.09	.09	
86.83...	1.22	0.52	.10	.09	.09	.09	.09	*H* 19
89.14...	0−2	0.17−1	.04	.09	.09	.09	.09	
91.56...	1.34	0.64	.14	.09	.09	.09	.09	*H* 18
3697.15...	1.46	0.77	.21	.09	.09	.09	.09	*H* 17
3700.62...	.....	0.72−2	.82−1	.08	.09	.09	.09	
03.86...	1.60	0.90	.31	.09	.09	.09	.09	*H* 16
07.60...	.....	0.50−2	.60−1	.05	.095	.10	.10	
11.97...	1.74	1.04	.45	.13	.105	.10	.10	*H* 15
16.84...	.....	0.22−2	.31−1	.96−1	.08	.10	.10	
21.94...	1.89	1.19	.59	.23	.105	.10	.10	*H* 14
34.37...	2.05	1.36	.76	.37	.14	.105	.105	*H* 13
34.95...	0.26−1	0.50	.68	.36	.13	.11	.11	
37.70...	.....	0.40−2	.46−1	.03	.06	.11	.11	
40.20...	.....	0.84−3	.86−2	.60−1	.96−1	.11	.11	
41.70...	.....	.....	.71−2	.47−1	.00	.11	.11	
44.70...	.....	0.83−3	.91−2	.64−1	.03	.11	.11	2
46.20...	.....	0.23−2	.26−1	.95−1	.12	.11	.11	
48.70...	0.23−2	0.37−1	.40	.44	.24	.11	.11	3
50.15...	2.23	1.53	0.93	0.54	0.26	0.12	0.11	*H* 12

1. At log $F_0 = 0.20-1$, log $a = 0.15$.
2. At log $F_0 = 1.20$, log $a = 0.09$.
3. At log $F_0 = 0.48$, log $a = 0.50$.

The computations were carried through for the values $F_0 = 0.1, 0.5, 2, 5, 10, 25, 100$. Results are given in Table 2 and Figures 1 and 2. It is seen that the absorption in the center of the Balmer line is very high for small F_0 and decreases for larger values, until for very large F_0(log $F_0 = 2$) even H 12 at 3750 merges into the continuum (Fig. 1). For wave lengths between two lines the situation is just the opposite: for small F_0 no line is drawn out far enough to contribute any absorption, but for larger F_0 the absorption increases until it reaches the same limiting value as at the line centers (Fig. 2). Points nearer to the line center in the wings of the line may show a combination of the two

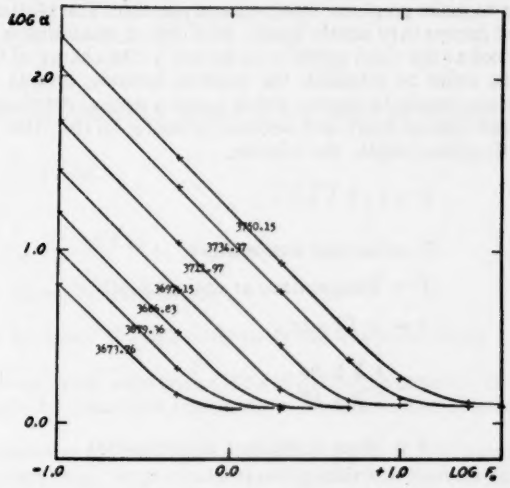

FIG. 1.—Absorption coefficient α in the centers of Balmer lines as a function of the normal field-strength F_0.

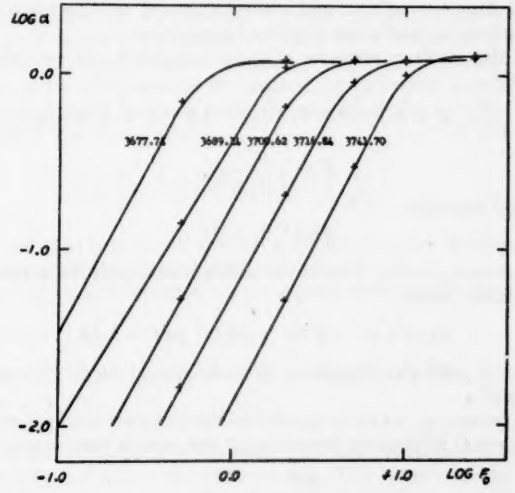

FIG. 2.—Absorption coefficient α between successive Balmer lines as a function of the normal field-strength F_0.

effects, passing through a maximum. In those cases a few additional values of a were computed, in order to make graphical interpolation possible. The plotting on a logarithmic scale made the curves very nearly linear, with only a small region of curvature.

4. We now proceed to the third question in section 1: the change of the field through the atmosphere. In order to establish the relation between optical depth and field strength, the relations should be known which connect optical depth and temperature, on the one hand, and optical depth and electron pressure, on the other. For the change of temperature with optical depth, the relation

$$T = T_0 \sqrt[4]{1 + C\tau} \tag{4}$$

was used, where

T_0 = Surface temperature,

T = Temperature at optical depth τ,

$$\tau = -\int k \rho d r , \tag{5}$$

$$C = \frac{3}{2} \frac{\bar{k}}{k} \frac{1}{4} \frac{h\nu}{kT},$$

in which

$\bar{k}$ = Mean coefficient of continuous absorption,

k = Coefficient of continuous absorption, both per unit mass.

The results of Pannekoek's computations for $\bar{k}$ and k were used,[10] which are given in the form $\bar{k} = \bar{\kappa} P x$ and $k = \kappa P x$; $\bar{\kappa}$ and κ are tabulated as functions of temperature; P is the electron pressure, and x the degree of ionization.

The change of the electron pressure with optical depth can be computed from the following relations:

$$\frac{x}{1-x} P = 10^{-5040(13.53/T)} \cdot T^{5/2} 10^{-0.48} = K \text{ (Saha)}, \tag{6}$$

$$P = \frac{x}{1+x} p , \tag{7}$$

where p is the total pressure.

$$g \rho d r = -dp , \tag{8}$$

in which g is the surface gravity. This is the well-known hydrostatic equation. It follows from this last equation that

$$\bar{k} g \rho d r = -k dp \qquad \text{or} \qquad g d\tau = k dp . \tag{9}$$

The relations (4)–(9) suffice to determine at each optical depth the value of T and P, and hence of F_0 and a.

5. Finally, the foregoing has to be applied to the integration of the equations of radiative transfer. The usual Eddington formulae for the case of pure scattering were used:

$$\frac{dH}{d\tau} = J - E , \tag{10}$$

$$\frac{dJ}{d\tau} = q^2 H , \tag{11}$$

[10] *Pub. Astr. Inst. U. Amsterdam*, No. 4, 1935.

where

$$q^2 = 3\left(1 + \frac{s}{k}\right). \tag{12}$$

In these formulae

s = Line absorption coefficient (scattering coefficient),

$$J = \frac{1}{4\pi} \int I \, d\omega,$$

$$H = \frac{1}{4\pi} \int I \cos \vartheta \, d\omega,$$

I = Intensity of radiation,

E = Intensity of black-body radiation at optical depth τ.

Under the assumptions made, equations (10) and (11) apply to each wave-length interval separately; hence the quantities appearing in these formulae should be defined accordingly.

The boundary condition for large optical depth is $J_\infty = E_\infty$. As boundary condition at the surface, the customary approximation $J_0 = 2H_0$ was used at first. Later some of the computations were repeated with the correct relation $J_0 = \sqrt{3}H_0$.[11, 12] These new computations indicated an increase in H_0 of about 4 per cent; all the results based on the first boundary condition were therefore increased by 4 per cent.

Because q^2 varies with optical depth in a way which cannot be given by a mathematical expression, no analytical solution of equations (10) and (11) was possible. Instead, numerical integration in the way outlined by Verweij[1] was performed. For that purpose a table of the relation q^2 versus τ is required for each wave length at which H_0 is to be computed. In order to obtain such tables, a graph of the variation of log F_0 with τ was constructed for each of the atmospheres considered, as indicated in section 4. For each wave length, then, log α could be read from the graphs of log α versus log F_0. On inserting the constants, it was found that

$$\log \frac{s}{k} = 6.86 + \log \alpha + \log \frac{y_2}{K\kappa}.$$

Here y_2 is the fraction of atoms in the second level, as given by Boltzmann's formula. For λ and κ the values at 3700 A were taken.

For the following twelve atmospheres computations were carried through:

$$\left.\begin{aligned} \theta_0 &= 0.50, \quad T_0 = 10{,}080°, \\ \theta_0 &= 0.40, \quad T_0 = 12{,}600°, \\ \theta_0 &= 0.30, \quad T_0 = 16{,}800°, \end{aligned}\right\} \log g = 2,4,6,8.$$

For log $g = 8$, only a few points along the spectrum were determined, since, in the region considered, no trace of a line spectrum is left. The results of the computations are given in Table 3. From these data the number of visible Balmer lines can be found. Figure 3 shows the dependence of this number on temperature and gravitation.

[11] E. Hopf, *Mathematical Problems of Radiative Equilibrium* (Cambridge: At the University Press, 1934), p. 46.

[12] S. Chandrasekhar, *Ap. J.*, **100**, 76, 1944.

TABLE 3

H_0 AS A FUNCTION OF λ, θ_0, g

λ	θ_0	LOG $g=2$			LOG $g=4$			LOG $g=6$			LOG $g=8$		
	No H	0.50	0.40	0.30	0.50	0.40	0.30	0.50	0.40	0.30	0.50	0.40	0.30
3659.42	33	0.20	0.20	0.20	0.20	0.20	0.20	0.20	0.20	0.20	0.20	0.20	0.20
63.41	29	.20	.20	.20	.....	.....	.....	.....	.....	.....	.....	.....	.....
73.76	23	.20	.....	.20	.....	.....	.....	.....	.....	.....	.....	.....	.....
75.25	.....	.21	.20	.21	.....	.....	.....	.....	.....	.....	.....	.....	.....
76.37	22	.....	.19	.....	.....	.....	.....	.....	.....	.....	.....	.....	.....
77.74	.....	.....	.....	.....	.20	.20	.....	.....	.....	.....	.....	.....	.....
79.36	21	.17	.....	.20	.....	.....	.....	.....	.....	.....	.....	.....	.....
81.10	.....	.....	.....	.21	.....	.....	.....	.....	.....	.....	.....	.....	.....
82.81	20	.....	.....	.....	.20	.....	.....	.....	.....	.....	.....	.....	.....
84.92	.....	.25	.23	.22	.20	.20	.....	.....	.....	.....	.....	.....	.....
86.83	.....	.....	.....	.....	.....	.20	.....	.....	.....	.....	.....	.....	.....
89.14	.....	.29	.25	.23	.....	.....	.....	.....	.....	.....	.....	.....	.....
91.56	18	.12	.13	.16	.....	.....	.....	.....	.20	.....	.....	.....	.....
94.18	.....	.35	.29	.25	.....	.....	.....	.....	.....	.....	.....	.....	.....
3697.15	17	.10	.12	.14	.19	.....	.....	.....	.....	.....	.....	.....	.....
3700.62	.....	.41	.28	.....	.21	.....	.....	.....	.....	.....	.....	.....	.....
01.62	.....	.....	.28	.....	.....	.....	.....	.....	.....	.....	.....	.....	.....
03.12	.....	.14	.....	.....	.....	.....	.....	.....	.....	.....	.....	.....	.....
03.86	16	.08	.10	.12	.18	.19	.20	.....	.....	.....	.19	.20	.20
04.60	.....	.14	.....	.....	.....	.....	.....	.....	.....	.....	.....	.....	.....
06.60	.....	.40	.31	.27	.....	.....	.....	.....	.....	.....	.....	.....	.....
07.60	.....	.45	.35	.29	.23	.21	.....	.....	.....	.....	.....	.....	.....
08.60	.....	.44	.34	.28	.....	.....	.....	.....	.....	.....	.....	.....	.....
11.35	.....	.11	.12	.14	.....	.....	.....	.....	.....	.....	.....	.....	.....
11.97	15	.06	.08	.11	.16	.18	.19	.19	.19	.....	.....	.....	.....
12.59	.....	.11	.12	.14	.....	.....	.....	.....	.....	.....	.....	.....	.....
15.34	.....	.47	.35	.29	.....	.....	.....	.....	.....	.....	.....	.....	.....
16.84	.....	.50	.37	.....	.25	.23	.21	.19	.....	.....	.....	.....	.....
18.34	.....	.46	.35	.29	.....	.....	.....	.....	.....	.....	.....	.....	.....
21.34	.....	.11	.11	.12	.....	.....	.....	.....	.....	.....	.....	.....	.....
21.94	14	.05	.07	.09	.....	.16	.18	.....	.....	.....	.....	.....	.....
22.54	.....	.11	.11	.12	.....	.....	.....	.....	.....	.....	.....	.....	.....
25.04	.....	.44	.34	.....	.....	.....	.....	.....	.....	.....	.....	.....	.....
26.54	.....	.53	.40	.32	.....	.....	.....	.....	.....	.....	.....	.....	.....
28.04	.....	.55	.41	.33	.....	.....	.....	.....	.....	.....	.....	.....	.....
29.54	.....	.53	.40	.32	.....	.....	.....	.....	.....	.....	.....	.....	.....
33.97	.....	.10	.10	.11	.....	.....	.....	.....	.....	.....	.....	.....	.....
34.37	13	.04	.06	.07	.10	.13	.15	.19	.19	.20	.....	.....	.....
34.95	.....	.10	.10	.11	.11	.....	.17	.....	.....	.....	.....	.....	.....
37.70	.....	.46	.35	.29	.....	.....	.....	.....	.....	.....	.....	.....	.....
40.20	.....	.57	.43	.33	.31	.28	.25	.....	.....	.....	.....	.....	.....
41.70	.....	.59	.44	.34	.33	.29	.25	.20	.19	.....	.....	.....	.....
43.20	.....	.59	.43	.34	.32	.29	.25	.....	.....	.....	.....	.....	.....
44.70	.....	.57	.43	.33	.....	.....	.....	.....	.....	.....	.....	.....	.....
46.20	.....	.50	.38	.....	.....	.....	.....	.....	.....	.....	.....	.....	.....
48.70	.....	.24	.21	.20	.12	.14	.15	.....	.....	.....	.....	.....	.....
50.15	12	0.03	0.04	0.06	0.08	0.10	0.13	0.18	0.18	0.19	0.19	0.19	0.20

6. The number of visible Balmer lines is the quantity most readily obtained from observations. Limitations to its dependability, however, are set by the possible rotation of the observed stars and by the resolving power of the spectrograph used.

Observational material was put at the writer's disposal through the kindness of Dr. C. D. Shane, director of the Lick Observatory. A large number of microdensitometer tracings on a small scale of spectra made by C. S. Yü were available, as well as others, taken by the writer at the Lick Observatory and traced on a larger scale.

The parameters entering into a comparison of theory and observations are the temperature and surface gravity of a star. The latter depends on mass and radius. For two classes of objects these quantities are known with fair accuracy. The first one consists of bright stars, as given, e.g., in Schlesinger's *Bright Star Catalogue*, which furnishes all the data required as far as dependable parallaxes are known. The second group is formed by eclipsing binaries. The data for these objects were taken from a publication by S. Gaposchkin.[13] As to a third source of observational material, we were fortunate in having access to the spectra of two white dwarfs.

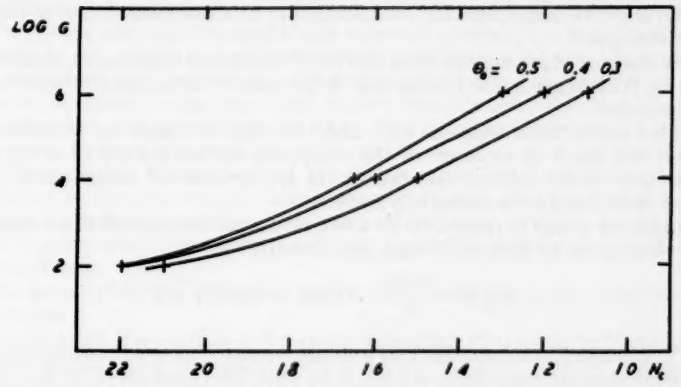

FIG. 3.—Last-resolved Balmer line N_e as a function of surface gravity G and surface temperature θ_0

The groups require a different treatment, and the single stars will be discussed first.

7. The mass of a star can be found from its absolute magnitude by the application of a mass-luminosity relation. In the reductions the form given by Russell and Moore[14] was used:

$$\log \mathcal{M} = -0.105\,(M - 5.23)\,, \tag{13}$$

in which $\mathcal{M}$ stands for the mass and M is the bolometric absolute magnitude. The corrections to be applied to visual magnitudes in order to reduce them to bolometric magnitudes are by no means easily determined. Hertzsprung has computed these corrections, assuming the stars to radiate like black bodies, but, as has been shown by Pannekoek[15] and Unsöld,[16] stellar radiation deviates from black-body radiation. From Pannekoek's work Kuiper[17] derived corrections to be applied to Hertzsprung's numbers. Some un-

[13] *Proc. Amer. Phil. Soc.*, Vol. 82, No. 3, 1940.

[14] *The Masses of the Stars* (Chicago: University of Chicago Press, 1940), p. 112.

[15] *M.N.*, 95, 529, 1935.

[16] *Zs. f. Ap.*, 8, 32, 1933; 8, 225, 1934.

[17] *Ap. J.*, 88, 429, 1938.

certainty may still exist as to these corrections, since they were derived from Pannekoek's theory, which, although it is qualitatively correct, still leaves discrepancies with observations. However, these corrections enter into log $\mathcal{M}$ only multiplied by 0.1, and hence they do not affect its value strongly.

The determination of the visual absolute magnitudes involves many more uncertainties, especially for the B stars. Spectroscopic determinations seemed to be the most reliable.

Many of the stars used here of classes B1–A7 have been classified by Morgan, Keenan, and Kellman in their *Atlas of Stellar Spectra*, in which data on the absolute magnitudes of the various subclasses are also given. It should be kept in mind, though, that the authors themselves do not consider these determinations as final. Dr. Morgan, moreover, kindly allowed the writer to use some of his unpublished classifications and absolute magnitudes. The probable errors range from 0.4 to 1.0 mag.

For many of the stars of classes B1–B8 (on the Victoria classification) Stebbins, Huffer, and Whitford[18] give spectral classifications, together with a list of the mean absolute magnitudes for each spectral subclass.

Finally, absolute magnitudes for a small number of A stars were found in the Mount Wilson Catalogue.[19]

For the stars for which none of these sources give absolute magnitudes, the parallaxes, as given by Schlesinger in the *Catalogue of Bright Stars*,[20] were used to derive the absolute magnitudes.

It follows easily from formulae (13) and (14) that a change in M amounting to $\Delta M = 1.0$ will result in a change of the computed surface gravity of $\Delta \log g = 0.3$. Hence, in spite of the existing uncertainties in M, the order of magnitude of log g, as computed, is believed to be essentially correct.

The radius of a star is related to its absolute magnitude and effective temperature by a formula, given by Russell, Dugan, and Stewart[21] as

$$\log R = \frac{5900}{T_e} - 0.2M_v - 0.02 + x\,, \tag{14}$$

where R is expressed in solar radii. This formula is based on a solar temperature of 6000° and a visual absolute magnitude of 4.83. If we take the values given by Kuiper,[17] viz., 5713° and 4.73, the constant -0.02 is changed into -0.09. The term x has the following values:

$T =$	8000°	10,000°	12,000°	15,000°	20,000°
$x =$	-0.01	-0.01	-0.02	-0.04	-0.06

The radius thus computed is that of the layer of the effective temperature of the star, or essentially that of the opaque disk. It is an open question how far the layers of smaller opacity extend and hence by how much log R should be increased. Radiation pressure or dynamical ejection might support the stellar atmosphere much higher than the negligibly small thickness of the photosphere found from computations, which do not take these effects into account.

Another difficult point in the discussion is that of the stellar temperatures. As mentioned before, the material for checking theory with observations consisted partly of a number of microdensitometer tracings made by Yü at the Lick Observatory. Yü has used the tracings to determine the color temperatures of these stars.[22] However, his de-

[18] *Ap. J.*, **91**, 20, 1940.

[19] *Mt. W. Contr.*, No. 511; *Ap. J.*, **81**, 187, 1935.

[20] New Haven: Yale University Observatory, 1940.

[21] *Astronomy*, 2 (Boston: Ginn & Co., 1938), 738.

[22] *Lick Obs. Bull.*, No. 375, 1926.

terminations seem to be affected by systematic errors,[23] and, besides, the reduction of color temperatures to effective temperatures is an uncertain procedure. Therefore, in Table 4 all temperatures are based on Kuiper's scale and the Henry Draper classification, since this classification underlies Kuiper's determinations.

For the relation between effective temperature T_e and surface temperature T_0, the approximation $T_e = 1.20\ T_0$, or $T_0 = \frac{5}{6} T_e$ was used; T_0 was rounded off to the nearest 50°.

In Table 4 the stars used are listed, together with the quantities essential in the computation of log g. Column 7 gives the computed number of observable Balmer lines N_c. Columns 8, 9, and 10 give the observed numbers N_{o1} on Yü's tracings, N_{o2} on the larger scale tracings, and the logarithm of the effective surface gravity, log g_e, which follows from the observed number of lines. Both g_e and g_e are expressed in solar units. In a few cases, observed line numbers were available from other sources, as indicated in the column "Remarks." Log g_e was always derived from the largest observed number indicated and was entered only if $N_c < N_o$.

As can be seen from the table, the agreement between observations and theory is not very satisfactory, especially if we realize that the N_{o1} are lower limits, owing to the small scale of the tracings. One might have expected an effect in a direction opposite to the one shown, viz., that the number observed would be smaller than the number predicted, because of limited resolving power of the spectrograph, etc. However, the number observed is, in general, larger than what follows from the computations. The case of β Orionis presents a striking discrepancy, and ζ Tauri, which is known to be a shell star, is an even stronger example, with $N_c = 14$, and $N_o = 32$, as given by Miss Losh.[24] In terms of Stark effect, this means that the field is weaker than would follow from the theory based on temperature and surface gravity. It does not seem probable that the temperatures are much lower than the ones assumed, and certainly not to the extent required to bring observations and theory into agreement. Some other possibilities will be discussed later.

8. The double stars will be treated briefly, since observations are available for only a few systems.

As is well known, it is possible to derive, for well-observed systems of eclipsing binaries, the relative dimensions of the components. If a mass-luminosity relation is assumed and if the spectrum of at least one of the components is known, it is possible to determine the absolute dimensions and the masses. Some modifications were made in the treatment of the extensive material compiled by Gaposchkin.[13] The temperature scale was changed slightly so as to agree with Kuiper's scale, used in the previous section. Furthermore, the mass-luminosity relation (13) was substituted for Gaposchkin's, and the ratio of the masses of two stars with known difference in brightness was computed from that relation. Table 5 gives the data for the five stars for which the lines could be counted. As before, the number of lines observed is, in almost every case, considerably larger than the number computed.

9. Dr. W. J. Luyten kindly put at the writer's disposal the spectra of two white dwarfs, taken at the McDonald Observatory. The stars are Co $-32°5613$ and o^2 Eri B;[25] both are A-type stars. The spectrum of o^2 Eri B shows the usual features of a white dwarf, namely, extremely broad hydrogen lines; the last visible member of the Balmer series is H 9. The lines in Co $-$ 32°5613 are far less broadened, but here also the continuum begins between H 9 and H 10. Luyten's value for the absolute magnitude of this star, $M = 10.1$, and equation (13) yield a value for the mass of 0.3 solar masses. It is known, however, that the white dwarfs are less luminous than the main-sequence stars

[23] A. Arnulf, D. Barbier, and D. Chalonge, *J. d. Obs.*, **19**, 149, 1936.

[24] *Pub. Obs. U. Michigan* **4**, 1, 1932.

[25] A description of these stars is given by W. J. Luyten, *Ap. J.*, **102**, 382, 1945.

TABLE 4

Star (1)	Spectrum (2)	Authority* (3)	M_v (4)	θ_0 (5)	log g_e (6)	N_e (7)	N_{01} (8)	N_{02} (9)	log g_e (10)	Remarks (11)
o Per	B1 IV	M	−4.7	0.26	−0.5	14–15	15	.....	−0.8	
ζ Per	B1 I	M	−5.5	.26	−1.0	15–16	16	.....	.....	
ϵ Per	B0.5 III	MKK	−4	.26	−0.6	14–15	14–15	.....	.....	
η Ori	B1 V	M	−3.8	.26	−0.5	14–15	14–15	.....	−0.6	
β CMa	B1 II–III	MKK	−4	.26	−0.5	14–15	15	.....	−1.4	Marshall†
β Cep	B1 IV	MKK	−2.5	.26	−0.1	14	16	.....	−1.7	Marshall†
ν Eri	B2s	SHW	−3.0	.30	−0.4	15	15–16	.....	−0.6	
γ Ori	B2 IV	MKK	−2.5	.30	−0.2	14	17–18	.....	−1.2	
χ^2 Ori	B2 I	M	−7.2	.30	−1.7	18	20	.....	−2.0	
α Vir	B1 III–IV	MKK	−3	.30	−0.4	15	13–14	.....	.....	
ζ Cas	B2.5 IV	MKK	−3	.33	−0.5	15	14–15	.....	−1.2	Struve‡
ϵ Cas	B3 III	MKK	−3.5	.33	−0.7	16	15	.....	.....	
π^4 Ori	B2s	SHW	−3.0	.33	−0.4	15	18	.....	−1.6	
η Aur	B3 V	MKK	−1.0	.33	+0.1	14	16	.....	−0.8	
ζ Tau	B3e	SHW	−2.2	.33	−0.3	14–15	18	.....	<-3.0	Losh§
η UMa	B3 V	MKK	−1.0	.33	+0.1	14	16–17	.....	−0.8	
δ Per	B5 III	MKK	−0.5	.39	0.0	15	15	.....	.....	
17 Tau	B5nea	SHW	−1.6	.39	−0.3	15–16	16–17	.....	−0.7	
20 Tau	B9s	SHW	−0.4	.39	+0.1	15	15–16	.....	−0.2	
η Tau	B5p	HD	−1.5	.39	−0.2	15–16	16–17	.....	−0.7	
τ Ori	B8	SHW	−0.8	.39	0.0	15	16	.....	−0.6	
γ CMa	B5	HD	−0.5	.39	+0.1	15	15–16	.....	−0.2	
κ Dra	B5e	SHW	−1.6	.39	−0.3	15–16	16–17	.....	−0.7	
67 Oph	B5 I–II	M	−5.5	.39	−1.4	18	15?	.....	−2.2	Struve‡
ζ Dra	B5	HD	+0.3	.39	+0.1	15	19:	.....	−2.0	Struve‡
τ Her	B5 IV	MKK	−1.0	.39	−0.1	15	16–17	.....	−0.7	Struve‡
ξ Tau	B8nn	SHW	−0.8	.50	−0.3	16	13	16–17	−0.5	
β Ori	B8 Ia	MKK	−6.5	.50	−2.0	20	19–20	26	−3:	Marshall†
β Tau	B8 III	MKK	−2.0	.50	−0.7	17	15–16	.....	.....	
α Leo	B8 V	MKK	0.0	.50	−0.1	16	14–15	16	.....	
β Lib	B8 V	MKK	0.0	.50	−0.1	16	15	.....	.....	
α Del	B8	HD	+0.1	.50	0.0	16	13–14	.....	.....	
α And	A0p	HD	+0.2	.57	−0.2	16–17	15–16	19–20	−1.4	
ν Tau	A0	HD	+0.4	.57	−0.1	16–17	15–16	.....	.....	
μ Lep	A0	HD	+0.7	.57	0.0	16	18	19–20	−1.4	
β Aur	A2 IV	MKK	+0.5	.57	−0.3	17	17	.....	.....	
θ Aur	A0p	MKK	−1?	.57	−0.6?	17–18	16	15–16	.....	
γ Gem	A1 V	MKK	+1	.57	0.0	16	18–19	.....	−1.0	
α CMa	A1 V	MKK	+1	.57	0.0	16	16–17	18–19	−1.0	
c Hya	A0	HD	+0.6	.57	−0.1	16	14	.....	.....	
θ UMa	A0	HD	+0.2	.57	−0.2	17	16–17	17	.....	
κ Hya	A0	HD	+0.2	.57	−0.2	17	16	15–16	.....	
η Leo	A0p	HD	(+0.7)	.57	−0.1	16	18–19	.....	−1.0	
β UMa	A1 V	MKK	+1	.57	0.0	16	16	19	−1.4	
γ UMa	A0 V	W	+0.5	.57	−0.1	16	18	.....	−1.0	
ϵ UMa	A0	HD	0.0	.57	−0.3	17	16–17	18–19	−1.0	
α CVn	A0p	MKK	−1?	.57	−0.6	17	15–16	.....	.....	
α Dra	A0p	HD	+0.5	.57	−0.1	16	15–16	19–20	−1.4	
α CrB	A0 V	MKK	+0.5	.57	−0.1	16	15–16	18–19	−1.0	
μ Ser	A0	HD	+0.4	.57	−0.1	16	15	.....	.....	
λ Oph	A0	HD	+1.1	.57	−0.1	16	15	.....	.....	
ϵ Her	A0	HD	+0.8	0.57	0.0	16	15	.....	.....	

* The authorities quoted in the third column for classification and absolute magnitudes are: M: W. W. Morgan, unpublished. MKK: Morgan, Keenan, and Kellman, *An Atlas of Stellar Spectra*. SHW: Stebbins, Huffer, and Whitford, *Ap. J.*, **91**, 20, 1940 W: Miss M. E. Walther of the Harvard Observatory, who kindly made some tentative classifications on the MKK system. HD: *Henry Draper Catalogue* and Schlesinger's *Bright Star Catalogue*.

† *Pub. Obs. U. Michigan*, **5**, 137, 1934.

‡ *Ap. J.*, **91**, 365, 1940.

§ *Pub. Obs. U. Michigan*, **4**, 1, 1932.

TABLE 4—*Continued*

Star (1)	Spectrum (2)	Author-ity* (3)	M_v (4)	θ_0 (5)	log g_c (6)	N_c (7)	N_{o1} (8)	N_{o2} (9)	log g_e (10)	Remarks (11)
γ Oph....	A0	HD	0.0	0.57	−0.3	17	13	.....	.....	
α Lyr....	A0 V	MKK	+0.5	.57	−0.1	16	16–17	18–19	−1.0	
γ Lyr....	B9 V	MKK	+0.5	.57	−0.1	16	17:	.....	.....	
7 Lac.....	A0 V	W	+0.5	.57	−0.1	16	14–15	17–18	−0.6	
θ Gem...	A2 I	W	−6.5	.62	−2.3	21	17	19	.....	
λ Gem...	A2	HD	+1.4	.62	0.0	16–17	15	18	−0.8	
θ Leo....	A4s	MtW	+1.0	.62	−0.1	16–17	17–18	.....	−0.6	
λ UMa...	A2 IV	MKK	+0.5	.62	−0.3	17	18	19	−1.4	
β Leo....	A3 V	MKK	+2.0	.62	+0.2	16	16–17	18–19	−0.8	
δ UMa...	A3 V	MKK	+2.0	.62	+0.2	16	13	17–18	−0.6	
ζ₁ UMa...	A2 V	MKK	+1.3	.62	−0.1	17	17	.....	.....	
ζ Vir.....	A3 V	MKK	+2.0	.62	+0.2	16	16	.....	.....	
γ UMi...	A3 II–III	MKK	−1.0	.62	−0.8	18	14	18	.....	
ε Ser.....	A2	MtW	+1.8	.62	+0.2	16	15	.....	.....	
α Cyg....	A2 I	M	−7.2	.62	−2.6	22	18–19	19–20	<−3:	Wright‖
β Eri.....	A3	HD	+1.5	.65	0.0	16–17	15	15–16	.....	
δ Leo.....	A3	MtW	+2.1	.65	+0.1	16–17	16	19?	−1.2:	
β Tri.....	A5 III	MKK	0.0	.71	−0.6	18:	15–16	19	−1.2:	
α Aql.....	A7 V	MKK	+2.5	.71	+0.1	16–17:	15	16–17	.....	
α Cep....	A7 V	MKK	+2.5	0.71	+0.1	16–17:	15	18	−0.8:	

‖ *Lick Obs. Bull.*, **10**, 100, 1921.

of the same mass. In Figure 1 of Kuiper's article on the empirical mass-luminosity relation[26] and in Figure 1 of Russell and Moore's book[14] it seems indicated that the mass of a white dwarf corresponds to a bolometric absolute magnitude of about 3.5 mag. brighter than that of the dwarf. Therefore, a mass of 0.75⊙ was adopted for this star. With a temperature of 10,000°, formula (14) then yields log g = 3.0 in solar units, or 7.4 absolute. For o^2 Eri B, Kuiper[26] gives log g = 7.6.

In the course of the computations of H_0, the net stream at the stellar surface, it was found that a one-to-one correspondence exists between this quantity and the value of q^2 (eq. [12]) at optical depth 0.05. It therefore seems reasonable to assume that a line will be separately visible if, for the F_0 prevailing at $\tau = 0.05$, the absorption coefficient of that line has not yet attained the value of the continuous band of absorption. It was found that log F_0 = 2 is only about 0.20 higher than the values of log F_0 in these two dwarfs. Table 6 gives log α for a range of wave lengths for log F_0 = 2 and 1.5. The former corresponds to log g = 8, the latter to log g = 6.6, which is probably far below the dynamical value of log g in the stars considered. It is seen from the table that, for the higher value of log g, H 10 should not be visible, whereas, at log g = 6.6, H 10 will not yet have merged into the continuum. Hence the conclusion seems justified that, in the two white dwarfs considered, the observations are in accordance with the theoretical expectations.

10. In this section some effects will be investigated which may be the cause of the discrepancies found.

a) Collisional broadening, which was neglected altogether, would tend to decrease the computed numbers still further. It was found, however, that, on the basis of the theory of Weisskopf,[27] the collisional broadening is negligibly small in comparison with the Stark broadening applied.

[26] *Ap. J.*, **95**, 472, 1938.

[27] *Phys. Zs.*, **34**, 1, 1933.

b) The discrepancy between observation and theory is in the sense that the theoretical field strength seems to be too large or that the Stark broadening has been exaggerated. If the half-width of the Stark pattern is taken equal to the distance of the third-last component from the center, then the factor $\{n(n-1)+2\}$ is changed into $\{n(n-3)+2\}$. This is equivalent to taking, for the field strength at which the lines begin to merge, about 1.15 its present value; this adds 0.06 to log F_0. As can be seen from Figures 1 and 2, this will hardly ever increase N_e by one unit, and hence this correction will not remove the difficulty.

Inglis and Teller[28] have published an important investigation on the depression of series limits. They conclude that if n is the upper quantum number of the last line separately visible, the electrons do not contribute to the field at temperatures $T > 10^5/n$. Unsöld[29] reached a similar conclusion, for $T > (4.6 \times 10^5)/n$. If we adopt the first limit, this would mean that the value of P used is too large by a factor of 2. Cor-

TABLE 5

DOUBLE STARS

Star	Spectrum	N_e	N_{e2}	Star	Spectrum	N_e	N_{e2}
AR Aur	B9	17–18	19	β Lyr	B5–B8p	19	18
YZ Cas	A3	18–19	21–22	β Per	B8	16–17	18–19
α CrB	A0	16–17	18–19				

TABLE 6

LOG α FOR LOG $F_0 = 2$ AND 1.50

λ	Identification	log α	
		log $F_0 = 2$	log $F_0 = 1.50$
3970.08	*H*7	0.44	.....
60	.....	.36	.....
50	.....	.14	.....
40	.....	.89−1	.....
30	.....	.75−1	.....
20	.....	.80−1	.....
10	.....	.96−1	.....
00	.....	.12	.....
3889.05	*H*8	.19	0.64
80	.....	.17	.20
71	.....	.10	.52−1
62	.....	.045	.30−1
53	.....	.03	.56−1
44	.....	.06	.08
35.39	*H*9	.09	.40
26	.....	.09	.12
17	.....	.09	.79−1
08	.....	.09	.98−1
3797.90	*H*10	0.08	0.19

[28] *Ap. J.*, **90**, 439, 1939.

[29] *Vierteljahrsschrift der Astronomischen Gesellschaft*, Vol. **78**, No. 4, 1943.

recting log P by 0.30 comes to the same as correcting log g by 0.60, since P is very nearly proportional to $g^{1/2}$. This reduction would remove many, though not all, discrepancies observed, as can be seen from Table 4.

c) Another way of interpreting the effect found is that the electrical field actually present is weaker because the electron pressure is lower than the one assumed. On the assumption that the ionization corresponds to the case of thermodynamical equilibrium, this would mean that the mean density of the absorbing material is lower, or that the pressure gradient is smaller, than what would follow from the dynamical gravitation GM/R^2. A reduction by a factor as large as 50 seems to be indicated by the values of log g_e in Table 4, and for ζ Draconis and some others even by more than 100. Similar effects were found by Pannekoek and Reesinck[30] and by Schalén.[31] The latter, using Verweij's computations, finds for α Cygni a surface gravity of log $g = 1.2$, whereas the dynamical value is 2.5. Pannekoek and Reesinck find log $g = 0.4$, -0.1, and -0.2 for the cepheids δ Cephei, α Ursae Minoris, and ζ Geminorum; this would lead to masses for these stars smaller than the sun's mass. Pannekoek then concludes that a strong radiation pressure must be present, which might eventually surpass the gravitational forces and result in an outward flow of gas with very small pressure gradient.

In this connection the work of Elvey and Struve[32] and of Shajn[33] should be mentioned. Elvey and Struve conclude from the shape of the curve of growth in three supergiants that considerable turbulence must be present. Shajn finds a confirmation of outward streaming gases in supergiants. From a solution for galactic rotation of supergiants he finds a K-term of -5 km/sec, which he interprets as arising from an outward motion of the absorbing gases.

Finally, we may note here the increasing number of stars which have been found to possess extended atmospheres, and we recall the unsolved problem of the support of the solar corona.

In many investigations it has been assumed that the effect of decreased effective gravity can be attributed to the action of radiation pressure. A critical study shows, however, that, in general, the effect of radiation pressure is quite negligible. At first sight, one would be inclined to compute the net outward flux H, integrated over all frequencies, multiply it by the mean coefficient of mass absorption $\bar{k}$, and put the impulse communicated to the absorbing mass equal to $H\bar{k}/c$. This is essentially Eddington's procedure.[34] However, in doing so, one overlooks the important fact that the spectral region through which most of the outward flux passes is quite different from the spectral region of highest opacity. Hence the radiation passes mostly unobstructed, and no radiation pressure ensues. One must therefore consider both the absorption coefficient and the flux of radiation in their dependence on frequency.

The following treatment is due to Dr. Menzel, to whom the writer is indebted for permission to quote it here. Let

N_n = Number of H atoms per cubic centimeter in the nth quantum state;

N_i = Number of H ions per cubic centimeter;

$N = \Sigma N_n$;

$a_{\nu n}$ = Atomic coefficient of continuous absorption for frequency ν of an atom in the nth quantum state;

[30] *B.A.N.*, **3**, 47, 1925; **8**, 175, 1937.

[31] *Upsala U. Arsskrift*, No. 8, 1936.

[32] *Ap. J.*, **79**, 409, 1934.

[33] *Bull. Abastumani Obs.*, **7**, 83, 1943.

[34] *The Internal Constitution of the Stars* (Cambridge: At the University Press, 1926), §§ 233, 247, 248.

$a_{\nu n} \neq 0$ only to the violet of the nth series limit ;

ν_n = Frequency of the nth series limit ;

a_ν = Absorption coefficient per cubic centimeter for frequency ν ;

F_ν = Flux of radiation at frequency ν .

For F_ν the following expression is assumed:

$$F_\nu = \frac{2\pi h\nu^3}{c^2} \frac{1}{e^{h\nu/\kappa T} - 1} W ,$$

in which W is the dilution factor. The following relations exist:

$$\frac{N_n}{N_1} = \frac{g_n}{g_1} e^{-h(\nu_1 - \nu_n)/\kappa T} = n^2 e^{-h(\nu_1 - \nu_n)/\kappa T} ,$$

$$a_{\nu n} = \frac{\pi e^2}{m c} \cdot \frac{2^4}{3\pi\sqrt{3}} \frac{R^3}{\nu^3} \cdot \frac{1}{Rn^5} = \frac{1}{n^5} a_{\nu 1} = \text{Const.} \frac{1}{n^5} \frac{1}{\nu^3} ,$$

$$a_\nu = N_1 a_{\nu 1} + N_2 a_{\nu 2} + \ldots .$$

The impulse on the material in 1 cm³ resulting from absorption of radiation in the frequency interval ν to $\nu + d\nu$ is

$$\frac{F_\nu a_\nu d_\nu}{c} = \frac{a_{\nu 1}}{c} N_1 e^{-h\nu_1/\kappa T} \left(e^{h\nu_1/\kappa T} + \frac{1}{2^3} e^{h\nu_2/\kappa T} + \frac{1}{3^3} e^{h\nu_3/\kappa T} + \ldots \right) \times W \frac{2\pi h}{c^2} \frac{1}{e^{h\nu/\kappa T} - 1} d\nu .$$

Integrating this over all frequencies, we obtain

$$\text{Const. } N_1 e^{-h\nu_1/\kappa T} \left[\int_{\nu_1}^{\infty} \frac{e^{h\nu_1/\kappa T}}{e^{h\nu/\kappa T} - 1} d\nu + \frac{1}{2^3} \int_{\nu_2}^{\infty} \frac{e^{h\nu_2/\kappa T}}{e^{h\nu/\kappa T} - 1} d\nu + \ldots \right]$$

$$\sim \text{const. } N_1 e^{-h\nu_1/\kappa T} T \left(1 + \frac{1}{2^3} + \frac{1}{3^3} \ldots \right),$$

in which the constant is equal to 9.12×10^{-18}. Attention may be called here to the fact that the contributions from the continua other than the Lyman continuum are, in fact, negligible and independent of temperature. With increasing temperature the population of the higher levels increases, but the frequency of maximum intensity moves to the violet, and these two factors just balance. So much for the impulse arising from the absorption of radiation.

The impulse communicated per second to the hydrogen atoms and ions in 1 cm³ by the force of gravitation is equal to $(N + N_i) m_H g$, in which m_H is the mass of one hydrogen atom.

From the two expressions given and from the condition that the layer be semitransparent, Menzel computes the ratio of radiation pressure to gas pressure. The result found is that, for temperatures of 10,000°–15,000° and $\log g = 4$, this ratio is 0.001 to 0.01 and hence entirely negligible. Even in a completely opaque atmosphere the number of atoms that can be supported by radiation pressure is of the order of $10^{-10} \times$ the number present.

It must therefore be concluded that radiation pressure is not the explanation for the discrepancy found.

d) If a Milne-Eddington model of the atmosphere is assumed, in which s/k is constant through the atmosphere, then the line depth R (1 − residual intensity) in a line profile is given by

$$R = \frac{1}{2}\frac{s}{k} - \frac{3}{8}\left(\frac{s}{k}\right)^2 \cdots \qquad \text{for} \quad \frac{s}{k} \leqslant 1,$$

$$R = 1 - \left(\frac{k}{s}\right)^{1/2} + \frac{1}{2}\left(\frac{k}{s}\right)^{3/2} \cdots \qquad \text{for} \quad \frac{s}{k} \geqslant 1,$$

according to Pannekoek and van Albada.[35] It follows that the contrast between the line centers ($s/k > 1$) and line wings ($s/k < 1$) will be increased if s/k decreases. Therefore, the discrepancy found may have been caused by the use of too small a value for k. Moreover, the larger k is, the smaller is the pressure that corresponds to a certain value of the optical depth, and this again tends to make the line spectrum extend farther into the violet. The computations discussed here were carried through at a time when the war had cut off the writer nearly completely from contact with important developments abroad. For this reason the absorption by negative hydrogen has not been considered in the computations. It is a fortunate circumstance, however, that this source of absorption appears to be negligible at the temperatures considered originally. It may come in, however, at the lower temperatures for which line numbers were extrapolated. The discrepancies are by no means limited to these lower temperatures, and, therefore, the cause must be sought elsewhere.

Two effects that may influence the continuous absorption will be discussed here: electron scattering and admixture of other elements besides hydrogen. The scattering per electron is equal to

$$\sigma_e = \frac{8\pi}{3}\left(\frac{e^2}{mc^2}\right)^2.$$

If the atmosphere consists of hydrogen only, of which a fraction x is ionized, then there will be x electrons for every hydrogen atom. It follows that the electron scattering, σ, per gram of hydrogen will be equal to

$$\sigma = \frac{x}{m_H} \times \frac{8\pi}{3}\left(\frac{e^2}{mc^2}\right)^2 = 0.42x.$$

On the other hand, the mass-absorption coefficient per gram of hydrogen is given by $k = \kappa x P_e$. It follows that

$$\frac{\sigma}{k} = \frac{0.42}{\kappa P_e}. \qquad (15)$$

Electron scattering is predominant over atomic continuous absorption if $\sigma/k \geqslant 1$; this will be the case for $\log \kappa P_e \leqslant -0.38$. If for κ the values given by Pannekoek[10] are used, the resulting values of $\log P_e$ at which σ becomes larger than k are found to be about 0.2 smaller than those given by Greenstein.[36] Since the details of neither computation are available, it is not clear what causes the difference. The order of magnitude, however, is the same in both cases.

In the computations of P_e as a function of optical depth the electron scattering was neglected. It was found there that $\log \kappa P_e$ fulfils condition (15) only for $\log g = 2$ and only for the outer layers, as deep down as $\tau = 0.10$. The effect of an additional factor 3 in k is found to come approximately to the same as reducing $\log g$ by 0.8 at most. Although this correction is appreciable, it does not explain all the discrepancies in the

[35] *Pub. Astr. Inst. U. Amsterdam*, No. 6, Part 2, 1946.

[36] *Ap. J.*, **95**, 299, 1942.

supergiants. Moreover, corrections for electron scattering are negligible in the main-sequence stars. Hence electron scattering does not solve our problem either.

The influence of the admixture of other elements besides hydrogen has been treated by Greenstein.[36] He finds that the mean opacity per gram is much smaller for *He* than for *H* at almost all temperatures; only at $\theta = 0.3$ are they comparable. Hence the influence of *He* is very small, unless it greatly exceeds *H* by mass. For the elements *C*, *N*, *O*, and *Si*, Greenstein finds negligible contributions to the general opacity.

11. The general conclusion of this discussion must therefore be that the discrepancy found to exist between the theory, as developed here, and observation cannot be explained satisfactorily. Observational evidence deviates from the theoretical expectations in the sense that the stars considered seem to have effective gravities as much as a hundred times smaller than the dynamical surface gravities GM/R^2. The results of the present investigation seem to indicate that the theory which assumes the stellar atmospheres to be in a state of equilibrium, in which the force of gravitation is balanced by the gradients of gas and radiation pressures, is inadequate. Extensive study of shell stars, together with fundamental theoretical investigations, may lead to a correct interpretation of the observed phenomena.

The writer wishes to express her indebtedness to Dr. A. Pannekoek, of Amsterdam, who suggested the subject of this investigation and whose advice and support under the most difficult circumstances were invaluable; to Dr. D. H. Menzel, associate director of the Harvard College Observatory, for encouragement and many elucidating discussions; to Dr. B. J. Bok, associate director of the Harvard College Observatory, for continued interest and support; to Dr. C. D. Shane, director of the Lick Observatory, for permission to use the ultraviolet spectrograph; and to the American Association of University Women, and Radcliffe College, who, by the award of two International Study Grants and a fellowship, made it possible to finish the present study at the Harvard College Observatory.

ON THE PRESENCE OF POLARIZATION IN THE CONTINUOUS RADIATION OF STARS. II*

W. A. HILTNER
Yerkes and McDonald Observatories
Received February 25, 1949

ABSTRACT

Observations are presented which establish that radiation from distant galactic stars is polarized and that this polarization is independent of wave length. An attempt was made to establish a relationship between polarization and reddening. Although a close correlation is not evident, polarization has not been observed in unreddened stars. A possible mechanism for explaining the observations is briefly discussed.

Photometric observations for the detection of partially polarized radiation from eclipsing binaries have been in progress at Yerkes Observatory for several years, with a view to establishing observationally the effect pointed out by Chandrasekhar,[1] that the continuous radiation of early-type stars should be polarized.[2] On the assumption that the opacity of early-type stars is due to scattering by electrons, the continuous radiation emerging from a star should be polarized with a maximum of polarization of 11 per cent at the limb. Since the presence of this polarization can be detected only when the early-type star is partially eclipsed by a larger late-type companion of the system, the effect is masked by radiation from this companion so that the expected maximum effect is only of the order of 1.2 per cent.[2] Photographic observations of RY Per suggested that the proper amount of polarization may be present. However, the confirmation is not so definitive as one could desire, and consequently the problem was pursued by photoelectric techniques which are capable of appreciably higher accuracy.

There are two methods generally used for the detection of polarized light by photoelectric receivers. First, there is the simple method of placing an analyzer, such as a Nicol prism (or Glan-Thompson) or Polaroid in front of the photocell and then rotating the analyzer through 90° and measuring the light-intensity in the two planes. The second method is that of rapidly rotating the analyzer in front of the photocell and then measuring the AC component of the photocell output.[3] The latter system is usually referred to as the "flicker method." Each method has its merits. The former method is simple and straightforward. It measures the percentage of polarization directly and should be free of a magnitude error. Also it has the advantage of working at extremely low light-levels at any wave length to which cathodes are sensitive. Photocells of the nonmultiplier type can be used at maximum efficiency at very low light-levels. The latter method has the advantage that it is capable of somewhat higher speed of detection and measurement. For the detection and measurement of polarization in stars the resulting accuracy in either method is determined by the seeing fluctuations.

In the fall of 1946 a photoelectric photometer[4] was constructed at Yerkes Observa-

* *Contributions from the McDonald Observatory, University of Texas*, No. 168. The greater part of this paper was presented at the fall meeting of the Midwest Group of Astronomers held at Yerkes Observatory on October 23, 1948.

[1] *Ap. J.*, **103**, 365, 1946.

[2] W. A. Hiltner, *Ap. J.*, **106**, 231, 1947.

[3] R. C. Williams and W. A. Hiltner, *Pub. Obs. U. Michigan*, **8**, 45, 1940, and *Ap. J.*, **98**, 43, 1943; Öhman, *Ark. f. mat., astr., och fysik*, Vol. **323**, No. 1, 1945; J. S. Hall, *A.J.*, **54**, 39, 1948.

[4] The instrument was briefly described in *Ap. J.*, **108**, 56, 1948.

tory, in view of investigating the problem discussed above as well as others. The instrument, however, was not used for polarization measurements until July 5, 1948.

In the fall of 1947 a photoelectric light-curve was obtained of CQ Cep. The light-curves in the ultraviolet and yellow have been briefly described;[5] and, since it is now generally accepted that some of the observed characteristics of light-curves of Wolf-Rayet stars can be explained in terms of electron scattering,[6] it was felt that this eclipsing binary should be investigated for polarization. However, the system falls far short of the ideal eclipsing binary for the detecting of polarization at the limb. For example, the eclipses are 0.47 and 0.39 mag. before ellipticity is removed, while in the ideal system the early-type star would have a dark companion, that is, no secondary minimum. In spite of the above, it was considered important to observe the system, even if only negative results were obtained. The first observations of July 5, 1948, of CQ Cep and a comparison star (to eliminate any systematic errors that may have been in the instrument) showed[7] that radiation from CQ Cep was polarized by 10 per cent with the position angle of the electric vector maximum at 62°. Observations on the following nights soon showed that the amount of polarization was independent of phase. The observations were continued for the duration of the observing period (one month). The individual observations are given in graph form in Figure 1.

The observing procedure was as follows: Polaroid was placed on the optical axis of the telescope (the cassegrain focus was employed) and mounted in such a way that it could take either of two positions which differed by 90° in position angle. A measurement of the light-intensity was made first at one position, then at the other position, and then back to the original. The whole cassegrain head of the telescope was then rotated to another position angle and the above measurements repeated. The difference in magnitude corresponding to the two positions of the Polaroid was determined and plotted against position angle of the electric vector of the Polaroid in its first position. If polarization is present, then a sine-curve should result. A typical tracing obtained with a Brown recorder is shown in Figure 2.

Since considerable caution must be employed in measurements of polarization for possible systematic errors, the following sources of errors were investigated: (1) hour angle (errors may arise here by flexure in the telescope and the earth's atmosphere); (2) residual polarization in the telescope; (3) color error in the photometer (a quartz-fluorite field lens was employed which has a flat field over the spectral region to which the antimony-caesium surface is sensitive); (4) polarization by the color filters; (5) cathode more sensitive to one plane of polarization than to another. It was not possible to make isolated tests for systematic errors resulting from each effect. The procedure was that of varying one variable, such as hour angle or filters or position of cathode with respect to the plane of polarization of the Polaroid, and then observing the amount of polarization in the stars under investigation. Since no systematic errors were detected (a systematic error of 0.005 mag. can easily be observed), the observations were made of CQ Cep under all combinations of hour angle, filters, and cathode positions as plotted in Figure 1.

On July 8, 1948, it was discovered that a second Wolf-Rayet star, HD 211853, also showed polarization. In this case the amount of polarization was 8 per cent, and the electric vector maximum had a position angle of 44°. Similar observations for systematic errors were made on this star simultaneously with those on CQ Cep. Again all the observations are presented together in Figure 2.

There were two by-products of the above observations for systematic errors. First,

[5] W. A. Hiltner, *A.J.*, **53**, 198, 1948.

[6] Z. Kopal and M. Shapley, *Ap. J.*, **104**, 160, 1946.

[7] *Nature*, **163**, 283, 1949. The discovery of the constant polarization in CQ Cep and the fact that other stars such as Z Lac (a cepheid) showed the same effect was communicated to Dr. John S. Hall and other interested astronomers in early July.

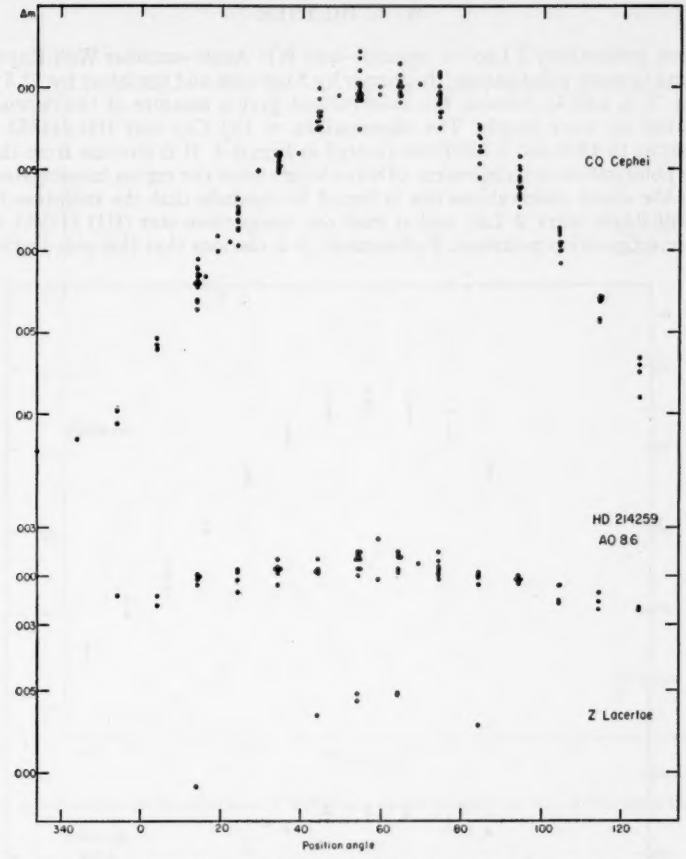

FIG. 1.—Polarization observations of CQ Cep, HD 214259, and Z Lac. All observations obtained between July 5, 1948, and August 7, 1948, are included.

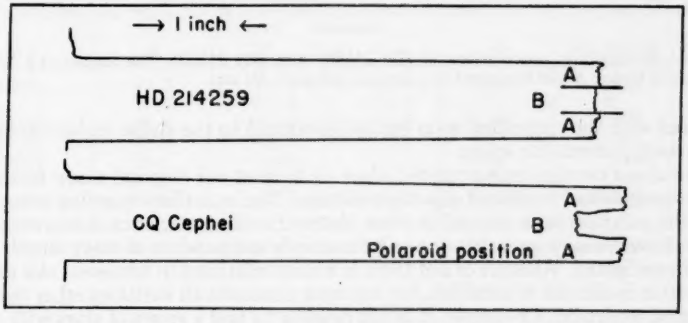

FIG. 2.—Typical tracing of CQ Cep and the control star HD 214259. The position angle of the electric vector of the Polaroid is 64° at position *A* and 154° at position *B*.

other stars, particularly Z Lac—a cepheid—and WN Anon—another Wolf-Rayet star—were found to show polarization, the former by 5 per cent and the latter by 12.3 per cent (see Figs. 1, 3, and 4). Second, the observations gave a measure of the dependence of polarization on wave length. The observations of CQ Cep and HD 211853 for two wave lengths (λ 4200 and λ 5300) are plotted in Figure 4. It is obvious from this figure that the polarization is independent of wave length over the region investigated.

From the above observations one is forced to conclude that the radiation from the three Wolf-Rayet stars, Z Lac, and at least one comparison star (HD 211903, which is a giant or subgiant) is polarized. Furthermore, it is obvious that this polarization is not

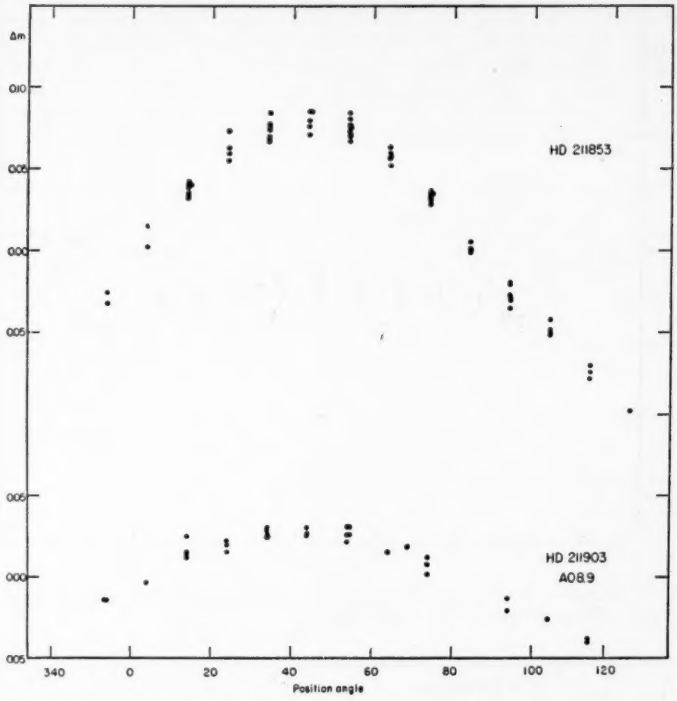

FIG. 3.—Polarization observations of HD 211853 and HD 211903. The former is a Wolf-Rayet spectroscopic binary, while the latter is a giant or subgiant A0 star.

associated with the individual stars but is introduced to the stellar radiation in its passage through interstellar space.

If the above conclusion is accepted, then we have at our disposal a new factor for the study of interstellar clouds and galactic structure. The immediate question arises whether or not the polarization is related to other observable characteristics of interstellar medium. We have already seen that the polarization is independent of wave length over the region investigated. Whether or not there is a close relationship between color excess and polarization is difficult to establish, for one must eliminate all variables other than polarization and reddening. Obviously, it is not possible to find a group of stars with the same distance and position, and with color excesses of varying amounts. However, it is well

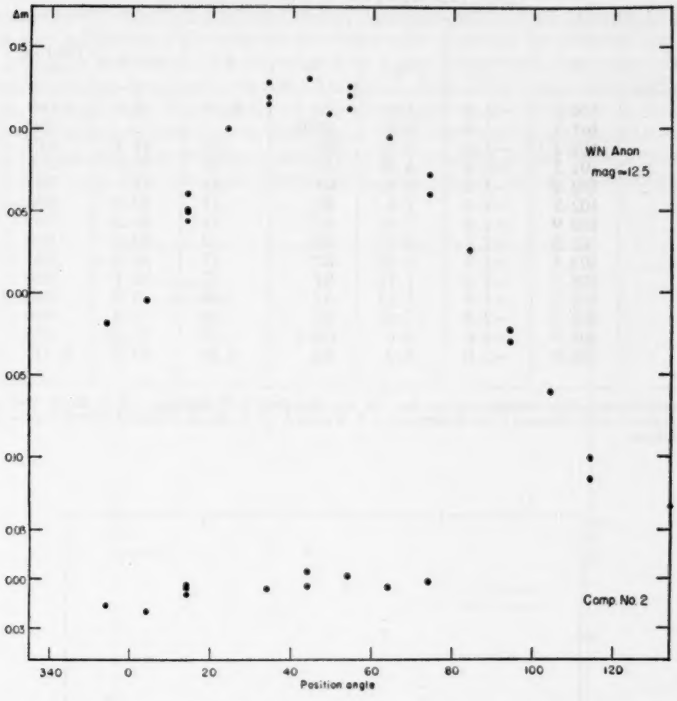

FIG. 4.—Polarization observations of WN Anon and a comparison star of the same magnitude

TABLE 1

SELECTED STARS IN CEPHEUS AND LACERTA

Star	l	b	m_{pv}	Sp.	Polarization*	Position Angle
WN Anon.....	70.3	+1.2	~12.5	WN5	0.125	44°
Comp.....	70.3	+1.2	~12.5	.....	0	.....
HD 211853.....	70.5	−0.8	9.0	WN6	.084	44
HD 211903.....	70.6	−0.7	8.9	A0	.030	44
HD 214259.....	73.1	−0.9	8.7	A0	.012	62
CQ Cep.....	73.0	−1.4	9.2	WN6	.100	62
Z Lac.....	73.5	−1.7	Max 8.2	F8–K2	0.050	62

* Polarization is defined here as the difference in magnitude between the electric vector maximum and the electric vector minimum.

TABLE 2*

SELECTED MEMBERS OF PERSEUS CLUSTER

HD	l	b	m_{pv}	Sp.	E_{1}	$m_0 - M$	Polarization	Position Angle
12953	100.7	−2.4	5.67	A1	0.18	11.0	0.060	109
13136	101.5	−4.0	8.0	M2Ib	.....	.....	.060	112
13267	101.3	−3.0	6.36	B8	.16	11.3	.070	110
13476	101.2	−2.0	6.39	A2	.26	10.7	.076	112
13854	102.2	−3.3	6.46	B1	.18	11.8	.055	115
13866	102.3	−3.6	7.4	B2	.14	10.6	.080	115
14535	102.9	−2.8	7.35	A2	.31	10.8	.050	110
14542	102.8	−2.7	6.85	B9	.33	10.6	.040	119
14818	103.4	−3.3	6.26	B2	.27	10.5	.065	115
14956	103.2	−2.2	7.16	B2	.37	10.7	.060	121
15316	103.5	−1.9	7.12	A2	.40	9.9	.080	117
15497	103.8	−2.0	7.01	B5	.46	9.9	.080	113
15642	104.9	−4.0	8.6	O9.5	.05	11.6	.055	116
15690	104.0	−2.0	8.2	B2	0.39	11.1	0.12	.....

* The spectral class and the distance modulus, $m_0 - M$, are taken from W. P. Bidelman, *Ap. J.*, **98**, 61, 1943; and the color excess, E_1, is taken from J. Stebbins, C. M. Huffer, and A. E. Whitford, *Ap. J.*, **91**, 20, 1940, but corrected to the spectral class given by Bidelman.

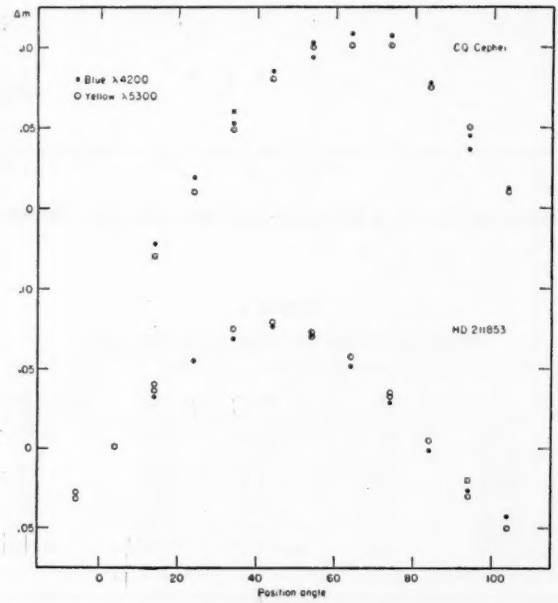

FIG. 5.—Polarization observations of CQ Cep and HD 211853 with blue (λ 4200) and yellow (λ 5300) filters.

known that the color excess of the stars in h and χ Per varies rapidly with galactic latitude. Consequently, this cluster is remarkably well suited for the present investigation.

A number of the brighter stars in the double cluster with color excesses from 0.05 to 0.46 and which Bidelman[8] considered members were observed for polarization with the 12-inch refractor at Yerkes Observatory. Also a few foreground stars were observed in order to detect any systematic errors. HD 16727, HD 13137, and HD 11857 were selected for this purpose. The results of this investigation are recorded in Table 2 and shown graphically in Figure 5. It is seen that a close relationship of polarization and reddening is not present. The average polarization for members of the Perseus cluster is 6.8 per cent. However, there are real differences in polarization for the various members of the cluster.

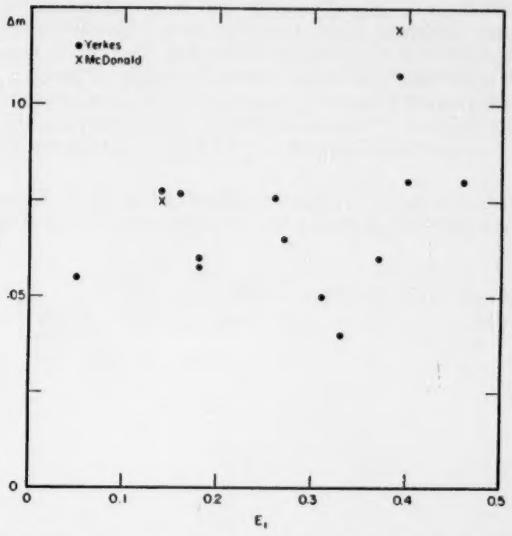

FIG. 6.—Polarization of members of h and χ Per plotted against color excess

The question now arises whether or not there is any correlation between polarization and interstellar *Ca* II K, since all members of h and χ Per have strong interstellar K lines. A correlation here does not appear at all probable, for HD 14633 (with strong interstellar K, color excess -0.07, and approximately the same distance as h and χ Per) does not show any significant polarization. The galactic latitude of this star is $-17°$.

The most logical conclusion that one can reach from the above is that a positive color excess is a necessary but not sufficient condition for polarization. This conclusion is borne out by observations of BD+31°642 and BD+31°643, B1 III and B5 V, respectively, at approximately the same distance (200 parsecs). The former has a color excess of 0.12, while the latter shows interstellar λ 4430 and has a color excess of approximately 0.4. The author is indebted to Dr. W. W. Morgan for the spectroscopic and parallax data quoted in the preceding paragraphs.

As yet there is no explanation for the presence of polarization in distant stars, and any explanation must meet a number of conditions. First, the mechanism must be independ-

[8] *Ap. J.*, 98, 61, 1943.

ent of wave length. Second, the mechanism must be operating over large distances. For example, WN Anon, HD 211853 and HD 211903 show polarization of different amounts but with the same position angle. Third, a positive color excess is necessary but not sufficient. Also it appears that the plane of polarization is associated with the galactic plane. Stars of low galactic latitude have a tendency to show polarization in which the electric vector maximum is approximately parallel to the galactic plane. This relationship, however, may not hold for all galactic longitudes, for a few scattered observations in Scutum and Cygnus indicate that this relationship does not hold at these longitudes. Likewise the amount of polarization appears to be greater near the galactic plane. This may be a consequence of greater concentration of interstellar dust or a more active mechanism or both.

If the polarization is a consequence of scattering by interstellar particles, it follows that these particles must be unsymmetrical, that is, elongated, and that these particles are subject to some alignment force. This force may take the form of magnetic fields, which, according to Alfven,[9] occupy interstellar space. These fields have been successfully employed by E. Fermi[10] in his investigations on the origin of the cosmic radiation. Since the interstellar particles are believed to be charged,[11] we may expect them to align if the particles are elongated and if there is a relative motion between the particles and the magnetic field frozen in. This alignment may be responsible for the observed effect.

It is a pleasure to thank Dr. S. Chandrasekhar and Dr. G. P. Kuiper for their advice and encouragement. This investigation has been supported by the American Philosophical Society.

[9] *Ark. f. mat., astr., och fysik,* Vol. **29B**, No. 2, 1943.

[10] *Phys. Rev.*, in press.

[11] L. Spitzer, *Ap. J.*, **93**, 369, 1941.

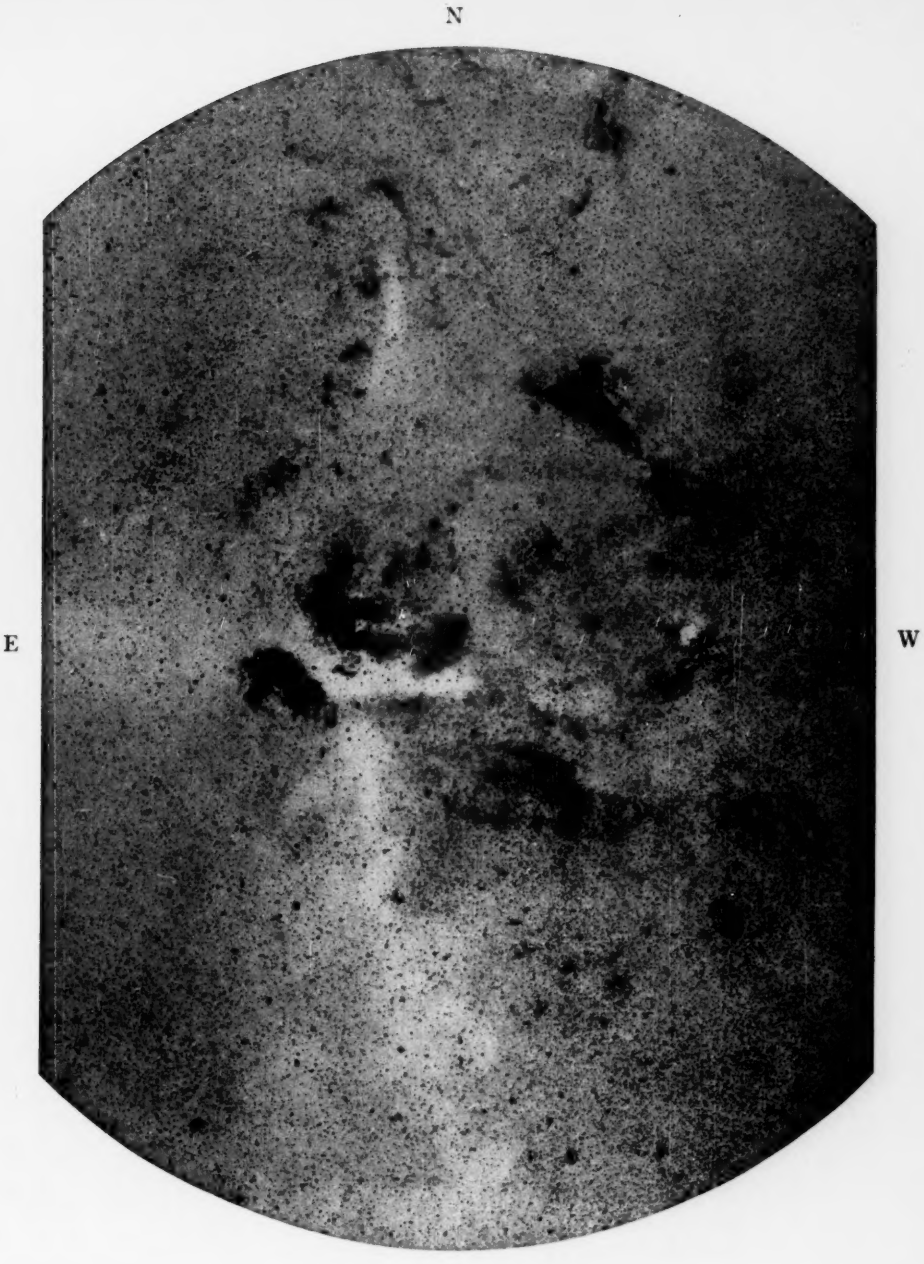

FIG. 1.—Region around γ Cygni. Scale: 1 cm = 27′

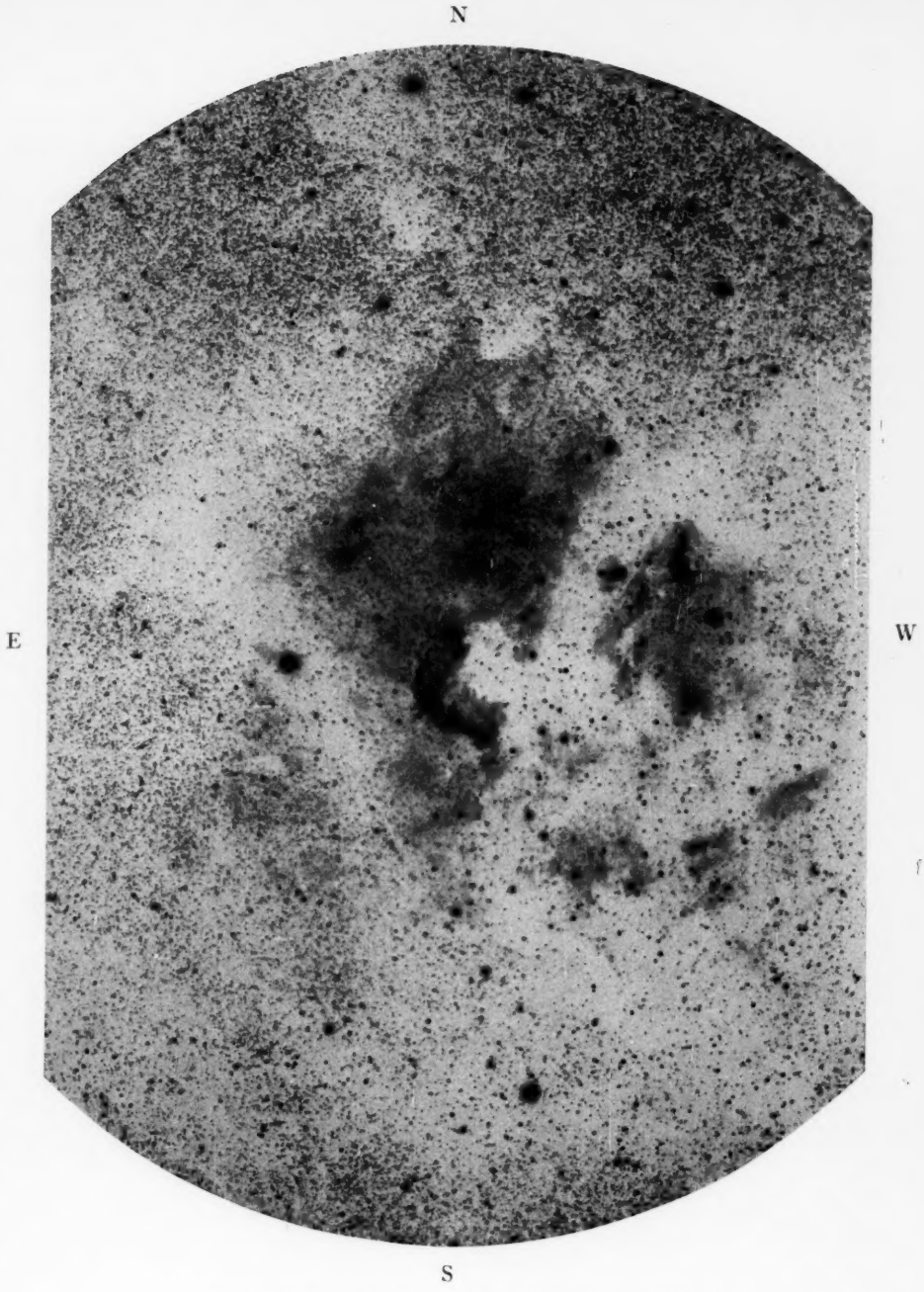

FIG. 2.—Region of the America nebula. Scale: 1 mm = 2'.5

PHOTOGRAPHIC STUDIES OF NEBULAE

VI. THE GREAT NEBULOUS REGION IN CYGNUS PHOTOGRAPHED IN RED LIGHT*

JOHN C. DUNCAN
Whitin Observatory, Wellesley College
Received February 14, 1949

ABSTRACT

The nebulous region in Cygnus photographed with the 18-inch Schmidt camera is illustrated and described.

The region in Cygnus at the head of the great rift in the Milky Way is well known to be replete with interesting objects, including variable stars, stars with remarkable spectra, star clouds, and nebulosities, both luminous and dark. In 1948 I photographed this region with the 18-inch, *f*/2 Schmidt camera on Palomar Mountain, using films of the very rapid red-sensitive emulsion Eastman 103*a*-E and filters that confined the effective light to the vicinity of $H\alpha$. The photographs record more than 100 square degrees of the sky, extending from near η Cygni northeastward to a position north of Deneb and the America nebula, and reveal the details and extent of the nebulosities more clearly than do photographs made with smaller cameras or in blue light or without filters.

The region around γ Cygni is shown in Figure 1 (negative Δ 1066; November 29, 1948; north is at the top). The exposure was 40 minutes through a red filter of Plexiglas, No. 160. The strength and detail of the large diffuse nebulae and of the long horizontal and vertical vacant lanes and the S-shaped luminous nebula near the top of the engraving should be noted. NGC 6888, the oval nebula 22 mm from the edge in the lower right quarter, appears greatly enhanced in red light. There are no defects that are likely to be deceptive except the ghost of γ Cygni, 4 mm northwest of that star in the center of the engraving, and a small hole in a diffuse nebula, 33 mm from the middle of the left edge.

Figure 2 shows the region of the America nebula (negative Δ 996; August 29, 1948; north is at the top). The exposure was 2 hours through an amber filter of Schott GG 11 glass. New detail appears especially within the borders of the Gulf of Mexico and over much of the southern half of the figure.

Not shown on Figures 1 and 2 are fainter and sparser parts of the great nebulous region. North of Figure 1 and west of Figure 2 the nebulosity lies in roughly parallel filaments that extend northeast-southwest. The most northerly of the filaments recorded is just west and north of o^1 and o^2 Cygni. South of Figure 1 are bright and dark features of the general character of those in the figure, but not so strongly displayed. Notable is a nebulous area about 2° in diameter, centered about 2° west of η Cygni and overlying the great parabolic dark marking Barnard 144.

Photographs made in this region with smaller Schmidt cameras, with and without filters, have been published by Otto Struve[1] and by Harold A. Lower.[2] The former are of an east-west strip centered on γ Cygni and show the nebulae near that star. The latter show the entire Cygnus region on a small scale.

* *Contributions from the Mount Wilson Observatory, Carnegie Institution of Washington*, No. 759.

[1] *Ap. J.*, **86**, 94, 1937.

[2] *Ap. J.*, **93**, 506, 1941.

SUPERTHERMIC PHENOMENA IN STELLAR ATMOSPHERES

III. THE CHROMOSPHERIC RADIATION FIELD

RICHARD N. THOMAS*
Harvard College Observatory
Received October 23, 1948

ABSTRACT

The solution for the chromospheric b_n values of Paper II is extended to the case in which the chromospheric radiation and absorption is included in the radiation field. That variety of the solution which takes into account absorption in the chromospheric Balmer lines predicts a Balmer decrement in the flash spectrum which agrees well with the observations. Earlier work on the theoretical Balmer decrement has neglected radiative excitation in the Balmer lines, and the assumption's physical usefulness is here questioned. The most likely N_e value and the relation between density and emission gradients are discussed.

I. ADDITIONAL COMPUTATIONS BASED ON THE APPROXIMATION OF PAPER II[1]

In the preceding paper[1] of this series we have considered the state of the hydrogen chromosphere when the only source of radiation is the conventional photosphere corresponding to a 6000° black body. Before proceeding to consider the modification of the radiation field caused by the chromospheric emission, we consider the following items:

TABLE 1

THE CHANGE OF b_n WITH T_e AND N_e

$N_e \cdot 10^{-11}$	1	2	4	∞	2	2
$T_e \cdot 10^{-4}$	3.5	3.5	3.5	3.5	3.0	2.0
$b_1 \cdot 10^{-6}$	4.30	2.07	1.02	.....	2.03	1.80
b_2	11.22	10.88	10.62	10.55	11.11	13.0
b_3	4.74	4.67	4.61	4.62	4.73	4.93
b_4	3.50	3.45	3.42	3.42	3.52	3.62
b_5	2.95	2.93	2.89	2.90	2.98	3.06
b_6	2.64	2.62	2.59	2.59	2.66	2.74
b_7	2.44	2.42	2.39	2.39	2.46	2.54
b_8	2.29	2.27	2.25	2.25	2.31	2.39
b_9	2.18	2.17	2.15	2.15	2.19	2.28
b_{10}	2.10	2.08	2.07	2.07	2.10	2.20

the effect of varying T_e and N_e on the b_n values, the most likely N_e value, and the hydrogen density gradient. The results of the last two items do not depend significantly on the b_n values and hence, by contrast with the results of Paper II, will not be altered by the higher approximations of Part II of the present paper.

a) VARIATION OF b_n WITH N_e AND T_e

Following the procedure outlined in Paper II and there demonstrated for the case $T_e = 35{,}000°$ and $N_e = 2 \cdot 10^{11}$, we obtain the results tabulated in Table 1, second to fourth and sixth to seventh columns. The latter two columns indicate the effect of temperature variation, for this first approximation, with constant N_e. The second to

* Now a Frank B. Jewett Fellow at the Institute for Advanced Study, Princeton, N.J.

[1] *Ap. J.*, **108**, 142, 1948.

fourth columns cover a range of only a factor of 4 in N_e, but it is seen that, to the extent that the present approximation is valid, the b_n for higher N_e do not differ significantly from those in the fourth column. To substantiate the assertion, the fifth column contains the b_n values, for $n > 1$, obtained by a solution for the case $N_e = \infty$. This last result should not be taken to have physical reality; for, before these conditions for N_e are reached, our assumption that only collisional excitation from level 1 is significant must break down. Table 1 is intended only to demonstrate the slowness of variation of b_n with N_e for the higher N_e values and under this first approximation. An estimate of the variation is required in subsection *c*. (The behavior of b_1, which is essentially inversely proportional to N_e, is excluded here.)

b) THE PROBABLE VALUE OF N_e

In Paper II we have adopted Wildt's suggested[2] value of $2 \cdot 10^{11}$ for N_e at the level of the chromosphere for which we have $T_e = 3.5 \cdot 10^4$. Roughly, Wildt assigns a height of some 500 km above the chromospheric base to this level. To obtain the above value of N_e, he ascribes the termination of the Balmer and Paschen series to Stark broadening and uses for the computation the Inglis-Teller formula relating the number of ions to the principal quantum number n of the last resolved series member. We have for this formula:

$$\log N_i = 23.26 - 7.5 \log n \,. \tag{1}$$

In the present case, only the number of ions enters, since our T_e exceeds the value $10^5/n$, the electron contribution dropping out because of the high thermal velocity. From Mitchell's data, one finds H 37 as the last resolved Balmer line; and H 40 for the Paschen series. We have, apparently, a difference of a factor of 2 between the electron density indicated by the two series. We note, however, that with the use of 35,000° for T_e we might expect thermal broadening to enter at some point. Let us inquire whether we can reconcile the Balmer and Paschen observations by considering thermal broadening.

We might expect the emission lines to be no longer distinct when the decrease in emission over the line contour is such that the intensity drop is 50 per cent at a point halfway to the next higher line in the series. We have the line contour fixed by the factor (apart from absorption, which does not enter here):

$$e^{-p^2} = e^{-[(\nu - \nu_0/\nu_0)(c/v)]^2} \,. \tag{2}$$

For a $(\nu - \nu_0)$ equal to the distance to the next higher series member, we have, for a T_e of 35,000°,

Balmer:

$$p_0 = \frac{4.88 \cdot 10^4 (2n+1)}{n^2 (n+1)^2} \left[1 - \left(\frac{2}{n}\right)^2\right]^{-1}; \tag{3}$$

Paschen:

$$p_0 = \frac{1.10 \cdot 10^5 (2n+1)}{n^2 (n+1)^2} \left[1 - \left(\frac{2}{n}\right)^2\right]^{-1}. \tag{4}$$

We desire an n such that, at $p_0/2$, e^{-p^2} will have the value $\frac{1}{2}$. We find this value at $n = 38$ for the Balmer series and $n = 50$ for the Paschen series. Thus we conclude that the series would no longer be resolvable from the continuum at these respective members and so find perfect agreement between predicted and observed termination of the Balmer series. Since the Paschen series should terminate from thermal broadening considerably later than the observed H 40, we conclude that the Stark broadening must be the true

[2] *Ap. J.*, **105**, 78, 1947.

termination factor here. Hence it would appear that the N_e value indicated by the Paschen series is the preferable one.

As there has been a wide range in the observed termination point of the Balmer series from different sets of eclipse observations, we can probably not insist very strongly on the exact agreement found here between prediction and observation. Nonetheless, the agreement between the several parameters resting on the value of T_e speaks well for the consistency of the data and renews confidence in the adopted value of T_e near 35,000°. In the remainder of the calculations, in particular in Part II, we shall then consider only the single case of $T_e = 35{,}000°$ and $N_e = 2 \cdot 10^{11}$, where it becomes necessary to use definite values of these parameters in the calculations. We shall, however, find the b_n values of the higher approximations insensitive to the N_e value, save for b_1.

c) THE HYDROGEN DENSITY GRADIENT

The procedure used by Wildt in obtaining the chromospheric emission gradient is, in brief, the following: The locus of the heights at which the various Balmer lines disappear gives an (emission, height) relation. We assume that the first point of appearance of each line corresponds to the threshold sensitivity of the photographic plate—and thus to the same energy. Therefore, we may write, ignoring absorption at the tips of the chromospheric lines,

$$E_{nn'} N_n = \text{Constant} ; \tag{5}$$

or, putting in the factors not constant or dependent upon n,

$$[A_{nn'} \nu_{nn'} n^2] \left[\frac{e^{X_n}}{T_e^{3/2}} b_n\right] [N_e^2(h)] = \text{Constant} \tag{6}$$

or

$$F(n) G(n, T_e, N_e) J(N_e) = \text{Constant} . \tag{7}$$

The symbols, apart from F, G, and J, are those of the preceding paper of the series.

If we now assume the atmosphere to be isothermal, we may seek the slope of the relation between the height h, at which a given line disappears, and the index n. We have:

$$\frac{dlnF}{dn} \Delta n + \left[\frac{\partial lnG}{\partial n} + \frac{\partial lnG}{\partial lnN_e} \frac{\partial lnN_e}{\partial h} \frac{\Delta h}{\Delta n}\right] \Delta n + \frac{dlnJ}{dh} \Delta h = 0 ; \tag{8}$$

$$\frac{\partial ln(FG)}{\partial n} \Delta n = -\left[\frac{\partial lnG}{\partial lnN_e} \frac{dlnN_e}{dh} + \frac{\partial lnJ}{\partial h}\right] \Delta h = -2\left[\frac{\partial lnG}{\partial lnN_e} \tfrac{1}{2} + 1\right] \frac{dlnN_e}{dh} \Delta h . \tag{9}$$

If the isothermal assumption holds, with the degree of ionization we have found in the atmosphere, $dlnN_e/dh$ is constant. If also the bracketed coefficient of $dlnN_e/dh$ in equation (9) is constant, we may plot the product FG against the height and take the slope. This is the procedure followed by Wildt, with the bracketed coefficient ignored. He has obtained the logarithmic gradient of N_e^2 rather than N_e; for his work assumed an atmosphere whose degree of ionization corresponds to a temperature of 4830°. Thus the emission gradient that Wildt obtained corresponded to the hydrogen density gradient. Here, however, we find the hydrogen essentially all ionized; hence we desire the electron density gradient. Ignoring the bracketed coefficient mentioned above and taking directly Wildt's emission gradient value, we should then interpret the results as giving a hydrogen density gradient just half that obtained by Wildt.

The relation between the density gradient and kinetic temperature follows from the equation of dynamic equilibrium. We have

$$\text{Logarithmic gradient} = -\frac{m_H g}{kT_e} \mu , \tag{10}$$

where g is the solar gravity and μ the mean molecular weight. The other symbols are conventional. Wildt uses a μ value of 1. Since we have an ionized atmosphere, we use $\frac{1}{2}$. Thus, the $\frac{1}{2}$'s in the density gradient and in the μ value cancel out, and we obtain the same kinetic temperature as in Wildt's earlier work.

The foregoing remarks follow, once we set the above-mentioned bracketed coefficient of $dlnN_e/dh$ in equation (9) equal to unity. If we allow other values than unity, we obtain:

$$1+\frac{1}{2}\frac{\partial lnG}{\partial lnN_e}=1+\frac{1}{2}\frac{\partial ln\, b_n}{\partial lnN_e}, \tag{11}$$

$$\frac{\partial lnN_e}{\partial h}=-\frac{1}{2}\frac{\Delta ln\,(FG)}{\Delta h}\left(1+\frac{1}{2}\frac{\partial ln\, b_n}{\partial lnN_e}\right)^{-1}, \tag{12}$$

$$T_e=\left(2\frac{m_H g}{k}\mu\right)\left(1+\frac{1}{2}\frac{\partial ln\, b_n}{\partial lnN_e}\right)\left(\frac{\Delta ln\,[FG]}{\Delta h}\right)^{-1}. \tag{13}$$

We use Table 1 to obtain an estimate of the $\partial lnb_n/\partial lnN_e$ term. We find that $\partial lnb_n/lnN_e$ has the value -0.035 for b_2 and -0.013 for b_9. The alteration in the slope is then but 2 and 1 per cent, respectively—an almost undetectable amount. This statement is particularly relevant when we realize that the slope is determined essentially from the higher series members, say for n greater than 10. Finally, we note that the correction term will be lessened when we consider the chromospheric radiation field; for, as we shall see in Part II, with the exception of b_1 the b_n determination does not depend upon N_e in the higher approximation. Thus we substantiate Wildt's conclusion that the kinetic temperature determination from the observed emission gradient is largely independent of the assumed conditions within the chromosphere. An analysis of the hydrogen density gradient, however, requires an identification of the kinetic temperature with the electron temperature before the observed emission gradient may be translated into actual density gradient.

Finally, we consider Wildt's use of Baumbach's coronal electron density measures[3] to check the density gradient. Using Baumbach's data, we may obtain equal confirmation of the present results. From these data, Wildt obtains an electron density of $10^{8.55}$ at a height of 14,500 km. Adopting the value $2\cdot10^{11}$ for the density at 500 km, we have

$$\frac{\Delta lnN_e}{\Delta h}=-\frac{2.75ln10}{14\cdot10^8}=-0.45\cdot10^{-8}\,\mathrm{cm}^{-1}. \tag{14}$$

Half of Wildt's density gradient is $-0.46\cdot10^{-8}$ cm^{-1}. The agreement is thus quite satisfactory. The present work and the work of Wildt—in spite of the differing results for the density gradient—both obtain an apparent confirmation from the same set of observational data because of the different assumptions as to the state of ionization in the chromosphere.

II. THE CHROMOSPHERIC EMISSION AND A SECOND APPROXIMATION TO THE b_n VALUES

In Part I and in Paper II[1] we considered the physical state of a hydrogen chromosphere characterized by a kinetic temperature T_e, which exceeds T_1, a black-body temperature characterizing the incident radiation field. We have treated the case in which the influence of the chromosphere, in its emission and absorption properties, might be neglected. Thus the b_n values tabulated in Paper II and Table 1 of the present paper characterize the chromosphere so long as the radiation field is less than or equal to that of the 6000° black-body distribution everywhere in the spectrum. Introducing the parameter S_ν as a multiplier of the 6000° black-body intensity distribution, we see that the

[3] *A.N.*, **263**, 121, 1937.

cases $S_\nu = 1$ and $S_\nu = 0$ cover the extreme range under the stated conditions. The range in b_n over these values of S_ν is found to be small.

The question arises as to the contribution of the chromospheric emission to the radiation field, particularly in the ultraviolet. Since the chromospheric emission occurs mostly in the Lyman series and Lyman continuum—if we are to accept the results of Paper II—there appears the possibility of deviations in the radiation field in the direction of an ultraviolet excess over the 6000° black-body distribution. With such a deviation, our earlier calculations must be modified to include the case $S > 1$ in some regions of the spectrum.

S may be expressed as a sum of two parts, B and C, in which B refers to the 6000° black-body contribution and C to the chromospheric emission. Once the b_n, T_e, and N_e are known throughout the chromosphere, C may be calculated. In a complete second approximation, C would be put into the equations as a function of the b_n, T_e, and N_e, and the b_n would be calculated. This complete approximation is not feasible at the present stage of investigation. We shall therefore proceed according to the following scheme. The results of the first approximation will be used to evaluate the ratio of intensity of the radiation field built up by the chromosphere alone to that of the 6000° black body. Where the ratio exceeds unity, we shall use the chromospheric field alone. Where the ratio is less than unity, we shall use the radiation field of the first approximation. The procedure seems to imply a cycle of successive approximation. We shall, however, find that, to a good approximation, only the chromospheric emission in the Lyman lines need be considered; and for the Lyman-line region a closed expression in terms of the b_n results.

Even with the closed expression for the S value in the Lyman lines, there exists, as in Paper II, a range of solutions depending upon the assumed value for S in the remainder of the spectrum. That is, there are the two extreme cases: $S = 1$ (no absorption lines) and $S = 0$ (no emission from the photosphere—a pure capture spectrum for the chromosphere). Solutions for each alternative will be carried through, and it will be shown that a solution corresponding to an intermediate value of S in the Balmer lines leads to a reasonable representation of the Balmer decrement in the solar flash spectrum.

In section *d* we evaluate the ratio of chromospheric emission to that of the 6000° black body. Section *e* presents a consideration of the influence of emission in the Lyman continuum. Section *f* contains the second approximation to the solution for the b_n. Section *g* demonstrates an attempt to represent the observed hydrogen flash spectrum with the results of section *f*.

d) THE S_ν VALUES RESULTING FROM THE CHROMOSPHERIC RADIATION FIELD

1. *General expressions for* S_ν.—Consider the geometrical situation of Figure 1. We again assume an exponential gradient for the electron density, with logarithmic gradient b_e. We have, for the contribution to the radiation field intensity at A due to the material at P,

$$\Delta I = {}_0E\, e^{-b_e w}\, e^{-N(\sigma)a_\nu}, \tag{15}$$

where, for a line,

$${}_0E = n_n h\nu_{nn'} A_{nn'} \frac{1}{4\pi}, \tag{16}$$

$$\begin{aligned} n_n &= N_e^2 b_n \left[\frac{h^2}{2\pi m kT_e}\right]^{3/2} \frac{\varpi_n}{2}\, e^{X_n} \\ &= b_n 2.45 n^2\, e^{4.42/n^2}, \end{aligned} \tag{17}$$

for $T_e = 3.5 \cdot 10^4$ and $N_e(x = 0) = 2 \cdot 10^{11}$. For a free-bound transition, we have

$$_0E = \frac{E_{\kappa n'}}{4\pi}\, d\nu = \frac{N_e^2}{4\pi}\frac{K}{T_e^{3/2}}\frac{e^{X_{n'}}}{n'^3}\; e^{-h\nu/kT_e} h\, d\nu . \tag{18}$$

Also:

$$N a_\nu = a_{\nu A} n_{n'} \int_0^\sigma e^{-b_e w} d\sigma , \tag{19}$$

where a_ν is the appropriate atomic absorption coefficient. Hence for the entire contribution along the direction θ we find

$$I = {}_0E \int^\infty e^{-b_e w}\, e^{-N(\sigma) a} d\sigma . \tag{20}$$

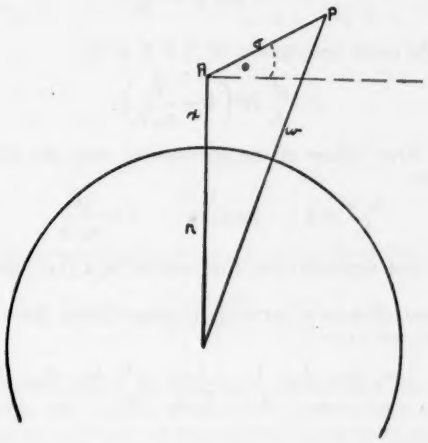

FIG. 1.—Geometrical situation

We may express w in terms of σ, θ (σ/r small). For convenience we take x equal to zero, i.e., measure the radius r to this point. We obtain

$$w \sim \sigma \sin\theta + \frac{\sigma^2}{2r} . \tag{21}$$

Whence, if we expand the integrand of equation (19) in powers of $(b_e \cdot w)$, we obtain

$$I = {}_0E \int_0^\infty \exp\left\{ - b_e \left[\sigma \left(\sin\theta + \frac{n_{n'} a}{b_e} \right) + \frac{\sigma^2}{2} \left(\frac{1}{r} - \frac{n_{n'} a}{b_e}\, b_e \sin\theta \right) \ldots \right] \right\} d\sigma . \tag{22}$$

A discussion of the values of I in different parts of the spectrum may be facilitated by considering special integrals for particular values of the absorption term, $n_{n'} a / b_e$.

Case a.—If the absorption is very small and we consider the tangential direction ($\theta = 0$), a consideration of the σ^2 term alone might be expected to yield a fair approximation to I. We obtain in this case

$$I \sim {}_0E \frac{1}{2} \left(\frac{2\pi r}{b_e} \right)^{1/2} . \tag{23a}$$

In the radial direction, the σ term—again neglecting the absorption—should give a good approximation. We obtain

$$I \sim \frac{{}_0E}{b_e}. \tag{23b}$$

In each case we note that we obtain an upper limit to I, and base the approximation on:

$$\frac{n_{n'}a}{b_e} \ll 1 .$$

Case β.—For intermediate values of the absorption we expect most of the contribution to the integral to come from the first-term coefficient of σ. We then have

$$I \sim \frac{{}_0E}{b_e} \frac{1}{\sin\theta + \dfrac{n_{n'}a}{b_e}} \tag{24a}$$

and, averaging over the outer hemisphere ($0 \leq \theta \leq \pi/2$),

$$I \sim \frac{{}_0E}{b_e} ln\left(1 + \frac{b_e}{n_{n'}a}\right). \tag{24b}$$

Case γ.—For very large values of the absorption, only the absorption term is significant. We have then

$$\frac{n_{n'}a}{b_e} \gg 1 \qquad \text{leads to} \qquad I \sim \frac{{}_0E}{n_{n'}a}. \tag{25a}$$

Thus the choice of case depends upon the value of $n_{n'}a$ (i.e., upon the amount of the absorption).

In case γ the S value takes on a particularly simple form. Re-writing equation (25*a*) by using equation (16), we have

$$I_{nn'} = \frac{n_n}{n_{n'}} \frac{h\nu_{nn'}A_{nn'}}{a_\nu} \frac{1}{4\pi} = \frac{b_n\varpi_n}{b_{n'}\varpi_{n'}} \frac{e^{X_n}}{e^{X_{n'}}} \frac{h\nu_{nn'}A_{nn'}}{a_\nu} \frac{1}{4\pi}, \tag{25b}$$

while we have the relation

$$a_\nu = \frac{\varpi_n}{\varpi_{n'}} \frac{c^2}{8\pi\nu^2} A_{nn'}. \tag{26}$$

Hence

$$I_{nn'} = \frac{b_n}{b_{n'}} \frac{e^{X_n}}{e^{X_{n'}}} \frac{2\nu^3 h}{c^2}. \tag{25c}$$

Thus for the ratio (S_ν) of this chromospheric field to the 6000° black-body field, for which

$$I_{bb} = \frac{2h\nu^3}{c^2}\left(e^{h\nu/kT_1} - 1\right)^{-1}, \tag{27}$$

we have

$$S_\nu = \frac{b_n}{b_{n'}} \frac{e^{Y_{n'n}} - 1}{e^{X_{n'n}}}. \tag{28a}$$

In the foregoing discussion we have considered only the spontaneous emission. It is readily shown that, to include the induced emission, we need only multiply the expression (25*c*) by the factor

$$\psi = \left[1 + \frac{c^2}{2h\nu^3} I_\nu S_\nu\right], \tag{29a}$$

in which $I_\nu S_\nu$ is the strength of the incident field as given by equation (25*c*). Hence

$$\psi = 1 + \frac{b_n e^{X_n}}{b_{n'} e^{X_{n'}}}. \tag{29b}$$

This term ψ will enter only in our final approximation and clearly differs from unity by only a small amount, and hence will be appreciable only in terms of the form $(1 - \psi)$. We have, then, the more correct expression for S_ν in case γ:

$$S_\nu = \left[\frac{b_n}{b_{n'}} \frac{e^{Y_{n'n}} - 1}{e^{X_{n'n}}}\right]\left[1 + \frac{b_n e^{X_n}}{b_{n'} e^{X_{n'}}}\right]. \tag{28b}$$

2. *Numerical value of* S_ν.—For the computation of S_ν the numerical values of $n_{n'}a/b_e$ are required. For the line absorption we have

$$\frac{n_{n'}a}{b_e} = \frac{1}{b_e}(2.45 n'^2 e^{4.42/n'^2} b_{n'})\left(\frac{\pi e^2 f_{nn'}}{mc}\left[\frac{1}{\sqrt{\pi}}\frac{\lambda_0}{v_0} e^{-p^2}\right]\right), \tag{30a}$$

where

$$p = \frac{c}{v_0}\frac{\nu - \nu_0}{\nu_0}.$$

Therefore,

$$\frac{n_{n'}a}{b_e} = \frac{2.9 \cdot 10^{-5} g_{n'n} n'^5 b_{n'} e^{4.42/n'^2}}{n^3\left[1 - \left(\frac{n'}{n}\right)^2\right]^4}. \tag{30b}$$

For the continuous absorption, the larger contribution is from the bound-free absorption. We have

$$\left(\frac{n_{n'}a}{b_e}\right)_{\text{eff}} = \frac{32\pi^2}{3^{3/2}} \frac{e^6 R}{ch^3\nu^3} \frac{1}{b_e} \sum_{n'} n_{n'} \frac{g_{II}}{n'^5} \tag{31a}$$

where g_{II} is a factor nearly unity, tabulated by Menzel and Pekeris.[4] For our present calculations it suffices to set g_{II} equal to unity. The summation is over all n' such that $X_{n'} \leqslant h\nu/kT_e$. The numerical value of expression (31*a*) is quite small unless $b_{n'}$ is large. In Paper II we found $b_1 = 2.07 \cdot 10^6$ for the T_e and N_e values here considered. Hence equation (31*a*) becomes

$$\left(\frac{n_{n'}a}{b_e}\right)_{\text{eff}} = 0.366\left(\frac{\nu_1}{\nu}\right)^3 \qquad \text{for} \qquad \nu > \nu_1. \tag{31b}$$

Absorption in the Balmer continuum is negligible. The free-free absorption may readily be shown to be much less than the bound-free.

We thus see immediately that case β, $(n_{n'}a/b_e) \sim 1$, applies to the continuous absorption. Hence equation (24*b*) should be used for the contribution of the chromospheric continuum.

If we use equation (30*b*) and the b_n values of Paper II, we obtain the $n_{n'}a/b_e$ values of Table 2. We see that case γ, $(n_{n'}a/b_e) \gg 1$, applies to the earlier members of the Lyman series, while case β applies to the higher series members. There thus occurs the required continuous grading of the higher series members into the continuum. For the Balmer and higher series, expression (23) holds as case α here applies. That is, we see that the density gradient term fixes the intensity in the Balmer and higher series, while the optical depth term fixes the intensity in the Lyman region. Thus we expect the chromospheric Lyman field to be isotropic (eq. [25]). On the other hand, since the radial density

[4] *M.N.*, **96**, 77, 1935.

gradient, $\exp(-b_e r)$, implies the density gradient, $\exp(-b_e y^2/2r)$, along the tangential ray, the Balmer and higher series field is nonisotropic (eqs. [23] and [24*a*]). The greatest intensity lies along the tangential direction.

In the preceding discussion we have considered the emission in the hemisphere lying above the point in question. The dependence of the Lyman emission on the optical depth term indicates that the same discussion holds over the inner hemisphere. For the Balmer transitions, however, we expect the emission to rise as θ approaches $-\pi/2$, so long as the atmosphere has the characteristics assumed for the chromosphere. We have, however, chosen the zero level in the lower chromosphere, and hence we expect the radiation field to conform to the 6000° atmosphere as we proceed inward. Thus there seems some justi-

TABLE 2

VALUES OF $n_{n'a}/b_e$ FROM EQUATION (30*b*)

	Lyman		Balmer		Paschen
$_2L$	$0.14 \cdot 10^4$	$_3H$	0.009	$_4P$	0.018
$_5L$	$.37 \cdot 10^2$	$_4H$	.0012	$_5P$	.0021
$_{10}L$	$0.41 \cdot 10$	$_{10}H$	$0.3 \cdot 10^{-4}$	$_{10}P$	$0.7 \cdot 10^{-4}$

TABLE 3

COMPARISON OF CHROMOSPHERIC EMISSION AND BLACK BODY IN THE LYMAN AND BALMER LINES

	Chromosphere (1)	Black Body 35,000° K (2)	Black Body 6000° K (3)	Ratio Col. (1): Col. (3) (4)
$_2L$	$4.2 \cdot 10^{-8}$	$0.82 \cdot 10^{-2}$	$0.88 \cdot 10^{-9}$	48
$_5L$	$9.3 \cdot 10^{-9}$	$0.74 \cdot 10^{-2}$	$.80 \cdot 10^{-11}$	$1.2 \cdot 10^2$
$_{10}L$	$6.6 \cdot 10^{-9}$	$0.64 \cdot 10^{-2}$	$.42 \cdot 10^{-11}$	$1.6 \cdot 10^2$
$_3H$	$0.92 \cdot 10^{-4}$	$2.6 \cdot 10^{-2}$	$.64 \cdot 10^{-3}$	0.14
$_5H$	$0.67 \cdot 10^{-5}$	.....	$.34 \cdot 10^{-3}$	0.02
$_{10}H$	$0.47 \cdot 10^{-6}$	.....	$0.23 \cdot 10^{-3}$	0.002

fication for taking the expression (23*a*) to characterize the maximum intensity contribution of the chromosphere to the Balmer emission. We shall, at any rate, proceed on this basis, noting the implicit assumption.

The expression (23*a*) does not lead to such a simple expression for the Balmer S_ν factor as does equation (25*a*) for the Lyman S_ν. However, we may compute the Balmer S_ν numerically. We must multiply equation (23*a*) by the Doppler distribution function to obtain the distribution in unit frequency interval. That is, we multiply by

$$f(v) = \frac{1}{v_0\sqrt{\pi}} \frac{c}{v_0} e^{-p^2} dv. \tag{32}$$

Hence for the Balmer emission we have

$$I_\nu d\nu = \frac{n_n h\nu_{nn'} A_{nn'}}{4\pi} \frac{1}{v_0\sqrt{\pi}} \frac{c}{\nu_0} e^{-p^2} \sqrt{\frac{\pi r}{2 b_e}}\, d\nu. \tag{33}$$

Table 3 contains the relation between chromospheric and assumed 6000° black-body

emission, using equations (33), (25*c*), and (27). For convenience, the results for a 35,000° black body are also given in Table 3.

In addition to the Table 3 values for the line emission, we need the values for the emission in the continuum. By combining equations (18), (24*b*), and (27) we obtain S in the Lyman continuum as follows:

$$S = 1.80 \cdot 10^{-7}\, e^{21.4\nu/\nu_1} \left(\frac{\nu_1}{\nu}\right)^3 ln \left[1 + \frac{1}{0.366}\left(\frac{\nu}{\nu_1}\right)^3\right]. \tag{34}$$

So, at $\nu = \nu_1$, $S = 4.6 \cdot 10^2$. The Balmer contribution is much smaller, amounting to an S of 29 at the Lyman limit and 10^{-4} at the Balmer limit. Thus, on the basis of the b_n values obtained in the first approximation, we may conclude that the assumed radiation field requires modification chiefly in the Lyman region. We proceed to consider the modification.

e) THE MODIFICATION OF THE EQUATIONS OF CONDITION DUE TO EMISSION IN THE LYMAN AND BALMER CONTINUA

While S is large for the Lyman continuum, its contribution to the solution of the equations of condition for b_n is small; for the bound-free excitations in the Lyman are few here. The correct expression for the Lyman bound-free excitations now is:

$$\int \bar{F}_{n'\kappa} d\nu = \int_{\nu_{n'}}^{\infty} \frac{E_{n'\kappa}}{h\nu}\, d\nu + \int_{\nu_1}^{\infty} S_\nu \frac{E_{n'\kappa}}{h\nu}\, d\nu, \tag{35}$$

where we have

$$E_{n'\kappa} d\nu = \frac{N_e^2 K}{T_e^{3/2}} \frac{e^{X_{n'}}}{n'^3} \left[\frac{b_{n'}\, e^{h\nu/kT_e} - 1}{e^{h\nu/kT_1} - 1}\right] h\, d\nu. \tag{36}$$

For $\nu > \nu_1$, we may drop the terms (-1) in the bracket. Substituting expression (34) in equation (35), we find the correction term to be added to the radiative ionizations to be

$$\int_{\nu_1}^{\infty} S_\nu \frac{E_{n'\kappa}}{h\nu}\, d\nu = \frac{N_e^2 K}{T_e^{3/2}} \frac{e^{X_{n'}}}{n'^3}\, 1.80 \cdot 10^{-7} b_{n'} \times \int_{\nu_1}^{\infty} e^{-h\nu/kT_e} \left(\frac{\nu_1}{\nu}\right)^3 ln \left[1 + \frac{1}{0.366}\left(\frac{\nu}{\nu_1}\right)^3\right] \frac{h\, d\nu}{h\nu}. \tag{37}$$

We may set an upper bound on the integral by putting the exponential term equal to its value at the lower integration limit. The integration then gives, for the upper limit,

$$\int_{\nu_1}^{\infty} S_\nu \frac{E_{n'\kappa}}{h\nu}\, d\nu < \left[\frac{N_e^2 K\, e^{X_{n'}}}{T_e^{3/2} n'^3}\right] b_{n'} 1.6 \cdot 10^{-9} \tag{38}$$

to be added to the result earlier obtained, which was

$$\int_{\nu_{n'}}^{\infty} \bar{F}_{n'\kappa} d\nu = \left[\frac{N_e^2 K\, e^{X_{n'}}}{T_e^{3/2} n'^3}\right] \left\{ b_{n'} \sum_{a=1}^{\infty} -E_i(-a\, Y_{n'}) - \sum_{a=1}^{\infty} -E_i\left(-Y_{n'}\left[a + \frac{T_1}{T_e}\right]\right)\right\}. \tag{39}$$

Since, for the large X,

$$-E_i(-X) \sim \frac{e^{-X}}{X}, \tag{40}$$

the modification on the original 6000° field caused by considering the Lyman continuum is clearly negligible for all $n > 1$. For the ground level, the ratio of the correction term to the original term is

$$1.6 \cdot 10^{-9} : \frac{e^{-25.8}}{25.8} = 6.4 \cdot 10^{3} \text{ as an upper limit.}$$

This ratio then is the S in the term giving the radiative ionizations from the ground level. The value of the term, using this upper limit for S, amounts to about 6 per cent of the remaining terms in the coefficient of b_1.

If we carry through similar calculations for level 2, also using the Balmer continuum, we obtain an upper limit of some 8 per cent to the contribution to the coefficient of b_2. We thus see that the modifications in the continuum add essentially nothing to the computations. We therefore omit any correction term arising from an S greater than unity in the continuum.

Summarizing the results of sections *d* and *e*, we find that the significant contribution by the chromosphere to the radiation field lies in the Lyman-line region. The expression for the contribution is given explicitly in terms of the b_n by equation (28*a*). We then proceed in the next section to compute the solution for the b_n under this modification.

f) THE SOLUTIONS FOR b_n UNDER THE SECOND APPROXIMATION

As mentioned in the introduction to Part II, we still have a range of solution after the radiation field is corrected for the chromospheric emission in the Lyman lines. The range arises from a choice of S value for the spectral region outside the Lyman lines. We consider first the case $S = 1$.

1. S = *1 for* n > *1 and for the continuum.*—The original equation of condition for level 1, equation (19) of Paper II, had terms of the following form:

$$b_{n''} - S\,\frac{b_1\, e^{X_{1n''}} - b_{n''}}{e^{Y_{1n''}} - 1}. \tag{41}$$

Substituting the expression (28*b*) for S, we obtain, for the expression (41),

$$b_{n''}\left[\frac{b_{n''}}{b_1}\,\frac{1}{e^{X_{1n''}}}\right]^2. \tag{42}$$

On the basis of the b_n values of Paper II, this expression has the value $3 \cdot 10^{-13}$ for $n'' = 2$, and somewhat smaller values for higher n. The summation over n'' of brackets of this form which contribute to the expression for b_1 gives a small value compared with the remaining terms in the expression. So we may neglect the contribution of equation (42) and obtain the explicit expression for b_1 thus:

$$b_1 = \frac{1.85 \cdot 10^{18}}{N_e T_e^{1/2}}\,\frac{1}{\phi}\,\frac{1}{2}\left\{-E_i(-X_1) + \bar{S}\sum_{a=1}^{\infty} -E_i\left(-Y_1\left[a + \frac{T_1}{T_e}\right]\right)\right\} e^{X_1},$$

where

$$\phi = \sum_{2}^{\infty} (f[n][X_{1n} + 1]P_n) + 1.54 \cdot 10^{-8}(X_1 + 2) + \frac{K\, e^{X_1}}{A N_e T_e^{1/2}}\,\frac{\bar{S}}{2}\sum_{a=1}^{\infty} -E_i(-aY_1). \tag{43}$$

This gives $b_1 = 4.6 \cdot 10^4$ in place of the value $2 \cdot 10^6$ obtained in the first approximation. This small value of b_1 renders invalid the process whereby we obtained expression (28*a*) for S_ν, because of the decrease in the value of $n_{n'}a/b_e$ for $n' = 1$, for Lyman terms beyond $L\gamma$, say. However, a solution which retains expression (28*a*) for S will provide an upper limit for the values of $b_n (n > 1)$ and a lower limit for the value of b_1, in the case where the remaining $S = 1$.

We note that terms of the form (41) occur also in the equation of condition for level n; and again the bracket corresponding to expression (42) may be set equal to zero. We note that the physical counterpart of this procedure is the assumption that the Lyman excitations balance the Lyman downward transitions. We shall return to the point in section *f*-2.

When we proceed to modify the equation of condition for level n, equation (19) of Paper II, we find the only term linking levels 1 and n is the collisional term—denoted by C_T—which may be expressed as

$$C_T = b_1 N_e \frac{A T_e^{1/2}}{K} f(n) [X_{1n} + 1] = 0.931 f(n) [X_{1n} + 1]. \tag{44}$$

We then obtain the equation for b_n:

$$b_n \left\{ \sum_2^{n-1} \frac{G_{n'n}}{n'^3} + \frac{\bar{S}_\nu}{2} \sum_{a=1}^{\infty} -E_i(-aY_n) \right\} e^{X_n} = \left[C_T + \frac{1}{2} \left\{ -E_i(-X_n) + \bar{S} \sum_{a=1}^{\infty} -E_i\left(-Y_n\left[a + \frac{T_1}{T_e}\right]\right) \right\} \right] e^{X_n} + \sum_2^{n-1} \left[b_{n'} S_\nu \frac{e^{X_{n'n}} - \frac{b_n}{b_{n'}}}{e^{Y_{n'n}} - 1} G_{n'n} \frac{e^{X_n}}{n'^3} \right] + \sum_{n+1}^{\infty} b_{n''} \left[G_{nn''} P_{n''} - S_\nu \frac{\frac{b_n}{b_{n''}} e^{X_{nn''}} - 1}{e^{Y_{nn''}} - 1} G_{nn''} P_{n''} \right]. \tag{45}$$

The equation is best solved numerically by expressing b_2 in terms of the remaining b_n, introducing this expression into the equations for b_n, and solving this last set of equations by iteration. Table 4 contains the results of this solution. The b_2 value has increased by a factor of 100 over the first approximation value.

2. *The case* S < *1 for* n > *1.*—This case would seem to correspond more nearly to the true situation in the chromosphere. That is, we have seen that the contribution of the chromospheric emission outside the Lyman region is small. Hence the photospheric field conditions the radiation field outside the Lyman region, and the first modification of the assumed 6000° black-body field must be that taking into account absorption lines. An overestimation of the influence of absorption lines should be provided by the assumption of a pure capture spectrum, outside the Lyman. That is, $S = 0$.

It would appear, therefore, that a limiting estimate for the influence of absorption lines on the b_n values would result from a solution of equation (45) with S placed equal to zero. The solution of this equation, differing only in the neglect of collisional excitation from the ground level, has already been carried through, both for the case of the solar chromosphere[5] and for a particular case[6] of the planetary nebula problem. The numerical results

[5] Menzel and Cillié, *Ap. J.*, **85**, 88, 1937.

[6] Menzel and Baker, *Ap. J.*, **88**, 52, 1938.

of these previous solutions give $b_n < 1$ for $n > 2$. Also, however, these solutions give (although this consequence has not always been explicitly stated) an infinite value to b_2. (This consequence is seen immediately in eq. [45], with $S = 0$; for the coefficient of b_2 in the equation for b_2 vanishes.) Consequently, it is dubious how far such solutions correspond to any physical reality, for the following reasons.

The above solutions and equation (45) with $S = 0$ correspond to two physical assumptions: (A-1) There are no radiative excitations from levels other than the first. (A-2) Upward transitions exactly balance downward transitions in the Lyman lines. Assumption (A-2) is contained implicitly when we take the expression (42) equal to zero and has thus been shown to be a reasonable assumption. (One sees, physically, the reason for an infinite b_2 from these two assumptions; for the atoms entering level 2 by cascade from above cannot leave it.) In any given physical situation, the radiation field cannot be completely null but must have some small value, at least. With the corresponding very large value of b_2, the number of radiative excitations in the Balmer cannot, therefore, a priori be neglected as statement (A-1) assumes. It is necessary to inquire whether these radiative excitations are as numerous as the other processes that are

TABLE 4

b_n VALUES FOR ${}_nS=1$, $n>1$

b_1	b_2	b_3	b_4	b_5	b_6	b_7	b_8	b_9	b_{10}
$4.6\cdot10^4$	$1.02\cdot10^3$	52.	18.0	10.65	7.85	6.5	5.65	5.1	4.8

included. From a purely formal mathematical standpoint, it is seen that assumption (A-1) corresponds to setting the product $b_2 \cdot {}_2S$ equal to zero; whereas in the limiting case that ${}_2S$ approaches zero this quantity becomes the indeterminate form $\infty \cdot 0$. We consider, then, the form of the condition to replace assumption (A-1) for small values of S, i.e., weak radiation field.

a) The solution for a weak radiation field.—A correct formulation of the conditions describing a weak radiation field must evaluate the radiative Balmer excitations. For this purpose we re-write the equation for level 2 from equation (45) thus:

$$b_2\left\{\sum_3^\infty \frac{G_{2n''}}{n''^3}\frac{{}_2S_\nu}{e^{Y_{2n''}}-1}+\frac{{}_2\bar{S}}{2}\sum_{a=1}^\infty -E_i(-aY_2)\right\}e^{X_2}=\left[C_T+\tfrac{1}{2}\{-E_i(-X_2)\}\right.$$
$$\left.+\frac{{}_2\bar{S}}{2}\sum_{a=1}^\infty -E_i\left(-Y_n\left[a+\frac{T_1}{T_e}\right]\right)\right]e^{X_2}+\sum_3^\infty b_{n''}\left[1+\frac{{}_2S}{e^{Y_{2n}}-1}\right]G_{2n''}P_{n''}. \tag{46}$$

If we assume ${}_2S$ is the same for all Balmer levels and take ${}_2\bar{S} = {}_2S_\nu = {}_2S$, we may solve for $({}_2S \cdot b_2)$. A consideration of the numerical values of the terms in the coefficient of b_2 in equation (46) shows that the ${}_2S$ value must be that corresponding to the early members of the Balmer series, e.g., the depth of $H\alpha$. We obtain

$$b_2 \cdot {}_2S = \bar{C}_2 + e^{-X_2}\sum_3^\infty b_{n''}\eta_{2n''}. \tag{47}$$

The values of the new symbols used are apparent by comparison of equations (46) and (47). Hence the equation for b_n becomes

$$b_n\left\{\sum_{2}^{n-1}\frac{G_{n'n}}{n'^3}+\frac{{}_n\bar{S}}{2}\sum_{a=1}^{\infty}-E_i(-aY_n)+H_{2n}({}_2S_\nu-\eta_{2n}\bar{e}^{X_n})\right\}e^{X_n}$$

$$=\left\{(C_{Tn}+\bar{C}_2e^{X_{2n}}H_{2n})+\frac{1}{2}\left(-E_i[-X_n]+{}_n\bar{S}\sum_{a=1}^{\infty}-E_i\left[-Y_n\left(a+\frac{T_1}{T_e}\right)\right]\right)\right\}e^{X_n} \tag{48}$$

$$+\sum_{3}^{n-1}b_{n'}\left[\eta_{2n'}H_{2n}+\frac{{}_{n'}S_\nu G_{nn'}e^{X_n}}{n'^3}\,\frac{e^{X_{n'n}}-\dfrac{b_n}{b_{n'}}}{e^{Y_{n'n}}-1}\right]+\sum_{n+1}^{\infty}b_{n''}\left[(\eta_{2n''}H_{2n}+G_{nn''}P_{n''})\right.$$

$$\left.-{}_nS_\nu\,\frac{\dfrac{b_n}{b_{n''}}\,e^{X_{nn''}}-1}{e^{Y_{nn''}}-1}\,G_{nn''}P_{n''}\right].$$

Equation (48) is similar to the equation obtained from equation (45) by expressing b_2 in terms of the remaining b_n. If, in equation (48), we neglect ${}_2S$ with respect to the term in η_{2n}, which neglect is completely justified numerically, the equations are identical. Thus the solution of equation (48), which neglects absorption other than in the Balmer lines—and makes no assumption on this latter—gives the b_n values for $n > 2$ that are contained in Table 4. The value for b_2 depends upon the assumed value of ${}_2S$.

The b_n values for no radiation field result from a solution of equation (48) with $S = 0$ throughout. The resulting b_n values, for $n > 2$, are tabulated in Table 5. The cor-

TABLE 5

b_n VALUES FOR ${}_nS=0$, $n>2$; ${}_2S=0.0049$

b_1	b_2	b_3	b_4	b_5	b_6	b_7	b_8	b_9	b_{10}
$3.4\cdot10^6$	$5.5\cdot10^5$	154	29.8	14.1	9.4	7.3	6.1	5.3	4.8

responding values of b_1 and b_2 are discussed below. These results for b_2, $n > 2$, might be compared with the earlier results[5, 6] on a pure capture spectrum. Since these earlier results gave b_n less than 1, the difference is appreciable.

β) An upper limit for the b_n *values for* $S < 1$.—Assumptions (A-1) and (A-2) are of interest only in so far as they represent the conditions in the chromosphere. We have seen (A-1) to be unlikely. Statement (A-2) results from setting expression (42) equal to zero, and this procedure now becomes doubtful because of the large b_2 obtained for small ${}_2S$. We therefore remove the restriction on equation (42) and consider the alteration in the solution. Equation (42) then contributes to the numerator of expression (43) for b_1:

$$\sum_{2}^{\infty}b_n\left[\frac{b_n}{b_1}\,e^{-X_{1n}}\right]^2\frac{G_{1n}}{n^3}e^{X_n}. \tag{49}$$

And we add to the coefficient of b_n in equations (45) and (46)

$$\left[\frac{b_n}{b_1}\,e^{-X_{1n}}\right]^2G_{1n}. \tag{50}$$

The term has numerical significance only for b_1 and b_2.

Consider the alteration in the value of b_1. From equation (47) we see b_2 increase directly as ${}_2S^{-1}$. The term (49) causes a significant alteration in the b_1 value only for such small ${}_2S$ that (from eq. [43]):

$$\tfrac{1}{2}\left[-E_i(-X_1)\right] e^{X_1} \sim \sum_2^\infty b_n \left[\frac{b_n}{b_1}\, e^{-X_{1n}}\right]^2 \frac{G_{1n}}{n^3}\, e^{X_n} \sim b_2 \left[\frac{b_2}{b_1}\, e^{-X_{12}}\right]^2 \frac{G_{12}}{8}\, e^{X_2}. \quad (51)$$

As ${}_2S$ decreases, b_2 increases relative to b_1 until the term on the left of equation (51) becomes much less than the term on the right. Thus, while earlier we had from equation (43)

$$b_1 = \tfrac{1}{2}\, e^{X_1}\left[-E_i(-X_1)\right] \cdot 4.85 \cdot 10^5, \quad (52)$$

we now have, for these small values of ${}_2S$,

$$b_1 = 4.85 \cdot 10^5 b_2 \left[\frac{b_2}{b_1}\, e^{-X_{12}}\right]^2 G_{12} P_2. \quad (53)$$

Solving for b_2/b_1, we obtain

$$\frac{b_2}{b_1} \leqslant 1.63 \cdot 10^{-1}. \quad (54)$$

Since equation (52) gives $b_1 = 4.6 \cdot 10^4$, we therefore must use equation (53) for $b_2 > 7.5 \cdot 10^3$. The value (54) is the maximum allowable for b_2/b_1, set by the term (50). We may determine the smallest value of ${}_2S$ at which b_2 still increases with decreasing ${}_2S$. This minimum occurs when (referring to eq. [46])

$${}_2S_\nu \left[\sum_3^\infty \frac{G_{2n''}}{n''^3} \frac{1}{e^{Y_{2n''}} - 1} + \frac{1}{2}\sum_{a=1}^\infty -E_i(-aY_2)\right] \sim \left[\frac{b_2}{b_1}\, e^{-X_{12}}\right]^2 G_1^2. \quad (55)$$

The coefficient of ${}_2S$ has the value 0.0068. Using the b_2/b_1 from equation (54), we obtain for this minimum ${}_2S$ the value $0.49 \cdot 10^{-2}$. That is, we have a residual intensity in the line equal to 0.5 per cent of the 6000° black-body continuum. This would be a very black line, much blacker than the observed Balmer lines. Even in our first solution, Paper II, we obtained a chromospheric emission alone exceeding this value. We conclude, then, that we cannot expect this limiting ${}_2S$ value in the chromosphere.

We can now place explicit upper bounds upon the b_n values, whatever the value of ${}_2S$. The solution of equation (48), with S set equal to zero, can be shown to represent an upper limit to the solution for the b_n for $n > 2$ (cf. appendix). It has been shown in the previous paragraph that ${}_2S = 0.005$ represents the smallest value of ${}_2S$ for which b_2 will increase with decreasing ${}_2S$. The use of this value of ${}_2S$ and the $b_n (n > 2)$ values of Table 5 in equation (47) will therefore set an upper limit to b_2. The ratio (40) sets an upper limit to b_1. The values of b_2 and b_1 tabulated in Table 5 represent this upper limit. Since b_2, hence b_1, is inversely proportional to ${}_2S$ for ${}_2S$ larger than the value used above, the b_1 and b_2 values corresponding to a larger ${}_2S$ (say, the observed Balmer depth of about 0.1) may be immediately written down from the Table 5 values.

Summarizing the results of the b_n computations, one may say that Table 5 represents an upper limit to the b_n values, for an arbitrary ${}_2S$. For a given ${}_2S$, the discussion in the appendix and the b_n values there tabulated represent a closer approximation to the physical situation that we should expect for the solar chromosphere. In this exceedingly rough investigation the set of values contained in the appendix are not so useful as are the limiting values given in Table 5; for the proper ${}_2S$ value is not known and the degree of error introduced by the original assumptions made in the present treatment is even more uncertain. Thus, in regard to the latter, since the low values of ${}_2S$ cause such large

b_2, we might expect collisional excitation from the second level, which we have neglected, to become important. In regard to the uncertainty in ${}_2S$, a complete treatment must couple the solution onto the photosphere and the more conventional radiation transfer problems. Therefore, at this stage of investigation it becomes essential to form an estimate of the degree of promise shown by the present methods. Such an estimate may conceivably be obtained by inquiring how well the present computations represent the Balmer flash spectrum. With the relatively high population of level 2 obtained even for small ${}_2S$, some absorption effects are to be expected. Previous attempts to calculate the Balmer decrement in the flash spectrum have omitted absorption. Therefore, when absorption effects are included, an estimate of the upper limit of such effects should be made. For this reason Table 5 is essential.

g) ABSORPTION VALUES AND THE FLASH SPECTRUM

We use equation (30*b*) and various values of b_2 to tabulate values of the expression

$$N\alpha = \frac{n_{n'}\alpha}{2}\left(\frac{2\pi r}{b_e}\right)^{1/2} \tag{56}$$

in Table 6.

TABLE 6

VALUES OF $(n_{n'}\alpha/2)\sqrt{2\pi r/b_e}$ FOR THE BALMER SERIES

b_2	$5.5\cdot10^5$	$2.7\cdot10^4$	$1.02\cdot10^3$	10.9
${}_3H$	$1.44\cdot10^5$	$0.73\cdot10^3$	$0.27\cdot10^2$	0.28
${}_4H$	$0.66\cdot10^3$	$0.33\cdot10^2$	1.24	.01
${}_{10}H$	$0.50\cdot10^2$	2.5	0.094	0.001
${}_{13}H$	$0.21\cdot10^2$	1.05	0.040	.....
${}_{15}H$	$0.14\cdot10^2$	0.67	0.026	.....
${}_{20}H$	5.6	0.27	0.01	.....
${}_{25}H$	2.8	0.14	0.005	.....
${}_{30}H$	1.6	0.08	0.003	.....

We seek an expression for the Balmer emission in terms of the b_n and the absorption term given in equation (56). We have, for the emission reaching the observer along the tangential direction from the point P of Figure 1 (setting $y = \sigma[\theta = 0]$),

$$\text{Net emission} = {}_TE_{nn'} = {}_0E_{nn'}n_n(y)\; e^{-N(y)\alpha_\nu}, \tag{57}$$

where

$$n(y) = n_0\, e^{-b_e x}\, e^{-b_e y^2/2r} = n_i\, e^{-b_e y^2/2r}. \tag{58}$$

To obtain the total emission, we integrate along y. We may expand the exponent to obtain

$${}_TE_{nn'} = {}_0E_{nn'}n_{in}\int_{-\infty}^{\infty} e^{-b_e y^2/2r}\left[1 - (N\alpha) + \frac{(N\alpha)^2}{2} - \ldots\right] dy; \tag{59}$$

whence

$$\begin{aligned} {}_TE_{nn'} = {}_0E_{nn'}N_n\Big[1 - \frac{N\alpha}{1!} + \frac{(N\alpha)^2}{2!}(1+I_2) - \frac{(N\alpha)^3}{3!}(1+3I_2) + \ldots \\ + (-1)^m\frac{(N\alpha)^m}{m!}\Big(1 + \frac{m!}{2!(m-2)!}I_2 + \frac{m!}{4!(m-4)!}I_4 + \ldots\Big) + \ldots\Big], \end{aligned} \tag{60a}$$

where

$$I_j = \frac{2}{\sqrt{\pi}} \int_0^\infty e^{-s^2} g^j(s^2)\, ds\,, \qquad g(s^2) = \frac{2}{\sqrt{\pi}} \int_0^s e^{-s^2} ds\,, \qquad I_2 = 0.338\,,$$

$$I_4 = 0.198\ldots, \qquad N = n_i \frac{1}{2} \sqrt{\frac{2\pi r}{b_e}}, \qquad s = \sqrt{\frac{b_e}{2r}}\, y\,.$$

To compare these results to the flash spectrum, we recall that chromospheric "heights" refer to the integrated emission above the height given. Hence we must integrate equation (60) over x, recalling that

$$n_i = n_0 e^{-b_e x}\,. \tag{61}$$

We then have to multiply the terms of equation (60*a*) by $1/b_e(j+1)$, where j is the power of N occurring in the expansion, omitting the N in the coefficient of the bracket. Further, we take into account the Doppler broadening of the line by multiplying by the line-of-sight velocity-distribution function and integrating over v. Since α contains e^{-p^2} and the distribution function is given by equation (32), we obtain a coefficient $1/\sqrt{i+1}$, where i is the power of α occurring in the term. The resultant of the two coefficients is: $1/b_e(m+1)^{-3/2}$, and we have for the final expression for the emission,

$${}_TE_{nn'} = {}_0E_{nn'0}N_n\Big[1 + \Sigma(-1)^m \frac{(N\alpha)^m}{m!}(m+1)^{-3/2} \Big(1 + \frac{m}{2!\,(m-2)!}\, I_2 + \ldots\Big)\Big]\,. \tag{60b}$$

This expression is based upon the assumption that the values of b_n and T_e remain constant above the chromospheric level in question. The $(N\alpha)$ value is that tabulated in Table 6, using the various b_2 values of interest. We see that for the higher b_2 values—the cases most likely to correspond to reality—the expression (60*b*) converges only for the higher series members. That is, the whole atmospheric region along the tangential path contributes to the observed emission for these higher series members. For the earlier members the region in the vicinity of A in Figure 1 will not contribute because of the heavy absorption; hence we expect the emission to be characteristic of the upper atmosphere, where the assumption of constancy of T_e is most likely to depart seriously from reality. Therefore, for comparison of our prediction with observation, we are interested in the later series members.

An asymptotic formula for b_n comes readily from our solution of equation (48) with ${}_nS = 0$. We obtain

$$b_n \to \Big(\sum_2^{n-1} \frac{G_{n'n}}{n'^3}\Big)^{-1} \Big\{ (C_T + \bar{C}_2 e^{X_{2n}} H_{2n}) + \tfrac{1}{2}[-E_i(-X_n)] + e^{-X_n}\Big[\sum_3^{n-1} b_{n'}\eta_{2n'}H_{2n} + \sum_{n+1}^{\infty} b_{n''}G_{nn''}P_{n''}\Big]\Big\}\,, \tag{61a}$$

ignoring terms whose contribution is less than 0.01 in b_n. The summation over $b_{n'}$ is determined by the earlier b_n values and in any event does not change in value for $n-1$ greater than about 9. We have, further, the asymptotic form (small X_n):

$$-E_i(-X_n) \to -0.577 - \ln X_n + \frac{X_n}{1.1!} + \ldots. \tag{62}$$

So we finally obtain

$$b_n \to \left(\sum_2^{n-1} \frac{G_{n'n}}{n'^3}\right)^{-1} \left\{ \left(-0.94 + \frac{X_n}{2} + ln n \right) + 8.15 \cdot 10^3 \, e^{-X_n} H_{2n} + \sum_{n+1}^{\infty} b_{n''} G_{nn''} P_{n''} \, e^{-X_n} \right\}, \tag{61b}$$

which leads to the b_n values of Table 7, which supplements Table 5, and both apply to either of the first two columns of Table 6.

TABLE 7

b_n FOR LARGER n—CONDITIONS OF TABLE 4

n	10	13	15	20	25	30
b_n	4.74	3.90	3.57	3.03	2.78	2.63

TABLE 8

EMISSION IN THE FLASH SPECTRUM

n	($_2S = 0.1$) LOG E_{COMPUTED}	OBSERVED		LOG $E_{\text{PAPER II}}$	($_2S = 0.005$) LOG E_{EXTREME}
		log $E_{670\text{ km}}$	log $E_{1500\text{ km}}$		
10	14.27	14.11	13.67	14.17	†
13	13.96	13.98*	.....	13.77	†
15	13.78	13.80	13.33	13.57	†
20	13.38	13.51	13.01	13.15	†
25	13.07	13.28	12.71	12.83	12.80
30	12.81	13.08	12.6	12.57	12.63

* This value seems high in the observational work by 0.03 or so.

† Absorption too high for the absorption expansion to converge (cf. comments in text).

Using the third column of Table 6 (corresponding to $_2S = 0.1$) and Table 7, we obtain the predicted line intensities in the second column of Table 8. In the third column of Table 8 we tabulate the observed intensities, taken from the work of Menzel and Cillié[7] as applying to a height of 670 km. In the fourth column we tabulate the results observed for a height of 1500 km. In the fifth column we give the predictions based on our solution for the b_n of Paper II. In the sixth column we give the results for the extreme value of $b_2 = 5.5 \cdot 10^5$ ($_2S = 0.005$). The relative values of the observed intensities are far more accurate than the absolute values. Hence, a comparison of the decrements, predicted and observed, rather than the absolute intensities should provide a reasonable criterion of the closeness of the representation. The observed decrement of the third column does indeed fall between that predicted by the 0.1 and 0.005 values for $_2S$. Further, the

[7] *Harvard Obs. Circ.*, No. 410, October, 1935.

absolute value of the emission differs only by a factor of 2, or the square root of this in the assumed value of N_e.

The difference between the two predicted values of the decrement comes almost completely from the absorption term. The change of b_n with n for large n is very small. Thus the comparison of prediction and observation would appear to indicate that the observed decrement requires a rather high population of the second level in the chromosphere. This result suggests that the central intensity of the hydrogen lines in the normal solar spectrum, at least in the early Balmer lines, may be largely fixed by the chromosphere.

APPENDIX

We have indicated that the correction terms given in equations (49) and (50) are nontrivial for high enough b_2, i.e., small enough ${}_2S$. In carrying through the solution given Table 5 and discussed in the subsequent remarks, we have, however, neglected the throw-back influence of the terms added to b_2 and b_1 on equation (48). Since we here seek merely to place an upper bound on the b_n values—particularly for b_2—this neglect of the throw-back terms seems justified. However, we may indicate the alteration in equation (48).

Equation (45) for b_n may be corrected by adding the term

$$\left(\frac{b_n}{b_1}\, e^{-X_{1n}}\right)^2 G_{1n}\, e^{X_n}. \tag{A-1}$$

We then obtain, in place of equation (47),

$$b_2 \cdot {}_2S = C_2 \cdot \epsilon^{-1} + \epsilon^{-1}\, e^{-X_2} \Sigma\, b_{n''} \eta_{2n''}\,, \tag{A-2}$$

where $C_2 < \bar{C}_2$ by virtue of the C_T term dropping out of $\bar{C}_2$. And, for the case of ${}_nS = 0$, $n > 2$, equation (48) becomes

$$b_n \left\{ \sum_2^{n-1} \frac{G_{n'n}}{n'^3} - H_{2n}\eta_{2n}\, e^{-X_n}\, \frac{\mu_n}{\epsilon} \right\} e^{X_n} = \left\{ \left[C_2\, \frac{\mu_n}{\epsilon}\, H_{2n}\, e^{X_{2n}} + \tfrac{1}{2}\left(-E_i[-X_n] \right) \right] e^{X_n} + \sum_3^{n-1} b_{n'} H_{2n}\eta_{2n'}\, \frac{\mu_n}{\epsilon} + \sum_{n+1}^{\infty} b_{n''} \left[G_{nn''} P_{n''} + H_{2n}\eta_{2n''}\, \frac{\mu_n}{\epsilon} \right] \right\}, \tag{A-3}$$

where

$$\mu_n = 1 + \frac{\left[\dfrac{N_e T_e^{1/2}}{0.163}\, \dfrac{A}{K}\, f_n(X_{1n}+1)\left(1 - \dfrac{b_n}{b_1}\right) \right]}{S_2} \left[\frac{G_{2n}}{8\,(e^{X_{2n}} - 1)} \right]^{-1} e^{-X_{2n}}$$

or

$$\mu_n = 1 + \frac{a_n}{{}_2S}\, d_n^{-1}\, e^{-X_{2n}}, \qquad \epsilon = 1 + \frac{\left[\left(\dfrac{b_2}{b_1}\, e^{-X_{12}} \right)^2 G_{1n} - a_2 \right]}{{}_2S}\, d_2^{-1}. \tag{A-4}$$

Thus, equation (A-2) differs from the ${}_nS = 0$ expression for equation (48) in the presence of the factor μ_n/ϵ and the decrease in the constant term on the right-hand side of

the equation. Numerically, one obtains $\mu/\epsilon < 1$. This result suffices, numerically, to give b_n less than the values tabulated in Table 5. The value of ${}_2S$ at which b_2 no longer increases with decreasing S drops, however, from $S = 0.005$ to $S = 0.0015$, being given by the S at which ϵ is 2.

It does not seem worth while at this stage to discuss the alteration in Table 8 on the basis of a solution of equation (A-3). The significant change in higher approximations should be that resulting from an inclusion of collisional excitation from levels other than the ground level. Thus the above limit to the blackness of the line should rise as we consider collisional excitation from the second level, and the b_2 value should rise. Also a consideration of the effect of a temperature gradient on the integrated emission should be made, and the solution should be joined to the lower atmosphere in the manner already mentioned.

For convenience, the solution of equations (A-3) for ${}_2S = 0.1$, 0.05, 0.000 (and ${}_nS = 0$, $n > 2$) are tabulated for b_1–b_{10} in Table A-1.

TABLE A-1

s	b_1	b_2	b_3	b_4	b_5	b_6	b_7	b_8	b_9	b_{10}
0.1.....	$4.8\cdot10^4$	$0.78\cdot10^4$	45.2	8.90	4.48	3.11	2.54	2.19	1.96	1.83
0.05.....	$7.7\cdot10^4$	$1.25\cdot10^4$	33.5	6.75	3.50	2.50	2.07	1.82	1.64	1.52
0.....	$2.4\cdot10^5$	$3.9\cdot10^4$	2.08	1.44	1.24	1.15	1.10	1.06	1.03	1.02

SUPERTHERMIC PHENOMENA IN STELLAR ATMOSPHERES

IV. THE WOLF-RAYET ATMOSPHERE

RICHARD N. THOMAS*
Institute for Advanced Study, Princeton, New Jersey
Received November 30, 1948

ABSTRACT

The structure of the Wolf-Rayet atmosphere is considered from the standpoint of stratification and support. It is concluded that the neglect of deviations from the Boltzmann-Saha relations in earlier analysis obscured an ambiguity in the interpretation of the observations and that a homogeneous atmosphere with $T_e > T_r$ is as acceptable as a stratified atmosphere with T_e increasing downward. Analysis of the density gradient in V 444 Cygni leads to the conclusion that nonisotropic macroscopic motions of velocity equal to that inferred from the emission-band width suffice for support of the atmosphere. Comparison of the (ionization, band-width) correlation with the velocities required for support suggests that the ionization increases outward in at least the lower atmosphere.

The main problem of an extended atmosphere has been that of support. It now appears that the support mechanism is a system of microscopic and macroscopic motions. In the previous papers[1] of the series we have considered the case of the solar chromosphere, where the microscopic motion alone, in the form of an atmospheric kinetic temperature T_e greater than the radiation temperature T_r, suffices for support. In the present paper we consider the Wolf-Rayet atmosphere, where it appears that macroscopic motions contribute directly to the atmospheric support, rather than indirectly through the production of the condition $T_e > T_r$. In Section I we investigate the consequences of the condition $T_e > T_r$ on the structure of the Wolf-Rayet atmosphere, particularly in regard to the question of stratification. In Section II we investigate the combination of microscopic and macroscopic motions required to give the observed density gradient in the atmosphere of V 444 Cygni.

I. PSEUDO-STRATIFICATION

In a detailed analysis of several Wolf-Rayet objects Aller[2] finds a direct variation of excitation temperature and of the product of ion and electron density with ionization potential. He interprets these results as strong evidence for statification, with the more highly ionized material coming from the lower atmosphere, where the temperature and electron density are greater. The analysis rests on the assumption of the applicability of the (unmodified) Boltzmann-Saha equations. We note, however, that our theoretical analysis of the case $T_e > T_r$, in which we considered departures from the Boltzmann-Saha relations, indicates the absence of any unique excitation temperature. Indeed, we obtained in all levels an overpopulation relative to the Boltzmann distribution at T_e, with relative overpopulation decreasing toward the series limit. In such circumstances we expect to obtain a dependence of excitation temperature upon excitation level if we analyze the observed line intensities via the Boltzmann-Saha method. Since our calculations applied to a section of an atmosphere small enough to be uniform, the result would appear to cast doubt on the uniqueness of interpreting this (temperature, ionization) correlation as an indicator of stratification. We proceed to consider the $T_e > T_r$ effect

* Frank B. Jewett Fellow for 1948–49.

[1] Thomas, Papers I–III, *Ap. J.*, **108**, 130, 1948; **108**, 142, 1948; **109**, 480, 1949.

[2] *Ap. J.*, **97**, 135, 1943.

on the b_n values for the general case. It does not seem possible to obtain so complete a solution for the general as for the hydrogenic case, but some information relevant to the interpretation of the excitation temperatures and densities derived by Aller results.

a) THE b_n VALUES

In describing an atmosphere wherein $T_e > T_r$, the detailed balancing condition on each level must give way to the less restricted condition of steady-state population in each level. We then have, for the equation of condition on level n,

$$\sum_{n''} F_{n''n} + \sum_{n'} F_{n'n} + \sum_{n'} \bar{C}_{n'n} = \sum_{n'} F_{nn'} + \sum_{n''} F_{nn''} + \sum_{n''} \bar{C}_{nn''} . \tag{1}$$

The F's refer to spontaneous and radiation-induced transitions; the C's to the resultant between collisional excitations and de-excitations. For the continuum we use the quantum number κ and replace the sum over n'' by an integral over κ, or ν. We have

$$E_\kappa = h\frac{R}{\kappa^2} = \frac{m v^2}{2}, \tag{2}$$

$$F_{n'n} = 4\pi \int_0^\infty I_\nu S_\nu N_{n'} a_{n'n} \frac{d\nu}{h\nu} = \frac{4\pi^2 e^2}{m c} I_\nu S_\nu N_{n'} \frac{f_{n'n}}{h\nu}, \tag{3}$$

and

$$F_{nn'} = N_n \frac{\varpi_{n'}}{\varpi_n} \frac{4\pi^2 e^2}{m c}\left[\frac{2h\nu^3}{c^2} + I_\nu S_\nu\right]\frac{f_{n'n}}{h\nu}. \tag{4}$$

For $F_{\kappa n}$, etc., we multiply by $d\kappa = d\nu \cdot \kappa^3/2R$, replacing n'' by $i\kappa$, and the sum over n'' by an integral over κ. We have written $S_\nu I_\nu(T_r)$ as the intensity of the radiation field. $I_\nu(T_r)$ is the Planck function at T_r. We may write, for the population of level n,

$$N_n = b_n N_i N_e \left(\frac{h^2}{2\pi m k T_e}\right)^{3/2} \frac{\varpi_n}{2\varpi_i} e^{X_n}. \tag{5}$$

The notation is conventional, except that we set

$$X_n = \frac{\chi_n - \chi_i}{kT_e}, \qquad X_{nn''} = X_n - X_{n''}, \qquad Y_{nn''} = \frac{h\nu_{nn''}}{kT_r}, \tag{6}$$

with χ_i the ionization potential of the ion one stage lower than ion i, and χ_n the excitation potential of level n. We are interested in the values of the b_n. The only modification over Papers I–III lies in the possibility of the atom in question being something besides hydrogen. We may write

$$\bar{C}_{nn''} = 4\pi^2 a_0^2 N_n N_e \left(\frac{m}{2\pi k T_e}\right)^{3/2}\left(1 - \frac{b_{n''}}{b_n}\right)\int_{v_0}^\infty v^3 Q_{nn''} e^{-mv^2/2kT_e} dv . \tag{7}$$

Introduce

$$I_{nn''} = \int_{q_0}^\infty Q_{nn''} q^3 e^{-q^2} dq . \tag{8}$$

If we set

$$\tau = \left(\frac{2\pi k T_e}{m}\right)^{1/2} a_0^2 \frac{m c^3}{4\pi^2 e^2} \tag{9}$$

and substitute equations (2)–(7) in equation (1), we obtain, after some algebra,

$$b_n\left\{\tau N_e\sum_{n''} I_{nn''}\left(1-\frac{b_{n''}}{b_n}\right)\varpi_n e^{X_n}+\sum_{n'}\left[1-S_\nu\frac{\dfrac{b_{n'}}{b_n}\,e^{X_{n'n}}-1}{e^{Y_{n'n}}-1}\right]\varpi_{n'}f_{n'n}\nu_{n'n}^2 e^{X_n}\right\}$$

$$=\left\{\sum_{n''} b_{n''}\varpi_n f_{nn''}\nu_{nn''}^2 e^{X_{n''}}\left(1-S_\nu\frac{\dfrac{b_n}{b_{n''}}\,e^{X_{nn''}}-1}{e^{Y_{nn''}}-1}\right)+\frac{1}{2R}\int_{\nu_n}^{\infty}\varpi_n f_{n\kappa}\nu^2\kappa^3 e^{-h(\nu-\nu_n)/kT_e}\right. \tag{10}$$

$$\left.\times\left(1-S_\nu\frac{b_n e^{h\nu/kT_e}-1}{e^{h\nu/kT_r}-1}\right)d\nu+\tau N_e\sum_{n'} b_{n'}I_{n'n}\left(1-\frac{b_n}{b_{n'}}\right)\varpi_{n'}e^{X_{n'}}\right\}.$$

From this equation (10) we would like to draw the conclusion that, in the general case, the b_n monotonically approach unity from above, with the exception of lines originating from metastable terms. We should then be able to conclude that any excitation temperature determined from relative line intensities would be a lower limit to the atmospheric kinetic temperature (eq. [14] ff.). Unfortunately, at the time of this writing, a rigorous proof of $b_n > 1$ for all n does not seem evident. We can, however, show strong reason for believing the statement true.

Consider equation (10) for b_1. The terms involving a summation over n' drop out. Suppose $b_1 < b_{n''}$ for all n'' (hence $b_1 < b_\kappa = 1$). Since

$$T_e > T_r\,, \qquad X_{nn''} < Y_{nn''}\,, \qquad \text{and} \qquad \exp(X_{nn''})-1 < \exp(Y_{nn''})-1\,,$$

then

$$\frac{\dfrac{b_1}{b_{n''}}\exp(X_{nn''})-1}{\exp(Y_{nn''})-1} < 1 > \frac{b_n e^{h\nu/kT_e}-1}{e^{h\nu/kT_r}-1}\,.$$

So the terms remaining on the right in equation (10) are positive (since $S_\nu \leqslant 1$ unless $b_1 > b_{n''}$ follows from Paper III). But

$$1-\frac{b_{n''}}{b_n} < 0\,.$$

Hence the left side of equation (10) is negative. These two results are contradictory, so we conclude $b_1 > b_{n''}$ for at least some n''. It does not appear that we can, without more specific calculation for each case, extend the result rigorously to conclude $b_1 > b_{n''}$ for all but a finite number of n''. (In which case, since $b_{n''}$ must asymptotically approach 1 near the continuum, we would conclude that it approached from above; hence $b_n > 1$.) If, however, we approximate the structure of the ion by grouping all save the outer electron with the nucleus, we should, for the higher quantum orbits of the outer electron, approach the hydrogen configuration. And the developments of Papers II–III indicate that, for this hydrogen case and for $T_e > T_r$, $b_n > b_{n''} > 1$. While this hydrogenic approximation is hardly satisfactory to describe the spectrum, in the region of high quantum number we expect it to provide a sufficiently good approximation to the population of the energy states that the direction of approach of b_n to 1 will not be reversed from that in the exact case. Thus we have some confidence that, in general, $b_n > b_{n''} > 1$ for $T_e > T_r$.

We note that the N_i in equation (4) refers to the volume density of the ion one stage higher than that of N_n. In the calculations of Papers II–III we had $N_i = N_e$ and used

T_e and N_e as the observed parameters. Now, however, we must compute N_i from the relation

$$N_i = \sum_n {}_iN_n . \tag{11}$$

Thus we recognize that N_i has implicit in it the b_n of the ${}_iN_n$. Usually, we suspect, $N_i \sim {}_iN_1$, and the b is ${}_ib_1$. Thus, if N_j represents the volume density of the bare nucleus of the atom in question, ${}_{j-1}b_1$ is a measure of the ground-state population in the true hydrogenic configuration of the atom. We may use the explicit expression for b_1 given in equation (43) of Paper III to see how b_1 varies with the nuclear charge of the atom. We have, Paper III, equation (43),

$$b_1 = \frac{1.85 \cdot 10^{18}}{N_e T_e^{1/2}} \frac{1}{\phi} \frac{1}{2} \left\{ -E_i(-X_1) + \bar{S} \sum -E_i\left(- Y_1 \left[a + \frac{T_1}{T_e} \right] \right) \right\} e^{X_1}, \tag{12a}$$

$$\phi = \sum_2^\infty f(n)[X_{1n}+1)P_n + 1.54 \cdot 10^{-8} T_e (X_1+2) + \frac{K e^{X_1}}{A N_e T_e^{1/2}} \frac{\bar{S}}{2} \sum_{a=2}^\infty -E_i(-a Y_1). \tag{12b}$$

The factor $1.85 \cdot 10^{18}$ in equation (12*a*) is the ratio K/A of a numerical constant K from the radiative terms to the numerical constant A from the collisional cross-section term. A brief glance at the formal development of Paper II will show that, for nuclear charge Z, K should be replaced by KZ^4. The terms X_n and Y_n, which are essentially the excitation energies of level n, contain the factor Z^2. Finally, P_n is $(\exp X_n)/n^3$. Since, for large X, $-E_i(-X) \sim (\exp -X)/X$, only the first term in each of equations (12*a*) and (12*b*) is significant for large Z. Hence we can see that b_1 varies with Z through the combination of terms, as follows:

$$b_1 \sim Z^4 \frac{1}{Z^2 e^{Z^2(X_2)}} \frac{1}{Z^2} = \frac{1}{e^{Z^2 X_2}}. \tag{13}$$

The Z^2 (exp Z^2X_2) alone enters from ϕ, as it furnishes the larger part of the term. Thus b_1 decreases rapidly with larger nuclear charge.

For example, in an ensemble containing both *H* I and *He* II, we should expect the b_1 of the ground state of hydrogen to exceed that of helium. Since the b_n decrease from b_1 toward b_∞, we also expect the ratio of $b_m : b_n$, $m < n$, to be less for *He* II than for *H* I, for the same m and n. Thus the correction term b_m/b_n which enters in the Boltzmann expression (cf. eq. [14] ff.) for relative line intensities should be less for *He* II (if corresponding lines are used), and we expect an excitation temperature determined from *He* II more nearly to approach the electron temperature (i.e., atmospheric kinetic temperature) than an excitation temperature determined from *H* I.

The remarks of the preceding paragraph apply to the situation when the n and m are the same for *He* II and *H* I. We note, however, that, while the Balmer series is in the usually accessible region for *H* I, it is the Pickering and Fowler series for *He* II. Thus for *He* II we usually deal with (m, n) pairs somewhat smaller than for *H* I, and so expect the correction term to be smaller still, in general. To these remarks, depending upon the particular line chosen, one can, of course, always find exception. In general, however, when comparing the hydrogen-like ion of two elements, we expect that ion having the greater nuclear charge to give b_m/b_n values more nearly approaching unity.

While the above comparison between atoms is reasonably rigorous, we might expect roughly similar results when comparing various stages of ionization within the same ion. We again draw on our approximation of considering the outer electron in high quantum orbits to be nearly in a hydrogen configuration. Then we might expect the values of the ${}_ib_n$, for corresponding n, to be less than those for ${}_jb_n$, $j < i$. That is, we might expect the same rough variation of b_m/b_n with ionization potential—the higher potential giving the closer approach to unity.

Thus, summarizing briefly, we expect the b_1 value for a given ion to be less than that for an ion of lesser positive charge. Within a given ion we expect—with the exception of metastable levels—a monotonic decrease of b_n with increasing excitation level above the ground state of the ion. The essential result for the succeeding section on electron temperature is $b_n/b_m > 1$, $n < m$; with the ratio decreasing with increasing stage of ionization.

b) PSEUDO-TEMPERATURE VALUES

The results on the b_n values lead immediately to the earlier-mentioned comments on the kinetic temperature of the atmosphere. We may write the ratio of observed line intensities, ignoring saturation effects, thus:

$$\frac{I_{ab}}{I_{cd}} = \frac{N_a A_{ab} h\nu_{ab}}{N_c A_{cd} h\nu_{cd}} = \frac{b_a e^{X_a}}{b_c e^{X_c}} \frac{\varpi_a}{\varpi_c} \frac{A_{ab}}{A_{cd}} \frac{h\nu_{ab}}{h\nu_{cd}}. \tag{14}$$

Hence

$$T_e = \frac{\nu_a - \nu_c}{ln \dfrac{I_{ab}}{I_{cd}} - ln \dfrac{A_a \nu_a \varpi_a}{A_c \nu_c \varpi_c} - ln \dfrac{b_a}{b_c}} \frac{k}{h}. \tag{14a}$$

Now if $\nu_a > \nu_b$, then $b_a > b_c$ in general by the preceding discussion. Hence we will compute a T_e that is too small if, as is customarily done, we omit the term $-ln\, b_a/b_c$ from the denominator. And, as mentioned, we will obtain a systematic dependence of T_e on ionization level. This dependence may, in turn, be interpreted erroneously as evidence of stratification. These remarks are not meant to imply that one may not observe—in stratified atmospheres—a varying set of kinetic temperatures. Rather, the analysis of intensity ratios for kinetic temperature should include the b_n term, so that spurious stratification indications may be removed. Unfortunately, of course, such a knowledge of the b_n presupposes a detailed analysis of the atmosphere similar to that of Papers II–III for the solar chromosphere. Lacking such an analysis, we can conclude no more than that the computed excitation temperatures are only lower limits to a mean atmospheric kinetic temperature.

At this point we consider the numerical plausibility of the above suggestions. That is, Aller's spectroscopic data for several Wolf-Rayet objects provides a list of line intensities from which, by forcing agreement of T_e in equation (14*a*) for several lines, we might obtain an estimate of the b_n ratios. The nicest such use of the data would be for the $4^2F - m^2G$ *He* II series for the carbon stars, in which lines for $m = 12, 9, 8$, and 7 are measured; for this ion has just the hydrogen configuration. Unfortunately, the line intensities do not seem to be sufficiently self-consistent to obtain numerical results in this case, where, in the denominator of equation (14*a*), we depend on the difference of nearly equal quantities. The measured intensities of the lines are reasonably small, and Aller cautions against too great faith in accuracies of 10–20 per cent, which is the margin needed here. If we consider the *He* II $3^2D - m^2F$ series, we find stronger lines, but only two of them in the accessible range. Substituting numerical data in equation (14*a*) from Aller's paper, we obtain as typical results:

$$\begin{aligned}
\text{BD}+43^\circ 3571: \quad & \frac{T_e}{35000} = \frac{0.398}{0.784 - ln \dfrac{b_4}{b_5}}; \\
\text{BD}+35^\circ 4001: \quad & \frac{T_e}{35000} = \frac{0.398}{0.325 - ln \dfrac{b_4}{b_5}}; \\
\text{BD}+37^\circ 3821: \quad & \frac{T_e}{35000} = \frac{0.398}{0.564 - ln \dfrac{b_4}{b_5}}.
\end{aligned} \tag{15}$$

In the preceding papers of the series we treated the case of *H* I at $T_e = 35{,}000°$ and $N_e = 2 \cdot 10^{11}$, $T_r = 6000°$. The b_n values are not particularly sensitive to the N_e values, although this particular N_e value is nearly that in the Wolf-Rayet atmosphere. Thus these b_n values should be reasonably appropriate for *He* II at $T_e = 140{,}000°$ and $T_r = 25{,}000°$ (temperatures not a great deal different from those we might expect to characterize the Wolf-Rayet stars). From Paper III we obtain as a final, upper limit for the ratio b_4/b_5 the value 2.1. The first approximation, of Paper II, gives a lower limit of 1.18. If we use this value of $ln\ b_4/b_5$ to be somewhere between 0.74 and 0.165, the T_e values are of the order of $5 \cdot 10^{4°}$–$5 \cdot 10^{5°}$ K. Much significance cannot, of course, be attached to these results, beyond noting that the values form a reasonably self-consistent set and that the values are not absurd—in a numerical sense—relative to the other quantities of equation (15). From these lines, λ 3203 and λ 4686 alone, we cannot, however, find information on the decrease of b_n/b_m with larger n.

An interpretation of the Wolf-Rayet spectrum in the light of the above suggestions would indicate atmospheric kinetic temperatures of the order of $5 \cdot 10^{4°}$–$5 \cdot 10^{5°}$ K. It might be expected that one could use the results of the radial density distribution in V444 Cygni, as in the case of the solar chromosphere, to obtain the mean kinetic temperature and thus check the above values. However, by contrast with the solar case, a discussion (Sec. II) of the density gradient indicates that the system of macroscopic motions provides a considerable amount of momentum as well as energy transfer. In this case, one does not have an atmosphere in which the density gradient follows from the kinetic temperature alone.

c) PSEUDO-DENSITY EFFECTS

We turn, now, to consider the apparent increase of N_iN_e with the degree of ionization. Aller interprets this result as further evidence for the more highly ionized ions coming from the lower atmosphere, where N_e is greater. We note that equation (14) is used to obtain this result, neglecting, however, the b_n values and using a T_e from the earlier (T_e, ionization-level) relation. We have, for the equation,

$$N_iN_e = \varpi_i \frac{E_{nn'} T_e^{3/2} e^{-X_n}}{b_n A_{nn'} \varpi_n} \cdot \text{constant} . \tag{16}$$

We note, then, that at least part of Aller's computed increase of N_iN_e is a simple consequence of the use of a varying T_e and the neglect of b_n. Although b_n decreases with increased ionization level, the omission of b_n in Aller's calculations does not suffice to compensate for the pseudo-rise of $T_e^{3/2}e^{-X_n}$; for a consideration of equations (14) shows that the spurious variation of e^{-X_n} overcompensates this neglect of b_n. Hence the pseudo-N_iN_e should increase somewhat more rapidly than the $T_e^{3/2}$ due to this pseudo-temperature effect. A comparison of Aller's Figures 3 and 4, which show the apparent dependence of T_e and N_iN_e on ionization potential, shows an increase of N_iN_e considerably more rapid than this $T_e^{3/2}$. One may then still have some residual increase of N_iN_e other than the above pseudo-increase, although the amount is uncertain. The interpretation of such an increase is hardly unique, even though stratification is one possibility. We note that the departure from thermodynamic equilibrium suggests a rise in the number of ions at the higher stage of ionization. Thus, for example, our analysis of the hydrogen chromosphere showed hydrogen 99.5 per cent in the *H* II stage. This result is a considerable contrast with that obtained when we use the photospheric 6000° value rather than the chromospheric 35,000°. The same situation presents itself in the higher chromosphere, where it seems highly probable that *He* II will be more abundant than *He* I.

The net result of this discussion on the apparent increase of N_iN_e lies first in a recognition of the pseudo-increase due to the pseudo-temperature effect and, second, in a realization of the impossibility of a priori attributing a possible still present increase of N_eN_i uniquely to stratification.

II. KINEMATIC STATE

In the preceding section we simply showed that the condition $T_e > T_r$ in a uniform atmosphere leads to a spectrum exhibiting many of the characteristics usually attributed solely to a stratified atmosphere. Thus the remarks indicate the nonuniqueness of a particular model, without, however, containing a positive guide toward a more definite model. I have elsewhere suggested that the current simple expanding atmosphere model is incompatible with the band profiles and that the atmosphere is more likely nearly steady as a whole. In this section we suggest such an alternate Wolf-Rayet atmosphere model, basing the model largely on the inferences drawn from a study of the atmospheric support problem. We proceed to consider the manner of support.

The condition $T_e > T_r$, which formed the basis of the discussion in Section I, implies the existence of some system of energy transport other than radiation. A natural identification is that of this energy system with a mass motion in the atmosphere. In the solar chromosphere, as treated in Papers I–III, there was a significant assumption made on such mechanical-energy transport, namely, that one could neglect momentum transport from the mechanical system. This assumption implies the possibility of a direct interpretation of the atmospheric density gradient in terms of static gravitational equilibrium to obtain the atmospheric kinetic temperature. The more general case arises when the system of mass motion must be analyzed for momentum, as well as for energy transfer. We ask which of these cases holds in the Wolf-Rayet atmosphere.

We consider the quantitative aspects of the suggestion that the mass motion contributes in large part to the support of the atmosphere. We cannot from the following computations conclude that other support mechanisms are not operative. But we can investigate whether the velocities needed to support the atmosphere by momentum transfer are of the same order of magnitude as those inferred from the emission-band widths, and thus whether other support mechanisms are necessary.

We use for data the analysis by Kopal and Mrs. Shapley[3] of the atmosphere of V444 Cygni. The results of the analysis indicate that the opacity in the atmosphere arises chiefly from electron scattering, and so the atmosphere structure is given numerically in terms of electron density. Since the atmospheric hydrogen must be nearly all ionized, the electron density gradient cannot differ greatly from the mass density gradient. We use the results for an orbital inclination of 80°, which are contained in Table 8 of Shapley and Kopal.[3] Following the authors, we adopt $10\odot$ for the mass of the star. We take a mean molecular weight of $\frac{1}{2}$.

Consider, first, the possibility that the momentum transfer from the mass motion is small and that the atmosphere is therefore in static gravitational equilibrium at temperature T_e. We have the equation of condition:

$$\rho_0 T_{e0} \frac{k}{\mu m_H} = p_0 = \int_{r=r_0}^{\rho=0} g \rho \, dr . \tag{17}$$

For r_0 we take the smallest radius in Table 8. We evaluate the right side of equation (17) numerically and obtain

$$T_{e0} = 1.1 \cdot 10^{7\circ} \mathrm{K} . \tag{17a}$$

Even by comparison with the T_e values suggested in Section I from Aller's data, this value seems high.

We ask, then, what change in the dynamic state of the atmosphere is required to give

[3] *Ap. J.*, **104**, 160, 1946.

the observed density gradient and get T_{e0} a value of the order 10^5–10^6? We therefore replace equation (17) by the conventional hydrodynamic equation of motion:

$$\frac{\partial \rho v}{\partial t} + \nabla \cdot v \rho v = -g\rho - \nabla p . \tag{18}$$

If we assume no more than the existence of some kind of mass motion, a complete spherical symmetry is not, in general, required, nor can we neglect $\partial/\partial t$. The stability of the spectrum suggests, however, that, if we assume a random distribution of the mass motion (in location, not direction) and take averages in equation (18) over angular sectors of the atmosphere large with respect to the scale of distribution of the mass motion, we might ignore all derivatives but $\partial/\partial r$. Further, we shall assume that the macroscopic motions in question are radial only. We then have

$$\int_\omega \frac{1}{r^2}\frac{\partial}{\partial r}(r^2 \rho v^2)\, d\omega + \int_\omega \frac{\partial p}{\partial r}\, d\omega = -g \int \rho\, d\omega , \tag{19}$$

where ω is the solid angle of the above-mentioned angular sector. Let us further assume that we may take $\partial/\partial r$ outside the integral sign, in equation (19).[4] We then have, denoting by a bar the average over ω,

$$\frac{1}{r^2}\frac{\partial}{\partial r}(r^2 \overline{\rho v^2}) = -\frac{\partial \bar{p}}{\partial r} = -g\bar{\rho} \tag{20}$$

or

$$\frac{\partial}{\partial r}\overline{\rho v^2} + \frac{2\overline{\rho v^2}}{r} = -\frac{\partial \bar{p}}{\partial r} - g\bar{\rho} . \tag{20a}[5]$$

Now from equation (20) we expect to obtain a $\overline{v^2}$ which is an average velocity effective in momentum transfer. From the widths of the emission bands, however, we obtain (an upper limit to) the largest velocities of the macroscopic motion. Hence we must find that the velocities required in equation (20) are less than the band widths, if the dynamic support suggestion is tenable. From equation (20*a*) we obtain an upper limit to $\overline{v^2}$; for we have

$$r_0^2 \overline{\rho_0 v_0^2} = \int r^2 \left(g\bar{\rho} + \frac{\partial \bar{p}}{\partial r} \right) dr . \tag{21}$$

Since $\partial \bar{p}/\partial r < 0$, we obtain an upper limit to $\overline{v^2}$ by neglecting $\partial \bar{p}/\partial r$. Evaluating the integral remaining from Shapley and Kopal's data,[3] we obtain (at the same level referred to in eq. [17*a*])

$$\frac{1}{\bar{\rho}_0}\overline{\rho_0 v_0^2} < 45 \cdot 10^{14}\ \mathrm{cm^2/sec^2} . \tag{21a}$$

We note further that if we seek a solution harmonious with $T_e = 10^{5°}$–$10^{6°}$ K, equation (17) indicates that neglect of the $\partial \bar{p}/\partial r$ term introduces an error of only some 10 per cent. We may attempt to set a lower limit by considering equation (20*a*). We note that the two terms on the left are of opposite sign. Hence, neglecting one, we underestimate the other. Neglecting the second term and integrating, we get

$$\overline{\rho_0 v_0^2} + \overline{p_0} > \int_{r_0}^{\rho=0} g\bar{\rho}\, dr . \tag{22}$$

[4] While it is not, in general, true that $\partial\bar{\rho}/\partial r = \overline{\partial\rho/\partial r}$, it does not seem that the uncertainty so introduced is greater than that already present.

[5] The "extra" $(1/r)$ term comes from the assumed anisotropy of the macroscopic motion. We note that it has been habitually ignored in treatments of the turbulent support of extended stellar atmospheres.

Since the right sides of equations (22) and (17) are identical, we have

$$\frac{1}{\bar{\rho}_0}\overline{\rho_0 T_{e0}}+\frac{1}{\bar{\rho}_0}\overline{\rho_0 v_0^2}\frac{\mu m_H}{k}>1.1\cdot 10^{7\circ}\mathrm{K}. \tag{22a}$$

Again, since we wish $T_{e0}\sim 10^5$–10^6, and even though it is hardly to be expected that ρ_0, T_0, and v_0 are uncorrelated, dropping the first term on the left of equation (22*a*) should not alter the inequality. We then obtain

$$\frac{1}{\bar{\rho}_0}\overline{\rho_0 v_0^2}>18\cdot 10^{14}\ \mathrm{cm^2/sec^2}, \tag{22b}$$

again at the same level as for equation (17). We thus have the rough guide for the mass-averaged velocity effective in the momentum transfer,

$$400\ \mathrm{km/sec}\gtrsim v\gtrsim 700\ \mathrm{km/sec}\ .$$

If we carry through the computations for a level at twice the *radius*, we obtain

$$250\ \mathrm{km/sec}\gtrsim v\gtrsim 300\ \mathrm{km/sec}\ .$$

On the basis of these kinematic results we may make two remarks on the model of the atmosphere.

1. Beals classifies V 444 Cygni as WN5.5 in his Wolf-Rayet sequence. We reproduce in Table 1 Beals's typical values[6] for the (ionization, velocity) correlation for types WN5

TABLE 1

Atom	*He* I	*He* II	*N* IV	*N* V
λ	5875	5411	3483	4605
Ionization (e.v.)	24.5	54.2	77.0	97.4
WN5	.....	1361	.....	640
WN6	1815	1550	1235	487

and WN6. The profiles of $H\delta$ and $H\gamma$ published by Beals for V 444 Cygni agree with the Table 1 values by showing widths of $\pm\sim 2000$ km/sec. It then seems safe to conclude that the velocities required for the dynamic support of the atmosphere do not exceed those actually observed.

2. We have seen above that the velocities required for support decrease as we go higher in the atmosphere. Further, the observed maximum velocities for *N* v lie very close to the minimal average values computed from equation (22), while those for *H* and *He* lie safely above. We conclude, therefore, that the velocities decrease outward,[7] and that the (ionization, velocity) correlation indicates an increase in excitation level of the atmosphere outward. Thus while the Section I remarks on the condition $T_e > T_r$ indicate that we do not need to interpret the observations as giving an increase of excitation inward, the present section suggests that some measure of stratification exists—in the opposite direction.

I am greatly indebted to Dr. M. Schwarzschild for much discussion over the content and mode of presentation of the preceding.

[6] *XIII colloque d'astrophysique* (Actualités scientifiques et industrielles," No. 901), 1, 109.

[7] We note here Swings's remark (*Ap. J.*, 95, 127, 1942) to the effect that the presence of absorption cores in some of the emission bands demands (Rosseland, *Theoretical Astrophysics* [Oxford: Clarendon Press, 1936], p. 294) decelerated motion.

NONRADIAL OSCILLATIONS OF THE STANDARD MODEL

ZDENĚK KOPAL
Center of Analysis, Massachusetts Institute of Technology and Harvard College Observatory
Received November 26, 1948

ABSTRACT

The differential equations governing small nonradial oscillations of compressible-gas spheres are set up correctly to the order of accuracy to which the changes in the gravitational potential produced by such oscillations can be ignored. Explicit forms of these equations are obtained for the polytropic family of models and are integrated mechanically, for the case of the standard model (polytrope $n = 3$), by means of the Rockefeller differential analyzer of Massachusetts Institute of Technology, with the aim of ascertaining free periods of the lowest three "gravitational" oscillations which correspond to the second-, third-, and fourth-harmonic disturbance. A whole march of the corresponding pressure and density variation throughout the interior of the oscillating configuration is tabulated for all characteristic frequencies established in this paper, and the frequencies themselves are ultimately corrected for the main part of the error inherent in our initial neglect of the accompanying gravity changes, by Cowling's perturbation method.

The abstract problem of nonradial oscillations of compressible gaseous configurations is one of considerable interest for double-star astronomy. Consider a close binary system, the components of which revolve in Keplerian orbits around their common center of gravity. If their orbits happen to be eccentric—and the orbits of most real binaries are characterized by some eccentricity—the mutual tidal distortion of the components will vary, to a first approximation, as the inverse cube of the instantaneous radius vector of the relative orbit. If the orbital period is long in comparison with free periods in which the components can oscillate nonradially, the corresponding tidal distortion will be of the nature of a forced oscillation, the amount of which will differ but little from that given by the equilibrium theory of tides. However, should the period of the orbit become comparable with any free period of nonradial oscillation, the corresponding tidal harmonic may be enhanced by resonance beyond the equilibrium limit and may give rise to observable phenomena which defy conventional explanation. Several phenomena in certain eclipsing systems, such as the apparent excess or deficiency of photometric ellipticity,[1] or asymmetry of light-curves,[2] are indeed suggestive of resonance; but this explanation cannot be put on a firm basis until more light has been thrown on possible free periods of oscillation of compressible-gas configurations characterized by a high degree of central condensation.

The general oscillations of a heterogeneous sphere of compressible fluid present a mathematical problem of considerable complexity. Rosseland[3] was the first to show that small nonradial oscillations are governed by a linear differential equation of fourth order, the explicit form of which was eventually obtained by Pekeris.[4] Nothing is known, however, about the solutions of this equation beyond the simplest case of an initially homogeneous sphere, for which an instability with respect to all nonradial oscillations was established by Pekeris.

In order to simplify the problem and gain some insight into the nature of its characteristic frequency spectrum, Emden[5] conceived the idea of ignoring the effect of the displacement upon the gravitational potential in the outer parts of a centrally condensed

[1] Cf. Kopal, *Harvard Bull.*, No. 910, 1939.
[2] Taylor, *Ap. J.*, **94**, 46, 1941.
[3] *Oslo Pub.*, No. 2, 1932.
[4] *Ap. J.*, **88**, 189, 1938.
[5] *Gaskugeln* (Leipzig and Berlin: B. G. Teubner, 1907), p. 448.

configuration—a simplification which reduced the order of the governing differential equation from fourth to second. His work was, however, vitiated by inconsistent approximations made in considering the equation of continuity, which he reduced, in fact, to the form appropriate to a homogeneous incompressible fluid. The correct formulation of a problem so simplified was later given by Cowling,[6] who investigated numerically the fundamental modes of the second-harmonic oscillations of Eddington's well-known "standard model" for two different values of the ratio of specific heats, as well as certain of its overtones. The aim of the present investigation will be to investigate free frequencies in which the standard model can oscillate nonradially in greater detail than has been done so far, and to do so by more powerful numerical methods than have hitherto been brought to bear on our problem. In what follows, we shall extend Cowling's analysis to the domain of lower overtones characteristic of the second-harmonic oscillation and shall investigate—for the first time—the properties of the third- and fourth-harmonic free oscillations of the same model. In the first part of this paper approximate wave equations of nonradial oscillations will be deduced. In the second part we shall describe the way in which our wave equations can be solved by mechanical means, while the concluding third part will be devoted to a general discussion of the results.

I. EQUATIONS OF THE PROBLEM

Consider the oscillations of a gas sphere under the influence of its own gravity, which are so small that squares of amplitudes of the displacements and of their derivatives can be ignored in comparison with their first powers. In setting up the requisite equations of motion, we shall neglect viscous forces and assume that the motion of any individual gas particle takes place adiabatically. Let the pressure P, density ρ, and gravitational potential V at any point be altered by δP, $\delta\rho$, and δV, respectively, and let the vector displacement of material from its equilibrium be $\boldsymbol{h}$. Then, within the scheme of our approximation, the Eulerian equations of motion can be written as follows:

$$\rho \frac{\partial^2 \boldsymbol{h}}{\partial t^2} + \text{grad } \delta P + \delta\rho \text{ grad } V + \rho \text{ grad } \delta V = 0 , \tag{1}$$

where t denotes the time, and the equation of continuity becomes

$$\delta\rho + \text{div}(\rho \boldsymbol{h}) = 0 . \tag{2}$$

Consistent with our assumption of a simply harmonic motion, we shall seek such solutions of the foregoing system of equations for which

$$\frac{\partial^2 \boldsymbol{h}}{\partial t^2} + \sigma^2 \boldsymbol{h} = 0 , \tag{3}$$

where $\sigma = 2\pi/P$, P being the period of the respective oscillation.

Equations (1) and (2) represent a simultaneous system of fourth order, the solution of which represents, in any case, a problem of great mathematical complexity. In order to simplify it to some extent, let us—following Emden,[5] Rosseland,[3] and Cowling[6]—ignore the variation δV of the gravitational potential on the left-hand side of equation (1). If the mass of our configuration is largely condensed toward its center—which is certain to be true for most real stars—the variation in density accompanying the oscillations will produce but minor variation of the gravitational potential through most of the interior, the neglect of which should not affect appreciably the characteristic features of our problem. On the other hand, the advantage of such a neglect is the reduction of our mathematical problem to the solution of a single differential equation of second order.

[6] *M.N.*, **101**, 367, 1942.

In order to deduce this equation, let us begin by eliminating $\boldsymbol{h}$ between equations (1) and (3). Inserting equation (3) in equation (1) and taking the divergence of both sides, we obtain

$$\sigma^2 \operatorname{div}(\rho \boldsymbol{h}) = \operatorname{div}\{\operatorname{grad} \delta P + \delta\rho \operatorname{grad} V\}. \tag{4}$$

According to the equation of continuity, $\operatorname{div}(\rho \boldsymbol{h}) = -\delta\rho$; while the equation of hydrostatic equilibrium asserts that

$$\operatorname{grad} P = -\rho \operatorname{grad} V. \tag{5}$$

If, furthermore, use is made of the identity

$$\operatorname{div} \operatorname{grad} \delta P = \nabla^2 \delta P,$$

where ∇^2 denotes the Laplacean operator, the equations (1) of motion can be reduced to

$$\sigma^2 \delta\rho = \operatorname{div}\left(\frac{\delta\rho}{\rho} \operatorname{grad} P\right) - \nabla^2 \delta P. \tag{6}$$

Now we shall consider oscillations in which δP and $\delta\rho$ are products of a surface harmonic of order j and a function of the distance r from the center of our configuration. Then

$$\nabla^2 \delta P = \frac{1}{r^2 \partial r}\left\{ r^2 \frac{\partial \delta P}{\partial r}\right\} - \frac{j(j+1)}{r^2} \delta P, \tag{7}$$

and

$$\operatorname{div}\left(\frac{\delta\rho}{\rho} \operatorname{grad} P\right) = \frac{1}{r^2 \partial r}\left(r^2 \frac{\delta\rho}{\rho} \frac{\partial P}{\partial r}\right), \tag{8}$$

while, furthermore, the radial component δr of vector $\boldsymbol{h}$ follows from equations (1) and (3) as

$$\rho\sigma^2 \delta r = \frac{\partial \delta P}{\partial r} - \frac{\delta\rho}{\rho} \frac{\partial P}{\partial r}. \tag{9}$$

Inserting equations (7), (8), and (9) in equation (6), we obtain

$$\delta\rho = -\frac{\partial}{r^2 \partial r}(\rho r^2 \delta r) + \frac{j(j+1)}{\sigma^2 r^2} \delta P. \tag{10}$$

For an ordinary gas the relation between the adiabatic changes in pressure and density of a given element of fluid is given by

$$\delta P + \delta r \frac{\partial P}{\partial r} = c^2\left(\delta\rho + \delta r \frac{\partial \rho}{\partial r}\right), \tag{11}$$

where

$$c^2 = \gamma \frac{P}{\rho},$$

γ being the ratio of specific heats.[7] Under the conditions prevailing in stellar interiors γ is likely to be a variable quantity. The limits of its possible variation are, however, so narrow that an assumption of constant value of γ should be adequate for all practical purposes.

[7] In ordinary gas, c would be the Laplacean velocity of sound. If the matter were incompressible, $c = \infty$.

Eliminating $\delta\rho$ from equations (9) and (10) by the use of equation (11), we can reduce the fundamental equations of our problem to

$$\frac{d\zeta}{dr} - \frac{g}{c^2}\zeta = \left\{\frac{j(j+1)}{\sigma^2} - \frac{r^2}{c^2}\right\}\frac{\eta}{\rho}, \tag{12}$$

$$\frac{d\eta}{dr} + \frac{g}{c^2}\eta = \left\{\sigma^2 + \frac{g}{\rho}\frac{d\rho}{dr} + \frac{g^2}{c^2}\right\}\frac{\rho}{r^2}\zeta, \tag{13}$$

where we have abbreviated

$$\zeta = r^2\delta r,$$

$$\eta = \delta P,$$

and g is the local gravity related to the pressure gradient by the equation of hydrostatic equilibrium, $dP/dr = -g\rho$.

The boundary conditions of our problem call for a node (no displacement) at the center and a loop (no variation in pressure) at the free surface of the oscillating configuration, i.e., they require that $\delta r = 0$ at $r = 0$, while $\delta P = 0$ at a value of r_1 for which $\rho(r_1) = 0$. These conditions can be satisfied only for certain values of σ, the ensemble of which represents the frequency spectrum of the oscillating configuration.

In order to investigate the nature of this spectrum, we have to commit ourselves to a definite distribution of density in the interior of the oscillating configuration. In what follows we shall assume, with Cowling,[6] that the distribution in density is polytropic, i.e., that the pressure and density are related by

$$P = K\rho^{1+1/n},$$

where K and $0 \leqslant n \leqslant 5$ are constants. If, as usual, we put

$$\rho = \rho_c\theta^n$$

and

$$r = r_0 x, \qquad r_0^2 = \frac{(1+n)P_c}{4\pi G\rho_c^2},$$

G being the gravitational constant, the function θ is found to satisfy the well-known Emden equation,

$$\frac{1}{x^2}\frac{d}{dx}\left(x^2\frac{d\theta}{dx}\right) + \theta^n = 0, \tag{14}$$

subject to the conditions that, when $x = 0$, $\theta = 1$ and $(d\theta/dx) = 0$.[8]

If, after Cowling, we set

$$\frac{\delta r}{r_0}\theta^{(1+n)/\gamma} = z, \tag{15}$$

$$\frac{\delta P}{P_c}\theta^{-(1+n)/\gamma} = w, \tag{16}$$

[8] These are the so-called "E-solutions" of Emden's eq. (14). In what follows, the solutions of eq. (14) regular at the origin will exclusively be considered in connection with our oscillation problem. All statements made hereafter on the oscillatory properties of polytropic stars do not necessarily have a bearing on the polytropes for which θ is characterized by a singularity at the origin (F- or M-solutions).

and abbreviate

$$\frac{2(1+n)}{\gamma-n}=Q,$$

$$\frac{\sigma^2(1+n)}{4\pi G\rho_c}=\alpha,$$

our fundamental equations (12) and (13) can be shown to reduce to

$$\frac{dw}{dx}=Q\theta^{-Q}\left\{\alpha+\frac{(Q-n)(n+1)}{2}\frac{\theta'^2}{\theta}\right\}, \tag{17}$$

$$\frac{d}{dx}(x^2z)=w\theta^Q\left\{\frac{j(j+1)}{\alpha}-\frac{x^2}{\gamma\theta}\right\}, \tag{18}$$

where $\theta'=d\theta/dx$. Abbreviating

$$\theta^{-Q}\left\{\alpha+\tfrac{1}{2}(Q-n)(n+1)\frac{\theta'^2}{\theta}\right\}=f,$$

$$\theta^Q\left\{\frac{j(j+1)}{\alpha}-\frac{x^2}{\gamma\theta}\right\}=g,$$

we can, by elimination, reduce the system of equations (17)–(18) to a single second-order self-adjoint equation of the form

$$\frac{d}{dx}\left\{\frac{1}{g}\frac{dv}{dx}\right\}-\frac{f}{x^2}v=0; \tag{19}$$

or, alternatively,

$$\frac{d}{dx}\left\{\frac{x^2}{f}\frac{dw}{dx}\right\}-gw=0, \tag{20}$$

where $v=x^2z$. It has been pointed out by Cowling[6] that if α is very large or very small (which implies very short or very long period of free oscillation), equations (19) and (20) reduce to the Sturm-Liouville type,[9] and the theory of the Sturm-Liouville equation permits us to infer that equation (19) then has an infinite number of solutions with α indefinitely large, while equation (20) admits of an infinite number of solutions with α indefinitely small. Hence, an infinite number of oscillations with indefinitely long periods is possible, as well as an infinite number of indefinitely small periods.

The solutions—if any—corresponding to finite values of α cannot, however, be found otherwise than by a trial-and-error process of numerical integration. In the special cases investigated by Cowling ($n=3, j=2, \gamma=\frac{4}{3}$ and $\frac{5}{3}$) a single oscillation of intermediate period was found such that δr and $-\delta\rho$ were of the same sign at all points of any assigned

[9] This reduction involves the neglect, in f, of a term of the order of θ'^2/θ in comparison with α or, in g, of a term of the order of $1/\alpha$ in comparison with $1/\theta$. Provided that α is sufficiently large (or small), this is indeed legitimate everywhere except in the immediate neighborhood of the boundary and where $\theta\to 0$ and where, consequently, both f and g are bound to change signs. It might, therefore, be objected that such an approximation is bound to fail at the point where the outer boundary condition is given. In reality, however, the condition $\delta P=0$ cannot be expected to hold good exactly where $\rho=0$ because of the probable failure of our adiabatic condition in the outer low-temperature fringe, but rather at a certain depth inside our configuration, where θ, though small, remains finite. Last, it should be mentioned that the nature of the frequency spectrum of free oscillations of each polytrope in the range of extreme values of α will be different for the E-, M-, or F-solutions of Emden's eq. (14) governing θ; but a closer study of these differences would be of mainly theoretical interest and take us too far from the main objective of this investigation.

radius, which will hereafter be referred to as the fundamental "(f) mode." In addition, Cowling established the existence of oscillations of shorter as well as longer periods, which he referred to as the pressure (p) and gravity (g) oscillations, respectively; they exhibit an increasing number of nodes and loops in the interior of the oscillating configuration. Long periods of free oscillations are of particular interest to the students of close binary systems, because their consequences are more readily observable as well as because of the possibility of resonance with the period of the orbit. In what follows we shall, therefore, extend Cowling's analysis of the frequency spectrum of nonradial oscillations of the polytrope $n = 3$ (Eddington's "standard model") not only to the realm of second-harmonic g oscillations of higher order but to the third- and fourth-harmonic f and g oscillations as well.

In the absence of any direct practicable method for estimating the eigenvalues of our problem, their determination will evidently call for a large number of numerical integrations with trial values of α. If such integrations had to be carried out on ordinary desk-type computing machines, the weight of routine work might easily become prohibitive. Fortunately for science, powerful mechanical devices have been developed in recent years to cope with extensive amounts of numerical integration; and of such machines, the one best suited for the solution of ordinary differential equations of not too great complexity appears to be the differential analyzer as developed at the Massachusetts Institute of Technology by V. Bush, S. H. Caldwell, and their school in the past twenty years. The underlying principles of this analogue-type machine are perhaps too well known to be repeated here; its latest model was adequately described by Bush and Caldwell in a paper, to which the interested reader is referred for fuller detail.[10] It is provided with 18 integrators, only half of which will actually be needed for the solution of our problem, and its accuracy of approximately four significant figures will be ample for a survey work of this type. The present writer was fortunate enough to be in a position to enlist, for the purpose of this investigation, the services of the new Rockefeller differential analyzer of the Center of Analysis, M.I.T., and of a trained staff of operators whose collaboration materially facilitated our task. Since, in spite of the pioneer work by Rosseland, an application of the differential analyzer to astronomical problems still remains somewhat of a novelty, in what follows we shall describe in some detail—as an illustration of the general type of procedure—the way in which our present problem had to be formulated to make it susceptible of a solution on the analyzer.

II. SOLUTION OF THE EQUATIONS

In order to prepare equations (17)–(18) for integration on the differential analyzer, let us consider them in the form

$$\frac{dw}{dx} = fz\,, \tag{17.1}$$

$$\frac{d(x^2 z)}{dx} = gw\,, \tag{18.1}$$

where

$$f = f_1 - f_2\,, \qquad g = \frac{j(j+1)}{\alpha}\, g_1 - g_2\,, \qquad f_1 = \frac{1}{g_1} = \theta^{-Q}\,,$$

$$f_2 = \tfrac{1}{2}(n+1)(n-Q)\frac{\theta'^2}{\theta^{Q+1}}\,, \qquad g_2 = \frac{x^2}{\gamma}\,\theta^{Q-1}\,,$$

are functions of the independent variable, which, once we adopt definite values of Q and γ, can be regarded as known. In what follows, they will be evaluated with the aid of

[10] *J. Franklin Inst.*, **240**, 255, 1945.

the *British Association Tables*[11] of numerical solutions of the Emden equation (14) for $n = 3$ before the start of the integrations and will be brought into the machine by means of three separate input tables. The constants a and $j(j+1)/a$, for which a great many trial values may have to be adopted in the course of our investigation, will be absorbed in the gear ratios of the differential analyzer, which can be changed with great facility.

Equations (17.1) and (18.1), integrated symbolically with respect to x, yield

$$w = \int\int z\,dx\,, \tag{17.2}$$

$$z = x^{-2}\int gw\,dx\,. \tag{18.2}$$

The former equation is now in the form suitable for integration on the analyzer; the latter is not, because its right-hand side consists of a product x^{-2} times the integral of gw; and any product to be evaluated on the analyzer must first be transformed so as to relegate both factors behind the integral sign. This can be accomplished by use of the well-known rule for partial integration, which asserts that

$$uv = \int u\,dv + \int v\,du$$

and permits us, therefore, to re-write equation (18.2) in the form

$$z = \int x^{-2}d\left[\int gw\,dx\right] + \int\left[\int gw\,dx\right]d\,x^{-2}\,, \tag{18.3}$$

which the logic of the machine can better understand.

Equations (17.2) and (18.3) now lend themselves readily to a mechanical solution on the differential analyzer, the actual setup of which is diagrammatically shown in Figure 1; the notations used are those of Bush and Caldwell.[10] A total of nine integrators was necessary for this purpose, two of which were used to generate x^{-2} from x by integrating an auxiliary differential equation,[12]

$$\frac{d}{dx}\frac{1}{x} + \frac{1}{x^2} = 0\,.$$

As the reader may notice on the diagram, advantage has been taken, in one instance, of inverse integration to generate g_1 as a reciprocal of f_1, thus eliminating the need of an additional input table.

In the immediate neighborhood of the origin the reciprocal of x would be so large as to necessitate a great many changes of the scale factors—an operation which requires human intervention and correspondingly prolongs the solution time. In order to circumvent it, the solutions of equations (17) and (18) were expanded, near the origin, in ascending powers of x, and these series were used to ascertain the values of the initial conditions at $x = 0.1$, from which the solution was continued by mechanical means.

Suppose that, near the origin, the solution of equations (17) and (18) can be represented by

$$w = a_0x^m + a_2x^{m+2} + \ldots\,, \tag{21}$$

$$z = b_0x^n + b_2x^{n+2} + \ldots\,, \tag{22}$$

terms involving odd powers of x being ruled out on account of spherical symmetry. The indicial equation asserts that

$$m = n + 1 = j \qquad \text{and} \qquad b_0 = \frac{j}{a}\,a_0\,; \tag{23}$$

[11] Vol. 2: *Emden Functions* (London, 1932).

[12] Cf. Bush and Caldwell, *op. cit.*, p. 314, Fig. 43.

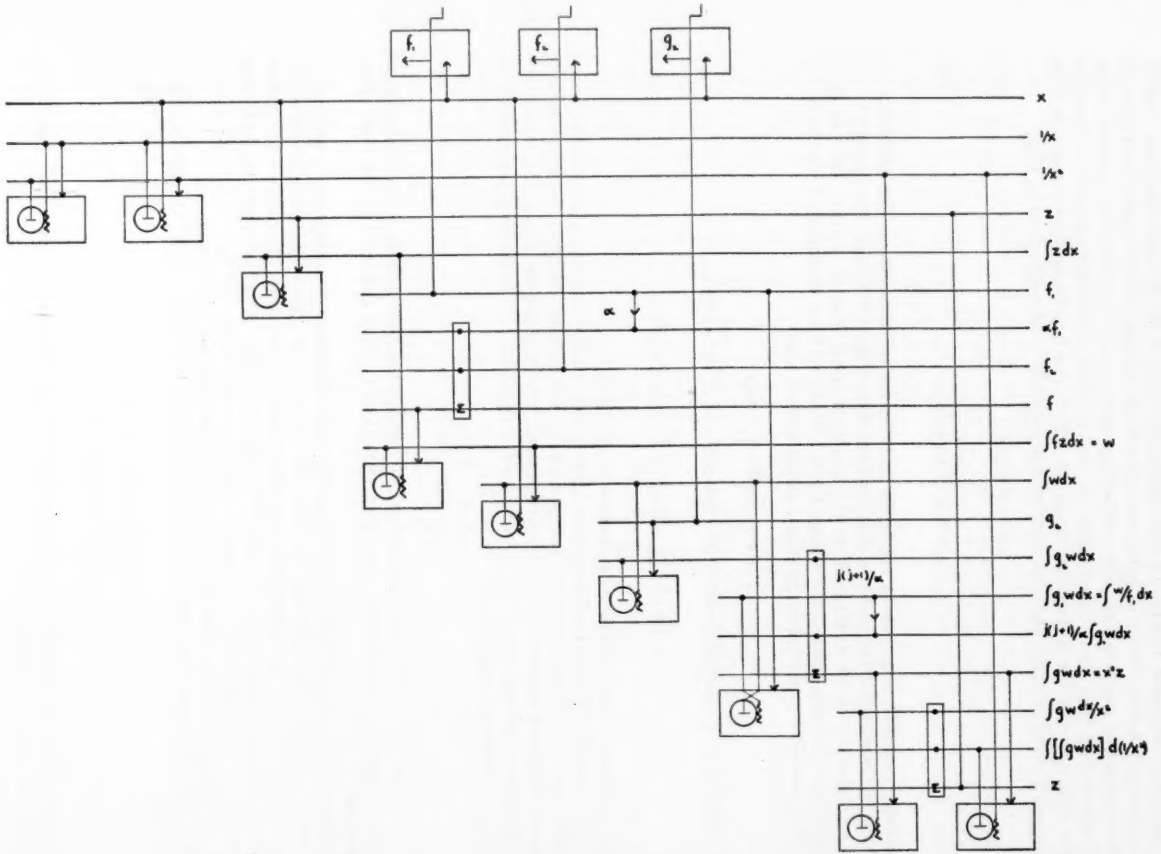

FIG. 1.—A schematic arrangement of the differential analyzer, showing equipment used for the mechanical solution of equations (17)–(18)

these are the only conditions for which a nonvanishing solution of our system of equations in ascending powers of x is possible. Moreover, we find that

$$-\frac{a_2}{a_0}=\frac{j(j+3)(n-Q)(n+1)}{3\sigma\alpha(2j+3)}-\frac{jQ}{\sigma(2j+3)}+\frac{3\alpha}{10(2j+3)},$$

$$-\frac{b_2}{b_0}=\frac{j(j+1)(n-Q)(n+1)}{3\sigma\alpha(2j+3)}+\frac{(j+1)Q}{\sigma(2j+3)}+\frac{3\alpha(i+2)}{10j(2j+3)}.$$

Higher terms of degree up to the sixth have been explicitly evaluated but are too long to be quoted here.

Cowling's numerical integrations[6] for $j = 2$ were carried out under the assumption that $b_0 = 1$. Moreover, it is obvious that b_0 must vanish if $j = 0$. This leads us to normalize our integrations by putting

$$b_0 = \tfrac{1}{2}j\,,$$

which, by equation (19), yields

$$a_0 = \tfrac{1}{2}\alpha\,.$$

Therefore, for the sake of consistency with Cowling's results, we put

$$w=\tfrac{1}{2}\alpha x^j\left\{1+\frac{a_2}{a_0}x^2+\ldots\right\} \tag{21.1}$$

and

$$z=\tfrac{1}{2}jx^{j-1}\left\{1+\frac{b_2}{b_0}x^2+\ldots\right\}. \tag{22.1}$$

Terms in these expansions of orders up to the sixth were used to predict the requisite values of the boundary conditions at $x = 0.1$, and the solution hence forward continued until the boundary was reached.

As a rule the integrations were started, for each j, with trial values of α. If the latter was too large, the values of w near $x_1 = 6.8968\ldots$ tended to $+\infty$ for the fundamental mode or the g_2 oscillation, and to $-\infty$ for the g_1 oscillation, while for small values of α the converse was true. By successive trials a pair of arbitrarily close values of α was established for which w tended to the opposite extremes in the immediate neighborhood of the boundary. Each such pair necessarily bracketed an eigenvalue of our oscillation problem, whose index refers to the number of loops of the corresponding oscillation in the interior. In actual practice, all trial runs—a great number of which was required—were performed on the differential analyzer, which permitted δ an accuracy of the order of one part in 10.[4] As soon as any one eigenvalue was sufficiently closely bracketed, we reverted, however, to the process of numerical integration, keeping one more decimal place, and completed the final runs by hand. It is these final hand-made runs which were used as a basis for the numerical results presented in this paper. If, for example, the values of z and w appropriate for each particular oscillation are known throughout the interior, the variations in radius, pressure, and density can be evaluated from equations (15), (16), and (11), which in our particular case ($n = 3$ and $\gamma = \frac{5}{3}$) take the explicit forms

$$\frac{\delta r}{r_0}=z\theta^{-2.4}, \qquad \frac{\delta P}{P_c}=w\theta^{2.4},$$

$$\frac{\delta\rho}{\rho_c}=\tfrac{3}{5}\{w\theta^{1.4}-z\theta'\theta^{-1.4}\},$$

where θ and θ' can again be taken from the *British Association Tables*.[11]

Tables of $\delta r/r_0$, $\delta P/P_c$, and $\delta\rho/\rho_c$ as a function of x for all oscillations investigated by the writer are collected in Tables 1–3. Table 1 describes the properties of a second-harmonic g_2 oscillation, while Tables 2 and 3 summarize the properties of the f, g_1, and g_2 oscillations for $j = 3$ and $j = 4$. The variation of the respective quantities is diagrammatically shown in Figures 2, 3, and 4, while Table 4 lists the characteristic values of α. The behavior of the quantities $\delta r/r$, $\delta P/P_c$, and $\delta\rho/\rho_c$ for various modes of different harmonic oscillation is further illustrated in Figures 2, 3, and 4, based on the numerical results summarized in Tables 1–3.

III. DISCUSSION OF THE RESULTS

An inspection of the numerical data summarized in the foregoing tables and shown on the preceding graphs leads to the following conclusions and general observations.

The existence and characteristic frequency of fundamental modes—such that δr and $-\delta\rho$ are of the same sign throughout the interior—has been established for the third- and fourth-harmonic oscillation of the standard model, as well as the existence and frequencies of two gravitational overtones of periods longer than the fundamental period. The g oscillations of increasing order are characterized by an increasing number of nodes and loops in the interior. For the fundamental mode of any g oscillation of even order, a displacement (or the corresponding variation in pressure or density) around the center and near the surface is in the same direction; for modes of odd orders the opposite is true.

The displacements $\delta r/r$ accompanying the fundamental modes of the second-, third-, and fourth-harmonic oscillation, normalized in conformity with equations (21.1)–(22.1), are much greater near the surface than in central portions of the oscillating configuration. For the g_1 mode, this is true to a much smaller extent; while for the g_2 and higher modes of gravitational oscillation the displacements remain appreciable only in the central portions. Conversely, if the amplitudes of various modes of nonradial oscillation were all normalized to unity on the surface, the displacement accompanying the fundamental mode would be appreciable only near the surface, while those accompanying higher modes would be far larger in the interior than on the surface—the larger, the higher the mode. Free oscillations in modes of high order can, therefore, be expected to suffer greatly from any kind of damping, the fundamental mode being the one which is likely to be least affected.

The variation in pressure and density, normalized consistently with equations (21.1)–(22.1), is confined largely to the deep interior of the oscillating configuration, and its range diminishes rapidly for any harmonic, with increasing order of the corresponding mode.

Having investigated certain free nonradial oscillations of the standard model corresponding to the second, third, and fourth harmonic, we find it, furthermore, of interest to compare them with a purely radial oscillation (corresponding to $j = 0$), the properties of which were extensively investigated by Schwarzschild.[13] Unlike the nonradial oscillations, those corresponding to $j = 0$ do not include the g oscillations, all "overtones" of the fundamental mode of radial oscillation being of the nature of p oscillations. This fundamental mode alone, therefore, lends itself to a comparison with those of nonradial oscillation. Schwarzschild's tabulated values of the displacement $\delta r/r \equiv \xi_1$ have been normalized so as to render $\xi_1 = 1$ at the boundary of the oscillating configuration. From his Table 4 we find that, for $\gamma = \frac{5}{3}$, $\xi_1 = 0.04457$ at $x = 0$, whereas the expansion (22.1) of our system of equations (17)–(18) near the origin reduces to $z = -\alpha x/10$ and, therefore, $\delta r/r \to -\alpha/10$ as $r \to 0$. A discrepancy in sign of the limiting value of ξ_1 between

[13] *Ap. J.*, **94**, 245, 1941.

TABLE 1

$\alpha_3 = .0723$				$\alpha_3 = .0723$			
x	$\delta r/r_0$	$\delta P/P_0$	$\delta\rho/\rho_0$	x	$\delta r/r_0$	$\delta P/P_0$	$\delta\rho/\rho_0$
0	.0000	.0000000	.00000				
.1	.0987	.0003508	.00217	3.6	-.00733	.0005200	.0011493
.2	.1897	.001282	.00817	3.7	.00398	.0004562	.0011248
.3	.2664	.002480	.01661	3.8	.0151	.0003980	.0010844
.4	.3238	.003538	.02561	3.9	.0261	.0003455	.0010320
.5	.3590	.004102	.03329	4.0	.0370	.0002985	.0009727
.6	.3718	.003969	.03825	4.1	.0478	.0002568	.0009069
.7	.3636	.003132	.03974	4.2	.0584	.0002199	.0008427
.8	.3375	.001754	.03780	4.3	.0689	.0001878	.0007765
.9	.2977	.000104	.03304	4.4	.0794	.0001593	.0007111
1.0	.2486	-.001531	.02642	4.5	.0898	.0001348	.0006480
1.1	.1945	-.002910	.01898	4.6	.1003	.0001135	.0005875
1.2	.1393	-.003883	.01167	4.7	.1107	.00009508	.0005297
1.3	.08611	-.004393	.006171	4.8	.1212	.00007926	.0004753
1.4	.03706	-.004464	-.000117	4.9	.1317	.00006589	.0004244
1.5	-.006290	-.004178	-.004328	5.0	.1423	.00005410	.0003769
1.6	-.04314	-.003633	-.008605	5.1	.1532	.00004424	.0003330
1.7	-.07319	-.002943	-.008008	5.2	.1643	.00003590	.0002924
1.8	-.09862	-.002200	-.008470	5.3	.1757	.00002887	.0002552
1.9	-.1139	-.001477	-.008240	5.4	.1871	.00002297	.0002209
2.0	-.1256	-.0008223	-.007541	5.5	.1989	.00001808	.0001897
2.1	-.1324	-.0002652	-.006566	5.6	.2112	.00001400	.0001614
2.2	-.1351	.0001837	-.005471	5.7	.2241	.00001088	.0001356
2.3	-.1343	.0005261	-.004358	5.8	.2378	.000007981	.0001127
2.4	-.1307	.0007708	-.003306	5.9	.2526	.000005824	.0000921
2.5	-.1249	.0009308	-.002358	6.0	.2691	.000004125	.0000739
2.6	-.1173	.0010212	-.001534	6.1	.288	.000002815	.0000579
2.7	-.1084	.0010568	-.0008430	6.2	.31	.000001828	.000044
2.8	-.09853	.0010511	-.0002799	6.3	.34	.000001110	.000032
2.9	-.08788	.0010156	.0001668	6.4	.37	.000000613	.000022
3.0	-.07686	.0009597	.0006102	6.5	.41	.000000294	.000014
3.1	-.06523	.0008913	.0007831	6.6	.5	.000000113	.000008
3.2	-.05342	.0008182	.0009407	6.7	.5	.000000029	.000003
3.3	-.04195	.0007389	.0010589	6.8	.5	.000000003	.000001
3.4	-.03032	.0006624	.0011234				
3.5	-.01876	.0005890	.0011514				

TABLE 2

	a_1 = .2428			a_2 = .1735			a_3 = .1071		
x	$\delta\tau/\tau_0$	$\delta P/P_0$	$\delta\rho/\rho_0$	$\delta\tau/\tau_0$	$\delta P/P_0$	$\delta\rho/\rho_0$	$\rho\tau/\tau_0$	$\delta P/P_0$	$\delta\rho/\rho_0$
0.0	.00000	.0000000	.0000000	.00000	.0000000	.000000	.0000	.000000	.0000000
.1	.01493	.0001198	.0003687	.01489	.0000855	.000347	.0148	.000052	.0003245
.2	.05886	.0009189	.002851	.05822	.0006470	.002661	.0587	.000392	.002442
.3	.1294	.002993	.009098	.1282	.001992	.008368	.1289	.001119	.007423
.4	.2227	.006225	.01995	.2129	.004155	.01797	.1918	.002168	.01522
.5	.3341	.01075	.03531	.3113	.006884	.03095	.2844	.003247	.02466
.6	.4584	.01602	.05423	.4140	.009730	.04597	.3267	.004002	.03393
.7	.5904	.02141	.07514	.5140	.01218	.06122	.3711	.004154	.04119
.8	.7252	.02628	.09619	.6063	.01380	.07488	.3930	.003591	.04505
.9	.8587	.03010	.1158	.6834	.01432	.08546	.3914	.002395	.04498
1.0	.9875	.03253	.1320	.7452	.01389	.09203	.3678	.000799	.04124
1.1	1.109	.03348	.1445	.7896	.01204	.09432	.3263	-.000904	.03473
.2	1.222	.03296	.1526	.8180	.009033	.09257	.2715	-.002438	.02656
.3	1.327	.03124	.1563	.8258	.006785	.08745	.2087	-.003606	.01798
.4	1.423	.02861	.1561	.8203	.005811	.07978	.1429	-.004313	.009904
1.5	1.510	.02539	.1525	.8019	.000973	.07053	.0782	-.004563	.003005
1.6	1.590	.02190	.1463	.7726	-.001539	.06051	.0178	-.004392	-.002389
.7	1.666	.01838	.1383	.7348	-.003613	.05042	-.0363	-.003931	-.006203
.8	1.736	.01504	.1291	.6905	-.005206	.04080	-.0828	-.003284	-.008564
.9	1.804	.01201	.1193	.6417	-.006328	.03200	-.1207	-.002551	-.009703
2.0	1.871	.009367	.1094	.5898	-.007019	.02421	-.1505	-.001815	-.009890
2.1	1.940	.007140	.09972	.5362	-.007350	.01762	-.1727	-.001134	-.009414
.2	2.012	.005329	.09057	.4819	-.007389	.01192	-.1879	-.0005429	-.008509
.3	2.089	.003905	.08208	.4277	-.007209	.007338	-.1968	-.0000672	-.007366
.4	2.172	.002830	.07432	.3740	-.006872	.003673	-.2003	+.0003211	-.006132
2.5	2.264	.002056	.06737	.3214	-.006432	.0008148	-.1994	.0006889	-.004918
2.6	2.366	.001532	.06118	.2699	-.005934	-.001387	-.1948	.0007887	-.003787
.7	2.480	.001214	.05574	.2197	-.005410	-.002983	-.1872	.0009049	-.002777
.8	2.608	.001057	.05100	.1709	-.004887	-.004138	-.1773	.0009624	-.001906
.9	2.753	.001023	.04689	.1232	-.004380	-.004926	-.1656	.0009751	-.001174
3.0	2.916	.001080	.04336	.0766	-.003902	-.005426	-.1524	.0009549	-.000577
3.1	3.100	.001200	.04033	.0309	-.003459	-.005702	-.1383	.0009119	-.000102
.2	3.307	.001382	.03776	-.0141	-.003055	-.005809	-.1234	.0008542	.000268
.3	3.541	.001548	.03566	-.0586	-.002689	-.005788	-.1081	.0007878	.000644
.4	3.804	.001740	.03371	-.1029	-.002362	-.005677	-.0926	.0007176	.000744
3.5	4.099	.001931	.03213	-.1473	-.002072	-.005504	-.0767	.0006469	.000882
3.6	4.431	.002111	.03080	-.1922	-.001814	-.005283	-.0609	.0005784	.000989
.7	4.803	.002275	.02967	-.2377	-.001588	-.005042	-.0450	.0005135	.001017
.8	5.219	.002417	.02870	-.2843	-.001388	-.004779	-.0290	.0004530	.001035
.9	5.688	.002535	.02786	-.3320	-.001213	-.004511	-.0130	.0003973	.001028
4.0	6.207	.002627	.02713	-.3812	-.001060	-.004243	.0030	.0003487	.001003
4.1	6.790	.002692	.02649	-.4321	-.0009263	-.003979	.019	.0003014	.000967
.2	7.441	.002729	.02590	-.4857	-.0008089	-.003722	.035	.0002609	.000921
.3	8.167	.002739	.02535	-.5418	-.0007056	-.003474	.051	.0002248	.000869
.4	8.976	.002723	.02482	-.6008	-.0006155	-.003236	.067	.0001930	.000813
4.5	9.877	.002682	.02429	-.6635	-.0005360	-.003008	.083	.0001651	.000756
4.6	10.88	.002617	.02375	-.7294	-.0004681	-.002791	.100	.0001408	.0006990
.7	11.99	.002530	.02318	-.7996	-.0004045	-.002583	.117	.0001192	.000642
.8	13.24	.002423	.02258	-.8742	-.0003501	-.002386	.134	.0001006	.000587
.9	14.61	.002299	.02193	-.9541	-.0003030	-.002198	.152	.00008447	.000533
5.0	16.14	.002160	.02122	-1.039	-.0002594	-.002018	.171	.00007050	.000483
5.1	17.84	.002007	.02045	-1.131	-.0002217	-.001847	.190	.00005845	.000434
.2	19.72	.001845	.01960	-1.228	-.0001882	-.001682	.209	.00004813	.000387
.3	21.80	.001675	.01867	-1.333	-.0001586	-.001524	.228	.00003930	.000344
.4	24.11	.001501	.01767	-1.445	-.0001325	-.001374	.249	.00003176	.000303
5.5	26.66	.001324	.01657	-1.568	-.0001095	-.001230	.272	.00002536	.000265
5.6	29.48	.001149	.01538	-1.696	-.00008926	-.001091	.294	.00001998	.000229
.7	32.60	.0009791	.01414	-1.835	-.00007166	-.0009677	.318	.00001550	.000196
.8	36.04	.0008158	.01281	-1.994	-.00005648	-.0008207	.340	.00001179	.000165
.9	39.84	.0006622	.01142	-2.143	-.00004346	-.0007095	.366	.000008764	.000137
6.0	44.02	.0005210	.009978	-2.314	-.00003252	-.0005949	.391	.000006335	.000112
6.1	48.63	.0003945	.008504	-2.495	-.00002348	-.0004871	.419	.000004419	.0000893
.2	53.85	.0002848	.007027	-2.688	-.00001619	-.0003868	.449	.000002943	.0000689
.3	59.5	.0001928	.005568	-2.888	-.00001061	-.0002950	.480	.000001844	.0000511
.4	65.5	.0001200	.00417	-3.08	-.00000672	-.0002126	.519	.000001052	.0000360
6.5	72.0	.0000659	.00287	-3.24	-.00000319	-.0001441	.576	.000000539	.0000233
6.6	79.1	.0000294	.00172	-3.39	-.00000145	-.000083	.643	.000000223	.0000132
.7	86.8	.0000089	.00079	-3.7	-.00000044	-.000038	.72	.000000062	.0000058
6.8	95.1	.0000010	.00019	-6.1	-.00000005	-.000010	.72	.000000006	.0000013

TABLE 3

	α_1 = .2527			α_2 = .2026			α_3 = .1347		
x	$\delta r/r_0$	$\delta P/P_0$	$\delta\rho/\rho_0$	$\delta r/r_0$	$\delta P/P_0$	$\delta\rho/\rho_0$	$\delta r/r_0$	$\delta P/P_0$	$\delta\rho/\rho_0$
0.0	.00000	.000000	.000000	.00000	.000000	.000000	.0000	.0000000	.000000
.1	.00199	.000012	.000047	.00199	.000010	.000045	.0019	.0000065	.000042
.2	.01554	.000188	.000720	.01539	.000149	.000690	.0150	.0000964	.000643
.3	.05063	.000880	.003406	.04956	.000686	.003228	.0470	.0004239	.002923
.4	.1144	.002495	.009810	.1102	.001891	.009140	.1002	.0011097	.007928
.5	.2104	.005254	.021129	.1984	.003876	.01940	.1706	.0020867	.01591
.6	.3382	.009161	.03832	.3109	.006500	.03401	.2502	.0031100	.02601
.7	.4944	.013868	.06029	.4411	.009384	.06184	.3271	.0038869	.03644
.8	.6730	.01884	.08557	.5802	.01202	.07097	.3905	.0040080	.04510
.9	.8666	.02341	.1119	.7186	.01392	.08908	.4319	.0035693	.05029
1.0	1.068	.02703	.1371	.8476	.01474	.1041	.4464	.0024853	.05110
1.1	1.269	.02932	.1588	.9600	.01438	.1145	.4331	.000906	.04762
.2	1.464	.03012	.1757	1.0511	.01291	.1196	.3948	-.000783	.04072
.3	1.650	.02946	.1870	1.1181	.01068	.1195	.3365	-.002320	.03170
.4	1.823	.02765	.1927	1.1603	.007756	.1147	.2644	-.003499	.02192
1.5	1.981	.02495	.1930	1.1788	.004706	.1064	.1849	-.004217	.01256
1.6	2.128	.02173	.1890	1.1757	.001776	.09665	.1040	-.004466	.00445
.7	2.258	.01830	.1815	1.1540	-.000836	.08358	.0263	-.004313	-.00197
.8	2.379	.01494	.1716	1.1169	-.003004	.07110	-.0448	-.003860	-.00659
.9	2.492	.01184	.1601	1.0676	-.004875	.05900	-.1047	-.003223	-.00953
2.0	2.600	.009124	.1480	1.0090	-.006855	.04775	-.1587	-.002504	-.01104
2.1	2.706	.006848	.1357	.9439	-.006593	.03768	-.2003	-.001788	-.01143
.2	2.814	.005024	.1239	.8745	-.006564	.02891	-.2319	-.001124	-.01101
.3	2.926	.003633	.1128	.8027	-.007014	.02147	-.2544	-.0006530	-.01009
.4	3.047	.002533	.1026	.7299	-.006849	.01530	-.2686	-.0000871	-.008865
2.5	3.180	.001970	.0934	.6570	-.006526	.01028	-.2756	.0002730	-.007620
2.6	3.327	.001589	.0853	.5851	-.006100	.006277	-.2766	.0005352	-.006176
.7	3.493	.001431	.0781	.5144	-.005616	.003137	-.2727	.0007123	-.004915
.8	3.680	.001446	.0719	.4453	-.005109	.000722	-.2647	.0008195	-.003777
.9	3.894	.001691	.0665	.3779	-.004606	-.001095	-.2535	.0008714	-.002786
3.0	4.139	.001824	.0620	.3120	-.004120	-.002435	-.2400	.0008816	-.001948
3.1	4.419	.002120	.0582	.2475	-.003664	-.003391	-.2245	.0008616	-.001253
.2	4.739	.002446	.0550	.1842	-.003244	-.004047	-.2077	.0008209	-.000692
.3	5.100	.002781	.0523	.1217	-.002863	-.004471	-.1897	.0007670	-.000248
.4	5.514	.003113	.0501	.0598	-.002521	-.004718	-.1711	.0007059	.000099
3.5	5.986	.003431	.04825	-.0022	-.002216	-.004828	-.1521	.0006418	.000367
3.6	6.520	.003726	.04674	-.0647	-.001947	-.004843	-.1328	.0005777	.000548
.7	7.127	.003986	.04550	-.128	-.001710	-.004785	-.1133	.0005158	.000679
.8	7.816	.004212	.04449	- 193	-.001502	-.004678	-.0937	.0004574	.000767
.9	8.595	.004398	.04365	-.259	-.001320	-.004531	-.0741	.0004032	.000818
4.0	9.475	.004543	.04295	-.328	-.001160	-.004361	-.0542	.0003536	.000843
4.1	10.47	.004645	.04234	-.401	-.001021	-.004183	-.0343	.0003088	.000845
.2	11.59	.004706	.04180	-.477	-.0008991	-.003993	-.0143	.0002688	.000832
.3	12.86	.004725	.04132	-.557	-.0007922	-.003799	.0059	.0002324	.000807
.4	14.28	.004703	.04083	-.644	-.0006982	-.003609	.0254	.0002008	.000774
4.5	15.88	.004640	.04032	-.736	-.0006153	-.003416	.0473	.0001728	.000736
4.6	17.68	.004540	.03977	-.834	-.0005419	-.003228	.0688	.0001481	.000692
.7	19.71	.004403	.03917	-.941	-.0004768	-.003044	.0904	.0001264	.000647
.8	21.99	.004234	.03849	-1.056	-.0004187	-.002862	.1128	.0001075	.000601
.9	24.54	.004034	.03770	-1.182	-.0003668	-.002686	.1367	.0000909	.000565
5.0	27.40	.003807	.03679	-1.317	-.0003202	-.002511	.1594	.00007662	.000509
5.1	30.62	.003557	.03575	-1.464	-.0002782	-.002339	.184	.00006414	.000464
.2	34.23	.003287	.03458	-1.628	-.0002404	-.002172	.210	.00005333	.000421
.3	38.26	.003001	.03319	-1.801	-.0002062	-.002005	.237	.00004400	.000378
.4	42.78	.002706	.03166	-1.995	-.0001753	-.001840	.265	.00003596	.000338
5.5	47.84	.002403	.02996	-2.21	-.0001475	-.001679	.294	.00002908	.000299
5.6	53.51	.002100	.02807	-2.44	-.0001225	-.001517	.326	.00002321	.000263
.7	59.87	.001800	.02599	-2.69	-.0001002	-.001357	.357	.00001824	.000228
.8	67.00	.001509	.02374	-2.97	-.00008039	-.001199	.392	.00001406	.000195
.9	75.02	.001234	.02135	-3.28	-.00006304	-.001044	.428	.00001062	.000165
6.0	84.04	.000978	.01882	-3.62	-.00004803	-.000892	.466	.00000778	.000136
6.1	94.26	.000746	.01619	-3.99	-.00003530	-.000744	.505	.00000551	.000110
.2	105.0	.000542	.01347	-4.42	-.00002477	-.000602	.547	.00000373	.000087
.3	118.8	.000370	.01079	-4.9	-.00001634	-.00047	.58	.00000238	.000065
.4	133	.000232	.00816	-5.6	-.00000989	-.00036	.63	.00000139	.000048
6.5	149	.000127	.00563	-6.3	-.00000527	-.00025	.7	.00000724	.000031
6.6	166	.0000586	.00339	-7.2	-.00000230	-.00014	.8	.000000308	.000018
.7	185	.0000170	.00156	-8.	-.00000068	-.00007	.9	.000000090	.000008
6.8	206	.0000019	.00037	-10.	-.00000008	-.00002	1.0	.000000010	0

Schwarzschild and us is readily explained if we remember that Schwarzschild has integrated Eddington's complete equation of small radial oscillations of the form

$$\frac{d^2\xi_1}{dr^2}+\left\{\frac{4}{r}-\frac{\gamma g}{c^2}\right\}\frac{d\xi_1}{dr}+\left\{\sigma^2+(4-3\gamma)\frac{g}{r}\right\}\xi_1=0\,, \tag{24}$$

whereas our equations (12) and (13) are approximations obtained by neglecting the variation δV in the gravitational potential arising from the oscillation. If, in equation

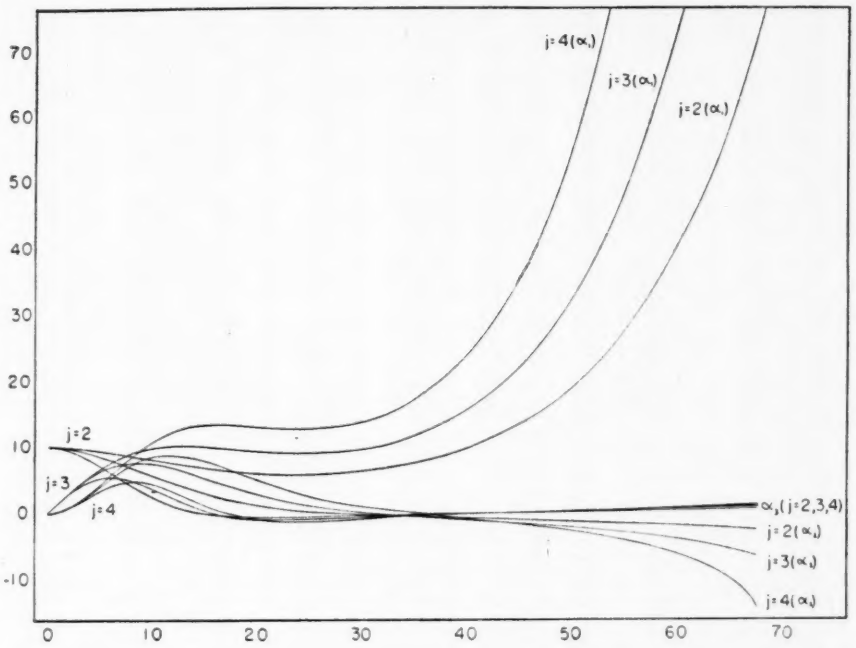

FIG. 2.—The variation of the displacement $\delta r/r$ in the interior of a polytrope $n = 3$, produced by the first three modes of free nonradial oscillation corresponding to the second, third, and fourth harmonic. Abscissae = x; ordinates = $\delta r/r$.

(12), we set $j = 0$, eliminate between equations (12) and (13), and remember that our $\zeta = r^2\delta r = r^3\xi_1$, the eliminant takes the form

$$\frac{d^2\xi_1}{dr^2}+\left\{\frac{4}{r}-\frac{\gamma g}{c^2}\right\}\frac{d\xi_1}{dr}+\left\{\sigma^2+(4-3\gamma)\frac{g}{r}\right\}\xi_1=4\pi G\rho\xi_1\,, \tag{25}$$

which differs from Eddington's equation (24) only in the term on its right-hand side.

It was pointed out at the outset that the neglect of δV in the equations of motion permitted us to restrict the order of the equation governing nonradial oscillations to two. In the limiting case of $j = 0$, where the corresponding wave equation is inherently of

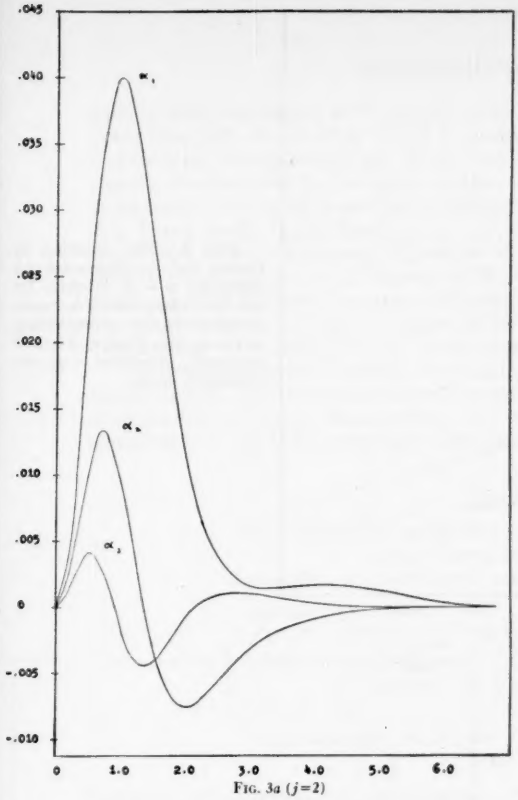

FIG. 3a ($j=2$)

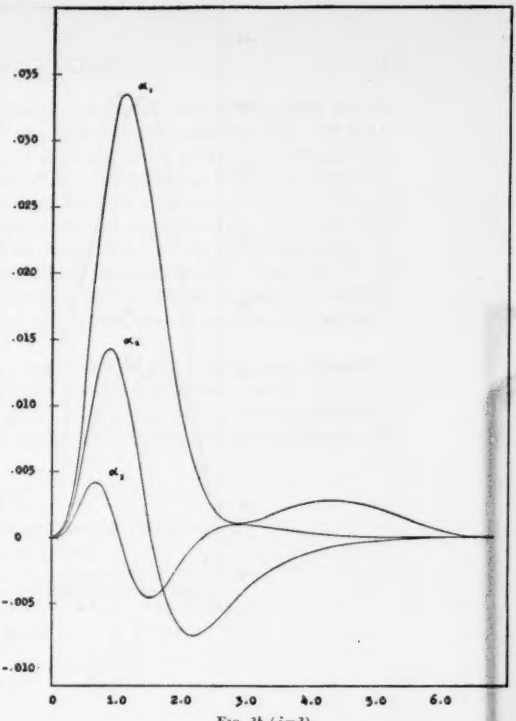

FIG. 3b ($j=3$)

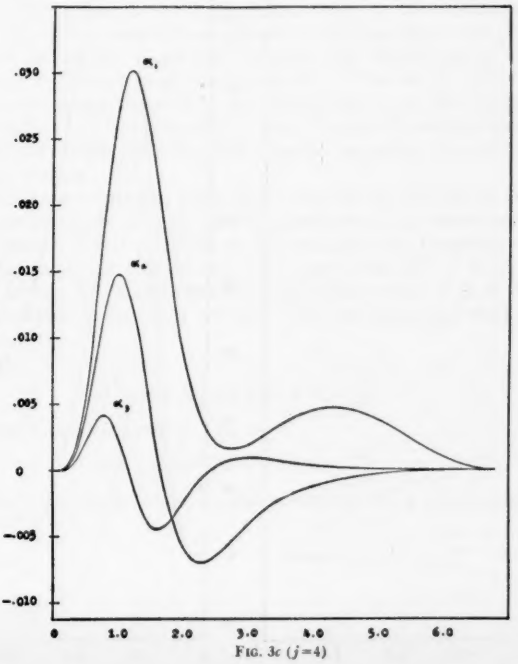

FIG. 3c ($j=4$)

FIG. 3.—The variation in pressure $\delta P/P_c$ in the interior of a polytrope $n = 3$, invoked by the first three modes of free nonradial oscillation corresponding to the second, third, and fourth harmonic. Abscissae = x; ordinates = $\delta P/P_c$.

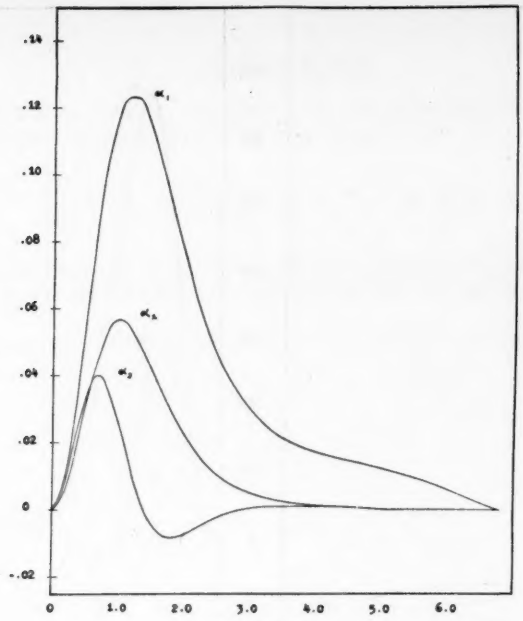

FIG. 4.—The variation in density $\delta\rho/\rho_c$ in the interior of a polytrope $n = 3$, invoked by the first three modes of free non-radial oscillation corresponding to the second, third, and fourth harmonic. Abscissae = x; ordinates = $\delta\rho/\rho_c$.

FIG. 4*a* ($j=2$)

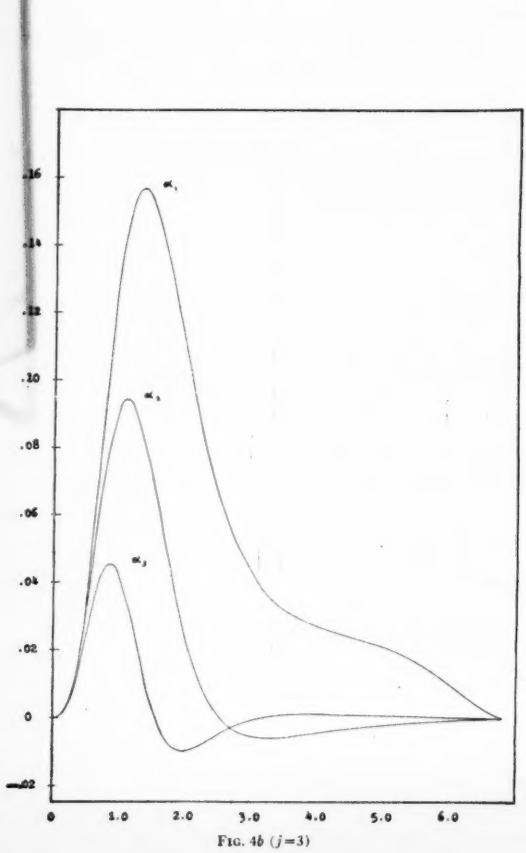

FIG. 4*b* ($j=3$)

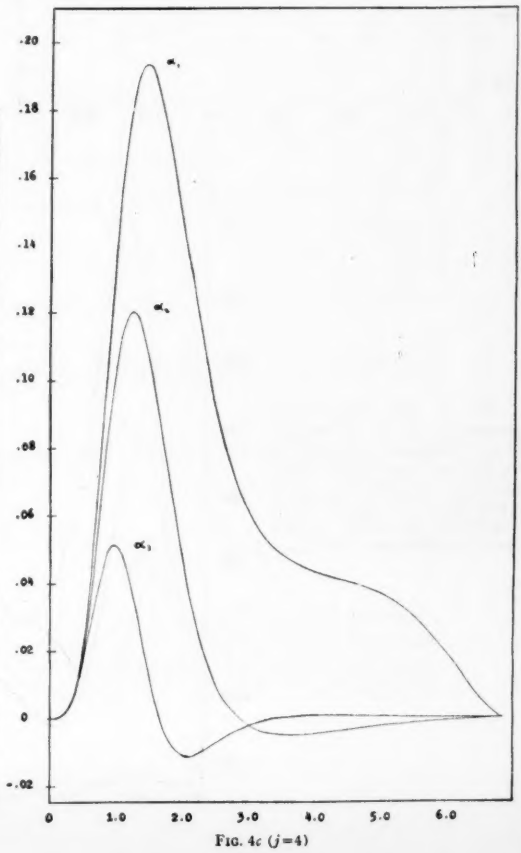

FIG. 4*c* ($j=4$)

second order, the neglect of δV turned out to result in an equation actually more complicated than (24). As can be surmised on general grounds, the error arising from the spurious term on the right-hand side of equation (24) is likely to be greater, the smaller the density concentration in the interior of the oscillating configuration, and is always likely to be appreciable in the immediate neighborhood of the star's center, where the value of ρ/ρ_c is not small. In the limiting case of a homogeneous configuration, equation (25) would lead to quite erroneous frequencies of free oscillation.[14] If on the other hand, the density concentration in the interior of the oscillating configuration is high—as in the polytrope $n = 3$, where the ratio of its mean density to the central density is 0.018456 . . . —the error caused by the neglect of δV in our equations of motion was actually evaluated by Cowling[6] and found to be minor.

The foregoing remarks make it clear that a comparison of the fundamental modes of radial oscillation of the standard model as governed by the complete equation (24), and of nonradial oscillation characterized by $j = 2, 3, 4$ as governed by the approximate equations (12) and (13), would have little meaning near the center of the oscillating con-

TABLE 4

CHARACTERISTIC VALUES OF α FOR NONRADIAL OSCILLATION OF A POLYTROPE $n=3$, $\gamma=\frac{5}{3}$

Oscillation	$j=2$	$j=3$	$j=4$	Frequency
f	0.2325*	0.2428	0.2527	α_1
g_1	0.1308*	0.1735	0.2026	α_2
g_2	0.0723	0.1071	0.1347	α_3

* After Cowling, *M.N.*, **101**, 367, 1942.

figuration but is possible at the boundary, where the effects of our neglect of δV are known to be minor. The values of the displacements $\delta r/r$ of the fundamental modes for $j = 0, 2, 3$, and 4, normalized to a unit amplitude at the boundary, are given in Table 5. An inspection of the tabulated values discloses that the displacements invoked by the fundamental mode of oscillation in all four cases are, on the whole, very similar and diminish slowly with increasing value of j. Any damping which they may encounter is, therefore, likely to affect the fundamental modes of nonradial oscillations in much the same way as that of the radial pulsation. The same is, moreover, true of the variation of δP and $\delta\rho$ along any radius.

An outstanding difference between radial and nonradial oscillations is, however, found in the behavior of the pressure, density, and temperature at the center of the oscillating configuration. For purely radial oscillations, for example, the boundary conditions requiring that there be a node ($\delta r = 0$) at the center and a loop ($\delta P = 0$) on the boundary do not imply that δP (or $\delta\rho$) would have any particular value at $x = 0$. The indicial equation (23) alone makes it, however, evident that, for nonradial oscillations, the re-

[14] I.e., it would yield

$$\sigma^2 = \tfrac{4}{3}\pi G\gamma\rho_c\left\{i(2i+5) + 3 - \frac{7}{\gamma}\right\},$$

whereas the true value of σ, consistent with eq. (24), is

$$\sigma^2 = \tfrac{4}{3}\pi G\gamma\rho_c\left\{i(2i+5) + 3 - \frac{4}{\gamma}\right\}.$$

For the fundamental mode ($i = 0$), eq. (25) would lead to instability for $\gamma < \frac{7}{4}$, whereas, in reality, the configuration is stable for $\gamma < \frac{4}{3}$.

quirement $\delta r = 0$ necessarily implies that $\delta P = \delta \rho = 0$ at the center of the oscillating configuration, i.e., that the origin is singular in so far as it is a node *and* a loop at the same time. This means that, whereas purely radial oscillations of stellar configurations are likely to be accompanied by periodic changes in central pressure, density, and temperature, nonradial oscillations apparently cannot invoke such changes—a fact which may lead us to expect a good deal of difference in the observable surface phenomena attending such motions.

TABLE 5

DISPLACEMENT $\delta r/r$ OF THE FUNDAMENTAL MODES

x	$j=0$*	$j=2$	$j=3$	$j=4$
0	0.0446	.....	.....	.....
1.0	0.0475	0.104	0.066	0.032
1.5	0.0520	0.088	0.067	0.040
2.0	0.0589	0.078	0.063	0.039
2.5	0.0695	0.075	0.061	0.038
3.0	0.0852	0.081	0.065	0.041
3.5	0.109	0.096	0.078	0.052
4.0	0.143	0.124	0.103	0.071
4.5	0.193	0.170	0.147	0.106
5.0	0.266	0.240	0.215	0.165
5.5	0.373	0.349	0.275	0.262
6.0	0.528	0.509	0.489	0.424
6.2	0.608	0.593	0.577	0.517
6.4	0.701	0.689	0.678	0.629
6.5	0.753	0.742	0.734	0.693
6.6	0.808	0.800	0.794	0.761
6.7	0.868	0.862	0.858	0.835
6.8	0.933	0.929	0.927	0.915
6.897	1.000	1.000	1.000	1.000

* After Schwarzschild, *Ap. J.*, **94**, 245, 1941.

TABLE 6

DEFINITIVE VALUES OF α (CORRECTED FOR THE NEGLECT OF δV)

Oscillation	$j=0$	$j=2$	$j=3$	$j=4$	Frequency
f	0.228*	0.214†	0.226	0.237	α_1
g_1	.....	.117†	.160	.190	α_2
g_2	.....	0.062	0.097	0.125	α_3

* After Schwarzschild, *Ap. J.*, **94**, 245, 1941.
† After Cowling, *M.N.*, **101**, 367, 1942.

In concluding the present study, one additional possible refinement should be pointed out. It has been frequently mentioned before that one approximation inherent in the equations of motion treated in this paper was our neglect of the disturbance δV of the gravitational potential caused by the oscillations. Reasons were listed to show why, for configurations exhibiting a pronounced degree of central condensation, this should be a relatively harmless assumption. Moreover, the extent of the error introduced into our determination of the characteristic frequencies α by the neglect of δV was also investigated by Cowling by the usual perturbation methods, and expressions were established,

for the corrections to the approximate values of the characteristic frequencies listed in Table 4, which should pretty nearly rectify the effects of our neglect of δV. The evaluation of these corrections requires additional quadratures. We have evaluated such corrections to the frequencies of all modes investigated in the present paper, using Cowling's method, and have applied them to the corresponding α's of Table 4. The outcome was Table 6, which contains the final values of all characteristic frequencies corrected for the neglect of δV. As many decimals are retained in this table as are considered to be significant. A glance at these values discloses that, to the extent of our present knowledge, no serious cases of coupling between the fundamental and higher modes are likely to arise except, possibly, for the second-harmonic oscillations for which the squares of periods of the f, g_1, and g_2 oscillations are roughly in the ratio 2:1.

In conclusion, the writer considers it a pleasure to record his indebtedness to the National Science Fund of the National Academy of Sciences and to its chairman, Dr. Harlow Shapley, for a generous grant of one thousand dollars which helped to defray the costs of the numerical work involved in the present investigation. The runs on the Rockefeller differential analyzer of the Center of Analysis, Massachusetts Institute of Technology, were carried out under the supervision of Mr. Bernard T. Svihel, research associate of the Institute. Last but not least, the writer is deeply indebted to Miss Katherine E. Kavanagh, staff member of the Center of Analysis, who carried out all final numerical integration by hand and rendered invaluable assistance in all phases of the whole work.

AN ATLAS OF IDENTIFICATION CHARTS OF WHITE DWARFS

WILLEM J. LUYTEN
University of Minnesota
Received February 23, 1949

ABSTRACT

Identification charts are given for 96 white dwarfs, together with magnitudes and color indices.

In view of the considerable interest attached to white dwarfs and degenerate stars and the difficulty generally experienced in identifying these faint objects in the sky, it might not be without value to publish an atlas of identification charts for them. The set of charts shown herewith gives such identification for 96 white dwarfs. A catalogue of these stars, giving the 1950 positions, the photographic magnitudes, and the color indices, all estimated by the writer, is presented in Table 1. This includes all white dwarfs now known with the exception of Sirius B, Procyon B, o_2 Eridani B, and *o* Ceti B, for which no identification is necessary, BPM 11534 = L 158-61 (*Harvard Announcement Card* 926) and Nos. 2, 3, 4, 7, and 28 from the list given by Zwicky and Humason,[1] for which no suitable chart plates were available. Two binaries, viz., LDS 1 and LDS 500, both of which appear to be composed of a pair of stars intermediate between the main sequence and the white dwarfs, have also been included. In addition, it should be mentioned that several other stars here listed may well turn out, upon later observation, to be likewise "intermediates" and not genuine white dwarfs of the o_2 Eridani type or fainter. However, it appears reasonably certain that all stars included are at least somewhat degenerate.

For those stars which are components of binaries, additional data are given in Table 2, which requires no further explanation.

All plates used for the present reproductions were taken with the 36-inch reflector of the Steward Observatory at Tucson (by P. D. Jose or the writer) or with the 60-inch reflector of the Córdoba Observatory (by M. Dartayet or David MacLeish). All were "blue" plates with the 103*a*-O emulsion, except for No. 37 (L 145–141) for which an excellent long exposure on a 103*a*-E emulsion without filter was available.

All charts are shown with north up, west to the right; in the original they have all been enlarged to the uniform scale of 1 mm = 15″ which, in the reproductions, has been reduced to 1 mm = 18″.8; the area of each field is therefore roughly 19′ × 19′. Since the images on most of the Córdoba plates were so small that difficulties with reproduction might have ensued, all the Córdoba enlargements were made slightly out of focus. In general, the star to be identified lies in the center of the area, though I have deviated from this rule if by so doing a bright star or a characteristic star group could be brought into the field. In the case of binaries with components of different color, the white star has been indicated by the *longer* line, the red star by the shorter line.

[1] *Ap. J.*, **105**, 399, 1947.

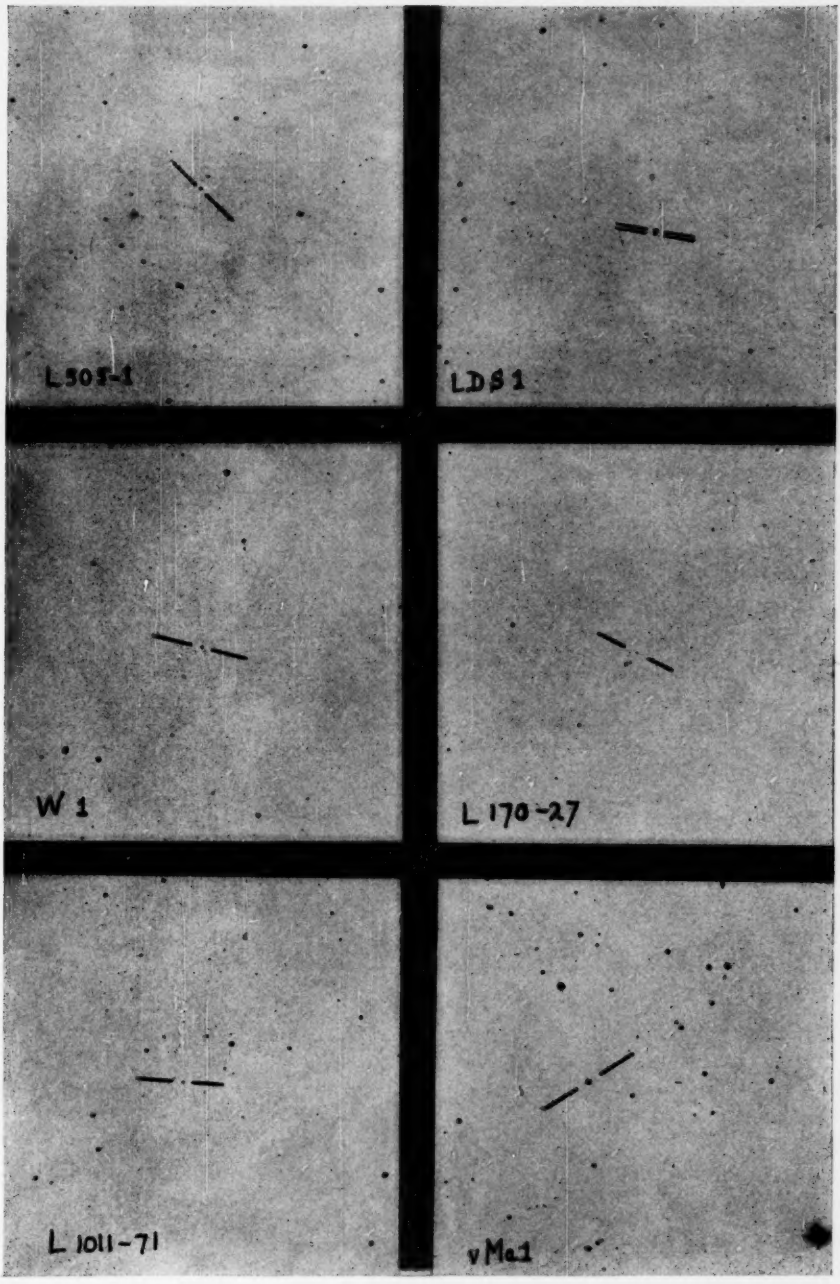

FIG. 1

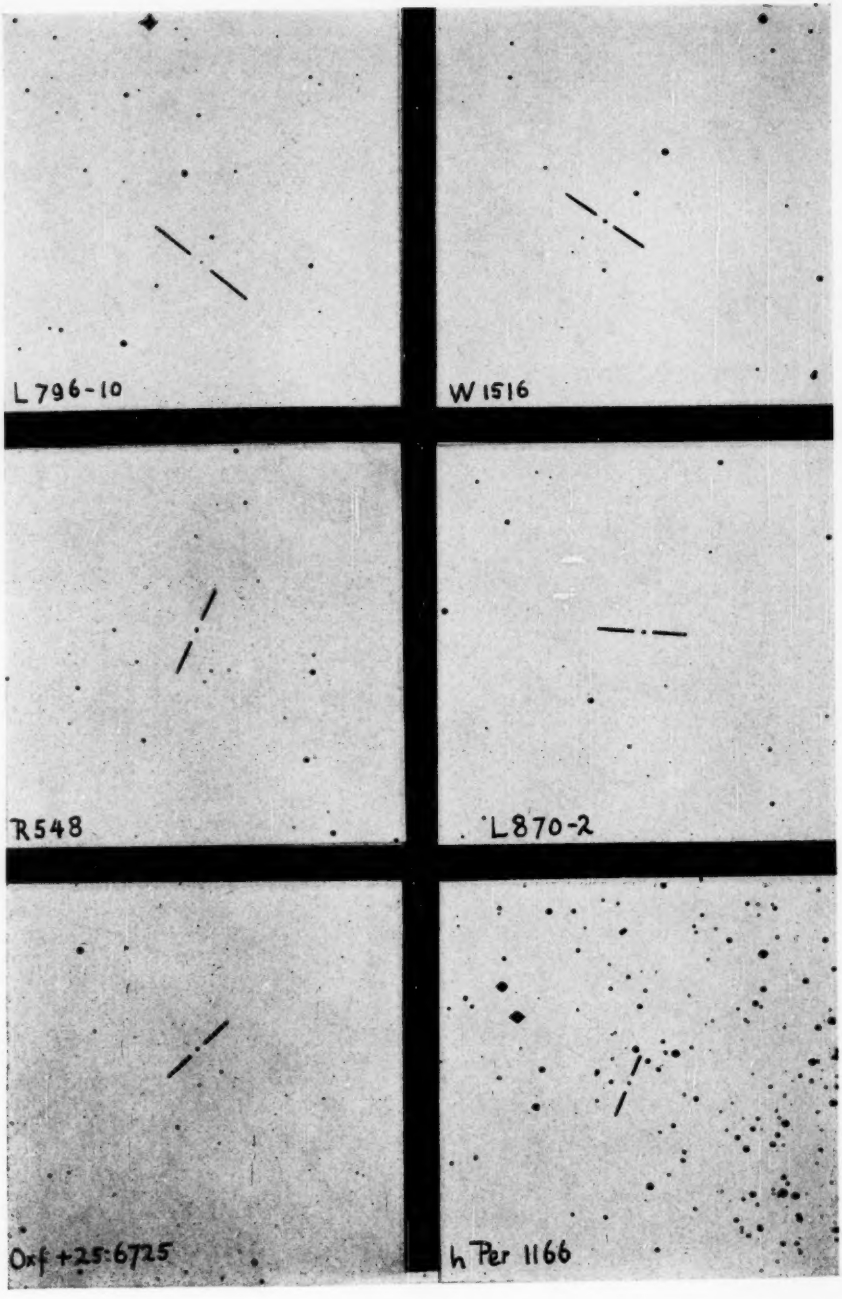

FIG. 2

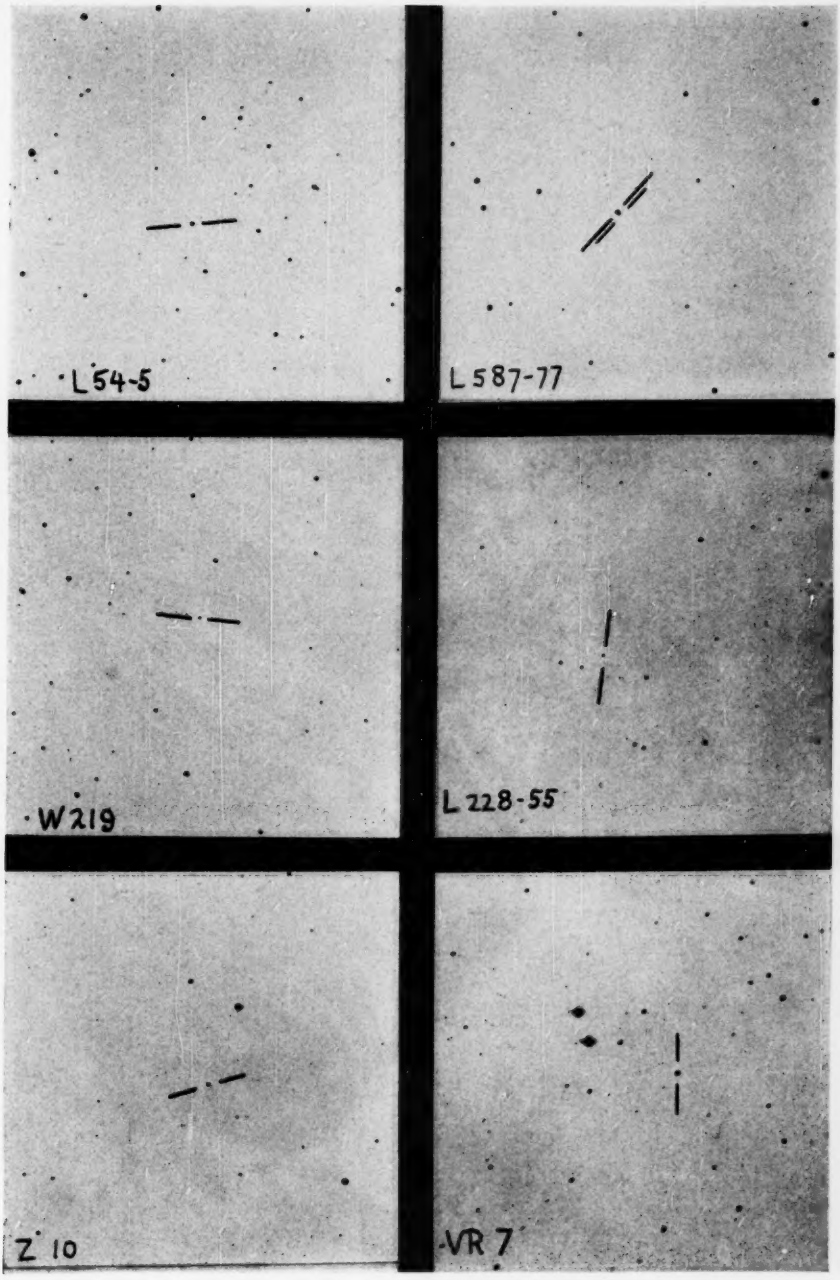

FIG. 3

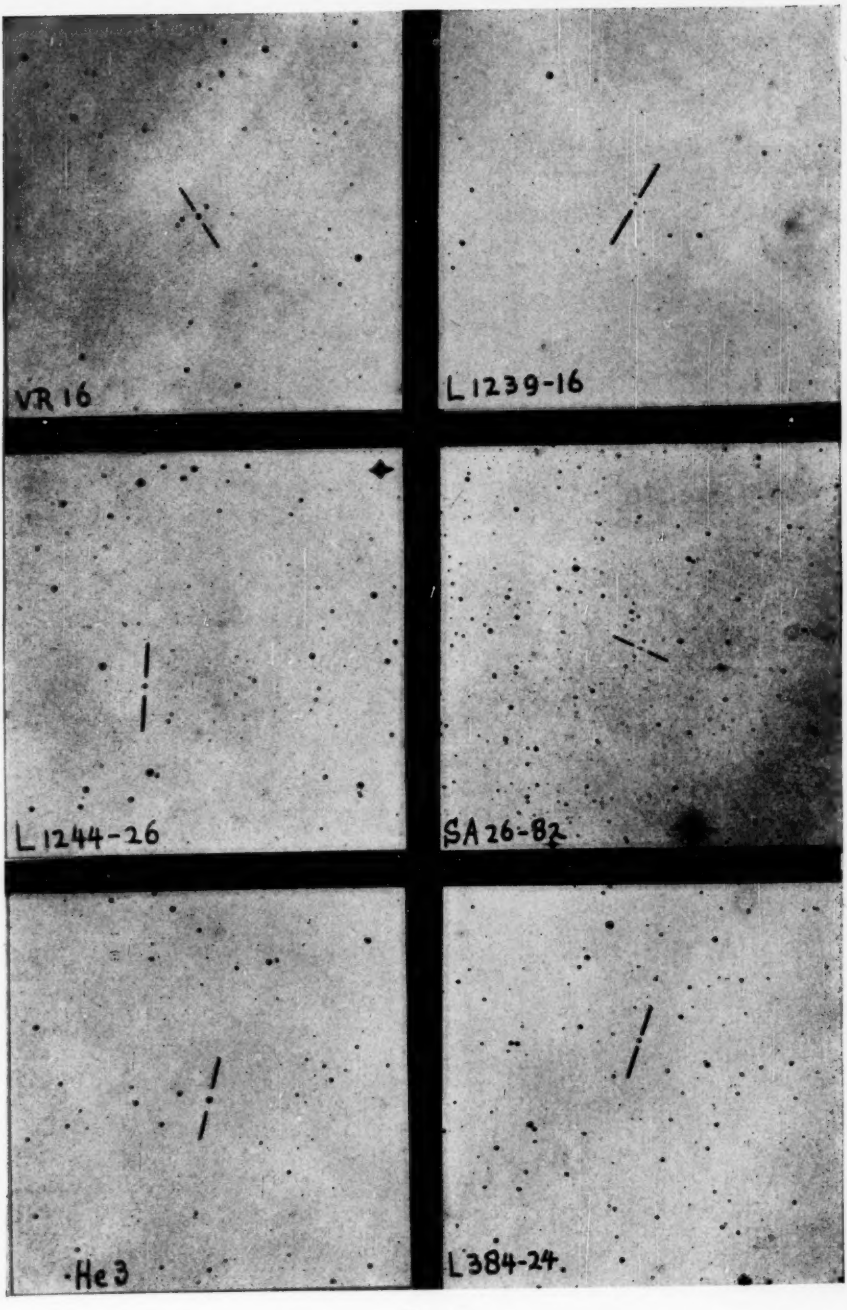

FIG. 4

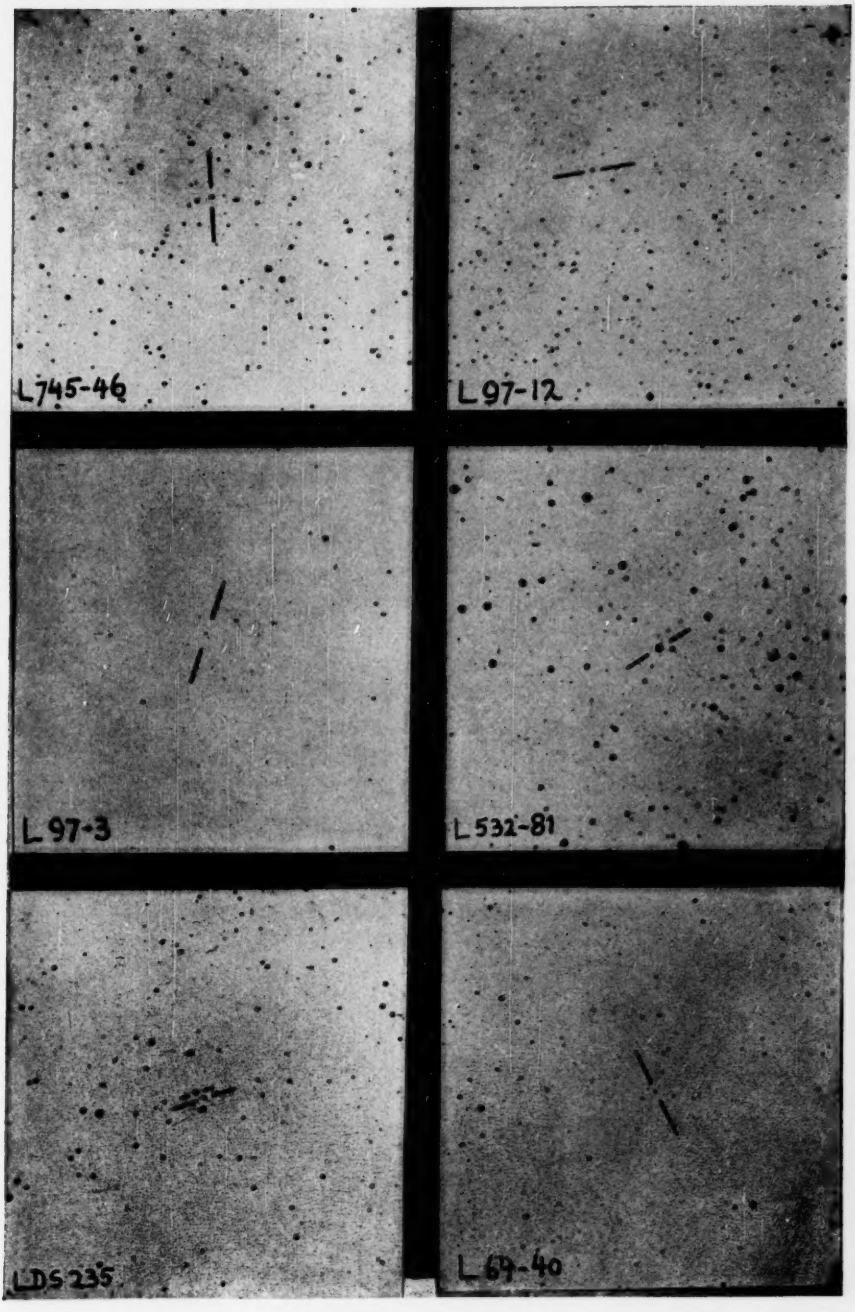

FIG. 5

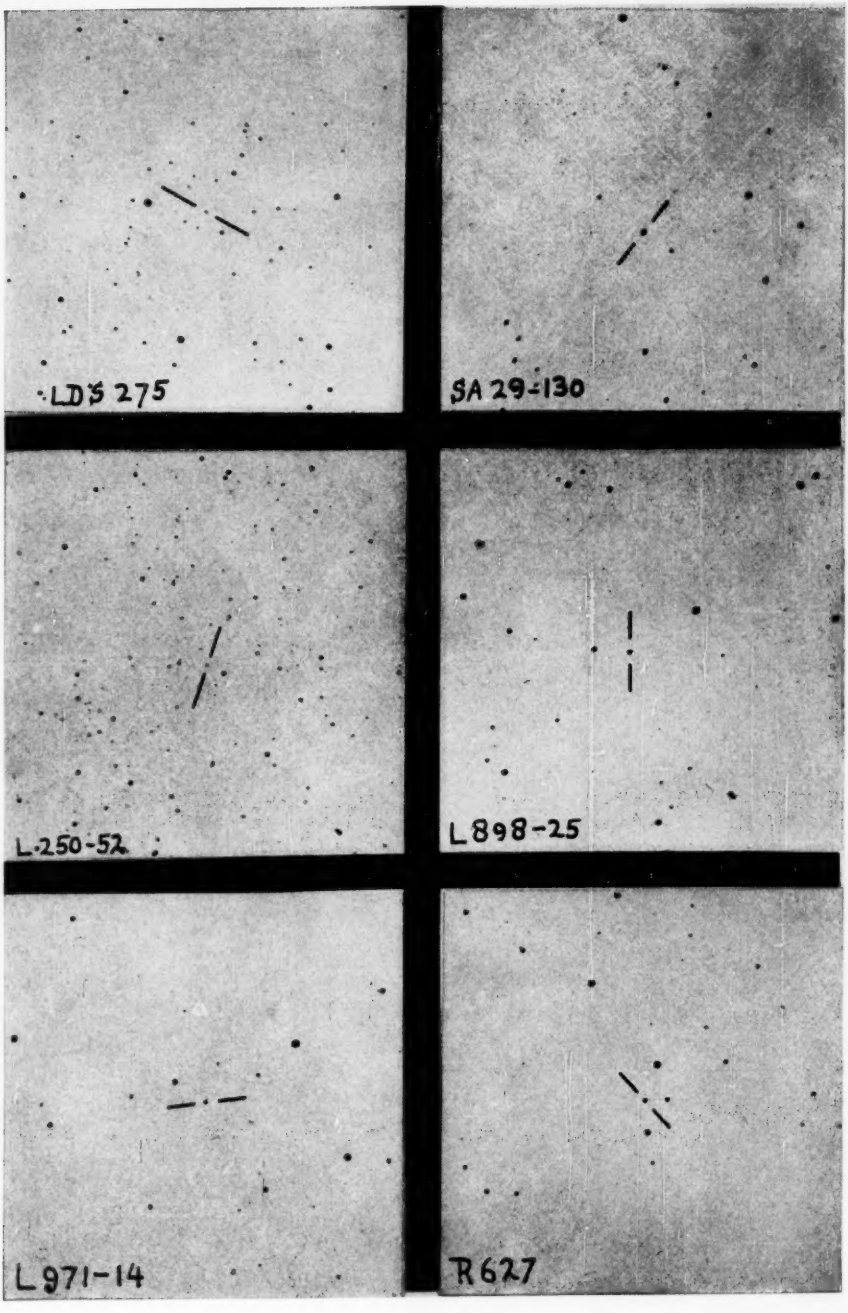

FIG. 6

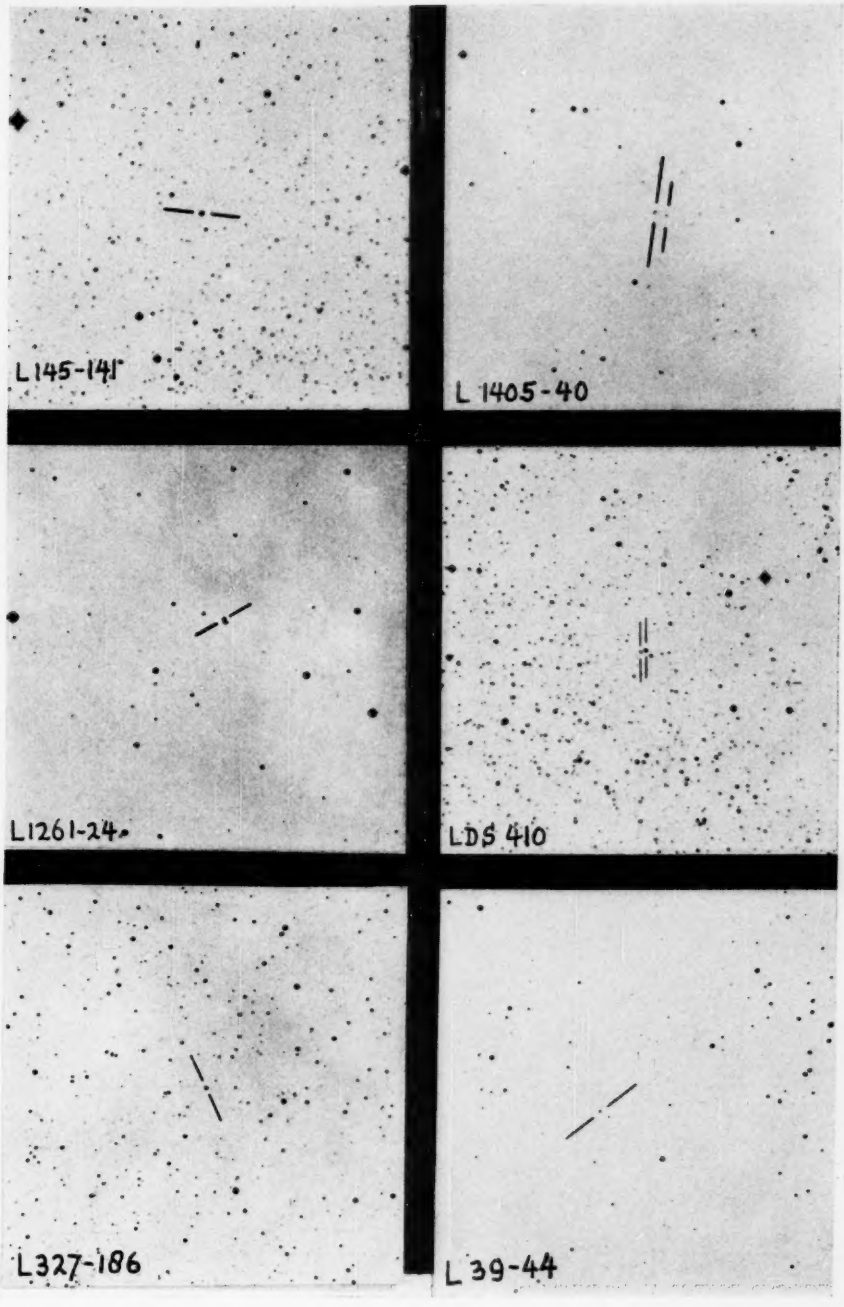

FIG. 7

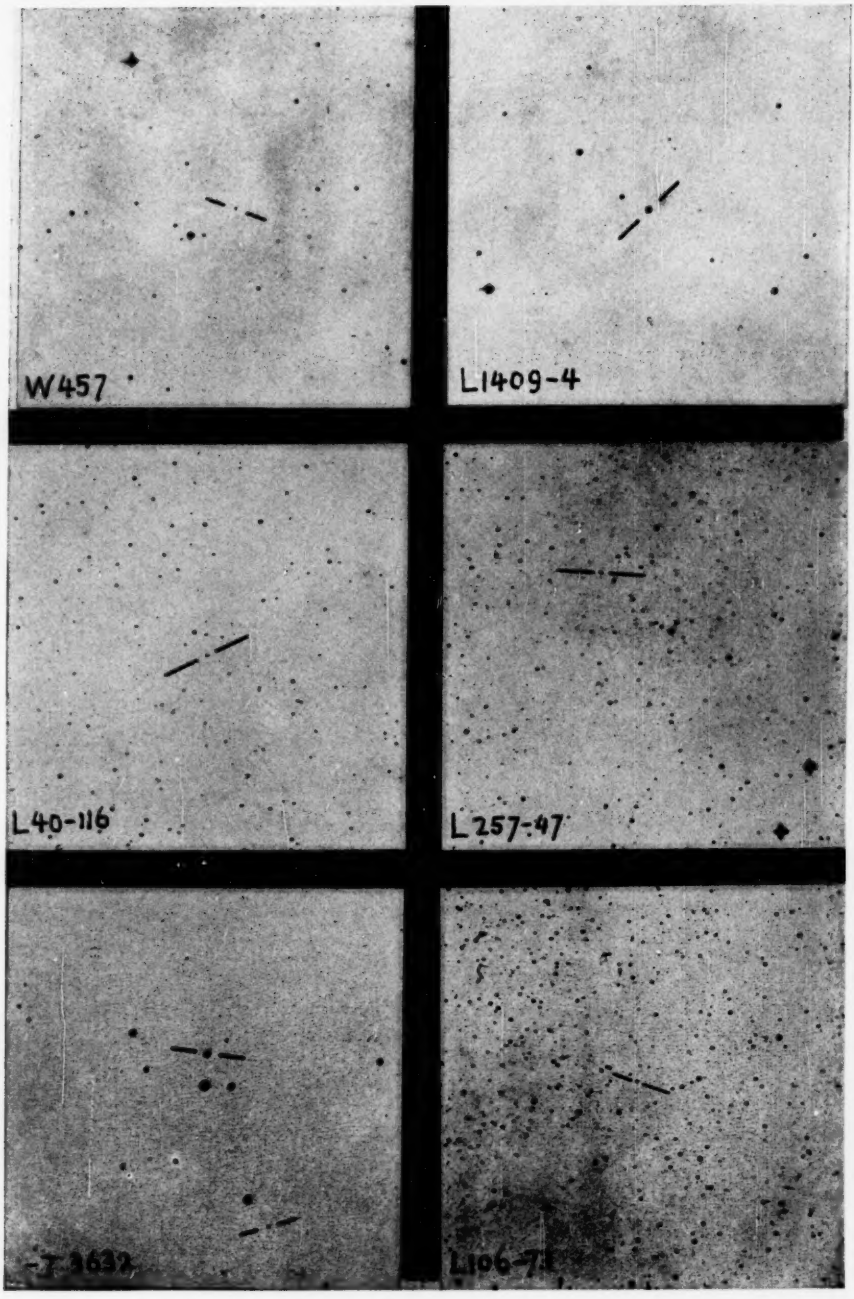

FIG. 8

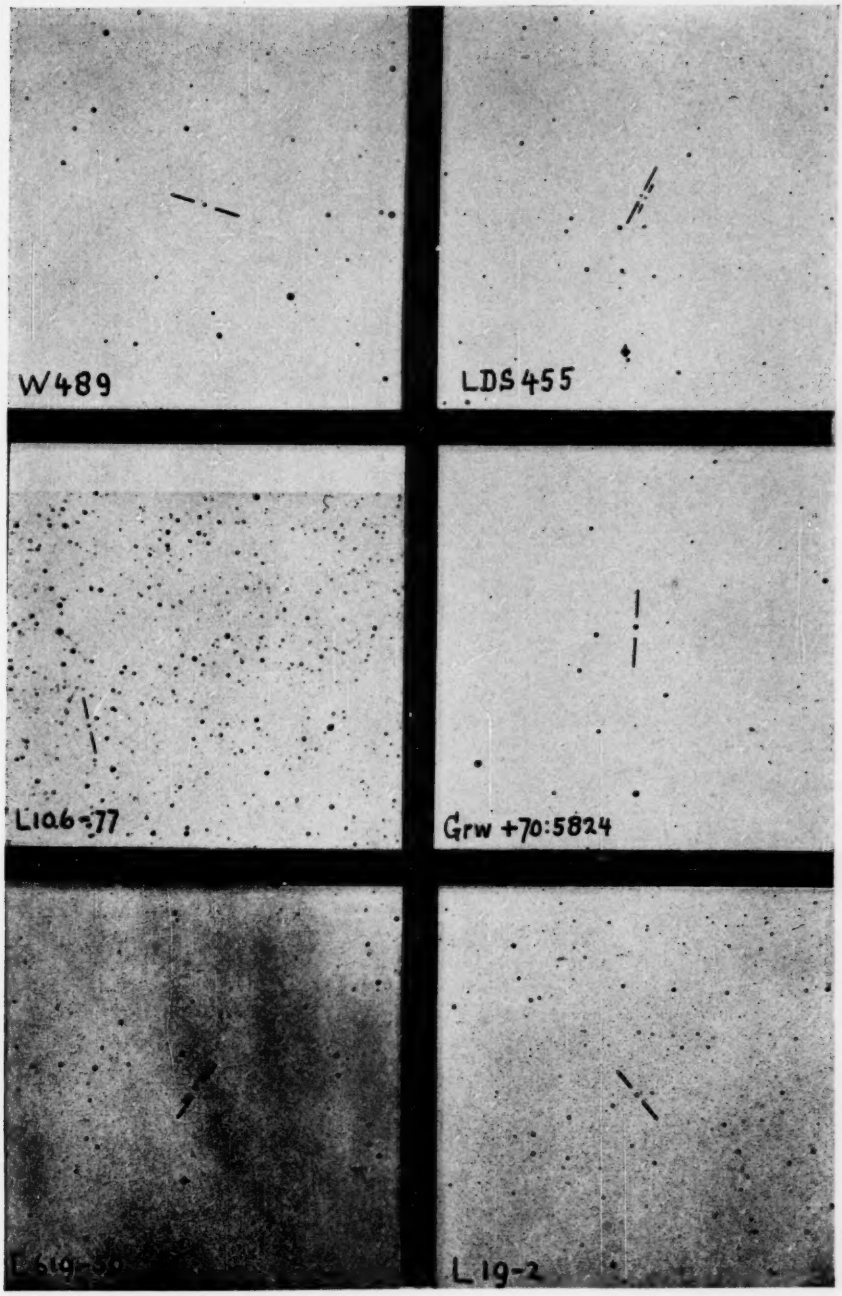

FIG. 9

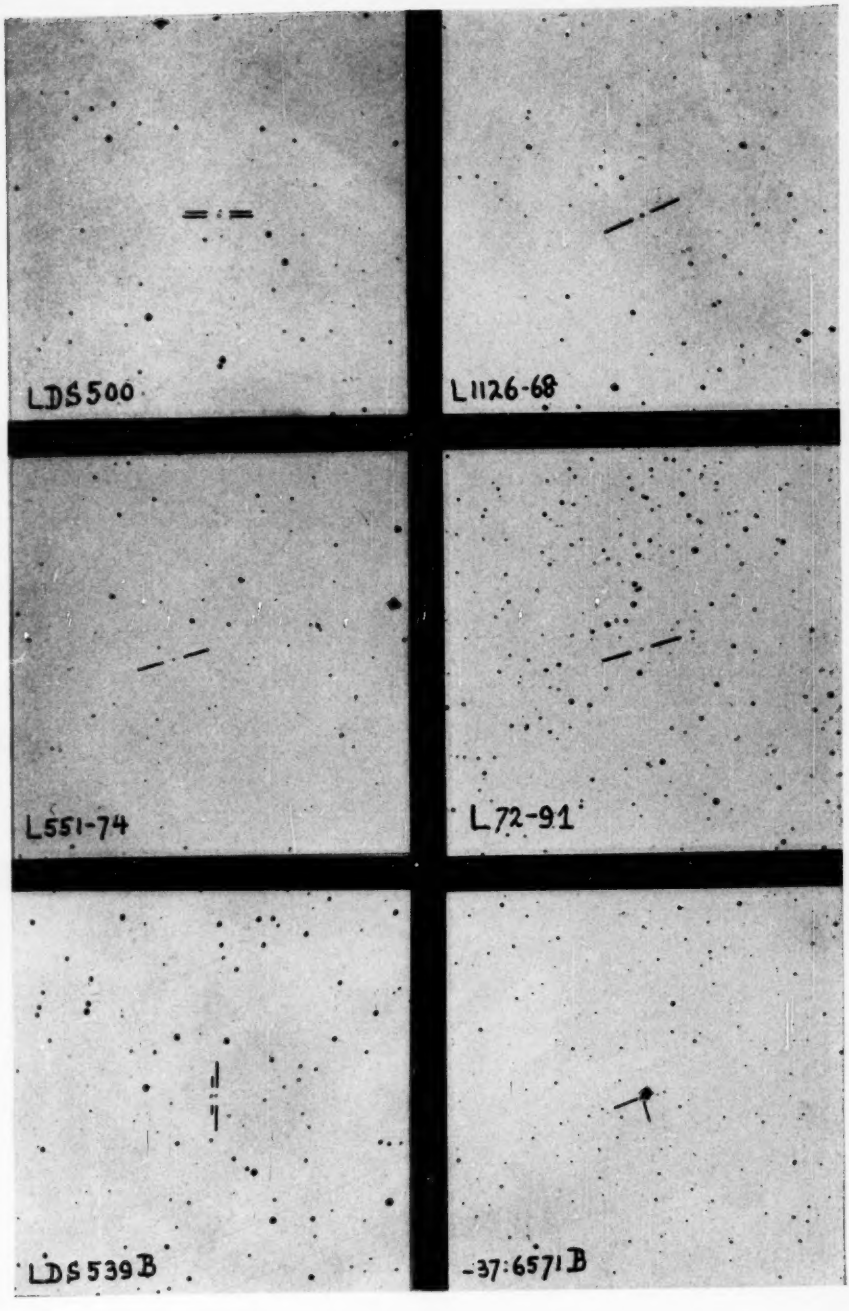

FIG. 10

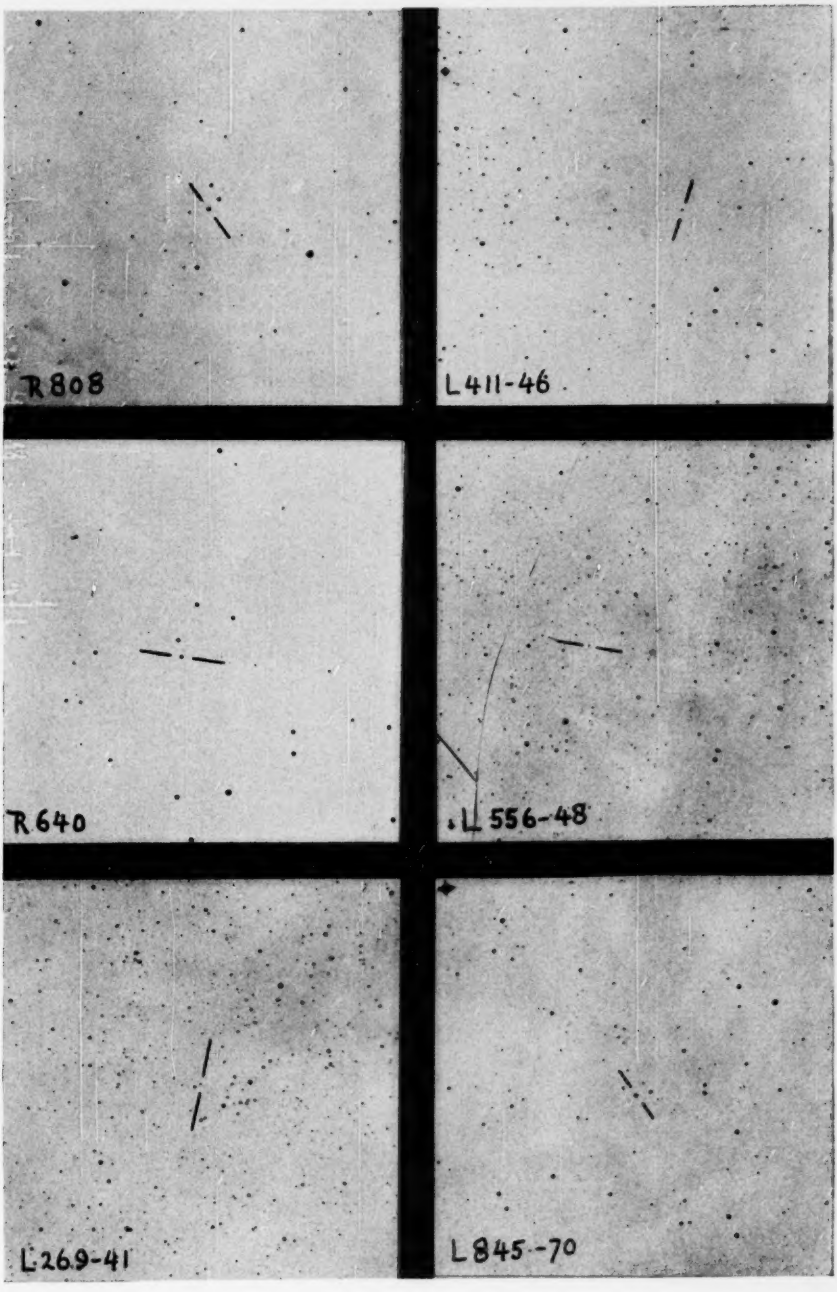

FIG. 11

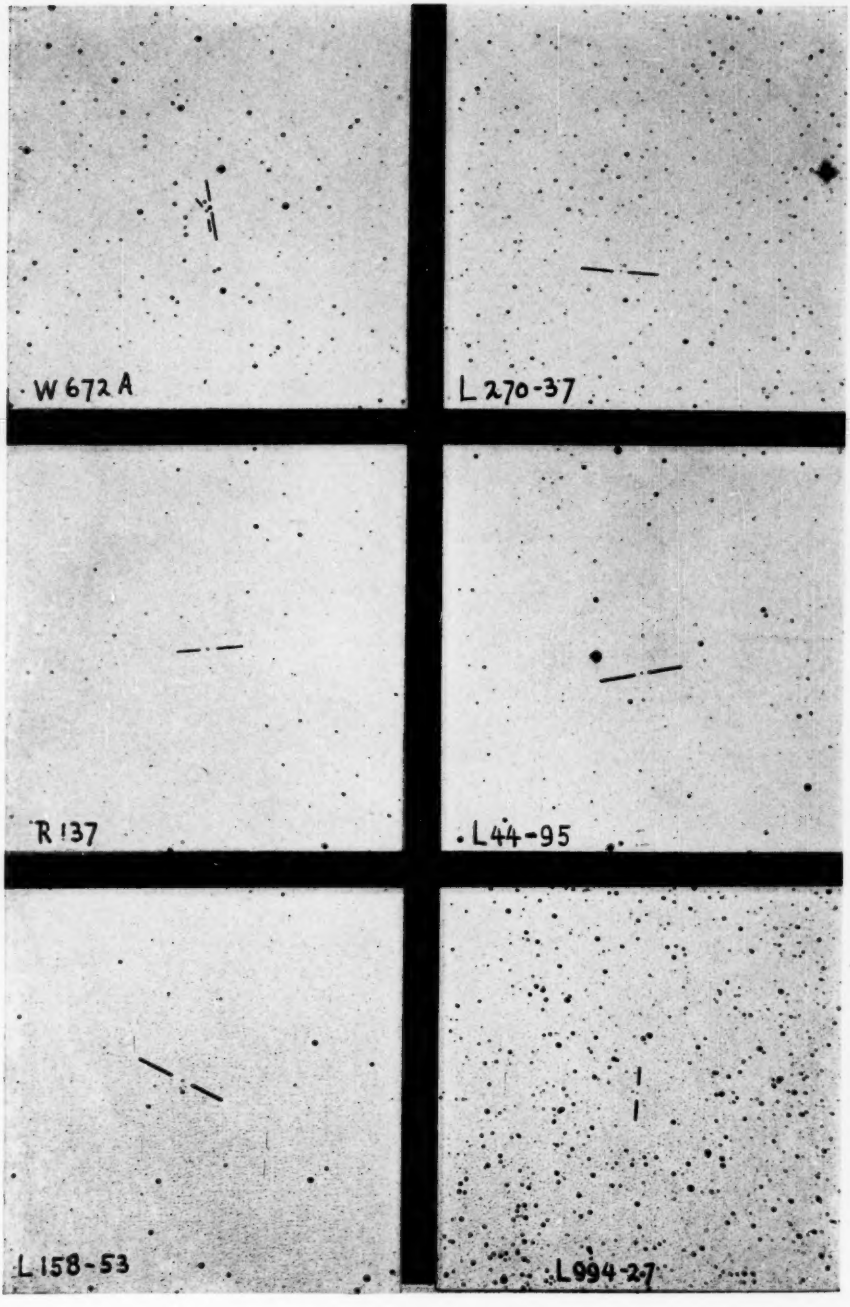

FIG. 12

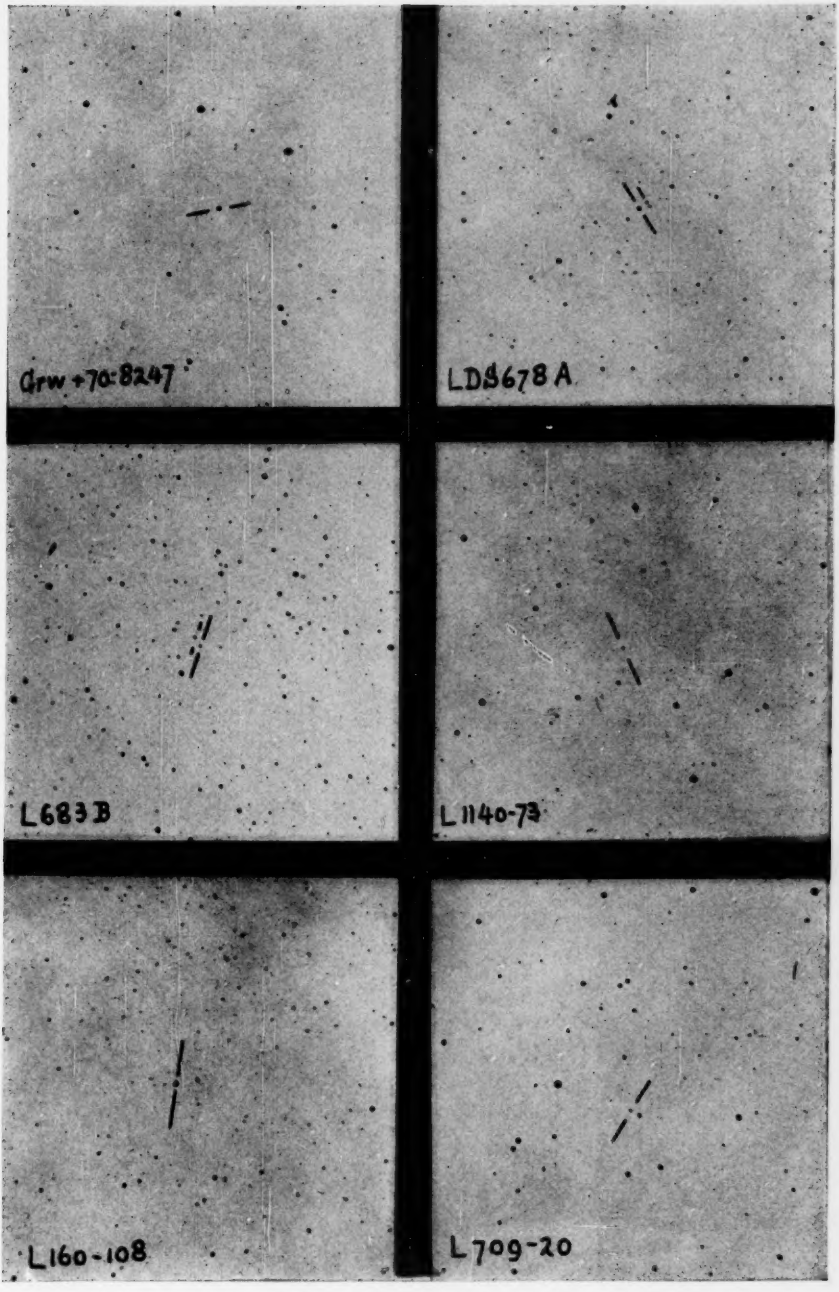

FIG. 13

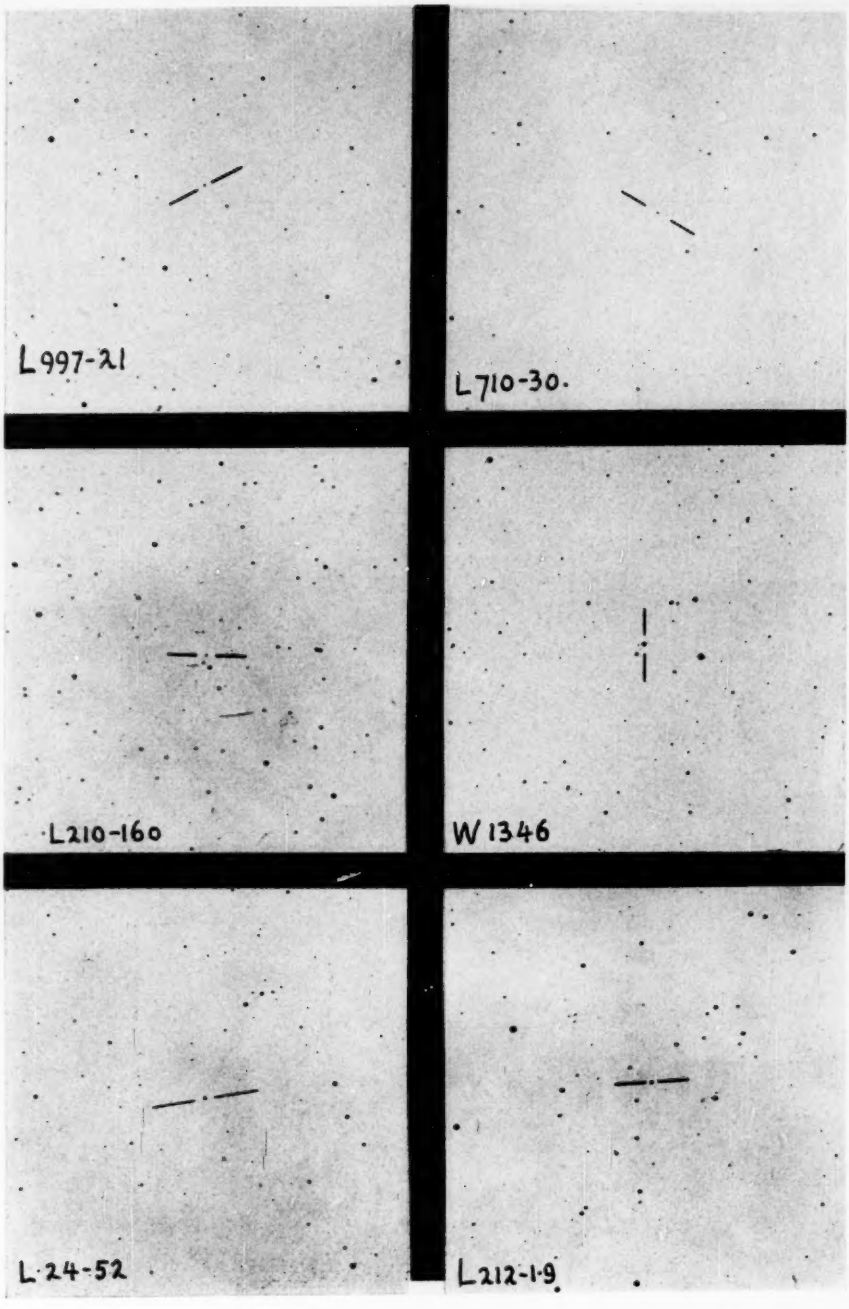

FIG. 14

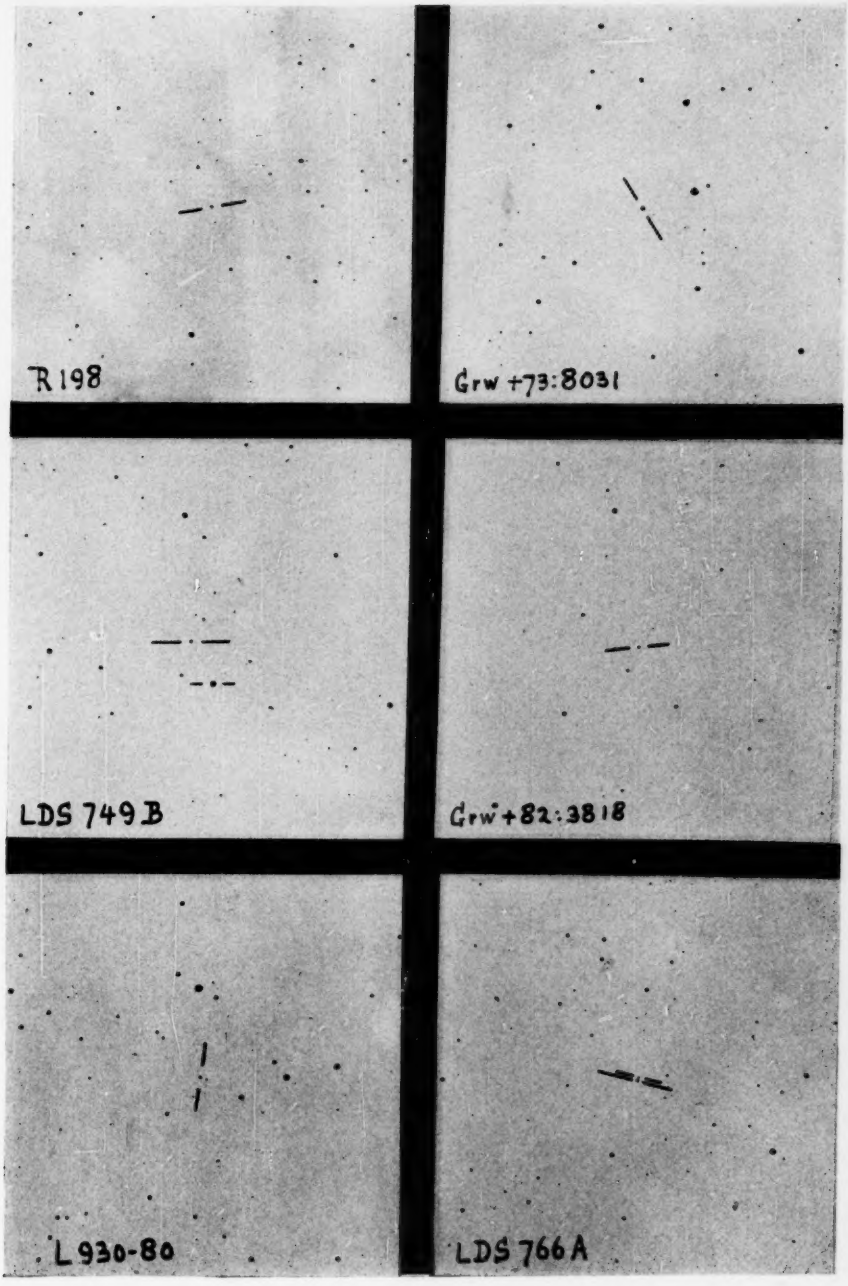

FIG. 15

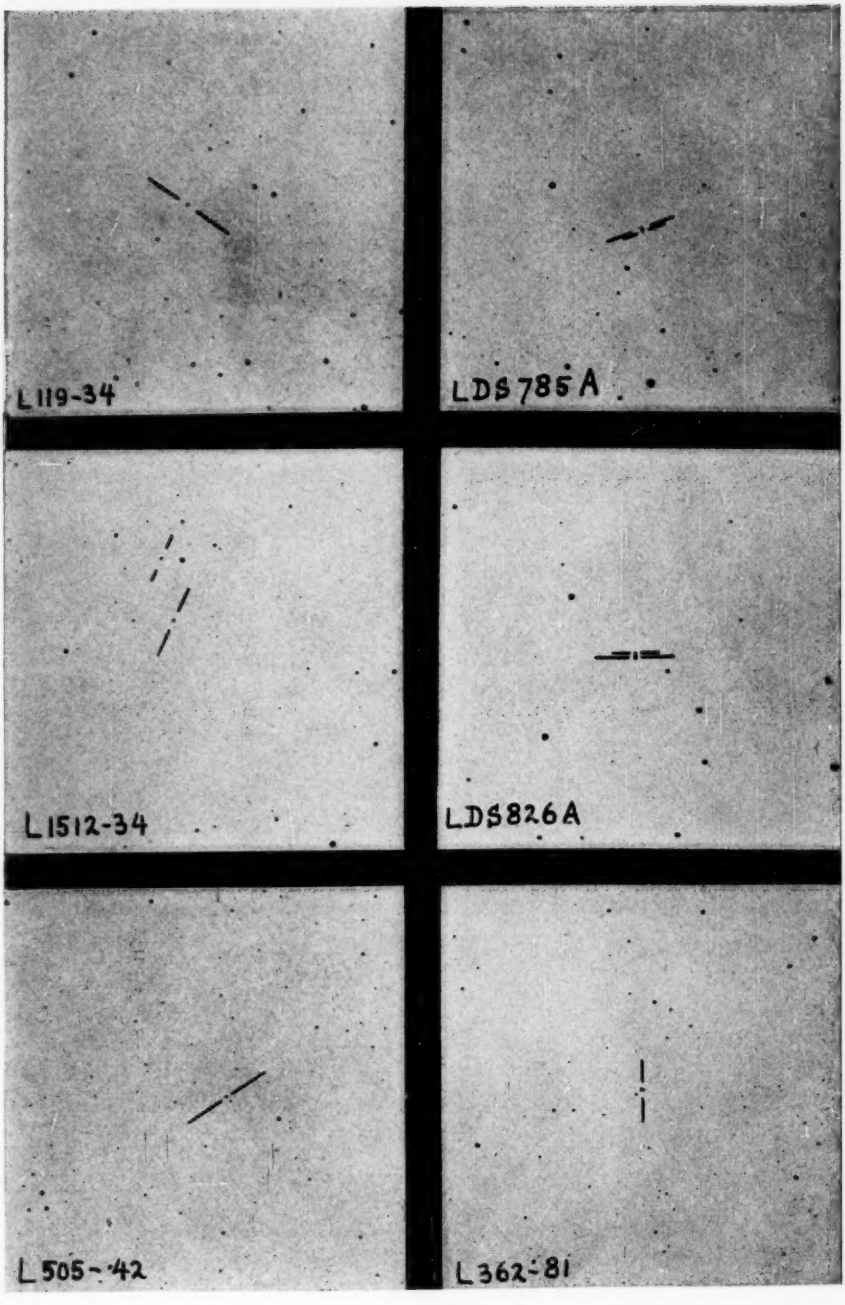

FIG. 16

TABLE 1

POSITIONS, MAGNITUDES, AND COLORS FOR WHITE DWARFS

No.	Designation	1950 Pos.		m_{pg}	I.C.
		α	δ		
1	L 505-1	0^h00^m1	−34°30′	14.5	+0.2
2	LDS 1	08.7	−21 00	12.2	*
3	W 1	11.1	+ 0 03	14.8	+0.1
4	L 170-27	24.3	−55 42	14.6	0.0
5	L 1011-71	33.1	+ 1 37	15.2	+0.3
6	v Ma 1	0 46.5	+ 5 11	12.6	+0.4
7	L 796-10	53.3	−11 45	15.1	+0.3
8	W 1516	1 15.4	+15 56	14.0	−0.2
9	R 548	33.7	−11 36	13.9	+0.2
10	L 870-2	35.5	− 5 16	12.8	+0.2
11	Oxf +25:6725	2 05.9	+25 00	12.8	0.0
12	h Per 1166	14.0	+56 53	13.4	−0.3
13	L 54-5	55.8	−70 34	14.0	+0.1
14	L 587-77 A	3 26.8	−27 34	13.9	−0.1*
15	W 219	41.6	+18 18	15.2	+0.3
16	L 228-55	3 42.3	−51 33	14.8	+0.1
17	Z 10	4 07.3	+17 54	14.4	−0.2
18	VR 7	21.0	+16 14	14.0	−0.3
19	VR 16	25.7	+16 52	13.7	−0.3
20	L 1239-16=Z 9	29.4	+17 38	14.1	0.0
21	L 1244-26	6 12.4	+17 45	12.9	−0.4
22	SA 26-82	39.6	+44 43	16.2	0.0
23	He 3	44.3	+37 36	11.7	−0.3
24	L 384-24	7 32.0	−42 47	14.4	0.0
25	L 745-46 A	38.0	−17 17	12.8	−0.1*
26	L 97-12	7 52.8	−67 38	14.9	+0.4
27	L 97-3	8 06.4	−66 09	13.6	0.0
28	L 532-81	39.7	−32 47	11.8	−0.2
29	LDS 235 B	45.3	−18 48	14.7	−0.1*
30	L 64-40	9 28.6	−71 20	16.2	+0.2
31	LDS 275 AB	9 35.0	−37 07	14.2	0.0*
32	SA 29-130	43.5	+44 08	13.0	+0.1
33	L 250-52	10 53.3	−55 04	13.0	−0.3
34	L 898-25	55.1	− 7 15	14.4	+0.1
35	L 971-14	11 15.8	− 2 58	15.0	0.0
36	R 627	11 21.7	+21 39	13.8	+0.3
37	L 145-141	42.9	−64 34	11.8	−0.3
38	L 1405-40 A	47.7	+25 35	15.3	+0.1*
39	L 1261-24	54.2	+18 39	15.3	+0.2
40	LDS 410 AB	12 25.6	−71 13	15.6	+1.1*
41	L 327-186	12 36.0	−49 32	14.0	0.0
42	L 39-44=38-80	41.3	−79 53	17.4	+0.2
43	W 457	57.7	+ 3 46	16.0	+0.5
44	Z 43=L 1409-4	13 14.0	+29 22	12.0	0.0
45	L 40-116	14.8	−78 09	17.0	+0.5
46	L 258-46	13 23.0	−51 26	15.0	0.0
47	BD−7:3632	27.7	− 8 18	11.9	+0.1
48	L 106-73	34.5	−67 49	16.1	−0.3
49	W 489	34.3	+ 3 58	15.4	+1.1
50	LDS 455 A	34.3	−16 04	14.9	0.0*

* Double stars; listed in Table 2.

TABLE 1—*Continued*

No.	Designation	1950 Pos.		m_{pg}	I.C.
		α	δ		
51	L 106-77	13^h37^m5	−67°55′	15.3	−0.2
52	Grw +70: 5824	37.8	+70 33	12.3	−0.1
53	L 619-49/50 B	48.1	−27 18	15.0	+0.1*
54	L 19-2	14 25.4	−81 07	13.0	0.0
55	LDS 500 AB	40.0	−40 57	13.2	+0.3*
56	L 1126-68	14 48.4	+ 7 47	15.0	0.0
57	L 551-74	15 20.1	−34 01	14.7	0.0
58	L 72-91	24.3	−74 55	16.7	−0.4
59	LDS 539 B	41.9	−38 10	14.9	+0.3*
60	CPD −37: 6571 B	44.2	−37 45	13.2	0.0*
61	R 808	15 59.6	+36 58	14.1	0.0
62	R 640	16 26.8	+36 51	13.4	+0.3
63	L 411-46	27.0	−41 59	15.6	+0.4:
64	L 556-48	47.4	−32 44	16.0	−0.1
65	L 269-41	57.8	−52 43	15.5	−0.2
66	L 845-70	17 08.5	−14 45	14.3	+0.2
67	W 672 A	16.2	+ 2 00	14.2	0.0*
68	L 270-37	33.2	−54 24	16.3	+0.4
69	R 137	18 24.8	+ 4 02	13.8	−0.3
70	L 44-95	34.7	−78 08	15.2	0.0
71	L 158-53	18 37.6	−61 56	15.2	+0.2
72	L 994-27	57.6	− 1 30	17.0	+0.4
73	Grw +70: 8247	19 00.6	+70 34	12.7	−0.2
74	LDS 678 A	17.7	− 7 46	11.9	−0.3*
75	LDS 683 B	32.9	−13 36	15.2	−0.1*
76	L 1140-73	19 41.9	+ 8 47	14.2	0.0
77	L 160-108	44.8	−63 07	11.8	+0.2
78	L 709-20	52.9	−20 37	14.6	0.0
79	L 997-21	54.0	− 1 09	13.6	0.0
80	L 710-30	20 07.3	−21 55	14.4	+0.2
81	L 219-160	20 18.3	−58 31	16.2	−0.1
82	W 1346	32.3	+24 55	11.2	−0.2
83	L 24-52	21 05.2	−82 01	14.4	+0.2
84	L 212-19	15.8	−56 03	15.0	+0.2
85	R 198	24.8	+54 59	14.4	−0.4
86	Grw +73: 8031	21 26.6	+73 25	12.6	−0.3
87	LDS 749 B	29.6	0 00	14.2	0.0*
88	Grw +82: 3818	36.7	+82 49	12.5	−0.1
89	L 930-80	45.0	− 7 58	14.2	0.0
90	LDS 766 A	54.9	−43 42	14.0	+0.1*
91	L 119-34	22 16.2	−65 44	14.8	0.0
92	LDS 785 A	24.6	−34 27	14.7	+0.2*
93	L 1512-34 B	23 41.4	+32 15	13.0	+0.1*
94	LDS 826 A	51.5	−33 33	14.6	0.0*
95	L 505-42	51.7	−36 50	14.8	+0.3
96	L 362-81	59.6	−43 25	12.8	+0.2

TABLE 2

DOUBLE STARS*

No.	A		B		p	s
	m_{pg}	I.C.	m_{pg}	I.C.		
2	12.4	+0.2	14.8	+0.5	168°	8".4
14	13.9	−0.1	15.6	+1.7	226	7.7
25	12.8	−0.1	16.9	+1.8	276	21.0
29	12.6	+1.0	14.7	−0.1	236	30.0
31	14.9	−0.1	15.1	0.0	36	3.6
38	15.3	+0.1	16.2	+1.3	250	36.2
40	15.7	+1.1	17.7	+1.0	108	15.3
50	14.9	0.0	15.2	+1.6	241	14.0
53	13.9	+1.4	15.0	+0.1	234	8.2
55	13.4	+0.3	14.9	+0.3	0	12.3
59	14.7	+1.1	14.9	+0.3	265	10.3
60	6.8	+0.8	13.2	0.0	130	14.7
67	14.3	0.0	15.6	+1.5	137	12.3
74	11.9	−0.3	13.7	+1.8	308	27.2
75	15.1	+1.2	15.4	−0.1	205	28.2
87	11.0	+1.0	14.2	0.0	28	132.8
90	14.0	+0.1	15.4	+1.3	329	9.0
92	14.7	+0.2	14.7	+1.5	197	9.4
93	13.0	+0.1	13.4	+1.3	9	174.0
94	14.6	0.0	15.0	+1.3	359	7.0

* The average date of the observations is 1944.5.

NOTES

A NEW STAR OF LARGE PROPER MOTION (L 726-8)

1. *Introduction.*—When the Bruce Proper Motion Survey was originally planned in 1926, it was found that, while the systematic plan required 1009 pairs of plates for a complete coverage of the Southern Hemisphere, early-epoch plates—taken between 1896 and 1911—were available for only 950 regions. Among the 59 missing plates, 34 had centers at declinations $-2\frac{1}{2}°$ or $-7\frac{1}{2}°$, and 25 others at various declinations between $-10°$ and $-45°$. As it was felt that the regions in the former group were accessible from the Northern Hemisphere and that a large part of this area had, in fact, been blinked by Wolf and Ross, nothing was done to complete this area, although this decision now appears to have been an error of judgment. When the writer began the taking of the new plates for the survey in 1929, first-epoch plates were taken immediately for all the 25 areas south of declination -10, and these plates were repeated by the Harvard Observatory during 1944–1946.

Although the time interval of the resulting pairs is only about half that in the regular series, it was felt that blinking these pairs would at least provide information on the motions larger than $0''.1$ annually. In the course of this examination a star was found with a proper motion larger than that of any star discovered in the survey; in addition, this star appears to possess so many other interesting features that it may well become the most important star found during the entire twenty-five years spent thus far on the Bruce Proper Motion Survey, and as such it would seem to merit individual description and publication.

2. *Observational.*—On October 29, 1947, while blinking Bruce Region 726 centered at 1^h30^m, $-17\frac{1}{2}°$, the eighth star found was of the fourteenth magnitude and possessed a proper motion of about $3''.3$ in 81°. Since the direction of motion indicated that it was probably not a high-velocity star and that it might, therefore, have a large parallax, further observations for parallax, magnitude, color, and spectrum were planned. Carpenter, at the Steward Observatory in Tucson, obtained a color plate which showed the star to be extremely red, while Page, at McDonald, obtained a spectrogram of the star under the co-operative arrangement then in effect between Minnesota and McDonald. This spectrogram showed the star to be of late spectral class—about M6—with both hydrogen and ionized calcium lines in emission. A further spectrogram was obtained by Struve in November, 1948; a series of parallax plates was taken by Carpenter with the 36-inch Steward reflector at Tucson in August and again in December, 1948; a large-scale plate was taken by Humason at Mount Wilson (for the purpose of measuring the separation of the components), and a large number of photometric comparisons was made by the writer during a brief visit to Tucson in September, 1948. In addition, micrometric observations of the star have been communicated by Van Biesbroeck at McDonald and Van den Bos at Johannesburg, and the radial velocities of the two components as measured on Mount Wilson spectrograms were communicated by Joy. Photoelectric observations to test the constancy of light are in progress at Tucson, while by agreement with Kuiper the last remaining hours of the co-operative agreement between Minnesota and Yerkes-McDonald are to be utilized to take plates of the star with the 40-inch refractor of the Yerkes Observatory for the purpose of parallax and orbital-motion determination. However, as these plates have not yet been received, it has not been possible to include the results of their measurements in the present paper.

The scientific and geographic variety of these observations is enumerated here in de-

tail, not only to show the truly co-operative spirit in astronomy and to enable the present writer to express his deep appreciation for this co-operation—for without the help of the Steward, McDonald, and Mount Wilson observatories this paper would not have been written, and without the plates loaned by the Harvard Observatory the star would not even have been discovered—but also to illustrate the difficulty of operation, and even of scientific survival, of a small, inadequately equipped observatory in our modern age of very faint objects, requiring large telescopes for observation.

3. *Photometric.*—Observations were made by the writer with the 36-inch reflector at Tucson, on 103*a*-G plates with a No. 12 filter and on 103*a*-O plates, using Selected Area 92 for comparison, with the following results:

Photovisual magnitude: 11.93 ± 0.03 (m.e.), 6 plates,

Photographic magnitude: 13.69 ± 0.05 , 9 plates.

Previous experience indicates that the photographic magnitudes determined in this way—with an aluminized mirror—are too faint for red stars when compared to the International scale; and the color index may well be somewhat less than the value of +1.76 implied by the above data, though this effect is counterbalanced to some extent by the fact that the observed color index is probably slightly too small, owing to the strong emission lines of ionized calcium.

4. *Binary character.*—The first plates taken at Tucson showed the image to be definitely elongated. Photographic and visual observations of the star which I am permitted to quote here gave the following results:

1948.72.....	117°.9,	1".65,	VBs 82",
1948.77.....	116.1,	1.51,	100-inch pg,
1948.93.....	120.4,	1.42,	B 27".

There are as yet no photographic estimates of the magnitude difference, but measures made on the Tucson photometric plates indicate no appreciable difference in position of the center of light on blue and yellow plates; and we may therefore conclude that the colors of the two components are approximately the same. The visual-magnitude difference appears to be around 0.5.

5. *Spectroscopic.*—From the spectra taken with the prime-focus and with the quartz *f*/1 spectrograph on the McDonald telescope the spectral class is estimated as dM6e. Since the small separation of the components did not make it possible to obtain their spectra separately, this is presumably mainly the spectral class of the primary. Joy at Mount Wilson, however, has kindly communicated the results of his observations and has allowed me to quote them here. He finds emission lines present in the spectra of both components; measures of these lines give a radial velocity of +29 km/sec for the brighter component (4 pls.) and of +32 km/sec for the fainter component (1 pl.). A reproduction of the McDonald spectrogram is shown in Figure 1.

6. *Variability.*—The individual values obtained for the photovisual and photographic magnitudes of the star vary considerably, especially in the case of the photographic magnitude, though not more than could be expected for so difficult an object—always low above the disturbing glare and smoke of the city. However, a plate taken by Carpenter on December 7, 1948, with five exposures, for parallax purposes, shows a pronounced fluctuation in brightness. In order to determine this accurately, the photographic and photovisual magnitudes of seven comparison stars were first obtained from the plates containing comparisons of the star field with that of S.A. 92. These magnitudes are shown in Table 1, and the identifications of the comparison stars are shown in Figure 1. The

photographic magnitude of each of the five images of the proper-motion star was then determined by estimating its brightness relative to the corresponding images of these comparison stars. The results which represent the averages of estimates made by Miss Helen Hughes and the writer are shown in the third column of Table 2, while the variation itself is clearly shown in the reproduction of this particular Tucson plate in the accompanying illustration. The original negative was developed until a noticeable sky-fog showed (moon at first quarter); yet there are no traces of nonuniformity in this background fog in the neighborhood of the star images, and variation in the sensitivity of the plate may therefore be practically discounted.

In the absence of further information it would not be possible to decide to which component the light-variation must be attributed. There is, however, further evidence obtained from the accurate measures of positions of the images. Since the plate in question

TABLE 1

MAGNITUDES OF COMPARISON STARS FOR L 726-8

Star	Pv	Pg	Star	Pv	Pg
a	10.4	10.9	e	13.1	13.5
b	12.0	12.2	f	13.0	13.6
c	12.0	12.5	g	14.4	14.6
d	12.6	13.0			

TABLE 2

VARIATION IN LIGHT OF L 726-8

	Date 1948 (U.T.)	m(pg)	$L_{(tot)}$	L_B	B'/B		Date 1948 (U.T.)	m(pg)	$L_{(tot)}$	L_B	B'/B
1	Dec 7.194	13.71	1.0	0.39	1.0	4	Dec 7.2015	13.01	1.87	1.26	3.2
2	7.196	11.86	5.4	4.79	12.3	5	7.204	13.07	1.76	1.16	3.0
3	7.198	12.78	2.3	1.69	4.3						

was taken for parallax purposes, it was measured and reduced in the same way as all the others, but it soon became apparent that its measured position was very discordant with the rest of the plates, in that the position of the parallax star was 0.0083 mm farther to the east than that on Plate 11687, which was taken only 25 minutes earlier and which agreed with the other plates. The image of the parallax star was of normal brightness on this earlier plate; furthermore, the brightest image on Plate 11688 gave the largest discordance. This suggests that it was the *fainter*, following component which increased in brightness, thus shifting the center of light of the combined image eastward.

Assuming $\Delta m = 0.5$ (pg), we may now calculate the corresponding light-changes. At normal brightness we then have $L_A = 0.61$, $L_B = 0.39$, expressed in terms of the combined normal light. The increased brightness of the fainter component B as thus calculated is shown in the fifth column of Table 2, and the ratio of increase in the sixth column. Finally, the center of light of the combined image has been calculated on this same assumption, and it is found that the average for these five images should lie 9 μ to the east of the center of light of the normal star. Accordingly, a correction of -0.0090 mm has been applied to the right-ascension measures on this plate; this removes all the discrepancy and results in a more concordant parallax.

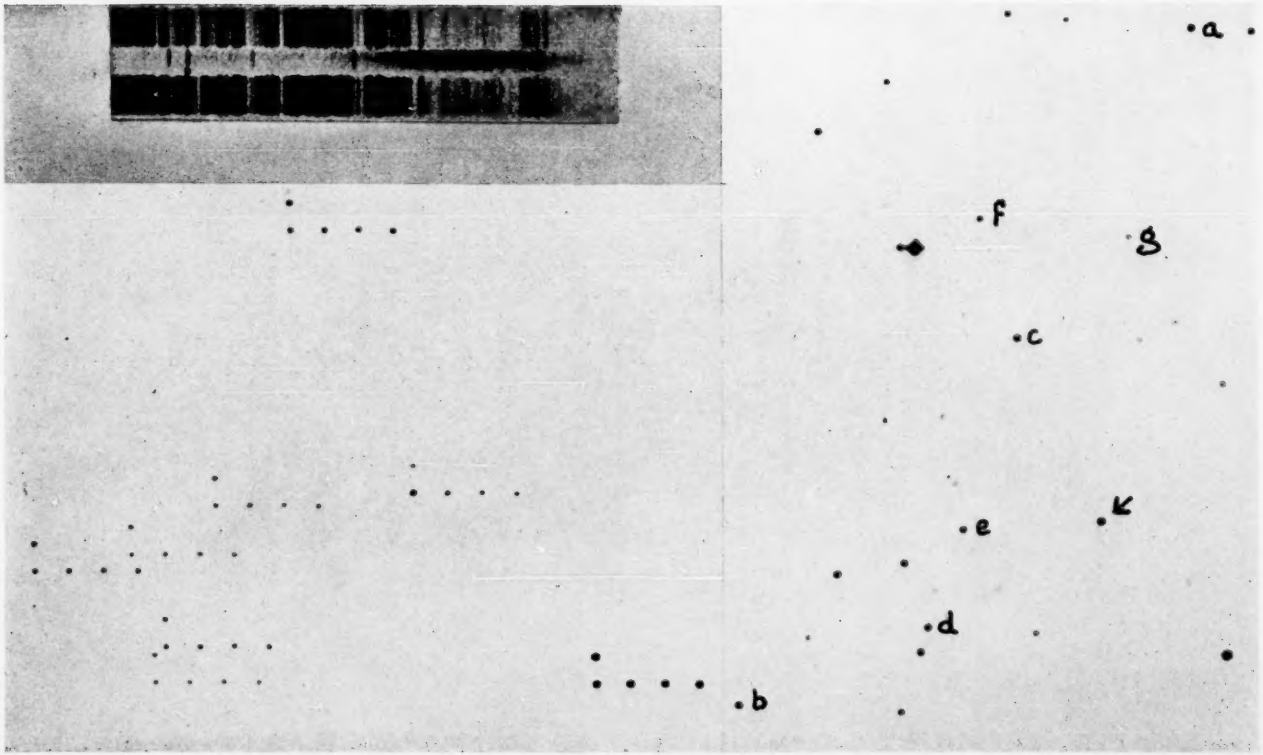

FIG. 1.—(*Above*) Spectrum of L 726-8 taken at McDonald Observatory, showing emission lines of *H* and *K* Ca II. (*Right*) Field of L 726-8. North is at top. The two brightest stars are BD-18°279 (*upper*) and BD-18°275 (*lower*). (*Lower left*) Multiple exposure of field, taken by Carpenter at Tucson, showing sudden brightening of L 726-8 on December 7, 1948. The interval of time between the first and last exposures was approximately 20 minutes. The chart plate is photovisual; the multiple exposure is photographic.

We may tentatively conclude that the observed sudden brightening of the star is real, in which case it would appear to be similar to the variations found by van Maanen in BD+44:2051(B)[1] and in Ross 882.[2] Table 3 gives the comparable data for these three stars, the third and fourth columns show the apparent photographic magnitudes at normal light and in the observed maximum, while the last two columns show the corresponding absolute magnitudes.

It will be noticed that all three stars are very late M dwarfs of nearly the same spectral class and that all three spectra contain emission lines. However, for the first two stars we merely know that variability exists, but Carpenter's plate of December 7, 1948, gives the first observation of the extreme rapidity of the change—to twelve times the original luminosity in less than 3 minutes (if the increase is, indeed, due to the fainter component). The average sustained luminosity increase of a supernova amounts to barely 5 per cent during the same period. Plotting the light-curve of the variation and extrapolating to the probable termination time of the flare, we find that the phenomenon appears to have lasted only about 20 minutes in the present case. During this time we find that the extra amount of energy radiated—i.e., over and above the normal radiation during that time—amounted to about 4000 seconds of normal radiation. Accepting provisionally

TABLE 3

VARIATION IN LIGHT OF DWARF M STARS

Star	Sp.	m_n	m_{max}	M_n	M_{max}
BD+44°2051(B)	dM6e	16.0	14.2	17.2	15.4
Ross 882	dM6e	13.2	11.8	14.0	12.6
L 726-8	dM6e	14.7	12.0	18.5	15.8

the data presented later, we find that the star is about two hundred thousand times less luminous than the sun, photographically, and that its total energy radiation in the photographic region, therefore, should be of the order of 10^{28} ergs per second. The total extra energy produced during the outburst would then be of the order of 4×10^{31} ergs—equivalent to 4.4×10^{4} tons of energy. This must be considered as a bare minimum, since the true parallax of the star may well be considerably smaller than the value used here, while, moreover, it would appear reasonably certain that there was some energy production outside the photographic region. In itself the amount is not large—equal to the sun's radiation during 1/100 second—though, compared to the star's normal radiation, it represents a significant amount, while, furthermore, the rapidity of the change suggests some explosive origin. It might be tempting to speculate on the possibility of the collision of the star with some large dark body which perhaps could temporarily raise the temperature locally enough to dissolve the molecular bands in the spectrum, were it not for the fact that the phenomenon appears to be associated with the presence of the emission lines and may well be periodic or semiperiodic (SS Cygni type?). It is hoped, however, that intensive photographic, photovisual, photoelectric, and spectroscopic observations of this star will be undertaken in the near future, with a view to examining any possible correlation between light-changes and those in color, spectrum, or strength of the emission lines, and thus aiding in the clearing-up of this mystery.

7. *Positional.*—Discussion of the astrometric data has been postponed to the last in view of the corrections to be applied because of section 6. A plate taken by the writer with the 36-inch reflector at Tucson when the star was nearly in opposition—and on the meridian—was used to determine its accurate position. Reducing the measures by means

[1] *Ap. J.*, **91**, 505, 1940. [2] *Pub. A.S.P.*, **57**, 216, 1945.

of the *Hyderabad Astrographic Catalogue* (Pl. 851, Zone −18, taken November 27, 1916) and correcting for precession, parallax, proper motion, secular proper motion of the comparison stars, and differential refraction due to the extreme redness of the star, we find for the position of the proper-motion star for the equinox and epoch of 1950.0:

$$\text{R.A.}, 1^h36^m25^s.40 ; \qquad \text{Dec.}, -18°12'41''.7 .$$

A provisional value for the proper motion was derived from this same Tucson plate and the original Harvard plate taken by the writer on January 5, 1930, and by using the same comparison stars as for the parallax measures. With this provisional value for the proper motion, which still included a small term dependent upon the parallax, final values for the proper motion and parallax were derived from measures of eight parallax plates taken by Carpenter with the 36-inch reflector at Tucson. Seven comparison stars were used on all plates; referred to the average position of these seven stars on all eight plates, the right-ascension co-ordinate of the parallax star is given for each of these plates in Table 4. The measures are expressed in millimeters (1 mm = 44".6 on these plates)

TABLE 4

CO-ORDINATES IN RIGHT ASCENSION

Plate	1948	X (Mm)	Plate	1948	X (Mm)
T 11395	Aug. 8	−0.0022	T 11687	Dec. 7	+0.0066
11396	9	− .0008	11688	7	+ .0059
11397	9	+ .0032	11699	29	+ .0050
11398	9	−0.0001	11700	29	+0.0056

and are referred to a purely arbitrary zero point—the average of the first four positions. The values given represent the average of measures made by Miss Helen Hughes and the writer.

The original measure on Plate 11688 gave a position of +0.0149; to this the correction of −0.0090 mm mentioned in section 6 has been applied.

From these measures the following values for the proper motion and the parallax are then derived (all are relative values):

$$\mu_\alpha \cos\delta = +3''.308 \pm 0''.037 \text{ (m.e.)}, \qquad \mu_\delta = +0''.570 \pm 0''.037 ,$$

$$p = 0''.561 \pm 0''.067 .$$

The value of this parallax, if substantiated, would render the present star the second nearest star in space, slightly closer even than BD+4°.3561 (Barnard's star, p = 0".544 ± 0".003). Experience with inaccurate reflector parallaxes indicates that they are often too large; in addition, in the present case it should be pointed out that the parallax star is a visual binary but is not resolved on the parallax plates; hence a further source of systematic error is introduced. The mean errors given above, while representing the data, are, after all, internal mean errors, and the real errors may well be much larger. It would, however, appear entirely safe to say that the star is probably nearer than 4 parsecs and may be nearer than $2\frac{1}{2}$ parsecs. A really definitive value of the parallax will probably not be derived until the pair has completed one orbital revolution—which may take 20–25 years.

8. *Orbital motion.*—If the present parallax is approximately correct, the absolute magnitudes of the components would be around 18.0 and 18.5, respectively, and the com-

bined mass can be expected to be not more than one-ninth that of the sun. With $p = 0''.56$, $s = 1''.5$ gives a linear separation of the order of 3 a.u. and an expected period of 15 years or so, with an average annual change in position angle of 15°. No data are now available from which this could be substantiated or refuted, but it is hoped that, when the Yerkes parallax plates become available, a first indication of this orbital motion may be derived. Observations made over the next 5 years should give at least an approximate answer to the question and hence also a correction to the parallax or to the mass or to both.

9. *Summary.*—Even though the very large parallax derived here may well be substantially lowered in future, there seems to be no doubt that the star described here is one of unusual interest. Not only does it appear to be the nearest short-period binary—with the possible exception of Proxima Centauri—but its components must have the smallest stellar masses now determinable. The sudden flaring-up of the fainter component, if real, appears to be a rare phenomenon whose ultimate solution should aid materially in the solution of the more general problem of the sources of stellar energy. Finally, because of its nearness—though in spite of its unfavorable position as seen from the Northern Hemisphere—a long series of astrometric observations should give further evidence as to the existence or nonexistence of bodies of substellar masses. The data are summarized in Table 5.

TABLE 5

SUMMARY OF DATA ON L 726-8

R.A., $1^h36^m25^s.40$; Dec., $-18°12'41''.7$ (1950.0)

$\mu = 3''.355$ in $80°.3$, $p = 0''.56 \pm 0''.07$, $s = 1''.5$ in 118° (1948.8).

$T_a = +28$ km/sec $\quad \Theta = -14$ km/sec (toward $l = 55°$, $b = 0°$)

$T_\delta = +5$ km/sec $\quad \Pi = -32$ (toward $l = 145$, $b = 0$)

$V = +30$ km/sec $\quad Z = -22$ (toward $b = +90$)

	Photovisual	Photographic		Photovisual	Photographic
m_{tot}	11.93	13.69			
m_A	12.45	14.21	M_A	16.20	17.96
m_B	12.95	14.71	M_B	16.70	18.46
		I.C. +1.76		dM6e	

In conclusion, it is a pleasure to acknowledge here the financial support received in the making of the observations and measures reported here, and toward their publication, from the Graduate School of the University of Minnesota and from the Gould Fund of the National Academy of Sciences.

WILLEM J. LUYTEN

UNIVERSITY OF MINNESOTA

A LARGE NEW PLANETARY NEBULA

This hitherto unrecognized planetary nebula in Pegasus was discovered in the course of a preliminary survey of a set of plates made with the Jewett Schmidt telescope of the Harvard College Observatory. It appears on two exposures, each of 30 minutes on 103*a*-O emulsion. The object is also faintly visible on a plate of 190-minute exposure taken in 1941 with the 16-inch Metcalf doublet. It had been noted and marked on this plate at some time in the past, but its character was not recognized or verified.

The nebula is not listed in Parenago's catalogue,[1] and we find no subsequent reference to it. The relevant data are tabulated below.

Equatorial co-ordinates for 1950.0	23^h33^m4	$+30°\,11'$
Galactic co-ordinates	73°	$-30°$
Apparent ptg. mag. of central star	15.1	.....
Maximum observed angular diameter	5'.1	.....

Only two arcs are visible, each subtending approximately 65° at the central star. The latter was easily identified among those within the arcs with the aid of an exposure on 103*a*-E emulsion through a red filter.

A photographic-magnitude sequence was set up by means of two independent transfers on overlapping plates from Selected Area 67. No material for the establishment of a red sequence is available, but a rough calibration of the red plate indicates that the red index of the central star is about -0.5 mag.

Fifty-six galaxies brighter than 17.5 mag. were counted in an area of 4.2 square degrees surrounding the nebula. Since only objects clearly identified as galaxies on both plates were included, the true number must be somewhat larger. The observed frequency of galaxies agrees well with the mean distributions of Shapley[2] and Hubble,[3] and the area is therefore not abnormally obscured for its galactic latitude.

The angular diameter of this planetary is the fourth largest known, exceeded by NGC 6853, 7293, and 2474–2475.

F. D. MILLER
E. VAN DIEN

UNIVERSITY OF MICHIGAN OBSERVATORY
BOSSCHA-STERRENWACHT, LEMBANG, JAVA
March 5, 1949

A NEW VARIABLE STAR

This star (1900: $\alpha = 19^h55^m9$; $\delta = +33°42'$) is located in the flipper of the seal-shaped absorption cloud (Barnard No. 144) in Cygnus.

The photographic sequence in Table 1 (a chart is in Fig. 1) is based on twelve pairs of plates (six each with the Zeiss camera and the reflector), using the Mount Wilson magni-

TABLE 1

COMPARISON STAR SEQUENCE

Star	m_{pg}	m_{pv}	Star	m_{pg}	m_{pv}	Star	m_{pg}	m_{pv}
A	11.70	10.70	b	12.05	11.70	e	13.95	.....
B	11.56	11.08	c	12.80	11.60	f	12.46	12.27
a	11.76	11.69	d	13.70	.....	g	14.39	.....

tudes in Selected Area 65 as standards. The photovisual sequence was determined from three comparisons with Harvard Standard Region C-12, plus two polar pairs for stars A and B.

Table 2 contains the normal points and Figure 1 the light-curves obtained from 253

[1] *A.J. Soviet Union*, **23**, 69, 1946.

[2] *Harvard Obs. Reprint*, No. 194, 1940.

[3] *Ap. J.*, **84**, 517, 1936.

photographic and 54 photovisual estimates. The longest gap in the series of plates was the 110-day interval centered at JD 2431940. The observed ranges are from 12.1 to 14.2 mag. (pg) and from 10.9 to 12.2 mag. (pv). The color index thence varies from1.2 mag. at maximum to 2.0 at minimum. The star is probably a member of the R Coronae Borealis class.

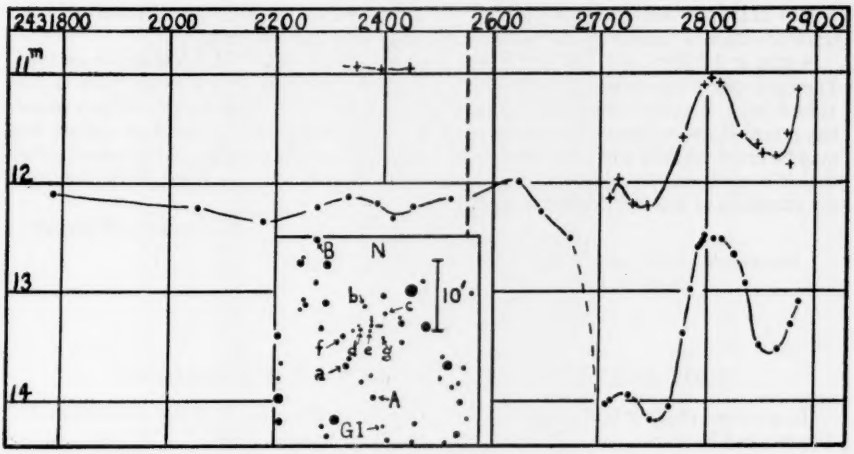

FIG. 1.—Photovisual (*upper*) and photographic light-curves; chart of the field

TABLE 2

PHOTOGRAPHIC AND PHOTOVISUAL NORMAL POINTS

JD 243+	n	m_{pg}	JD 243+	n	m_{pg}	JD 243+	n	m_{pv}
1784	6	12.10	2784	10	12.98	2348	3	10.93
2054	10	12.22	2792	11	12.59	2394	4	10.96
2178	6	12.36	2795	10	12.56	2443	2	10.95
2278	5	12.21	2796	10	12.54	2710	4	12.14
2335	8	12.12	2798	10	12.49	2718	2	11.99
2384	6	12.19	2806	10	12.51	2731	2	12.20
2417	5	12.31	2814	10	12.52	2745	1	12.22
2455	5	12.21	2824	10	12.66	2778	4	11.60
2522	4	12.15	2835	10	12.92	2798	4	11.11
2624	1	11.99	2849	10	13.49	2804	3	11.07
2645	2	12.26	2864	10	13.52	2821	3	11.10
2673	2	12.50	2878	10	13.30	2831	4	11.59
2706	10	14.02	2885	2	13.10	2848	4	11.66
2710	10	13.98				2851	3	11.74
2728	10	13.93				2864	4	11.77
2749	10	14.16				2874	3	11.56
2766	10	14.06				2878	3	11.84
2778	10	13.39				2885	1	11.17

BALFOUR S. WHITNEY

UNIVERSITY OF OKLAHOMA OBSERVATORY
NORMAN, OKLAHOMA
January 29, 1949

A REFLECTION NEBULA AND AN ASSOCIATED VARIABLE STAR

The star HD 222142 (9.2, B9) = BD+47°4220 (9.0) is in the south-preceding end of an obscured region 16′ long and 6′ wide which contains no other stars as bright as magnitude 15.5. A 60-minute exposure on an Eastman 103*a*-O plate with the 10-inch reflector shows traces of a few fainter stars. Small-scale plates indicate that the dark nebula may be much longer, but either less dense or at a greater distance outside these limits.

HD 222142 is surrounded by a faint patch of luminous nebulosity of radius 0′.9, no trace of which is visible on 10-minute exposures with the reflector.

A star at $23^h32^m.8$, +47°51′ (1900) has been estimated on 400 plates taken since 1942. The light-curve indicates a rapidly varying irregular variable with a range from 12.7 to <14.4 (m_{pg}). Fluctuations of 1 mag. have been observed in 1-day intervals. A long search has revealed no evidence of periodicity. The star is in the edge of the dark nebula and may be involved in it. The median absolute magnitude of the variable, on the assumptions that it is unobscured and is at the distance of the B9 star, is +5, a value which is normal for variables of the Orion nebula type.

BALFOUR S. WHITNEY

UNIVERSITY OF OKLAHOMA OBSERVATORY
March 19, 1949

NEW ABSORPTIONS IN THE URANUS ATMOSPHERE

In a recent publication[1] attention was called to an absorption in the atmospheres of Uranus and Neptune, not due to methane; the band is some 30–40 A wide and centered on 8270 A. On November 2, 1948, two additional features were found when Uranus was photographed with the same spectrograph (500-mm camera), but with only half the slit-width previously employed and on a contrasty plate (IV-N). The additional absorptions are situated at λ 7500 and λ 7524 and are remarkable for their sharpness. The spectrogram is reproduced in Figure 1, with a spectrum of Venus placed above it for comparison and with two later spectra of Uranus below. The latter confirm the reality of the narrow features; the lowest spectrogram, showing coarser grain, was obtained on I-N instead of IV-N.

During the months of December and January the writer, in collaboration with Dr. J. Phillips, examined a number of possible atmospheric gases in the Yerkes Observatory laboratory without finding a clue as to the identification of the new features. The Hilger spectrograph was used, which closely matches the dispersion of the McDonald Cassegrain spectrograph, about 200 A/mm in the near infrared. It was found that the absorptions are not caused by CH_4, C_2H_4, C_2H_6, CO, CO_2, or NH_3, and probably not by H_2S and N_2O. Dr. Phillips and the writer will publish the laboratory results more extensively in due course. In addition, Dr. Phillips has obtained a beautiful series of high-dispersion spectra (2.5 A/mm) of CH_4. They show no trace of CH_4 lines from about λ 7422 to λ 7594 with a path-length of 800 meter-atmospheres; this result practically rules out the possibility that the new features are CH_4 bands somehow strengthened as a result of the low Uranus temperature. The same holds true for a weaker absorption at λ 7471, reported below.

Obviously, improved Uranus spectra were highly desirable. It appeared that the McDonald infrared grating spectrograph (dispersion 50 A/mm)[2] was fast enough for the purpose, owing to the comparatively fast camera, *f*/3, employed. Dr. P. D. Jose, assisted

[1] *The Atmospheres of the Earth and Planets* (Chicago: University of Chicago Press, 1949), chap. xii; also *McDonald Observatory Contr.*, No. 161.

[2] W. A. Hiltner, *Ap. J.* **105**, 212, 1947.

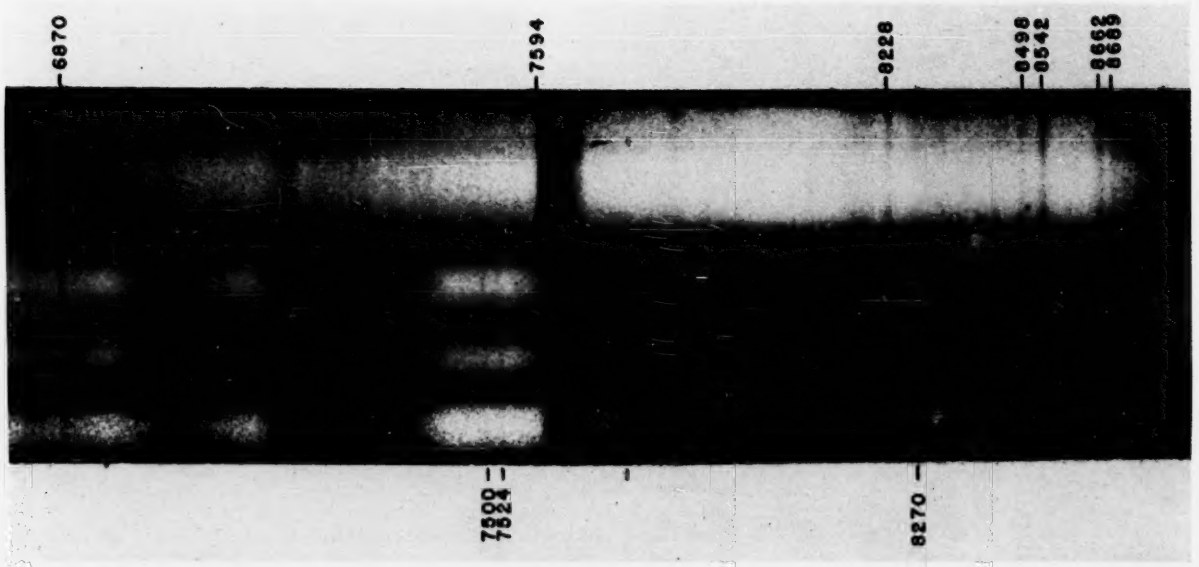

FIG. 1.—Three spectra of Uranus with Venus (*above*) for comparison. λλ 7500, 7524, and 8270 are unidentified; λ 8689 in Venus is due to CO_2

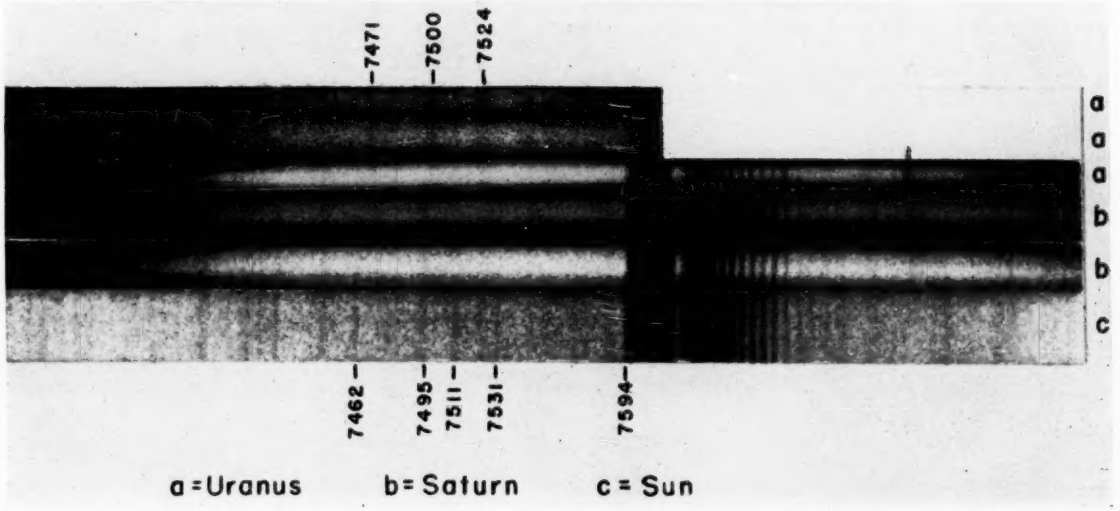

FIG. 2.—Spectra of Uranus showing unidentified bands at λλ 7471, 7500, and 7524. Saturn and sun for comparison

by Mr. W. C. Braun, kindly obtained several spectra of Uranus and Saturn, the best of which are reproduced in Figure 2. The absorptions at λ 7500 and λ 7524 are confirmed, and a third one, at λ 7471, is added. The grating spectra show that the three absorptions have a definite width and must therefore be unresolved molecular bands; the widths are, in order of wave length, about 2–3, 4, and 5 A, respectively.

In Figures 1 and 2 there is some similarity in appearance between the three new features and the somewhat stronger absorption at about λ 7731, marked on both plates. The λ 7731 absorption is due to CH_4, however, and appears broken up into numerous lines on Dr. Phillips' high-dispersion plates. The laboratory plates appear to rule out any relation between the λ 7731 band and the λ 7500 group.

NOTE ADDED IN PROOF

After the above was written, it was found that Neptune exhibits the same absorption bands, in nearly the same intensities; furthermore, the weak band suspected in Figure 2 at about λ 7546 is also seen in the Neptune spectrum and is therefore probably real. A fifth band may be present near λ 7570, but the presence of the Fraunhofer line λ 7569 makes this uncertain. The new system is therefore composed of four or five bands, nearly evenly spaced, of which λ 7500 and λ 7524 are the strongest.

GERARD P. KUIPER

YERKES AND MCDONALD OBSERVATORIES
April 10, 1949

THE SPECTRUM OF AR PAVONIS

AR Pavonis[1] was announced to be an eclipsing variable of P Cygni spectrum, by M. W. Mayall[2] in 1937. The magnitude estimations—900 in number—were made on Harvard chart plates, which cover the years from 1889 to 1936, and they led to the following elements:

$$\text{Min.} = \text{JD } 2411255 + 605^{d}E\,.$$

However, the determinations of the brightness do not fall upon a smooth light-curve. Quoting Mrs. Mayall's paper: "At times the maximum reaches 8.5 mag. or 9.0 mag. and at other times it is fainter than 11.0 mag. The observations at minimum are not sufficient to show any definite relation between the brightness at maximum and at minimum. The range between any one epoch is generally about three magnitudes, but the range varies and a bright minimum does not always follow a bright maximum." Mrs. Mayall's analysis of the photometric material suggested a 7-year wave and one of about 35 years superimposed upon the 605-day period. "Long-exposure photographs show no evidence of surrounding nebulosity or unevenness of star background which might account for the variation of magnitude at maxima."

The spectrum of AR Pavonis is known from three Harvard objective-prism plates taken in 1900, 1901, and 1908; the two first spectra showing "$H\beta$, $H\gamma$, $H\delta$, and $H\epsilon$ in emission with strong absorption edges toward the violet," and the third plate showing "bright lines near λ 4686 and λ 4640, in addition to the hydrogen lines." According to the published features, the star was included in Merrill and Burwell's list of Be and Ae stars[3] under the designation "MWC 600."

[1] $\alpha = 18^{h}15^{m}4$; $\delta = -66°6'$ [1950.0]. CPD−66°3307 = HV 7860.

[2] *Pub. A.A.S.*, **9**, 13, 1937; *Harvard Ann.*, **105**, 491, 1937; see also Campbell, *Pop. Astr.*, **45**, 95, 1937.

[3] *Ap. J.*, **98**, 153, 1943; *Mt. W. Contr.*, No. 682.

TABLE 1

THE SPECTRUM OF AR PAVONIS

Measured Wave Lengths*	Estimated Intensities†	Identifications‡
3670.77	1 E	*H* 3671.48
3671.69	A	
3672.95	1 E	*H* 3673.76
3674.36	A	
3675.49	1 E	*H* 3676.36
3678.66	1 E	*H* 3679.36
3681.91	1 E	*H* 3682.81
3685.93	1 E	*H* 3686.83
3689.46	A	
3690.52	1 E	*H* 3691.56
3696.47§	2 E	*H* 3697.15
3700.06	1 E	
3704.31	2 E	*H* 3703.86, *He* I 3705.00 (3), *He* I 3705.14 (1)
3711.60	2 E	*H* 3711.97
3714.78	1 E	
3715.92	A?	
3720.03	A	
3721.16	3 E	*H* 3721.94
3727.38	A	
3729.73	A?	
3732.35	A	
3733.70	2 E	*H* 3734.37, *He* I 3732.86 (1), *He* I 3732.99 (1)
3749.28	3 E	*H* 3750.15
3769.99	4 E	*H* 3770.63
3795.51	A	
3797.07	5 E	*H* 3797.90
3809.37	A?	
3817.64	A	
3818.70	1 E	*He* I 3819.61 (4), *He* I 3819.76 (1)
3833.10	A?	
3834.38	8 E	*H* 3835.39
3852.64	0 E	*Si* II 3853.66 (3)
3854.76	2 E	*Si* II 3856.02 (8)
3861.65	0–1 E	*Si* II 3862.59 (6)
3867.66	15 E	*He* I 3867.48 (2), *He* I 3867.63 (1), [*Ne* III] 3868.74
3886.62	A	
3888.14	20 E	*He* I 3888.65, *H* 3889.05
3962.57	A	
3963.72	5 E	*He* I 3964.73 (4)
3966.38	5 E	[*Ne* III] 3967.51
3969.17	20 E	*H* 3970.07
4008.23	0–1 E	*He* I 4009.22 (1)
4024.21	A	
4025.20	3 E	*He* I 4026.19 (5), *He* I 4026.36 (1)
4101.07	25 E	*H* 4101.74, *N* III 4103.37 (9)
4143.67	3 E	*He* I 4143.76 (2)
4174.56	A	
4231.94	6 E	*Fe* II 4233.17 (11)
4339.58	30 E	*H* 4340.47
4350.77	5 E	*Fe* II 4351.76 (9)

* From Plate I 132 of June 17, 1948, except *Hα*.

† "E" means emission; "A," absorption. No intensity estimations have been made for the *He* I 4922, [*O* III] 4959, and [*O* III] 5007 lines because they were present only on the 103*a*-O plates.

‡ The laboratory intensities are from Miss Moore's *Multiplet Table* (*Contr. Princeton U. Obs.*, No. 20, 1945).

§ Violet absorption?

TABLE 1—*Continued*

Measured Wave Lengths*	Estimated Intensities†	Identifications‡
4362.10	20 E	[*O* III] 4363.21
4369.39	A?	
4386.80	5 E	*He* I 4387.93 (3)
4469.90	A	
4470.71	8 E	*He* I 4471.48 (6), *He* I 4471.69 (1)
4480.14	0–1 E	*Mg* II 4481.23 (100)
4518.96	0–1 E	*Fe* II 4520.22 (7)
4521.59	0–1 E	*Fe* II 4522.63 (9)
4527.52	0 E	*Al* III 4529.18 (10)?
4540.67	1 E	*He* II 4541.59
4543.24	A	
4548.52	0–1 E	*Fe* II 4549.47 (10)
4554.55	0–1 E	*Fe* II 4555.89 (8)
4557.31	0–1 E	*Cr* II 4558.66 (100)
4583.06	1 E	*Fe* II 4583.83 (11)
4628.41	1 E	*Fe* II 4629.34 (7)
4632.65	1 E	*N* III 4634.16 (9)
4639.74‖	5 E	*N* III 4640.64 (10), *N* III 4641.90 (7)
4643.28	A	
4646.26‖	5 E	*C* III 4647.40 (20), *C* III 4650.16 (19), *C* III 4651.35 (18)
4679.82	A?	
4684.27	15 E	*He* II 4685.68
4710.47	A	
4712.02	1 E	*He* I 4713.14 (3), *He* I 4713.37 (1)
4860.44	30 E	*H* 4861.33
4920.60	E	*He* I 4921.93 (4)
4957.69	E	*O* III] 4958.91
5005.55	E	[*O* III] 5006.84
6561.94	300 E	*H* 6562.82

‖ Wide emission.

In order to study with more detail the spectrum of such a peculiar eclipsing star, the object has been included on the spectrographic program of the 60-inch reflecting telescope at the Bosque Alegre Astrophysical Station of the Córdoba Observatory. Five spectrograms (dispersion of about 42 A/mm) were obtained in June, 1948, on Eastman 103*a*-O and 103*a*-F emulsions, covering all the way from the ultraviolet region up to *Hα*. Figure 1 is an enlargement of the O plate obtained on June 17, 1948, showing the appearance of the spectrum from the ultraviolet to λ 5506. A reproduction of one of the F plates is not published because the exposure times of those plates were such that toward the red of *Hβ* only *Hα* is present. Table 1 lists the measured wave lengths of both the emission and the absorption features and the estimated intensities and the identifications of the bright lines.

Our spectrograms of AR Pavonis show a relatively strong early-type absorption spectrum, upon which a set of emission lines of *H*, *Mg* II, *Fe* II, *Si* II, *Cr* II, *He* I, *He* II, [*O* III], [*Ne* III], *C* III, and *N* III appear superimposed. *Si* II 4128–31 are either absent or extremely weak and *Mg* II 4481 very weak. There may also be present a few emission lines which cannot be detected without having widened spectrograms and/or using emulsions of more contrast; *N* III 4097 is probably among them—on our enlargement it is just possible to guess it.

Some of the emission lines are accompanied by a violet absorption, the strongest of

all the absorption lines belonging to *He* I 3888.65, a fact which is similar to the one previously observed in β Lyrae,[4] for instance.

The radial velocities, obtained from the measurement of the emission lines on the different spectrograms secured, are shown in Table 2.

The star will be kept on the observing program.

TABLE 2

RADIAL VELOCITIES FROM THE EMISSION LINES

Plate*	Date (1948)	U.T.	Exposure Time (Minutes)	Emulsion	Radial Velocity (Km/Sec)	No. of Lines
I 120	June 3	6:36	122	103*a*-O	−44.7	6
132	17	5:46	150	103*a*-O	−68.0	48
144	18	8:04	95	103*a*-F	−40.1	4
152	19	8:48	167	103*a*-F	−51.1	6
161	20	6:28	80	103*a*-O	−49.9	3

* The equivalent slit-width was 1.5 A.

JORGE SAHADE

OBSERVATORIO ASTRONÓMICO
CÓRDOBA, ARGENTINA
December 16, 1948

DISPLACED ABSORPTION LINES IN THE SPECTRUM OF UPSILON SAGITTARII*

1. On a spectrogram of υ Sagittarii taken at the McDonald Observatory on April 8, 1948, the *Hα* line shows a well-pronounced P Cygni structure. A strong absorption line is seen, displaced about 270 km/sec to the violet of the rather broad emission line normally present. Displaced components of other hydrogen lines and probably of two helium lines are visible as well. On a spectrogram taken 22 days later, not covering the *Hα* region, no displaced components are seen. Only one previous observation has been published of a strong absorption component at *Hα*, although this region of the spectrum has been studied on several occasions. Greenstein and Merrill[1] state: "Among the spectra available, only one plate (G 175, taken on July 24, 1928) shows a strong absorption component near *Hα*. The measured displacement with respect to the center of the bright line is −323 km/sec."

The P Cygni characteristic in the spectrum of υ Sagittarii is thus rather rare. But "violet satellites" of the hydrogen lines were first observed many years ago at Harvard, and Miss Maury's results concerning them[2] will be discussed below.

2. The displaced absorption lines observed at the McDonald Observatory are those of *Hα*, *Hβ*, *Hγ*, *Hδ*, and two lines probably arising from metastable levels of the helium atom, λ 3889 and λ 3965. The dispersion ranges from 16 A/mm at λ 3889 to 114 A/mm at *Hα*. Because of the low dispersion at *Hα*, little can be said of the structure of the absorption line. While it does not appear to be very narrow, the line is certainly considerably weaker than the normal absorption *Hα* of φ Cassiopeiae, an A5 supergiant. At *Hβ*

[4] J. G. Baker, *Harvard Ann.*, **105**, 107, 1937.

* *Contributions from the McDonald Observatory, University of Texas*, No. 167.

[1] *Ap. J.*, **104**, 177, 1946; *Mt. W. Contr.*, No. 723.

[2] *Harvard Bull.*, 824, 1925.

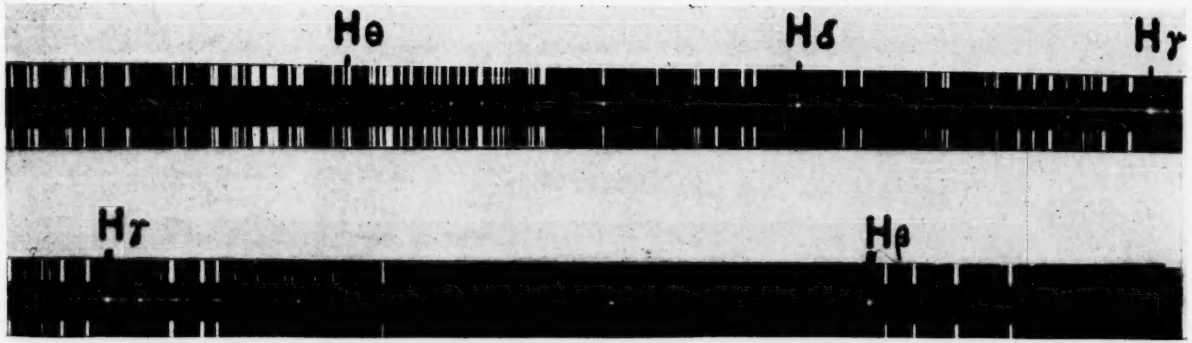

FIG. 1.—The spectrum of AR Pavonis taken on June 17, 1948

the displaced component is considerably stronger than the normal line, while the components of $H\gamma$ and $H\delta$ are definitely weaker than the stellar lines proper. As for the helium lines, the line ascribed to the displaced component of λ 3889 may be partly that due to $H\zeta$, though the weakness of the violet component of $H\epsilon$ makes this possibility unlikely. There is a strong stellar line normally at the position of the presumed violet satellite of λ 3965, but the displaced component is probably also present. The velocity differences measured between the displaced components and the stellar lines are given in the accompanying tabulation.

Line	Velocity (Km/Sec)	Line	Velocity (Km/Sec)
$H\alpha$	−270	$H\delta$	−320
$H\beta$	−300	He λ 3965	−280
$H\gamma$	−310	He λ 3889	−280

3. The peculiarities of the normal spectrum of υ Sagittarii have been emphasized by several investigators.[1, 3] The observable layers of the star appear to be characterized by an abnormally low hydrogen content, while the spectrum contains numerous high-excitation lines due to the rare gases and the ionized metals. These lines are abnormally strong in υ Sagittarii. The star has also been found to be the primary of a spectroscopic binary system. Wilson's orbit[4] represents recent observations well; the period is nearly 138 days, the eccentricity small. It was shown by Plaskett[5] that all absorption lines in the spectrum share in the velocity variation; no trace of the spectrum of the other component has yet been found.

4. It is of interest to determine whether the appearance of violet-displaced components of the hydrogen lines is associated with any particular phase of the spectroscopic orbit. The P Cygni structure of $H\alpha$ has been observed only twice, both times fairly near the phase at which an eclipse of the primary would occur, were the constants of the system such as to make this possible. From Wilson's elements the phase at which an eclipse of the primary might occur is about 20 days; the phases of the two observations of the strong displaced absorption component at $H\alpha$ are 10 and 35 days, respectively, for the Mount Wilson and McDonald observations. Miss Maury's observations made on Harvard objective-prism plates[2] support the view that the violet-displaced absorptions are limited to certain phases. She found, on occasion, strong displaced components of hydrogen and helium at a velocity of about −280 km/sec. These displaced components occurred *without exception* during an interval of about 4 weeks centered on phase 20 days, although many plates were available at other phases. However, Miss Maury emphasized that the phenomenon was unpredictable, for the spectrum was sometimes found to be normal even within the stated interval. This is in agreement with the Mount Wilson result[1] that several spectrograms obtained during this part of the cycle did *not* show a P Cygni structure of the $H\alpha$ line.

Miss Maury's results were based on spectra taken over many years. Somewhat later Plaskett[5] discussed the question of the violet satellites. He confirmed the existence of the displaced lines at about −300 km/sec and also observed components at −150 and −200 km/sec. In contradiction to Miss Maury's results, however, he stated that the dis-

[3] A. J. Cannon, *Harvard Ann.*, **56**, 108, 1912; J. S. Plaskett, *Pub. Dom. Ap. Obs., Victoria*, **4**, 1, 1927, and 111, 1928; W. W. Morgan, *Ap. J.*, **79**, 513, 1934, and *Pub. Yerkes Obs.*, Vol. 7, Part III, 1935; P. W. Merrill, *Pub. A.S.P.*, **51**, 218, 1939; J. L. Greenstein, *Ap. J.*, **91**, 438, 1940, and **97**, 252, 1943; H. F. Weaver, *Ap. J.*, **98**, 131, 1943; P. W. Merrill, *Pub. A.S.P.*, **55**, 242, 1943, and **56**, 42, 1944; and J. L. Greenstein and W. S. Adams, *Ap. J.*, **106**, 339, 1947; *Mt. W. Contr.*, No. 738.

[4] *Lick Obs. Bull.*, **8**, 132, 1915. The final value of V_0 given in this paper should be changed to +8.4 km/sec; this requires a further correction of −0.2 km/sec to reduce the velocity to the system of *Lick Pub.*, Vol. 16. In computing the radial velocity from Wilson's orbital elements, one should therefore use $V_0 = +8.2$ km/sec.

[5] *Op. cit.*

placed components were present throughout the entire cycle of the star, although they varied appreciably in intensity. This discrepancy between the two series of observations has not been explained. It is probably partly due to the fact that Plaskett's observations covered only about 1½ years. It seems that much more striking changes occurred in the spectrum during the period covered by Miss Maury's observations than during that covered by Plaskett's. The data given by the latter show that the −300 km/sec component, which is the most persistent of all, is definitely stronger during the third of the period centered on phase 20 days than it is during the remainder of the cycle; it does appear, however, that displaced components of lesser velocity and varying intensity (i.e., at $H\beta$) may occur at almost any phase of the orbit. The Harvard observations and those at the $H\alpha$ line agree in suggesting that the displaced components are strongest near the time at which the observed star is farthest from the earth.

The violet satellite lines will be seen only when the matter absorbing them is viewed against the background of the primary star. We may suppose, therefore, that these lines arise from matter traveling from the primary mainly toward the secondary star. If this explanation is correct, one would not expect to observe displaced components at other phases. An alternative hypothesis would be that matter is ejected from the primary star in all directions but that high velocities are attained only by the matter traveling in the general direction of the secondary. The very small light-variation found by S. Gaposchkin[6] implies that the fainter (unobserved) component of the system of υ Sagittarii possesses the higher surface brightness, and consequently it must be the smaller of the two stars. The hypothesis sketched above is consistent with this picture of the system.

We are familiar with the idea of stream motions in binary systems through the work of Struve on such stars as β Lyrae,[7] SX Cassiopeiae,[8] φ Persei,[9] and many others. In many instances the velocity differences between the lines arising from the streaming gases and those arising from the star are rather small, so that distortions of the radial velocity-curves result. In υ Sagittarii this is not the case. Another difference is the fact that the process of ejection of matter in υ Sagittarii appears to be markedly discontinuous, *appearing in some cycles but not in others*, while in those systems studied by Struve the stream motions appear to be continuous.

5. Aside from the violet components of the hydrogen and helium lines, the Harvard investigators have also found occasional changes in the *general* spectrum of υ Sagittarii. These take the form of a blurring or weakening of the low-temperature features of the spectrum (the *Ti* II lines, for example), so that the spectrum appears to be similar to that of a B8 star. The fullest development of this "B8 spectrum" was observed at Harvard only during the time when the displaced components occurred. A Yerkes spectrogram taken on April 25, 1911, shows this phase well. The *Ti* II lines are very noticeably weakened, and the metallic spectrum resembles cB9. The phase of this spectrogram is 55 days, near quadrature in the binary orbit. No displaced components are visible.

The important and puzzling complexities in the absorption and emission lines which have been studied at the Mount Wilson Observatory have not been considered in this discussion. The permanent existence of emitting masses of gas of both high and low velocity is shown by the emission lines in the red and infrared regions of the spectrum. The importance of continuous observations throughout the orbital period of this binary system is apparent, especially if such observations could be made during the more active periods of the system.

W. P. BIDELMAN

YERKES OBSERVATORY
January 21, 1949

[6] *A.J.*, **51**, 109, 1945.
[7] *Ap. J.*, **93**, 104, 1941.
[8] *Ap. J.*, **99**, 89, 1944.
[9] *Pop. Astr.*, **49**, 129, 1941.

A CATALOGUE OF THE BRIGHTER METALLIC-LINE STARS

A program of obtaining spectra of the *Henry Draper* type B8–A5 stars brighter than the fifth magnitude and north of declination −20° has recently been completed by a group under the direction of W. W. Morgan at the Yerkes Observatory. An examination of these spectra, obtained with a small spectrograph attached to the 40-inch telescope having a dispersion of about 60 A/mm at $H\gamma$, has revealed a number of new members of the "metallic-line" star class of peculiar A stars. The criteria distinguishing this group have been listed by Roman, Morgan, and Eggen[1] as follows: (1) The K line is considerably weaker than would be expected for the average metallic-line type; (2) there is no possibility of explaining the spectrum in terms of one or two normal stars; and (3) the metallic-line stars show no obvious similarity to recognized "shell-spectrum" types and are readily distinguishable from the "silicon"-"strontium"-"europium" groups.

TABLE 1

THE BRIGHTER METALLIC-LINE STARS

Star	α (1900)	δ (1900)	*m*	*Ca* II K	Metallic Lines	*H* Lines	HD Type
α Gem B	7^h28^m2	+32° 6′	2.85	A1	A5	A5	A0
60 Leo	10 57.0	+20 43	4.42	A1	A5	A5	A0
ζ Eri	3 11.0	− 9 11	4.90	A2	A7	A8	A3
ζ UMa(ft)	13 19.9	+55 27	3.96	A2	A7	A8	A2
λ Vir	14 13.7	−12 55	4.60	A2	A7	A8	A2
υ Oph	16 22.4	− 8 9	4.68	A2	A7	A7	A2
ω Tau	4 11.4	+20 20	4.80	A2	F5 IV=F0 II–III	F0	A3
15 UMa	9 1.8	+52 0	4.54	A2	F5 IV=F0 II–III	F0	A3p
25 ν^2 Dra*	17 30.3	+55 14	4.95	A2	F5 IV=F0 II–III	F0	A5
ξ Cep	22 0.9	+64 8	4.57	A2	F5 IV=F0 II–III	F0	A3
88 Tau	4 30.2	+ 9 57	4.38	A3	A7	A8	A3
μ Ori	5 56.9	+ 9 39	4.19	A3	A7	A8	A2
ε Ser	15 45.8	+ 4 47	3.75	A3	F0	A5	A2
ζ Lyr A	18 41.3	+37 30	4.29	A4	F0	A7	A3
μ Aqr	20 47.3	− 9 22	4.80	A4	F5 IV=F0 II–III	F0	A3
τ UMa	9 2.7	+63 55	4.74	A5	F6 II	F0	A5, F5
15 Vul	19 57.0	+27 29	4.74	A6	F5 IV=F0 II–III	A8	A5
θ Cep	20 27.9	+62 39	4.28	A6	F5 IV=F0 II–III	A8	A5
δ Cap	21 41.5	−16 35	2.98	A6	F5 IV=F0 II–III	F2	A5

* Both members of the binary, ν Draconis, seem to exhibit peculiar spectra. The K-line and metallic-line types of 24 ν^1 Draconis are A4 and A7, respectively, sufficiently different to indicate that the star is probably peculiar but not different enough to justify designating it as a metallic-line star. Two other bright, northern A stars, α Cancri and μ Aurigae, have similar spectra.

Table 1 contains 19 stars which differ sufficiently in their K-line and metallic-line types as to be considered definite members of the metallic-line class, and it is probably complete for stars brighter than the fifth magnitude and north of declination −20°. Seven were previously known to be metallic-line stars, and four of these were used as standards in classifying the twelve new members.

It may be of interest to compare the total of 19 stars in Table 1, which we assume to be complete, with the total number of A and F stars lying within the same limits of brightness and declination. The *Henry Draper* types of all the objects listed lie between A0 and A5, and the *Henry Draper Catalogue* contains 225 stars (excluding those exhibiting composite spectra) within these limits. Therefore, it seems reasonable to suppose that, to a given limiting apparent magnitude, nearly 10 per cent of all stars classified as A0–A5 on objective-prism plates will be metallic-line stars. It has been shown,[1, 2] how-

[1] *Ap. J.*, **107**, 107, 1948.

[2] W. W. Morgan and W. P. Bidelman, *Ap. J.*, **104**, 245, 1946.

ever, that the intrinsic colors of the metallic-line stars correspond to the type derived from the metallic lines and that the absolute magnitudes are similar to main-sequence objects of early F type. Taking the mean absolute magnitude of the metallic-line stars in Table 1 as +2.5 and that of the A0–A5 stars in the *Henry Draper Catalogue* as +1.0, the latter will occupy a volume of space some eight times larger than that occupied by the metallic-line stars. Therefore, in classifying A0–A5 stars from objective-prism plates and reducing the results to a given volume of space, over 40 per cent of the stars thus classified would be metallic-line stars. Since the metallic-line types of the stars listed range from A5 to F6, we may regard them as A5–F6 main-sequence stars and compare them with the total number of normal A5–F6 main-sequence stars within the same limits of brightness and declination. This is essentially a comparison per volume of space and indicates that the metallic-line stars represent about 15 per cent of the total number of A5–F6 stars.

ARNE SLETTEBAK

YERKES OBSERVATORY
February 17, 1949

UPPER LIMITS ON THE ABUNDANCES OF INTERSTELLAR *Li* AND *Be**

The discovery[1, 2, 3] that the *Li* line at λ 6707.8 A is moderately strong in the spectra of certain N-type stars suggests that thermonuclear reactions in these stars have not yet converted *Li* into *He* and that the primitive abundance of *Li* in the prestellar stage was considerably higher than the low value now obtaining in the sun. If this explanation is correct, one might expect *Li*, perhaps together with *Be* and *B*, to be relatively abundant also in interstellar space.

While the *B* atom has no accessible resonance lines, the resonance lines of *Li* I at λ 6707.74 and λ 6707.89 and of *Be* II at λ 3130.416 and λ 3131.064 fall in the observable region of the spectrum. A search for these lines in the spectra of distant B stars was therefore made with the coudé spectrograph of the 100-inch telescope at the Mount Wilson Observatory.

The stars examined are given in Table 1, together with their color excesses and distances,[4] and the cameras used in the ultraviolet and red. For χ^2 Ori the distance is taken from unpublished work by W. W. Morgan on B-type supergiant stars. For the plates taken in the ultraviolet, half the grating was covered to reduce the scattered light. The emulsions used were Eastman II*a*-O and 103*a*-E for the ultraviolet and red, respectively. The resonance lines of *Li* and *Na* could be photographed at the same time, and the red plates were all taken during an investigation of the components of interstellar D lines.

No certain trace of either the *Li* or the *Be* lines could be detected on the spectrograms obtained. The maximum equivalent width which would escape resolution may be conservatively estimated as 0.01, 0.02, and 0.07 A with the 114-, 73-, and 32-inch camera, respectively, in the first order, which was used for the red plates. Since the ultraviolet spectra were photographed in the second order, the maximum equivalent width of either of the *Be* II lines in the four stars investigated is 0.035 A.

The corresponding upper limits for the total number of *Li* I and *Be* II atoms in the

* This article is based on observations made by the author as guest investigator at the Mt. Wilson and Palomar Observatories.

[1] A. McKellar, *Pub. A.S.P.*, **52**, 407, 1940; *Observatory*, **64**, 4, 1941.

[2] R. S. Sanford, *Ap. J.*, **99**, 145, 1944.

[3] A. McKellar and W. H. Stilwell, *J.R.A.S. Canada*, **38**, 237, 1944.

[4] J. Stebbins, C. M. Huffer, and A. E. Whitford, *Ap. J.*, **91**, 20, 1940.

line of sight, per square centimeter, may be computed from the standard formulae for lines on the linear portion of the curve of growth. If these values are divided by the distances in Table 1, upper limits on the density are obtained. For *Li* I, the two lines overlap, and the effective oscillator strength is about 1; computed upper limits on the density of *Li* I range from about 2×10^{-11} cm^{-3} for HD 199478 to 2×10^{-10} cm^{-3} for HD 212978 and HD 217050. If we omit these last two stars in Table 1, we find an average upper limit of about 5×10^{-11} cm^{-3}. These values may be compared with an over-all average density[5] for *Na* I of 7×10^{-9} cm^{-3}. The *Be* II lines would be resolvable, and the oscillator strength of the stronger line is about $\frac{1}{2}$. Therefore the total number of absorbing *Be* II atoms in the line of sight to each of the 4 stars observed in the ultraviolet is less than 8.0×10^{11} per square centimeter. The corresponding space density of *Be* II atoms is less than about 9×10^{-10} cm^{-3} for the three stars at about 300 pc, and about one-fourth this value for χ^2 Ori.

To compare the total abundance of *Li* and *Be* with that of *Na*, it is necessary to take the relative ionization into account. The ionization potentials of *Li* I and *Na* I are 5.37

TABLE 1

LIST OF STARS OBSERVED

STAR		E_1 (MAG.)	r (PC)	CAMERA USED FOR	
				Ultraviolet	Red
HD 30836	3 Ori	0.00	230	.....	73
36822	37 Ori	+ .04	420	.....	73
36861	λ^1 Ori	+ .01	420	32	73
37468	σ Ori	+ .06	290	.....	73
41117	χ^2 Ori	+ .19	1200	32	32
197345	α Cyg	− .05	280	32	114
190429br		.....	.....	.....	32
199478		+ .22	870	.....	73
212978		+ .01	440	.....	32
217050		+0.02	290	32	32

and 5.12 volts, respectively. This difference is so small that it has only a very small effect on the relative ionization. However, one must also consider Strömgren's correction[6] to the ionization equation, which takes into account the actual probability of ionization from the ground state and which is surprisingly different for these two atoms. Since the absorption coefficient of unexcited *Li* I near the series limit is apparently about twenty times the corresponding value for *Na* I,[7] the number of Li^+ ions per neutral *Li* atom will be about twenty times the corresponding value for *Na*. Thus the upper limit on the total number of *Li* atoms in interstellar space per cubic centimeter is increased to about one-tenth of the corresponding number of *Na* atoms.

In the sun this *Li-Na* ratio is found[8] to be about 6×10^{-6}. In the N star WZ Cas, and

[5] L. Spitzer, Jr., *Ap. J.*, **108**, 276, 1948. On p. 303, 10^{-8} atoms/cm^3 should be replaced by 10^{-9} atoms/cm^3; correct values are given in the summary on p. 304 and in the abstract.

[6] *Ap. J.*, **108**, 242, 1948.

[7] M. Rudkjøbing, *Dr. Kgl. Danske Vidensk. Selskab. Mat.-fys. Medd.*, Vol. **18**, No. 2, 1940; B. Trumpy, *Zs. f. Phys.*, **71**, 720, 1931.

[8] H. N. Russell, *Ap. J.*, **70**, 11, 1929.

probably also[2] in WX Cyg, the value of this ratio appears to be considerably greater. The observed equivalent width[3] of the two blended D lines in WZ Cas is 56 A, while the corresponding equivalent width for *Li* is 8.4 A. Both lines are presumably on the square-root section of the curve of growth. The damping constant γ for impact of *Li* with neutral *H* atoms should be about four-ninths as great as that for *Na*, since for such impacts γ is proportional to the square of the quantum number of the excited state. Thus we find that the ratio of neutral atoms of *Li* and *Na* in WZ Cas is about 5×10^{-2}. Since the relative ionization of *Li* is unlikely to be greater than that of *Na*, the over-all *Li-Na* ratio is not likely to exceed 5×10^{-2}. Thus the dispersion used in the present work is not sufficient to detect interstellar *Li* if its abundance relative to *Na* is no greater than in WZ Cas.

According to V. M. Goldschmidt,[9] the relative abundance of *Li* in the surface rocks of the earth and in stony meteorites is found to be considerably greater than in the sun, with *Li-Na* ratios of 7.6×10^{-3} and 2.3×10^{-3} for the earth and for meteorites, respectively. According to H. Brown,[10] the best value for the *Li-Na* ratio in stony meteorites is about 1.3×10^{-3}; however, this value is not believed to be precise to better than a factor of 2. These values of the *Li-Na* ratio are appreciably less than the upper limit found in WZ Cas; a *Li* abundance of this order would apparently be difficult to detect in interstellar space.

The upper limit on the density of *Be* is substantially less than that for *Li*. The first and second ionization potentials of *Be* are 9.28 and 18.13, respectively. It is evident from Strömgren's calculations[6] that the ratio of *Ca* III to *Ca* II is about 10 for the conditions of physical interest in interstellar space; the ionization potential of *Ca* II is 11.82 volts. One may infer that the ratio of *Be* II to *Be* I is even greater. On the other hand, the ratio of *Be* III to *Be* II should be very low in an *H* I region, where the ionizing radiation beyond the Lyman limit will mostly be absorbed. In *H* II regions, on the other hand, the ratio of *Be* III to *Be* II may considerably exceed unity, since the continuous absorption coefficient for an unexcited *Be* II atom is likely to be large, as in the isoelectronic atom *Li* I. According to present evidence,[5,6] the interstellar lines are formed mostly in obscuring clouds, where the hydrogen is neutral. If this assumption is correct for the four particular stars observed, then it follows that the total number of *Be* atoms in all stages of ionization in the line of sight to these stars is equal to the corresponding number of Be^+ ions. The average density of *Na* in space is somewhat uncertain, but a value of about 2×10^{-6} cm^3 is consistent with an average interstellar gas density of one *H* atom per cubic centimeter. The over-all *Be-Na* ratio in interstellar space on the basis of these assumptions is therefore less than 5×10^{-4} in the line of sight to the three near stars photographed and one-fourth of this, or about 10^{-4}, for χ^2 Ori.

These values are remarkably low. In the sun the *Be-Na* ratio is found[8] to be 4×10^{-6}. In meteorites and the earth's crust the *Be-Na* ratio appears to be about 4×10^{-4}, with again a possible error[10] of a factor of 2. While the upper limit in interstellar space should be decreased somewhat to allow for observational selection—the stars observed were those in which the D lines were unusually strong—it must be admitted that this upper limit is in any case highly tentative. The state of ionization of *Be* is not definitely known; and the average density of *Na* ions in space is about equally uncertain. Further work is desirable to indicate whether the *Be-Na* ratio is definitely less in interstellar space than in our planetary system. Such a conclusion, if confirmed, might have important cosmogonic consequences.

LYMAN SPITZER, JR.

PRINCETON UNIVERSITY OBSERVATORY
April 19, 1949

[9] "Geochemische Verteilungsgesetze der Elemente. IX. Die Mengenverhältnisse der Elemente und der Atom Arten," *Skrft. Utg. Norsk. Vidensk.-Akad. Oslo, Mat.-Nat. Kl., 1937*, No. 4 (Oslo, 1938).

[10] Informal communication.

THE ISOTHERMAL FUNCTION

Many years ago we made an extensive integration of the equation[1]

$$\frac{1}{\xi^2}\frac{d}{d\xi}\left(\xi^2\frac{d\psi}{d\xi}\right)=e^{-\psi},$$

which governs the distribution of matter in hydrostatic equilibrium under its own gravitation and at a constant temperature. This integration has been used in the various investigations of stellar models with isothermal cores which have been carried out at this observatory.[2] In view of the increasing importance of such models for stellar structure,[3] we have thought that it may be useful to publish our integration of the isothermal function.

In addition to the usual quantities, we have also tabulated the homology invariant functions

$$u=\frac{\xi\, e^{-\psi}}{\psi'} \quad \text{and} \quad v=\xi\psi',$$

which are useful in the construction of composite models.

We believe that the tabulated entries after rounding the last figure should be reliable to one or two units.

S. CHANDRASEKHAR
GORDON W. WARES

YERKES OBSERVATORY
March 14, 1949

WAVE LENGTHS OF THE (0, 0) BAND HEADS IN THE INFRARED SYSTEM OF *CN*

Recently Herzberg and Phillips published in this *Journal*[1] a new assignment of vibrational quantum numbers to the infrared *CN* bands near 10930 A. These bands were photographed at the National Bureau of Standards,[2] more than ten years ago, with the spectrograph in which is mounted the Anderson concave grating with 7500 lines per inch. The dispersion in the first-order spectrum is 10 A/mm. The light-source was an arc between graphite electrodes carrying 15 amperes from a 220-volt D.C. circuit. Measurements of three to ten spectrograms gave the following mean values for the wave lengths of the band heads: 10871.71 (2), 10925.74 (10), and 10963.75 (8). The numbers in parentheses are estimated intensities. A strong feature at 11048.42 (10) is probably a blend of several rotation lines.

C. C. KIESS

NATIONAL BUREAU OF STANDARDS
March 31, 1949

[1] For the notation see S. Chandrasekhar, *Introduction to the Study of Stellar Structure* (Chicago: University of Chicago Press, 1939), pp. 155–170.

[2] S. Chandrasekhar and L. R. Henrich, *Ap. J.*, **94**, 525, 1941; S. Chandrasekhar and M. Schönberg, *Ap. J.*, **96**, 161, 1942; M. Harrison, *Ap. J.*, **103**, 193, 1946, and **105**, 322, 1947; and P. Ledoux, *Ap. J.*, **105**, 305, 1947.

[3] A. Reiz, *Ann. d'ap*, **10**, 301, 1947; M. Schwarzschild and R. Richardson, *Ap. J.*, **108**, 373, 1948.

[1] *Ap. J.*, **108**, 163, 1948.

[2] *J. Res. Nat. Bur. Standards*, **20**, 37, 1938.

TABLE 1

ξ	ψ	$e^{-\psi}$	$-\psi'$	u	v	$\xi^2\psi'$	$\rho_c/\bar{\rho}$
0	0.00000000	1.0000000	0.0000000	3.000000	0.000000	0.000000	1.000000
.1	0.00166583	0.9983355	0.0333000	2.998002	0.003330	0.000333	1.001000
.2	0.00665337	0.9933687	0.0664010	2.992028	0.013280	0.002656	1.004001
.3	0.01493288	0.9851780	0.0991076	2.982145	0.029732	0.008920	1.009004
.4	0.02645548	0.9738914	0.1312320	2.968456	0.052493	0.020997	1.016012
.5	0.04115396	0.9596814	0.1625969	2.951106	0.081298	0.040649	1.025030
.6	0.05894408	0.9427595	0.1930388	2.930270	0.115823	0.069494	1.036061
.7	0.07972601	0.9233693	0.2224100	2.906158	0.155687	0.108981	1.049113
.8	0.10338606	0.9017788	0.2505811	2.879000	0.200465	0.160372	1.064193
.9	0.12979853	0.8782724	0.2774418	2.849049	0.249698	0.224728	1.081308
1.0	0.15882769	0.8531434	0.3029014	2.816571	0.302901	0.302902	1.100467
1.1	0.19032975	0.8266865	0.3268897	2.781841	0.359579	0.395537	1.121683
1.2	0.22415488	0.7991913	0.3493560	2.745136	0.419227	0.503073	1.144964
1.3	0.26014913	0.7709366	0.3702684	2.706733	0.481349	0.625754	1.170322
1.4	0.29815626	0.7421854	0.3896126	2.666904	0.545458	0.763641	1.197771
1.5	0.33801943	0.7131814	0.4073907	2.625912	0.611086	0.916629	1.227323
1.6	0.37958273	0.6841468	0.4236191	2.584007	0.677791	1.084465	1.258993
1.7	0.42269255	0.6552801	0.4383270	2.541427	0.745156	1.266765	1.292795
1.8	0.46719876	0.6267555	0.4515543	2.498393	0.812798	1.463036	1.328744
1.9	0.51295569	0.5987233	0.4633503	2.455106	0.880366	1.672695	1.366856
2.0	0.55982298	0.5713102	0.4737714	2.411755	0.947543	1.895086	1.407148
2.1	0.60766620	0.5446204	0.4828796	2.368505	1.014047	2.129499	1.449637
2.2	0.65635733	0.5187375	0.4907410	2.325509	1.079630	2.375186	1.494339
2.3	0.70577514	0.4937257	0.4974247	2.282897	1.144077	2.631377	1.541272
2.4	0.75580536	0.4696322	0.5030011	2.240785	1.207203	2.897286	1.590454
2.5	0.80634082	0.4464889	0.5075413	2.199274	1.268853	3.172133	1.641903
2.6	0.85728143	0.4243140	0.5111157	2.158447	1.328901	3.455142	1.695637
2.7	0.90853409	0.4031147	0.5137938	2.118378	1.387243	3.745557	1.751675
2.8	0.96001257	0.3828881	0.5156432	2.079125	1.443801	4.042643	1.810037
2.9	1.01163730	0.3636231	0.5167295	2.040733	1.498516	4.345695	1.870740
3.0	1.06333512	0.3453023	0.5171153	2.003242	1.551346	4.654038	1.933805
3.1	1.11503902	0.3279025	0.5168608	1.966676	1.602268	4.967032	1.999249
3.2	1.16668782	0.3113966	0.5160225	1.931057	1.651272	5.284070	2.067093
3.3	1.21822587	0.2957544	0.5146545	1.896397	1.698360	5.604588	2.137356
3.4	1.26960276	0.2809432	0.5128074	1.862701	1.743545	5.928054	2.210056
3.5	1.32077295	0.2669289	0.5105282	1.829970	1.786849	6.253970	2.285215
3.6	1.37169548	0.2536765	0.5078613	1.798198	1.828301	6.581882	2.362850
3.7	1.42233365	0.2411506	0.5048477	1.767379	1.867937	6.911365	2.442981
3.8	1.47265473	0.2293159	0.5015255	1.737500	1.905797	7.242028	2.525628
3.9	1.52262964	0.2181375	0.4979300	1.708546	1.941927	7.573515	2.610809
4.0	1.57223270	0.2075812	0.4940936	1.680501	1.976374	7.905498	2.698544
4.1	1.62144134	0.1976137	0.4900464	1.653346	2.009190	8.237680	2.788852
4.2	1.67023587	0.1882027	0.4858158	1.627060	2.040426	8.569791	2.881751
4.3	1.71859922	0.1793172	0.4814268	1.601622	2.070135	8.901582	2.977261
4.4	1.76651672	0.1709273	0.4769026	1.577010	2.098371	9.232834	3.075401
4.5	1.81397593	0.1630048	0.4722642	1.553202	2.125189	9.563350	3.176188
4.6	1.86096639	0.1555223	0.4675306	1.530173	2.150641	9.892947	3.279643
4.7	1.90747946	0.1484541	0.4627193	1.507900	2.174781	10.221469	3.385782
4.8	1.95350819	0.1417758	0.4578461	1.486359	2.197661	10.548774	3.494624
4.9	1.99904709	0.1354643	0.4529251	1.465529	2.219333	10.874732	3.606186
5.0	2.04409206	0.1294977	0.4479695	1.445385	2.239847	11.199237	3.720491
5.1	2.08864022	0.1238554	0.4429907	1.425905	2.259253	11.522188	3.837552
5.2	2.13268980	0.1185181	0.4379995	1.407065	2.277598	11.843512	3.957386
5.4	2.21929101	0.10868614	0.4280160	1.371222	2.311287	12.48095	4.205450
5.6	2.30389963	0.09986863	0.4180832	1.337687	2.341266	13.11109	4.464821
5.8	2.38653113	0.09194809	0.4082524	1.306297	2.367864	13.73361	4.735632
6.0	2.46721009	0.08482117	0.3985637	1.276903	2.391382	14.34829	5.018019
6.2	2.54596816	0.07839712	0.3890481	1.249363	2.412098	14.95501	5.312111
6.4	2.62284247	0.07259622	0.3797295	1.223544	2.430269	15.55372	5.618034
6.6	2.69787426	0.06734853	0.3706253	1.199325	2.446127	16.14444	5.935914
6.8	2.77110773	0.06259263	0.3617480	1.176592	2.459886	16.72723	6.265872
7.0	2.84258916	0.05827459	0.3531060	1.155240	2.471742	17.30219	6.608026
7.2	2.91236613	0.05434699	0.3447041	1.135172	2.481870	17.86946	6.962493
7.4	2.98048696	0.05076811	0.3365447	1.116298	2.490431	18.42919	7.329388
7.6	3.04700018	0.04750121	0.3286278	1.098535	2.497571	18.98154	7.708822
7.8	3.11195416	0.04451388	0.3209520	1.081808	2.503425	19.52672	8.100900
8.0	3.17539683	0.04177752	0.3135141	1.066045	2.508113	20.06490	8.505731
8.2	3.23737538	0.03926682	0.3063100	1.051183	2.511742	20.59628	8.923422

TABLE 1-Continued

ξ	ψ	$e^{-\psi}$	ψ'	u	v	$\xi^2\psi'$	R/F
8.2	3.23737538	0.03926682	0.3063100	1.051183	2.511742	20.59628	8.923422
8.4	3.29793612	0.03695937	0.2993351	1.037161	2.514415	21.12108	9.354065
8.6	3.35712434	0.03483529	0.2925838	1.023924	2.516221	21.63950	9.797763
8.8	3.41498415	0.03287693	0.2860501	1.011421	2.517241	22.15172	10.254614
9.0	3.47155848	0.03106857	0.2797279	0.999604	2.517551	22.65796	10.724708
9.2	3.52686898	0.02939623	0.2736107	0.988431	2.517218	23.15841	11.208136
9.4	3.58101599	0.02784739	0.2676920	0.977861	2.516305	23.65327	11.704994
9.6	3.63397856	0.02641090	0.2619652	0.967856	2.514866	24.14271	12.215363
9.8	3.68581441	0.02507674	0.2564237	0.958383	2.512952	24.62693	12.739332
10.0	3.73655997	0.02383596	0.2510612	0.949408	2.510612	25.10612	13.276975

ξ	ψ	$e^{-\psi}$	ψ'	u	v
10	3.73655997	0.02383596	0.2510612	0.949408	2.510612
11	3.97511952	0.018777057	0.2267131	0.911053	2.493844
12	4.19117842	0.015128447	0.2059457	0.881501	2.471348
13	4.38799408	0.012425629	0.1881317	0.858618	2.445712
14	4.56825346	0.010376066	0.1727558	0.840869	2.418581
15	4.73417833	0.008789668	0.1594003	0.827132	2.391005
16	4.88761436	0.007539388	0.1477278	0.816571	2.363645
17	5.03010344	0.006538134	0.1374657	0.808553	2.336917
18	5.16294168	0.005724834	0.1283929	0.802591	2.311072
19	5.28722535	0.005055769	0.1203294	0.798305	2.286259
20	5.40388741	0.004499057	0.1131274	0.795397	2.262548
21	5.51372659	0.004031057	0.1066652	0.793625	2.239969
22	5.61743057	0.003633966	0.1008417	0.792800	2.218517
23	5.71559468	0.003294191	0.0955726	0.792763	2.198170
24	5.80873691	0.003001218	0.0907872	0.793385	2.178893
25	5.89731020	0.002746823	0.0864256	0.794563	2.160640
26	5.98171237	0.002524500	0.0824371	0.796207	2.143365
27	6.06229439	0.002329051	0.0787786	0.798242	2.127022
28	6.13936715	0.002156288	0.0754129	0.800607	2.111561
29	6.21320709	0.002002804	0.0723080	0.803249	2.096932
30	6.28406094	0.001865808	0.06943642	0.806122	2.083093
32	6.41767169	0.0016324527	0.06429989	0.812420	2.057596
34	6.54171438	0.0014420143	0.05984538	0.819253	2.034743
36	6.65742606	0.0012844482	0.05595102	0.826440	2.014237
38	6.76582795	0.0011524929	0.05252153	0.833843	1.995818
40	6.86777147	0.0010407939	0.04948146	0.841361	1.979258
42	6.96397286	0.0009453334	0.04677039	0.848913	1.964356
44	7.05503961	0.0008630486	0.04433949	0.856441	1.950938
46	7.14149083	0.0007915711	0.04214884	0.863897	1.938847
48	7.22377312	0.0007290465	0.04016560	0.871249	1.927949
50	7.30227320	0.0006740049	0.03836248	0.878469	1.918124
52	7.37732783	0.0006252695			
54	7.44923187	0.0005818884			
55	7.4840848	0.00056195727	0.03450171	0.895830	1.897594
60	7.6484895	0.00047676374	0.03136331	0.912079	1.881799
65	7.7986151	0.00041030281	0.02876508	0.927155	1.869730
70	7.9368274	0.00035733838	0.02658032	0.941060	1.860622
75	8.0649553	0.00031436516	0.02471855	0.953834	1.853891
80	8.1844398	0.00027896067	0.02311346	0.965535	1.849077
85	8.2964345	0.00024940449	0.02171552	0.976232	1.845819
90	8.4018769	0.00022444568	0.02048701	0.985996	1.843831
95	8.5015380	0.00020315568	0.01939874	0.994899	1.842880
100	8.5960597	0.00018483267	0.01842785	1.003007	1.842785
105	8.6859815	0.00016893754	0.01755609	1.010387	1.843389
110	8.7717612	0.00015505026	0.01676883	1.017097	1.844571
115	8.8537906	0.00014283927	0.01605414	1.023195	1.846226
120	8.9324072	0.00013203980	0.01540223	1.028733	1.848268
125	9.0079040	0.00012243822	0.01480503	1.033755	1.850629
130	9.0805373	0.00011386042	0.01425576	1.038307	1.853249
135	9.1505319	0.00010616332	0.01374870	1.042429	1.856075
140	9.2180866	0.00009922837	0.01327906	1.046156	1.859068

TABLE 1-Continued

ξ	ψ	$e^{-\psi}$	ψ'	u	v
140	9.2160866	0.00009922837	0.01327906	1.046156	1.859068
145	9.2833780	0.00009295659	0.01284271	1.049522	1.862193
150	9.3465633	0.00008726481	0.01243613	1.052556	1.865420
155	9.4077838	0.00008208266	0.01205627	1.055286	1.868722
160	9.4671661	0.00007735030	0.01170049	1.057738	1.872078
165	9.5246250	0.00007301651	0.01136650	1.059933	1.875473
170	9.5808640	0.00006903728	0.01105226	1.061895	1.878884
175	9.6353776	0.00006537454	0.01075605	1.063638	1.882309
180	9.6884519	0.00006199531			
200	9.8878344	0.00005078815	0.00949605	1.069683	1.899210
225	10.1124639	0.00004057072	0.00851205	1.072411	1.915211
250	10.3150266	0.00003313148	0.00771984	1.072933	1.929960
275	10.4996104	0.00002754718	0.00706674	1.071990	1.943354
300	10.6692309	0.00002324940	0.00651806	1.070076	1.955418
325	10.8261826	0.00001987232	0.00604992	1.067536	1.966224
350	10.9722557	0.00001717156	0.00564538	1.064596	1.975883
375	11.1088768	0.00001497876	0.00529198	1.061425	1.984493
400	11.2372028	0.00001317482	0.00498042	1.058130	1.992168
425	11.3581863	0.00001167353	0.00470353	1.054793	1.999000
450	11.4726215	0.00001041127	0.00445574	1.051469	2.005083
475	11.5811785	0.00000934024	0.00423262	1.048196	2.010495
500	11.6844281	0.00000842398	0.00403061	1.045001	2.015305
525	11.7828607	0.00000763429	0.00384682	1.041900	2.019581
550	11.8769011	0.00000694908	0.00367888	1.038902	2.023384
575	11.9669199	0.00000635086	0.00352479	1.036018	2.026754
600	12.0532422	0.00000582563	0.00338290	1.033250	2.029740
625	12.1361551	0.00000536209	0.00325182	1.030596	2.032388
650	12.2159134	0.00000495103	0.00313035	1.028056	2.034728
675	12.2927442	0.00000458489	0.00301747	1.025628	2.036792
700	12.3668510	0.00000425740	0.00291229	1.023313	2.038603
725	12.4384166	0.00000396336			
750	12.5076063	0.00000369841	0.00272209	1.019001	2.041568
800	12.6394420	0.00000324160	0.00255478	1.015071	2.043824
850	12.7634002	0.00000286368	0.00240644	1.011509	2.045474
900	12.8803509	0.00000254762	0.00227403	1.008280	2.046627
950	12.9910281	0.00000228070	0.00215514	1.005348	2.047383
1000	13.0960569	0.00000205331	0.00204780	1.002691	2.047800
1050	13.1959740	0.00000185806	0.00195043	1.000277	2.047952
1100	13.2912436	0.00000168922	0.00186170	0.998089	2.047870
1150	13.3822697	0.00000154225	0.00178052	0.996105	2.047598
1200	13.4694066	0.00000141355	0.00170599	0.994296	2.047188
1250	13.5529661	0.00000130023	0.00163731	0.992660	2.046638
1300	13.6332245	0.00000119996	0.00157384	0.991171	2.045992
1350	13.7104273	0.00000111080	0.00151500	0.989825	2.045250
1400	13.7847941	0.00000103119	0.00146032	0.988599	2.044448
1450	13.8565218	0.00000095981	0.00140938	0.987481	2.043601
1500	13.9257878	0.00000089558	0.00136180	0.986473	2.042700
1550	13.9927521	0.00000083757	0.00131726	0.985565	2.041753
1600	14.0575601	0.00000078501	0.00127550	0.984734	2.040800
1650	14.1203437	0.00000073724	0.00123625	0.983989	2.039813
1700	14.1812233	0.00000069370	0.00119930	0.983318	2.038810
1750	14.2403091	0.00000065390	0.00116446	0.982711	2.037805
1800	14.2977019	0.00000061742	0.00113156	0.982159	2.036808
1850	14.3534945	0.00000058392	0.00110043	0.981671	2.035796
1900	14.4077722	0.00000055307	0.00107094	0.981234	2.034786
1950	14.4606138	0.00000052460	0.00104297	0.980840	2.033792
2000	14.5120922	0.00000049826	0.00101639	0.980501	2.032780
2050	14.5622750	0.00000047389	0.00099112	0.980194	2.031796
2100	14.6112247	0.00000045125	0.00096706	0.979922	2.030826
2150	14.6589998	0.00000043020			
2200	14.7056544	0.00000041059			

THE FUNCTIONS $G_{n,m}(\tau)$ AND $G'_{n,m}(\tau)$ OF ORDER 6 ($m = 6$ AND $m \geq n$)

In the appendix to the author's paper, "On the Radiative Equilibrium of a Stellar Atmosphere. XXIV,"[1] the various auxiliary functions needed in the approximate solution of the X- and Y-equations have been tabulated. Now for evaluating "the corrected second approximation" for cases in which the characteristic function $\Psi(\mu)$ contains a term in μ^4, we require the functions $G_{n,m}(\tau)$ and $G'_{n,m}(\tau)$ for all orders up to 6 ($m \geq n$ and $m \leq 6$). The functions of order up to 5 have been tabulated in Paper XXIV (Table 2, pp. 109 and 110).[2] We now supplement this table by the functions of order 6.

S. CHANDRASEKHAR

YERKES OBSERVATORY
March 14, 1949

[1] *Ap. J.*, **108**, 92, 1942.

[2] By an oversight, the primes which distinguish the functions $G_{n,m}$ and $G'_{n,m}$ do not appear in the headings of the columns. It may, therefore, be noted that in each case $G'_{n,m}$ is the *second* function tabulated: thus the functions tabulated on p. 109 are, respectively, $G_{11}, G'_{11}, G_{12}, G'_{12}, G_{13}, G'_{13}$, etc.

ERRATA

In Volume **109**, page 312, line 8, *for* Mimas *read* Tethys.

In Volume **109**, page 325 (W. Gleissberg, "The Predictability of the Probable Features of the Sunspot Cycles"), the entries under "Predicted" in Table 2 for t_r, R_M, t_l, and t_f should read <45, >82, <64, >38 and <34, >112, <66, >60 for cycles 16 and 17, respectively, instead of these same numbers without the inequality signs.

TABLE 2-Continued

τ	G_{16}	G'_{16}	G_{26}	G'_{26}	G_{36}	G'_{36}
0	0	0	0	0	0	0
0.01	0.010009	0.009997	0.001933	0.001932	0.000984	0.000984
0.02	0.017188	0.017139	0.003760	0.003758	0.001937	0.001937
0.03	0.023282	0.023173	0.005499	0.005495	0.002861	0.002860
0.04	0.028669	0.028477	0.007160	0.007150	0.003756	0.003754
0.05	0.033530	0.033232	0.008749	0.008732	0.004624	0.004620
0.06	0.037972	0.037548	0.010272	0.010246	0.005466	0.005459
0.07	0.042069	0.041498	0.011735	0.011694	0.006283	0.006271
0.08	0.045872	0.045133	0.013140	0.013083	0.007075	0.007058
0.09	0.049419	0.048493	0.014491	0.014413	0.007844	0.007820
0.10	0.052742	0.051610	0.015791	0.015689	0.008590	0.008558
0.11	0.055865	0.054508	0.017043	0.016914	0.009314	0.009272
0.12	0.058807	0.057208	0.018250	0.018088	0.010018	0.009964
0.13	0.061587	0.059729	0.019414	0.019215	0.010700	0.010633
0.14	0.064219	0.062084	0.020536	0.020297	0.011363	0.011281
0.15	0.066714	0.064287	0.021619	0.021335	0.012007	0.011908
0.16	0.069084	0.066349	0.022665	0.022332	0.012633	0.012514
0.17	0.071338	0.068280	0.023675	0.023288	0.013240	0.013101
0.18	0.073484	0.070089	0.024650	0.024205	0.013830	0.013668
0.19	0.075530	0.071784	0.025593	0.025086	0.014404	0.014217
0.20	0.077483	0.073372	0.026504	0.025930	0.014961	0.014747
0.25	0.086037	0.079912	0.030633	0.029657	0.017520	0.017137
0.30	0.092962	0.084549	0.034142	0.032655	0.019743	0.019135
0.35	0.098643	0.087715	0.037139	0.035038	0.021676	0.020788
0.40	0.103350	0.089722	0.039708	0.036896	0.023361	0.022137
0.45	0.107280	0.090804	0.041520	0.038306	0.024830	0.023218
0.50	0.110583	0.091143	0.043820	0.039332	0.026114	0.024065
0.6	0.115736	0.090136	0.046886	0.040445	0.028218	0.025163
0.7	0.119470	0.087549	0.049195	0.040586	0.029833	0.025622
0.8	0.122208	0.083948	0.050940	0.040019	0.031076	0.025595
0.9	0.124235	0.079726	0.052267	0.038945	0.032036	0.025199
1.0	0.125747	0.075159	0.053279	0.037514	0.032779	0.024532

τ	G_{46}	G'_{46}	G_{56}	G'_{56}	G_{66}	G'_{66}
0	0	0	0	0	0	0
0.01	0.000658	0.000658	0.000494	0.000494	0.000395	0.000395
0.02	0.001297	0.001297	0.000975	0.000975	0.000780	0.000780
0.03	0.001920	0.001919	0.001443	0.001443	0.001156	0.001156
0.04	0.002526	0.002524	0.001900	0.001899	0.001523	0.001522
0.05	0.003115	0.003113	0.002346	0.002344	0.001880	0.001879
0.06	0.003689	0.003685	0.002780	0.002777	0.002229	0.002227
0.07	0.004247	0.004241	0.003203	0.003198	0.002569	0.002566
0.08	0.004791	0.004782	0.003615	0.003608	0.002706	0.002896
0.09	0.005320	0.005307	0.004017	0.004008	0.003225	0.003218
0.10	0.005835	0.005817	0.004408	0.004396	0.003540	0.003531
0.11	0.006336	0.006313	0.004790	0.004774	0.003848	0.003836
0.12	0.006878	0.006795	0.005163	0.005142	0.004149	0.004133
0.13	0.007300	0.007262	0.005525	0.005500	0.004442	0.004423
0.14	0.007762	0.007716	0.005879	0.005848	0.004728	0.004704
0.15	0.008213	0.008157	0.006224	0.006186	0.005007	0.004978
0.16	0.008651	0.008585	0.006560	0.006515	0.005279	0.005244
0.17	0.009078	0.009000	0.006888	0.006834	0.005544	0.005503
0.18	0.009494	0.009403	0.007208	0.007144	0.005803	0.005755
0.19	0.009899	0.009793	0.007519	0.007446	0.006056	0.006000
0.20	0.010294	0.010172	0.007823	0.007739	0.006303	0.006238
0.25	0.012118	0.011895	0.009232	0.009078	0.007448	0.007331
0.30	0.013717	0.013359	0.010474	0.010225	0.008462	0.008271
0.35	0.015121	0.014591	0.011570	0.011199	0.009359	0.009074
0.40	0.016354	0.015617	0.012537	0.012017	0.010152	0.009752
0.45	0.017438	0.016457	0.013391	0.012696	0.010855	0.010319
0.50	0.018392	0.017133	0.014145	0.013250	0.011477	0.010786
0.6	0.019970	0.018064	0.015401	0.014034	0.012517	0.011456
0.7	0.021196	0.018532	0.016384	0.014460	0.013335	0.011836
0.8	0.022150	0.018639	0.017153	0.014605	0.013978	0.011984
0.9	0.022894	0.018467	0.017757	0.014524	0.014485	0.011895
1.0	0.023474	0.018084	0.018231	0.014273	0.014884	0.011771

INDEX TO VOLUME 109

INDEX TO SUBJECTS

TW Andromedae, Spectrographic Observations of. *W. A. Hiltner, Burke Smith, and O. Struve* . . . 95

Anharmonic Pulsations of the Standard Model. *Martin Schwarzschild and Malcolm P. Savedoff* . . . 298

Bands in the Photographic Infrared Spectra of Long-Period Variables, New. *J. J. Nassau, G. B. van Albada, and P. C. Keenan* . . . 333

Be, Upper Limits on the Abundances of Interstellar *Li* and. *Lyman Spitzer, Jr.* . . . 548

Bright H and K Lines of Calcium, Stars Whose Spectra Have. *Alfred H. Joy and Ralph E. Wilson* . . . 231

Ca II, Oscillator Strengths for the Continua of. *Louis C. Green* . . . 289

Calcium, Stars Whose Spectra Have Bright H and K Lines of. *Alfred H. Joy and Ralph E. Wilson* . . . 231

α Canis Minoris and α Persei, Spectrophotometry of the F Stars. III. *Jesse L. Greenstein and W. A. Hiltner* . . . 265

β Cephei, The Radial Velocity of. *Mogens Rudkjøbing* . . . 331

Cepheus, A Bright Region in. *A. Marguerite Risley* . . . 314

CH_4 in the Solar Spectrum, Telluric Bands of. *Robert R. McMath, Orren C. Mohler, and Leo Goldberg* . . . 17

CN, Wave Lengths of the (0, 0) Band Heads in the Infrared System of. *C. C. Kiess* . . . 551

Contours of Absorption Lines, Theoretical. *Daniel L. Harris III* . . . 53

T Coronae Borealis, High-Dispersion Spectrograms of. *Roscoe F. Sanford* . . . 81

Cosmological Model, A Nonhomogeneous. *Guy C. Omer, Jr.* . . . 164

Curves of Growth for the Formation of Absorption Lines According to the Milne-Eddington Model, Exact. I. Total Flux. *Marshal H. Wrubel* . . . 66

XZ Cygni, The Radial Velocity of. *O. Struve and A. Van Hoof* . . . 215

Degenerate Stellar Configurations near the Limiting Mass, The Structure of. *Anders Reiz* 303

Dynamical Friction. *Marvin Lee White* . . . 159

Eclipsing Star XZ Sagittarii, New Spectrographic Observations of the. *Jorge Sahade* . . . 439

Eclipsing Variable SW Lacertae, Spectrographic Observations of the. *Otto Struve* . . . 436

Eclipsing Variable RS Sagittarii, Spectrographic Observations of the. *Jorge Sahade* . . . 116

Editor's Note . . . 179

Electron Density near the Earth's Orbit, An Upper Limit to the. *Fred L. Whipple and Joseph L. Gossner* . . . 380

Errata 555

Erratum 336

Functions $G_{n,m}(\tau)$ and $G'_{n,m}(\tau)$ of Order 6 ($m = 6$ and $m \geqslant n$), The. *S. Chandrasekhar* . 555

HD 190918, The Wolf-Rayet Spectroscopic Binary. *O. C. Wilson* 76

Interstellar H and K, Molecular Lines, and Radial Velocities in the Spectra of 300 O and B Stars, Observations of. *Walter S. Adams* 354

Interstellar *Li* and *Be*, Upper Limits on the Abundances of. *Lyman Spitzer, Jr.* 548

Interstellar Matter, The Temperature of. II. *Lyman Spitzer, Jr.* 337

Isothermal Function, The. *S. Chandrasekhar and Gordon W. Wares* 551

SW Lacertae, Spectrographic Observations of the Eclipsing Variable. *Otto Struve* . . . 436

Li and *Be*, Upper Limits on the Abundances of Interstellar. *Lyman Spitzer, Jr.* 548

Longitude of Periastron, Further Note on the Distribution of the. *Elizabeth L. Scott* . . 446

Longitude of Periastron of Spectroscopic Binaries, Distribution of the. *Elizabeth L. Scott* . 194

Luminosity Function, Variations in the Stellar. II. A Region in Orion. *S. W. McCuskey* . 139

Luminosity Function, Variations in the Stellar. III. A Region in Auriga. *S. W. McCuskey* 444

RR Lyrae from Coudé Spectrograms, Radial Velocities of. *Roscoe F. Sanford* 208

Metallic-Line Stars, Analysis of the. II. *Jesse L. Greenstein* 121

Metallic-Line Stars, A Catalogue of the Brighter. *Arne Slettebak* 547

Molecular Band at λ 3682 in the Spectra of Late-Type Stars, Identification of a. *George H. Herbig* 109

Molecular Lines, and Radial Velocities in the Spectra of 300 O and B stars, Observations of Interstellar H and K. *Walter S. Adams* 354

M-Type Stars in Cygnus, A Study of. *J. J. Nassau and G. B. van Albada* 391

Multiplet Intensities for the Nebular Lines $^4S - {}^2D$ of *O* II. *L. H. Aller, C. W. Ufford, and J. H. Van Vleck* 42

N_2^+ Flashes at Twilight and Dawn, Comparison of the *Na* and. *P. Swings and M. Nicolet* 327

Na and N_2^+ Flashes at Twilight and Dawn, Comparison of the. *P. Swings and M. Nicolet* 327

Nebula and an Associated Variable Star, A Reflection. *Balfour S. Whitney* 540

Nebulae, Photographic Studies of. VI. The Great Nebulous Region in Cygnus Photographed in Red Light. *John C. Duncan* 479

Noncoherent Scattering, On the Formation of Absorption Lines by. *Guido Münch* . . 275

Nonradial Oscillations of the Standard Model. *Zdeněk Kopal* 509

O II, Multiplet Intensities for the Nebular Lines $^4S - {}^2D$ of. *L. H. Aller, C. W. Ufford, and J. H. Van Vleck* 42

Oscillator Strengths for the Continua of *Ca* II. *Louis C. Green* 289

AR Pavonis, The Spectrum of. *Jorge Sahade* 541

γ Pegasi, The Atmosphere of. *Lawrence H. Aller* 244

α Persei, Spectrophotometry of the F Stars α Canis Minoris and. III. *Jesse L. Greenstein and W. A. Hiltner* . . . 265

Photoelectric Observations of W Virginis. *Katherine C. Gordon and Gerald E. Kron* . . 177

Planetary Nebula, A Large New. *F. D. Miller and E. van Dien* . . . 537

Planetary Nebulae," Note on the Paper, "The Absorption-Line Spectra of the Central Stars of the. *Lawrence H. Aller* . . . 179

Planetary and Satellite Distances, The Law of. *Gerard P. Kuiper* . . . 308

Polarization in the Continuous Radiation of Stars, On the Presence of. II. *W. A. Hiltner* . 471

Radial Velocities of RR Lyrae from Coudé Spectrograms. *Roscoe F. Sanford* . . . 208

Radial Velocities in the Spectra of 300 O and B Stars, Observations of Interstellar H and K, Molecular Lines, and. *Walter S. Adams* . . . 354

Radial Velocity of β Cephei, The. *Mogens Rudkjøbing* . . . 331

Radial Velocity of XZ Cygni, The. *O. Struve and A. Van Hoof* . . . 215

Radial-Velocity Measures of Eight Stars Formerly Assigned to the β Cephei Group, An Analysis of. *John F. Heard* . . . 185

Radial-Velocity Observations with the Bruce Spectrograph. *Daniel M. Popper* . . . 100

Reviews:

CAMBI, ENZO. *Eleven and Fifteen-Place Tables of Bessel Functions of the First Kind, to All Significant Orders* . . . 182

Centennial Symposia (Otto Struve) . . . 180

COMPUTATION LABORATORY OF THE NATIONAL APPLIED MATHEMATICS LABORATORIES, NATIONAL BUREAU OF STANDARDS. *Tables of Bessel Functions of Fractional Order*, Vol. 1 . . . 182

FLUEGGE, S. "An Introduction to Nuclear Physics," and *Nuclear Physics Tables*, by J. MATTAUCH . . . 182

HOSMER, GEORGE L., and JAMES M. ROBBINS. *Practical Astronomy* (Daniel L. Harris III) . . . 183

JÁNOSSY, L. *Cosmic Rays* . . . 183

KENNON, WILLIAM L. *Astronomy* (Daniel L. Harris III) . . . 184

MATTAUCH, J. *Nuclear Physics Tables* and "An Introduction to Nuclear Physics," by S. FLUEGGE . . . 182

NASSAU, JASON J. *Practical Astronomy* (Daniel L. Harris III) . . . 183

ROBBINS, JAMES M., and GEORGE L. HOSMER. *Practical Astronomy* (Daniel L. Harris III) . . . 183

Rotating Star, The Oscillations of a. *T. G. Cowling and R. A. Newing* . . . 149

υ Sagittarii, Displaced Absorption Lines in the Spectrum of. *W. P. Bidelman* . . . 544

XZ Sagittarii, New Spectrographic Observations of the Eclipsing Star. *Jorge Sahade* . . 439

RS Sagittarii, Spectrographic Observations of the Eclipsing Variable. *Jorge Sahade* . . 116

Solar Lines in the Spectral Region 1.52–1.75 μ, New. *Leo Goldberg, Orren C. Mohler, and Robert R. McMath* . . . 28

Solar Spectra, Analysis of the First Rocket Ultraviolet. *E. Durand, J. J. Oberly, and R. Tousey* 1

Solar Spectrum, Telluric Bands of CH_4 in the. *Robert R. McMath, Orren C. Mohler, and Leo Goldberg* 17

Spectra of the Central Stars of the Planetary Nebulae," Note on the Paper, "The Absorption-Line. *Lawrence H. Aller* 179

Spectra with Emission Lines in the Obscuring Clouds of Ophiuchus and Scorpius, Stellar. *Otto Struve and Mogens Rudkjøbing* 92

Spectra in Milky Way Regions, Stellar. I. A Region in Aquila. *S. W. McCuskey* . . . 426

Spectrograms of T Coronae Borealis, High-Dispersion. *Roscoe F. Sanford* 81

Spectrographic Observations of TW Andromedae. *W. A. Hiltner, Burke Smith, and O. Struve* 95

Spectrographic Observations of the Eclipsing Star XZ Sagittarii, New. *Jorge Sahade* . 439

Spectrographic Observations of the Eclipsing Variable SW Lacertae. *Otto Struve* . . . 436

Spectrographic Observations of the Eclipsing Variable RS Sagittarii. *Jorge Sahade* . . 116

Spectrophotometry of the F Stars α Canis Minoris and α Persei. III. *Jesse L. Greenstein and W. A. Hiltner* 265

Spectroscopic Binaries, Distribution of the Longitude of Periastron of. *Elizabeth L. Scott* 194

Spectroscopic Binary HD 190918, The Wolf-Rayet. *O. C. Wilson* 76

Spectrum of AR Pavonis, The. *Jorge Sahade* 541

Spectrum of *v* Sagittarii, Displaced Absorption Lines in the. *W. P. Bidelman* 544

Star of Large Proper Motion (L 726-8), A New. *Willem J. Luyten* 532

Stark Effect of the Higher Balmer Lines in Stars of Spectral Types A and B, The. *Elsa van Dien* 452

Stellar Atmospheres, Superthermic Phenomena in. III. The Chromospheric Radiation Field. *Richard N. Thomas* 480

Stellar Atmospheres, Superthermic Phenomena in. IV. The Wolf-Rayet Atmosphere. *Richard N. Thomas* 500

Sunspot Cycles, The Predictability of the Probable Features of the. *W. Gleissberg* . . 321

Uranus Atmosphere, New Absorptions in the. *Gerard P. Kuiper* 540

Variable Star, A New. *Balfour S. Whitney* 538

Variable Star, A Reflection Nebula and an Associated. *Balfour S. Whitney* 540

Variables, New Bands in the Photographic Infrared Spectra of Long-Period. *J. J. Nassau, G. B. van Albada, and P. C. Keenan* 333

W Virginis, Photoelectric Observations of. *Katherine C. Cordon and Gerald E. Kron* . . 177

White Dwarfs, An Atlas of Identification Charts of. *Willem J. Luyten* 528

Wolf-Rayet Spectroscopic Binary HD 190918, The. *O. C. Wilson* 76

INDEX TO AUTHORS

ADAMS, WALTER S. Observations of Interstellar H and K, Molecular Lines, and Radial Velocities in the Spectra of 300 O and B Stars 354

ALLER, L. H., C. W. UFFORD, and J. H. VAN VLECK. Multiplet Intensities for the Nebular Lines $^4S - {}^2D$ of *O* II 42

ALLER, LAWRENCE H. The Atmosphere of γ Pegasi 244

ALLER, LAWRENCE H. Note on the Paper, "The Absorption-Line Spectra of the Central Stars of the Planetary Nebulae" 179

BIDELMAN, W. P. Displaced Absorption Lines in the Spectrum of υ Sagittarii . . . 544

CHANDRASEKHAR, S. The Functions $G_{n,m}(\tau)$ and $G'_{n,m}(\tau)$ of Order 6 ($m = 6$ and $m \geqslant n$) 555

CHANDRASEKHAR, S., and GORDON W. WARES. The Isothermal Function 551

COWLING, T. G., and R. A. NEWING. The Oscillations of a Rotating Star 149

DUNCAN, JOHN C. Photographic Studies of Nebulae. VI. The Great Nebulous Region in Cygnus Photographed in Red Light 479

DURAND, E., J. J. OBERLY, and R. TOUSEY. Analysis of the First Rocket Ultraviolet Solar Spectra 1

GLEISSBERG, W. The Predictability of the Probable Features of the Sunspot Cycles . . 321

GOLDBERG, LEO, ROBERT R. MCMATH, and ORREN C. MOHLER. New Solar Lines in the Spectral Region 1.52–1.75 μ 28

GOLDBERG, LEO, ROBERT R. MCMATH, and ORREN C. MOHLER. Telluric Bands of CH_4 in the Solar Spectrum 17

GORDON, KATHERINE C., and GERALD E. KRON. Photoelectric Observations of W Virginis 177

GOSSNER, JOSEPH L., and FRED L. WHIPPLE. An Upper Limit to the Electron Density near the Earth's Orbit 380

GREEN, LOUIS C. Oscillator Strengths for the Continua of *Ca* II 289

GREENSTEIN, JESSE L. Analysis of the Metallic-Line Stars. II 121

GREENSTEIN, JESSE L., and W. A. HILTNER. Spectrophotometry of the F Stars α Canis Minoris and α Persei. III 265

HARRIS, DANIEL L. III. Review of: *Astronomy*, William L. Kennon 184

HARRIS, DANIEL L. III. Review of: *Practical Astronomy*, George E. Hosmer and James M. Robbins 183

HARRIS, DANIEL L. III. Review of: *Practical Astronomy*, Jason J. Nassau 183

HARRIS, DANIEL L. III. Theoretical Contours of Absorption Lines 53

HEARD, JOHN F. An Analysis of Radial-Velocity Measures of Eight Stars Formerly Assigned to the β Cephei Group 185

HERBIG, GEORGE H. Identification of a Molecular Band at λ 3682 in the Spectra of Late-Type Stars . . . 109

HILTNER, W. A. On the Presence of Polarization in the Continuous Radiation of Stars. II 471

HILTNER, W. A., BURKE SMITH, and O. STRUVE. Spectrographic Observations of TW Andromedae . . . 95

HILTNER, W. A., and JESSE L. GREENSTEIN. Spectrophotometry of the F Stars α Canis Minoris and α Persei. III . . . 265

JOY, ALFRED H., and RALPH E. WILSON. Stars Whose Spectra Have Bright H and K Lines of Calcium . . . 231

KEENAN, P. C., J. J. NASSAU, and G. B. VAN ALBADA. New Bands in the Photographic Infrared Spectra of Long-Period Variables . . . 333

KIESS, C. C. Wave Lengths of the (0, 0) Band Heads in the Infrared System of *CN* . . . 551

KOPAL, ZDENĚK. Nonradial Oscillations of the Standard Model . . . 509

KRON, GERALD E., and KATHERINE C. GORDON. Photoelectric Observations of W Virginis 177

KUIPER, GERARD P. The Law of Planetary and Satellite Distances . . . 308

KUIPER, GERARD P. New Absorptions in the Uranus Atmosphere . . . 540

LUYTEN, WILLEM J. An Atlas of Identification Charts of White Dwarfs . . . 528

LUYTEN, WILLEM J. A New Star of Large Proper Motion (L 726-8) . . . 532

MCCUSKEY, S. W. Stellar Spectra in Milky Way Regions. I. A Region in Aquila . . . 426

MCCUSKEY, S. W. Variations in the Stellar Luminosity Function. II. A Region in Orion 139

MCCUSKEY, S. W. Variations in the Stellar Luminosity Function. III. A Region in Auriga 414

MCMATH, ROBERT R., LEO GOLDBERG, and ORREN C. MOHLER. New Solar Lines in the Spectral Region 1.52–1.75 μ . . . 28

MCMATH, ROBERT R., LEO GOLDBERG, and ORREN C. MOHLER. Telluric Bands of CH_4 in the Solar Spectrum . . . 17

MILLER, F. D., and E. VAN DIEN. A Large New Planetary Nebula . . . 537

MOHLER, ORREN C., ROBERT R. MCMATH, and LEO GOLDBERG. New Solar Lines in the Spectral Region 1.52–1.75 μ . . . 28

MOHLER, ORREN C., ROBERT R. MCMATH, and LEO GOLDBERG. Telluric Bands of CH_4 in the Solar Spectrum . . . 17

MÜNCH, GUIDO. On the Formation of Absorption Lines by Noncoherent Scattering . . . 275

NASSAU, J. J., and G. B. VAN ALBADA. A Study of M-Type Stars in Cygnus . . . 391

NASSAU J. J., G.B. VAN ALBADA and P. C. KEENAN. New Bands in the Photographic Infrared Spectra of Long-Period Variables . . . 333

NEWING, R. A., and T. G. COWLING. The Oscillations of a Rotating Star . . . 149

NICOLET, M., and P. SWINGS. Comparison of the *Na* and N_2^+ Flashes at Twilight and Dawn . . . 327

OBERLY, J. J., E. DURAND, and R. TOUSEY. Analysis of the First Rocket Ultraviolet Solar Spectra . . . 1

OMER, GUY C., JR. A Nonhomogeneous Cosmological Model 164

POPPER, DANIEL M. Radial-Velocity Observations with the Bruce Spectrograph . . . 100

REIZ, ANDERS. The Structure of Degenerate Stellar Configurations near the Limiting Mass 303

RISLEY, A. MARGUERITE. A Bright Region in Cepheus 314

RUDKJØBING, MOGENS. The Radial Velocity of β Cephei 331

RUDKJØBING, MOGENS, and OTTO STRUVE. Stellar Spectra with Emission Lines in the Obscuring Clouds of Ophiuchus and Scorpius 92

SAHADE, JORGE. New Spectrographic Investigations of the Eclipsing Star XZ Sagittarii . 439

SAHADE, JORGE. Spectrographic Observations of the Eclipsing Variable RS Sagittarii . 116

SAHADE, JORGE. The Spectrum of AR Pavonis 541

SANFORD, ROSCOE F. High-Dispersion Spectrograms of T Coronae Borealis 81

SANFORD, ROSCOE F. Radial Velocities of RR Lyrae from Coudé Spectrograms . . . 208

SAVEDOFF, MALCOLM P., and MARTIN SCHWARZSCHILD. Anharmonic Pulsations of the Standard Model 298

SCHWARZSCHILD, MARTIN, and MALCOLM P. SAVEDOFF. Anharmonic Pulsations of the Standard Model 298

SCOTT, ELIZABETH L. Distribution of the Longitude of Periastron of Spectroscopic Binaries 194

SCOTT, ELIZABETH L. Further Note on the Distribution of the Longitude of Periastron . 446

SLETTEBAK, ARNE. A Catalogue of the Brighter Metallic-Line Stars 547

SMITH, BURKE, W. A. HILTNER, and O. STRUVE. Spectrographic Observations of TW Andromedae 95

SPITZER, LYMAN, JR. The Temperature of Interstellar Matter. II 337

SPITZER, LYMAN, JR. Upper Limits on the Abundances of Interstellar *Li* and *Be*. . . 548

STRUVE, O., W. A. HILTNER, and BURKE SMITH. Spectrographic Observations of TW Andromedae 95

STRUVE, O., and A. VAN HOOF. The Radial Velocity of XZ Cygni 215

STRUVE, OTTO. Review of: *Centennial Symposia* 180

STRUVE, OTTO. Spectrographic Observations of the Eclipsing Variable SW Lacertae . . 436

STRUVE, OTTO, and MOGENS RUDKJØBING. Stellar Spectra with Emission Lines in the Obscuring Clouds of Ophiuchus and Scorpius 92

SWINGS, P., and M. NICOLET. Comparison of the *Na* and N_2^+ Flashes at Twilight and Dawn 327

THOMAS, RICHARD N. Superthermic Phenomena in Stellar Atmospheres. III. The Chromospheric Radiation Field 480

THOMAS, RICHARD N. Superthermic Phenomena in Stellar Atmospheres. IV. The Wolf-Rayet Atmosphere 500

TOUSEY, R., E. DURAND, and J. J. OBERLY. Analysis of the First Rocket Ultraviolet Solar Spectra 1

UFFORD, C. W., L. H. ALLER, and J. H. VAN VLECK. Multiplet Intensities for the Nebular Lines $^4S - {}^2D$ of *O* II 42

VAN ALBADA, G. B., and J. J. Nassau. A Study of M-Type Stars in Cygnus 391

VAN ALBADA, G. B., J. J. Nassau, and P. C. KEENAN. New Bands in the Photographic Infrared Spectra of Long-Period Variables 333

VAN DIEN, E., and F. D. MILLER. A Large New Planetary Nebula 537

VAN DIEN, ELSA. The Stark Effect of the Higher Balmer Lines in Stars of Spectral Types A and B 452

VAN HOOF, A., and O. STRUVE. The Radial Velocity of XZ Cygni 215

VAN VLECK, J. H., L. H. ALLER, and C. W. UFFORD. Multiplet Intensities for the Nebular Lines $^4S - {}^2D$ of *O* II 42

WARES, GORDON W., and S. CHANDRASEKHAR. The Isothermal Function 551

WHIPPLE, FRED L., and JOSEPH L. GOSSNER. An Upper Limit to the Electron Density near the Earth's Orbit 380

WHITE, MARVIN LEE. Dynamical Friction 159

WHITNEY, BALFOUR S. A New Variable Star 538

WHITNEY, BALFOUR S. A Reflection Nebula and an Associated Variable Star 540

WILSON, O. C. The Wolf-Rayet Spectroscopic Binary HD 190918 76

WILSON, RALPH E., and ALFRED H. JOY. Stars Whose Spectra Have Bright H and K Lines of Calcium 231

WRUBEL, MARSHAL H. Exact Curves of Growth for the Formation of Absorption Lines According to the Milne-Eddington Model. I. Total Flux 66

THE OBSERVATORY

FOUNDED 1877

* * *

A Magazine presenting current developments in Astronomy by means of Articles, Correspondence, Notes on discoveries and Reviews of important astronomical books. The papers read at the Meetings (Astronomical & Geophysical) of the Royal Astronomical Society and the discussions which follow are also fully reported.

* * *

Annual subscription for 6 issues, post free, 15/–
should be sent to

The Editors, ROYAL OBSERVATORY
Greenwich, London S.E., 10

The FACE of the MOON

BY RALPH B. BALDWIN

An answer, in terms of the meteorite theory, to the question of how the moon came to exist in its present form.

The study of the moon—a mirror for the study of the earth.

256 pages. 6¼"×9¼". Illustrated. $5.00.

THE UNIVERSITY OF CHICAGO PRESS

POPULAR ASTRONOMY

A magazine now in its fifty-seventh year, devoted to the elementary aspects of Astronomy and allied sciences.

Published monthly, except July and September.

Yearly subscription rates: Domestic $4.00; Canadian $4.25; Foreign $4.50.

Address

POPULAR ASTRONOMY
CARLETON COLLEGE
NORTHFIELD, MINNESOTA, U.S.A.

ASTROPHYSICAL MONOGRAPHS

Sponsored by the Editors of the Astrophysical Journal

PRINCIPLES OF STELLAR DYNAMICS

By S. CHANDRASEKHAR

In this monograph the dynamical methods of interpreting the motions in the galaxy, spiral nebulae, and star clusters are developed from a coherent point of view. "This book should exert a profound influence on the future developments in the field of galactic dynamics. I can recommend its study unreservedly to newcomers in the field and to those who already have a passing acquaintance with its problems. The experts can profit from reading it."—BART J. BOK, in *Science*. 1942. $3.00

AN ATLAS OF STELLAR SPECTRA. By W. W. MORGAN, PHILIP C. KEENAN, and EDITH KELLMAN

This work represents approximately ten years of spectrographic observations with the 40-inch telescope at Yerkes Observatory. It consists of fifty-five photographic prints, size 8 by 10 inches, in a portfolio. In the booklet accompanying the prints a complete summary of the spectral classification is given. The atlas and text have been prepared with the needs of the stellar astronomer in mind and the whole work is technical in nature. 1943. $20.00

SPECTRA OF LONG-PERIOD VARIABLE STARS

By PAUL W. MERRILL

This monograph is devoted largely to the observational side of the subject, but some discussion of the physical significance of various spectral features is included. A brief introduction and a historical chapter are inserted for the benefit of the reader who is not a specialist in stellar spectra. "To one wishing an intimate view of our present knowledge of the spectra of long-period variable stars, whether he be a student, astronomer, physicist, or chemist, the present monograph is recommended."—J. H. MOORE in *Astronomical Society of the Pacific*. 1940. *Paper*, $2.50

THE MASSES OF THE STARS, WITH A GENERAL CATALOGUE OF DYNAMICAL PARALLAXES

By HENRY NORRIS RUSSELL and CHARLOTTE E. MOORE

"Astrophysicists will be grateful to the authors for so thorough an examination of available knowledge. . . . We may be permitted to congratulate the senior author on this magnificent outgrowth from an idea which germinated in his mind thirty years ago."—PROFESSOR A. S. EDDINGTON, *The Observatory* (England). 1940. *Paper*, $4.50

AN INTRODUCTION TO THE STUDY OF STELLAR STRUCTURE. By S. CHANDRASEKHAR

Treats in a deductive manner the subject of stellar interiors. The necessary physical theories and mathematical methods are fully explained. Includes accounts of the foundations of thermodynamics, the theory of radiation, the quantum theory of a perfect gas, and a discussion of the elements of nuclear physics. "The material is throughout presented with enviable crispness and clarity of expression. The work will undoubtedly become an indispensable handbook for future researchers in this field."—*Nature* (England). 1939. $10.00

THE DISTRIBUTION OF THE STARS IN SPACE

By BART J. BOK

". . . . an extremely important contribution to the field of galactic structure, invaluable alike to both students and research workers in the field."—*Science*. The large number and variety of researches carried out in this field during the past fifteen years are discussed critically in this study with clarity and dispatch. 1937. *Paper*, $2.50

THE UNIVERSITY OF CHICAGO PRESS